2011

Hydroxyl-bridged lanthanide amino acid clusters and hexatantalum and hexatungsten chloride clusters: synthesis, characterization, and relevance to biomedical imaging

David Alan Rotsch
University of Iowa

HYDROXYL-BRIDGED LANTHANIDE AMINO ACID CLUSTERS AND HEXATANTALUM AND HEXATUNGSTEN CHLORIDE CLUSTERS: SYNTHESIS, CHARACTERIZATION, AND RELEVANCE TO BIOMEDICAL IMAGING

by

David Alan Rotsch

An Abstract

Of a thesis submitted in partial fulfillment
of the requirements for the Doctor of
Philosophy degree in Chemistry
in the Graduate College of
The University of Iowa

May 2011

Thesis Supervisor: Associate Professor Louis Messerle

ABSTRACT

The synthesis and characterization of polynuclear lanthanide complexes and tungsten chloride clusters are detailed. The relevance of these complexes to MRI contrast agents, physiological parameter reporting MRI contrast agents, and X-ray computed tomography contrast agents is discussed. Polylanthanides, in particular polygadolinium and polyeuropium(II) complexes, represent a paradigm shift in contrast agent design.

Base hydrolysis of aqueous $Ln(ClO_4)_3$ in the presence of L-histidine and alkali metal halide anions (Cl^-, Br^-, and I^-) yields the pentadecalanthanide(III) complexes $[Ln_{15}(\mu_5\text{-}X)(\mu_3\text{-}OH)_{20}(his^{+/-})_{10}(his^-)_5(OH)_7]^{12+}$ (X = Cl^- or Br^-; $his^{+/-}$ = zwitterionic histidine, his^- = histidinate) and $[Ln_{15}(\mu_5\text{-}OH)(I)_2(\mu_3\text{-}OH)_{20}(his^{+/-})_{10}(his^-)_5(OH)_7]^{10+}$ for Ln = Y, Eu, Gd, Tb, Nd, and La (abbreviated Ln_{15}–his X). Base hydrolysis of $Ln(ClO_4)_3$ in the presence of L-histidine without added halide yields the complex $[Ln_{15}(\mu_5\text{-}OH)\text{-}(\mu_3\text{-}OH)_{20}(his^{+/-})_{10}(his^-)_5(OH)_7]^{12+}$ (Ln_{15}-his OH) for Ln = Eu and Tb. These latter complexes represent the first halide-free complexes of this structure type. Solution studies revealed the latter complex's ability to capture halides (Cl^-, Br^-, and I^-) to generate the corresponding Ln_{15}-his X complexes described above. All new complexes were characterized by single-crystal X-ray diffraction.

Polyeruopium(III) complexes were studied by electrochemistry and spectrofluorimetry. Diffusion coefficients of Eu_{15}-his X complexes were determined to be between 2.0 $x10^{-7}$ and 1.2 $x10^{-6}$ cm^2/s. From fluorescence studies, approximately 22 waters were found to coordinate to the inner sphere of the Eu(III) ions in Eu_{15}-his X. Fluorescence data supported the coordination of strong-field ligands, such as carboxylates and hydroxides. It was also found that the hydrogens of μ_3-OH ligands are capable of exchanging with bulk D_2O. Electrospray ionization mass spectroscopy (ESI-MS) on the Eu(III)-based clusters showed mass-to-charge peaks representative of the intact cluster core minus several counter ions and ligands.

Yttrium analogues were prepared for ^{13}C and ^{89}Y NMR spectroscopy studies. The ^{13}C NMR spectra exhibited two sets of resonances for histidine. One set matches that of free-histidine in aqueous solution, and the other most likely represents yttrium-coordinated histidine. ^{89}Y NMR spectra exhibited two resonances and correlate with the solid-state structure.

Solution-state studies of the Ln_{15}-his X complexes suggest that the Ln_{15}-his X clusters maintain the observed solid-state structure in solution.

Inner-ligand-substituted hexanuclear tantalum and tungsten chloride clusters were also investigated. Substitution of inner chlorines by metathesis of the robust cluster cores in solution proved to be challenging. Solid-state synthesis to obtain mixed oxygen-chlorine hexatantalum clusters resulted in ampoule explosions because of side reactions between the reactants and the quartz ampoule. Solid-state routes towards tungsten clusters with mixed inner ligands yielded the $(H_3O)_2[\alpha/\beta\text{-}W_6(\mu_2\text{-}O)_6\text{-}(\mu_2\text{-}Cl)_6Cl_6]\cdot X(H_2O)$ ($X_\alpha = 4$; $X_\beta = 6$) complexes.

Abstract Approved: ________________________________
Thesis Supervisor

____
Title and Department

____
Date

HYDROXYL-BRIDGED LANTHANIDE AMINO ACID CLUSTERS AND HEXATANTALUM AND HEXATUNGSTEN CHLORIDE CLUSTERS: SYNTHESIS, CHARACTERIZATION, AND RELEVANCE TO BIOMEDICAL IMAGING

by

David Alan Rotsch

A thesis submitted in partial fulfillment
of the requirements for the Doctor of
Philosophy degree in Chemistry
in the Graduate College of
The University of Iowa

May 2011

Thesis Supervisor: Associate Professor Louis Messerle

Graduate College
The University of Iowa
Iowa City, Iowa

CERTIFICATE OF APPROVAL

PH.D. THESIS

This is to certify that the Ph.D. thesis of

David Alan Rotsch

has been approved by the Examining Committee
for the thesis requirement for the Doctor of Philosophy
degree in Chemistry at the May 2011 graduation.

Thesis Committee: ___________________________________
Louis Messerle, Thesis Supervisor

____
Ned B. Bowden

____
Darrell P. Eyman

____
Edward G. Gillan

____
Alan Stolpen

To my family, especially my wife and son.

There is nothing like looking around, if you want to find something.
You certainly usually find something, if you look, but it is not always quite the something you were after

J.R.R. Tolkien

ACKNOWLEDGMENTS

There is a long list of people that will need to be thanked for helping me develop professionally and personally. For all of those whom I do not specifically thank here, I would like to extend my sincere appreciation and thanks.

First and foremost I would like to thank Prof. Lou Messerle for his guidance and personal support throughout my time here at Iowa. I find myself fortunate to have had the privilege of working with someone like you. Two of the most valuable lessons I have learned from you are (1) how to be the "devil's advocate" when it comes to making conclusions and (2) how you never miss something until you don't have it. You have been an excellent advisor especially knowing when to allow me to venture in my own directions and when to reign me back in.

There are several people within the Chemistry Department at the University of Iowa who should receive recognition I would like to thank Dale Swenson for collecting X-ray data, solving crystal structures, and helping me understand all the little nuances of solving crystal structures. Peter Hatch, for making all the crazy glassware I asked of him and for personal conversations. I would like to thank Sharon Robertson and Janet Kugley for their friendship and all of their help and guidance.

My Messerle group colleagues, both past and present. John Thurston, Adil Mohammad, Ross Bemowski, Jeremy Hubbard, Tom Wood, Chris Kassl, and Justine Olson have all enhanced the graduate school experience and provided a wonderful atmosphere in which to work. I am very thankful to John for helping me cope with the early years of graduate school. I would especially like to thank Adil for his support and particular brand of entertainment. To those of you who suffered through reading my thesis prior to Lou's editing, my sincere apologies and thanks. To the undergraduates who assisted me through the years, I would like to offer my sincere thanks.

There are several friends that I have gained during my graduate career here at Iowa and I would like to thank each and every one of them for being apart of my graduate school journey and making my life richer in the process. In particular I would like to thank Tim Paschkewitz, Perry Motsegood, Mike Ivanov, Kristina Rogers, Gordy Hunter, Joe Cannistra, and Beth Elaqua. I will not forget the good times that we have had especially during tailgating, intramurals, and city leagues. I will especially miss those afternoon runs with Tim, Mike and Perry.

Most of all I would like to thank my wife Kristen. She has been kind enough to put up with everything that I had to offer these past several years. I thank you for your patience and understanding. I thank you for picking up the slack when I was under pressure. Your support and encouragement throughout my graduate career was more appreciated than you will ever know. Finally, thank you for our son. He has brought me more joy than I ever thought imaginable. Hopefully he will encompass the best of us both.

Lastly I would like to thank the rest of my family. Your continual questioning of “when are you going to graduate” and other forms of encouragement provided extra incentive for me to finish my degree.

ABSTRACT

The synthesis and characterization of polynuclear lanthanide complexes and tungsten chloride clusters are detailed. The relevance of these complexes to MRI contrast agents, physiological parameter reporting MRI contrast agents, and X-ray computed tomography contrast agents is discussed. Polylanthanides, in particular polygadolinium and polyeuropium(II) complexes, represent a paradigm shift in contrast agent design.

Base hydrolysis of aqueous $Ln(ClO_4)_3$ in the presence of L-histidine and alkali metal halide anions (Cl^-, Br^-, and I^-) yields the pentadecalanthanide(III) complexes $[Ln_{15}(\mu_5\text{-}X)(\mu_3\text{-}OH)_{20}(his^{+/-})_{10}(his^-)_5(OH)_7]^{12+}$ (X = Cl^- or Br^-; $his^{+/-}$ = zwitterionic histidine, his^- = histidinate) and $[Ln_{15}(\mu_5\text{-}OH)(I)_2(\mu_3\text{-}OH)_{20}(his^{+/-})_{10}(his^-)_5(OH_2)_7]^{10+}$ for Ln = Y, Eu, Gd, Tb, Nd, and La (abbreviated Ln_{15}–his X). Base hydrolysis of $Ln(ClO_4)_3$ in the presence of L-histidine without added halide yields the complex $[Ln_{15}(\mu_5\text{-}OH)\text{-}(\mu_3\text{-}OH)_{20}(his^{+/-})_{10}(his^-)_5(OH)_7]^{12+}$ (Ln_{15}-his OH) for Ln = Eu and Tb. These latter complexes represent the first halide-free complexes of this structure type. Solution studies revealed the latter complex's ability to capture halides (Cl^-, Br^-, and I^-) to generate the corresponding Ln_{15}-his X complexes described above. All new complexes were characterized by single-crystal X-ray diffraction.

Polyeruopium(III) complexes were studied by electrochemistry and spectrofluorimetry. Diffusion coefficients of Eu_{15}-his X complexes were determined to be between 2.0 $x10^{-7}$ and 1.2 $x10^{-6}$ cm^2/s. From fluorescence studies, approximately 22 waters were found to coordinate to the inner sphere of the Eu(III) ions in Eu_{15}-his X. Fluorescence data supported the coordination of strong-field ligands, such as carboxylates and hydroxides. It was also found that the hydrogens of μ_3-OH ligands are capable of exchanging with bulk D_2O. Electrospray ionization mass spectroscopy (ESI-MS) on the Eu(III)-based clusters showed mass-to-charge peaks representative of the intact cluster core minus several counter ions and ligands.

Yttrium analogues were prepared for ^{13}C and ^{89}Y NMR spectroscopy studies. The ^{13}C NMR spectra exhibited two sets of resonances for histidine. One set matches that of free-histidine in aqueous solution, and the other most likely represents yttrium-coordinated histidine. ^{89}Y NMR spectra exhibited two resonances and correlate with the solid-state structure.

Solution-state studies of the Ln_{15}-his X complexes suggest that the Ln_{15}-his X clusters maintain the observed solid-state structure in solution.

Inner-ligand-substituted hexanuclear tantalum and tungsten chloride clusters were also investigated. Substitution of inner chlorines by metathesis of the robust cluster cores in solution proved to be challenging. Solid-state synthesis to obtain mixed oxygen-chlorine hexatantalum clusters resulted in ampoule explosions because of side reactions between the reactants and the quartz ampoule. Solid-state routes towards tungsten clusters with mixed inner ligands yielded the $(H_3O)_2[\alpha/\beta\text{-}W_6(\mu_2\text{-}O)_6\text{-}(\mu_2\text{-}Cl)_6Cl_6]\cdot X(H_2O)$ ($X_\alpha = 4$; $X_\beta = 6$) complexes.

TABLE OF CONTENTS

LIST OF TABLES

LIST OF FIGURES

LIST OF SCHEMES

CHAPTER 1:
INTRODUCTION

Biomedical X-Ray Imaging and MRI

Wilhelm Röntgen's discovery of X-rays and the first X-ray image of his wife's hand in 1895 (Figure 1.1), have paved the way for noninvasive medical imaging. Medical imaging creates images of the human body (or parts and function thereof) for diagnosis. Diagnostic imaging has become an integral part of the treatment of disease. A variety of techniques are used in order to exploit different physical phenomena that allow for physiological and clinical interpretations. These techniques include X-ray radiography, X-ray computed tomography (CT), ultrasonography, nuclear medicine imaging (positron emission tomography, PET, single-photon emission computed tomography, SPECT), and magnetic resonance imaging (MRI).[1]

X-ray imaging is the earliest diagnostic imaging technique.[2] It has been used primarily to evaluate broken bones, cavities, swallowed objects, lungs, blood vessels, and breasts.[3] However, this technique is limited to two-dimensional planar images. CT has provided three-dimensional images of an anatomical area by obtaining multiple images taken via helical rotation. CT is commonly used to evaluate organs, colon health, presence of tumors, pulmonary embolism, abdominal aortic aneurysms, and spinal injuries.[3] Both planar and CT imaging have inherent risks as they employ X-rays. X-ray radiation is classified as a carcinogen by the World Health Organization's International Agency for Research on Cancer and the U.S. government.[4] Dosages of X-ray radiation are usually monitored, and patients are only permitted a limited amount of X-ray exposure per year.

MRI, on the other hand, does not subject patients to ionizing radiation. Instead, MRI probes the properties of living tissues, in particular the nuclei of certain atoms within these living tissues. Among the elements in the periodic table, hydrogen is the

Figure 1.1: First X-ray image of Wilhelm Röntgen's wife's hand (left) and Wilhelm Röntgen (right).[5]

simplest and of the greatest importance biologically. Hydrogen is one of the most easily detected nuclei and is the most abundant atom, comprising two-thirds of all the atoms in living tissue.[1, 6] MRI uses hydrogen in tissue water and body fat to produce images. MRI is typically used to evaluate blood vessels, breasts, organs, and the presence of tumors.[3] Herein is described how X-ray imaging and MRI work and contrast agents (CA) for both techniques.

How Do X-Ray and CT Work?

Medical images are created by detecting the effects that a region of the patient's body has on a suitable probe. For transmission imaging, the body must be partially transparent to the probe. If the probe in question passes through the body without interacting, then no difference between tissues is observed. Similarly, if the probe is completely blocked, nothing of interest can be observed. If, instead, a probe is only partially absorbed, scattered, or reflected by the body, small differences in the probe's interactions with various tissues may be observed.

A beam of X-ray photons is such a probe. In planar imaging, X-rays are directed towards the anatomic region of interest for a fraction of a second, and the transmitted X-ray shadow is captured on film.[2, 7] Various body tissues attenuate the X-ray beam by different amounts. Attenuation by a tissue is directly related to the thickness and chemical makeup of the tissue; for example, the lungs are chemically similar to muscle but are only about a third as dense to X-rays. Consequently, lungs have an X-ray attenuation that is a third of that of muscle. The more a tissue absorbs or scatters X-ray photons, the less X-ray energy that passes through the body to the film, and the less exposed the developing film will be. This technique creates a two-dimensional image of the anatomic region being targeted.

CT is capable of creating a three-dimensional image by generating multiple adjacent transverse slice images, acquired helically, and combining the results. One way to think of this is to imagine the body as consisting of thin, flat, longitudinal slices of tissue (Figure 1.2). If each slice is irradiated with X-rays, a transmitted image would be obtained. If those images where then placed on top of one another, the images obscure one another, and the three dimensional aspect of the anatomy is lost. CT preserves and extracts the different images corresponding to multiple and separate images of the body without tissue overlay in order to render tomographic images.

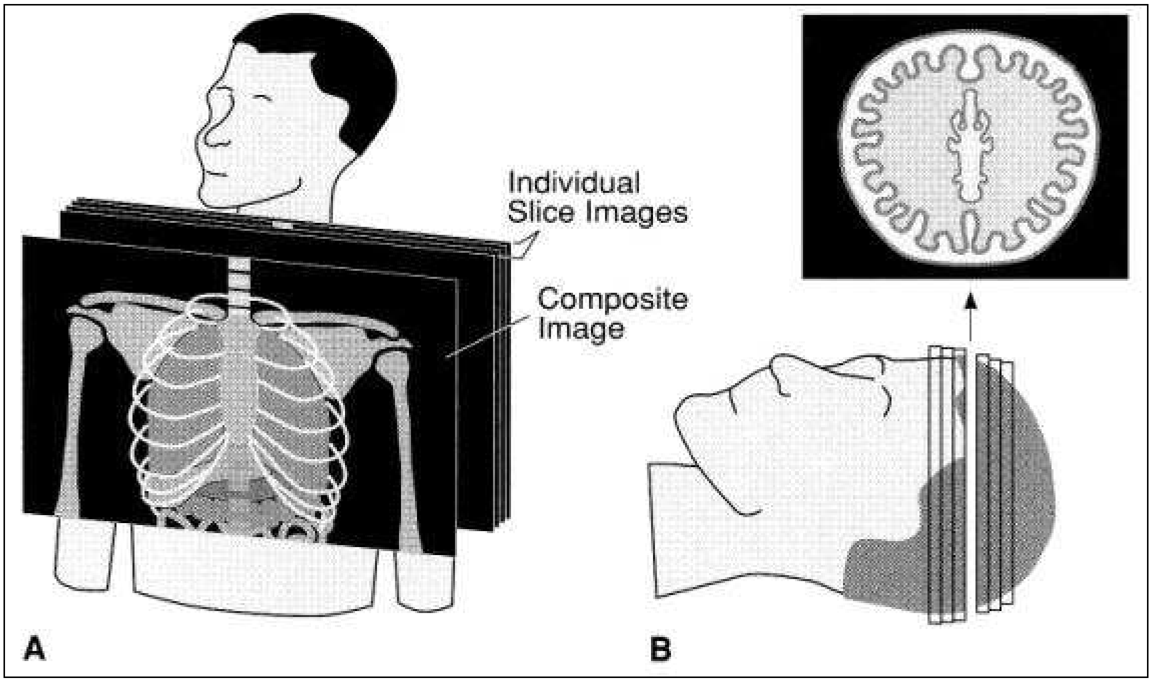

Figure 1.2: CT is capable of creating a three-dimensional image by generating multiple adjacent transverse slice images. A). An ordinary X-ray film (depicted as the front film) is the composite that would result from the superpositioning of the set of separate films of the individual (longitudinal) slices. B). With CT, it is possible to obtain the individual (transverse) slice images separately.[2]

Interaction of X-Rays With Matter

There are a number of mechanisms by which electromagnetic radiation can interact with matter. X-Ray photons at typical diagnostic energies interact with matter by means of Compton scattering and by a lesser extent the photoelectric effect.[2, 8] At diagnostic energies, Compton interactions primarily occur with soft tissues, while photoelectric effects are primarily observed for bone and denser materials. In Compton events, incident X-ray photons decrease in energy by inelastic scattering as a result of interaction with matter (Figure 1.3).

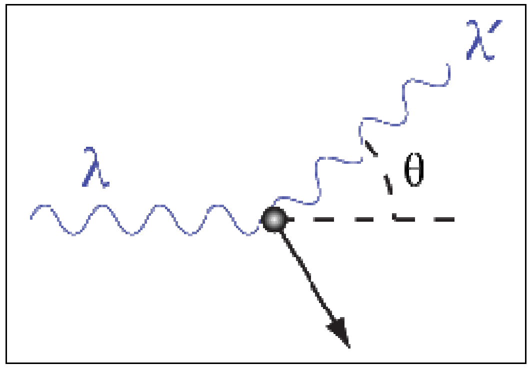

Figure 1.3: Compton Scattering: A photon of wavelength λ comes in from the left, collides with a target at rest, transfer energy, and a new photon of longer wavelength (lower energy), λ', emerges at an angle θ. Figure was adapted from Reference 2.

Part of the energy is transferred to a scattering electron, which recoils and is ejected from its atom, and the rest of the energy is taken by the scattered, lower-energy incident photon. In a photoelectric event, all of the incoming energy is transferred to the atom, resulting in the emission of electrons (Figure 1.4).

The attenuation of a material is dependent on several factors: (1) the thickness of the material, (2) the density of the material, (3) its elemental composition, and (4) the X-ray photon energy.[2, 8] Materials that are thick, dense, and have a chemical makeup that consists of higher atomic number elements will have large attenuation coefficients, while materials with opposite characteristics will have lower attenuation coefficients.

The dependency of the attenuation of a material on the thickness of that material is shown in Equation 1.1[2]

$$\Delta n = -\mu \cdot n \cdot \Delta x \tag{1.1}$$

where Δn is the change in the number of photons in an X-ray beam targeted at the material of interest, μ is the linear attenuation coefficient, n is the initial number of X-ray

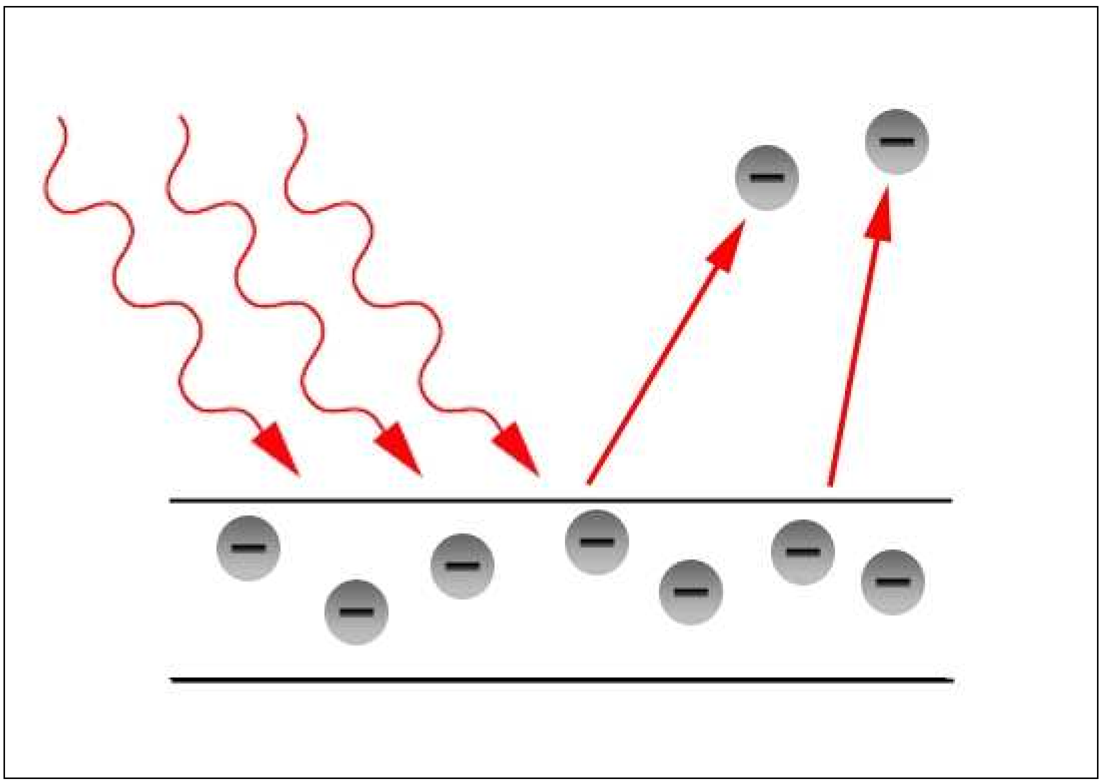

Figure 1.4: Photoelectric effect: Incoming photons come in from the upper left, collide with a target at rest, transfer energy, and lead to electron emission from the target. Figure was adapted from Reference 2.

photons, and Δx is the thickness of the material of interest. This equation is expressed in terms of numbers of photons; a more practical way to describe the linear attenuation coefficient is in terms of intensity of the incident radiation (Equation 1.2):[2]

$$\mu = -\frac{\Delta I}{I} \cdot \Delta x \tag{1.2}$$

where I is the incident intensity of incoming X-ray photons. Figure 1.5 depicts linear attenuation coefficients for several materials.

The linear attenuation coefficient is a function of the density, ρ, the effective atomic number of the irradiated material, Z, and the effective energy of the photons that constitute the beam, *hv* (Equation 1.3):[2]

$$\mu = \mu(\rho, Z, hv) \tag{1.3}$$

Separation of the density dependence from the linear attenuation coefficient yields the mass attenuation coefficient, [μ/ρ](Z,*hv*) (Equation 1.4):[2]

$$\Delta I = -\left[\frac{\mu}{\rho}\right] \cdot \rho \cdot I \cdot \Delta x \tag{1.4}$$

Figure 1.6 depicts linear attenuation coefficients for several materials. The mass attenuation coefficient can be further partitioned into photoelectric and Compton components. The two interaction mechanisms vary based on atomic number and photon energy. Away from the absorption edges, the photoelectric effect varies with photon energy and the effective atomic number of the material as approximately $(Z/hv)^3$.[2] At diagnostic X-ray energies, the Compton interaction decreases slowly with *hv* and, with the important exception of hydrogen, is nearly independent of Z. These interactions are described in the literature.[2, 8]

In short, the ability to form clinical images is based on the attenuation of X-ray photons by the various elements in tissues in a patient's body.

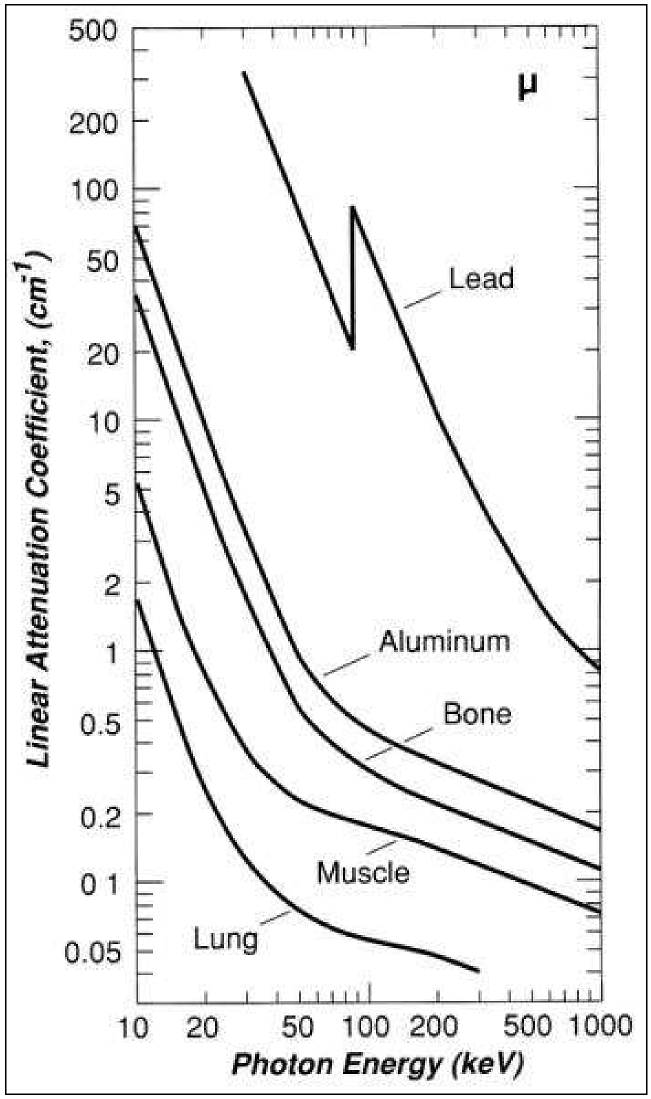

Figure 1.5: Linear attenuation coefficient as a function of monochromatic photon energy for several materials.[2]

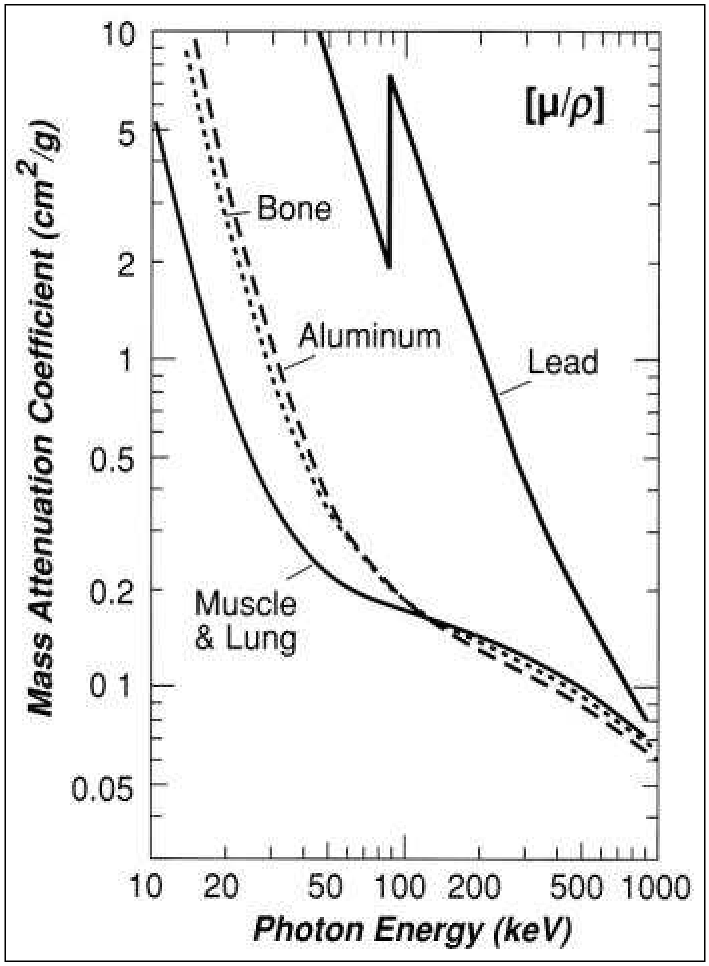

Figure 1.6: Mass attenuation coefficient as a function of monochromatic photon energy for several materials.[2]

X-Ray Contrast Agents

Shortly after the discovery of X-rays, contrast media were developed for diagnostic imaging. The first example of this was studied by Wolf Becher.[9] Becher commented that hollow inner organs can be imaged by introducing solvents of metallic salts to absorb X-rays.[10] This was demonstrated by opacifying the gastrointestinal tract of white mice and guinea pigs with lead acetate. The use of contrast media to enhance X-ray images quickly progressed. However, the toxicity of heavy metal agents soon became apparent. Ernest Sehrwald was the first to suggest the use of iodinated organic compounds.[10] He performed *in vitro* experiments on the ability of halides to absorb X-rays and thus paved the way for the application of molecular, as apposed to ionic iodine compounds as contrast media.

X-Ray contrast agents (CA) work on the same principle as how X-rays interact with matter. X-Ray CA do not affect the material that they are present in; instead, the CA enters the material and attenuates X-ray photons.[2] This causes the material that may have been previously transparent (or only partially visible) by X-ray imaging to become opaque and thus visible by X-ray imaging. Figures 1.7, 1.8, and 1.9 demonstrate the ability of an X-ray CA to increase the visibility of targeted tissues. Figure 1.7 depicts a normal X-ray image of the chest, where only certain anatomical features are visible. Differences in tissues, such as in the cardiovascular system, are difficult to observe. Figure 1.8 demonstrates the ability of an X-ray contrast agent to enhance the contrast of one particular tissue over another. Images A and B from Figure 1.8 can be subtracted from one another in order to obtain an image of the particular target region. Figure 1.9 demonstrates the ability of contrast agents to help differentiate between healthy and diseased tissue.

These CA must have certain properties, such as (1) water solubility, (2) high attenuation of X-ray photons, (3) specific *in vivo* distribution that can be selectively

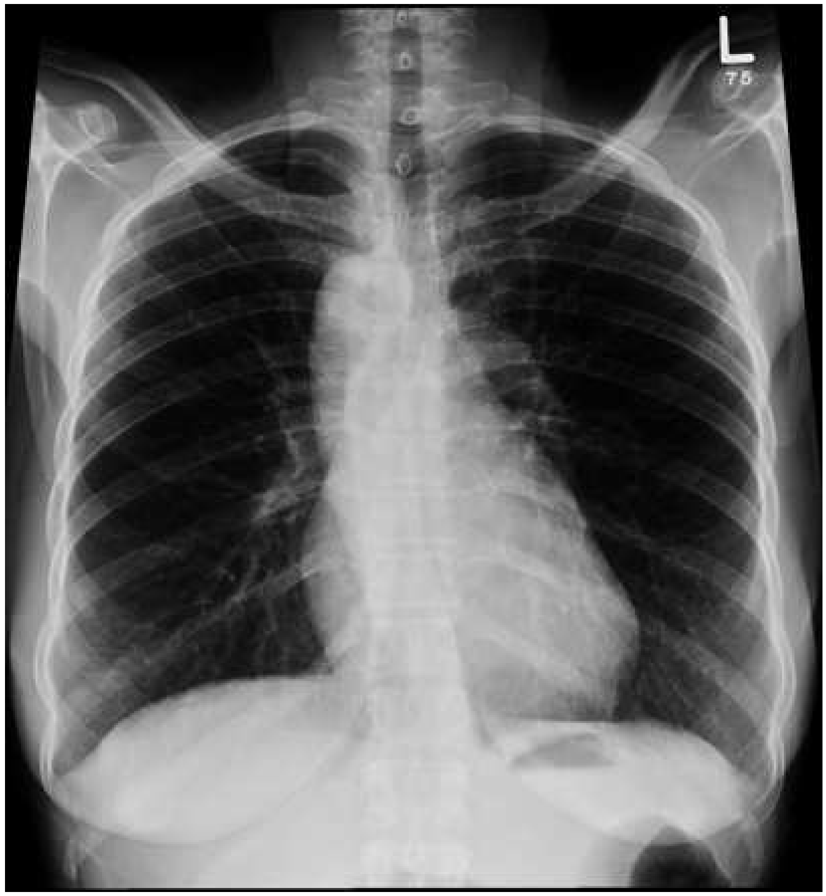

Figure 1.7: Chest X-ray depicting aortic artery without CA. The lungs, heart, ribs and several other bones are visible but the aorta is not.[11]

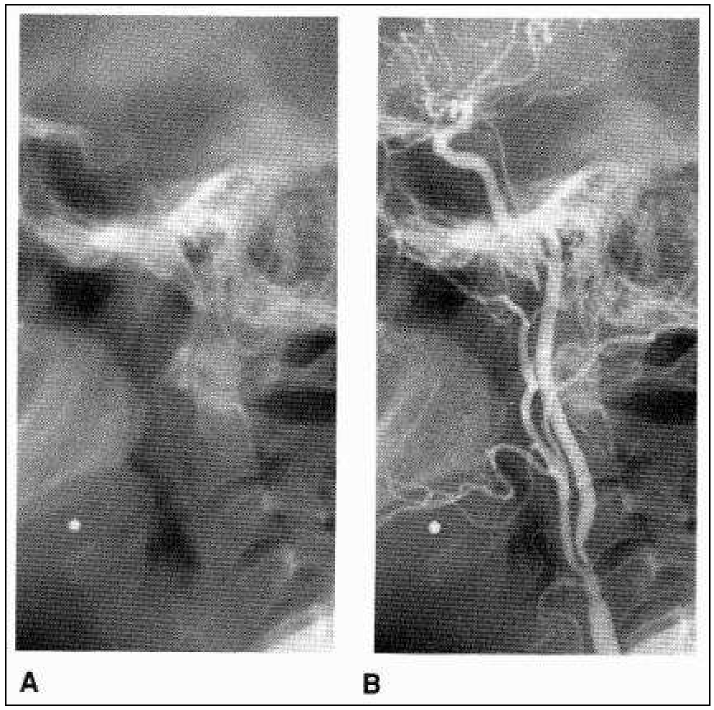

Figure 1.8: X-ray image of the carotid artery without (A) and with (B) iodinated contrast agent.[2]

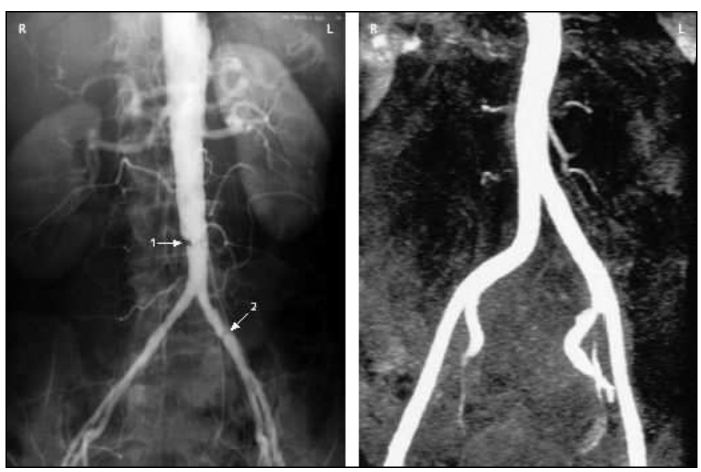

Figure 1.9: Enlarged abdominal X-ray depicting aorta with CA. The CA was injected through a fine catheter passed up the artery from the right groin. The left image depicts a diseased artery (arterial disease is depicted by the arrows), while the right image depicts healthy tissue.[12]

delivered to particular organs, (4) *in vivo* stability (including the excretability and toxicity of the CA), and (5) biocompatibility with biological environments. An added bonus would include a long shelf-life of the compound and the thermal stability needed for sterilization.

Current Clinical X-Ray Contrast Agents

Elements with high atomic numbers, such as bromine, iodine, barium, bismuth and lead, are useful contrast enhancers. Strontium bromide and lithium and sodium iodide were studied as the first water-soluble contrast agents.[10] Iodine took the leading role in contrast agent design and synthesis because of its high absorption coefficient (attenuation), chemical versatility, and relative inertness. Compounds like sodium iodide are not used today because free iodide is toxic in high concentrations, affecting the thyroid and other organs.[7] Organically-bound and, thus, more chemically stable, iodine is better tolerated by patients. The historic development of organic iodinated X-ray CA was based on minimizing CA toxicity. This toxicity was mainly attributed to hydrophilicity of the molecule and the osmolality and viscosity of preparation. Several current clinical X-ray CA are depicted in Figures 1.10, 1.11, and 1.12.

Problems with Clinical X-Ray Contrast Agents

Organic iodinated CA are very stable. However, under certain circumstances they are degraded, particularly by deiodination. There have been several reports that discuss the degradation of iodinated complexes triggered by glucose,[13] copper ion,[13] laser excitation (λ = 308 nm),[14] ultraviolet irradiation,[14] and certain metabolic pathways.[15]

The osmolality of a CA solution is proportional to the number of independent particles in the solution and is strongly influenced by both the concentration of the CA and the temperature of the solution.[7] Current CA can be classified into three different groups, high-osmolar (~1500 mosm kg^{-1}), low-osmolar (600-700 mosm kg^{-1}) and

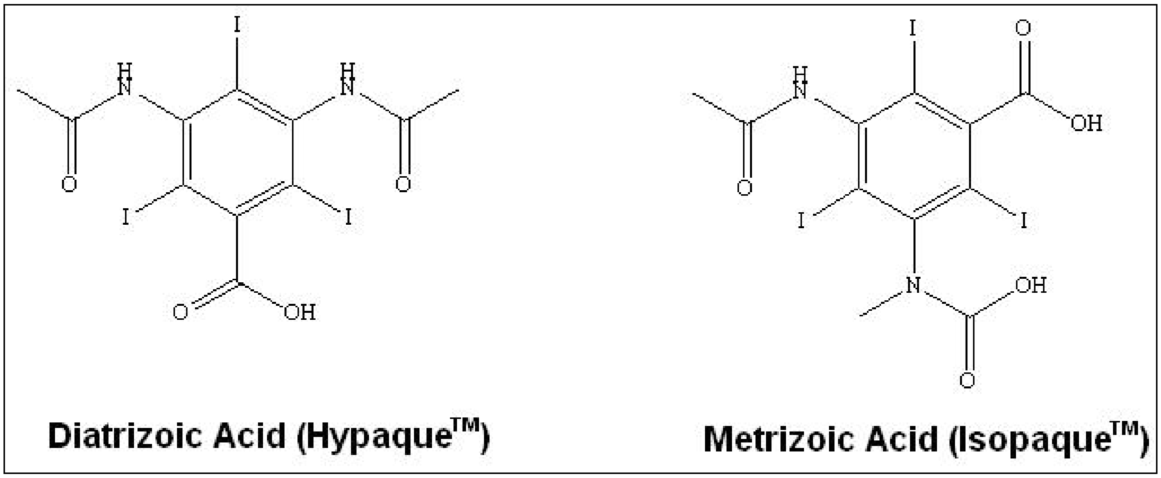

Figure 1.10: Clinically approved high osmolar (charged) X-ray CA: Hypaque™ = 1550 milliosmol kg^{-1} (mosm kg^{-1}); Isopaque™ = 2100 mosm kg^{-1}.[7]

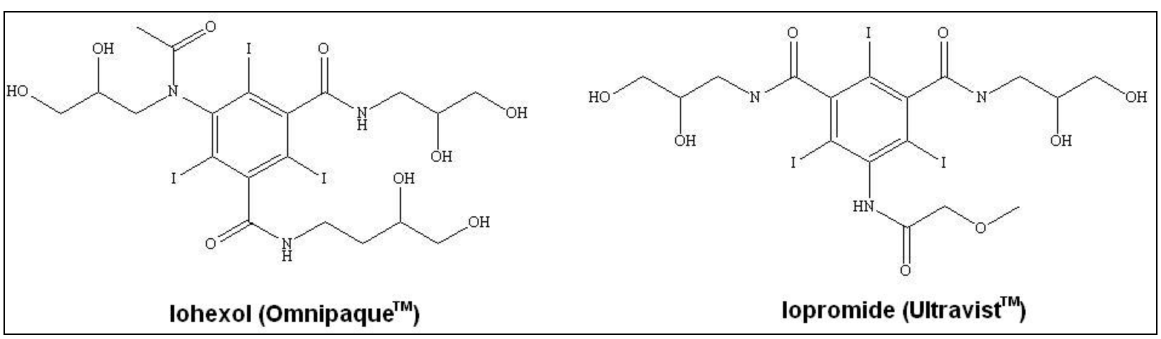

Figure 1.11: Clinically approved low osmolar (neutral) X-ray CA: Omnipaque™ = 884 mosm kg^{-1}; Ultravist™ = 774 mosm kg^{-1}.[7]

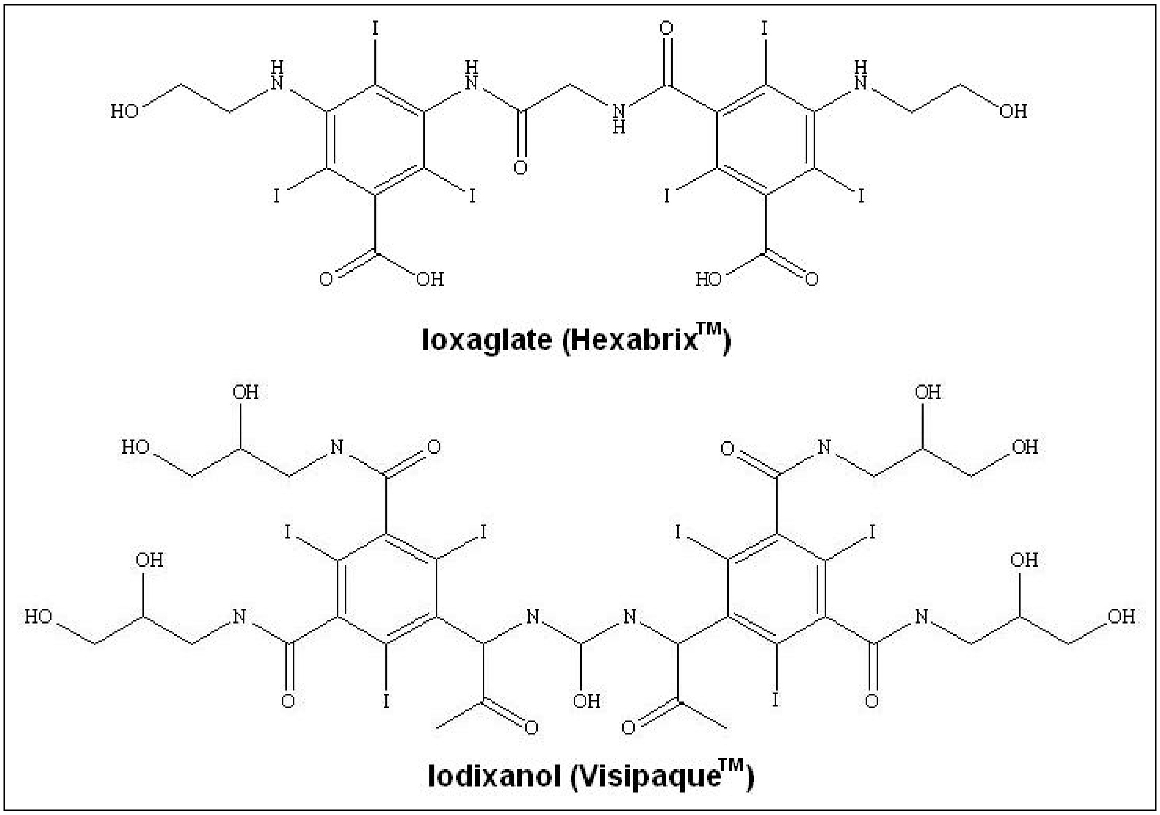

Figure 1.12: Clinically approved isotonic X-ray CA: Ioxaglate™ = 580 mosm kg^{-1}; Visipaque™ = 290 mosm kg^{-1}.[7]

isotonic, which has similar osmolality to that of blood (300 mosm kg^{-1}).[7] High osmolality is directly related to certain types of side-effects such as pain at the injection site, cardiovascular effects (changes in heart rate and blood pressure), and diuresis. The closer the osmolality is to that of blood, the lower is the overall side-effect profile.

The largest concern with X-ray CA is osmotic shock,[7, 16] the sudden change in the solute concentration around a cell, causing a rapid change in the movement of water across the cell membrane. Under high concentration of either salts, substrates or any solute in the supernatant, water is drawn out of the cells through osmosis. This inhibits the transport of substrates and cofactors into the cell, thus “shocking” the cell.

A New Paradigm for X-Ray Contrast Agents

One way to circumvent the problem of osmotic shock and the discomfort associated with injections of X-ray CA is to use either isotonic X-ray CA or to use an uncharged compound that has equal or greater attenuation of X-ray photons than current clinical CA. Octahedral halide clusters of tantalum (Ta) and tungsten (W) should have multiplied attenuation, compared to iodinated organic complexes, in X-ray imaging because of their closer absorption match to the emission spectra of radiological equipment. These transition metal clusters also have higher atomic number and, as previously discussed, will improve attenuation. Attenuation studies have demonstrated the theoretical potential of octahedral transition metal halide clusters as contrast media with multiplied attenuation as compared to conventional agents.[17]

How Does MRI Work?

MRI is one of the most powerful diagnostic imaging techniques available today. Its development was the result of the discovery that atomic nuclei that possess a spin angular momentum will interact with a magnetic field.[1, 18] This phenomenon is most commonly exploited by chemists in order to deduce molecular structures via nuclear magnetic resonance (NMR) spectroscopy. Both MRI and NMR spectroscopy work via the same basic physical principles. The largest difference between the two is that MRI uses magnetic field gradients to spatially encode nuclei, while NMR spectroscopy uses either an electromagnetic, permanent magnet or a single superconducting magnet to align nuclei.[18a, 19] The other difference is that NMR spectroscopy employs small glass tubes containing the sample that are spun within a magnetic field, while MRI employs a bed in which a patient is placed and then moved into the magnet field. The basic principle that these techniques utilize is that nuclei can be aligned in a magnetic field and their spin vector subsequently flipped by application of specific radio frequencies (RF).[1, 18] While within a magnetic field, these nuclei will realign themselves with the magnetic field.

This produces a signal that can be detected by RF receivers. For MRI, the data from these nuclei can be compiled, translated, and converted into an image. NMR spectroscopy is capable of observing many nuclei. MRI, as currently used clinically, on the other hand specifically observes abundant water and fat protons (hydrogens). MRI is capable of distinguishing between the chemical environments of protons in different types of healthy tissue, such as muscle and fat. Furthermore, the chemical environment of the protons in diseased tissue generally differs greatly from healthy tissue of the same type, although this is not always the case. Contrast agents enhance signal-to-noise (or contrast-to-noise) ratios so that tumors and lesions can be differentiated from normal tissue.

NMR Phenomenon and Proton Properties Critical for MRI

Hydrogen nuclei possess a spin angular momentum. This nuclear spin is composed of the spins of individual protons and neutrons. When placed in an external magnetic field, hydrogen nuclei can be pictured as microscopic compass needles, orientating themselves along the external magnetic field (B_o).[1, 18] Quantum mechanical considerations for spinning charged nuclei allow them to be oriented in discrete directions that correspond to an energy level of the nucleus (Figure 1.13). Following classical arguments, the positively-charged protons with spin angular momentum in a nucleus constitute a ring current with negligible dimension, which in turn gives rise to a dipolar magnetic moment, μ.[1, 18] This magnetic moment is like the nuclear spin and aligns parallel to the rotation axis of the nucleus.

A magnetic moment, when placed in a magnetic field, possesses a magnetic energy. The energy states of the nucleus are given by m_I (Equation 1.5):[18a]

$$E_{mI} = -m_I \cdot \gamma \cdot B_o \tag{1.5}$$

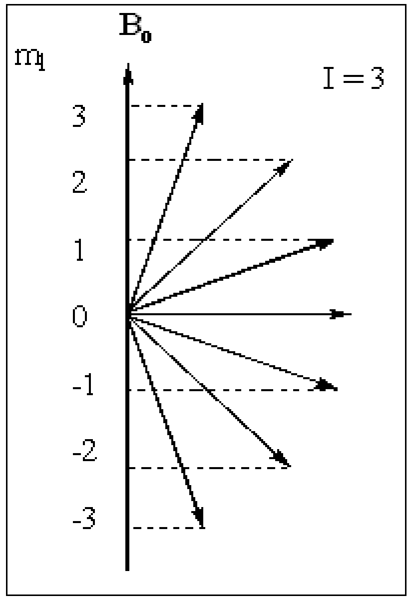

Figure 1.13: Possible orientations for the spin vector of a nucleus with spin quantum number I = 3, in the presence of an external magnetic field B_o. Figure adapted from Reference 18a.

where m_I is the magnetic quantum number, γ is the gyromagnetic ratio (a constant for each nucleus type), and B_o is the applied magnetic field. The energy difference between two neighboring m-states is, for a given nucleus (Equation 1.6):[18a]

$$\Delta E = \gamma \cdot \hbar \cdot B_o \tag{1.6}$$

and thus proportional to the magnetic field. This is exemplified for a nucleus with a spin quantum number of I = ½ in Figure 1.14. A nucleus can change energy states but only to a neighboring state. In order to move up to a higher energy, the nucleus must be supplied with the necessary energy difference, ΔE, in the form of electromagnetic radiation. In order to move to a lower energy state, the nucleus must emit the energy difference, ΔE.

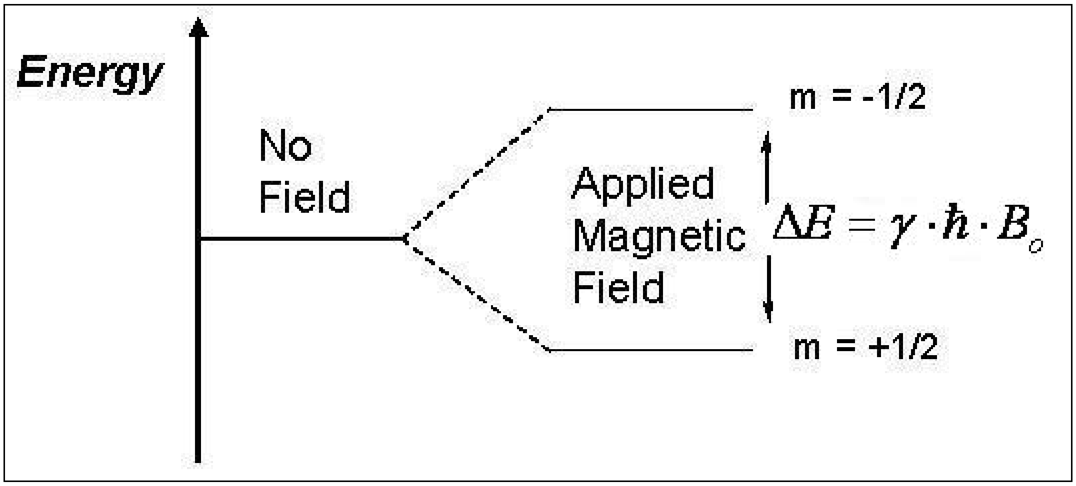

Figure 1.14: Energy-term scheme for nucleus with spin quantum number of I = ½.
Figure adapted from Reference 18a.

Both energy transitions must obey the following relationship (Equation 1.7):[18a]

$$\Delta E = h \cdot v_o \tag{1.7}$$

for the frequency v_o of the electromagnetic radiation. Combination of Equations 1.6 and 1.7 yields Equation 1.8:[18a]

$$h \cdot v_o = \gamma \cdot \hbar \cdot B_o \tag{1.8}$$

which allows for the determination of angular frequency, $\omega_o = 2\pi v_o$ for the electromagnetic radiation at an energy transition (Equation 1.9):[18a]

$$\omega_o = \gamma \cdot B_o \tag{1.9}$$

While aligned with the magnetic field, the nuclei begin to precess due to torque experienced from coupling between the dipolar magnetic moment and the external magnetic field (Figure 1.15) The angular velocity (ω_L) of this motion can be related to the magnetic field strength through physical arguments of torque and angular momentum vector laws (Equation 1.10):[6, 18a]

$$\omega_L = -\gamma \cdot B_o \tag{1.10}$$

The angular velocity is called the 'Larmor frequency'. The Larmor frequency is thus unique to the nucleus being observed and dependent on the magnetic field strength.

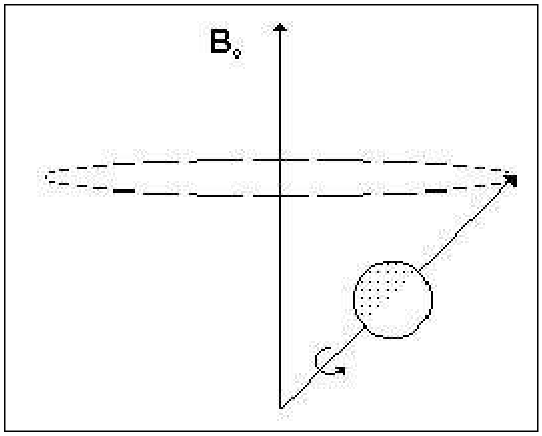

Figure 1.15: A hydrogen atom precesses about an applied magnetic field. Figure adapted from Reference 18a.

A typical high field-strength MRI scanner may have field strengths of 10,000 Gauss (one Tesla). The resonant frequency for hydrogen in this field is 42.6 million cycles per second (MHz). Magnetic field gradients are introduced to subtly adjust B_o and consequently affect the Larmor frequency of the protons. This allows for spatial encoding of protons within the body. In this manner, MRI is able to provide sensitive information on the environments of the protons, their density, and their physical location.

Nucleus Relaxation Times

As stated before, a nuclei's spin vector aligned in a magnetic field may be flipped with an RF pulse. The nucleus, while still spinning, will then realign with the magnetic field at the Larmor frequency of that nucleus. A detector is placed along an axis perpendicular to the imposed magnetic field (B_o). The signal that is observed is actually the decay of the perpendicular component as the nucleus realigns with B_o.[6] Thus, it is important to understand what effects the relaxation of the observed nucleus. The return to alignment with the magnetic field depends on specific *rate constants*, $1/T_1$ and $1/T_2$. T_1 and T_2 are commonly referred to as *relaxation times*, because these terms are the inverse rate at which the nucleus returns to its resting position after excitation with RF energy.[1, 6, 18a]

A spin in a high-energy state can transition to a low-energy state either via spontaneous or stimulated emission. The likelihood of a spontaneous emission is very low and insignificant; thus, the majority of transitions occur through stimulated processes.[18a] The fluctuating magnetic environment surrounding the observed nucleus, otherwise known as the lattice, is enough to stimulate relaxation. T_1 is therefore referred to as the spin-lattice relaxation time, and is enthalpic in nature.

T_2 is referred to as the spin-spin relaxation time and is entropic in nature. When nuclei are tipped with an RF pulse, such as a 90^o tip, the nuclei align in the plane perpendicular to B_o in phase, that is they are all spinning at relatively the same rate. However, these spins start to deviate from one another and dephase. This is the result of fluctuations in angular velocity of individual spins caused by fluctuating magnetic fields that are caused by the random motion of molecules.[6, 18a] The spins dephase, and this leads to a net signal decrease.

Since MRI deals with protons of water molecules, protons will be the nucleus discussed hereon. T_1 and T_2 values of pure water at MRI-relevant field strengths are approximately 2.5-3 seconds.[6, 20] Some characteristic T_1 and T_2 values encountered in the human body in a 1.0 Tesla magnetic field are listed in Table 1.1.[1] Multiple factors effect T_1 and T_2. These factors are important in MRI because they have direct impact on the magnetic behavior of the protons and thus the MRI results.

Some of the spin-lattice interactions that are relevant to MRI are local fluctuations in magnetic field strength near the protons caused by thermal motion of magnetic particles in close proximity to the protons being observed.[1] Random collisions occur between water and other molecules that make up the magnetic environment. Dipole-dipole interactions cause fluctuations in the magnetic signal, which results in different observed proton signals.

Table 1.1: A list of the typical T_1 and T_2 values for tissues in the human body at 1.0 T. Proton densities are relative to blood.

Tissue	Proton Density	T_1 (ms)	T_2 (ms)
Pancreas	0.97	275	45
Liver	1.00	250	45
Blood	1.00	525	260
Kidney cortex	1.03	400	70
Brain (gray matter)	1.05	475	120
Cerebrospinal fluid	1.08	2000	250
Fat	1.09	150	150
Brain (white matter)	1.10	300	133
Muscle	1.10	450	65

Note: Proton density data taken from Reference 1 was not defined and error limits were not provided.

In addition to thermal motion, magnetic interactions with large biologically-important molecules such as proteins affect the relaxation of protons.[6] Most of these molecules are polar and have an uneven distribution of charge on their surface. Also, the motion of these large molecules affects the proton's relaxation. This occurs because, as protons interact with these large, slowly moving molecules, the protons themselves move slower. This interaction reduces frequencies of magnetic fluctuations because the water molecules are moving at a lower rate of speed. As a result of slowing, more magnetic fluctuations occur at the resonant Larmor frequency. These interactions cause an increase in relaxation and thus a shortening of T_1.[6]

Paramagnetic atoms produce the largest fluctuations in the magnetic environment of protons. Paramagnetic atoms contain unpaired electrons that possess spin, and, by the right hand rule in physics, create their own magnetic field. They can be considered tiny, spinning magnets. These atoms are able to create magnetism that is approximately 1000 times greater than nuclear magnetism.[6] Paramagnetic atoms have a profound effect on the T_1 and T_2 of protons.[21]

In aqueous solution, dipolar magnetic interactions exist between the electronic magnetic moment of the paramagnetic atom and the much smaller magnetic moments of protons of nearby water molecules. Molecular motions cause random fluctuations in this dipolar magnetic interaction and reduce both T_1 and T_2 of the water protons.

MRI Contrast Agents

MRI contrast agents (CA) were developed to enhance contrast in images obtained by MRI. Most of these agents are based on paramagnetic atoms because paramagnetism has such a large effect on T_1 and T_2.[1, 6, 19] Even without CA, MRI images demonstrate contrast between different tissues, as seen in Figure 1.16, because of inherent tissue differences. These differences include proton spin density, T_1, T_2, resonant frequency, chemical shift, and magnetic susceptibility, as well as flow, perfusion, or other molecular motions.[21] Some combination of these properties gives rise to the signal intensity.

Image contrast can be increased by two ways: (1) the physical parameters associated with the imaging method can be manipulated, or (2) a drug (CA) can be administered that alters physical characteristics of the tissue.[22] Figure 1.17 shows a MRI scan without and with CA. The introduction of the CA can enhance the signal from damaged or diseased tissue. In this particular image, the introduction of a CA provides a more detailed image of an already obvious abnormality. Contrast can be positive or negative depending on whether the tissue of interest being imaged is brightened or darkened after the CA has been introduced. The ideal CA would be one that increases

Figure 1.16: Full cross-sectional MRI of a male.[23]

the contrast between normal and abnormal tissue, by preferentially adjusting the signal intensity of one of the two tissues, and then be readily excretable with no toxic side effects. Gadolinium(III) (Gd(III)) is the paramagnetic ion of choice for MRI CA because Gd(III) has the largest effective magnetic moment of all atoms or ions.[20]

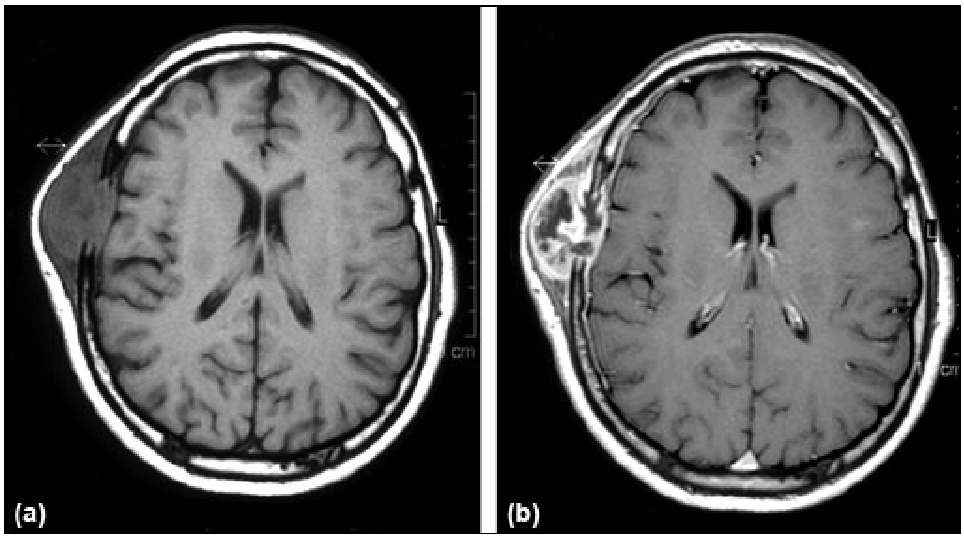

Figure 1.17: MRI image of a brain containing a tumor of the frontal bone (a) without and (b) with Gd(III) CA.[24]

Relaxivity of Metal Complexes

The parameter used to quantify the ability of a metal complex to influence proton relaxation rates is known as relaxivity, r_1. Relaxivity is expressed in units of $mM^{-1}\ s^{-1}$, and can be considered a concentration-dependent relaxation time. The relaxivity of a complex at 20 ^{o}C is governed by Equation 1.11**:**[25]

$$r_1 = C \cdot q \cdot \mu_{eff}^2 \cdot \tau_c \cdot r^{-6} \tag{1.11}$$

where C is a constant, q is the number of inner-sphere waters, μ_{eff} is the effective magnetic moment, τ_c is the molecular correlation time , and r is the Gd···H distance.

Number of Bound Waters: q

Current clinical contrast agents are usually based on Gd(III) chelate complexes where q is one. Based on Equation 1.11, increasing the number of inner-sphere waters increases the relaxivity of the complex. However, by increasing q, the reactivity of the complex also increases.[20] This leads to an instability of the complex that may lead to release of Gd(III) ion. Even though outer-sphere waters may interact with the Gd(III) center, these effects on T_1 and T_2 are less than that of those on water molecules directly coordinated to the metal center.

Gd···H Distance: r

The r^{-6} dependence on the Gd···H distance means that inner-sphere water molecules are more effectively relaxed than outer-sphere waters. Consequently, a shorter Gd···H distance will dramatically increase proton relaxivity. An increase in relaxivity can be accomplished by (1) chemically inducing an orientation of bound water molecules, such that the protons are closer to the metal center or unpaired spin density, or (2) delocalizing the unpaired spin density toward the water through atomic or molecular orbitals of the metal ion, the chelating ligand, or the bound water itself.[26]

It is also possible that using ligands that exchange with protons on water and have smaller coordination radii will increase relaxivity. For example, we postulate H-exchange between μ_3-OH ligands in Gd(III) clusters and bulk H_2O. The Gd···H distance between a bound hydroxide is significantly smaller than that for bound water and should increase the relaxivity of these clusters.

Molecular Correlation Time: τ_c

The molecular correlation time (τ_c) is determined by the rotational correlation time, τ_r, the electronic correlation time, τ_s, and the proton residence lifetime, τ_m (i.e. the reciprocal of the water exchange rate, k_{ex}) as show in Equation 1.12.[20]

$$\tau_c^{-1} = \tau_r^{-1} + \tau_s^{-1} + \tau_m^{-1} \qquad (1.12)$$

Theory shows that maximum relaxivity occurs when the dipole-dipole correlation time is the inverse of the proton Larmour frequency, with optimal τ_{cl}'s of 7.4 ns at 0.5 T and 2.5 ns at 1.5 T.[20] There is considerable opportunity for improvement in τ_r and τ_m. τ_r is the single most important source for relaxivity enhancement.[26] The τ_r of simple Gd(III)-chelates is generally on the order of 10^{-10} s. Theory suggests that slowing τ_r to 10^{-8} s would significantly improve relaxivity. The most common method for increasing τ_r is to increase the size of the molecule. For example, Gd(DTPA) can "hitch a ride" on human serum albumin (HSA) protein and increase its relaxivity from 4 $mM^{-1}\ s^{-1}$ to 56 $mM^{-1}\ s^{-1}$.[27]

The electronic correlation time is field dependent based on nuclear magnetic relaxation dispersion (NMRD) studies. The zero-field value is highly sensitive to the coordination symmetry of the complex and the nature of the coordinating ligands.[27]

The proton residence lifetime characterizes the efficiency of the chemical exchange of water molecules from bulk solvent to inner-sphere.[21, 26]

The proton residence time is assumed to be equal to the water residence time, since proton exchange at physiological pH is determined by water exchange. A proton of a coordinated water molecule can exchange without the exchange of the entire water molecule.[21] In current clinical Gd(III) CA the water and proton exchange rates are approximately the same. Acidic or basic conditions may catalyze the exchange of protons.[27-28]

Contrast Agent Requirements

CAs have been designed and administered to patients in order to either enhance the contrast between normal and diseased tissue or to indicate organ function or blood flow.[21] MRI CA must have certain characteristics in order to function as CAs within biological systems. Some of these characteristics include (1) water solubility, (2) high relaxivity, (3) specific *in vivo* distribution, (4) *in vivo* stability (including the excretability and toxicity of the CA), and (5) biocompatibility with biological environments. An added bonus would include a long shelf-life of the compound.[21, 26, 29]

Specific *in vivo* distribution refers to the ability of the CA to localize in an area of the body being targeted for a short period of time without spreading into other nontarget regions. This is a basic theory for any imaging procedure, where detection of the agent is a function of its concentration within the target tissue.[26] To obtain information from an MRI study, the relaxation rate of the target tissue only needs to be enhanced as compared to its surrounding tissue. This allows for means other than concentration differences to be applied if the agent has a higher relaxivity in one particular tissue than another.[26]

Gadolinium ions, used in current clinical CA, are toxic at the levels used in clinical circumstances: a typical dose is 0.1 - 0.3 mmol/kg total body weight. This is because Gd(III) has a similar size-to-charge ratio as Ca(II). Gd(III) can disrupt essential Ca(II)-required signaling processes occurring in the body. This is one reason why the *in vivo* stability and toxicity of the CA is so important. Gd(III) MRI CA complexes are designed to stay intact and not break apart or dissociate to any degree in the body.[21, 29] However, 'the best laid plans of mice and men go often astray, and leave us naught but grief and pain' (Robert Burns, 1785). This will be discussed in future sections.

Current Clinical MRI Contrast Agents

All approved MRI CA are nine-coordinate Gd(III) complexes with a single ligand occupying eight coordination sites and the ninth coordination site take up by a coordinated water molecule (Figure 1.18). The first CA approved for clinical use was $[Gd(DTPA)(OH_2)]^{2-}$ (Magnevist™, DTPA = diethylenetriaminepentaacetic acid) in 1988 by Schering Company in Germany.[20] As of 1999, nearly 30 metric tons of gadolinium had been administered to patients worldwide, and approximately 30 % of all MRI exams included the use of CA.[20] The majority of CA incorporate a acyclic or macrocyclic ligand.

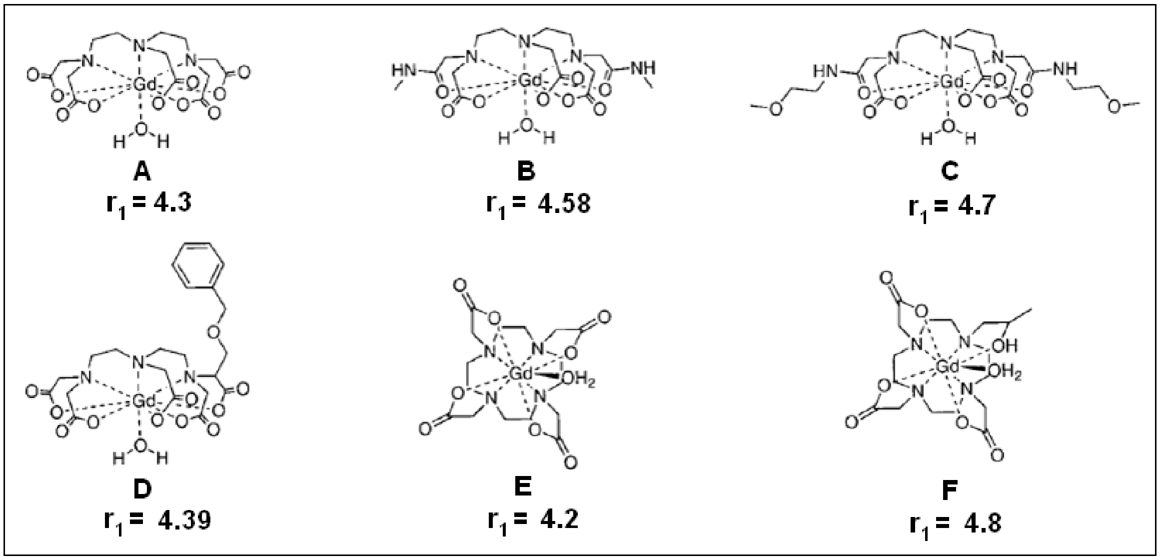

Figure 1.18: Clinically approved MRI CA with relaxivity values. All were approved as of 1999. A, $[Gd(DTPA)(OH_2)]^{2-}$ (Magnevist^{TM}); B, $[Gd(DTPA\text{-}BMA)(OH_2)]$ (Omniscan^{TM}); C, $[Gd(DTPA\text{-}BMEA)(OH_2)]$ (OptiMARK^{TM}); D, $[GD(BOPTA)(OH_2)]^{2-}$ (MultiHance^{TM}); E, $[Gd(DOTA)(OH_2)]^{-}$ (Dotarem^{TM}, approved for use outside the U.S.); F, $[GD(HP\text{-}DO3A)(OH_2)]$ (ProHance^{TM}). Figure adapted from reference 18a.

The vast majority of acyclic complexes are variations of DTPA. One or more of the pendant acetate groups of DTPA or the diethylenetriamine backbone are functionalized in order to enhance the overall relaxivity of the complex. These derivatives demonstrate similar stability and toxicity. The steric bulk helps to increase the molecular correlation time, alter the water exchange rates, and increase relaxivity. There is a positive correlation between the size of the substituent and the relaxivity of the resulting Gd(III) complex.

Polyazapolycarboxylate macrocycles are more lanthanide-specific ligands as compared to their acyclic counterparts.[20] These macrocyclic Gd(III) complexes have higher thermodynamic and kinetic stability compared to acyclic ligands like EDTA and DTPA.[22] Therefore, a ligand with higher complex stability and superior lanthanide selectivity would more than likely make a good foundation for improved MRI CA.[30]

One of the earliest polyazapolycarboxylate macrocycles studied was 1,4,7,10-tetraazacyclododecane-N,N”,N”N”’-tetraacetate (DOTA). The Gd(III) complex is in clinical use. This complex is more thermodynamically stable than Gd(DTPA), as the increased stability can be attributed to (1) a reduction in steric strain because of the formation of eight five-membered rings upon metal complexation and (2) the macrocycle effect, which is the primary basis of the four to eight order-of-magnitude increase in stability over that of complexes containing acyclic ligands.[22]

There are other complexes that have been designed to improve relaxivity. These efforts include increasing τ_r by attaching Gd(DTPA) and Gd(DOTA) to larger macromolecules in order to slow their rotation. The most common approaches are to conjugate functionalized chelates to polymers,[20] dendrimers,[20] or biological molecules.[20, 31] Other CA efforts include using nanoparticles[32] and nanomaterials.[33]

Problems with Clinical MRI Contrast Agents

There are a number of common side effects associated with MRI CA. Several of these side effects are considered normal and mild. Injections usually cause a significant amount of discomfort and pain to the patient and can last a period of a few hours to days. This side effect is a result of the high concentration of the CA required to significantly increase image contrast.[21, 34] The high concentration also means that the osmolality of the drug is higher than that of blood. The high osmolality causes discomfort and pain to the patient. Other side effects include allergic reaction, flushing, or redness of the skin leading to a sensitivity to touch and/or a strong itching sensation, hives on the skin, numerous serious medical issues (some of which can be fatal), dizziness and disorientation, and shortness of breath or an inability to “catch one’s breath.”[34]

A serious and more recently recognized side effect associated with Gd(III)-based CA is nephrogenic systemic fibrosis (NSF), a multisystemic fibrosing disorder, often fatal, which affects the skin and other organs of patients with renal insufficiency.[35] NSF causes a thickening and hardening of the skin, often leading to immobility and tightness or deformity of the joints. Autopsies of patients with this disease have shown systemic manifestations including fibrosis of the skeletal muscle, bone, lungs, pleura, pericardium, myocardium, kidney, testes, and dura.[35-36] Therefore there is a major need for Gd(III)-based CAs with greater solution stability and relaxivity, based on our current understanding of NSF.

A New Paradigm for MRI Contrast Agents

Considerable research has been performed in the development of CA with increased q and exchange rates or τ_r, including noncovalent association of Gd(III) chelates with albumin, chelates that increase q or water exchange rate, and Gd(III) chelates bonded to polymers or dendrimers. Chelate-polymer/dendrimer linkage flexibility and polymer backbone dynamics decrease relaxivity by reducing the rotational correlation of $Gd \cdots H_{water}$ vectors and the molecule, and gains can be further limited by slow water exchange. However, limited research has been performed on developing CA with multiple metal centers.[34]

Polyhedral polynuclear Gd(III) complexes have only recently demonstrated their potential for high r_1 from decreased τ_r and inner/outer-sphere water interactions with multiple Gd(III) centers. Additional relaxation may be possible from H-bonding to or exchange of water protons with μ_3-OH ligands.[17a]

Aqueous polyhedral polylanthanide chemistry was pioneered by Zak[37] and further developed by Gao,[38] Zheng,[39] and others. Base hydrolysis of Ln(III) yields discrete complexes with supporting ligands (e.g., amino acids, β-diketonates) and anion templates that divert oligomerization away from precipitation. Tetra-,[40] hexa-,[41] hepta-,[42] dodeca,[43] and pentadecalanthanide(III)[43-44] complexes have been studied for applications from agricultural chemisty to materials science, and several reviews have appeared.[45]

The combination of (1) multiple Gd(III) centers, (2) new relaxivity pathways involving H-exchange between μ_3-OH ligands in these clusters and bulk H_2O, (3) higher q, and (4) non-spherical structures are unique to these compounds and represent a paradigm shift in contrast agent design. This has recently been demonstrated in the literature.[17a]

Thesis Overview

The focus of this dissertation is to develop the solution chemistry of multinuclear metal complexes. The long-range goal is to modify these compounds so that they can serve as a new paradigm for contrast agents in X-ray and magnetic resonance imaging. We have been focused on developing the chemistry of polylanthanide complexes in order to determine their structural integrity in aqueous solutions. If these types of polynuclear complexes are to be applied to biomedical imaging, then their solution chemistry needs to be further understood.

The Messerle group has also focused on developing the chemistry of hexanuclear transition metal clusters. Chapter 7 discusses our efforts to produce inner-ligand substituted hexatantalum and hexatungsten oxo-chloride clusters.

CHAPTER 2:
SYNTHESIS AND STRUCTURAL CHARACTERIZATION OF HALIDE-'TEMPLATED' PENTADECANUCLEAR LANTHANIDE(III) COMPLEXES OF L-HISTIDINE (Ln_{15}–his X) (Ln = Y, Nd, Eu, AND Tb; X = Cl, Br, $(I)_2$-OH)

Introduction

Lanthanides are a group of chemical elements used in many facets of technology and medicine such as fluorescent bulb phosphors,[46] magnetic materials,[46b, 47] additives in metallurgy,[46] and pharmaceuticals.[21, 46b, 48] However, the lanthanides claim to fame is arguably their roles as nuclear magnetic resonance (NMR) shift reagents[34, 46a, 49] and magnetic resonance imaging (MRI) contrast agents (CA).[21, 34, 46a, 48] These remarkable utilities arise from the number of unpaired electrons of the Ln(III) ions, in particular Gd(III) (seven unpaired electrons).

Current gadolinium(III) MRI CAs have been associated with necrotizing systemic fibrosis (also referred to as nephrogenic systemic fibrosis, NSF), a multisystemic fibrosing disorder, often fatal, that affects the skin and other organs in patients with renal insufficiency.[35] Therefore, there is a major need for Gd(III)-based MRI CAs with greater solution stability and relaxivity (the signal enhancement from the use of CAs). Polynuclear lanthanide clusters are one possible solution to this problem, but their chemistry is relatively unexplored.

A common synthetic method for the formation of polynuclear complexes is direct hydrolysis or alcoholysis of a metal or its ion in the presence of supporting ligands such as carboxylates,[45a, 50] amines,[51] alcohols,[52] ketonates,[53] and alkoxides[52a, 54] that preclude overhydrolysis to poorly-defined oxo/hydroxo precipitates. Amino acids are an interesting class of ligands as they contain diverse functional groups capable of coordination. Zak,[37b] Gao,[38] Zheng,[42, 45a] and others have demonstrated that hydrothermal treatment or base hydrolysis of lanthanide salts leads to hydroxy-bridged polylanthanide complexes of varying nuclearities and geometries.

Polynuclear Ln(III) clusters can be divided into several classes, the most prominent of which are anion-templated polynuclear Ln(III) clusters. This structure type has led to more clusters than clusters only supported by organic ligands. Several reported templated complexes relevant to this chemistry are listed below:

Ln_4: Rhombohedral tetranuclear structure with μ_4-O^{2-} template: $[Ln_4L_2(NO_3)_4(MeOH)_2(\mu_4\text{-}O)]$ (Ln = Gd and Tb; L = 1,3-bis(2-hydroxy-3-methoxy-benzylamino)propan-2-ol)[38] and $Na_6[((C_6H_5SiO_2)_8)_2Ln_4(\mu_4\text{-}O)]$ (Ln = Gd and Nd)[55]

Ln_6: Octahedral structure with μ_6-O^{2-} template: $[Gd_6(\mu_6\text{-}O)(\mu_3\text{-}OH)_8(OH_2)_{12}(NO_3)_6]^{2+}$,[37a] $[Yb_6(\mu_6\text{-}O)(\mu_3\text{-}OH)_8(dmf)_{16}]^{8+}$ (dmf = dimethylformamide),[56] $[Ln_6(\mu_6\text{-}O)(\mu_3\text{-}OH)_8(OH_2)_{24}](ClO_4)_8$ (Ln = Nd, Gd),[41] $[Gd_6(\mu_6\text{-}O)(\mu_3\text{-}OH)_8(\eta_2\text{-}ClO_4)_2(OH_2)_{20}](ClO_4)_6$,[39] $[Ln_6(\mu_6\text{-}O(\mu_3\text{-}OH)_8(OH_2)_{24}]I_8(H_2O)_{12}$ (Ln = Nd, Eu, Tb, Dy)[57]

Ln_{12}: Four vertex-sharing cubanes in a square array with two μ_4-I templates: $[Ln_{12}(OH)_{16}I_2(\mu_3\text{-}tyr)_8(OH_2)_{20}](ClO_4)_{10}$ (Ln = Dy, Er; tyr = tyrosine)[43]

Ln_{15}: Five vertex-sharing cubanes in a pentagonal array with μ_5-X (X = Cl or Br) template: $[Ln_{15}(\mu_3\text{-}OH)_{20}(\mu_5\text{-}Cl)(\mu_3\text{-}tyr)_{10}(OH_2)(\mu\text{-}OH_2)_5(OH_2)_{18}](ClO_4)_{12}$ and related complexes (Ln = Eu, Nd, Gd, Pr)[43, 45]

Ln_{60}: Giant cage-like clusters consisting of vertex-sharing cubanes with μ_6-CO_3^{2-} templates: $[Er_{60}(L\text{-}thre)_{34}(\mu_6\text{-}CO_3)_8(\mu_3\text{-}OH)_{96}(\mu_2\text{-}O)(OH_2)_{18}]Br_{12}(ClO_4)_{18}(H_2O)_{40}$ (L-thre = L-threonine)[58] and $[Y_{60}(\mu_3\text{-}OH)_{96}(\mu\text{-}CO_3)_8(\mu_4\text{-}Br)_6(\mu_4\text{-}Cl)_6(his)_{24}](OH)_{32}$ (Messerle group, unpublished results)

Recently, it has been proposed that the main driving force for formation of high nuclearity polynuclear lanthanide-hydroxo complexes are template effects.[43] Indeed, it has been observed that a central spherical charge density, such as a halide or an oxo/hydroxo group, is a common structural feature in polynuclear lanthanide alkoxides.[52b, 59] However, the exact role of these anionic species has not been investigated. It is unclear whether the driving force is based on a negative charge density, ligand interactions, or a combination of both. This question can be probed by investigating the Ln_{12} and Ln_{15} complexes mentioned above. These complexes consist of tyrosine (an amino acid) coordinated to vertex-sharing cubanes organized around single or multiple central halides. If the halide template effect is the main driving force for the formation of these complexes, then complexes of similar core structure should be obtainable with any ligand capable of coordination that is analogous to the complexes' ligands, i.e., any other amino acid. No such clusters have yet been reported in the literature. This suggests that the amino acid ligand also plays a role in these structure types.

A main interest within the Messerle group is the development of polynuclear lanthanide clusters with the goal of isolating novel complexes for use as MRI or CT CAs and biomacromolecular crystallographic phasing agents. Herein is described (1) attempts to synthesize and crystallize polynuclear lanthanide clusters with triflate and tosylate anions instead of the ubiquitous perchlorate, (2) synthesis of new histidine-coordinated pentadecanuclear lanthanide complexes with various templating ions, $[Ln_{15}(\mu_5\text{-}X)(\mu_3\text{-}OH)_{20}(his)_{15}(OH)_7](ClO_4)_{12}$ (Ln = Y, Nd, Eu, and Tb; X = Cl, Br, $(I)_2$-OH), (3) solid-state structure of these new Ln_{15}–his X complexes, and (4) initial attempts to understand solution-state stability by means of recrystallization.

Results and Discussion

Towards Increased Water-Solubility Polynuclear Lanthanide Clusters

We attempted to synthesize perchlorate-free polynuclear lanthanide complexes from triflate and tosylate salts of Eu(III) and Y(III). Our goal in this regard was to synthesize a more water-soluble product. These attempts resulted in the isolation of crystalline Ln(III) triflate and tosylate starting materials (Figures 2.1 and 2.2). Aqueous base hydrolysis of LnA_3 (A = $CF_3SO_3^-$ or $CH_3C_6H_4SO_3^-$) in the presence of an amino acid gives LnA_3 starting material or insoluble precipitates. Even when solutions were concentrated to dryness, crystalline LnA_3 or amorphous powders formed. Figure 2.1 depicts $Eu(CF_3SO_3)_3$ ($Eu(OTf)_3$) and Figure 2.2 depicts $Eu(CH_3C_6H_4SO_3)_3$ ($Eu(OTs)_3$). In the solid-state structure of $Eu(OTf)_3$, the triflate anions of $Eu(OTf)_3$ orient themselves around the aquated Eu(III) cation in such a way that hydrogen bonding interaction are observed while manipulating the structure in the X-ray diffraction program. Interestingly, the solid-state structure of $Eu(OTs)_3$ exhibits Eu(III) coordination by two of the tosylate anions while the third remains separate in the crystal lattice.

Exchange reactions of polynuclear complexes with perchlorate counter ions and potassium salts (i.e., polylanthanide perchlorates and KCF_3SO_3 or $KCH_3C_6H_4SO_3$) were performed and were also unsuccessful. It is unclear why these reactions did not produce the desired results.

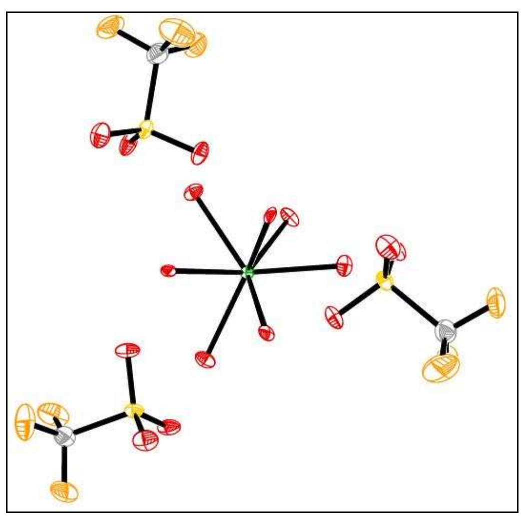

Figure 2.1: Depiction of $Eu(OTf)_3$ (OTf = $CH_3SO_3^-$). Color scheme: green, europium; yellow, sulfur; grey, carbon; orange, fluorine; red, oxygen.

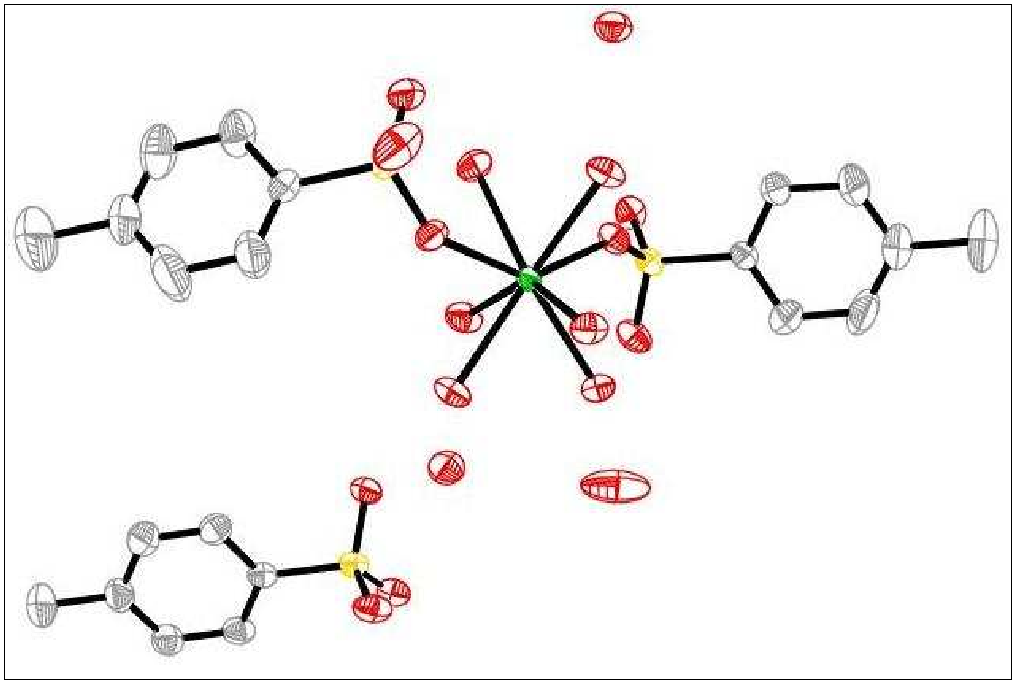

Figure 2.2: Depiction of $Eu(OTs)_3$ (OTs = $CH_3C_6H_4SO_3^-$). Color scheme: green, europium; yellow, sulfur; grey, carbon; red, oxygen.

Synthesis Characterization of

$[Ln_{15}(\mu_5\text{-}X)(\mu_3\text{-}OH)_{20}(his^{+/-})_{10}(his^-)_5(OH)_7](ClO_4)_{12}$

(Ln = Y, Nd, Eu, and Tb; X = Cl, Br, $(I)_2$-OH)

Aqueous hydrolysis of $Ln(ClO_4)_3$ in the presence of L-histidine and NaX (in the ratio 1:2:1 for $Ln(ClO_4)_3$:L-his:NaX) gives $[Ln_{15}(\mu_5\text{-}X)(\mu_3\text{-}OH)_{20}(his)_{15}(OH)_7](ClO_4)_{12}$ (Ln_{15}–his X) in 60 – 70 % isolable yields (Figure 2.3). Crystals obtained from this procedure are generally clear prisms, and only the neodymium(III) analogs exhibit any color (light purple). Europium(III) and terbium(III) complexes fluoresce, red and green respectively, when irradiated with long-wave ultraviolet (UV) light. The compounds are soluble in water, DMSO, and only marginally soluble in acetone, acetonitrile, and alcohols.

Product yields were dependent on solvent volume and did not vary with different starting material ratios. Prior synthetic work by Dr. Chang-Tong Yang, a former post-doc in the Messerle group, required a two-fold excess of L-histidine (L-his) and 15-fold excess of NaX for the synthesis of Ln_{15}–his X complexes, as compared to crystallographic data where the ratio of Ln:L-his:X is 1:1:1/15 (X = Cl or Br) and 1:1:2/15 (X = I). Ln_{15}–his X can be obtained in moderate yields (60 – 70 %) using starting material ratios seen in the crystallized product. Excess L-his may act as a buffer and help stabilize crystal growth. However, subsequent crystallizations after initial product growth resulted in precipitation of presumed lanthanide oxo-hydroxo solids that were independent of starting material ratios.

Successful formation of isolable crystals of Ln_{15}–his X complexes was pH dependent. Solutions with pH under 6 did not afford crystalline Ln_{15}–his X complexes, even when the solution was concentrated to near dryness. Instead, histidinium perchlorate crystallized followed by insoluble lanthanide oxo/hydroxo precipitates. Permanent insoluble precipitate formed when solutions were above pH = 7. However, if the precipitate was removed from the mother liquor via centrifugation or filtration, Ln_{15}–his X crystallized, albeit in diminished yields. The pH range of 6.2 – 6.4 proved most effective in producing Ln_{15}–his X crystalline complexes in high yields.

Previous approaches by Dr. Chang-Tong Yang in forming Ln_{15}–his X complexes used methanolic solutions (1:1 methanol:H_2O) and dilute conditions, nearly 50 mL of solvent for 1.0 mmol of $Ln(ClO_4)_3$. In this thesis we use 7 mL of deionized water for 1.0 mmol of $Ln(ClO_4)_3$. Dilute solutions produced the desired product in moderate to low yields, and only after extensive concentration by removal of solvent. By starting with a reduced volume, very little concentration was required. Previous methods also used dropwise addition of NaOH solution. This is not required as long as the reaction temperature is above 70 ^{o}C, at which NaOH can be added quickly by buret. Addition of base solution produced

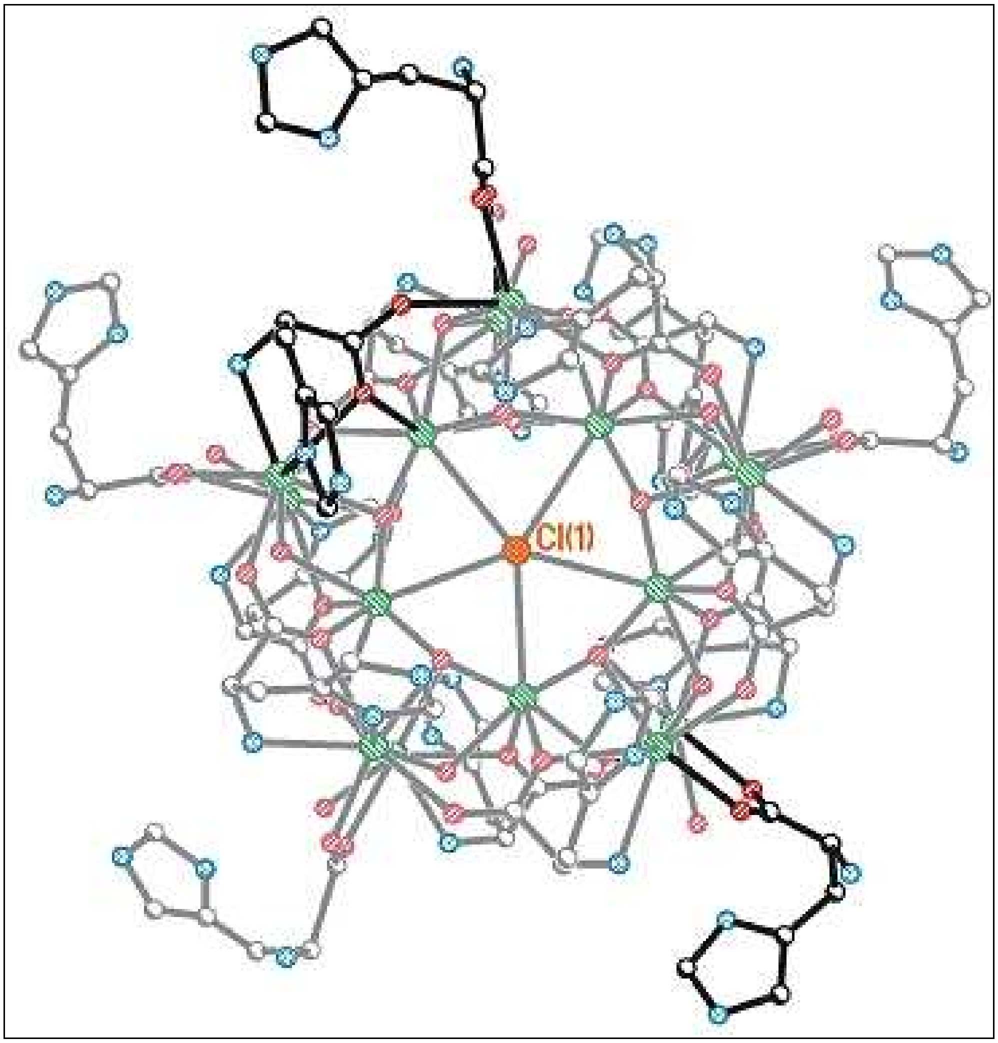

Figure 2.3: $[Ln_{15}(\mu_5\text{-}X)(\mu_3\text{-}OH)_{20}(his)_{15}(OH_2)_7](ClO_4)_{12}$ (Ln = Y, Eu, or Tb) crystal structure showing the coordination modes of the histidine ligands. Perchlorate anions omitted for clarity. Color scheme: green, Ln(III); orange, chloride; gray, carbon; blue, nitrogen; red, oxygen.

precipitation; however, with continued heating and stirring, the solution became homogenous within the 6.2 – 6.4 pH range.

Recrystallizations of $[Eu_{15}(\mu_5\text{-}Cl)(\mu_3\text{-}OH)_{20}(his^{+/-})_{10}(his^{-})_5(OH)_7](ClO_4)_{12}$, $[Eu_{15}(\mu_5\text{-}Br)(\mu_3\text{-}OH)_{20}(his^{+/-})_{10}(his^{-})_5(OH)_7](ClO_4)_{12}$, and $[Eu_{15}(\mu_5\text{-}OH)(I)_2(\mu_3\text{-}OH)_{20}(his^{+/-})_{10}(his^{-})_5(OH)_7](ClO_4)_8$ were attempted in order to understand the solution dynamics of these complexes; such recrystallizations have not yet been reported in the literature. Recrystallizations from deionized H_2O or 0.1 M $HClO_4$ (pH = 6.4) produced white insoluble precipitates. Eu_{15}–his X complexes (X = Cl, Br, $(I)_2$-OH) could only be recrystallized from L-his (0.1 M) buffered solutions at pH = 6.0 – 6.6. As in the initial synthesis of these complexes, pH was critical. Crystals would not form in solutions below pH = 6, and insoluble precipitates were obtained in solutions above pH = 6.8. The inability of these complexes to recrystallize from deionized H_2O or $HClO_4$ solutions (0.1 M, pH = 6.4) suggests that the stability of these complexes, in solution, was pH dependent and that the ligands are labile and capable of changing their bonding modes. Variable coordination or labile ligands are easily replaced with bulk solvent molecules, thereby allowing for further hydrolysis and precipitation.

In order to ascertain the validity of the above hypothesis regarding ligand lability and cluster compound solution-state stability, solution-state structures studies were investigated by ^{13}C NMR and ^{89}Y NMR spectroscopies. Yttrium(III) complexes that were isostructural to Ln_{15}–his X complexes were prepared because yttrium chemistry is very similar to that for Ln(III), ^{89}Y is NMR active (I = ½, 100 % abundant), and Y(III) is diamagnetic (unlike most Ln(III) ions) and allows for ^{13}C NMR spectroscopy.

The ^{13}C NMR spectrum of Y_{15}-his Cl exhibited two separate signals for L-histidine (Figure 2.4) in 50:50 D_2O/MeOD. One set of resonances matched with that of free L-histidine in 50:50 D_2O/MeOD solution: resonances with chemical shifts of δ 32.1, 58.5, 118.9, 135.7, 139.8, and 178.0 ppm. The other set of resonances is further downfield and most likely arises from L-histidine coordinated to Y(III): resonances with chemical shifts δ 32.9, 58.7, 120.8, 138.4, 142.1, and 186.1 ppm. The appearance of resonances matching with free L-histidine is suggestive of the lability of the histidine ligands. In order to test this, free histidine would need to be added to solutions of Y_{15}-his Cl studied by ^{89}Y NMR; such experiments were not performed. It is plausible to postulate that the exterior L-histidine ligands exchange more readily than the face-bound L-histidine because of multidentate coordination for the latter.

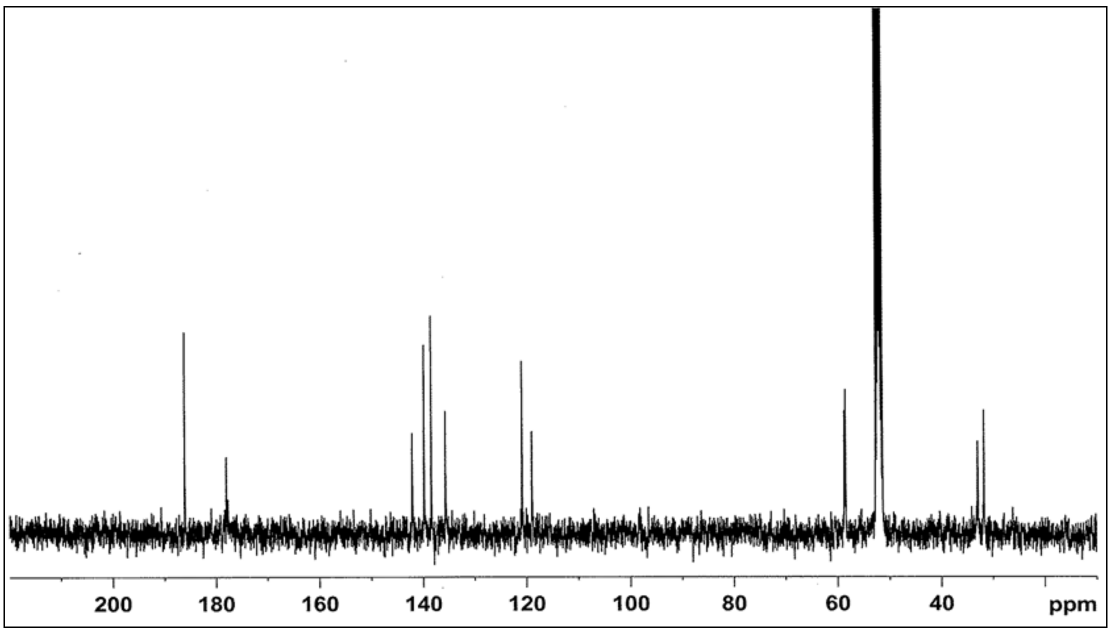

Figure 2.4: 400 MHz ^{13}C NMR spectrum of Y_{15}-his Cl in DMSO depicting L-histidine coordinated to Y(III) and free L-histidine in solution. Spectrum obtained by Dr. John Thurston, a former post-doc in the Messerle group.

^{89}Y NMR spectroscopy of Y_{15}-his Cl exhibited two separate Y(III) resonances consistent with solid-state structure, at δ 65 and 75 ppm (Figure 2.5) with an integration of 1:2, respectively. One resonance is significantly broadened compared to the other. This is assumed to arise from ^{89}Y-^{14}N quadrupolar coupling. This spectrum is also consistent with the solid-state structure, as the ten exterior Y(III) centers are coordinated

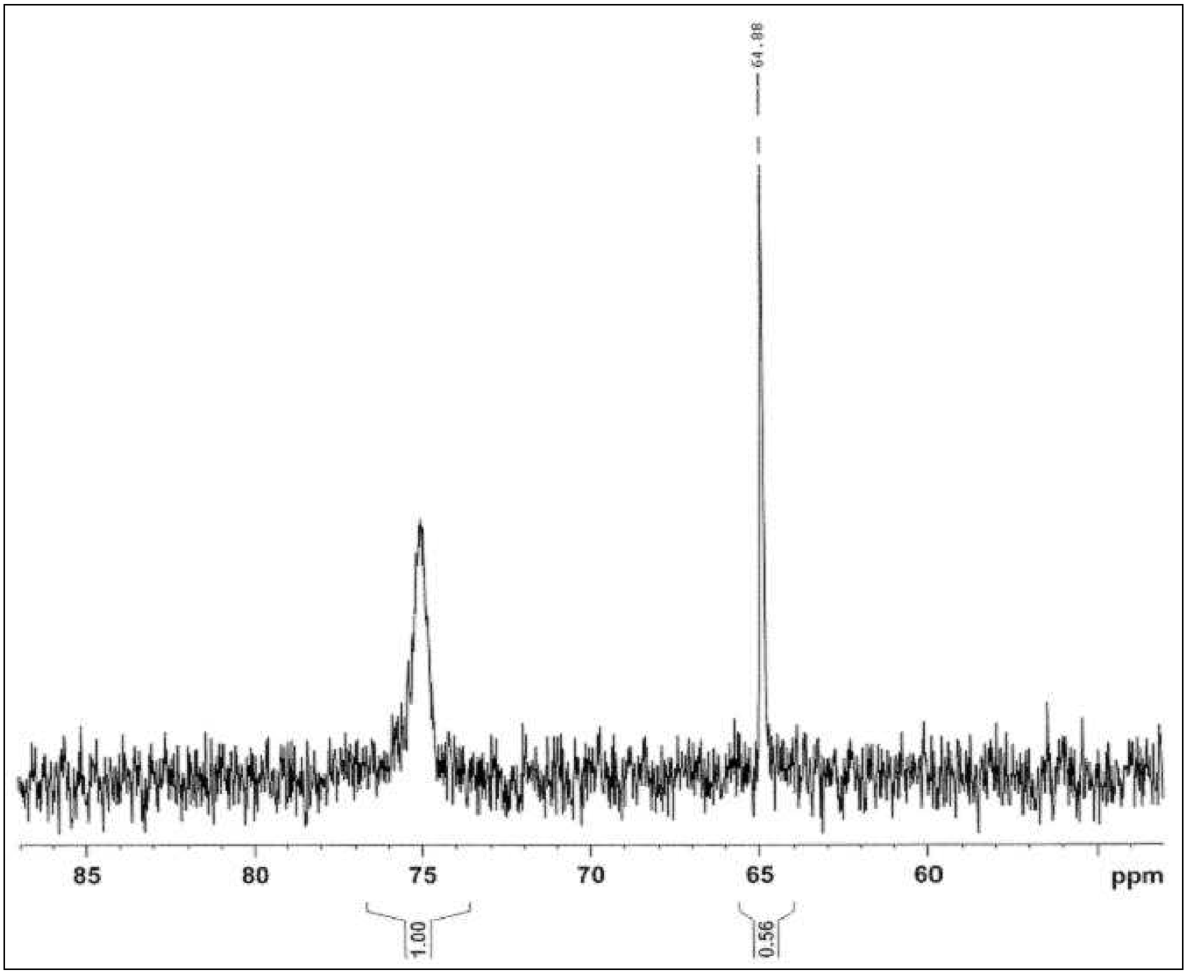

Figure 2.5: 400 MHz ^{89}Y NMR spectrum of Y_{15}-his Cl in MeOD depicting two resonances for two unique Y(III) centers. Broadening of the peak at δ 75 ppm is suspected to be from ^{14}N quadrupolar coupling or dynamic ligand exchange processes. Spectrum obtained by Dr. John Thurston, a former post-doc in the Messerle group.

by oxygen and nitrogen atoms and the five interior Y(III) centers are only coordinated by oxygen atoms. Another plausible explanation for the broadening is dynamic ligand exchange. Exterior Y(III) centers are coordinated by oxygens and nitrogens from face-bound-histidine ligands (Figures 2.3, 2.10 and Scheme 2.1a) as well as from oxygens from exterior L-histidine ligands. As previously discussed, these ligands may be labile and exchange with bulk solvent. This dynamic process would cause a change in the Y(III) environment that may give rise to another resonance at similar chemical shifts. The dynamic environment of the exterior Y(III) centers could be probed with variable temperature NMR spectroscopy studies. This data is consistent with stability of the cluster core, if not the complex as a whole. Identical spectra with similar integration are obtained several days after initial NMR experiments, further supporting the robustness of the cluster.

Electrospray ionization mass spectrometry (ESI-MS) was employed to probe the solution stability of the Ln_{15}–his X clusters. For example, ESI-MS of Eu_{15}–his Cl displayed a peak envelope centered at 980 amu, corresponding to [Eu_{15}–his Cl – $5ClO_4^-$ – 6 L-$his^{+/-}$]$^{5+}$. Specific m/z values matching a +3 charged species were also observed by ESI-MS (Figure 2.6). Similar results were obtained for each Eu_{15}–his X reported here. These results indicate that the integrity of the polynuclear core was maintained in solution during the course of ESI-MS studies.

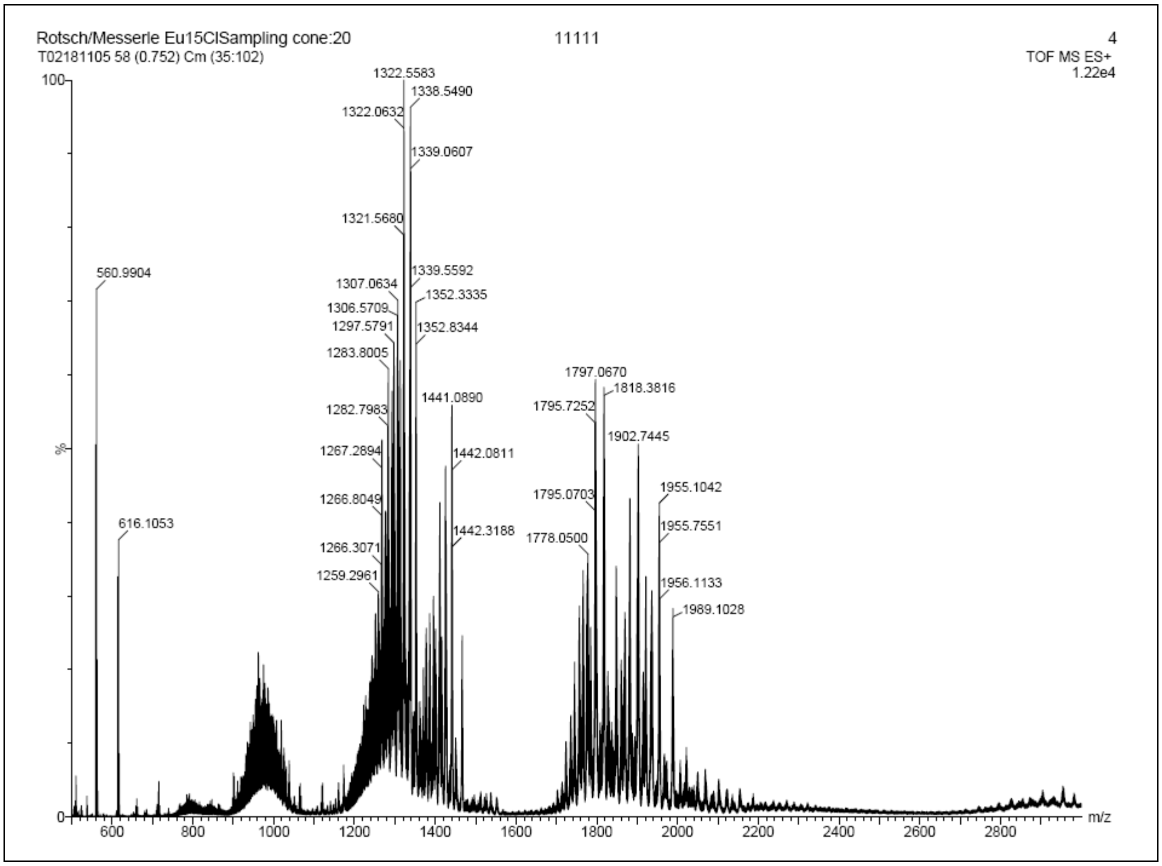

Figure 2.6: ESI-MS spectrum of Eu_{15}-his Cl in H_2O (% intensity vs. m/z). Peak envelopes centered at 980 amu corresponds to to [Eu_{15}–his Cl – $5ClO_4^-$ – 6 L-$his^{+/-}]^{5+}$. Peak envelopes at 1320 amu corresponds to [Eu_{15}–his Cl – $4ClO_4^-$ – 4 L-$his^{+/-}]^{4+}$; 1945 amu corresponds to [Eu_{15}–his Cl – $3ClO_4^-$ – L-$his^{+/-}]^{3+}$. Other peak envelopes representing other charged species are also observed.

Solid-State Structure of $[Ln_{15}(\mu_5\text{-X})(\mu_3\text{-OH})_{20}(his^{+/-})_{10}(his^-)_5(OH)_7](ClO_4)_{12}$ (Ln = Y, Nd, Eu, and Tb; X = Cl^-, Br^-, $(I^-)_2$-OH^-) via Single-Crystal X-Ray Diffractometry

The D_{5h}-symmetry core $[Ln_{15}(\mu_5\text{-X})(\mu_3\text{-OH})_{20}]^{24+}$ of $[Ln_{15}(\mu_5\text{-X})(\mu_3\text{-OH})_{20}(his^{+/-})_{10}(his^-)_5(OH)_7](ClO_4)_{12}$ (denoted as Ln_{15}-his X) is similar to the reported tyrosine analogs of $[Ln_{15}(\mu_5\text{-X})(\mu_3\text{-OH})_{20}]^{24+}$ (Ln = Nd, Gd, Eu, and Pr; X = Cl^- and Br^-; denoted as Ln_{15}-tyr X). Solid-state structural comparison of Ln_{15}–his X and the reported Ln_{15}–tyr

X reveals that the core structures are indeed comparable, even though they have different ligands. A structural comparison of Eu(III) analogs of these complexes, with available literature bond lengths and atomic separations, is summarized in Table 2.1.

Table 2.1: Selected mean bond lengths and atom separations (Å) for Eu_{15}-his-Cl and literature Eu_{15}-tyr-Cl.[43]

	Eu_{15}-his Cl (Å)	**Eu_{15}-tyr Cl (Å)[43]**
Eu···Eu (inner-inner)	3.8390(7)	3.896
Eu-μ_3-OH	2.415(7)	2.43(3)
Eu-O carboxalato	2.512(7)	2.51(8)
Eu-N amine	2.585(9)	2.63(3)
Eu-Cl	3.241(3)	3.31(3)

Both the reported Eu_{15}-tyr-Cl and the Eu_{15}-his-Cl clusters can be described as five vertex-sharing lanthanide tetrahedras forming a pentagon (Figure 2.8). It is easier to understand the structure by first observing the individual tetrahedra of Eu(III) and then the cubanes, $Eu_4(\mu_3\text{-}OH)_4$, that make up the pentadecanuclear europium cluster (Figure 2.7). Each Eu(III) tetrahedral face is capped by a triply-bridging hydroxo ligand forming quasi-cubanes (Figure 2.7 B). These cubanes then come together by sharing Eu(III) vertices to form the structure shown in Figure 2.9. Both faces of the pentagon are coordinated by tridentate tyrosine ligands or tetradentate histidine ligands. However, in contrast to the reported Eu_{15}-try-Cl, Eu_{15}-his-Cl has histidine ligands coordinating to the exterior of the pentagon. The remainder of the coordination sphere for exterior Eu(III) ions of Eu_{15}-tyr Cl is completed by water ligands to give a coordination number (CN) of 9 for each unique Eu(III) center.

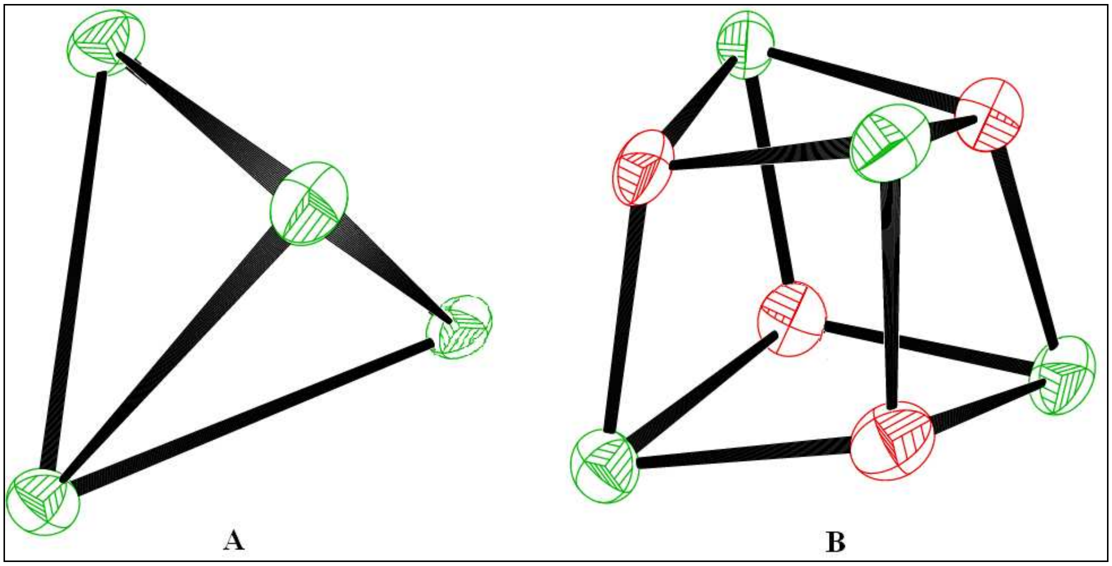

Figure 2.7: Depiction of tetrahedron of Eu(III) ions, (A), and quasi-cubane of $Eu_4(\mu_3\text{-}OH)_4$ with hydrogens omitted for clarity, (B). Color scheme: green, Eu(III); red, oxygen.

The Eu_{15}-his X complexes crystallized with varying CN for Eu(III) in identical skeletal positions. Five interior Eu(III) ions exhibited CN of 9, with coordination from the μ_5-X, six μ_3-OH, and two carboxyl oxygens as a result of face-coordinated histidines. Ten exterior Eu(III) ions are coordinated by three μ_3-OH, three carboxyl oxygens, an amine, an imidazole nitrogen and, in some cases, a water or hydroxide, for a CN of either 8 or 9. It is unclear if these exterior ligands are waters or hydroxides. Based on charge considerations, they are likely hydroxides. Presumably, any Eu(III) with a CN = 8 in the solid-state structure would increase to 9 from solvent molecules in the solution-state.

As seen in Table 2.1, minor differences in bond length were observed. In Eu_{15}-tyr Cl, ten tyrosine ligands coordinate in a μ_3: η^1:η^2:η^1 coordination mode.[45a] In Eu_{15}-his-Cl, fifteen histidine ligands coordinate in three distinct fashions: ten coordinate to the face of the pentagon utilizing all three functional groups in a μ_3: η^1:η^2:η^1:η^1 coordination mode (Scheme 2.1a), four coordinate to the edge of the pentagon by the carboxyl group in a μ_2 coordination mode (Scheme 2.1b), and the last histidine is bidentate through one carboxyl oxygen and the amine (Scheme 2.1c). Figure 2.3 shows the actual coordination within the molecule. The ten face histidines coordinate similarly to that seen for histidine-copper coordination complexes.[60] The coordination of the imidazole (the amino acid histidine's side-group) forces the imidazole rings to tilt towards the center of the pentagon, forming a cage. A perchlorate anion (or iodide anion in the case of Ln_{15}–his $(I)_2$-OH) rests within the cage on each face of the pentagon (Figure 2.10). There is also evidence for hydrogen bonding or electrostatic interactions from hydroxo hydrogens to perchlorate or iodide. Charge-balance considerations require that all face histidine ligands are in the zwitterionic state and all exterior histidine ligands have a single negative charge.

The coordination mode of histidine differs across the Ln(III) series of complexes reported here. Larger ionic radii allow for higher CNs and more space for functional group coordination (Scheme 2.2). Four of the five exterior histidine ligands of La_{15}–his Cl and Nd_{15}–his Cl coordinate in the same mode as seen in the smaller Eu_{15}–his X complexes. The fifth exterior histidine for La(III) and Nd(III) complexes coordinates in bidentate fashion through one carboxyl oxygen and the amine; however, it also coordinates to a separate Ln_{15}–his X cluster within the same crystalline lattice through the imidazole nitrogen (Scheme 2.2 d). This effectively forms a one-dimensional network of Ln_{15}–his X molecules (Figure 2.11). Smaller Ln_{15}-his X with Ln = Y(III), Eu(III), Gd(III), and Tb(III), crystallize only as single molecular units. Nd_{15}–his Br exhibited yet another new coordination mode for histidine. As before, four of the five exterior histidine ligands coordinate as seen in Eu_{15}–his X, but the fifth histidine is bidentate through the carboxyl group (Scheme 2.2c). Scheme 2.2 depicts the new L-histidine coordination modes of Ln_{15}-his X complexes made up of larger Ln(III) ions such as La(III) and Nd(III). Aside from the new histidine coordination modes, changing the Ln(III) ion size causes nominal bond length and angle changes that are most likely due to

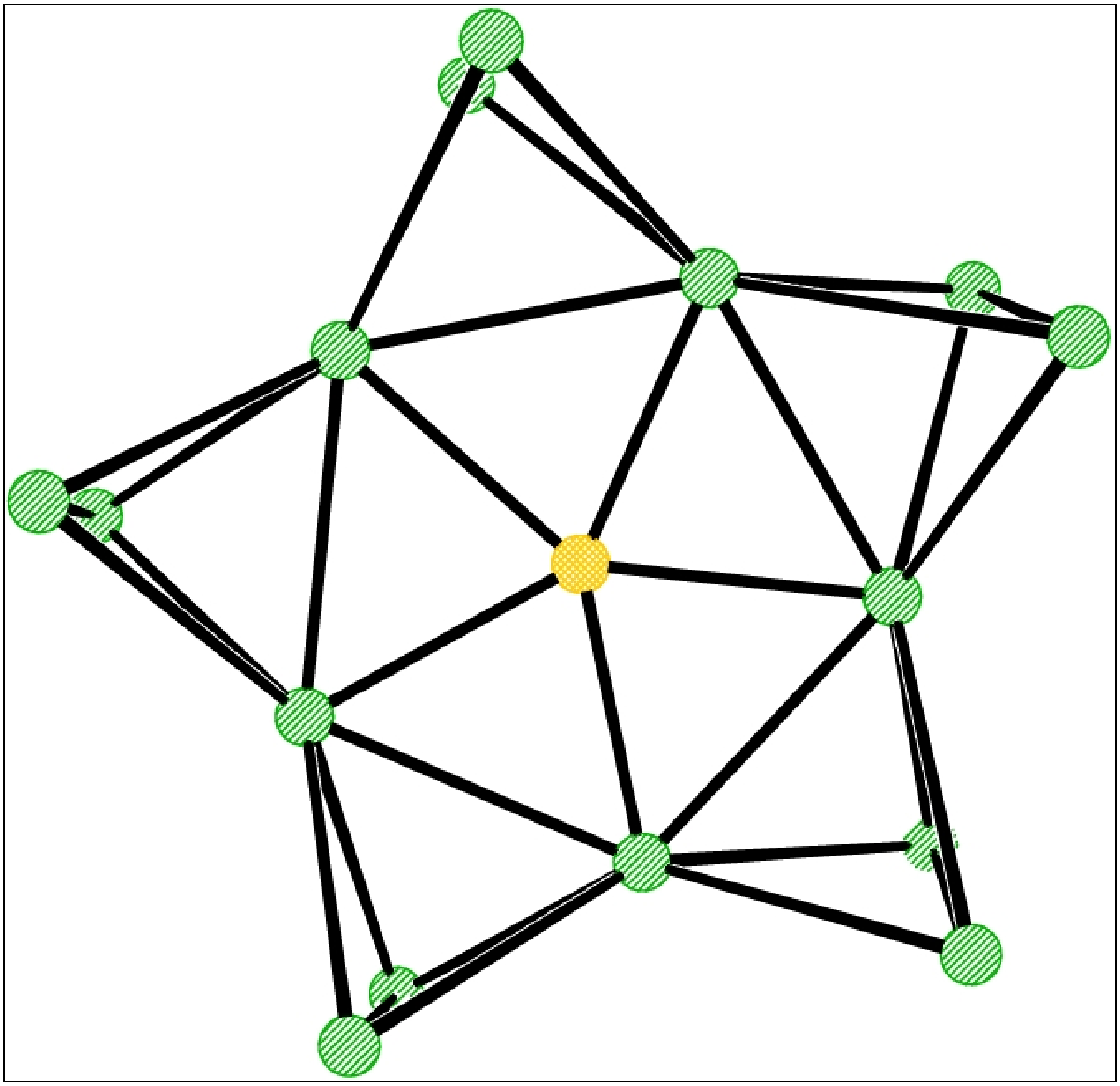

Figure 2.8: Skeletal view of Eu_{15}-his Cl with Eu(III) and μ_5-Cl depicted. All other ligands and anions omitted for clarity. Color scheme: green, Eu(III); yellow, chloride. This structure was also observed for Ln = Nd, Gd, Tb, and Y.

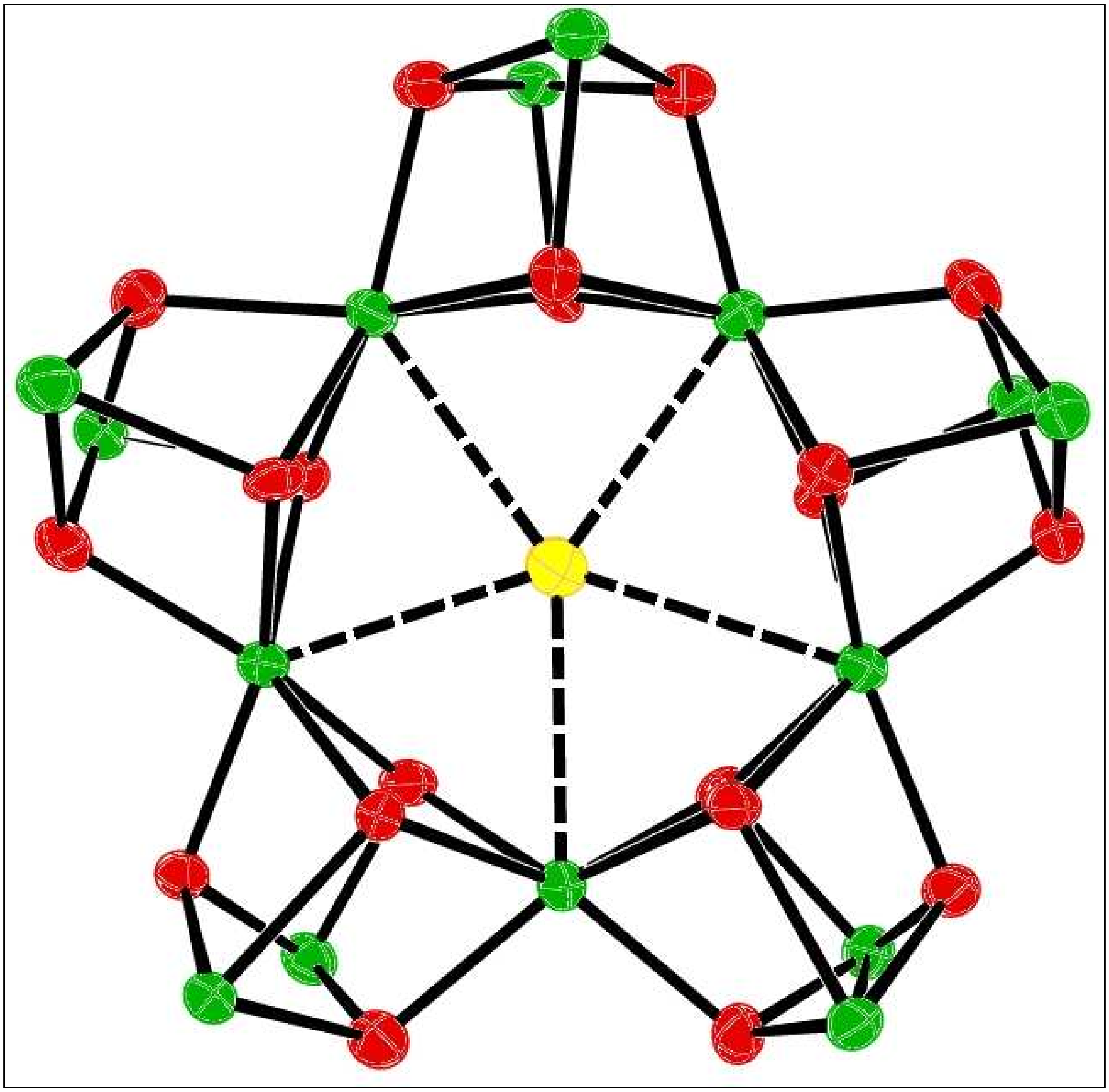

Figure 2.9: Skeletal view of Ln_{15}-his Cl with bridging hydroxides (μ_3-OH) and μ_5-Cl. All other ligands and anions omitted for clarity. Color scheme: green, Eu(III); yellow, chloride; red, oxygen. This structure was also observed for Ln = Nd, Gd, Tb, and Y.

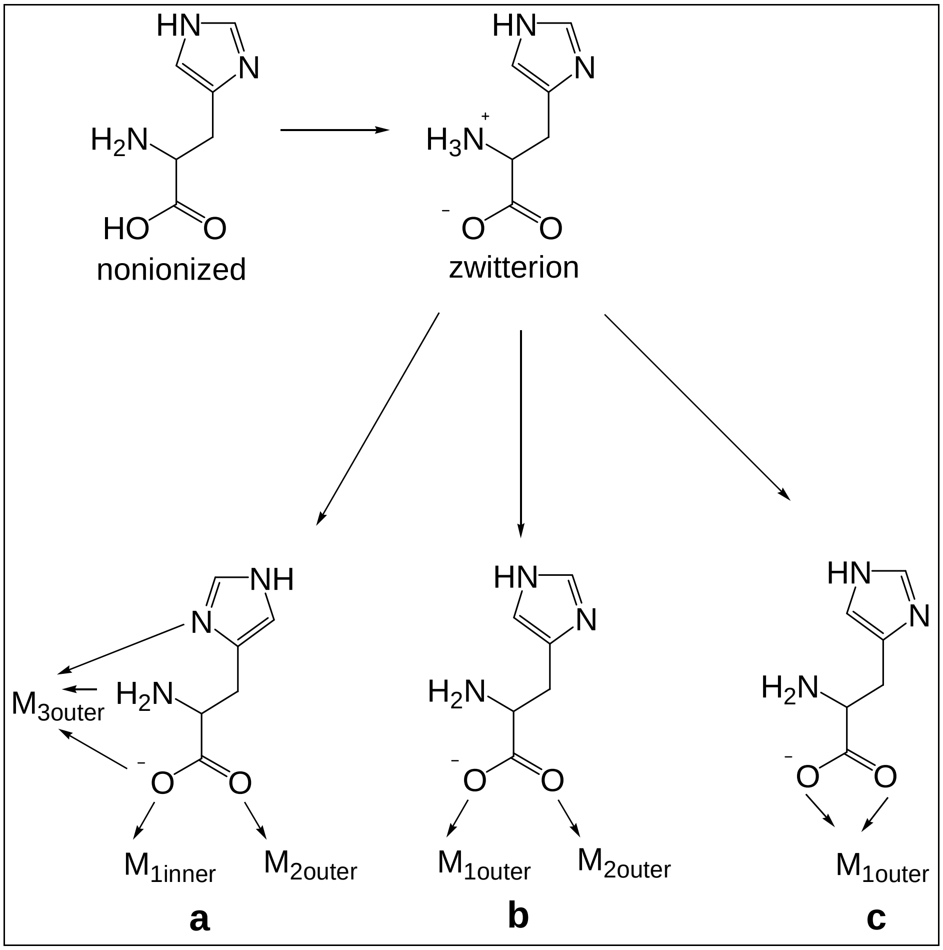

Scheme 2.1: L-histidine coordination modes in Ln_{15}–his X complexes (Ln = Y, Eu, Gd, and Tb).

Table 2.2: Selected mean atomic separations (Å), bond lengths (Å) and dihedral angles for Eu_{15}–his X and Nd_{15}-his X complexes.

	Nd_{15}-his Cl	**Eu_{15}-his Cl**	**Tb_{15}-his Cl**
Ln-μ_3-OH (inner-inner) (Å)	2.46(1)	2.404(7)	2.45(4)
Ln-μ_3-OH (inner-outer) (Å)	2.49(1)	2.412(7)	2.42(5)
Ln-μ_3-OH (outer-outer) (Å)	2.46(1)	2.417(7)	2.40(6)
Ln-μ_3-OH (outer-inner) (Å)	2.47(1)	2.426(7)	2.37(4)
μ_3-OH (inner) Displacement from Ln Tetrahedra (Å)	0.985	0.957	1.013
μ_3-OH (outer) Displacement from Ln Tetrahedra (Å)	0.936	0.923	0.939
Ln⋯Ln (inner-inner) (Å)	3.905(1)	3.8390(7)	3.807(7)
Ln⋯Ln (outer-outer) (Å)	4.065(1)	3.9797(7)	3.905(9)
Ln⋯Ln (inner-outer) (Å)	3.774(1)	3.7005(7)	3.734(5)
Tetrahedra Dihedral Angle (inner)	73.84°	73.98°	72.90°
Tetrahedra Dihedral Angle (outer)	71.66°	72.00°	72.25°
Cavity Area (Å^2)	26.243(4)	22.933(7)	24.898(8)
Cavity Diameter(Å)	4.213(4)	3.579(7)	4.139(8)
μ_5-X Displacement from InnerLn$_5$ Plane (Å)	0.0156	0.0085	0.2939
Ln-Ln-Ln (angle)	108.00°	107.95°	107.90°
Ln-X (Å)	3.358(4)	3.265(2)	3.095(3)

Note: The cavity areas does not take into consideration the ionic radii of the Ln(III).

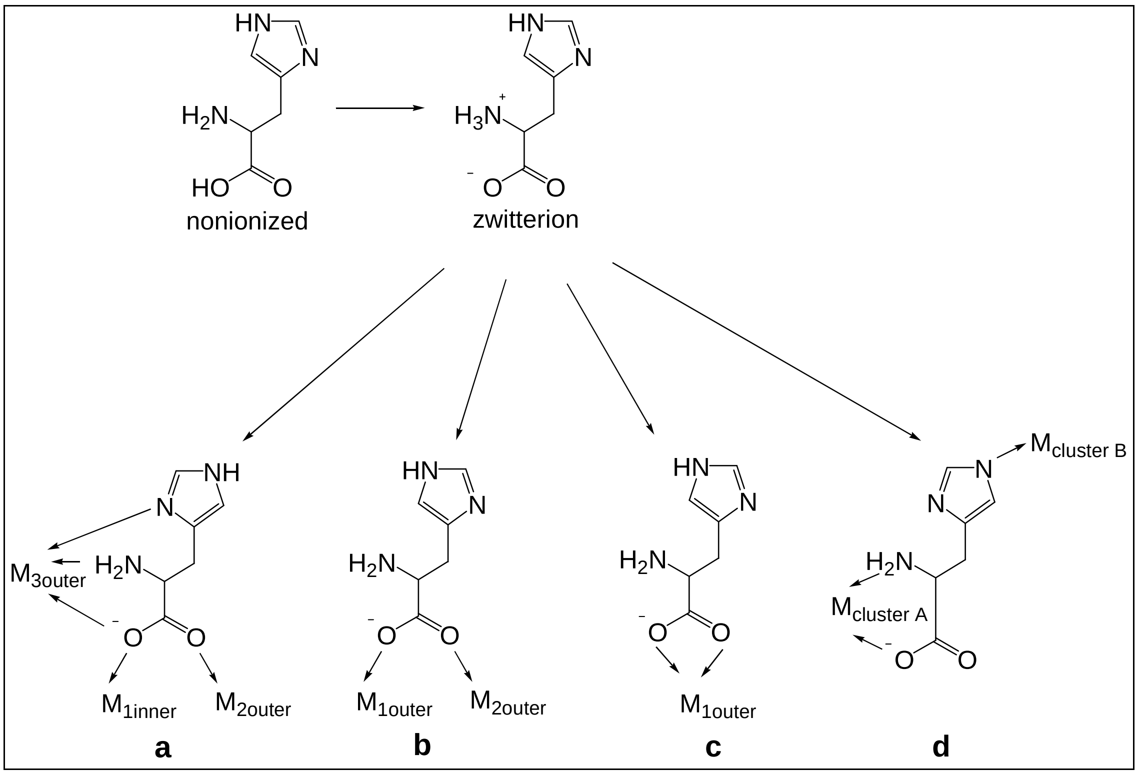

Scheme 2.2: L-histidine coordination modes for Ln_{15}-his X complexes (Ln = La and Nd).

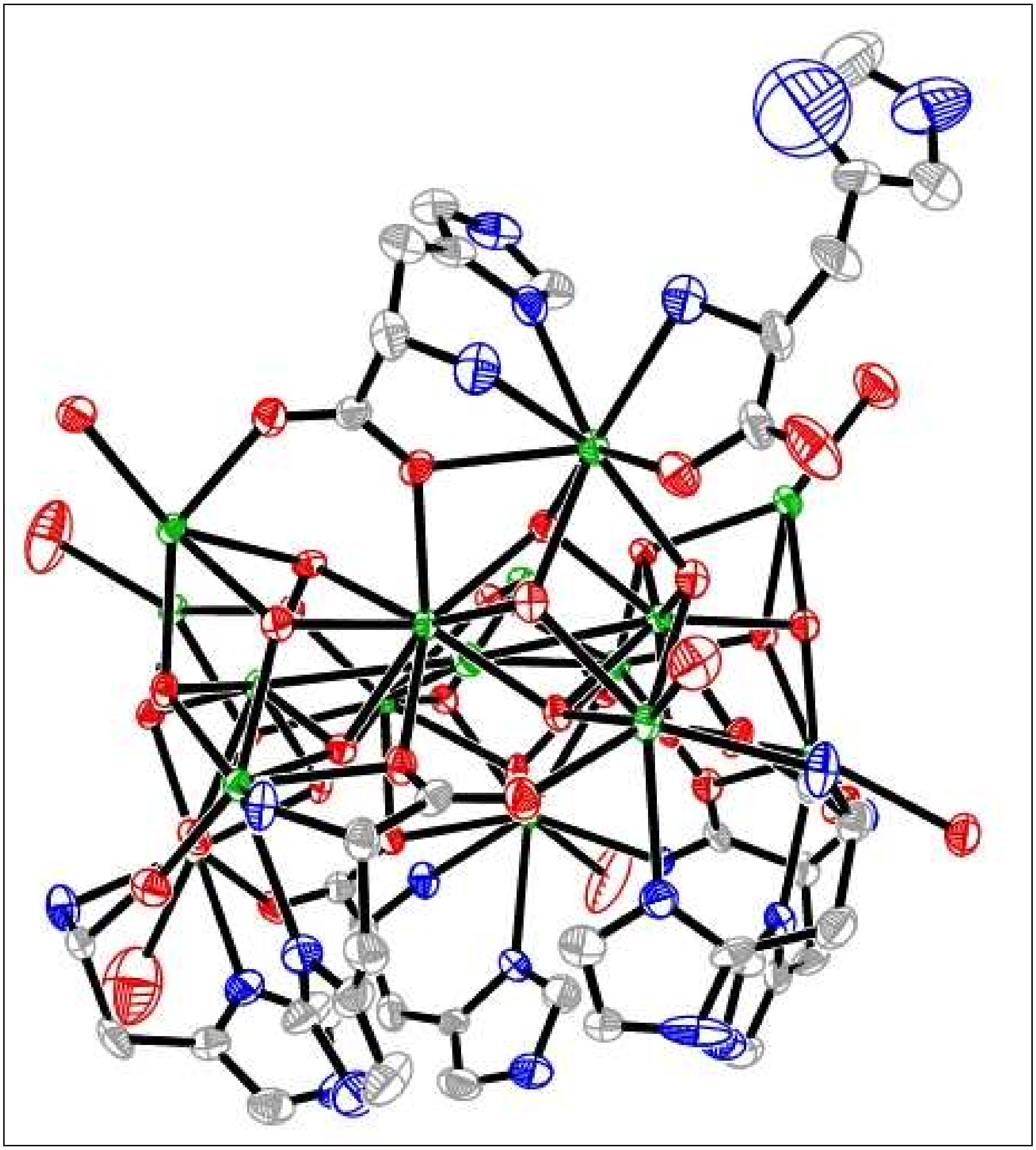

Figure 2.10: Depiction of Ln_{15}-his X with several ligands and anions omitted to demonstrate the cage that histidine forms on the faces of the complex. Two coordination modes can be observed: face-bound histidine, Scheme 2.1a and one exterior histidine, Scheme 2.1c. At the top of the figure, the face-bound histidine is directed away from the observer. The rest of the face of the complex is filled with histidines in such a coordination mode. This effectively results in the formation of a cage on the face of the cluster as depicted by the lower half of the figure.

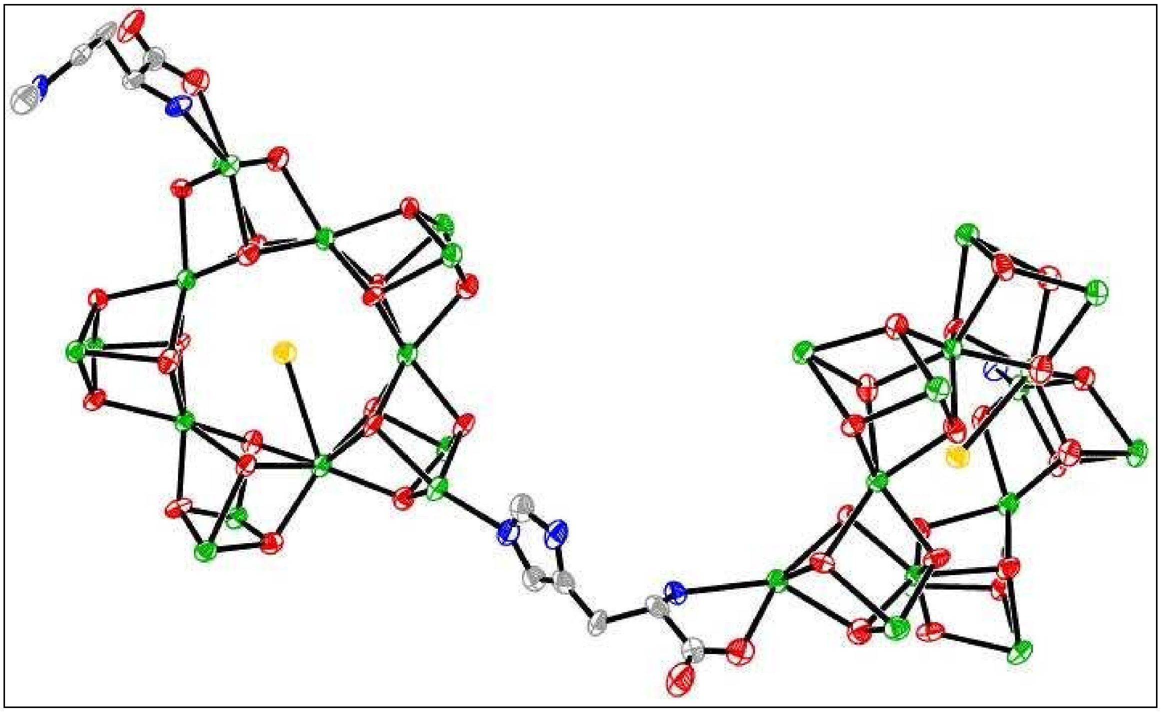

Figure 2.11: Depiction of one linkage unit of the one-dimensional network of Nd_{15}-his Cl clusters linked through L-histidine coordination. Color scheme: green, Nd(III); red, oxygen; blue, nitrogen; yellow chlorine.

the differences in the ionic radii of the lanthanide(III) (Table 2.2).

Some of the most interesting structural changes in Ln_{15}–his X complexes occur when substitutions in X are made. Bond length and angle changes observed for the Eu_{15}-his X series with varying X are analogous to the changes observed for the rest of the Ln_{15}-his X series when X is changed (i.e., structural changes in Eu_{15}-his Cl to Eu_{15}-his Br to Eu_{15}-his $(I)_2$-OH are similar to that observed in Nd_{15}-his Cl to Nd_{15}-his Br to Nd_{15}-his $(I)_2$-OH). Therefore, only the Eu_{15}-his X series will be discussed. Averaged atomic distances, bond lengths and angles are listed in Table 2.3. In summary, all Eu-μ_3-OH distances are statistically the same. Eu···Eu distances are shorter for interior Eu(III) as compared to exterior Eu(III). Shorter interior Eu···Eu distances result in inner μ_3-OH ligands extending further from the face of the Eu(III) tetrahedra than exterior μ_3-OH ligands.

Eu(III) tetrahedra are distorted from idealized tetrahedra by several degrees (idealized tetrahedra have dihedral angles of 70.5^o). These deviations are linear with halide size, i.e., larger halides correlate with an increase in deviations. Eu(III) ions with coordination Scheme 1c have larger Eu···Eu distances than those in Scheme 1b, causing larger inner dihedral angles than exterior dihedral angles by 1^o - 2^o. This can be accounted for by smaller inner Eu···Eu distances and larger exterior Eu···Eu distances.

The μ_3-OH deviation from the face of the Eu(III) tetrahedra and Eu(III) tetrahedral distortions could be the result of several factors. Hydrogen bonding or electrostatic interactions between the hydrogens of μ_3-OH and ClO_4^- or I^- could increase the distance of the interior hydroxo ligands from the face of the Eu(III) tetrahedra. Shorter inner Eu···Eu distances could also cause interior hydroxo ligands to extend away from the tetrahedral faces more than exterior hydroxo ligands because of less room between the Eu(III) ions. Another possible explanation for this deviation could be Eu(III)-μ_5-X interactions. The cavity area increases as halide size increases: Eu_{15} Cl, 22.933(7) Å^2; Eu_{15} Br, 25.721(9) Å^2; and Eu_{15} $(I)_2$-OH, 26.980(7) Å^2.

The 'templating' anion rests in the nearly-perfect pentagonal cavity formed by five inner Eu(III) ions. Eu(III)'s equally share the 'template' anion as seen in Figure 2.12. The average Eu-Cl distance of 3.265(2) Å is significantly larger than the sum of the individual ionic radii of Cl^- (1.81 Å) and Eu(III) (1.120 Å), reflecting primarily ionic interactions between the halide and the lanthanide. The same is true for Br^- (1.96 Å) and OH^- (1.34 Å). The average Eu-I distance of 4.876(3) Å is too large to postulate any interactions (I^- radius = 2.20 Å). Smaller anions deviate less than larger: OH^- by 0.0028 Å, Cl^- by 0.0085 Å, Br^- by 0.0157 Å, and I^- by 3.5618 Å (Figure 2.12). The small deviation observed for the hydroxide could also be a result of interactions with the iodides that are above and below the hydroxide's position. The large spherical anion

Table 2.3: Selected mean atomic separations (Å), bond lengths (Å) and dihedral angles for Eu_{15}–his X complexes.

	Eu_{15}–his Cl	**Eu_{15}–his Br**	**Eu_{15}–his $(I)_2$-OH**
Eu-μ_3-OH (inner-inner) (Å)	2.404(7)	2.420(9)	2.412(7)
Eu-μ_3-OH (inner-exterior) (Å)	2.412(7)	2.428(9)	2.405(7)
Eu-μ_3-OH (exterior-exterior) (Å)	2.417(7)	2.413(9)	2.424(7)
Eu-μ_3-OH (exterior-inner) (Å)	2.426(7)	2.411(9)	2.455(7)
μ_3-OH (inner) Displacement from Eu_4 (Å)	0.957	0.951	0.972
μ_3-OH (exterior) Displacement from Eu_4 (Å)	0.923	0.915	0.915
Eu···Eu (inner-inner) (Å)	3.8390(7)	3.8667(9)	3.9144(7)
Eu···Eu (exterior-exterior) (Å)	3.9797(7)	3.980(1)	3.9972(7)
Eu···Eu (inner-exterior) (Å)	3.7005(7)	3.748(1)	3.8058(7)
Tetrahedra Dihedral Angle (inner)	73.98°	74.10°	75.14°
Tetrahedra Dihedral Angle (exterior)	72.00°	72.86°	74.00°
Cavity Area (Å^2)	22.933(7)	25.721(9)	26.980(7)
Cavity Diameter (Å)	3.579(7)	4.123(9)	4.314(7)
μ_5-X Displacement from Inner Eu_5 Plane (Å)	0.0085	0.0157	3.5618 $(I)_2$ 0.0028 (OH)
Eu-Eu-Eu (angle)	107.95°	107.98°	107.98°
Eu-X (Å)	3.265(2)	3.266(1)	4.876(3) $(I)_2$ 3.333(3) (OH)

Note: The cavity diameters does not take into consideration the ionic radii of the Eu(III).

would be able to penetrate the molecules core cavity more effectively than a tetrahedral perchlorate anion. This could effectively decrease the lateral space available to the hydroxide and thus give rise to a much smaller deviation for the hydroxide as compared to chloride or bromide.

The iodide sits well above the inner Eu_5 plane because the cavity is too small to accommodate I^-. The cavity diameter for Eu_{15}–his Cl is 3.5790(7) Å and Cl^- diameter is 3.62 Å and so the Cl^- does not deviate much from planarity with the inner Eu(III). For Eu_{15}–his Br, the cavity diameter is 4.1225(9) Å and the Br^- diameter is 3.92 Å, thus allowing more deviation from planarity. The Eu_{15}–his $(I)_2$-OH complex has a diameter of 4.3143(7), and an iodide would require a larger diameter in order to fit (diameter 4.40 Å) within the cavity with small deviations from planarity. This would force the inner Eu···Eu distances to be approximately 5.65 Å apart, which in turn would force Eu-μ_3-OH bond distances to elongate proportionately. This elongation would be longer than the sum of the radii of the ions (Eu(III) 1.20 Å and OH^- 1.34 Å) and prohibit the hydroxo ligand from bridging three Eu(III) ions. Instead, the μ_3-OH would most likely become a μ_2-OH. These changes would distort the $Eu_4(\mu_3\text{-OH})_4$ ‘cubane’ enough to destroy the cluster or cause a need for more bridging ligands. Therefore, a hydroxide anion sits in the cavity instead of an iodide for the Eu_{15}–his $(I)_2$-OH cluster. The “templating effect” of the OH^- is discussed in a subsequent chapter.

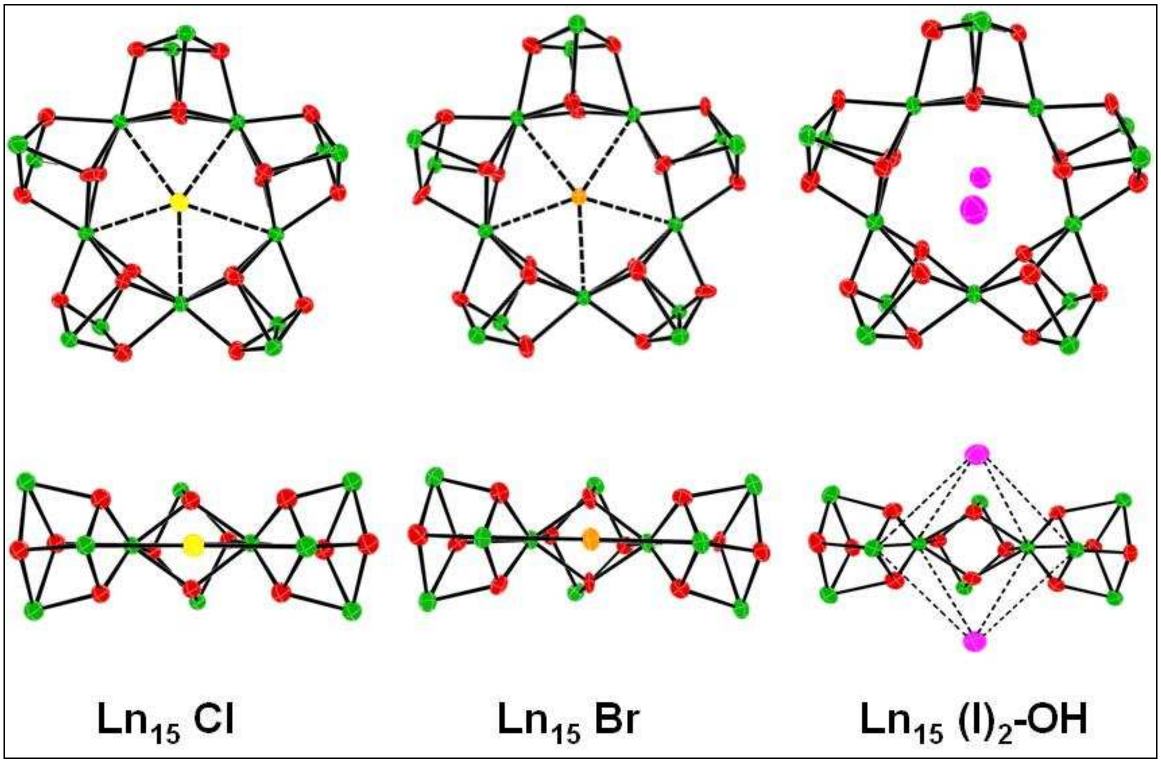

Figure 2.12: Ln_{15}-his X (X = Cl, Br, and $(I)_2$-OH) with Ln(III), μ_3-OH, and μ_5-X depicted. All other ligands are omitted for clarity. The μ_5-OH of Ln_{15}-his $(I)_2$-OH is omitted for clarity. The lower structures have two cubanes excised for clarity. Dotted lines do not indicate bonding, but are merely to help the viewer understand the positioning of the halide.

Conclusions

Base hydrolysis of aqueous $Ln(ClO_4)_3$ in the presence of L-histidine and sodium halides (chloride, bromide, or iodide) yields the pentadecalanthanide(III) complexes $[Ln_{15}(\mu_5\text{-}X)(\mu_3\text{-}OH)_{20}(his^{+/-})_{10}(his^-)_5(OH)_7]^{12+}$ (Ln = Y, Nd, Eu, and Tb; X = Cl^- Br^-; or $(I^-)_2$-OH; $his^{+/-}$ = zwitterionic histidine, his^- = histidinate). The synthetic approaches reported here improve upon former preparation methods for Ln_{15}-his X and provide specific guidelines for the formation and recrystallization of Ln_{15}-his X complexes.

$[Ln_{15}(\mu_5\text{-}X)(\mu_3\text{-}OH)_{20}(his^{+/-})_{10}(his^-)_5(OH)_7](ClO_4)_{12}$ can be synthesized with Ln = La, Nd, Eu, Y, and Tb with X = Cl, Br, or $(I)_2$-OH. Each Ln(III) yields isostructural cores with minor differences in bond length and atom separations that are contributed to the ionic radii differences. Larger Ln(III) ions such as La(III) and Nd(III) exhibit different coordination modes as compared to the smaller Ln(III) ions Eu(III), Tb(III), and Y(III). The different coordination modes of L-histidine also varying with size of Ln(III) ions. Larger Ln(III) ions have larger coordination spheres and allow for more diverse ligand coordination modes.

Altering the templating halide from Cl^-, to Br^-, and than to I^- while keeping the Ln(III) constant afforded isostructural complexes with minor variations in interatomic distances. The central cavity enlarges to accommodate the change in halide size, but only to a certain extent, as is evident with the Ln_{15}–his $(I)_2$-OH complex, where a hydroxo rests within the central plane of the molecule and iodide does not.

These types of polynuclear complexes have not yet been obtained in the absence of a templating anion. The synthesis of Ln_{15}–his $(I)_2$-OH supports the hypothesis that a negative charge at the center of the inner lanthanide pentagon is required for their formation. However, this effect does not seem to be the overriding factor for the formation of these clusters. Instead, the formation seems to be dependent on both template and amino acid ligand effects.

Recrystallization of Eu_{15}–his X complexes demonstrated the importance of including excess amino acid. ^{13}C NMR spectra for Y_{15}–his X complexes provided evidence supporting variable coordination and ligand lability of L-his ligands in solution. These spectra show two unique L-histidine molecules in solution. One set of resonances correlate with the ^{13}C NMR spectrum of free histidine in aqueous solution. Needed future experiments include ligand exchange reactions with labeled histidine molecules in order to test ligand exchange in solution.

The solution-state stability of Ln_{15}–his X complexes has been demonstrated through ESI-MS and ^{89}Y NMR spectroscopy. Although ESI-MS is a destructive technique, it provides m/z peaks consistent with fully intact core minus several anions and amino acids. ^{89}Y NMR spectra exhibit two unique Y(III) resonances differing from free Y(III) (YCl_3) and Y(III) in the presence of L-histidine. These data are consistent with solid-state structures that also exhibit two unique Y(III) centers.

Experimental

General Considerations

All syntheses were conducted in a fume hood or on an open bench top in 20-mL disposable scintillation vials equipped with stirbar. Heating and stirring were performed with a Pierce Reacti-Therm Stirring/Heating Module Series 550 equipped with an aluminum block machined to hold five 20-mL scintillation vials.

Stock 1.0 M solutions of $Eu(ClO_4)_3$, $Nd(ClO_4)_3$, $Tb(ClO_4)_3$, and $Y(ClO_4)_3$ were prepared via digestion at 90 to 100 ^oC of the appropriate oxide (Eu_2O_3, Nd_2O_3, and Y_2O_3, Metall Rare Earth Limited China) with new 60 or 70% perchloric acid (Fisher) followed by dilution with deionized water. Tb_2O_3 was obtained by reduction of Tb_4O_7 (Metall Rare Earth Limited) with hydrogen gas at 1000 ^oC, and was subsequently digested in perchloric acid in order to give a $Tb(ClO_4)_3$ stock solution.[61] Ln(III) triflates were prepared by digesting the appropriate oxide in triflic acid (CF_3SO_3H, SynQuest Labs) followed by dilution with deionized water to give a 1.0 M solution. Ln(III) tosylates were prepared by digesting the appropriate oxide in solutions of p-toluensulfonic acid ($CH_3C_6H_4SO_3H$, Sigma-Aldrich) followed by dilution with deionized water to make 1.0 M solutions. L-Histidine (Fisher) was used as received. Solid NaOH (Fisher) was used to make 0.3 M aqueous NaOH stock solutions. NaCl, NaBr, and NaI (Fisher) were used as received.

The presence of coordinated or free L-histidine was determined by the ninhydrin (1,2,3-indanetrione monohydrate, Matthew Coleman and Bell) test,[62] where several crystals of the material in question were dissolved in 1.0 mL of ninhydrin solution (0.4 g in 100 mL deionized H_2O) and heated. The solution turns royal blue in the presence of free L-histidine, while other colors (red, orange, yellow) and precipitation were indications of L-histidine coordinated to a lanthanide.

Single-crystal diffractometry was performed on a Nonius KappaCCD diffractometer with Mo K_α radiation equipped with a CCD area detector. Qualitative fluorescence was observed with a UVP Multi-Band UV-254/365 nm Mineralight Lamp for crystalline Eu(III) and Tb(III) complexes.

Electrospray ionization mass spectroscopy (ESI-MS) was performed on a Waters Q-TOF Premier mass spectrometer. Samples were introduced via direct infusion in Optima grade water (Fisher). Data was collected using a 20V sampling cone, 2.8 V capillary voltage, source temperature of 120 ^{o}C, and nitrogen desolvation gas temperature of 350 ^{o}C. Data processing was performed using the Mass Lynx software package.

Attempted Preparation of Polylanthanide Complexes from Triflate and Tosylate Salts

The hydrolysis of Ln(III) triflate or tosylate salts with NaOH to pH's ranging from 5 to 8 at elevated temperatures (90 ^{o}C) in aqueous media in the presence of α-amino acids (glycine, proline, valine, serine, or histidine) failed to give isolable products, instead giving gelatinous white precipitates. In reactions where a precipitate did not form, crystals of Ln(III) triflate or tosylate starting material were obtained, as confirmed by single-crystal X-ray diffraction.

Preparation of $[Eu_{15}(\mu_5\text{-}Cl)(\mu_3\text{-}OH)_{20}(his^{+/-})_{10}(his^{-})_5(OH)_7](ClO_4)_{12}$ via Base Hydrolysis of $Eu(ClO_4)_3$ in the Presence of L-Histidine

$Eu(ClO_4)_3$ (1.0 mL, 1.0 M) was diluted with 7 mL of deionized water. L-Histidine (3.104 g, 2.0 mmol) and NaCl (0.058g, 1.0 mmol) was added and dissolved in the solution. The pH of the starting mixture was typically between 1 and 2. The mixture was stirred and heated to 90-95 ^{o}C. NaOH solution (0.3 M) was added slowly until a pH of 6.2 or 6.4 was obtained (usually required 4 – 5 mL of base solution). Careful attention to pH is required in order to prevent the formation of unwanted oligomers or precipitation. Once the desired pH was obtained, the reaction mixture was removed from stirring and heating.

Upon addition of NaOH a fleeting precipitate was observed; however, the precipitate usually dissolved with continued heating and stirring. If permanent precipitation occurred, the mixture was centrifuged to separate the mother liquor from the precipitate. Permanent precipitation would normally occur at pH > 6.6. The mother liquor was then loosely capped and allowed to stand undisturbed at room temperature. Crystalline product suitable for X-ray analysis would form within several hours of reaction or overnight. Eu(III) crystal content was qualitatively checked by irradiating with long wave UV light, as crystals containing Eu(III) fluoresce pink/red.

Crystals were collected by gently scraping them off of the vial wall and bottom, followed by filtration through a medium porosity glass fritted funnel, and then washed with cold deionized water. Crystals were submitted for single-crystal X-ray diffraction covered with mother liquor. The remaining crystals were dried over calcium sulfate in a desiccator to yield 0.281 g (first crop yield of 67.0% based on $Eu(ClO_4)_3$) of $[Eu_{15}(\mu_5\text{-}Cl)(\mu_3\text{-}OH)_{20}(his^{+/-})_{10}(his^{-})_5(OH_2)_7](ClO_4)_{12}$ Typical dry yields were in the 60 – 70 % range based on $Eu(ClO_4)_3$. Attempts to obtain a second crop of crystals resulted in precipitation of amorphous solid.

Recrystallization of
$[Eu_{15}(\mu_5\text{-}Cl)(\mu_3\text{-}OH)_{20}(his^{+/-})_{10}(his^{-})_5(OH)_7](ClO_4)_{12}$

$[Eu_{15}(\mu_5\text{-}Cl)(\mu_3\text{-}OH)_{20}(his^{+/-})_{10}(his^{-})_5(OH)_7](ClO_4)_{12}$ (0.1 g, 1.59 x 10^{-2} mmol) was dissolved in 2.0 mL of hot L-histidine solution (0.1 M, pH = 6.4). Upon slow cooling to room temperature, clear colorless crystals suitable for X-ray analysis formed. If crystals did not form upon cooling, the solution was left uncapped at room temperature for slow evaporation of solvent. Crystals formed within several days. Eu(III) crystal content was qualitatively checked by irradiating with long-wave UV light.

Crystals were collected by gently scraping them off of the vial wall and bottom, followed by filtration through a medium porosity glass fritted funnel, and then washed with cold deionized water. Crystals were submitted for single-crystal X-ray diffraction covered with mother liquor. The remaining crystals were dried over calcium sulfate in a desiccator to yield $[Eu_{15}(\mu_5\text{-}Cl)(\mu_3\text{-}OH)_{20}(his^{+/-})_{10}(his^{-})_5(OH_2)_7](ClO_4)_{12}$ (first crop: 0.0678 g, 67.8% yield). Attempts to obtain a second crop of crystals resulted in precipitation of amorphous solid.

Preparation of $[Eu_{15}(\mu_5\text{-}Br)(\mu_3\text{-}OH)_{20}(his^{+/-})_{10}(his^{-})_5(OH)_7](ClO_4)_{12}$ via Base Hydrolysis of $Eu(ClO_4)_3$ in the Presence of L-Histidine

This synthetic preparation was similar to the pentadecanuclear Eu(III) chloride complex with the exception that NaBr (1.0 mmol) was used instead of NaCl. The solution was allowed to stand loosely capped and undisturbed at room temperature. No permanent precipitation was observed. Crystals of similar color and morphology to the Eu_{15}–his Cl complex formed overnight. Eu(III) crystal content was qualitatively checked by irradiating with a UV lamp. Yields comparable to the Eu_{15}–his Cl complex were observed, based on $Eu(ClO_4)_3$. The product was determined to be $[Eu_{15}(\mu_5\text{-}Br)(\mu_3\text{-}OH)_{20}(his^{+/-})_{10}(his^{-})_5(OH)_7](ClO_4)_{12}$ by X-ray diffraction data. Attempts to obtain a second crop of crystals resulted in precipitation of amorphous solid.

Recrystallization of

$[Eu_{15}(\mu_5\text{-}Br)(\mu_3\text{-}OH)_{20}(his^{+/-})_{10}(his^{-})_5(OH)_7](ClO_4)_{12}$

The recrystallization of $[Eu_{15}(\mu_5\text{-}Br)(\mu_3\text{-}OH)_{20}(his^{+/-})_{10}(his^{-})_5(OH)_7](ClO_4)_{12}$ followed the same procedure as Eu_{15}–his Cl. Eu(III) crystal content was qualitatively checked by irradiating with long-wave UV light. Yields comparable to the recrystallization of Eu_{15}–his Cl complex were observed. X-ray diffraction data was not collected.

Preparation of

$[Eu_{15}(\mu_5\text{-}OH)(I)_2(\mu_3\text{-}OH)_{20}(his^{+/-})_{10}(his^{-})_5(OH)_7](ClO_4)_{10}$

via Base Hydrolysis of $Eu(ClO_4)_3$ in the Presence of

L-Histidine

This synthesis was the same as for the Eu_{15}–his Cl and Eu_{15} Br mentioned above with the exception tha NaI (1.0 mmol) was used instead of NaCl or NaBr. No permanent precipitation was observed. Eu(III) crystal content was qualitatively checked by irradiating with long-wave UV light. Yields comparable to the Eu_{15}–his Cl complex were observed, based on $Eu(ClO_4)_3$. The product was determined to be $[Eu_{15}(\mu_5\text{-}OH)(I)_2(\mu_3\text{-}OH)_{20}(his^{+/-})_{10}(his^{-})_5(OH)_7](ClO_4)_{10}$ by X-ray diffraction data. Attempts to obtain a second crop of crystals resulted in precipitation of amorphous solid.

Recrystallization of

$[Eu_{15}(\mu_5\text{-}OH)(I)_2(\mu_3\text{-}OH)_{20}(his^{+/-})_{10}(his^{-})_5(OH)_7](ClO_4)_{12}$

The recrystallization of $[Eu_{15}(I)_2(OH)(\mu_3\text{-}OH)_{20}(his^{+/-})_{10}(his^{-})_5(OH)_7](ClO_4)_{12}$ followed the same procedure as Eu_{15}–his Cl. Eu(III) crystal content was qualitatively checked by irradiating with long-wave UV light. Yields comparable to the Eu_{15}–his Cl complex were observed. X-ray diffraction data was not collected.

Preparation of

$[Nd_{15}(\mu_5\text{-}Cl)(\mu_3\text{-}OH)_{20}(his^{+/-})_{10}(his^{-})_5(OH)_8](ClO_4)_{12}$ via

Base Hydrolysis of $Nd(ClO_4)_3$ in the Presence of

L-Histidine

This synthetic preparation was similar to the pentadecanuclear Eu(III) chloride complex except that $Nd(ClO_4)_3$ (1.0 mL, 1.0 M) was used instead of $Eu(ClO_4)_3$. The resulting solution was blue to light purple in color. The crystals retained the solution color. Nd(III) ions do not fluoresce as do Eu(III) (red/prink) or Tb(III) (green), therefore Nd(III) crystals content was qualitatively verified via a ninhydrin test. Yields comparable to the Eu_{15}–his Cl complex were observed, based on $Nd(ClO_4)_3$. The product was determined to be $[Eu_{15}(\mu_5\text{-}OH)(I)_2(\mu_3\text{-}OH)_{20}(his^{+/-})_{10}(his^{-})_5(OH)_7](ClO_4)_{10}$ by X-ray diffraction data. Attempts to obtain a second crop of crystals resulted in precipitation of amorphous solid.

Preparation of

$[Nd_{15}(\mu_5\text{-}Br)(\mu_3\text{-}OH)_{20}(his^{+/-})_{10}(his^{-})_5(OH)_8](ClO_4)_{12}$ via

Base Hydrolysis of $Nd(ClO_4)_3$ in the Presence of

L-Histidine

This synthesis followed the synthesis of Nd_{15}–his Cl with the exception that NaBr (1 mmol) was used instead of NaCl. Nd(III) crystal content was qualitatively verified via a ninhydrin test. Yields comparable to the Eu_{15}–his Cl complex were observed, based on $Nd(ClO_4)_3$. The product was determined to be $[Nd_{15}(\mu_5\text{-}Br)(\mu_3\text{-}OH)_{20}(his^{+/-})_{10}(his^{-})_5(OH)_8](ClO_4)_{12}$ by X-ray diffraction data. Attempts to obtain a second crop of crystals resulted in precipitation of amorphous solid.

Preparation of

$[Nd_{15}(\mu_5\text{-}OH)(I)_2(\mu_3\text{-}OH)_{20}(his^{+/-})_{10}(his^-)_5(OH)_8](ClO_4)_{12}$

via Base Hydrolysis of $Nd(ClO_4)_3$ in the Presence of

L-Histidine

This synthesis followed the synthesis of Nd_{15}–his Cl with the exception that NaI (1.0 mmol) was used instead of NaCl or NaBr. Nd(III) crystal content was qualitatively verified via a ninhydrin test. Yields comparable to the Eu_{15}–his Cl complex were observed, based on $Nd(ClO_4)_3$. Unit cell analysis was performed instead of structural analysis because of large mosaity in one of the three crystallographic axes. Attempts to obtain a second crop of crystals resulted in precipitation of amorphous solid.

Preparation of

$[Tb_{15}(\mu_5\text{-}Cl)(\mu_3\text{-}OH)_{20}(his^{+/-})_{10}(his^-)_5(OH)_7](ClO_4)_{12}$ via

Base Hydrolysis of $Tb(ClO_4)_3$ in the Presence of

L-Histidine

This synthetic preparation was similar to the pentadecanuclear europium(III) chloride complex except that $Tb(ClO_4)_3$ (1.0 mL, 1.0 M) was used instead of $Eu(ClO_4)_3$. The resulting solution was clear and colorless. Tb(III) crystals content was qualitatively verified via irradiating with a UV lamp (brilliant green fluorescence) and a ninhydrin test. Yields comparable to the Eu_{15}–his Cl complex were observed, based on $Tb(ClO_4)_3$. The product was determined to be $[Tb_{15}(\mu_5\text{-}Cl)(\mu_3\text{-}OH)_{20}(his^{+/-})_{10}(his^-)_5(OH)_7](ClO_4)_{12}$ by X-ray diffraction data. Attempts to obtain a second crop of crystals resulted in precipitation of amorphous solid.

Preparation of

$[Tb_{15}(\mu_5\text{-}Br)(\mu_3\text{-}OH)_{20}(his^{+/-})_{10}(his^-)_5(OH)_7](ClO_4)_{12}$ via

Base Hydrolysis of $Tb(ClO_4)_3$ in the Presence of

L-Histidine

This synthesis followed the synthesis of Tb_{15}–his Cl except NaBr (1mmol) was used instead of NaCl. Tb(III) crystal content was qualitatively verified via irradiating with a UV lamp (brilliant green fluorescence) and ninhydrin test. Yields comparable to the Eu_{15}–his Cl complex were observed, based on $Tb(ClO_4)_3$. The product was determined to be $[Tb_{15}(\mu_5\text{-}Br)(\mu_3\text{-}OH)_{20}(his^{+/-})_{10}(his^-)_5(OH)_7](ClO_4)_{12}$ by X-ray diffraction data. Attempts to obtain a second crop of crystals resulted in precipitation of amorphous solid.

Preparation of

$[Tb_{15}(\mu_5\text{-}OH)(I)_2(\mu_3\text{-}OH)_{20}(his^{+/-})_{10}(his^-)_5(OH)_7](ClO_4)_{12}$

via Base Hydrolysis of $Tb(ClO_4)_3$ in the Presence of

L-Histidine.

This synthesis followed the synthesis of Tb_{15}–his Cl except NaI (1mmol) was used instead of NaCl or NaBr. Tb(III) crystal content was qualitatively verified via irradiating with a UV lamp (brilliant green fluorescence) and ninhydrin test. Yields comparable to the Eu_{15}–his Cl complex were observed, based on $Tb(ClO_4)_3$. The product was determined to be $[Tb_{15}(\mu_5\text{-}OH)(I)_2(\mu_3\text{-}OH)_{20}(his^{+/-})_{10}(his^-)_5(OH)_7](ClO_4)_{12}$ by X-ray diffraction data. Attempts to obtain a second crop of crystals resulted in precipitation of amorphous solid.

Preparation of

$[La_{15}(\mu_5\text{-}Br)(\mu_3\text{-}OH)_{20}(his^{+/-})_{10}(his^{-})_5(OH)_{11}](ClO_4)_{12}$ via

Base Hydrolysis of $La(ClO_4)_3$ in the Presence of

L-Histidine

This synthetic preparation was similar to the pentadecanuclear europium(III) bromide complex except $La(ClO_4)_3$ (1.0 mL, 1.0 M) was used instead of $Eu(ClO_4)_3$. The resulting solution was clear and colorless. La(III) crystal content was qualitatively verified via ninhydrin test. Yields comparable to the Eu_{15}–his Cl complex were observed, based on $La(ClO_4)_3$. The product was determined to be $[La_{15}(\mu_5\text{-}Br)(\mu_3\text{-}OH)_{20}(his^{+/-})_{10}(his^{-})_5(OH)_{11}](ClO_4)_{12}$ by X-ray diffraction data. Attempts to obtain a second crop of crystals resulted in precipitation of amorphous solid.

X-Ray Diffractometry:

$[Eu_{15}(\mu_5\text{-}Cl)(\mu_3\text{-}OH)_{20}(his^{+/-})_{10}(his^{-})_5(OH)_7](ClO_4)_{12}$

A colorless prismatic crystal with dimensions of 0.36 x 0.26 x 0.18 mm^3 was mounted via grease on the tip of a glass fiber (epoxied to a brass pin) and placed on the diffractometer with the long crystal dimension approximately parallel to the diffractometer phi axis. Data were collected on a Nonius KappaCCD diffractometer (Mo K_α radiation, graphite monochromator) at 190 K (cold N_2 gas stream) using standard CCD data collection techniques. Lorentz and polarization corrections were applied to the 47857 data. A correction for absorption using the multi-scan technique was applied (T_{max} = 0.4849, T_{min} = 0.2824). Equivalent data were averaged yielding 44560 unique data (R-int = 0.0249, 41384 with $F > 4\sigma(F)$). Based on preliminary examination of the crystals, the space group P2(1) was assigned. The computer programs from the HKLint package were used for data reduction. Structure refinement was performed with the SHELXTL v6.1 software package.

The preliminary model of the structure was obtained using XS, a direct methods program. Least-squares refinement of the model vs. the data was performed with the XH program. Tables were made with the XCIF program. All non-hydrogen atoms were refined with anisotropic thermal parameters. All H atoms were included with the riding model using the XL program default values. Any restraints and constraints imposed on the data are described in the .cif files.

X-Ray Diffractometry: Recrystallized $[Eu_{15}(\mu_5\text{-}Cl)(\mu_3\text{-}OH)_{20}(his^{+/-})_{10}(his^{-})_5(OH)_7](ClO_4)_{12}$

A colorless prismatic crystal with dimensions of 0.24 x 0.18 x 0.16 mm^3 was mounted via grease on the tip of a glass fiber (epoxied to a brass pin) and placed on the diffractometer with the long crystal dimension approximately parallel to the diffractometer phi axis. Data were collected on a Nonius KappaCCD diffractometer (Mo K_α radiation, graphite monochromator) at 190 K (cold N_2 gas stream) using standard CCD data collection techniques. Lorentz and polarization corrections were applied to the 39611 data. A correction for absorption using the multi-scan technique was applied (T_{max} = 0.5418, T_{min} = 0.4205). Equivalent data were averaged yielding 20049 unique data (R-int = 0.0461, 16223 with $F > 4\sigma(F)$). Based on preliminary examination of the crystals, the space group C222(1) was assigned. The computer programs from the HKLint package were used for data reduction. Structure refinement was performed with the SHELXTL v6.1 software package.

The preliminary model of the structure was obtained using XS, a direct methods program. Least-squares refinement of the model vs. the data was performed with the XH program. Tables were made with the XCIF program. All non-hydrogen atoms were refined with anisotropic thermal parameters. All H atoms were included with the riding model using the XL program default values. Any restraints and constraints imposed on the data are described in the .cif files.

X-Ray Diffractometry:

[$Eu_{15}(\mu_5$-Br$)(\mu_3$-OH$)_{20}$(his$^{+/-})_{10}$(his$^{-})_5$(OH$)_7$](ClO$_4)_{12}$

A colorless prismatic crystal with dimensions of 0.36 x 0.32 x 0.16 mm^3 was mounted via grease on the tip of a glass fiber (epoxied to a brass pin) and placed on the diffractometer with the long crystal dimension approximately parallel to the diffractometer phi axis. Data were collected on a Nonius KappaCCD diffractometer (Mo K_α radiation, graphite monochromator) at 190 K (cold N_2 gas stream) using standard CCD data collection techniques. Lorentz and polarization corrections were applied to the 47572 data. A correction for absorption using the multi-scan technique was applied (T_{max} = 0.5055, T_{min} = 0.2694). Equivalent data were averaged yielding 47458 unique data (R-int = 0.0584, 37315 with $F > 4\sigma(F)$). Based on preliminary examination of the crystals, the space group P2(1) was assigned. The computer programs from the HKLint package were used for data reduction. Structure refinement was performed with the SHELXTL v6.1 software package.

The preliminary model of the structure was obtained using XS, a direct methods program. Least-squares refinement of the model vs. the data was performed with the XH program. Tables were made with the XCIF program. All non-hydrogen atoms were refined with anisotropic thermal parameters. All H atoms were included with the riding model using the XL program default values. Any restraints and constraints imposed on the data are described in the .cif files.

X-Ray Diffractometry: Recrystallized

[$Eu_{15}(\mu_5$-Br$)(\mu_3$-OH$)_{20}$(his$^{+/-})_{10}$(his$^{-})_5$(OH$)_7$](ClO$_4)_{12}$

A colorless prismatic crystal with dimensions of 0.22 x 0.14 x 0.12 mm^3 was mounted via grease on the tip of a glass fiber (epoxied to a brass pin) and placed on the diffractometer with the long crystal dimension approximately parallel to the diffractometer phi axis. Data were collected on a Nonius KappaCCD diffractometer (Mo

K_α radiation, graphite monochromator) at 190 K (cold N_2 gas stream) using standard CCD data collection techniques. Lorentz and polarization corrections were applied to the 46113 data. A correction for absorption using the multi-scan technique was applied (T_{max} = 0.5882, T_{min} = 0.4091). Equivalent data were averaged yielding 45448 unique data (R-int = 0.0342, 40577 with $F > 4\sigma(F)$). Based on preliminary examination of the crystals, the space group P2(1) was assigned. The computer programs from the HKLint package were used for data reduction. Structure refinement was performed with the SHELXTL v6.1 software package.

The preliminary model of the structure was obtained using XS, a direct methods program. Least-squares refinement of the model vs. the data was performed with the XH program. Tables were made with the XCIF program. All non-hydrogen atoms were refined with anisotropic thermal parameters. All H atoms were included with the riding model using the XL program default values. Any restraints and constraints imposed on the data are described in the .cif files.

X-Ray Diffractometry:

$[Eu_{15}(\mu_5\text{-}OH)(I)_2(\mu_3\text{-}OH)_{20}(his^{+/-})_{10}(his^-)_5(OH)_7](ClO_4)_{12}$

A colorless crystalline plate with dimensions of 0.32 x 0.20 x 0.10 mm^3 was mounted via grease on the tip of a glass fiber (epoxied to a brass pin) and placed on the diffractometer with the long crystal dimension approximately parallel to the diffractometer phi axis. Data were collected on a Nonius KappaCCD diffractometer (Mo K_α radiation, graphite monochromator) at 190 K (cold N_2 gas stream) using standard CCD data collection techniques. Lorentz and polarization corrections were applied to the 47333 data. A correction for absorption using the multi-scan technique was applied (T_{max} = 0.4908, T_{min} = 0.1765). Equivalent data were averaged yielding 47070 unique data (R-int = 0.0286, 43164 with $F > 4\sigma(F)$). Based on preliminary examination of the crystals, the space group P2(1) was assigned. The computer programs from the HKLint package were used for data reduction. Structure refinement was performed with the SHELXTL v6.1 software package.

The preliminary model of the structure was obtained using XS, a direct methods program. Least-squares refinement of the model vs. the data was performed with the XH program. Tables were made with the XCIF program. All non-hydrogen atoms were refined with anisotropic thermal parameters. All H atoms were included with the riding model using the XL program default values. Any restraints and constraints imposed on the data are described in the .cif files.

X-Ray Diffractometry: Recrystallized $[Eu_{15}(\mu_5\text{-}OH)(I)_2(\mu_3\text{-}OH)_{20}(his^{+/-})_{10}(his^{-})_5(OH)_7](ClO_4)_{12}$

A colorless prismatic crystal with dimensions of 0.34 x 0.18 x 0.16 mm^3 was mounted via grease on the tip of a glass fiber (epoxied to a brass pin) and placed on the diffractometer with the long crystal dimension approximately parallel to the diffractometer phi axis. Data were collected on a Nonius KappaCCD diffractometer (Mo K_α radiation, graphite monochromator) at 190 K (cold N_2 gas stream) using standard CCD data collection techniques. Lorentz and polarization corrections were applied to the 46273 data. A correction for absorption using the multi-scan technique was applied (T_{max} = 0.4980, T_{min} = 0.2779). Equivalent data were averaged yielding 46213 unique data (R-int = 0.0218, 43699 with $F > 4\sigma(F)$). Based on preliminary examination of the crystals, the space group P2(1) was assigned. The computer programs from the HKLint package were used for data reduction. Structure refinement was performed with the SHELXTL v6.1 software package.

The preliminary model of the structure was obtained using XS, a direct methods program. Least-squares refinement of the model vs. the data was performed with the XH program. Tables were made with the XCIF program. All non-hydrogen atoms were refined with anisotropic thermal parameters. All H atoms were included with the riding model using the XL program default values. Any restraints and constraints imposed on the data are described in the .cif files.

X-Ray Diffractometry:

$[Nd_{15}(\mu_5\text{-}Cl)(\mu_3\text{-}OH)_{20}(his^{+/-})_{10}(his^{-})_5(OH)_8](ClO_4)_{12}$

A blue prismatic crystal with dimensions of 0.26 x 0.26 x 0.245 mm^3 was mounted via grease on the tip of a glass fiber (epoxied to a brass pin) and placed on the diffractometer with the long crystal dimension approximately parallel to the diffractometer phi axis. Data were collected on a Nonius KappaCCD diffractometer (Mo K_α radiation, graphite monochromator) at 190 K (cold N_2 gas stream) using standard CCD data collection techniques. Lorentz and polarization corrections were applied to the 61370 data. A correction for absorption using the multi-scan technique was applied (T_{max} = 0.4436, T_{min} = 0.4257). Equivalent data were averaged yielding 34801 unique data (R-int = 0.0284, 31087 with $F > 4\sigma(F)$). Based on preliminary examination of the crystals, the space group P2(1)2(1)2(1) was assigned. The computer programs from the HKLint package were used for data reduction. Structure refinement was performed with the SHELXTL v6.1 software package.

The preliminary model of the structure was obtained using XS, a direct methods program. Least-squares refinement of the model vs. the data was performed with the XH program. Tables were made with the XCIF program. All non-hydrogen atoms were refined with anisotropic thermal parameters. All H atoms were included with the riding model using the XL program default values. Any restraints and constraints imposed on the data are described in the .cif files.

X-Ray Diffractometry:

$[Nd_{15}(\mu_5\text{-}Br)(\mu_3\text{-}OH)_{20}(his^{+/-})_{10}(his^{-})_5(OH)_8](ClO_4)_{12}$

A blue prismatic crystal with dimensions of 0..195 x 0.195 x 0.09 mm^3 was mounted via grease on the tip of a glass fiber (epoxied to a brass pin) and placed on the diffractometer with the long crystal dimension approximately parallel to the diffractometer phi axis. Data were collected on a Nonius KappaCCD diffractometer (Mo K_α radiation, graphite monochromator) at 150 K (cold N_2 gas stream) using standard CCD data collection techniques. Lorentz and polarization corrections were applied to the 69895 data. A correction for absorption using the multi-scan technique was applied (T_{max} = 0.7241, T_{min} = 0.5218). Equivalent data were averaged yielding 69400 unique data (R-int = 0.0635, 52366 with $F > 4\sigma(F)$). Based on preliminary examination of the crystals, the space group P2(1) was assigned. The computer programs from the HKLint package were used for data reduction. Structure refinement was performed with the SHELXTL v6.1 software package.

The preliminary model of the structure was obtained using XS, a direct methods program. Least-squares refinement of the model vs. the data was performed with the XH program. Tables were made with the XCIF program. All non-hydrogen atoms were refined with anisotropic thermal parameters. All H atoms were included with the riding model using the XL program default values. Any restraints and constraints imposed on the data are described in the .cif files.

X-Ray Diffractometry:

$[Nd_{15}(\mu_5\text{-}OH)(I)_2(\mu_3\text{-}OH)_{20}(his^{+/-})_{10}(his^{-})_5(OH)_8](ClO_4)_{12}$

A colorless prismatic crystal with dimensions of 0.17 x 0.16 x 0.14 mm3 was mounted via grease on the tip of a glass fiber (epoxied to a brass pin) and placed on the diffractometer with the long crystal dimension approximately parallel to the diffractometer phi axis. Data were collected on a Nonius KappaCCD diffractometer (Mo K_α radiation, graphite monochromator) at 190 K (cold N_2 gas stream) using standard CCD data collection techniques. Based on preliminary examination of the crystals, the space group P-1 was assigned. Because of mosaicity in one axis, full structural information could not be integrated to produce data suitable for structure refinement.

X-Ray Diffractometry:

$[Tb_{15}(\mu_5\text{-}Cl)(\mu_3\text{-}OH)_{20}(his^{+/-})_{10}(his^{-})_5(OH)_7](ClO_4)_{12}$

A colorless plate with dimensions of 0.135 x 0.12 x 0.03 mm^3 was mounted via grease on the tip of a glass fiber (epoxied to a brass pin) and placed on the diffractometer with the long crystal dimension approximately parallel to the diffractometer phi axis. Data were collected on a Nonius KappaCCD diffractometer (Mo K_α radiation, graphite monochromator) at 190 K (cold N_2 gas stream) using standard CCD data collection techniques. Lorentz and polarization corrections were applied to the 27265 data. A correction for absorption using the multi-scan technique was applied (T_{max} = 0.8551, T_{min} = 0.5301). Equivalent data were averaged yielding 27514 unique data (R-int = 0.1448, 12694 with $F > 4\sigma(F)$). Based on preliminary examination of the crystals, the space group P1 was assigned. The computer programs from the HKLint package were used for data reduction. Structure refinement was performed with the SHELXTL v6.1 software package.

The preliminary model of the structure was obtained using XS, a direct methods program. Least-squares refinement of the model vs. the data was performed with the XH program. Tables were made with the XCIF program. All non-hydrogen atoms were refined with anisotropic thermal parameters. All H atoms were included with the riding model using the XL program default values. Any restraints and constraints imposed on the data are described in the .cif files.

X-Ray Diffractometry:

$[Tb_{15}(\mu_5\text{-}Br)(\mu_3\text{-}OH)_{20}(his^{+/-})_{10}(his^{-})_5(OH)_7](ClO_4)_{12}$

A colorless prismatic crystal with dimensions of 0.19 x 0.15 x 0.115 mm^3 was mounted via grease on the tip of a glass fiber (epoxied to a brass pin) and placed on the diffractometer with the long crystal dimension approximately parallel to the diffractometer phi axis. Data were collected on a Nonius KappaCCD diffractometer (Mo

K_α radiation, graphite monochromator) at 190 K (cold N_2 gas stream) using standard CCD data collection techniques. Lorentz and polarization corrections were applied to the 18438 data. A correction for absorption using the multi-scan technique was applied (T_{max} = 0.5831, T_{min} = 0.4349). Equivalent data were averaged yielding 28166 unique data (R-int = 0.0000, 15701 with F > 4σ(F)). Based on preliminary examination of the crystals, the space group P1 was assigned. The computer programs from the HKLint package were used for data reduction. Structure refinement was performed with the SHELXTL v6.1 software package.

The preliminary model of the structure was obtained using XS, a direct methods program. Least-squares refinement of the model vs. the data was performed with the XH program. Tables were made with the XCIF program. All non-hydrogen atoms were refined with anisotropic thermal parameters. All H atoms were included with the riding model using the XL program default values. Any restraints and constraints imposed on the data are described in the .cif files.

X-Ray Diffractometry:

$[Tb_{15}(\mu_5\text{-}OH)(I)_2(\mu_3\text{-}OH)_{20}(his^{+/-})_{10}(his^{-})_5(OH)_7](ClO_4)_8$

A colorless prismatic plate with dimensions of 0.135 x 0.12 x 0.03 mm^3 was mounted via grease on the tip of a glass fiber (epoxied to a brass pin) and placed on the diffractometer with the long crystal dimension approximately parallel to the diffractometer phi axis. Data were collected on a Nonius KappaCCD diffractometer (Mo K_α radiation, graphite monochromator) at 190 K (cold N_2 gas stream) using standard CCD data collection techniques. Lorentz and polarization corrections were applied to the 27265 data. A correction for absorption using the multi-scan technique was applied (T_{max} = 0.8551, T_{min} = 0.5301). Equivalent data were averaged yielding 27514 unique data (R-int = 0.1448, 12694 with F > 4σ(F)). Based on preliminary examination of the crystals, the space group P1 was assigned. The computer programs from the HKLint package were used for data reduction. Structure refinement was performed with the SHELXTL v6.1 software package.

The preliminary model of the structure was obtained using XS, a direct methods program. Least-squares refinement of the model vs. the data was performed with the XH program. Tables were made with the XCIF program. All non-hydrogen atoms were refined with anisotropic thermal parameters. All H atoms were included with the riding model using the XL program default values. Any restraints and constraints imposed on the data are described in the .cif files.

X-Ray Diffractometry:

$[La_{15}(\mu_5\text{-}Br)(\mu_3\text{-}OH)_{20}(his^{+/-})_{10}(his^{-})_5(OH)_{11}](ClO_4)_{12}$

A colorless crystalline rod with dimensions of 0.30 x 0.07 x 0.07 mm^3 was mounted via grease on the tip of a glass fiber (epoxied to a brass pin) and placed on the diffractometer with the long crystal dimension approximately parallel to the diffractometer phi axis. Data were collected on a Nonius KappaCCD diffractometer (Mo K_α radiation, graphite monochromator) at 220 K (cold N_2 gas stream) using standard CCD data collection techniques. Lorentz and polarization corrections were applied to the 52490 data. A correction for absorption using the multi-scan technique was applied (T_{max} = 0.7919, T_{min} = 0.4202). Equivalent data were averaged yielding 31423 unique data (R-int = 0.1020, 16346 with $F > 4\sigma(F)$). Based on preliminary examination of the crystals, the space group P2(1)2(1)2(1) was assigned. The computer programs from the HKLint package were used for data reduction. Structure refinement was performed with the SHELXTL v6.1 software package.

The preliminary model of the structure was obtained using XS, a direct methods program. Least-squares refinement of the model vs. the data was performed with the XH program. Tables were made with the XCIF program. All non-hydrogen atoms were refined with anisotropic thermal parameters. All H atoms were included with the riding model using the XL program default values. Any restraints and constraints imposed on the data are described in the .cif files.

CHAPTER 3:
A 'TEMPLATING' μ_5-HYDROXIDE IN AMINO-ACID LIGATED PENTADECALANTHANIDE CHEMISTRY: SYNTHESIS, STRUCTURAL CHARACTERIZATION, AND HALIDE–FOR–HYDROXIDE LIGAND EXCHANGE REACTIONS

Introduction

Base hydrolysis of lanthanide(III) ions has long been known to lead at higher pH to poorly-characterized amorphous precipitates that are presumed to contain oxo and/or hydroxo ligands and to be polynuclear. Better-defined lanthanide hydrolysis and discrete polylanthanide chemistry have developed since the discovery by Zak and co-workers of octahedral hexalanthanide complexes with a central μ_6-oxo ligand from hydrothermal treatment of lanthanide(III) salts.[37] Ligands, in particular amino acids, that can intercept intermediate products during hydrolysis have been shown by Zheng,[43-45] Gao,[38, 63] Wang,[64] and coworkers to yield discrete complexes with nuclearities from four to fifteen, and even larger structures (some containing transition metals) have been reported recently.[58, 65] A common structural feature in many of these complexes is the μ_3-OH ligand formed during hydrolysis of the lanthanide(III) ions. A parallel nonaqueous chalcogenide polylanthanide chemistry and material science has been developed by Brennan,[66] Ibers,[59g] and others.

A particularly interesting subset of these polylanthanide(III) complexes are the D_{5h}-symmetry pentadecalanthanide (Ln_{15}) complexes $[Ln_{15}(\mu_3\text{-OH})_{20}(\mu_5\text{-Cl})(\mu_3\text{-tyr})_{10}(OH_2)(\mu\text{-}OH_2)_5(OH_2)_{18}](ClO_4)_{12}$ with L-tyrosine ligands and a central μ_5-halide, first reported by Zheng and co-workers.[43-44] These authors postulated that the μ_5-halide plays a templating role in the self-assembly of these large pentagonal structures. No supporting mechanistic information was provided by these authors. While mechanisms for formation of discrete amino-acid-ligated polylanthanide have been proposed in the literature,[45] the role of the halide in either templating or trapping a polylanthanide intermediate is unclear.

During our study of the base hydrolysis of lanthanide perchlorates in the presence of L-histidine, an amino acid with unreported polylanthanide hydrolysis chemistry, we discovered the first μ_5-halide-free Ln_{15} amino acid complex that does not require a halide template in order to self-assemble, the μ_5-hydroxo Ln_{15} complex $[Ln_{15}(\mu_5\text{-}OH)(\mu_3\text{-}OH)_{20}(his^{+/-})_{10}(his^{-})_5(OH)_7](ClO_4)_{12}$. We also show that reaction of the Ln_{15}-his OH complex with chloride, bromide, or iodide in histidine-buffered aqueous solution leads to formation of the Ln_{15}-his X (X = Cl, Br, or $(I)_2$-OH) histidine complex described in Chapter 2. This observation has implications for the mechanism of formation of halide-containing Ln_{15} amino acid (at least in the case of L-histidine) complexes.

Results and Discussion

Synthesis and Characterization of $[Ln_{15}(\mu_5\text{-}X)(\mu_3\text{-}OH)_{20}(his^{+/-})_{10}(his^{-})_5(OH)_7](ClO_4)_{12}$

Dropwise addition of aqueous NaOH to an aqueous solution of $Ln(ClO_4)_3$ (Ln = Eu or Tb; $Ln(ClO_4)_3$ prepared by digestion of Ln_2O_3 with non-chloride-contaminated $HClO_4$) and L-histidine in a 1:2 relative ratio at 90 °C leads to slight precipitation as the pH approaches 6.8. Centrifugation in order to remove a small amount of precipitate followed by concentration of the clear supernatant leads to crystals of $[Ln_{15}(\mu_5\text{-}OH)(\mu_3\text{-}OH)_{20}(his^{+/-})_{10}(his^{-})_5(OH)_7](ClO_4)_{12}$ (Figure 3.1) in 58% isolated yield. Europium(III) and terbium(III) complexes fluoresce, red and green respectively, when irradiated with long-wave ultraviolet (UV) light. The compounds are soluble in water, DMSO, and only marginally soluble in acetone, acetonitrile, and alcohols.

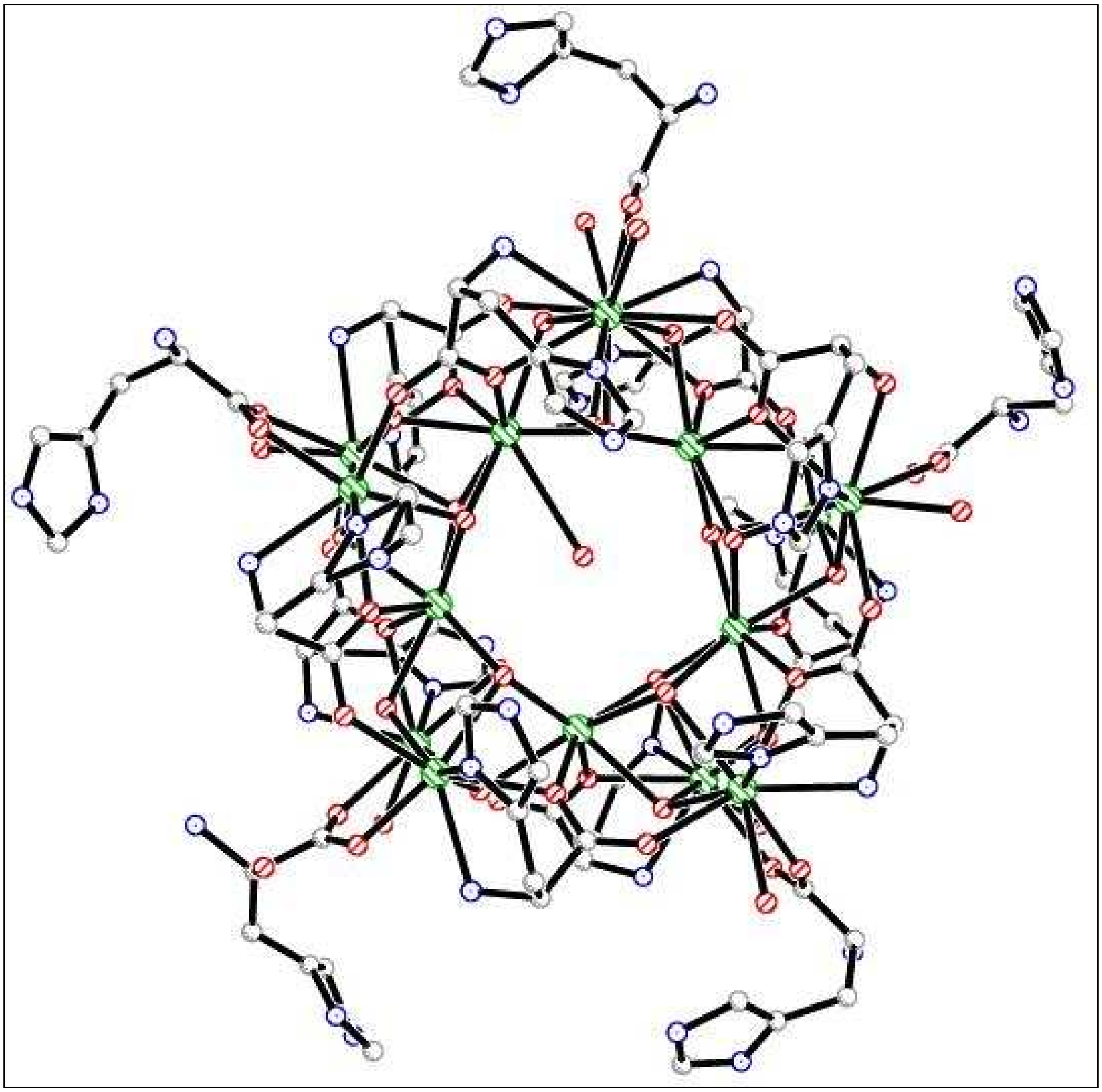

Figure 3.1: Perspective view of $[Eu_{15}(\mu_5\text{-}OH)(\mu_3\text{-}OH)_{20}(his)_{15}(OH_2)_7](ClO_4)_{12}$. Perchlorate anions omitted for clarity. Color scheme: green, Eu(III); gray, carbon; blue, nitrogen; red, oxygen.

The reaction conditions for the synthesis of $Ln_{15}(\mu_5\text{-OH})(\mu_3\text{-OH})_{20}(his^{+/-})_{10}(his^{-})_5(OH)_7](ClO_4)_{12}$ were very similar to that of $Ln_{15}(\mu_5\text{-X})(\mu_3\text{-OH})_{20}(his^{+/-})_{10}(his^{-})_5(OH)_7](ClO_4)_{12}$ (X = Cl, Br, or $(I)_2$-OH) with the exception that no NaX was added to the reaction. These reaction conditions are discussed in Chapter 2. The pH of the solution is critical in forming these complexes, with the pH range of 6.4 – 6.6 most effective in producing Ln_{15}–his OH crystalline complexes in high yields.

Recrystallizations of $[Eu_{15}(\mu_5\text{-OH})(\mu_3\text{-OH})_{20}(his^{+/-})_{10}(his^{-})_5(OH)_7](ClO_4)_{12}$ were performed under conditions identical to those discussed in Chapter 2 for Eu_{15}-his X (X = Cl, Br, and $(I)_2$-OH), with the exception that L-his buffered solutions were at pH = 5.8. As in the initial synthesis of these complexes, pH was critical. Crystals would not form in solutions below pH = 5.5, and insoluble precipitates were obtained in solutions above pH = 6.8.

Electrospray ionization mass spectrometry (ESI-MS) was employed to probe the solution stability of the Ln_{15}–his OH clusters. For example, ESI-MS of Eu_{15}–his OH displayed a peak envelope centered at 1313.57 amu, corresponding to $[Eu_{15}$–his OH – $4ClO_4^-$ – 4 L-$his^{+/-}]^{4+}$. Specific m/z values matching a +3 charged species were also observed by ESI-MS (Figure 3.2). These results indicate that the structural integrity of the polynuclear core was maintained in solution during the course of ESI-MS studies.

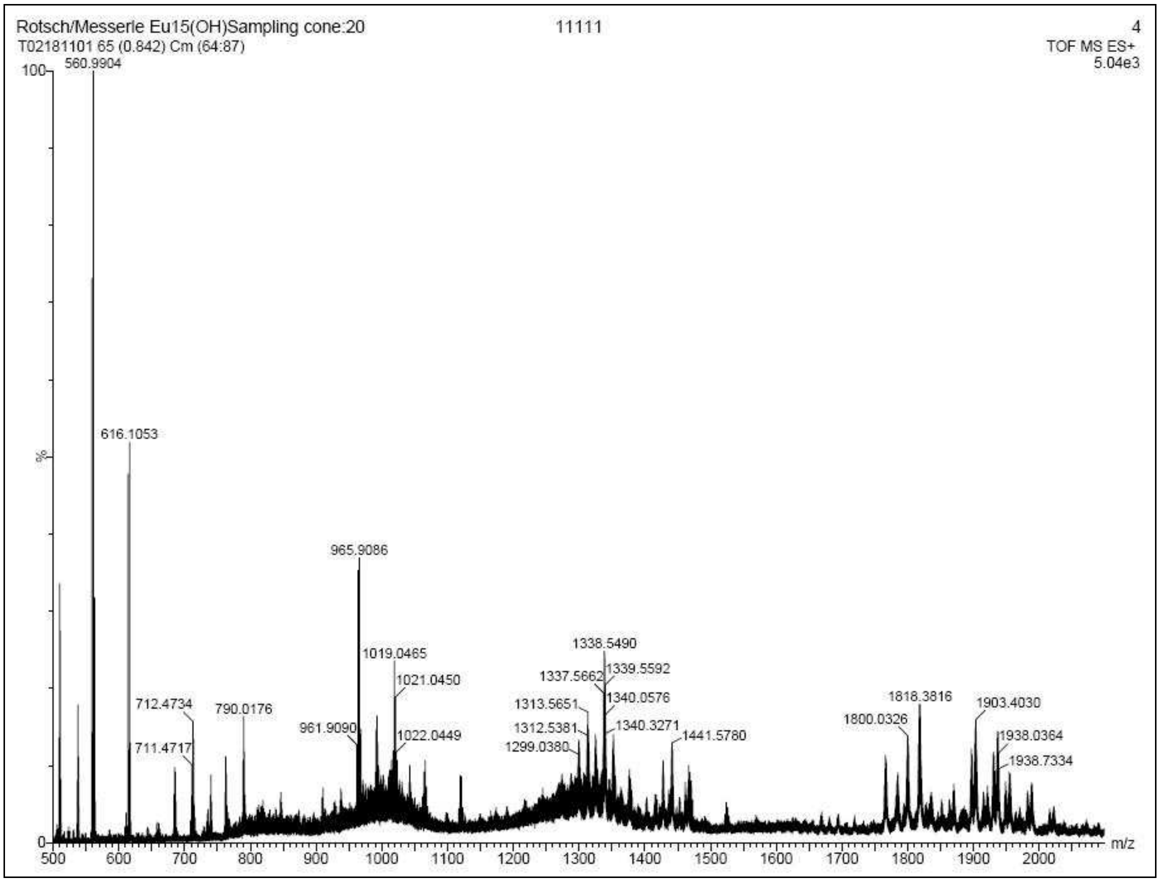

Figure 3.2: ESI-MS spectrum of Eu_{15}-his OH in H_2O (% intensity vs. m/z). Peak envelopes centered at 1313.57 amu corresponds to to [Eu_{15}–his OH – $4ClO_4^-$ – 4 L-$his^{+/-}$]$^{4+}$. Peak envelopes centered at 1019 amu corresponds to to [Eu_{15}–his OH – $4ClO_4^-$ – OH^- – 5 L-$his^{+/-}$]$^{4+}$. Other peak envelopes representing other charged species are also observed.

Comparative Solid-State Molecular Structures of

Ln_{15}-his μ_5-Cl and Ln_{15}-his μ_5-OH

The D_{5h}-symmetry core $[Ln_{15}(\mu_5\text{-X})(\mu_3\text{-OH})_{20}]^{24+}$ of $[Ln_{15}(\mu_5\text{-OH})(\mu_3\text{-OH})_{20}(his^{+/-})_{10}(his^-)_5(OH)_7](ClO_4)_{12}$ and $[Ln_{15}(\mu_5\text{-Cl})(\mu_3\text{-OH})_{20}(his^{+/-})_{10}(his^-)_5(OH)_7](ClO_4)_{12}$ (denoted as Ln_{15}-his OH and Ln_{15}-his X, respectively, Ln = Eu or Tb) can be described as five vertex-sharing lanthanide tetrahedra forming a pentagon (Figure 3.4). For simplicity, the Eu(III) complex will be discussed. It is easier to understand the structure by first observing the individual tetrahedra of Eu(III) and then the cubanes, Eu_4

(μ_3-OH)$_4$, that make up the pentadecanuclear europium cluster (Figure 3.3). Each Eu(III) tetrahedral face is capped by a triply-bridging hydroxo ligand, forming quasi-cubanes (Figure 3.3 B). These cubanes then come together by sharing Ln(III) vertices to form the structure shown in Figure 3.5.

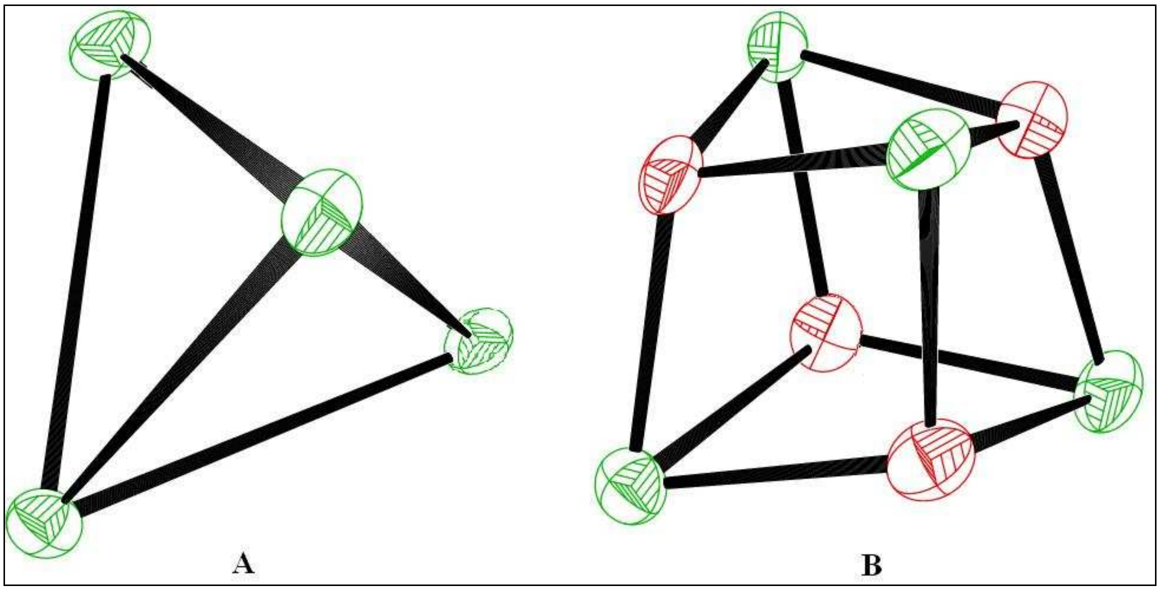

Figure 3.3: Depiction of tetrahedron of Eu(III) ions, (A), and quasi-cubane of $Eu_4(\mu_3\text{-}OH)_4$ with hydrogens omitted for clarity, (B). Color scheme: green, Eu(III); red, oxygen.

The cavities in which the μ_5-OH and μ_5-Cl are located are formed by five inner Eu(III) ions that make up a nearly perfect pentagon. Perchlorate anions are above and below the Eu_5 plane, almost trapping the central anion. The average Eu-μ_5-OH distance of 3.34(3) Å is significantly larger than the sum of the individual ionic radii of OH^- (1.34 Å) and Eu(III) (1.120 Å). Similarly, the average Eu-μ_5-Cl distance is 3.265(2) Å and is significantly larger than the sum of the individual ionic radii of Cl^- (1.81 Å) and Eu(III) (1.120 Å). The large average Eu-μ_5-anion (chloride or hydroxide) distances reflect

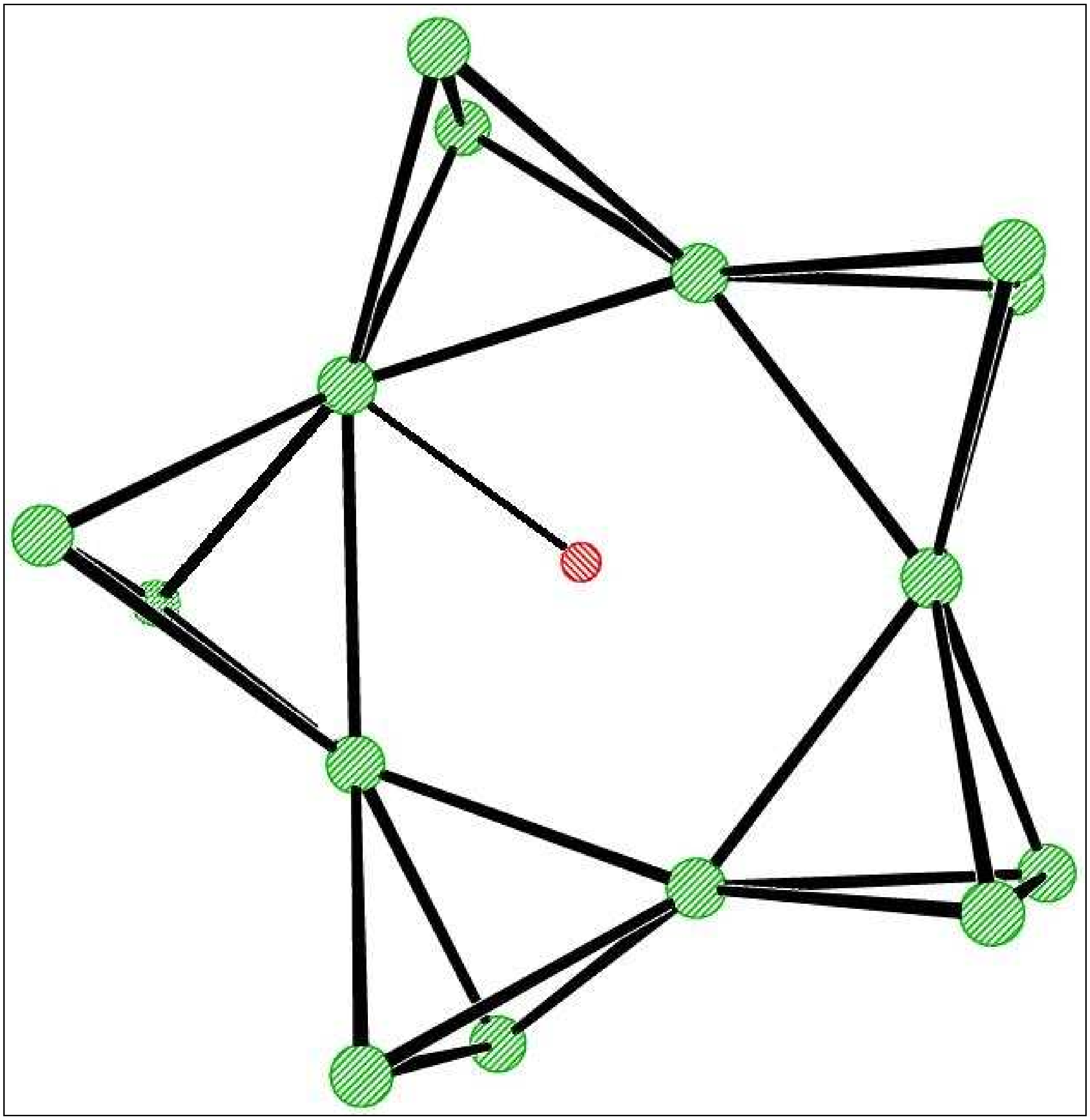

Figure 3.4: Skeletal view of Eu_{15}-his OH with Eu(III) and μ_5-OH depicted. All other ligands and anions omitted for clarity. Color scheme: green, Eu(III); red, oxygen. This structure was also observed for Ln = Tb.

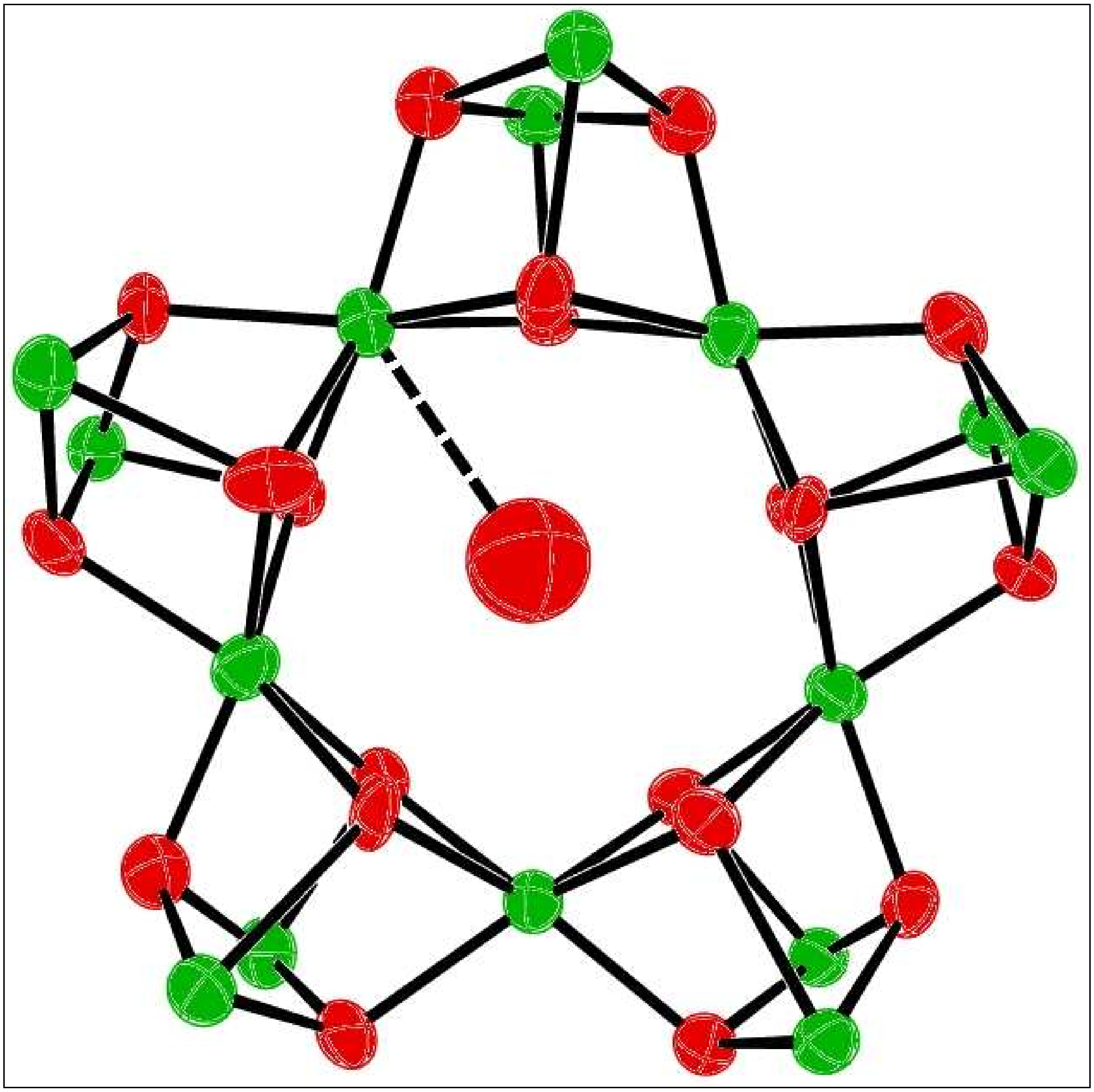

Figure 3.5: Skeletal view of Eu_{15}-his OH with bridging hydroxides (μ_3-OH) and μ_5-OH. All other ligands and anions omitted for clarity. Color scheme: green, Eu(III); red, oxygen. This structure was also observed for Ln = Tb.

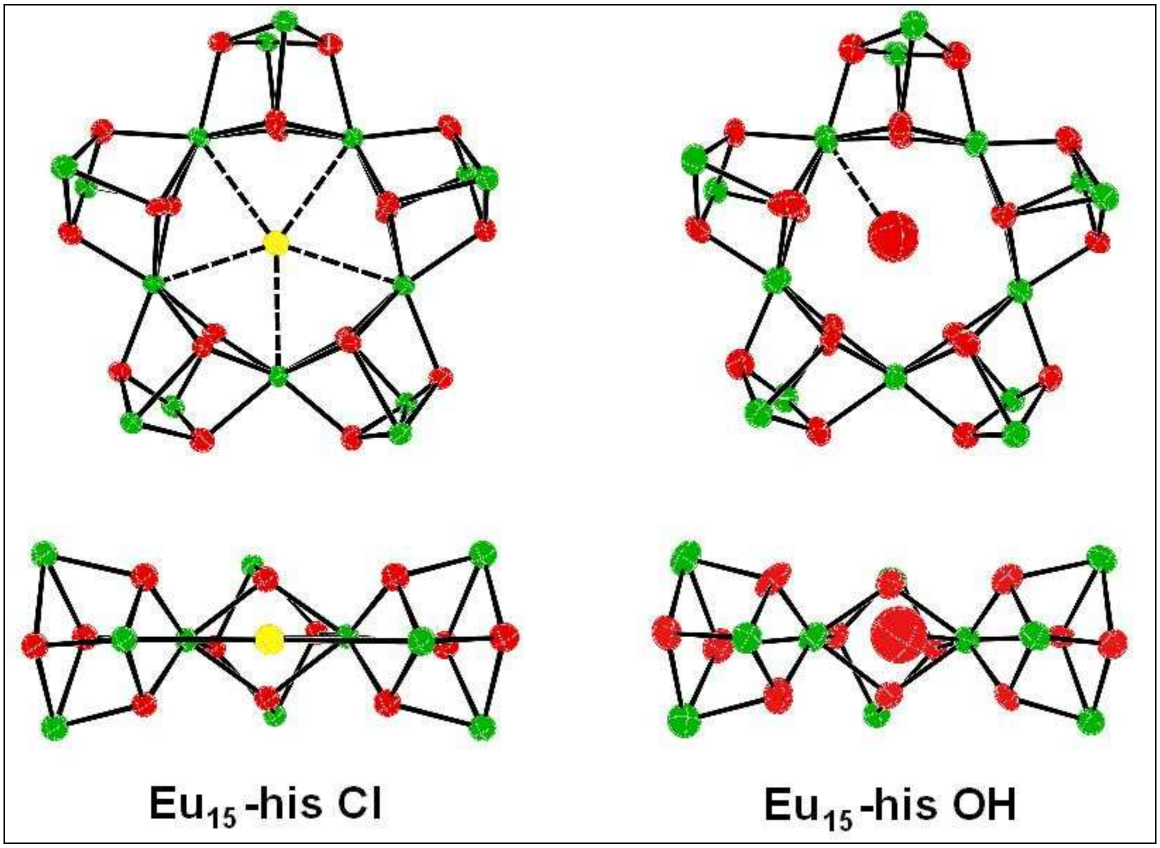

Figure 3.6: Eu_{15}-his Cl and Eu_{15}-his OH with Eu(III), μ_3-OH, and μ_5-X or μ_5-OH depicted. All other ligands are omitted for clarity. The lower structures have two cubanes excised for clarity. Dotted lines do not indicate bonding, but are merely to help the viewer understand the positioning of the halide.

primarily ionic interactions between the halide and the lanthanide. Figure 3.6 shows a skeletal comparison of Eu_{15}-his Cl to Eu_{15}-his OH.

Mean atomic distances, bond lengths, and angles for Eu_{15}-his Br and Eu_{15}-his $(I)_2$-OH are listed in Chapter 2, Table 2.3. For simplicity, only the Eu_{15}-his OH and Eu_{15}-his Cl will be compared. A comparison of mean atomic distances, bond lengths, and angles between the Eu_{15}-his OH and Eu_{15}-his Cl complexes is listed in Table 3.1. The cores of the Eu_{15}-his OH and Eu_{15}-his Cl complexes are very similar in terms of metrics. Eu-μ_3-OH bond distances are within experimental error for both structures. Each core is distorted in similar fashion, with the inner μ_3-OH ligands displaced from the Eu_3 plane more than the exterior μ_3-OH ligands. A plausible explanation as to why the inner μ_3-OH ligands deviate more from planarity than exterior μ_3-OH ligands is hydrogen bonding with centralized ClO_4^- anions. However, the inner μ_3-OH ligands are further out of plane, an average of 0.036 Å more for the Eu_{15}-his OH complex than the chloride complex. The opposite is observed for the exterior μ_3-OH ligands, where these ligands are closer to planarity, an average of 0.014 Å more for Eu_{15}-his OH than for Eu_{15}-his Cl. Considering that the average Eu···Eu distances in the plane of the inner faces of the tetrahedra is longer (0.08 Å longer for inner-inner, 0.109 Å longer for inner-exterior Eu···Eu distances) for Eu_{15}-his OH, it is unclear why these deviations are observed. The outer-outer Eu···Eu distances are comparable for the two complexes.

The longer Eu···Eu distances observed for the Eu_{15}-his OH complex give rise to greater distortion of the tetrahedra from idealized tetrahedra (an idealized tetrahedra has dihedral angles of 70.5^o). Eu_{15}-his OH tetrahedra increase their dihedral angels by 4.13^o on average while Eu_{15}-his Cl tetrahedral increase by 2.49^o on average.

Larger displacement for inner μ_3-OH ligand from the Eu_3 plane and greater deviation of the tetrahedra from idealized tetrahedra could be the results of interactions with the central anion. The μ_5-Cl is more evenly shared between the five inner Eu(III) ions and is thus more centralized in the pentagonal cavity than the μ_5-OH. In the solid-state, the μ_5-OH is located closer to three of the inner Eu(III) ions than the other two. However, the μ_5-OH has a very large thermal parameter (Figure 3.5), showing that the position of the μ_5-OH is not well defined. It is possible that the μ_5-OH is constantly oscillating (or switching) between all inner Eu(III) ions. Also, the μ_5-OH deviates from the pentagonal Eu_5 plane more than the μ_5-Cl does in the chloride structure. There is no data to characterize the possibility of hydrogen bonding between μ_3-OH ligands and the μ_5-OH or between the μ_5-OH and ClO_4^- anions in these complexes. However, hydrogen bonding interactions may affect the inner μ_3-OH interactions with Eu(III) ions. Conversely, it is also possible that because of the μ_5-OH mobility, it could come within close enough proximity to repel the interior μ_3-OH ligands and push them further from the interior of the pentagon.

Averaged atomic distances, bond lengths, and angles for Eu_{15}-his OH and Tb_{15}-his OH are listed in Table 3.1. The Tb_{15}-his OH complex structure is very similar to the Eu_{15}-his OH complex structure. Changing the lanthanide ion from Eu(III) to Tb(III) causes nominal bond length, non-bonded distance, and non-bonded angle changes that most likely result from differences in the ionic radii of the two lanthanides.

The L-histidine ligand coordination is identical to that discussed in Chapter 2. In brief, ten L-histidine ligands coordinate by all three functional groups to the face of the pentagon in a μ_3:η^1:η^2:η^1:η^1 coordination mode (see Scheme 2.1a), four coordinate to the edge of the pentagon by the carboxyl group in a μ_2-coordination mode (Scheme 2.1b), and the last histidine coordinates to the exterior of the pentagon in a bidentate fashion through one carboxyl oxygen and the amine (Scheme 2.1c). The pentagon-face-bound histidine ligands form a cage over the central cavity of the complex. In the solid-state, a perchlorate anion is in the middle of the cage. The perchlorate is most likely held in place by hydrogen bonding to μ_3-OH ligands and the histidine imidazoles. Charge-balance considerations require that all face histidine ligands are in the zwitterionic state and all exterior histidine ligands have a single negative charge.

Table 3.1: Selected mean atomic separations (Å), bond lengths (Å) and dihedral angles for Eu_{15}–his OH and Eu_{15}-his Cl complexes.

	Eu_{15}-his OH	**Eu_{15}-his Cl**
Eu-μ_3-OH (inner-inner)	2.41(1)	2.404(7)
Eu-μ_3-OH (inner-exterior)	2.40(1)	2.412(7)
Eu-μ_3-OH (exterior-exterior)	2.42(1)	2.417(7)
Eu-μ_3-OH (exterior-inner)	2.48(1)	2.426(7)
μ_3-OH (inner) Displacement from Eu Tetrahedron	0.9926	0.9565
μ_3-OH (exterior) Displacement from Eu Tetrahedron	0.9088	0.9231
Eu¨Eu (inner-inner)	3.918(1)	3.8390(7)
Eu¨Eu (exterior-exterior)	3.975(1)	3.9797(7)
Eu¨Eu (inner-exterior)	3.809(1)	3.7005(7)
Tetrahedron Dihedral Angle (inner)	75.25	73.98
Tetrahedron Dihedral Angle (exterior)	74.01	72.00
Cavity Area	26.407(7)	22.933(7)
Cavity Diameter	4.1924(7)	3.5790(7)
μ_5-X Displacement from Eu_5 Plane	0.0503	0.0085
Eu-Eu-Eu (angle)	108.00	107.95
Eu-μ_5-anion	3.34(3)	3.265(2)

Note: The cavity areas do not take into consideration the ionic radii of the Ln(III).

Table 3.2: Selected mean atomic separations (Å), bond lengths (Å) and dihedral angles for Eu_{15}–his OH and Tb_{15}-his OH complexes.

	Eu_{15}-his OH	**Tb_{15}-his OH**
Ln-μ_3-OH (inner-inner)	2.41(1)	2.39(5)
Ln-μ_3-OH (inner-exterior)	2.40(1)	2.40(5)
Ln-μ_3-OH (exterior-exterior)	2.42(1)	2.39(5)
Ln-μ_3-OH (exterior-inner)	2.48(1)	2.43(5)
μ_3-OH (inner) Displacement from Ln Tetrahedron	0.9926	1.010
μ_3-OH (exterior) Displacement from Ln Tetrahedron	0.9088	0.916
Ln···Ln (inner-inner)	3.918(1)	3.806(5)
Ln···Ln (exterior-exterior)	3.975(1)	3.922(5)
Ln···Ln (inner-exterior)	3.809(1)	3.669(5)
Tetrahedron Dihedral Angle (inner)	75.25	73.68
Tetrahedron Dihedral Angle (exterior)	74.01	71.84
Cavity Area	26.407(7)	24.757(5)
Cavity Diameter	4.1924(7)	4.109(5)
μ_5-X Displacement from Ln_5 Plane	0.0503	0.268
Ln-Ln-Ln (angle)	108.00	108.00
Ln-OH	3.34(3)	3.25(6)

Note: The cavity areas do not take into consideration the ionic radii of the Ln(III).

Conversion of

$[Ln_{15}(\mu_5\text{-}OH)(\mu_3\text{-}OH)_{20}(his^{+/-})_{10}(his^{-})_5(OH)_7](ClO_4)_{12}$ to

$[Ln_{15}(\mu_5\text{-}X)(\mu_3\text{-}OH)_{20}(his^{+/-})_{10}(his^{-})_5(OH)_7](ClO_4)_{12}$

X = Cl, Br, or $(I)_2$-OH

$[Ln_{15}(\mu_5\text{-}OH)(\mu_3\text{-}OH)_{20}(his^{+/-})_{10}(his^{-})_5(OH)_7](ClO_4)_{12}$ provides a novel starting point to probe the mechanism of formation of the Ln_{15} μ_5-halide histidine complexes discussed in Chapter 2. Addition of NaX (X = Cl, Br, or I) to a histidine-buffered (pH = 5.8) solution of $[Eu_{15}(\mu_5\text{-}OH)(\mu_3\text{-}OH)_{20}(his^{+/-})_{10}(his^{-})_5(OH)_7](ClO_4)_{12}$ followed by concentration of the solution yields crystals of $[Eu_{15}(\mu_5\text{-}Cl)(\mu_3\text{-}OH)_{20}(his^{+/-})_{10}(his^{-})_5(OH)_7](ClO_4)_{12}$ in 58% isolated yield, $[Eu_{15}(\mu_5\text{-}Br)(\mu_3\text{-}OH)_{20}(his^{+/-})_{10}(his^{-})_5(OH)_7](ClO_4)_{12}$ in 53% isolated yield, and $[Eu_{15}(\mu_5\text{-}OH)(I)_2(\mu_3\text{-}OH)_{20}(his^{+/-})_{10}(his^{-})_5(OH)_7](ClO_4)_{10}$ in 55% isolated yield, respectively. The identities of the μ_5-halide complexes were confirmed by single-crystal X-ray diffractometry and similarity of the unit cell parameters for a set of crystals from the isolated material.

The fact that the Eu_{15}-his μ_5-OH complex can be converted into the isostructural Eu_{15}-his μ_5-X complexes suggests that hydroxide anions can serve as a template not only for self-assembly of the tetralanthanide cubanes that make up the structure, through lanthanide vertex sharing, but also their condensation and assembly into the larger pentadecalanthanide structure. The μ_5-OH can then be displaced (either in an associative or dissociative manner) by an incoming halide. However, iodide is too large to fit within the cavity and displace the μ_5-OH. Instead, two iodides take up positions above and below the μ_5-OH. The observed conversion of Eu_{15}-his μ_5-OH to Eu_{15}-his μ_5-X discussed above does not rule out the possibility that these D_{5h}-symmetry pentadecalanthanide complexes are in equilibrium with smaller fragments that reassemble around a different template anion to form a new Ln_{15} complex. Instead, these results show that associative/dissociative anion exchange is a viable pathway that should be considered in the synthesis and reactivity of discrete polylanthanide complexes.

Conclusions

Base hydrolysis of aqueous $Ln(ClO_4)_3$ in the presence of L-histidine and absence of sodium halide yields the pentadecalanthanide(III) complexes $[Ln_{15}(\mu_5\text{-}OH)(\mu_3\text{-}OH)_{20}(his^{+/-})_{10}(his^{-})_5(OH)_7]^{12+}$ (Ln = Eu and Tb; $his^{+/-}$ = zwitterionic histidine, his^{-} = histidinate). ESI-MS of the Eu_{15}-his OH complex exhibited m/z signals consistent with fully-intact cluster cores minus several anions and amino acid ligands.

Conversions of Eu_{15}-his OH to isostructural halide versions $[Eu_{15}(\mu_5\text{-}Cl)(\mu_3\text{-}OH)_{20}(his^{+/-})_{10}(his^{-})_5(OH)_7]^{12+}$, $[Eu_{15}(\mu_5\text{-}Br)(\mu_3\text{-}OH)_{20}(his^{+/-})_{10}(his^{-})_5(OH)_7]^{12+}$, and $[Eu_{15}(\mu_5\text{-}OH)(I)_2(\mu_3\text{-}OH)_{20}(his^{+/-})_{10}(his^{-})_5(OH)_7]^{12+}$, were demonstrated. These conversions provide the first insight into the formation of Ln_{15}-his X complexes.

Experimental

General Considerations

All syntheses were performed in a fume hood or on an open bench top in 20-mL disposable scintillation vials equipped with a stirbar. Heating and stirring were performed on a Pierce Reacti-Therm Stirring/Heating Module Series 550 equipped with an aluminum block machined to hold five 20-mL scintillation vials.

Stock 1.0 M solutions of $Eu(ClO_4)_3$ and $Tb(ClO_4)_3$ were prepared via digestion of the appropriate oxide (Eu_2O_3, Tb_2O_3, Metall Rare Earth Limited China) with new 60 or 70% perchloric acid (Fisher) followed by dilution with distilled water. Tb_2O_3 was obtained by reduction of Tb_4O_7 (Metall Rare Earth Limited) with hydrogen gas at 1000 ^{o}C; subsequent digestion of Tb_2O_3 in perchloric acid gave $Tb(ClO_4)_3$ stock solution.[61] L-Histidine (Fisher) was used as received. Solid NaOH (Fisher) was used to make 0.3 M aqueous NaOH stock solutions. NaCl, NaBr, and NaI (Fisher) were used as received.

The presence of coordinated or free L-histidine was determined by the ninhydrin (1,2,3-indanetrione monohydrate, Matthew Coleman and Bell) test,[62] where several crystals of the material in question were dissolved in 1.0 mL of ninhydrin solution (0.4 g in 100 mL deionized H_2O) and heated. The solution turned royal blue in the presence of free L-histidine, while other colors (red, orange, yellow) and precipitation were indications of lanthanide-coordinated L-histidine.

Single-crystal diffractometry was performed on a Nonius KappaCCD diffractometer equipped with a CCD area detector. Qualitative fluorescence data was observed with a UVP Multi-Band UV-254/365 nm Mineralight Lamp for Eu(III) and Tb(III) complexes.

Electrospray ionization mass spectroscopy (ESI-MS) was performed on a Waters Q-TOF Premier mass spectrometer. Samples were introduced via direct infusion in Optima grade water (Fisher). Data was collected using a 20V sampling cone, 2.8 V capillary voltage, source temperature of 120 ^{o}C, and nitrogen desolvation gas temperature of 350 ^{o}C. Data processing was performed using the Mass Lynx software package.

Preparation of $[Eu_{15}(\mu_5\text{-}OH)(\mu_3\text{-}OH)_{20}(his^{+/-})_{10}(his^{-})_5(OH)_7](ClO_4)_{12}$ via Base Hydrolysis of $Eu(ClO_4)_3$ in the Presence of L-Histidine

L-Histidine (0.3104 g, 2.0 mmol) was dissolved in 7 mL of deionized water and $Eu(ClO_4)_3$ (1.0 mL, 1.0 M). The pH of the starting mixture was typically between 1 and 2. The mixture was stirred and heated to 90-95 ^{o}C. Aqueous NaOH (0.3 M) was then added slowly until a pH of 6.4 or 6.6 was obtained (usually between 4.5 and 5.5 mL of base). Careful attention to pH is required in order to prevent the formation of unwanted oligomers or precipitation. Once the desired pH was obtained, the reaction mixture was removed from stirring and heating.

The mother liquor was then loosely capped and allowed to stand undisturbed at room temperature. Crystals of various sizes suitable for X-ray analysis formed within several hours of reaction or overnight. Eu(III) crystal content was qualitatively checked by irradiating with a UV lamp and via a ninhydrin test as previously described.

Crystals were collected by gently scraping them off of the vial wall and bottom, followed by filtration through a medium-porosity glass-fritted funnel, and then washed with cold deionized water. Crystals were submitted for single-crystal X-ray diffraction covered with mother liquor. The remaining crystals were dried over calcium sulfate in a desiccator to yield 0.238 g (first crop yield of 56.9 % based on $Eu(ClO_4)_3$) of $[Eu_{15}(\mu_5\text{-}OH)(\mu_3\text{-}OH)_{20}(his^{+/-})_{10}(his^{-})_5(OH_2)_7](ClO_4)_{12}$ Typical dry yields were in the 50 – 60 % range based on $Eu(ClO_4)_3$. Attempts to obtain a second crop of crystals resulted in precipitation of amorphous solid.

Preparation of
$[Tb_{15}(\mu_5\text{-}OH)(\mu_3\text{-}OH)_{20}(his^{+/-})_{10}(his^{-})_5(OH)_7](ClO_4)_{12}$ via
Base Hydrolysis of $Tb(ClO_4)_3$ in the
Presence of L-Histidine

This synthetic preparation was similar to the pentadecanuclear europium(III) hydroxide complex except $Tb(ClO_4)_3$ (1.0 mL, 1.0 M) was used instead of $Eu(ClO_4)_3$. The resulting solution was clear and colorless. Tb(III) crystal content was qualitatively verified via irradiating with a UV lamp (brilliant green fluorescence) and a ninhydrin test. Yields comparable to the Eu_{15} OH complex were observed, based on $Tb(ClO_4)_3$. The product was determined to be $[Tb_{15}(\mu_5\text{-}OH)(\mu_3\text{-}OH)_{20}(his^{+/-})_{10}(his^{-})_5(OH)_7](ClO_4)_{12}$ by X-ray diffractometry.

Preparation of
$[Eu_{15}(\mu_5\text{-}Cl)(\mu_3\text{-}OH)_{20}(his^{+/-})_{10}(his^{-})_5(OH_2)_7](ClO_4)_{12}$ by
Recrystallization of
$[Eu_{15}(\mu_5\text{-}OH)(\mu_3\text{-}OH)_{20}(his^{+/-})_{10}(his^{-})_5(OH_2)_7](ClO_4)_{12}$ in
the Presence of L-Histidine and NaCl

$[Eu_{15}(\mu_5\text{-}OH)(\mu_3\text{-}OH)_{20}(his^{+/-})_{10}(his^{-})_5(OH)_7](ClO_4)_{12}$ (0.1 g, 1.59 x 10^{-2} mmol) and NaCl (0.001 g, 1.59 x 10^{-2} mmol) were dissolved in 2.0 mL of hot (~90 ^{o}C) L-histidine solution (0.1 M, pH = 5.8). Upon cooling, clear colorless crystals suitable for X-ray analysis formed. If crystals did not form upon cooling, the solution was left uncapped at room temperature for slow evaporation of solvent. Crystals would form within several days. Eu(III) crystal content was qualitatively checked by irradiating with a UV lamp. The product (first crop: 0.058 g, 58 % yield based on Eu_{15}-his OH) was determined to be $[Eu_{15}(\mu_5\text{-}Cl)(\mu_3\text{-}OH)_{20}(his^{+/-})_{10}(his^{-})_5(OH_2)_7](ClO_4)_{12}$ by X-ray diffractometry. No attempts were made to isolate a second crop.

Preparation of
$[Eu_{15}(\mu_5\text{-}Br)(\mu_3\text{-}OH)_{20}(his^{+/-})_{10}(his^{-})_5(OH_2)_7](ClO_4)_{12}$ by
Recrystallization of
$[Eu_{15}(\mu_5\text{-}OH)(\mu_3\text{-}OH)_{20}(his^{+/-})_{10}(his^{-})_5(OH_2)_7](ClO_4)_{12}$ in
the Presence of L-Histidine NaBr

The formation of $[Eu_{15}(\mu_5\text{-}Br)(\mu_3\text{-}OH)_{20}(his^{+/-})_{10}(his^{-})_5(OH)_7](ClO_4)_{12}$ from $[Eu_{15}(\mu_5\text{-}OH)(\mu_3\text{-}OH)_{20}(his^{+/-})_{10}(his^{-})_5(OH_2)_7](ClO_4)_{12}$ and NaBr (0.002 g, 1.59 x 10^{-2} mmol) followed the same procedure as the formation of $Eu_{15}Cl$ from $Eu_{15}OH$. Eu(III) crystal content was qualitatively checked by irradiating with a UV lamp. The product (first crop: 0.053 g, 53 % yield based on Eu_{15}-his OH) was determined to be $[Eu_{15}(\mu_5\text{-}Br)(\mu_3\text{-}OH)_{20}(his^{+/-})_{10}(his^{-})_5(OH_2)_7](ClO_4)_{12}$ by X-ray diffractometry. No attempts were made to isolate a second crop.

Preparation of

$[Eu_{15}(\mu_5\text{-}OH)(I)_2(\mu_3\text{-}OH)_{20}(his^{+/-})_{10}(his^{-})_5(OH_2)_7](ClO_4)_{10}$

by Recrystallization of

$[Eu_{15}(\mu_5\text{-}OH)(\mu_3\text{-}OH)_{20}(his^{+/-})_{10}(his^{-})_5(OH_2)_7](ClO_4)_{12}$ in

the Presence of L-Histidine and NaI

The formation of $[Eu_{15}(\mu_5\text{-}OH)(I)_2(\mu_3\text{-}OH)_{20}(his^{+/-})_{10}(his^{-})_5(OH)_7](ClO_4)_{12}$ from $[Eu_{15}(\mu_5\text{-}OH)(\mu_3\text{-}OH)_{20}(his^{+/-})_{10}(his^{-})_5(OH_2)_7](ClO_4)_{12}$ and NaI (0.004 g, 3.18x 10^{-2} mmol) followed the same procedure as the formation of Eu_{15} Cl from Eu_{15} OH. Eu(III) crystal content was qualitatively checked by irradiating with a UV lamp. The product (first crop: 0.055 g, 55 % yield based on Eu_{15}-his OH) was determined to be $[Eu_{15}(\mu_5\text{-}I)_2(OH)(\mu_3\text{-}OH)_{20}(his^{+/-})_{10}(his^{-})_5(OH_2)_7](ClO_4)_{10}$ by X-ray diffractometry. No attempts were made to isolate a second crop.

X-Ray Diffractometry:

$[Eu_{15}(\mu_5\text{-}OH)(\mu_3\text{-}OH)_{20}(his^{+/-})_{10}(his^{-})_5(OH)_7](ClO_4)_{12}$

A colorless prismatic crystal with dimensions of 0.36 x 0.26 x 0.18 mm^3 was mounted via grease on the tip of a glass fiber (epoxied to a brass pin) and placed on the diffractometer with the long crystal dimension approximately parallel to the diffractometer phi axis. Data were collected on a Nonius KappaCCD diffractometer (Mo K_α radiation, graphite monochromator) at 190 K (cold N_2 gas stream) using standard CCD data collection techniques. Lorentz and polarization corrections were applied to the 47857 data. A correction for absorption using the multi-scan technique was applied (T_{max} = 0.4849, T_{min} = 0.2824). Equivalent data were averaged yielding 44560 unique data (R-int = 0.0249, 41384 with $F > 4\sigma(F)$). Based on preliminary examination of the crystals, the space group P2(1) was assigned. The computer programs from the HKLint package were used for data reduction. Structure refinement was performed with the SHELXTL v6.1 software package.

The preliminary model of the structure was obtained using XS, a direct methods program. Least-squares refinement of the model vs. the data was performed with the XH program. Tables were made with the XCIF program. All non-hydrogen atoms were refined with anisotropic thermal parameters. All H atoms were included with the riding model using the XL program default values. Any restraints and constraints imposed on the data are described in the .cif files.

X-Ray Diffractometry:

$[Tb_{15}(\mu_5\text{-}OH)(\mu_3\text{-}OH)_{20}(his^{+/-})_{10}(his^{-})_5(OH)_7](ClO_4)_{12}$

A colorless prismatic plate with dimensions of 0.135 x 0.12 x 0.03 mm^3 was mounted via grease on the tip of a glass fiber (epoxied to a brass pin) and placed on the diffractometer with the long crystal dimension approximately parallel to the diffractometer phi axis. Data were collected on a Nonius KappaCCD diffractometer (Mo K_α radiation, graphite monochromator) at 190 K (cold N_2 gas stream) using standard CCD data collection techniques. Lorentz and polarization corrections were applied to the 27265 data. A correction for absorption using the multi-scan technique was applied (T_{max} = 0.8551, T_{min} = 0.5301). Equivalent data were averaged yielding 27514 unique data (R-int = 0.1448, 12694 with $F > 4\sigma(F)$). Based on preliminary examination of the crystals, the space group P1 was assigned. The computer programs from the HKLint package were used for data reduction. Structure refinement was performed with the SHELXTL v6.1 software package.

The preliminary model of the structure was obtained using XS, a direct methods program. Least-squares refinement of the model vs. the data was performed with the XH program. Tables were made with the XCIF program. All non-hydrogen atoms were refined with anisotropic thermal parameters. All H atoms were included with the riding model using the XL program default values. Any restraints and constraints imposed on the data are described in the .cif files.

X-Ray Diffractometry:

$[Eu_{15}(\mu_5\text{-}Cl)(\mu_3\text{-}OH)_{20}(his^{+/-})_{10}(his^{-})_5(OH_2)_7](ClO_4)_{12}$ from

$[Eu_{15}(\mu_5\text{-}OH)(\mu_3\text{-}OH)_{20}(his^{+/-})_{10}(his^{-})_5(OH)_7](ClO_4)_{12}$

A colorless prismatic crystal with dimensions of 0.24 x 0.18 x 0.16 mm^3 was mounted via grease on the tip of a glass fiber (epoxied to a brass pin) and placed on the diffractometer with the long crystal dimension approximately parallel to the diffractometer phi axis. Data were collected on a Nonius KappaCCD diffractometer (Mo K_α radiation, graphite monochromator) at 190 K (cold N_2 gas stream) using standard CCD data collection techniques. Lorentz and polarization corrections were applied to the 39611 data. A correction for absorption using the multi-scan technique was applied (T_{max} = 0.5418, T_{min} = 0.4205). Equivalent data were averaged yielding 20049 unique data (R-int = 0.0461, 16223 with $F > 4\sigma(F)$). Based on preliminary examination of the crystals, the space group C222(1) was assigned. The computer programs from the HKLint package were used for data reduction. Structure refinement was performed with the SHELXTL v6.1 software package.

The preliminary model of the structure was obtained using XS, a direct methods program. Least-squares refinement of the model vs. the data was performed with the XH program. Tables were made with the XCIF program. All non-hydrogen atoms were refined with anisotropic thermal parameters. All H atoms were included with the riding model using the XL program default values. Any restraints and constraints imposed on the data are described in the .cif files.

X-Ray Diffractometry:

$[Eu_{15}(\mu_5\text{-}Br)(\mu_3\text{-}OH)_{20}(his^{+/-})_{10}(his^{-})_5(OH_2)_7](ClO_4)_{12}$

from

$[Eu_{15}(\mu_5\text{-}OH)(\mu_3\text{-}OH)_{20}(his^{+/-})_{10}(his^{-})_5(OH)_7](ClO_4)_{12}$

A colorless prismatic crystal with dimensions of 0.22 x 0.14 x 0.12 mm^3 was mounted via grease on the tip of a glass fiber (epoxied to a brass pin) and placed on the diffractometer with the long crystal dimension approximately parallel to the diffractometer phi axis. Data were collected on a Nonius KappaCCD diffractometer (Mo K_α radiation, graphite monochromator) at 190 K (cold N_2 gas stream) using standard CCD data collection techniques. Lorentz and polarization corrections were applied to the 46113 data. A correction for absorption using the multi-scan technique was applied (T_{max} = 0.5882, T_{min} = 0.4091). Equivalent data were averaged yielding 45448 unique data (R-int = 0.0342, 40577 with $F > 4\sigma(F)$). Based on preliminary examination of the crystals, the space group P2(1) was assigned. The computer programs from the HKLint package were used for data reduction. Structure refinement was performed with the SHELXTL v6.1 software package.

The preliminary model of the structure was obtained using XS, a direct methods program. Least-squares refinement of the model vs. the data was performed with the XH program. Tables were made with the XCIF program. All non-hydrogen atoms were refined with anisotropic thermal parameters. All H atoms were included with the riding model using the XL program default values. Any restraints and constraints imposed on the data are described in the .cif files.

X-Ray Diffractometry:

[Eu_{15}(μ_5-OH)(I)$_2$(μ_3-OH)$_{20}$($his^{+/-}$)$_{10}$(his^-)$_5$(OH)$_7$](ClO_4)$_{10}$

from

[Eu_{15}(μ_5-OH)(μ_3-OH)$_{20}$($his^{+/-}$)$_{10}$(his^-)$_5$(OH)$_7$](ClO_4)$_{12}$

A colorless crystalline plate with dimensions of 0.32 x 0.20 x 0.10 mm^3 was mounted via grease on the tip of a glass fiber (epoxied to a brass pin) and placed on the diffractometer with the long crystal dimension approximately parallel to the diffractometer phi axis. Data were collected on a Nonius KappaCCD diffractometer (Mo K_α radiation, graphite monochromator) at 190 K (cold N_2 gas stream) using standard CCD data collection techniques. Lorentz and polarization corrections were applied to the 47333 data. A correction for absorption using the multi-scan technique was applied (T_{max} = 0.4908, T_{min} = 0.1765). Equivalent data were averaged yielding 47070 unique data (R-int = 0.0286, 43164 with $F > 4\sigma(F)$). Based on preliminary examination of the crystals, the space group P2(1) was assigned. The computer programs from the HKLint package were used for data reduction. Structure refinement was performed with the SHELXTL v6.1 software package.

The preliminary model of the structure was obtained using XS, a direct methods program. Least-squares refinement of the model vs. the data was performed with the XH program. Tables were made with the XCIF program. All non-hydrogen atoms were refined with anisotropic thermal parameters. All H atoms were included with the riding model using the XL program default values. Any restraints and constraints imposed on the data are described in the .cif files.

CHAPTER 4:

FLUORESCENCE STUDIES OF POLYEUROPIUM COMPLEXES

Introduction

Lanthanide luminescence has been exploited as probe ions in order to gain structural and analytical information, such as the determination of local symmetries in crystalline materials,[46a] inorganic glasses,[46a] and solutions.[46a, 67] Substitution of Ln(III) ions for Ca(II) or Zn(II) aids in the investigation of metal binding sites in biological molecules.[67-68] Ln(III) ion luminescence also facilitates the study of the effects of chemical and thermal treatments on catalysts.[69]

Particularly useful information such as formation constants,[70] stability constants,[71] and coordination environments[46a, 72] can be obtained from luminescence spectroscopy. The coordination environment may be probed by observing nephelauxetic effects on emissive transitions.[73] In the case of Eu(III) ion, the $^7F_0$ ground state and the $^5D_0$ state are unsplit.[46b, 73b] If there is more than one component seen for this transition, then multiple Eu(III) sites exist. These transitions have been observed to range between 17225 cm^{-1} to 17280 cm^{-1} (~580 nm to 578 nm) for Eu(III) complexes.[73] During attempts to understand this effect for the $^5D_0 \rightarrow {}^7F_0$ energy separation, Horrocks, et al., observed that the frequency of the $^5D_0 \rightarrow {}^7F_0$ transition correlates with the total formal charge on the ligands coordinated to Eu(III). Equation 4.1 was used to relate the frequency, v, to the total formal ligand charge, p.[73b]

$$v = -0.76p^2 + 2.22p + 17273 \tag{4.1}$$

Qualitative information regarding the coordination environment may also be obtained by observing transition intensity variations.[72] The $^5D_0 \rightarrow {}^7F_2$ transition observed at 615 nm is electric dipole in origin and, as such, its intensity is very sensitive to ligand field strength.[46b, 72] In contrast the $^5D_0 \rightarrow {}^7F_1$ transition observed at 591 nm retains its magnetic dipole character, and its radiative transition intensity is little effected by ligand field strength.[46b, 72] The relative intensities of the two transitions serve as a good indicator for the strength of the ligand field, including both the inner- and outer-sphere around Eu(III). By plotting the change in number of inner-sphere water molecules determined by use of Equation 4.2 (N_{H2O} is determined by equation 4.3) against the relative intensities of $^5D_0 \rightarrow {}^7F_2$ and $^5D_0 \rightarrow {}^7F_1$, $R_{E/M}$, (Equation 4.4) a difference between inner and outer-sphere interactions, may be observed[72]

$$\Delta N_{H2O} = 9 - N_{H2O} \tag{4.2}$$

$$N_{H2O} = 1.05k_{obs} - 0.44 \tag{4.3}$$

$$R_{E/M} = I(^5D_0 \rightarrow {}^7F_2) \ / \ I(^5D_0 \rightarrow {}^7F_1) \tag{4.4}$$

where N_{H2O} is the number of inner-sphere waters for the complex, ΔN_{H2O} is the change in the number of inner-sphere water molecules as compared to aqueous Eu(III) ion, k_{obs} is the reciprocal of the excited state lifetime, $I(^5D_0 \rightarrow {}^7F_2)$ and $I(^5D_0 \rightarrow {}^7F_1)$ are determined from the relative emission intensities for each transition. Highly-coordinating strong-field ligands (such as ethylenediaminetetraacetic acid (EDTA), Figure 4.1) exhibited large ΔN_{H2O} and displayed several $R_{E/M}$ values. These differences are seen in Figure 4.2.[72]

From fluorescence measurements, the total number of inner-sphere water molecules can be determined. The number of inner-sphere water molecules of metal ions is of paramount importance in understanding the nature and reactivity of metal complexes in solution. This is especially true for MRI contrast agents, where the relaxivity is directly dependent on the number of inner-sphere waters (q). For most metal ions and their complexes in solution, the determination of q is difficult or impossible. The luminescence of Ln(III) ions, in particular Eu(III) and Tb(III), offers a convenient method for the determination of q.

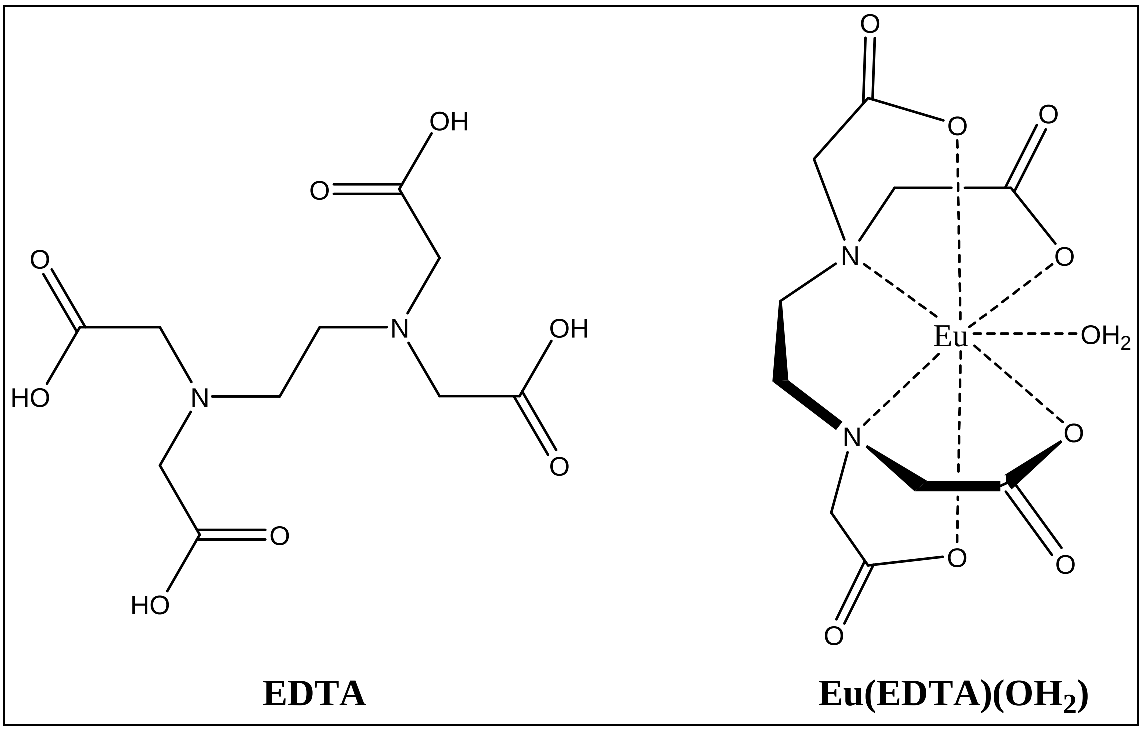

Figure 4.1: Depiction of ethylenediaminetetraacetic acid (EDTA) and Eu complexed by $EDTA^{4-}$ (the tetraacetate is coordinated) with a single inner-sphere water.

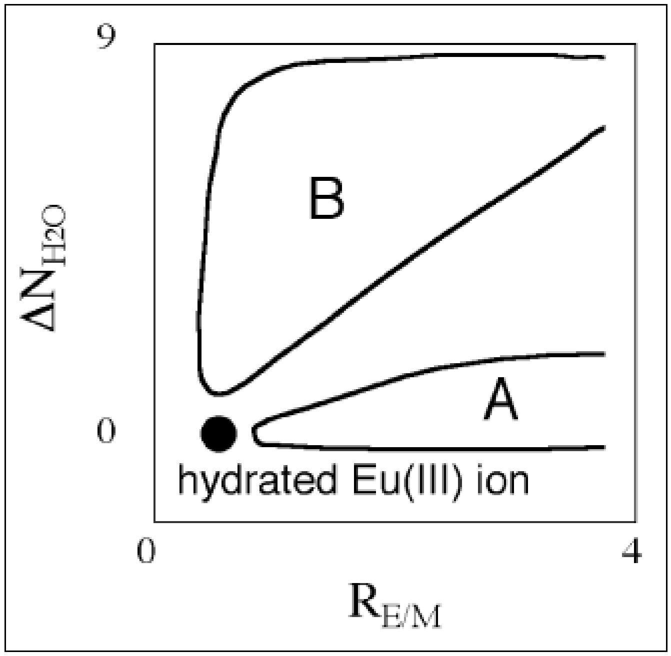

Figure 4.2: Schematic coordination environment diagram indicating areas corresponding to the characteristics of the interaction between Eu(III) and ligands. Plots in areas A and B are representative of outer-sphere and inner-sphere ligand coordinations, respectively.[72]

Early work on lanthanide luminescence established that OH (including H_2O) oscillators provide efficient non-radiative pathways for deexcitation of electronically excited-state Ln(III) ions.[74] In contrast, OD and D_2O oscillators are quite inefficient at deexcitation.[75] Work by Horrocks and Sudnick[76] calibrated the luminescence decay rates of a series of crystalline deutero and protio Eu(III) complexes, where q is known from X-ray diffraction studies. This work formulated Equation 4.5:

$$q = A[\tau_{H2O}^{-1} - \tau_{D20}^{-1}] \qquad (4.5)$$

where the constant A was determined to be 1.05 (water molecules·ms) for Eu(III) and 4.2 (water molecules·ms) for Tb(III).[76]

Even though this equation has proven very useful in the determination of q for Eu(III) complexes in aqueous solutions, it frequently gives non-integer q-values.[76] This can be accounted for by several reasons. First, the Eu(III) ion may form more than one type of complex with a particular ligand in solution. The presence of multiple Eu(III) species in solution can be verified by observing multiple signals for the $^7F_0 \rightarrow {}^5D_0$ excitation transition. The two states are non-degenerate and are dependent on the identity of the atoms in the first coordination sphere (i.e., two different Eu(III) species will give two different $^7F_0 \rightarrow {}^5D_0$ transitions).[76] If the Eu(III) ion is in two different coordination environments with different q-values, the q-value determined by Equation 4.5 depends on the rate of exchange of the Eu(III) between its different coordination environments. For example, if the Eu(III) ion is in coordination environments containing differing numbers of inner-sphere water molecules, and fast exchange between the two environments occurs, the q-value will be non-integral because it will be the weighted average of the q-values measured.

Second, ligands containing X-H oscillators can also shorten a Eu(III) excited state lifetime to varying degrees. This is especially true for X-H moieties that contain exchangeable hydrogen atoms, in particular oscillators such as alcoholic O-H and amine N-H in which the O or N are directly coordinated to the Eu(III).

A third reason for non-integral and larger than expected q-values is that outer-sphere water molecules are known to shorten excited state lifetimes. With these difficulties in mind, Equation 4.5 was modified to Equation 4.5a:

$$q = A[\tau_{H2O}^{-1} - \tau_{D20}^{-1} - k_{XH}] \qquad (4.5a)$$

$$k_{XH} = \alpha - \beta n_{OH} - \gamma n_{NH} - \delta n_{O=CNH} \qquad (4.5b)$$

where n_{OH} is the number of alcoholic O-H oscillators, n_{NH} is the number of amine N-H oscillators, and $n_{O=CHN}$ is the number of amide N-H oscillators in the first coordination sphere. Equation 4.5b is the k_{XH} term in Equation 4.5a. In Equation 4.5b α is 0.31 and the contributions of each oscillator are $\beta = 0.45$ ms^{-1}, $\gamma = 0.99$ ms^{-1}, and $\delta = 0.075$ ms^{-1}. The A value is the quenching of excited-state Eu(III) by second coordination sphere water molecules.

This analysis has only been performed on mononuclear species. The Messerle group's interests lay in the determination of the solution-state structure of polynuclear lanthanide clusters in aqueous media and the relationship to the solid-state structure. The number of inner-sphere water molecules is also of great importance as it is directly related to the viability of gadolinium(III) complexes as MRI contrast agents. The experiments described here are solely concerned with Eu(III) (with similar ionic radis to Gd(III)) complexes. Herein we report attempts to elucidate the solution-state structure of our polyeuropium complexes via spectrofluorimetry.

Results and Discussion

Fluorescence Profiles

The solution excitation and emission fluorescence profiles of $Eu(ClO_4)_3$, Eu_4 proline and all Eu_{15}-his X (X = Cl, Br, $(I)_2$-OH, OH) are shown in Figures 4.6 to 4.11, respectively. Figure 4.3 is a representative structure of the Eu_{15}-his X clusters mentioned. The solid-state excitation and emission fluorescence profiles for all Eu_{15}-his X are shown in Figures 4.12 through 4.15. Emissive transitions that were of interest to this research are the $^5D_0 \rightarrow {}^7F_0$, $^5D_0 \rightarrow {}^7F_1$, and $^5D_0 \rightarrow {}^7F_2$ transitions that were observed at 580 nm, 591 nm, and 613 nm, respectively.

The ground state $^7F_0$ and the excited state $^5D_0$ of europium(III) ions are nondegenerate and are not split by ligand field effects. Each Eu(III) environment may, in theory, give rise to different peaks in the $^5D_0 \rightarrow {}^7F_0$ emission spectrum, and the number of emission peaks may reflect the number of Eu(III) species present. However, this phenomenon is not apparent in the solution- or solid-state fluorescence profiles of the Eu_{15}-his X complexes (Figure 4.3). This may be accounted for by the relatively small

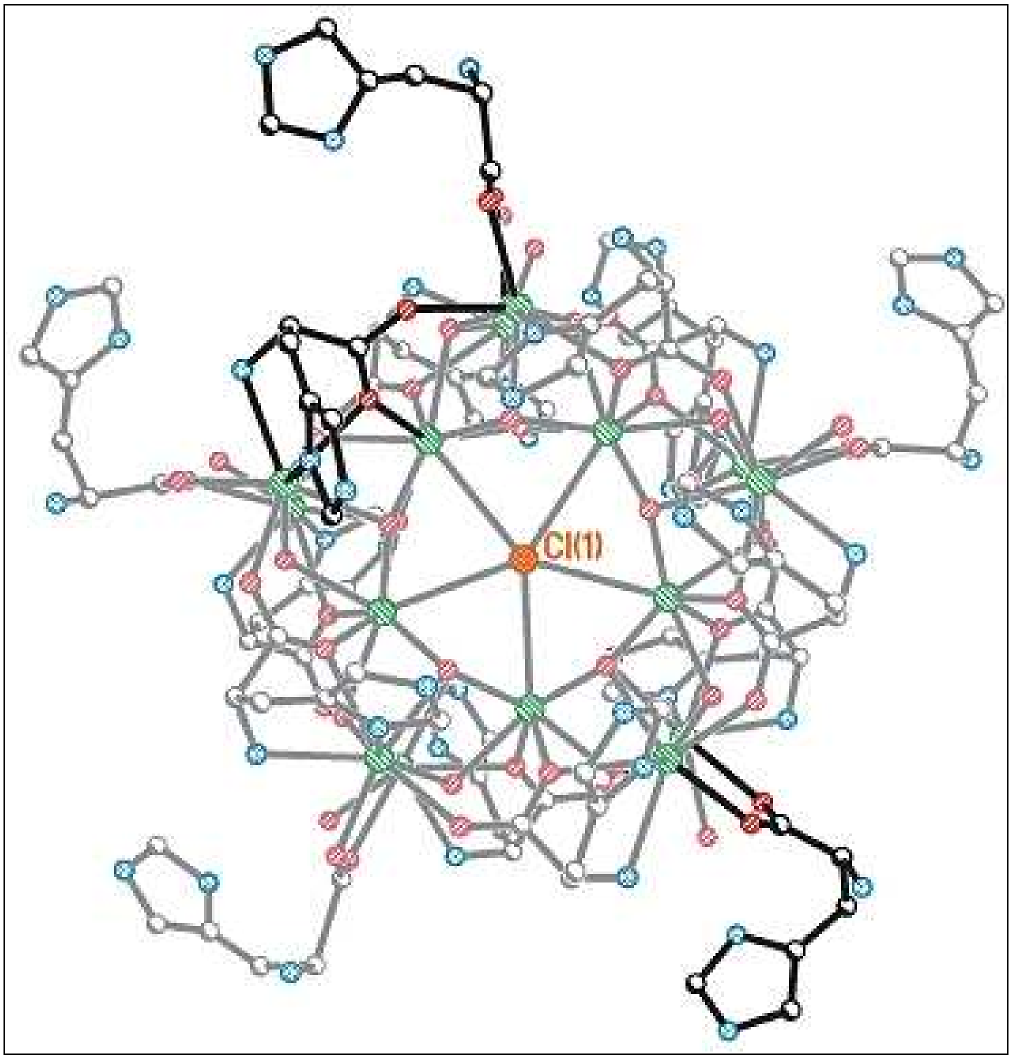

Figure 4.3: $[Eu_{15}(\mu_5\text{-}X)(\mu_3\text{-}OH)_{20}(his)_{15}(OH_2)_7](ClO_4)_{12}$ crystal structure showing the coordination modes of the histidine ligands. Perchlorate anions omitted for clarity. Color scheme: green, Eu(III); orange, chloride; gray, carbon, blue, nitrogen; red, oxygen. Identical structures are observed for Ln = Gd, Tb, and Y.

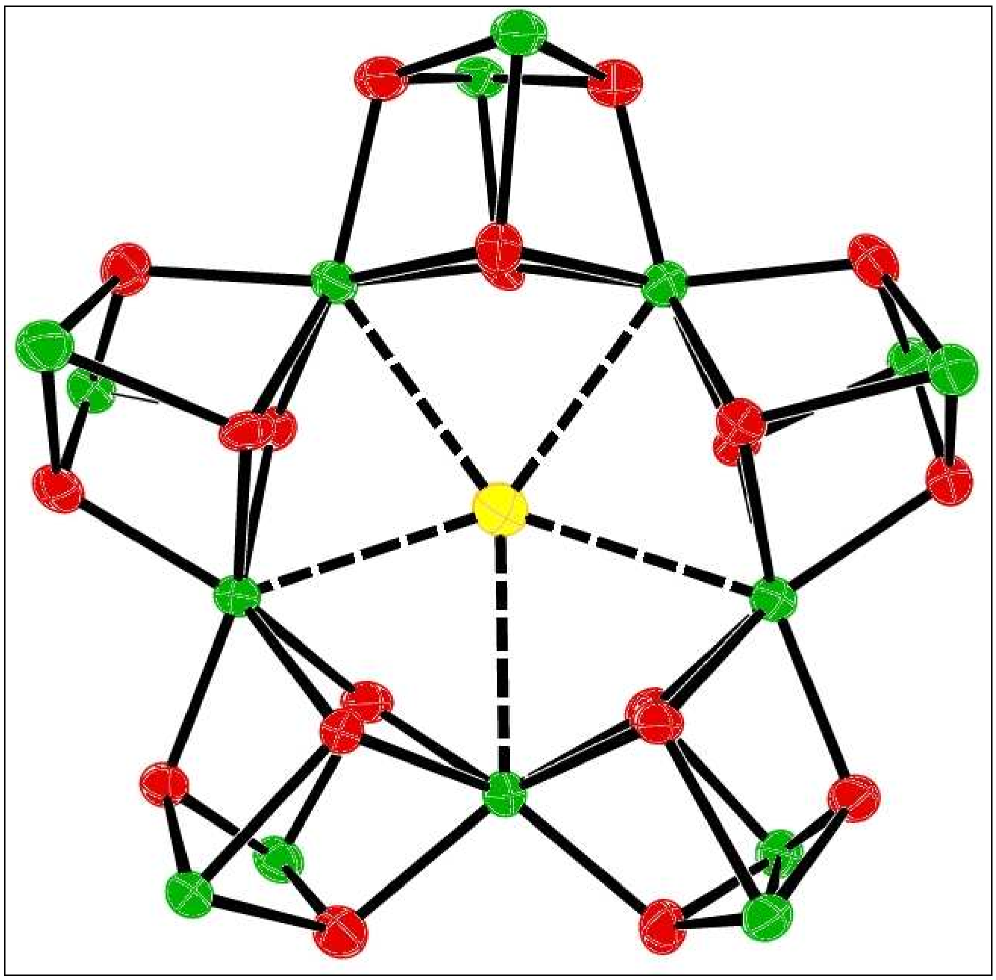

Figure 4.4: Skeletal view of Eu_{15}-his Cl with bridging hydroxides and μ_5-Cl. All other ligands and anions omitted for clarity. Color scheme: green, Eu(III); yellow, chloride; red, oxygen. It is apparent even without ligands that there are two unique Eu(III) centers: five interior and ten exterior.

environmental differences between the two unique Eu(III) centers (Figure 4.4). If this were the case, both emissions would be observed in nearly identical positions. Another plausible explanation is that one transition for one Eu(III) center is observed at 580 nm and the other transition is enveloped by the $^5D_0 \rightarrow {}^7F_1$ transition centered at 591 nm. The latter of the two arguments is much less likely. This is evident by applying Equation 4.1 to the observed emission frequencies in order to determine the total formal charge of the ligands coordinated to the Eu(III) ion. The corresponding frequency for the observed transitions at 580 nm and 591 nm are 17235 cm^{-1} and 16920 cm^{-1}, which correspond to *v*-values of -5 and -20, respectively. From crystallographic data the coordination sphere of each inner Eu(III) ion is filled with nine negatively-charged bridging ligands. Exterior Eu(III) ions are coordinated by six negatively-charged bridging ligands. Since the negatively-charged ligands are shared amongst several Eu(III) ions, the charge of the ligands can be considered to be shared, and a calculated formal charge of -5 is reasonable. A total formal charge of -20 is improbable; therefore the most plausible explanation for the absence of the second $^5D_0 \rightarrow {}^7F_0$ transition is the first argument.

The solid-state structures of Eu_{15}-his X complexes are well-defined, while the solution-state structure is not. Comparison of the fluorescence profiles of solid-state data and solution-state could provide insight into the solution-state structure. Fluorescence profiles of both the solution- and solid-state Eu_{15}-his X complexes are identical, with the exception that the solid-state profiles exhibit sharper and more defined peaks. It is also important to note that the fluorescence profiles show little if any change with varying X. Splitting observed in the $^5D_0 \rightarrow {}^7F_1$ and $^5D_0 \rightarrow {}^7F_2$ transitions can be accounted for by ligand field effects. The ligand field in a complex ion removes degeneracy of a given $^{2S+1}L_J$ term partly or completely, resulting, in many cases, in individual transitions with more than one line.[46b] These splitting patterns provide information concerning the coordination environment of the Eu(III) ion. One such example was the application of

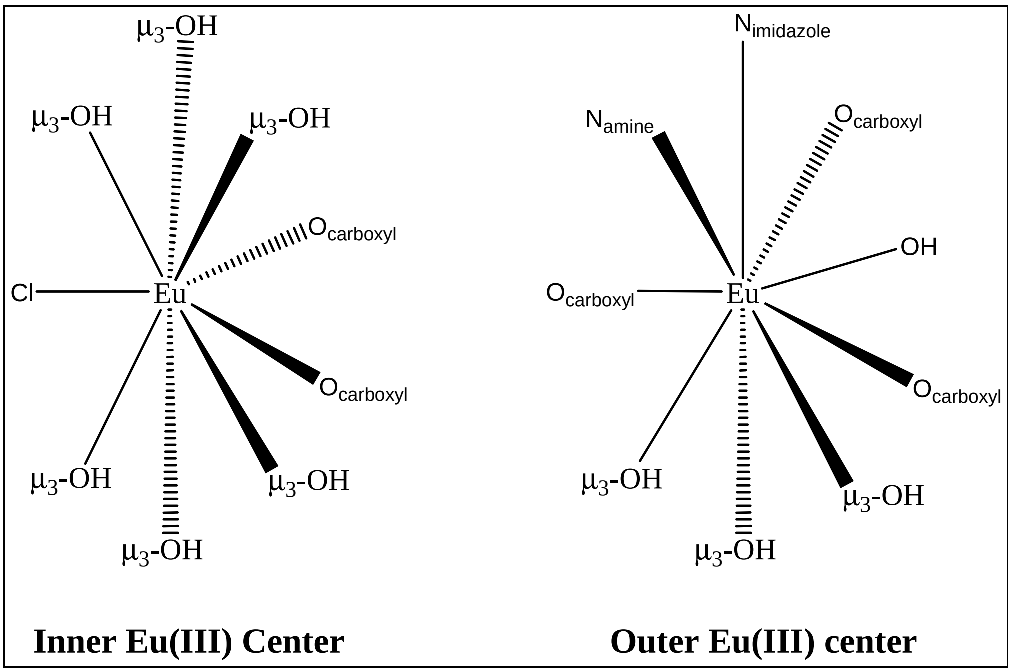

Figure 4.5: Depiction of Eu(III) environments in Eu_{15}-his Cl. Similar environments are observed for each Eu_{15}-his X, where X = Br, $(I)_2$-OH, and OH.

luminescence spectroscopy to assign the geometry of Eu(III) in $[Eu(terpy)_3](ClO_4)_3$ before the crystallographic details were available.[77] However, in the complex systems of Eu_{15}-his X, assigning the geometric position of Eu(III) ions is much more difficult. This is especially true since these systems have multiple Eu(III) ions in different geometric positions, and the transitions that would allow for geometric determinations overlap. However, since the solution- and solid-state excitation and emission profiles are identical, it can be assumed that the Eu(III) ions observed during excitation and emission are in similar if not identical coordination geometries.

Although the ligated geometry of the Eu(III) ions for Eu_{15}-his X complexes cannot be determined from fluorescence studies, information regarding the type of ligand interactions may be examined. As seen in Figure 4.1, highly-coordinating strong-field ligands reside in the region marked as B, and non-coordinating weak-field ligands reside in the region marked A. By applying Equations 4.2, 4.3 and 4.4 to the Eu_{15}-his X data, ΔN_{H2O} is found to range between seven and five, and $R_{E/M}$ ranges from 1.2 to 1.6 for the Eu_{15}-his X complexes. Using Figure 4.1, the plotted values are within the B region of the plot, indicating that the Eu(III) ions observed in the fluorescence spectra are coordinated by strong-field ligands. This data supports what is expected from crystallographic analyses, where the Eu(III) ions are coordinated by hydroxides and carboxylates.

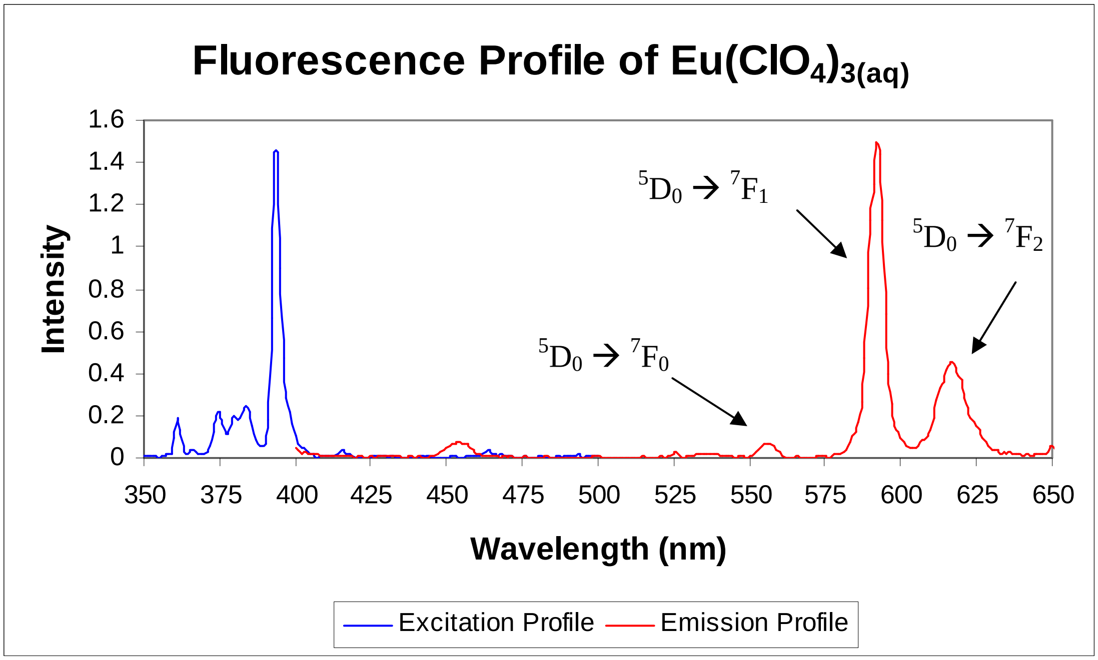

Figure 4.6: Excitation and emission profile of $Eu(ClO_4)_3$ in aqueous media.

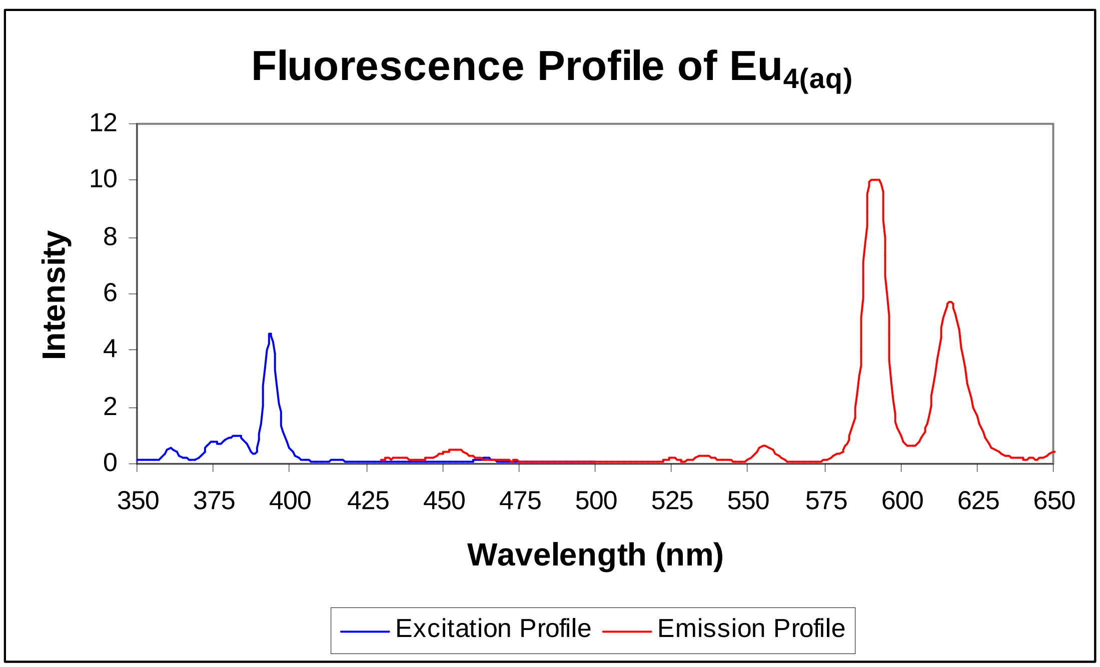

Figure 4.7: Excitation and emission profile of $[Eu_4(\mu_3\text{-}OH)_4(pro)_6(OH_2)_7](ClO_4)_6$ in aqueous media.

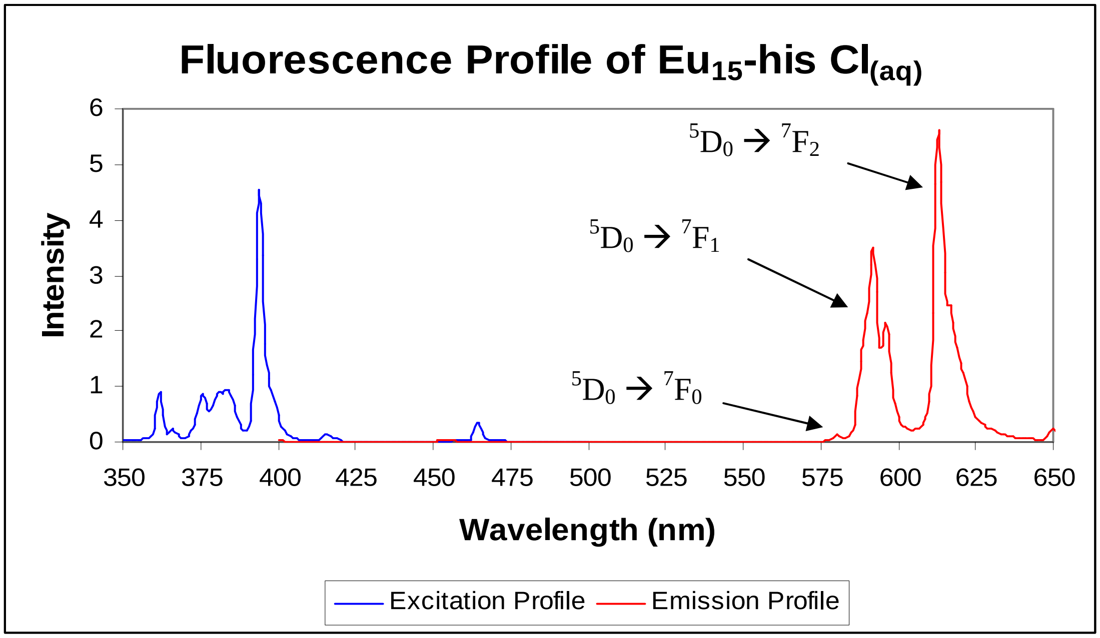

Figure 4.8: Excitation and emission profile of $[Eu_{15}(\mu_5\text{-}Cl)(\mu_3\text{-}OH)_{20}(his^{+/-})_{10}(his^{-})_5(OH)_7](ClO_4)_{12}$ in aqueous media.

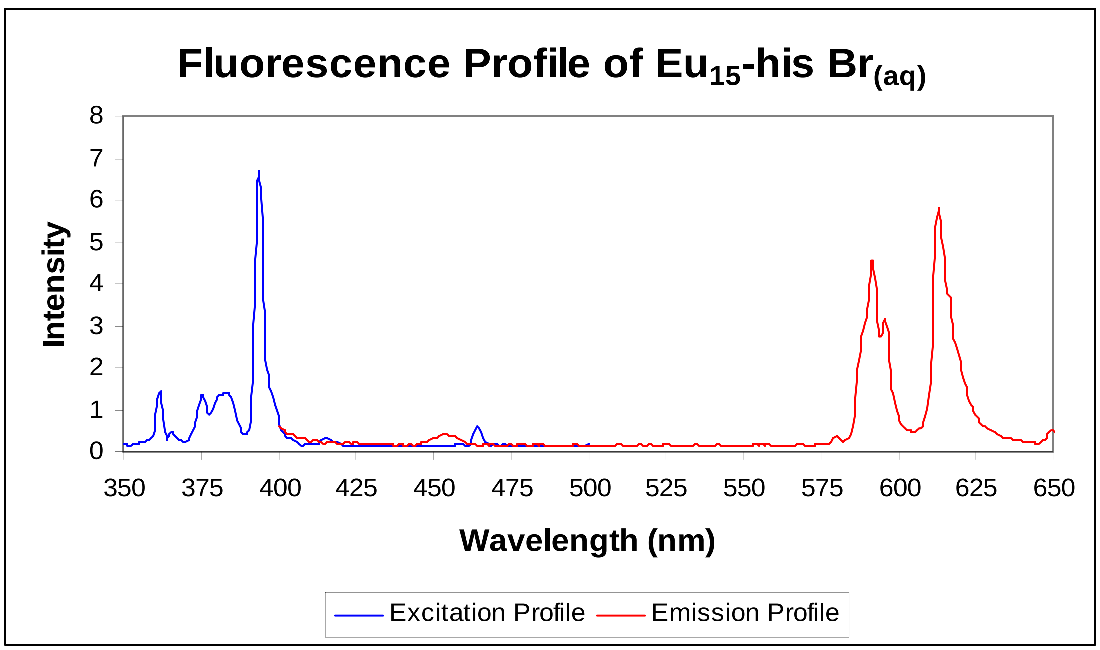

Figure 4.9: Excitation and emission profile of $[Eu_{15}(\mu_5\text{-}Br)(\mu_3\text{-}OH)_{20}(his^{+/-})_{10}(his^{-})_5(OH)_7](ClO_4)_{12}$ in aqueous media.

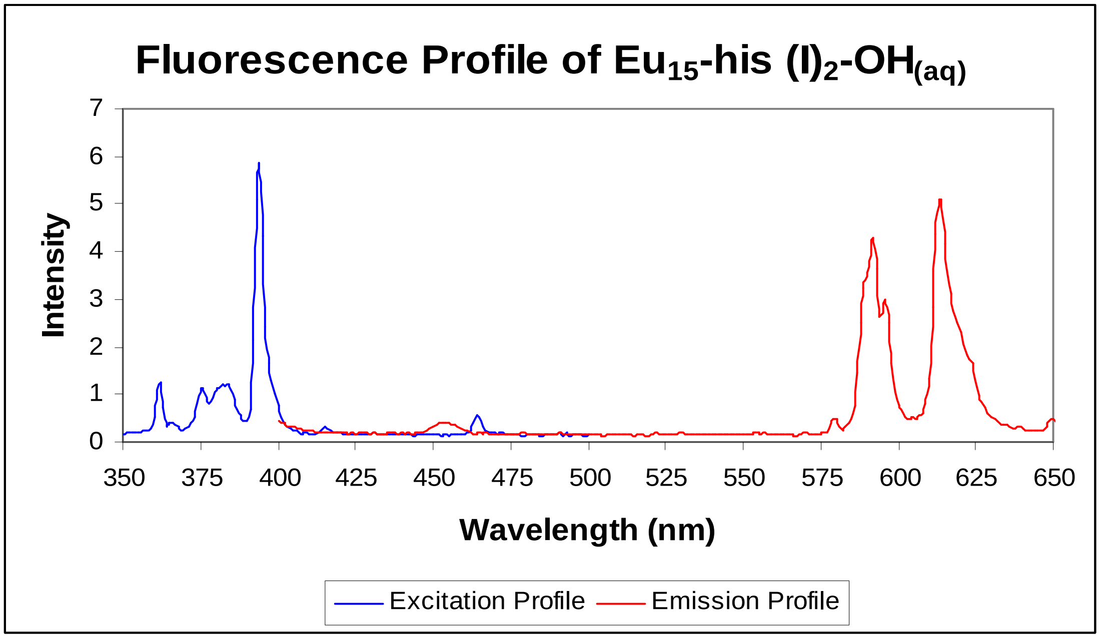

Figure 4.10: Excitation and emission profile of $[Eu_{15}(\mu_5\text{-}OH)(I)_2(\mu_3\text{-}OH)_{20}(his^{+/-})_{10}(his^{-})_5(OH)_7](ClO_4)_{10}$ in aqueous media.

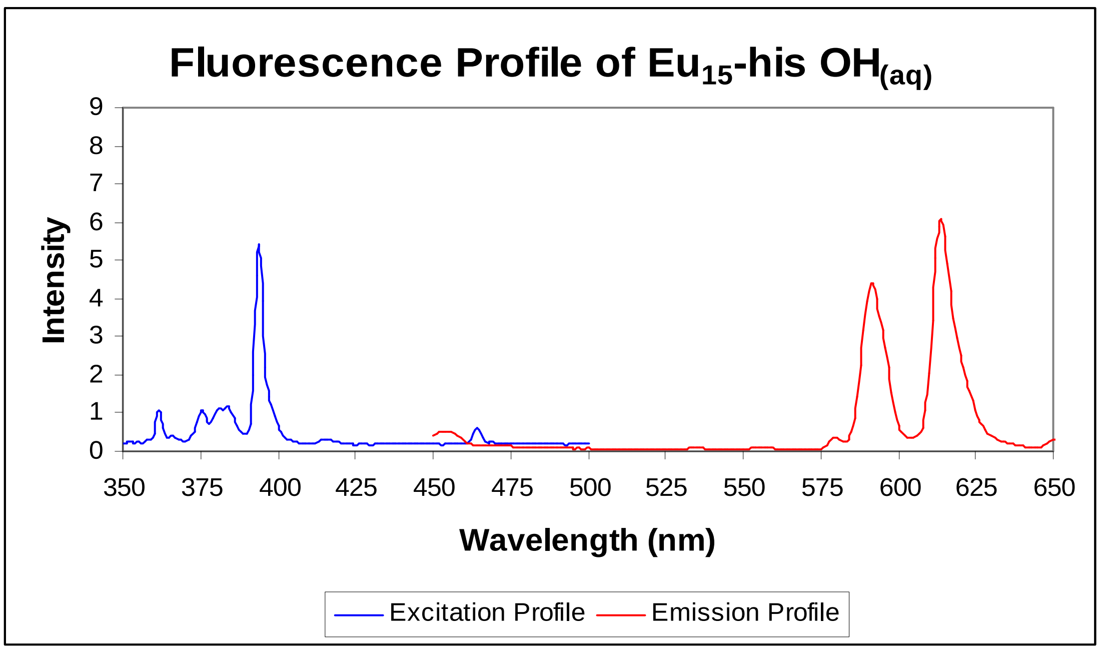

Figure 4.11: Excitation and emission profile of $[Eu_{15}(\mu_5\text{-}OH)(\mu_3\text{-}OH)_{20}(his^{+/-})_{10}(his^{-})_5(OH)_7](ClO_4)_{12}$ in aqueous media.

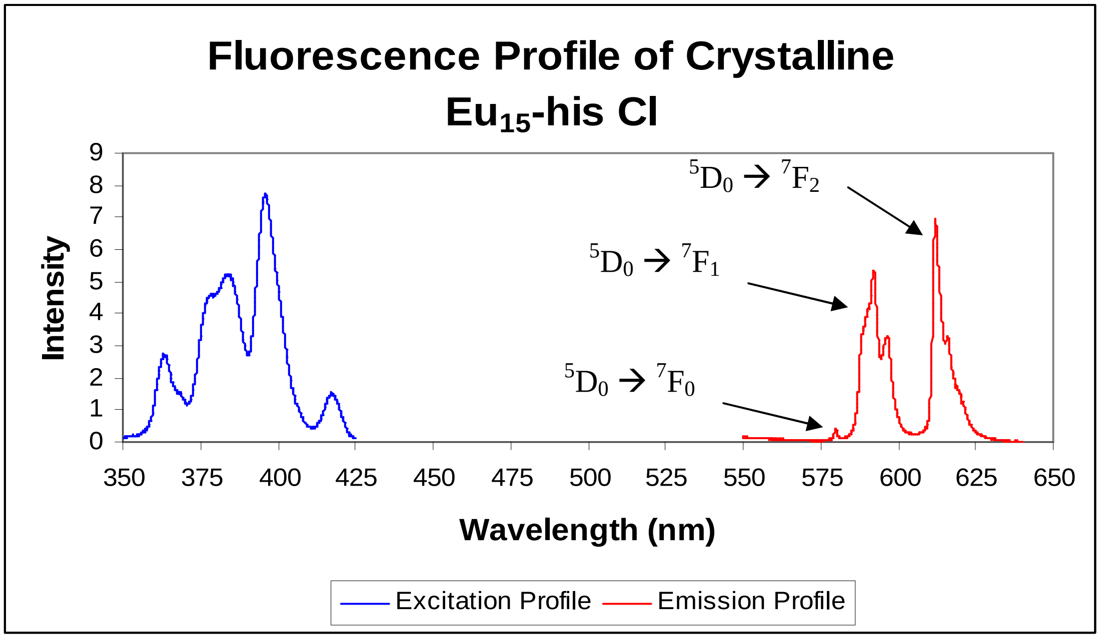

Figure 4.12: Excitation and emission profile of crystalline $[Eu_{15}(\mu_5\text{-}Cl)(\mu_3\text{-}OH)_{20}(his^{+/-})_{10}(his^{-})_5(OH)_7](ClO_4)_{12}$.

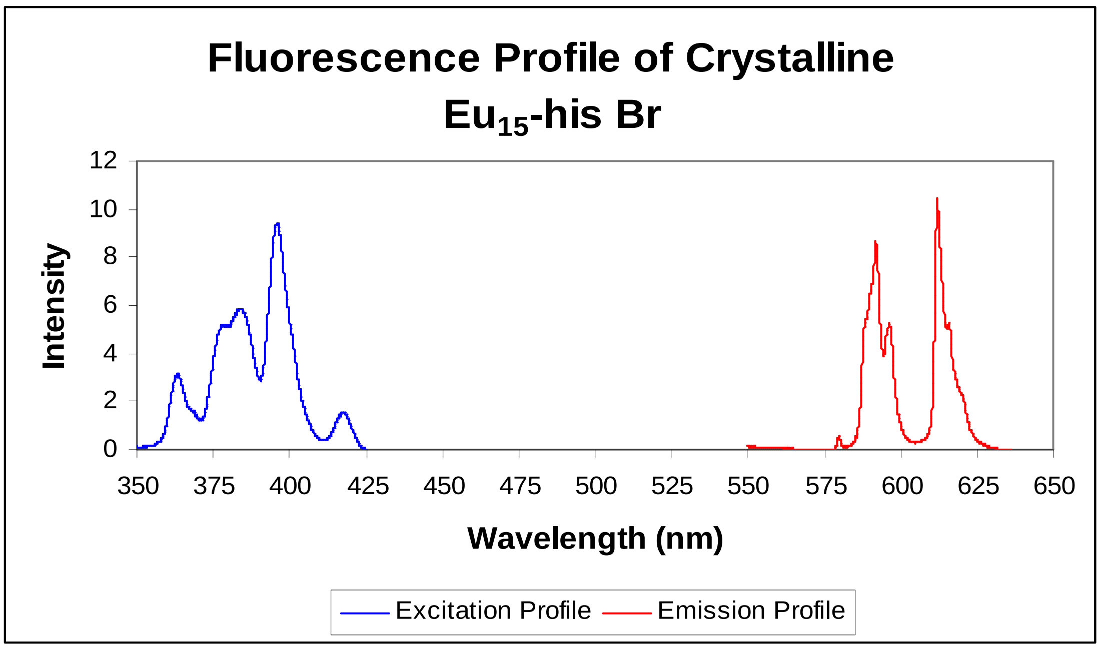

Figure 4.13: Excitation and emission profile of crystalline $[Eu_{15}(\mu_5\text{-}Br)(\mu_3\text{-}OH)_{20}(his^{+/-})_{10}(his^{-})_5(OH)_7](ClO_4)_{12}$.

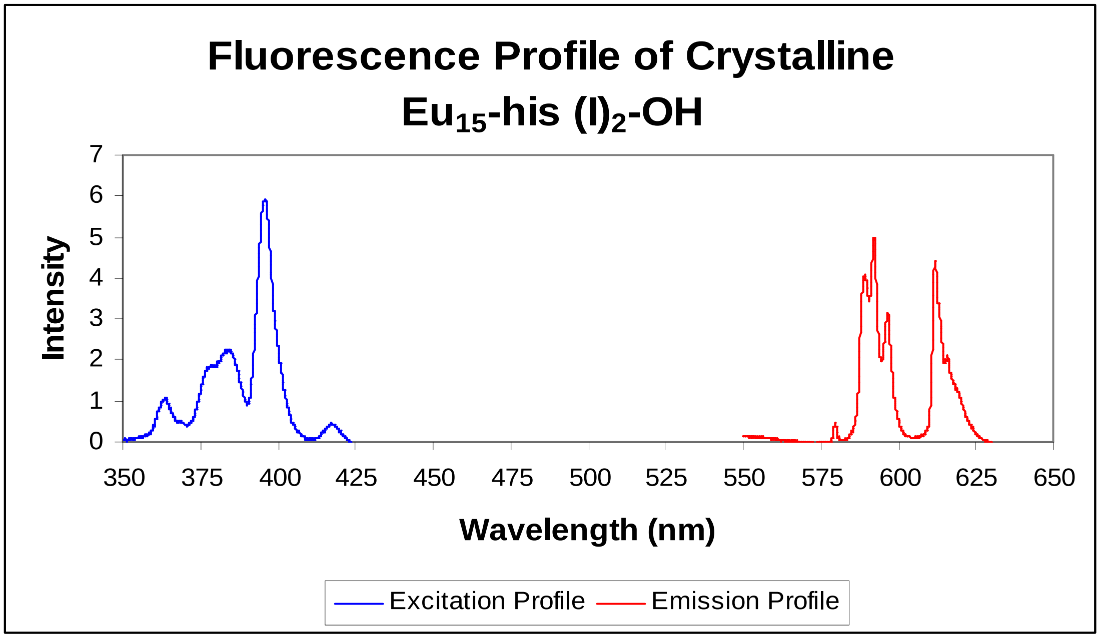

Figure 4.14: Excitation and emission profile of crystalline $[Eu_{15}(\mu_5\text{-}OH)(I)_2(\mu_3\text{-}OH)_{20}(his^{+/-})_{10}(his^{-})_5(OH)_7](ClO_4)_{10}$.

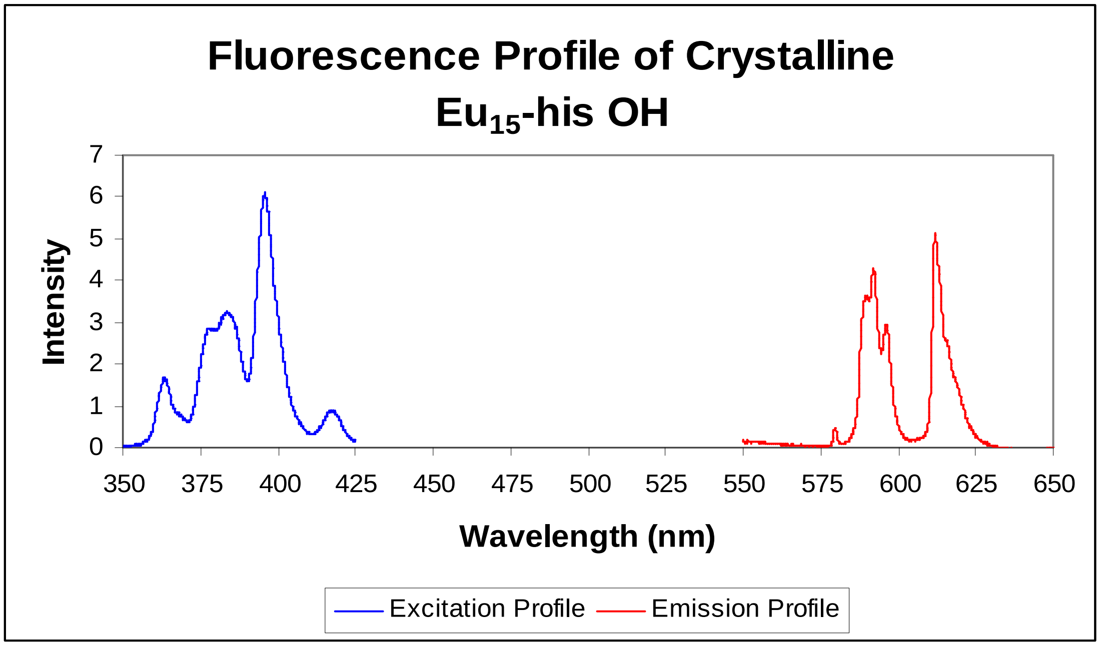

Figure 4.15: Excitation and emission profile of crystalline $[Eu_{15}(\mu_5\text{-}OH)(\mu_3\text{-}OH)_{20}(his^{+/-})_{10}(his^{-})_5(OH)_7](ClO_4)_{12}$.

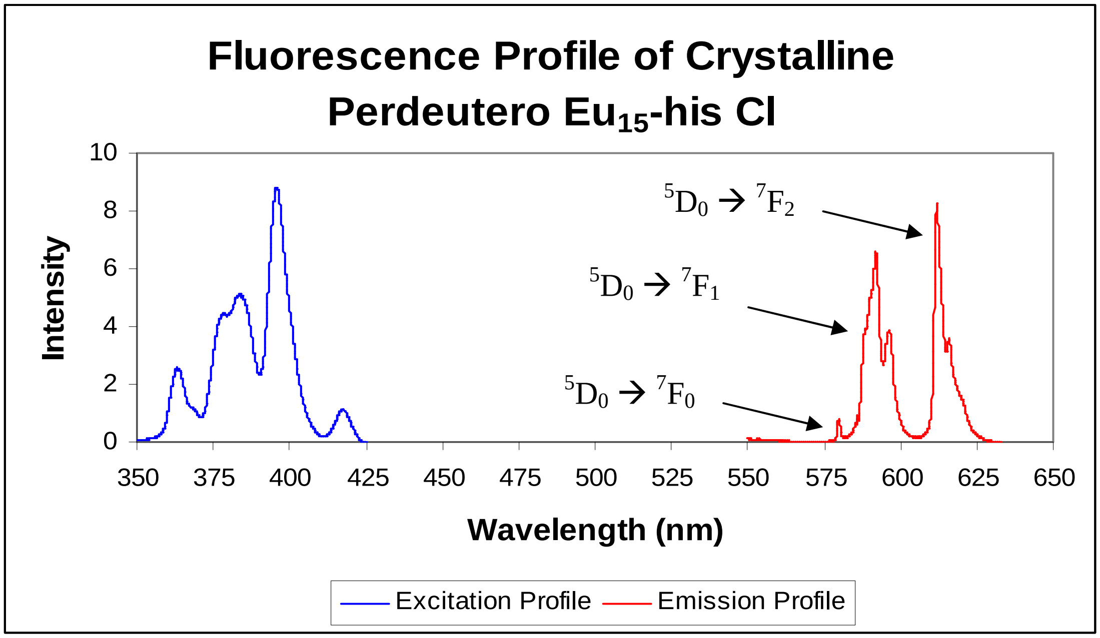

Figure 4.16: Excitation and emission profile of crystalline perdeutero $[Eu_{15}(\mu_5\text{-}Cl)(\mu_3\text{-}OD)_{20}(his^{+/-})_{10}(his^{-})_5(OD)_7](ClO_4)_{12}$.

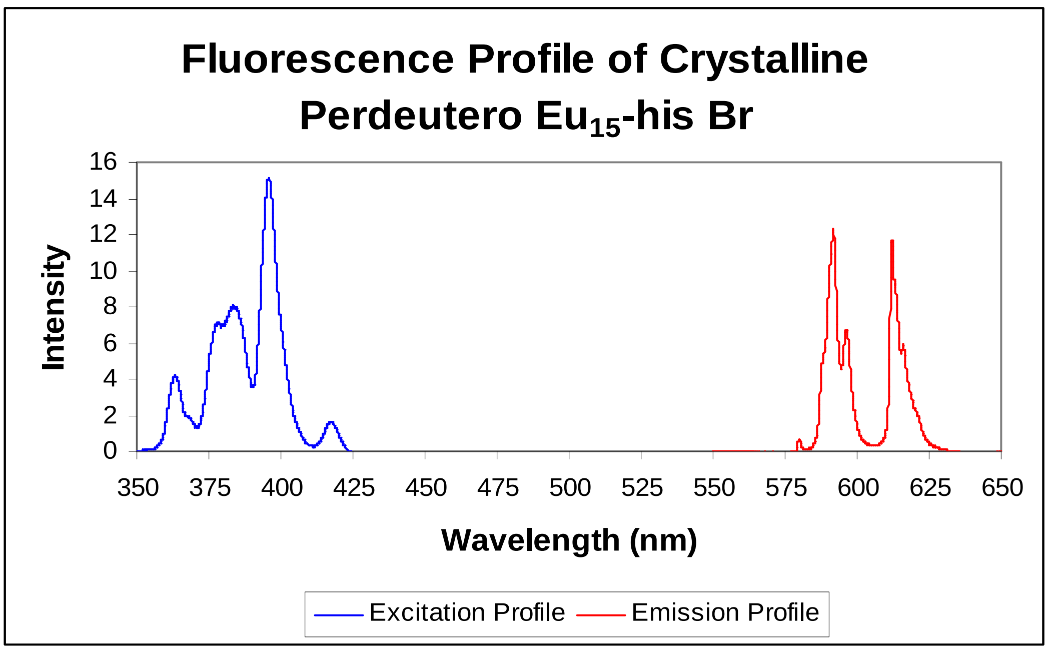

Figure 4.17: Excitation and emission profile of crystalline perdeutero $[Eu_{15}(\mu_5\text{-}Br)(\mu_3\text{-}OD)_{20}(his^{+/-})_{10}(his^{-})_5(OD)_7](ClO_4)_{12}$.

Fluorescence Lifetime Measurements

The luminescence from solution and solid-state samples of Eu_{15}-his X were analyzed for the luminescence decay constants of europium(III) ions. The fluorescence lifetimes were determined from the slope of $\ln(I/I_o)$ vs. time, where I is the intensity, I_o is the maximum intensity, and the slope of the line was $1/\tau$ ($1/\tau$, decay constant, and τ is the fluorescence lifetime). Fluorescence lifetimes were measured for the $^5D_0 \rightarrow ^7F_0$, $^5D_0 \rightarrow ^7F_1$, and $^5D_0 \rightarrow ^7F_2$ transitions of Eu(III). The lifetimes of each transition ($^5D_0 \rightarrow ^7F_0$, $^5D_0 \rightarrow ^7F_1$, and $^5D_0 \rightarrow ^7F_2$) were within experimental error of each other. For this reason, only the lifetimes from the $^5D_0 \rightarrow ^7F_0$ transition are discussed. The fluorescence lifetimes are listed in Table 4.1 for protio and perdeutero samples.

Table 4.1: Fluorescence lifetimes of $Eu(ClO_4)_{3(aq)}$ and Eu_{15}-his X complexes in solution (H_2O or D_2O) and as solids (protio or perdeutero).

Compound	**τ_{H20} (ms)**	**τ_{D20} (ms)**
$Eu(ClO_4)_3$	0.115(2)	3.675
Eu_{15} Cl	0.26(2)	1.05(2)
Eu_{15} Cl solid	0.261(5)	1.38(1)
Eu_{15} Br	0.26(6)	0.95(2)
Eu_{15} Br solid	0.270(6)	1.44(5)
Eu_{15} $(I)_2$-OH	0.25(4)	2.83(6)
Eu_{15} $(I)_2$-OH solid	0.274(5)	0.97(4)
Eu_{15} OH	0.20(3)	2.68(2)
Eu_{15} OH solid	0.233(3)	0.96(4)

The observed fluorescence lifetimes for each sample were single exponential curves from which the decay constants were determined through linear regression and converted to fluorescence lifetimes. The luminescence intensity from Eu(III) as a function of time was used to calculate the decay constants. Equation 4.5a was used to calculate q-values, and these values are given in Table 4.2 and Table 4.3. Since Equation 4.5a was developed from, and used to determine q for mononuclear species, there is some question as to whether the equation applies to polynuclear species. The largest concern when employing this equation is whether or not the calculated q-value is representative of the cluster as a whole or if the value is intended for an individual Eu(III) center. While employing Equation 4.5a for Eu_{15}-his X clusters, several of the variables were used or omitted during the determination of q. For example, it is unclear whether the triply-bridging hydroxyl's affect each Eu(III) center equally or partially. With this in mind, Equation 4.5a was employed with n_{OH} = 20 (total number of OH ligands per structure and n_{NH} was set to 10), 3 (total number of OH ligands coordinated to each Eu(III) and n_{NH} was set to 2), and 1 (assuming that each OH only partially affects each Eu(III) and n_{NH} was set to 1). Both cases provided q-values that were reasonable based on expected values from crystallographic data. Since there are no reports using Equation 4.5a for polynuclear complexes, the application of this equation, assuming that it holds only for individual Eu(III) ions and assuming that it holds for polynuclear complexes, will be discussed.

Table 4.2 lists the calculated q-values assuming that Equation 4.5a provides values that are representative of individual Eu(III) ions. When n_{OH} = 3 or 1, positive q-values of 5.3 to 7.3 and 4.3 to 6.4, respectively, are obtained. Assuming that these q-values are representative of individual Eu(III) ions, when multiplied by the number of Eu(III) ions capable of inner-sphere coordination by water, these values can be used to calculate the total number of inner-sphere waters per Eu_{15}-his X complex. In this case, ten Eu(III) ions are capable of such coordination, assuming that the structure observed in the solid-state is stable in solution. The resulting q-values (q' and q" in Table 4.2) now range between 43 and 63 inner-sphere waters per complex. Neither of these values correlates with what is expected from crystallographic data. There are several possible reasons for why higher-than-expected q-values are obtained. It is possible that Equation 4.5a does not hold for polynuclear complexes or that the q-values are not representative of individual Eu(III) ions.

Table 4.2: Calculated q-values for $Eu(ClO_4)_{3(aq)}$ and Eu_{15}-his X complexes in solution and as solids using Equation 4.5a assuming the equation represents q-values for individual Eu(III) ions.

Compound	**q**	**q'**	**q"**
$Eu(ClO_4)_3$	9.006	9.006	9.006
Eu_{15} Cl	2.80(3)	5.36(1)	4.38(2)
Eu_{15} Cl solid	3.10(2)	5.67(4)	4.69(4)
Eu_{15} Br	2.8(3)	5.3(6)	4.3(5)
Eu_{15} Br solid	2.99(9)	5.6(2)	4.6(1)
Eu_{15} $(I)_2$-OH	2.83(6)	3.7(3)	5.3(5)
Eu_{15} $(I)_2$-OH solid	2.77(2)	5.34(5)	4.36(4)
Eu_{15} OH	4.8(5)	7.3(8)	6.4(7)
Eu_{15} OH solid	3.28(7)	5.8(1)	4.9(1)

Note: q neglects the contributions from all oscillators in equation 4.5a; q' n_{OH} = 3; q" n_{OH} = 1.

The q-values (2.7 to 4.8) calculated using Equation 4.5 are more reasonable than those calculated using the extended equation (Equation 4.5a). This could be because the relative contributions of each oscillator are not correct (i.e., $\beta n_{OH} = 0.45$ ms^{-1}, $\gamma n_{NH} = 0.99$ ms^{-1}, and $\delta n_{O=CNH} = 0.075$ ms^{-1} are incorrect for polynuclear complexes). It may be possible that the contributions should be much lower than those reported. The oscillators in the Eu_{15}-his X complexes (OH and NH) are being shared among several Eu(III) ions, and it is unclear how the oscillator effects each Eu(III). Does each OH oscillator contribute a full 0.45 or a fraction of that to each Eu(III) that it coordinates? If the contribution is a fraction of the reported contribution, then a significant difference in the calculated values for these complexes would be observed.

The identity of the μ_3-OH and exterior OH ligands is not confirmed because the hydrogen atoms are not observed in the crystallographic data. It is possible that these ligands could be oxo ligands or even waters. If the μ_3-OH ligands are indeed oxo ligands then the contribution from OH oscillators in Equation 4.5 does not apply to these complexes. If the suspected μ_3-OH ligands are actually waters, then the q-values (q' and q") calculated using Equation 4.5a are more plausible. Both of these possibilities have significant ramifications on the understanding of these complexes (i.e., ligand charge would need to be reassigned).

If, instead, we assume that Equation 4.5a holds for polynuclear complexes, q-values of 22.1 to 24 are obtained (Table 4.3). It was suggested in Chapter 2 that several of the amino acid ligands exhibit variable coordination between two separate coordination modes, and this would alter the q-value of the Eu(III) ions coordinated by these dynamic ligands. Our data also suggests that the amino acid ligands are very labile and may be exchangeable with water molecules. With these possibilities in mind, the q-values of 22 to 24 per Eu_{15}-his X complex are reasonable. From crystallographic data, ten exterior Eu(III) ions coordinate to only seven hydroxides (charge considerations suggest hydroxide ligands, though it is unclear if the ligands are truly hydroxides or waters), providing seven Eu(III) ions with coordination numbers of nine and leaving the remaining Eu(III) ions with coordination numbers of eight. Eu(III) is capable of coordinating up to nine ligands. Presumably, the eight-coordinate Eu(III) ions become nine-coordinate in solution with coordination by water molecules. Also, if the exterior ligands are labile, as experiments suggest (Chapter 2), the exterior Eu(III) ions could easily coordinate several more water molecules. From this argument a q-value of 20 or more, in solution, for the entire cluster is reasonable.

Comparison of the q-values in Table 4.2 and 4.3, shows that Equation 4.5a provides q-values that correlate better with crystallographic data, assuming the q-values represent the cluster as a whole. Based on crystallographic data and solution-state data (^{13}C and ^{89}Y NMR spectroscopy), the values in Table 4.3 are more reasonable than those in Table 4.2. However, the q-values obtained for the solid-state samples are much higher than what would be expected from crystallographic data. It is possible, as previously suggested, that several of the μ_3-OH ligands may actually be water ligands. This would increase the expected number of inner-sphere water molecules significantly. Another explanation that may be more plausible is that Equation 4.5a requires alterations in order to provide an adequate estimation for the number of inner-sphere water molecules for polynuclear complexes. Modifying Equation 4.5a represents future work.

Table 4.3: Calculated q-values for $Eu(ClO_4)_{3(aq)}$ and Eu_{15}-his X complexes in solution and as solids using Equation 4.5a assuming the equation represents q-values for the cluster as a whole.

Compound	**q***	**q****
$Eu(ClO_4)_3$	9.006	9.006
Eu_{15} Cl	1.31(5)	22.1(1)
Eu_{15} Cl solid	3.10(2)	23.9(2)
Eu_{15} Br	1.28(3)	22.0(5)
Eu_{15} Br solid	2.99(9)	23.8(8)
Eu_{15} $(I)_2$-OH	1.97(6)	22.7(3)
Eu_{15} $(I)_2$-OH solid	2.57(7)	23.7(8)
Eu_{15} OH	4.8(5)	23.0(8)
Eu_{15} OH solid	3.26(1)	24.0(9)

Note: q* neglects the contributions from all oscillators in equation 4.5a; q** n_{OH} = 20.

Comparison of the fluorescence lifetimes from Table 4.1 of protio Eu_{15}-his X complexes dissolved in D_2O with synthesized perdeutero Eu_{15}-his X complexes provides insight into the ability of coordinated O-H oscillators to exchange with bulk water. Scheme 4.1 depicts a possible μ_3-OH hydrogen exchange with the deuterium of D_2O. The fluorescence lifetimes for the protio analogs, in both the solution- and solid-state, match. However, the protio analogue dissolved in D_2O does not match with the perdeutero analog. The values are in close agreement but are not exact, suggesting slightly different coordination environments for the observed Eu(III) ions. A possible explanation for these differences may be attributed to incomplete exchange of all O-H oscillators of the protio analog with bulk D_2O. It is possible that less sterically-hindered exterior μ_3-OH ligands exchange most rapidly with bulk D_2O. It is possible, but less likely, that more sterically-hindered interior μ_3-OH ligands will exchange, though possibly at a much slower rate. We postulate that the interior μ_3-OH ligands are protected via bulky groups that form barriers to protect the inner ligands and thus make solvent exchange processes more difficult.

The fluorescence lifetimes for both the solution-state and solid-state of protio Eu_{15}-his X complexes are the same within experimental error. This correlation suggests that the solution-state structure is very similar, if not identical to, that of the solid-state structure, further supporting solution-state stability of these Ln_{15}-his X complexes.

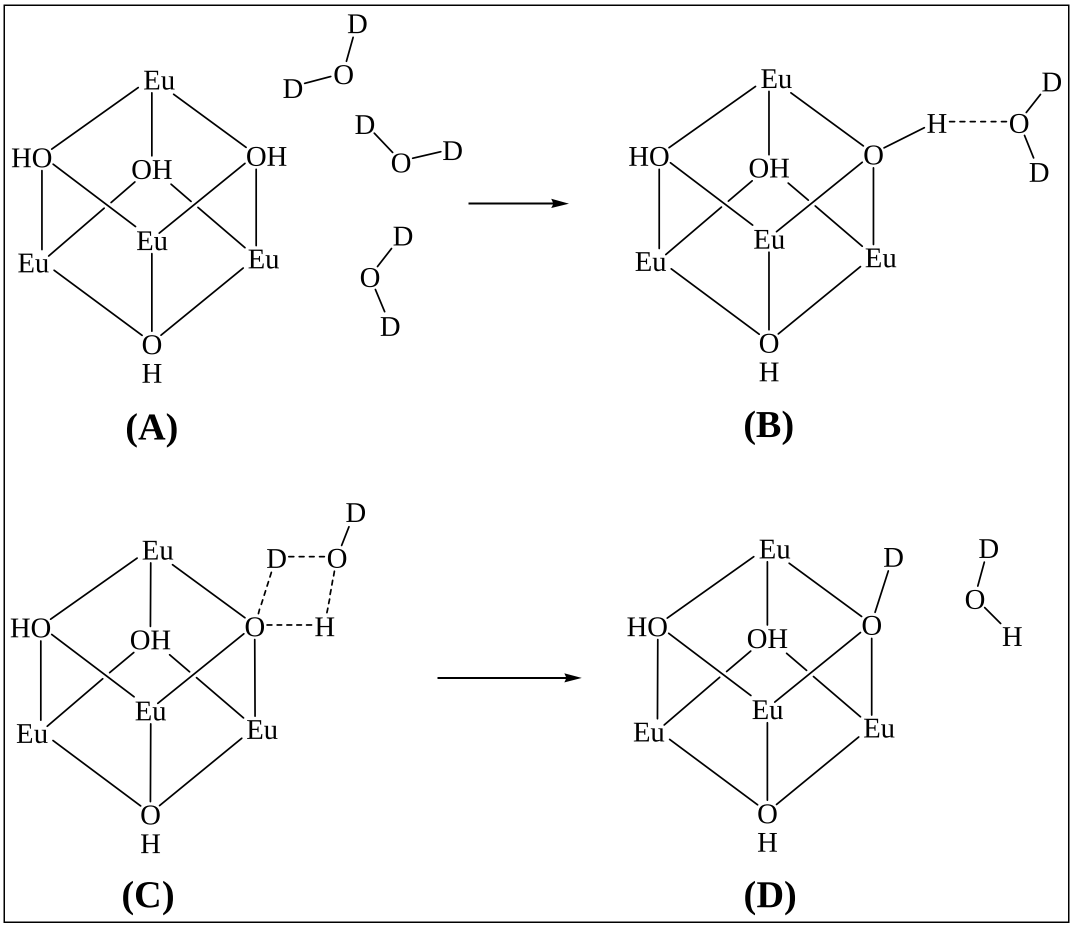

Scheme 4.1: Schematic demonstrating possible hydrogen, from μ_3-OH, exchange with a deuteron from bulk D_2O. Only one cubane is shown with all ligands except μ_3-OH excised for clarity. (A) bulk solvent around abbreviated molecule, (B) interaction between oxygen of D_2O and hydrogen of μ_3-OH, (C) transition state, (D) exchange of hydrogen for deuterium.

Conclusions

Fluorescence excitation and emission spectra were obtained for all Eu_{15}-his X complexes. The same transition shifts and splittings were observed for both the solution- and solid-state Eu_{15}-his X samples. Two unique Eu(III) centers are observed from crystallographic data and, as such, two $^5D_0 \rightarrow {}^7F_0$ transitions were expected. This was not observed and could be explained by slight environmental differences that may not significantly affect the transition energies. The two transitions most likely overlap one another.

Based on the energy shift of the $^5D_0 \rightarrow {}^7F_0$ transition, it was determined that the ligand environment around the Eu(III) centers was comprised of a total formal ligand charge of -5. From crystallographic data, one set of Eu(III) ions are coordinated by nine negatively-charged bridging ligands, and the other set of Eu(III) ions are coordinated by five negatively-charged bridging ligands, one negatively-charged ligand and one positively-charged ligand. Since the negatively-charged ligands are shared with other Eu(III) ions, the charge can be considered shared as well. By this argument the calculated total formal ligand charge seems sensible. It was also determined that the Eu(III) ions are coordinated by strong-field ligands.

Fluorescence lifetimes were determined for all Eu_{15}-his X complexes. This data was used to determine the number of inner-sphere water molecules, q. As there was some question as to whether Equation 4.5a would hold for multinuclear complexes, q was calculated with several factors in mind. It was determined that Equation 4.5a, in its current form, was inadequate to accurately calculate the total number of inner-sphere water molecules for multinuclear complexes. However, given that this is the only available model for the determination of inner-sphere water molecules for lanthanide complexes, q-values were calculated. The values obtained from Equation 4.5a correlated better with crystallographic data assuming the q-values represented the polyeuropium complexes as a whole than it did assuming the values represented individual Eu(III) ions.

From Equation 4.5a, it was determined that 22 – 24 waters are within the inner-sphere of Eu(III) ions in the Eu_{15}-his X complexes. In the solution-state, these values are reasonable. Eu_{15}-his X complexes crystallize with seven OH ligands that presumably exchange with solvent when dissolved. Also, several of the Eu(III) ions' coordination spheres are unsaturated and capable of further coordination; this, coupled with labile amino acid ligands, supports the ability of Eu_{15}-his X complexes to coordinate more waters than that expected from crystallographic data. However, the q-values calculated for the solid-state samples were much higher than what was expected. These values could be the result of the unconfirmed identity of μ_3-OH and exterior OH ligands or unreliable q-values, calculated from an equation that does not hold for polynuclear complexes.

The fluorescence data suggests that the solid-state structure of Eu_{15}-his X is maintained in the solution-state, based on similar fluorescence lifetimes and q-values. However, better theory is needed in order to confirm the total number of inner-sphere water molecules for Eu_{15}-his X complexes.

Fluorescence lifetime measurements in D_2O also confirmed the ability of several μ_3-OH hydrogens to exchange with solvent. This ability allows these complexes to interact with more water molecules than those that are directly coordinated to the metal center, which in turn could multiply the relaxivity of the Gd(III) analogs of these complexes.

Experimental

General Considerations:

The protio compounds were prepared as previously described in Chapter 2. D_2O was purchased from Sigma Aldrich and stored in a desiccator. The solutions used in these studies were made by dissolving 0.1 g of sample in 10 mL of solvent (H_2O or D_2O). Solutions were purged with $Ar_{(g)}$ for 10 minutes prior to excitation.

Solid-state fluorescence emission lifetimes were observed from finely-ground dried product. The solid was placed in a cylindrical quartz tube (inner diameter, 4 mm; outer diameter, 5 mm) which was then placed into a quartz cuvette filled with distilled water. The quartz cylinder was angled away from the excitation source and detector.

Initial solution excitation spectra were obtained on a Hewlett Packard 8453 UV-Visible spectrophotometer. Solution excitation and emission profiles were obtained on a Spectrophotometer**.** Solid-state fluorescence profiles were obtained on Jasco FP-6500 Research fluorescence spectrometer with an EFA-383 epifluorescence attachment. Lifetime measurements were obtained on a Photon Technology International (PTI) GL-3300 nitrogen laser in line with a PTI GL-302 dye laser. The Dye laser was tuned using 2-[1,1'-biphenyl]-4-yl-6-phenyl-benzoxazole (PBBO, Exciton Co.) dye in toluene/ethanol (7/3; 3.0 x 10^{-3} M) solution. Excitation wavelength was set to 393 nm, and emission lifetimes were observed at 580 nm, 591 nm, and 613 nm. Samples were placed in quartz cuvettes. A PTI Photomuliplier detection system Model 814 was placed 90 degrees from the excitation source. The signal was fed to a Tektronix TDS 2022 two-channel digital storage oscilliscope. The Wavestar program was used to import the oscilloscope signal to the computer and later exported as a Microsoft Excel file for analysis.

Preparation of Perdeutero Sodium Hydroxide (NaOD)

NaOH (2.4 g, 60 mmol) pellets were placed in a Schlenk flask and dissolved in a minimal amount of D_2O. The mixture was heated with water bath (90 ^oC) and dried *in vacuo*. Under inert atmosphere conditions, D_2O was added to the solid and the mixture stirred until the white solid dissolved. The mixture was again dried *in vacuo*. This procedure was repeated three times in order to ensure that all protons had exchanged for deuterons. The resulting white powder was dissolved in 100 mL of D_2O and then transferred and stored in a plastic container with septum in a desiccator.

Preparation of Perdeutero $[Eu_{15}(\mu_5\text{-}Cl)(\mu_3\text{-}OD)_{20}(his^{+/-})_{10}(his^{-})_5(OD_2)_7](ClO_4)_{12}$ (D-Eu_{15}–his Cl)

D-Eu_{15}–his Cl was synthesized by modification of the synthesis of $[Eu_{15}(\mu_5\text{-}Cl)(\mu_3\text{-}OH)_{20}(his^{+/-})_{10}(his^{-})_5(OH_2)_7](ClO_4)_{12}$. A Schlenk flask was charged with $Eu(ClO_4)_3$ (1.0 mL, 1.0 M, in deionized H_2O), L-histidine (0.3104 g, 2.0 mmol), and NaCl (0.058 g, 1.0 mmol). The mixture was heated with water bath (90 ^oC) and dried *in vacuo*. Under inert atmosphere conditions, D_2O was added to the solid and the mixture stirred until the $Eu(ClO_4)_3$ and L-histidine dissolved. The mixture was again dried *in vacuo*. This procedure was repeated three times in order to ensure that all protons had exchanged for deuterons. The solid was dissolved in 10.0 mL of D_2O and heated at 90 ^oC. NaOD (0.6 M) was added dropwise until incipient precipitation was observed. The solution was filtered via a Schlenk frit and left as a clear solution in order to grow crystals, which formed overnight. The crystals were isolated on a Schlenk frit and washed with cold D_2O, and stored in a desiccator prior to use.

Preparation of Perdeutero $[Eu_{15}(\mu_5\text{-}Br)(\mu_3\text{-}OD)_{20}(his^{+/-})_{10}(his^{-})_5(OD_2)_7](ClO_4)_{12}$ (D-Eu_{15}–his Br)

The synthesis and isolation of D-Eu_{15}–his Br was the same as for D-Eu_{15}–his Cl with the exception that NaBr was used instead of NaCl.

Preparation of Perdeutero $[Eu_{15}(\mu_5\text{-}OH)(I)_2(\mu_3\text{-}OD)_{20}(his^{+/-})_{10}(his^{-})_5(OD_2)_7](ClO_4)_{10}$ (D-Eu_{15}–his $(I)_2$-OH)

The synthesis and isolation of D-Eu_{15}–his $(I)_2$-OH was the same as for D-Eu_{15}–his Cl with the exception that NaI was used instead of NaCl.

Preparation of Perdeutero

$[Eu_{15}(\mu_5\text{-}OH)(\mu_3\text{-}OD)_{20}(his^{+/-})_{10}(his^{-})_5(OD_2)_7](ClO_4)_{12}$

(D-Eu_{15}–his OH)

The synthesis and isolation of D-Eu_{15}–his OH was the same as for D-Eu_{15}–his Cl with the exception that no NaX was added.

CHAPTER 5:
ELECTROCHEMICAL STUDIES OF POLYEUROPIUM COMPLEXES

Introduction

Electrochemical studies of metal complexes can reveal useful information including, but not limited to, redox potentials, thermodynamic stability, and diffusion coefficients.[78] Reversible electrochemistry of mononuclear species with one observed reduction or oxidation is well understood. Electrochemistry of polynuclear complexes is interesting because of its ability to investigate multiple redox events. The most widely-cited electrochemistry of polynuclear complexes involves polyoxometallates (POMs) and hexanuclear transition metal complexes.[79]

POMs are large inorganic polyatomic ions usually consisting of three or more octahedral transition metal oxyanions (MO_6), linked together by shared oxides.[79b] The framework of MO_6 encloses one or more tetrahedrally-coordinated heteroatoms, such as PO_4^{3-} or SiO_4^{4-}, in POM heteropolyanions.[79b] These compounds have been used in a wide range of applications in material science, medicine, catalysis, and pigmenting owing to their rich electrochemical and photophysical properties. The ability to accept several electrons is one particularly interesting property of POMs.[79a, b] Redox chemistry of POMs can be altered by changing the metal or type of POM (i.e. Keggin- or Dawson-type).[79a, b, 80]

Octahedral hexanuclear transition metal clusters can also accept multiple electrons. The electrochemistry of hexanuclear clusters is dependent upon the ligands as well as the type of cluster, whether octahedral face-bridged or edge-bridged.[81] Edge-bridged clusters often exhibit a greater number of accessible redox potentials than do face-bridged.[25, 79d]

In contrast to the reported electrochemistry of the aforementioned polynuclear complexes, there has been little discussion of the electrochemistry of polynuclear lanthanide complexes. The majority of literature reports focus on mononuclear species.[78b, c, 82] Of the published electrochemical studies of polynuclear lanthanide complexes, two report upon the electrochemical dynamics. Westin, et. al. reported a mixed Eu(II)/Eu(III) valence polynuclear alkoxide (Figure 5.1) and determined that oxidation of the mixed-valent $[Eu_4(OPr^i)_{10}(HOPr^i)_3]\cdot 2HOPr^i$ by $O_{2(g)}$ affords trivalent $Eu_5O(OPr^i)_{13}$ (Figure 5.2).[52c] The reduction of $Eu_5O(OPr^i)_{13}$ with Eu metal, however, did not afford the $[Eu_4(OPr^i)_{10}(HOPr^i)_3]$ $2HOPr^i$ complex. No further electrochemical characterization was reported. Another report on dinuclear europium(III) β-diketonate complexes determined that cathodic peaks observed by cyclic voltammetry (CV) arose from ligands and that no metal-centered redox processes were observed.[78c]

The solution-state structure and solution chemistry of polynuclear lanthanide complexes is of significant interest to the Messerle reserach group. Herein is described the electrochemical characterization of Eu_{15}–his X complexes.

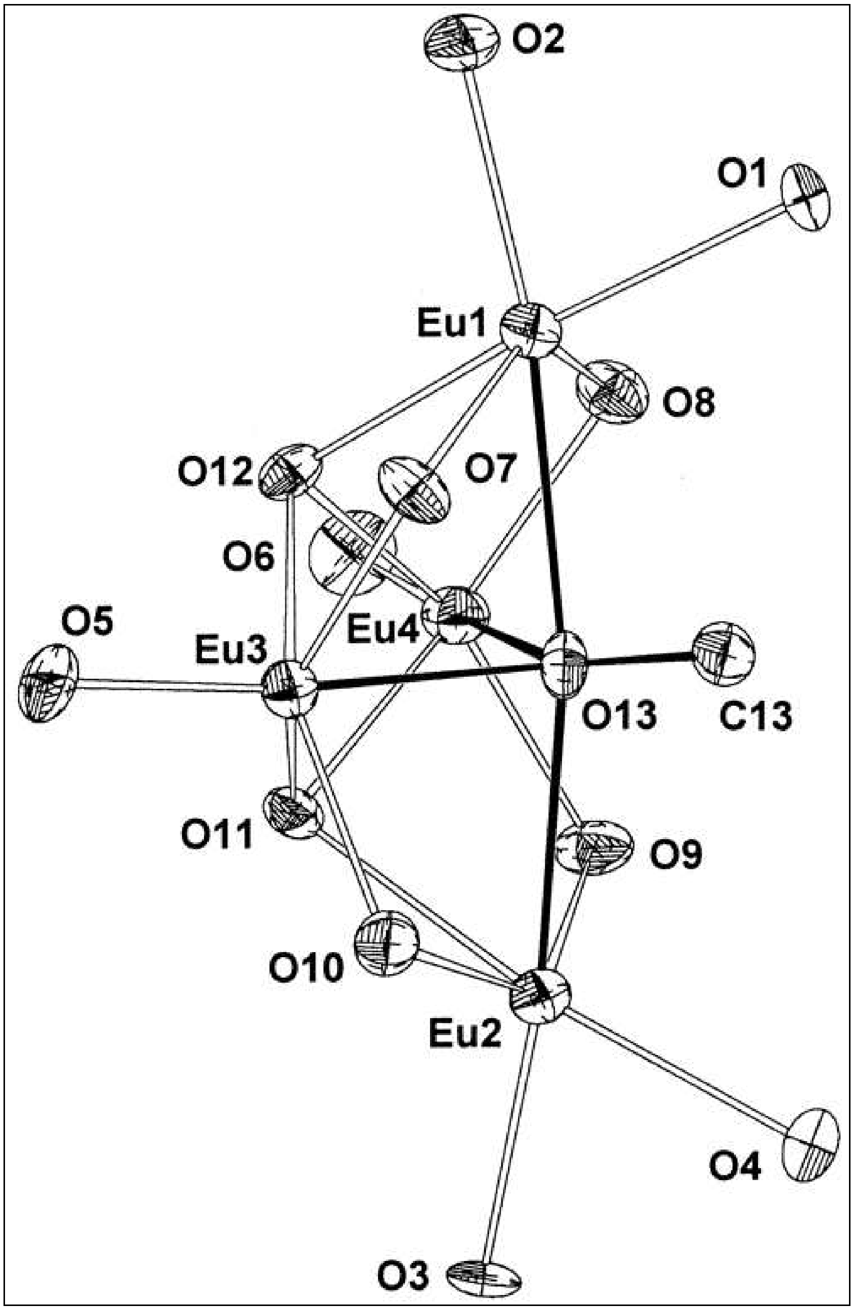

Figure 5.1: ORTEP view (30% probability displacement ellipsoids) of $[Eu_4(OPr^i)_{10}(HOPr^i)_3]\cdot 2HOPr^i$, showing the molecular structure of the metal-oxygen core. Only one molecule from the asymmetric unit is shown.[52c]

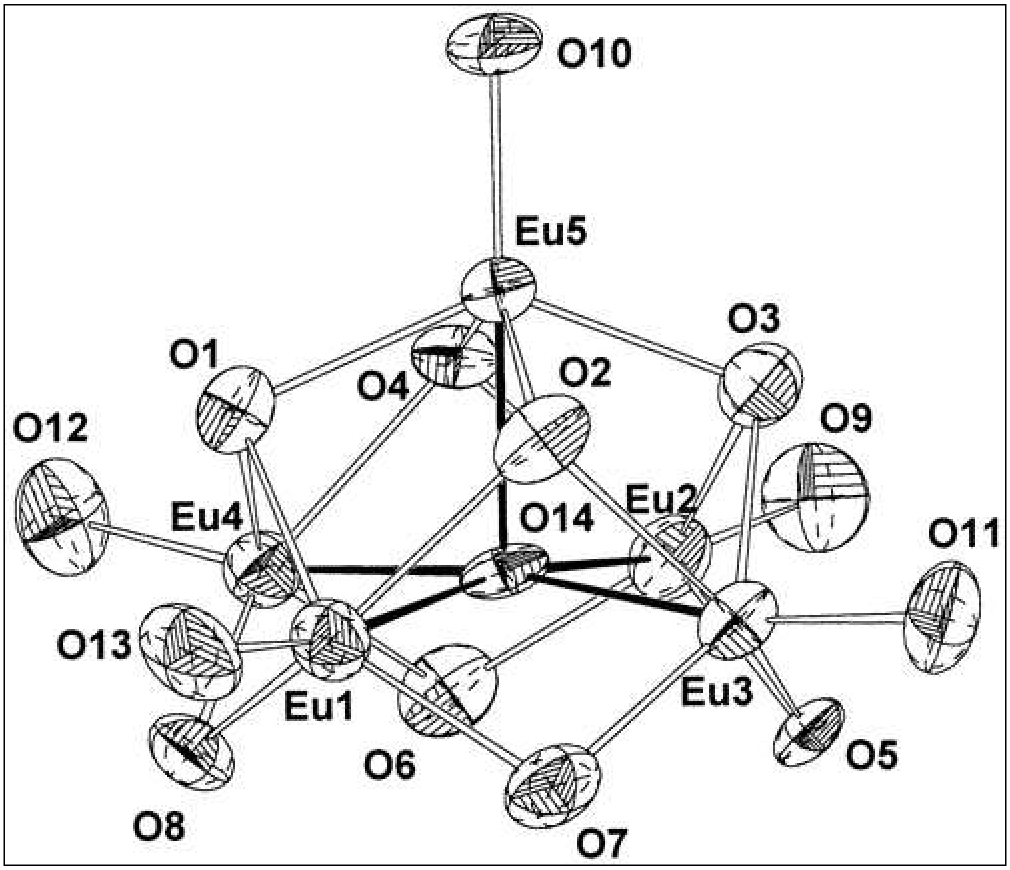

Figure 5.2: ORTEP view (30% probability displacement ellipsoids) of $Eu_5O(OPr^i)_{13}$, showing the molecular structure of the metal-oxygen core.[52c]

Results and Discussion

Cyclic voltammetry (CV) is an electrochemical technique commonly employed in the electrochemical study of a compound. This technique allows for rapid observation of the redox behavior of a compound over a wide potential range. CV consists of cycling the potential of an electrode immersed in an unstirred solution and measuring the resulting current. Potential perturbations of an analyte solution by a working electrode give rise to the observed current. The potential drop between the working and counter electrode is monitored indirectly by the potentiostat by a third electrode. This reference electrode has its own redox potential and insures that the potentials desired are actually applied. Common reference electrodes are saturated calomel electrode (SCE), silver/silver chloride electrode (Ag/AgCl), or a silver/silver oxide reference electrode (Ag/AgO). The Ag/AgO electrode is called a quasi reference electrode because its standard potential changes. Potential is dropped across solution between the working and reference electrode and can be considered as an excitation signal. This signal is a linear potential scan with a triangular waveform as shown in Figure 5.3.[83] The triangular potential is swept between two chosen values. The excitation signal in Figure 5.3 causes the potential to sweep negatively from +0.8 V to -0.2 V, at which point the scan direction is reversed and sweeps positively back to the original potential of + 0.8 V. The dotted lines represent a second scan.[83]

A cyclic voltammogram is obtained by measuring the current at the working electrode during the potential scan. The voltammogram is a plot of the current response versus the applied potential. Figure 5.4 shows a typical CV for a platinum working electrode in an aqueous solution containing 6.0 mM $K_3Fe(CN)_6$ as the electroactive species in 1.0 M KNO_3 as the supporting electrolyte. The initial potential (E_i) of 0.8 V applied (a) is chosen to avoid any electrolysis of $Fe(CN)_6^{3-}$ when the electrode is switched on. The forward scan in the negative direction is indicated by an arrow. $Fe^{III}(CN)_6^{3-}$ begins to reduce when a sufficient negative potential is reached (b). Moving to an even more negative potential rapidly increases the cathodic current response (b → d) until the concentration of $Fe^{III}(CN)_6^{3-}$ at the electrode surface is substantially diminished, causing the current peak (d). The current decays (d → g) as the solution adjacent to the electrode is depleted of $Fe^{III}(CN)_6^{3-}$ due to its electrolytic conversion to $Fe^{II}(CN)_6^{4-}$. The scan direction is switched to positive at -0.15 V (f) for the reverse scan. The potential is still strong enough to reduce $Fe^{III}(CN)_6^{3-}$, so cathodic current continues even though the

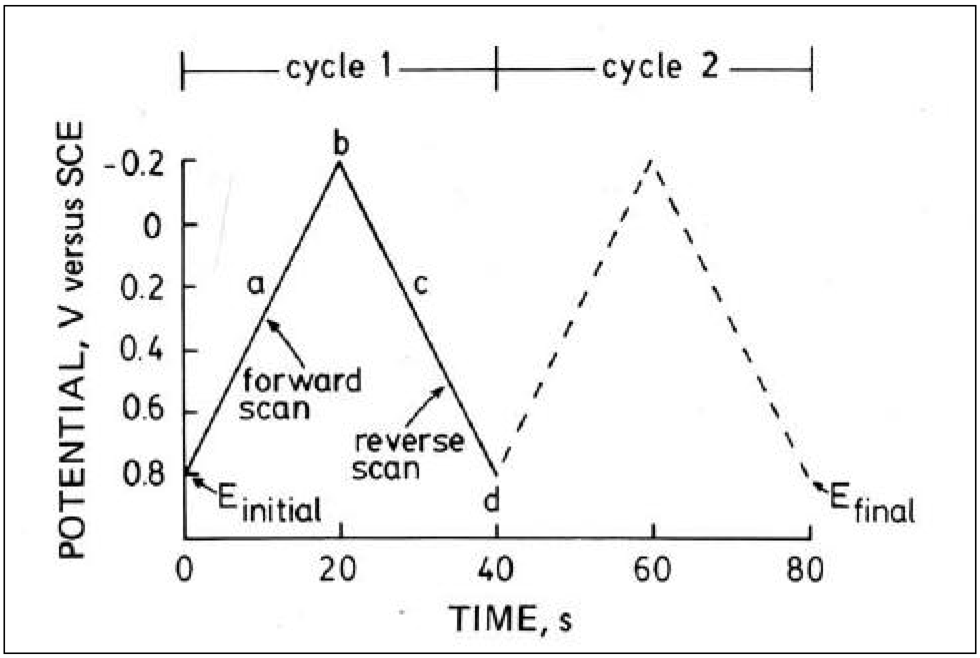

Figure 5.3: Typical signal for cyclic voltammetry, a triangular potential waveform with switching potentials at 0.8 V and -0.2 V versus SCE.[83]

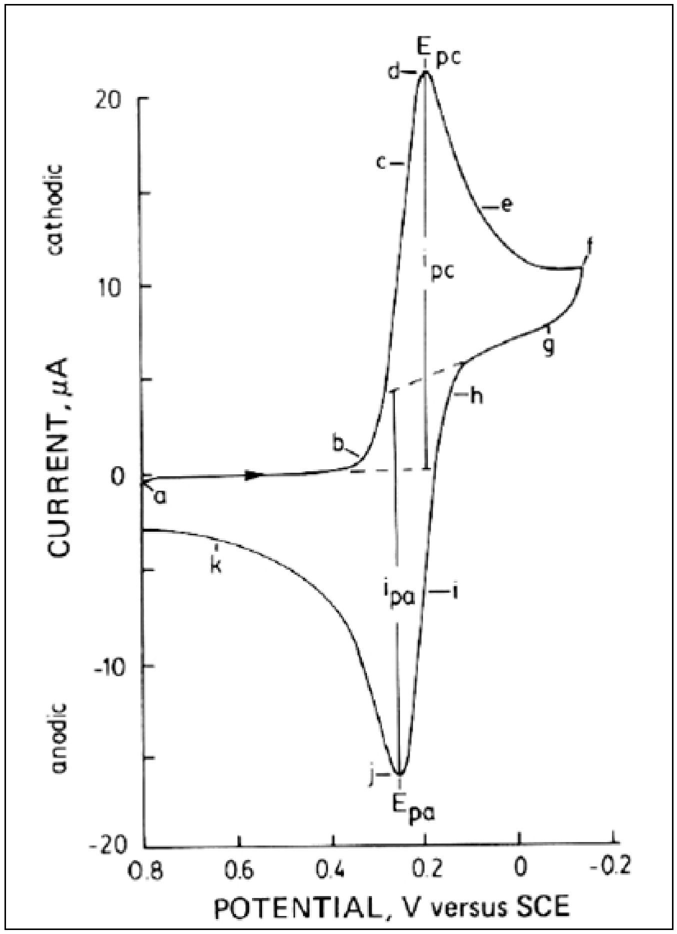

Figure 5.4: Cyclic voltammogram of 6 mM $K_3Fe(CN)_6$ in 1 M KNO_3. Scan initiated at 0.8 V versus SCE in negative direction at 50 mV/s. Platinum electrode, area = 2.54 mm^2.[83]

potential is now scanning in the positive direction. When the potential of the electrode becomes strong enough to oxidize $Fe^{II}(CN)_6^{4-}$, which has been accumulating adjacent to the electrode, anodic current response is observed (i → k). The anodic peak (j) is observed when the $Fe^{II}(CN)_6^{4-}$ surrounding the electrode is diminished. The first cycle is then complete when the potential reaches +0.8 V. The example here provide a basic and fundamental overview of a CV experiment. Several important parameters that can be obtained from CVs include cathodic and anodic peak currents (ip,c and ip,a), cathodic and anodic peak potentials ($E_{p,c}$ and $E_{p.a}$), standard redox potentials (E^o), and half-wave potential for the redox couple ($E_{1/2} = E_{p,a} + E_{p,c/2}$). For a fully reversible redox reaction, the Nernst equation predicts a potential peak splitting of 57.8 mV.

In preliminary experiments, CV was performed in dimethyl sulfoxide (DMSO) on L-histidine and perchlorate solutions without Eu(III) present. Negligible current (i), was observed in the potential window of 0 to -4 V vs. Ag quasi reference electrode (Ag QRE). DMSO was selected as the solvent for two reasons: (1) organic solvents allow for a wider potential range of study; and (2) aside from dimethyl formamide (DMF), DMSO is the only organic solvents that fully dissolves Eu_{15}-his X. Figure 5.5 shows the i-V response (CV) of $Eu(ClO_4)_3$ in DMSO at different scan rates, v = 0.01 to 0.12 V/s. Figure 5.6 shows the CV of $[Eu_4(\mu_3\text{-}OH)_4(pro)_6(OH_2)_7]^{6-}$ in DMSO at different scan rates, v = 0.01 to 0.12 V/s. The CVs of $[Eu_{15}(\mu_5\text{-}X)(\mu_3\text{-}OH)_{20}(his^{+/-})_{10}(his^-)_5(OH)_7]^{12-}$ in DMSO at different scan rates, v = 0.01 to 0.12 V/s, are shown in Figures 5.7 for X = Cl, 5.8 for X = Br, 5.9 for X = $(I)_2$-OH, and 5.10 for X= OH. The redox potentials of these complexes were determined from CVs not shown here. Common reference electrodes such as saturated calomel (SCE) or Ag/AgCl electrodes are aqueous-based and incompatible with organic solvents. Thus, a Ag QRE was employed in the DMSO solvent systems. The reference electrode was standardized against the $[Ru(NH_3)_6]Cl_3$ redox system and potentials for $Eu(ClO_4)_3$, Eu_4, and all Eu_{15}-his X are given in Table 5.1. When CVs of $Eu(ClO_4)_3$ are compared to those of polyeuropium complexes, the peak potentials for polyeuropium complexes shift to more negative potentials in DMSO. It is unclear if there were multiple species in solution. CV is a very sensitive technique but lacks selectivity. This makes interpretation difficult especially in a system where the number of electrons being transferred and the solution-state species are unknown. Redox stability is measured by the reduction potentials of the $Eu^{III}_{complex}/Eu^{II}_{complex}$ couple, with more negative potential meaning lower redox stability against oxidation. This observation has been demonstrated in literature using monoeuropium complexes with chelating ligands and macrocycles.[78b, 84]

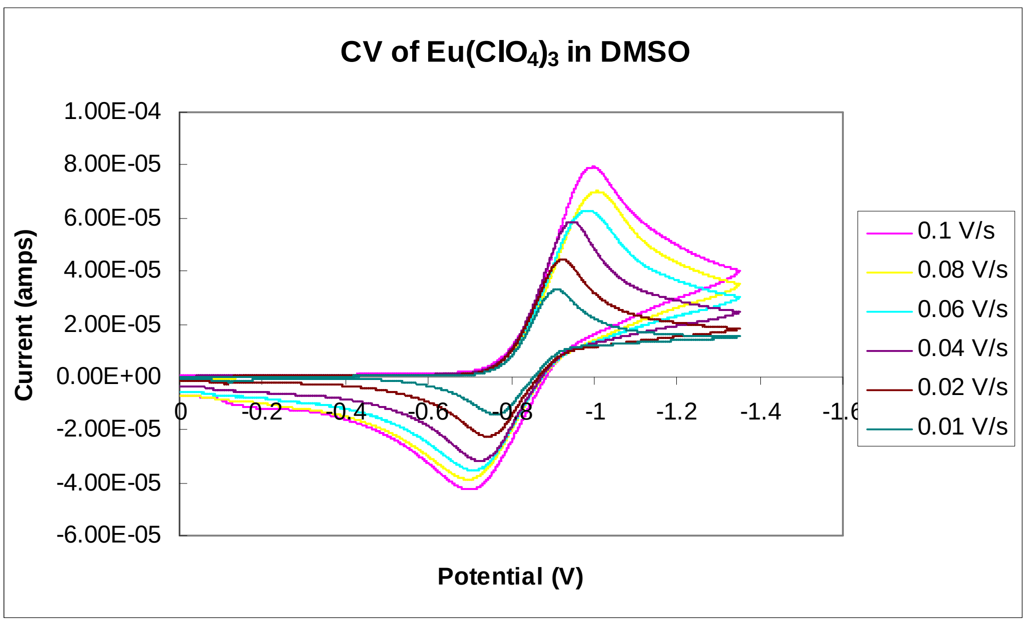

Figure 5.5: Cyclic voltammogram of $Eu(ClO_4)_3$ in DMSO at multiple scan rates with tetrabutylammonium perchlorate as the supporting electrolyte.

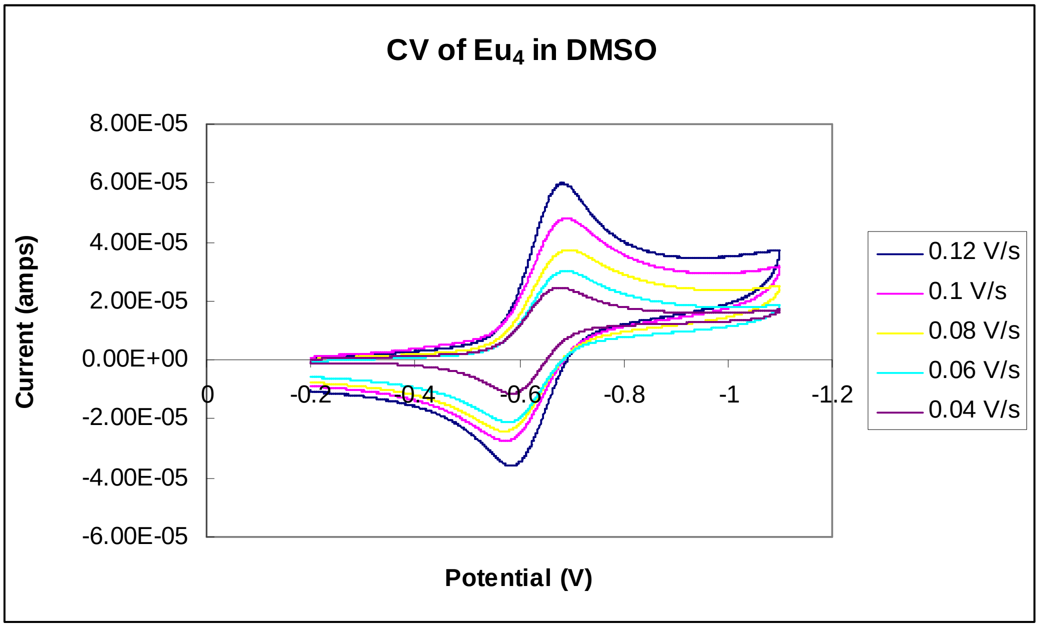

Figure 5.6: Cyclic voltammogram of $[Eu_4(\mu_3\text{-}OH)_4(pro)_6(OH)_2](ClO_4)_6$ in DMSO at multiple scan rates with tetrabutylammonium perchlorate as the supporting electrolyte.

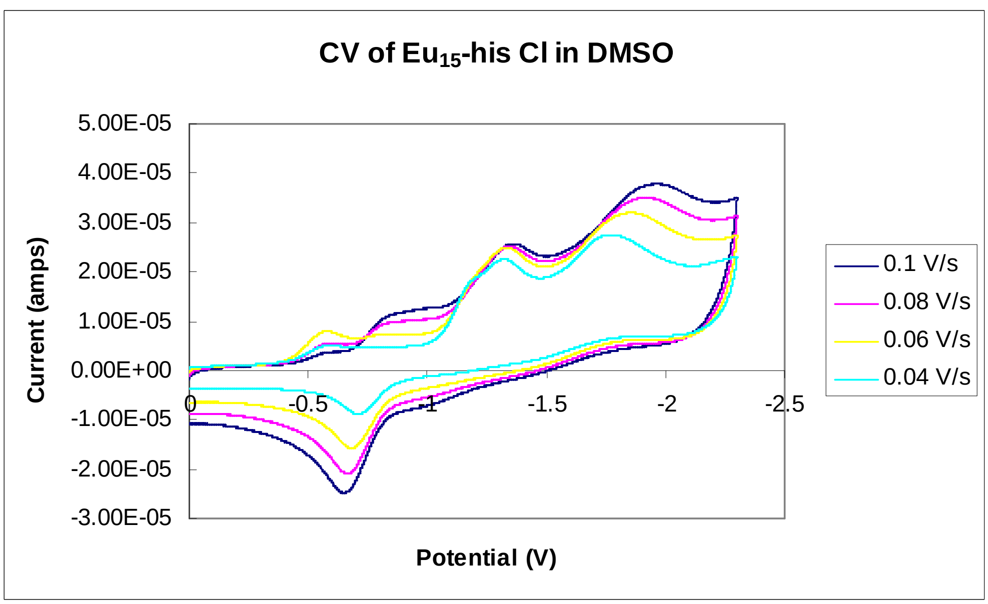

Figure 5.7: Cyclic voltammogram of $[Eu_{15}(\mu_5\text{-}Cl)(\mu_3\text{-}OH)_{20}(his^{+/-})_{10}(his^{-})_5(OH)_7](ClO_4)_{12}$ in DMSO at multiple scan rates with tetrabutylammonium perchlorate as the supporting electrolyte.

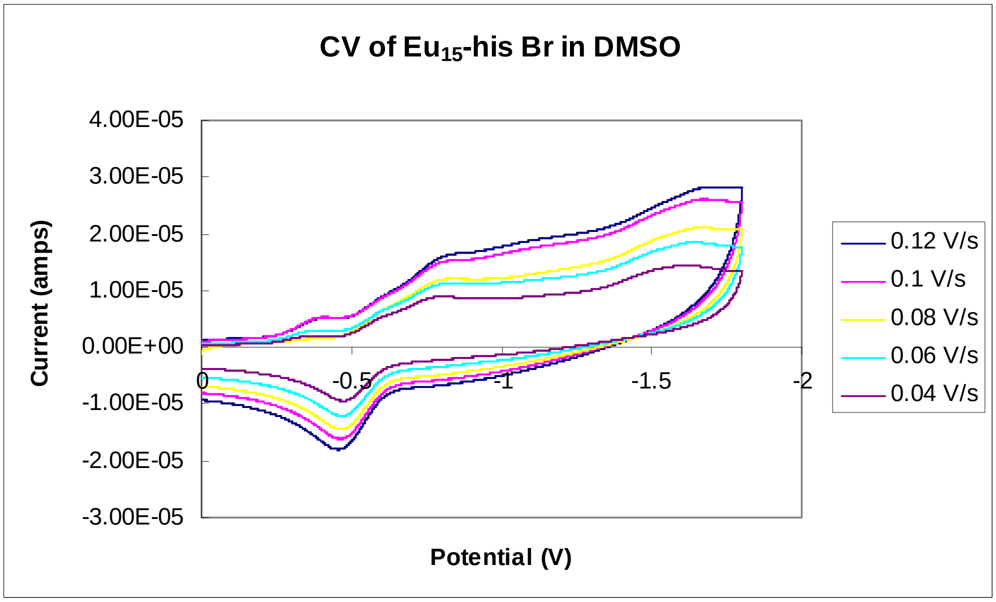

Figure 5.8: Cyclic voltammogram of $[Eu_{15}(\mu_5\text{-Br})(\mu_3\text{-OH})_{20}(his^{+/-})_{10}(his^{-})_5(OH)_7](ClO_4)_{12}$ in DMSO at multiple scan rates with tetrabutylammonium perchlorate as the supporting electrolyte.

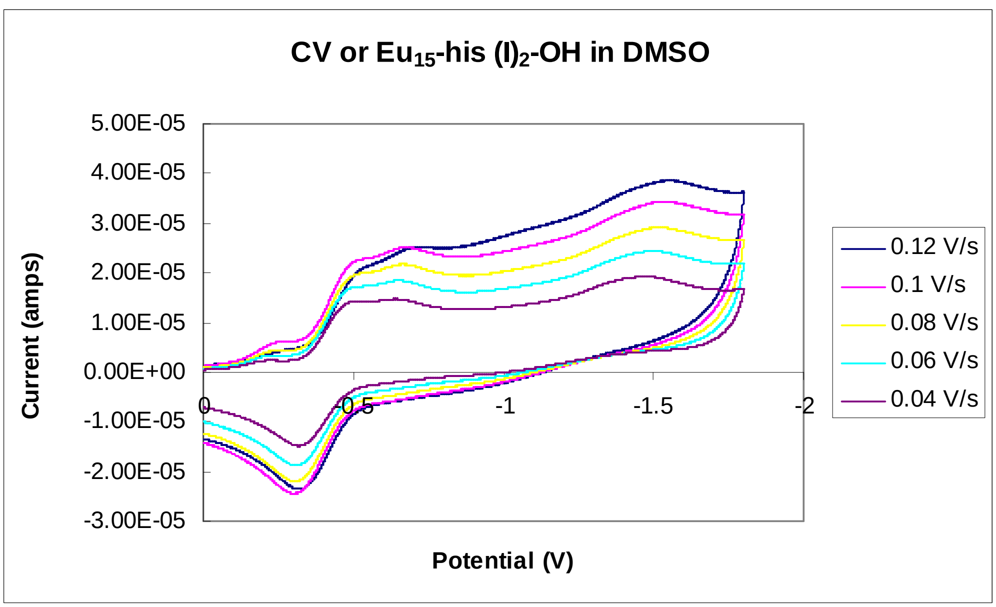

Figure 5.9: Cyclic voltammogram of $[Eu_{15}(\mu_5\text{-OH})(I)_2(\mu_3\text{-OH})_{20}(his^{+/-})_{10}(his^{-})_5(OH)_7]$ $(ClO_4)_{10}$ in DMSO at multiple scan rates with tetrabutylammonium perchlorate as the supporting electrolyte.

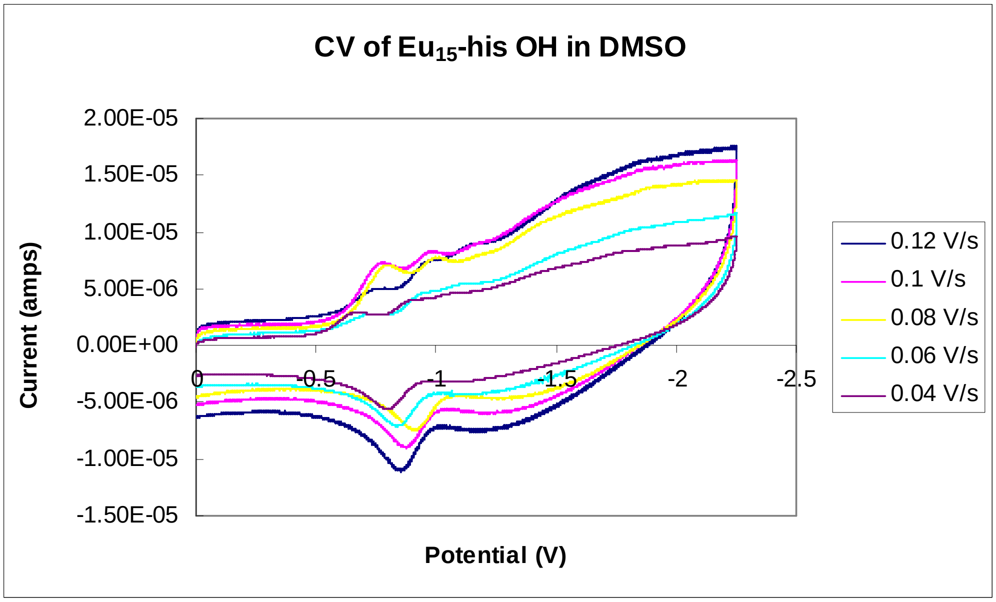

Figure 5.10: Cyclic voltammogram of $[Eu_{15}(\mu_5\text{-}OH)(\mu_3\text{-}OH)_{20}(his^{+/-})_{10}(his^{-})_5(OH)_7](ClO_4)_{12}$ in DMSO at multiple scan rates with tetrabutylammonium perchlorate as the supporting electrolyte.

The redox potential of a given $Eu^{III}L/Eu^{II}L$ (L = ligand) couple depends on the relative thermodynamic stabilities of the $Eu^{III}L$ and $Eu^{II}L$ complexes (Equation 5.1). The higher the stability constant for the oxidized complex ($Eu^{III}L$), as compared to that of the reduced form ($Eu^{II}L$), the more negative the redox potential will be. Differences in E^o between the complexed and uncomplexed one-electron redox couples ($\Delta E_{1/2}$) is directly related to the ratio of the stability constants:

$$\Delta E_{1/2} = E_{1/2,complexed} - E_{1/2,uncomplexed} = \frac{RT}{F}\ln\left(\frac{K^{II}}{K^{III}}\right) \qquad (5.1)$$

where K^{III} and K^{II} are the thermodynamic stability constants of the oxidized and reduced forms, respectively, R is the gas constant, T is temperature, and F is Faraday's constant.[78b] By these arguments, the reduced Eu_{15}-his X complexes are less stable than the oxidized form.

Table 5.1: List of reduction potentials for several Eu(III) complexes at 25 ^{o}C.

Compound	**$E_{1/2}$ vs SHE (V)**
$Eu(ClO_4)_3$	-0.36
Eu_4	-0.40
Eu_{15}-his Cl	-0.41
Eu_{15}-his Br	-0.42
Eu_{15}-his $(I)_2$-OH	-0.40
Eu_{15}-his OH	-0.40

For a reversible redox reaction, Ox + ne^- = Red (Ox = Eu(III), Red = Eu(II) in this work), the current response from a CV is given by the following equation:

$$i_p = 2.99x10^5 n(\alpha n_a)^{1/2} AC_o^* D_o^{1/2} v^{1/2} \quad (5.2)$$

where i_p is the peak current (Amps), n is the number of electrons transferred, α is the transfer coefficient, n_a is the number of electrons transferred in the rate-determining step, A is the surface area of the working electrode (cm^2), C_o^* is the concentration of species Ox (mol/cm^3), D_o is the diffusion coefficient of species Ox (in cm^2/s), and v is the scan rate (V/s).[78a] The αn_a term can be obtained from the E_p at i = i_p and potential, $E_{p/2}$, at i = $i_{p/2}$:

$$\left| E_{p/2} - E_p \right| = 1.857 \frac{RT}{\alpha n_a} F = \frac{0.0477}{\alpha n_a} \quad at \;\; 25^o C \quad (5.3)$$

where F and R are Faraday and molar gas constants, respectively.[78a] Determination of parameters such as D_o and C_o^* is possible using both Equations 5.2 and 5.3.

Diffusion coefficients for the complexes were determined by plotting i_p vs $v^{1/2}$ and are listed in Table 5.2. The slope of the expected linear agreement is then m = 2.99 $x10^5 n(\alpha n_\alpha)^{1/2} AC_o^* D_o^{1/2}$, for a known C_o^*, D_o can be calculated. These D_o values were verified by another electrochemical experiment, rotating disk electrode voltammetry

(RDE). CV uses a linear sweep waveform that is cycled, whereas RDE voltammetry uses a linear sweep waveform that is not cycled. The difference is the electrode in RDE is rotated in order to create convection of the solution. This convection continuously supplies fresh analyte to the electrode surface, thus the current response is no longer diffusion limited. Instead, a steady-state current response is obtained. The steady-state current response shows a sigmoid shape on a current versus potential plot (voltammogram). Important parameters to consider in RDE are the rotation rate of the electrode (*w*) and the viscosity of the solution (*v*). The voltammogram that results from an RDE experiment shares characteristics with those from CV experiments. Due to the steady-state flux of reactant to the electrode surface, the resulting i-V curve is sigmoidal. Similarly to CV, a scan is initiated at a potential where no faradaic current flows, ramped linearly until sufficiently past the E^o required for electrolysis of the redox species. Thus, as shown in Figures 5.11 through 5.16, the current can be quantified by measuring the limiting current (i_l) plateau that arises from the steady-state electrolysis. The magnitude of current as measured from zero current to a best-fit line through the final current plateau is a good estimate of i_l. When a compound has more than one redox event possible, several plateaus will be observed in the RDE voltammogram. Figure 5.11 shows the RDE voltammogram of $Eu(ClO_4)_3$ in DMSO at different rotation rates, 400 – 1400 rpm (at 200 rpm intervals). Figure 5.12 shows the RDE voltammogram of $[Eu_4(\mu_3\text{-}OH)_4(pro)_6(OH)_2]^{6+}$ in DMSO at different rotation rates, 400 – 1400 rpm (at 200 rpm intervals). The RDE voltammograms of $[Eu_{15}(\mu_5\text{-}X)(\mu_3\text{-}OH)_{20}(his^{+/-})_{10}(his^{-})_5(OH)_7]^{12+}$ in DMSO at different rotation rates, 400 – 1400 rpm, are shown in Figures 5.13 for X =Cl, 5.14 for X = Br, 5.15 for X = $(I)_2$-OH, and 5.16 for X= OH. The current response from RDE voltammetry is given by the Levich equation:

$$i_l = 0.620 nFAD_o^{2/3}\omega^{1/2}v^{-1/6}C_o^* \qquad (5.4)$$

where i_l is the limiting peak current (Amps), n is the number of electrons in the rate-determining step, F is Faraday's constant, A is the area of the electrode (cm^2), D is the diffusion coefficient (cm^2/s), ω is the angular frequency of rotation (2π x rotation rate, s^{-1}), ν is the kinematic viscosity of solution (for DMSO, 1.861 x10^{-2} cm^2/s),[85] and C_o^* is the concentration of species Ox (mol/cm^3).[78a] Diffusion coefficients for the complexes were determined by plotting i_p vs $\omega^{1/2}$. The slope of the expected linear agreement is then $m = 0.620nFAC_o^*D_o^{2/3}$; for a known C_o^*, D_o can be calculated.

Table 5.2: Table of experimental and theoretical diffusion coefficients for several Eu(III) complexes.

	D_o in DMSO (x10^{-6} cm^2/s)	**Theoretical D_o Range (x10^{-6} cm^2/s)**
$Eu(ClO_4)_3$	4.77	N/A
Eu_4	2.99	1.88
Eu_{15} Cl	0.12(7)	2.82 - 6.17
Eu_{15} Br	0.17(6)	2.83 - 6.11
Eu_{15} $(I)_2$-(OH)	0.2(1)	2.78 - 6.07
Eu_{15} OH	0.2(2)	3.06 - 6.12

Theoretical diffusion coefficients listed in Table 5.2, were calculated using the Einstein-Stokes equation:

$$D = \frac{k_B T}{6\pi\eta\ r} \tag{5.5}$$

where D is the diffusion coefficient (cm^2/s), k_B is Boltzmann's constant, T is the absolute temperature (K), η is the viscosity, and r is the radius of the molecule. Rearrangement of Equation 5.5 results in a simple ratio by which to compare similar systems:[78a]

$$r_1 D_1 \approx r_2 D_2 \tag{5.6}$$

where r_1 is the radius (Å) of compound 1, D_1 is the diffusion coefficient of compound 1, r_2 is the radius (Å) for compound 2, and D_2 is the diffusion coefficient of compound 2. The radii of compounds 1 and 2 were determined from X-ray crystallographic data. Theoretical diffusion coefficients were calculated from the CVs of $Eu(ClO_4)_3$ in DMSO as compound 1. The ratio in Equation 5.6 is a reasonable estimate for spherical molecules and will be used here as a gross approximation.

The theoretical diffusion coefficients were calculated from two different crystallographic radii. It has been demonstrated that several of the ligands on Eu_{15}-his Cl are dynamic and very labile, thus both radii were used as shown in Table 5.3. The fully ligated molecule (Figure 5.15) and molecule with excised exterior ligands (Figure 5.16) are both shown.

Table 5.3: Crystallographic radii used to determine theoretical diffusion coefficients.

Compound	**Fully Ligated radius (Å)**	**Exterior Ligands Excised (Å)**
Eu_{15}-his Cl	10.825	4.955
Eu_{15}-his Br	10.802	5.002
Eu_{15}-his $(I)_2$-OH	10.990	5.037
Eu_{15}-his OH	9.995	4.998

The measured diffusion coefficients are slower than the theoretical diffusion coefficients. Despite estimating theoretical values by Equation 5.6, these values provide valuable information concerning the identity of the species in solution. It is expected for the calculated values to be larger than theoretical values since the latter do not account for ligand-solvent interactions. Also, because Eu_{15}-his X complexes are not spherical, as assumed by Equation 5.5, the diffusional movement through solution is not considered

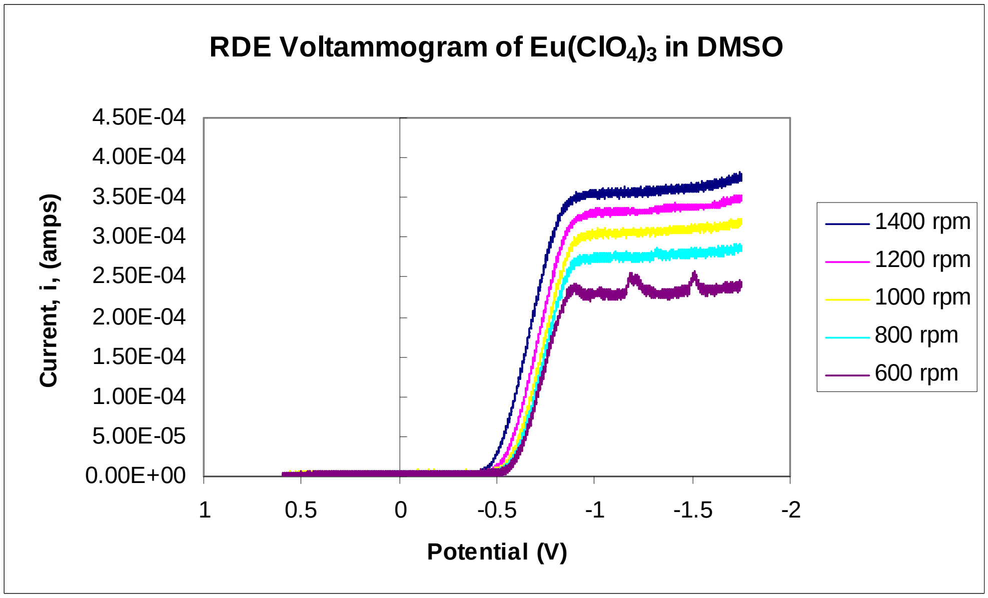

Figure 5.11: Rotating disk electrode (RDE) voltammogram of $Eu(ClO_4)_3$ in DMSO at multiple rotation rates with tetrabutylammonium perchlorate as the supporting electrolyte. The blips in the 600 rpm scan are from physically bumping the apparatus.

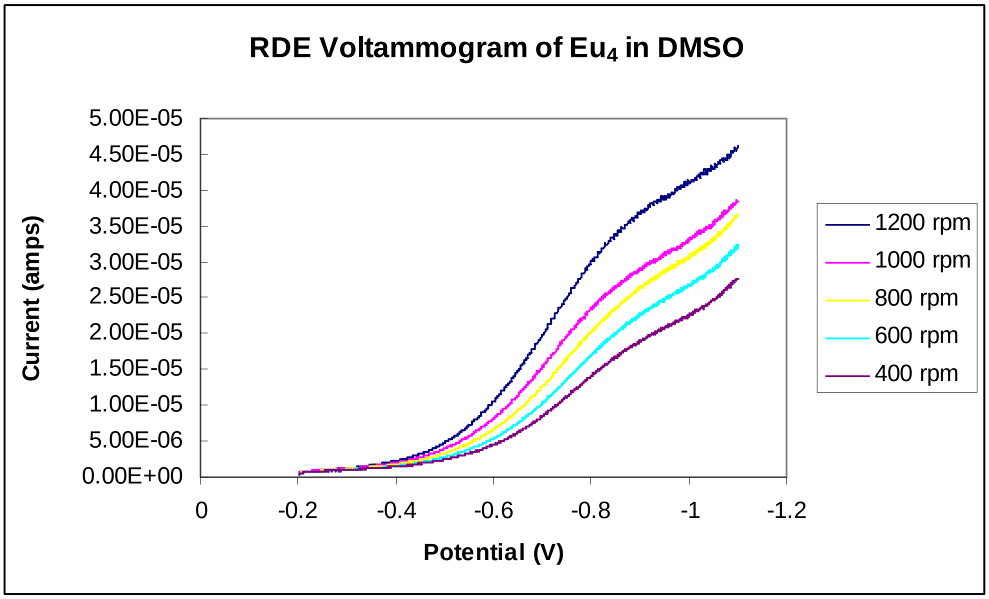

Figure 5.12: RDE voltammogram of $[Eu_4(\mu_3\text{-}OH)_4(pro)_6(OH)_2](ClO_4)_6$ in DMSO at multiple rotation rates with tetrabutylammonium perchlorate as the supporting electrolyte.

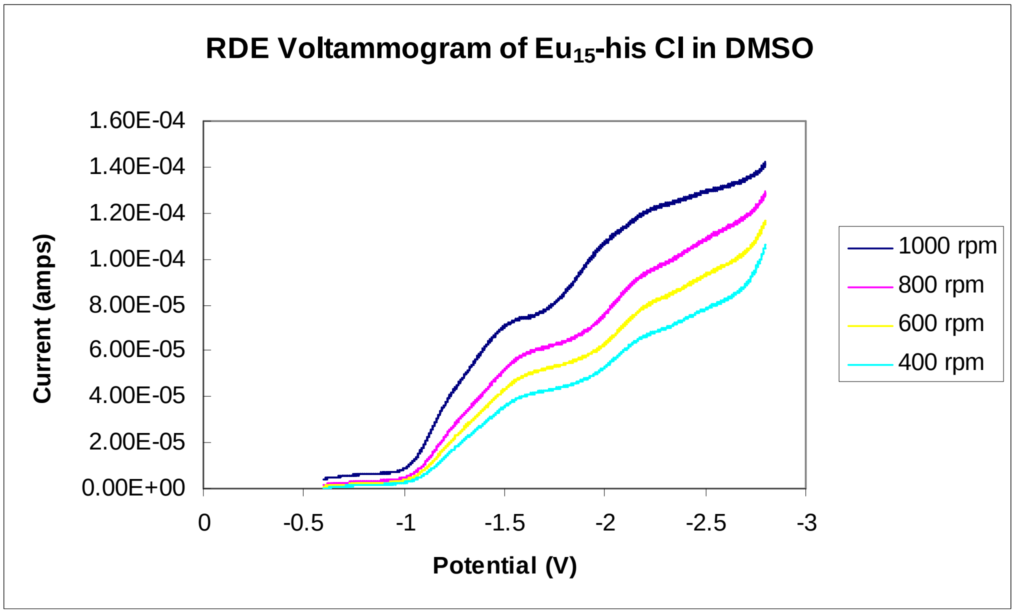

Figure 5.13: RDE voltammogram of $[Eu_{15}(\mu_5\text{-}Cl)(\mu_3\text{-}OH)_{20}(his^{+/-})_{10}(his^{-})_5(OH)_7](ClO_4)_{12}$ in DMSO at multiple rotation rates tetrabutylammonium perchlorate as the supporting electrolyte.

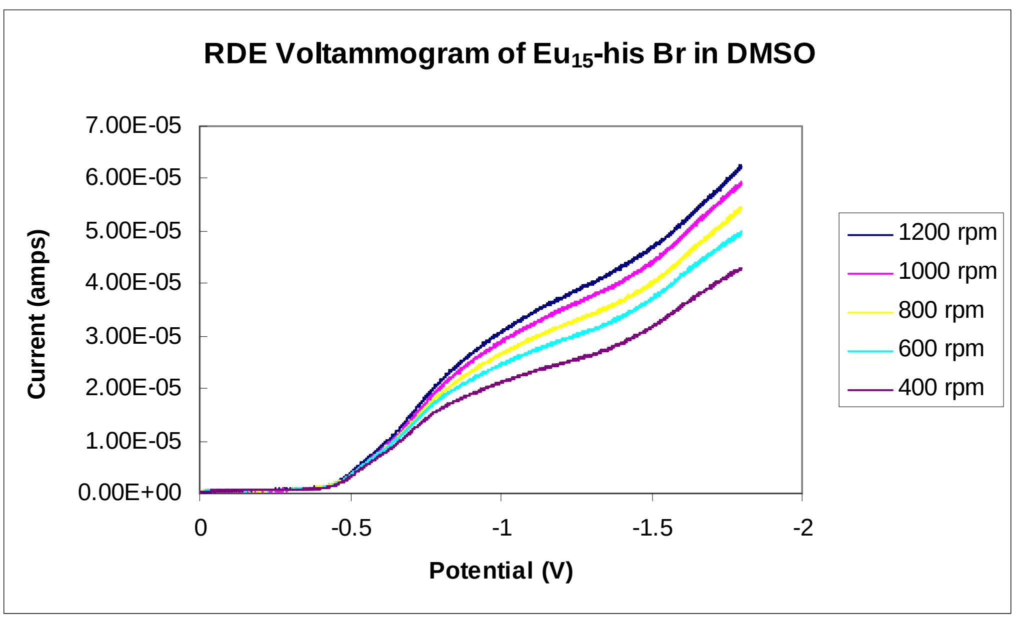

Figure 5.14: RDE voltammogram of $[Eu_{15}(\mu_5\text{-}Br)(\mu_3\text{-}OH)_{20}(his^{+/-})_{10}(his^{-})_5(OH)_7](ClO_4)_{12}$ in DMSO at multiple rotation rates with tetrabutylammonium perchlorate as the supporting electrolyte.

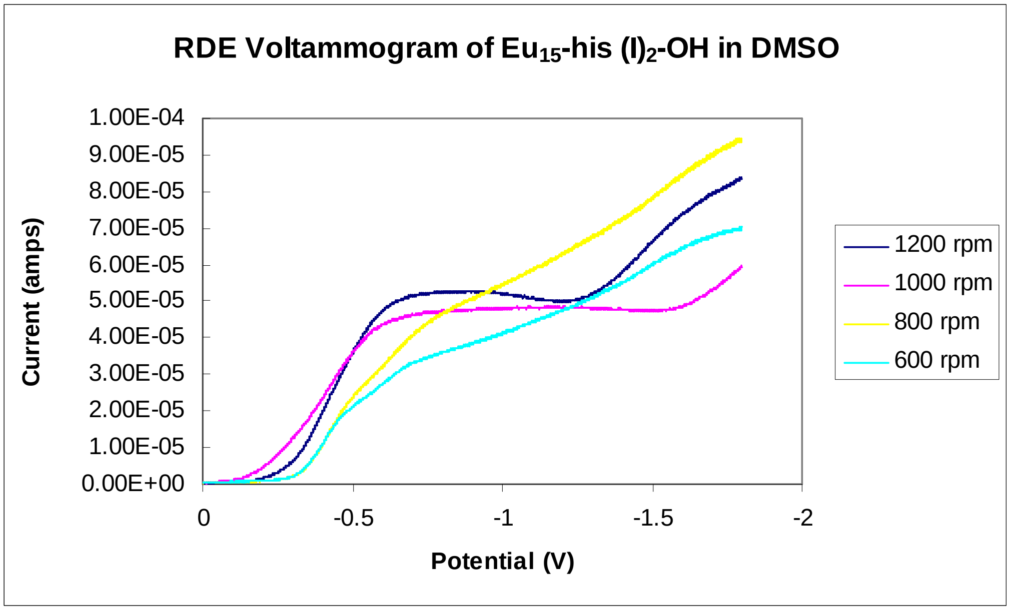

Figure 5.15: RDE voltammogram of $[Eu_{15}(\mu_5\text{-}OH)(I)_2(\mu_3\text{-}OH)_{20}(his^{+/-})_{10}(his^{-})_5(OH)_7](ClO_4)_{10}$ in DMSO at multiple rotation rates with tetrabutylammonium perchlorate as the supporting electrolyte.

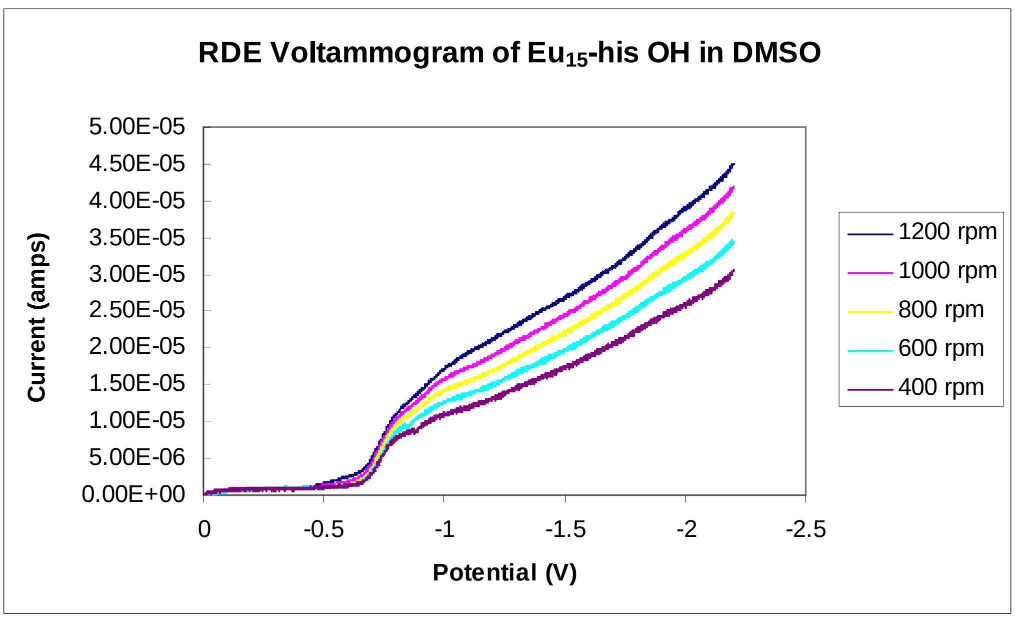

Figure 5.16: RDE voltammogram of $[Eu_{15}(\mu_5\text{-}OH)(\mu_3\text{-}OH)_{20}(his^{+/-})_{10}(his^{-})_5(OH)_7](ClO_4)_{12}$ in DMSO at multiple rotation rates with tetrabutylammonium perchlorate as the supporting electrolyte.

in the equation. Solvent interactions with DMSO, a highly coordinating solvent, would slow the diffusion of a complex in solution. Since the experimental D_o values are slower than the theoretical D_o, it is reasonable to conclude that there are solvent interactions with the Eu_{15}-his X complexes. It is unclear if the interactions are between Eu-coordinated histidine ligands and DMSO or between the Eu_{15}-his X core and DMSO. In either case, the D_o values are much lower than that for $Eu(ClO_4)_3$ in DMSO. This suggests that the species observed in the Eu_{15}-his X trials is much larger than that of $Eu(ClO_4)_3$. It is unclear if the Eu_{15}-his X core is maintained in DMSO solution.

Cyclic and rotating disk voltammograms both suggest multiple one-electron reductions during potential perturbation. There are no corresponding anodic (oxidative) waves observed in the CVs of the Eu_{15}-his X complexes; however, the oxidation wave of Eu(II) is observable. The lack of complementary oxidative peaks for each reductive peak has several implications. First, the reduction of these complexes may be an irreversible process. The irreversibility may arise because of destruction or degradation of the polynuclear complex. The decreased charge on the metal center decreases the Lewis acidity of the metal and, thus, decreases the stability of the interaction with hard Lewis bases (i.e. the carboxylate groups). It is possible that this destabilization causes the ligand coordination to become more labile and thus exchangeable with solvent molecules, effectively causing the destruction of the complex. Other possibilities which could account for observed irreversibility are given in Figure 5.19.[78a] Several of the paths depicted could be possible for Eu_{15}-his X complexes. Heterogeneous electron transfer reactions ($O + ne^- \rightarrow R$) at the electrode surface are the simplest case of redox reactions. Many of the possible pathways shown arise because of reaction kinetics. Several pathways in Figure 5.19, however, also involve kinetic considerations, such as homogeneous reactions (reactions in bulk solvent). Kinetic considerations are more significant in the homogenous case. These possibilities were not experimentally studied.

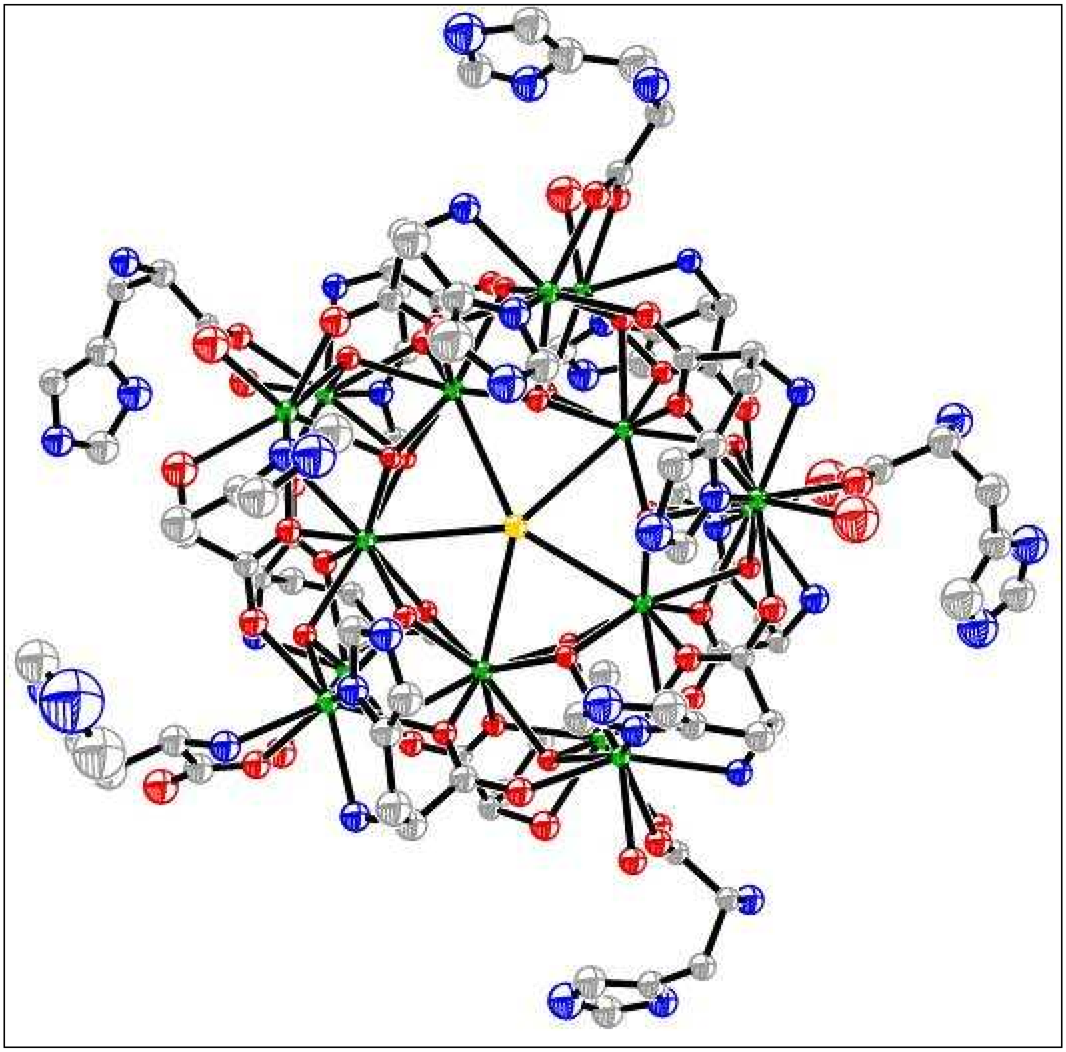

Figure 5.17: $[Eu_{15}(\mu_5\text{-}X)(\mu_3\text{-}OH)_{20}(his)_{15}(OH_2)_7](ClO_4)_{12,}$ fully ligated. Perchlorate anions omitted for clarity. Color scheme: green, Eu(III);yellow, chloride; gray, carbon, blue, nitrogen; red, oxygen.

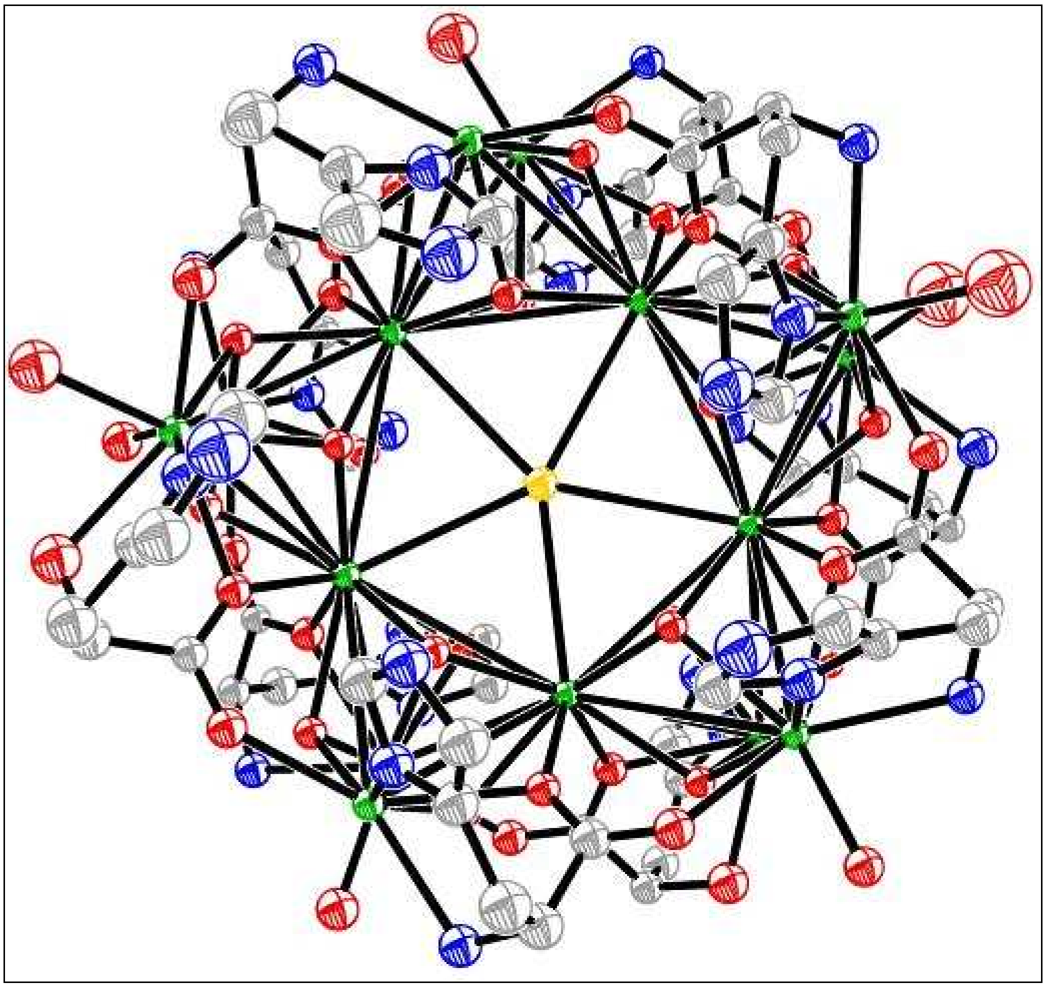

Figure 5.18: $[Eu_{15}(\mu_5\text{-}X)(\mu_3\text{-}OH)_{20}(his)_{15}(OH_2)_7](ClO_4)_{12}$, exterior ligands excised. Perchlorate anions omitted for clarity. Color scheme: green, Eu(III);yellow, chloride; gray, carbon, blue, nitrogen; red, oxygen.

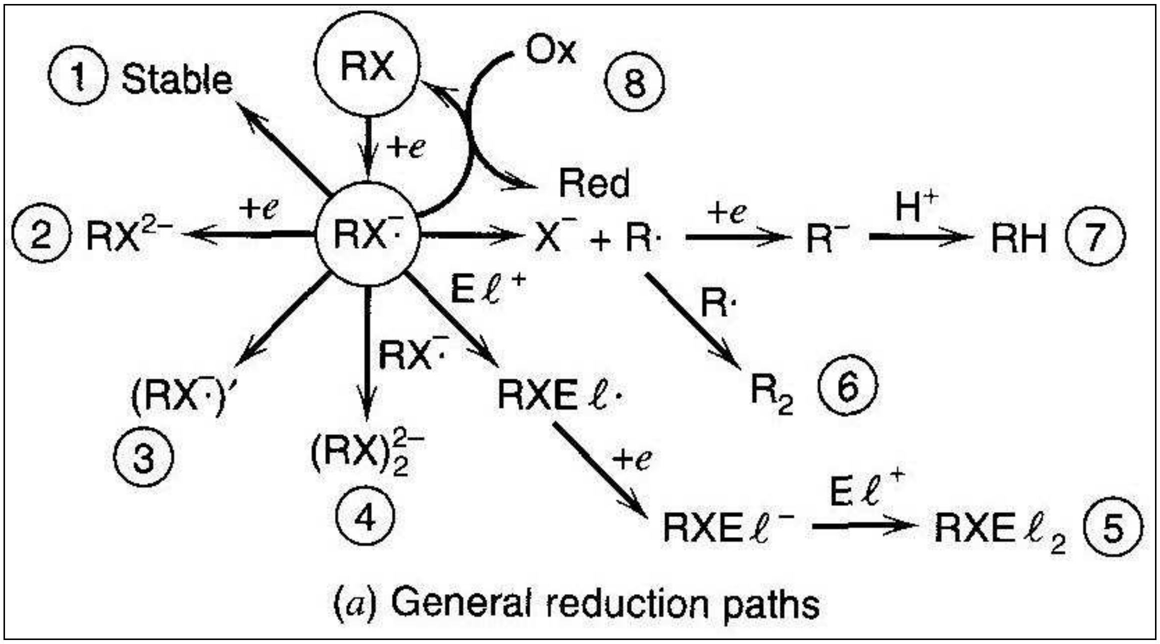

Figure 5.19: Schematic representation of possible reaction paths following reduction of species RX. (a) Reduction paths leading to (1) stable reduced species, such as a radical anion; (2) uptake of a second electron; (3) rearrangement; (4) dimerization; (5) reaction with an electrophile to produce a radical followed by an additional electron transfer and further reaction; (6) loss of X^- followed by dimerization; (7) loss of X^- followed by a second electron transfer and protonation; (8) reaction with an oxidized species, Ox, in solution.[78a]

The numerous possibilities for the fate of the Eu_{15}-his X complexes demonstrates the need for more rigorous and exploratory investigation into the solution kinetics of these system. This may be achieved experimentally but also through the use of modeling and electrochemical simulations.

Another possible explanation for the lack of a corresponding oxidative wave is that the perchlorate anion, an oxidative (E^o = 0.56 V) species that is used as the counterion for these complexes, is not merely a spectator ion.[86] It is possible that as Eu_{15}^{III}-his X complexes are reduced to Eu_{15}^{II}-his X, they are immediately oxidized back to Eu_{15}^{III}-his X by perchlorate. For this reason, attempts to produce the tosylate and triflate salts of these complexes have been performed. These attempts are commented upon in Chapter 2. Eu(II) is also known to be susceptible to photooxidation.[87] Competitive oxidative processes may explain the lack of corresponding oxidative peaks in voltammetric studies.

Conclusions

Redox potentials and diffusion coefficients were determined from electrochemical measurements of the Eu_{15}-his X series. Diffusion coefficients were slower than theoretically-calculated values based on crystallographic radii. This suggests solute-solvent interaction. The diffusion coefficients are also much slower than that of $Eu(ClO_4)_3$ in DMSO, suggesting that the species observed in the Eu_{15}-his X studies is much larger than that of $Eu(ClO_4)_3$. It appears that Eu_{15}-his X complexes are capable of multiple one-electron reductions. However, because the redox potentials of Eu_{15}-his X complexes shift to more negative values as compared to that of aqueous Eu(III), these reduced complexes are not as electrochemically stable as the oxidized forms. The absence of complementary oxidative waves in CV analysis further suggests instability of these reduced complexes. It is possible that these complexes begin to disassemble/degrade upon reduction based on changes in Lewis acidity. Other possibilities include the immediate oxidation of the reduced complex by competitive oxidative processes, such as chemical oxidation by perchlorate ion or photooxidation. Many of these possibilities are summarized in Figure 5.19.

Overall, the electrochemistry of Eu_{15}-his X complexes may be much more convoluted than expected. Kinetic relationships of oxidized and reduced forms and subsequent electron transfer leads to many questions, most of which have not been addressed by the work presented. Further electrochemical study of these systems should focus on these aspects and will be aided by CV simulations and modeling.

Experimental

General Considerations:

All electrochemical experiments were performed in anhydrous dimethyl sulfoxide (DMSO, Acros) with tetrabutylammonium perchlorate (TBAP, Fluka) in 100-fold excess as the supporting electrolyte. Eu_{15}-his X samples were collected and dried on a frit prior to use. In a typical experiment 0.1 g of Eu_{15}-his X was dissolved in 10 mL of anhydrous DMSO under inert atmosphere conditions. Analyte solutions were purged with $Ar_{(g)}$ for 10 minutes prior to use.

Cyclic voltammetry (CV) was performed at 25 +/-1 ^{o}C under $Ar_{(g)}$ atmosphere with a CH Instruments Model 760B Series Electrochemical Analyzer/Workstation interfaced to a PC. A three electrode system was utilized: glassy carbon working electrode (CH Instruments Inc., Part Number CHI 104, surface area 0.0562 cm^2), Pt wire counter electrode (Alfa Aesar), and a Ag QRE (prepared from polished silver wire (Strem) immersed in concentrated HNO_3 for five minutes and then washed with de-ionized H_2O). Cyclic voltammograms were recorded at different scan rates in order to determine electrochemical parameters such as diffusion coefficients (D_o) of the complexes. D_o values were calculated using a modified Radles-Sevčik equation (Equation 5.2).[78a]

Rotating disk electrode (RDE) voltammetry experiments were conducted at 25 +/-1 ^{o}C under $Ar_{(g)}$ atmosphere with a CH Instruments Model 760B Series Electrochemical Analyzer/Workstation in conjunction with a Pine Instruments Company Analytical Rotator with an ASR Speed Controller. A three electrode system was utilized: glassy carbon working electrode (Pine Instruments Company Glassy Carbon E2A Electrode, surface area 0.3512 cm^2), Pt wire counter electrode (Alfa Aesar), and a Ag QRE (prepared from polished silver wire (Strem) immersed in concentrated HNO_3 for five minutes and then washed with de-ionized H_2O). RDE voltammograms of Eu(III) were recorded at different rotation rates in order to determine electrochemical parameters such as diffusion coefficients, D_o of Eu(III) complexes. D_o were calculated by the Levich equation (Equation 5.4).[78a]

Electrode areas were calculated from CV data of $K_3[FeCN_6]$ by the Radles-Sevčik equation, using 7.6 x 10^{-6} cm^2/s as D_o.[78a]

CHAPTER 6:
TOWARDS THE SYNTHESIS OF POLYEUROPIUM(II) COMPLEXES

Introduction

Superoxide and other reactive oxygen species (ROS) have been implicated in aging, cancers, and reperfusion injury in acute myocardial infarction (heart attack). The ability to monitor ROS would also provide the ability to monitor tumor response to therapy. In order to study temporal changes in ROS concentration, a noninvasive method for their detection is needed. Magnetic resonance imaging (MRI) is a noninvasive diagnostic imaging method.[18a, 21, 88] MRI has been used primarily to image pathological alterations in living tissue, such as tumors, and may be adaptable for the detection of ROS. MRI exploits the inherent and sometimes subtle differences in tissues. The need for better S/N (signal-to-noise or contrast-to-noise) in imaging has led to the development of MRI contrast agents (CA). These CA are often based on gadolinium(III) (Gd(III)) because of the half-filled f-orbitals leading to seven unpaired electrons.[21] Paramagnetic Gd(III) decreases the relaxation times of nearby water protons in tissues and thus causes signal variations. However, current clinical Gd(III) CAs are not capable of serving as ROS reporters because of the absence of accessible redox chemistry in aqueous solution.

ROS are strong oxidizing agents, and this chemical property affords a method for their detection and quantification. Equation 6.1 gives the MRI signal obtained by the relaxivity of water protons where C is a constant, q is the number of inner-sphere waters, μ_{eff} is the effective magnetic moment, τ_c is the molecular correlation time, and r is the Gd(III)···proton distance.[25]

$$r_1 = C \cdot q \cdot \mu_{eff}^2 \cdot \tau_c \cdot r^{-6} \tag{6.1}$$

The effective magnetic moment (governed by the number of unpaired electrons in the molecule) will make a large impact on the relaxivity of the water protons. By increasing the number of unpaired electrons in a molecule, the signal observed will increase geometrically. The number of electrons in a molecule can be altered by oxidation (removal of electrons) or reduction (addition of electrons) of the molecule. Gd(III)-based CA are not redox-active and are therefore unsuitable for measuring ROS levels. Redox pairs such as Mn(II)/Mn(III) have been developed to detect blood oxygen pressures via MRI.[89] However, the two redox states exhibit similar relaxivities at MRI-relevant frequencies, and therefore do not provide useful images. The paramagnetic redox pair Eu(II)/Eu(III) may prove to be very effective redox-reporting CA. Eu(II) is isoelectronic to Gd(III) and exhibits similar MRI detectability, while Eu(III) has a dramatically weaker signal.[90] It is proposed that upon oxidation by ROS, Eu(II) will be oxidized to Eu(III) and the MRI signal will decrease dramatically. Eu(II)/Eu(III) systems are ideal MRI active ROS reporters provided that Eu ions can be stabilized for biocompatibility by suitable ligands.

The halides of the rare-earths in the oxidation state +2 have been known for nearly a century, but divalent complexes in aqueous media are rare. Most divalent lanthanide complexes consist of organometallic molecules in organic solvents,[52b, 91] mixed valence metal clusters,[52b, c] complex oxides,[92] or perovskite solid-state structures.[93] Nearly all reported aqueous divalent lanthanides complexes are mononuclear chelates.[18a, 52b, 78c, 82a, 82c-h, 94] Starynowicz prepared europous complexes (Figures 6.1 and 6.2) by electrochemical methods[82c-h] and isolated crystalline Eu(II) complexes from bulk reduction using an H-shaped electrolyser with sintered glass diaphragm, mercury cathode, and platinum anode (Figure 6.3). A stream of nitrogen gas was passed over the analyte solution in order to preclude dioxygen and to evaporate solvent. Crystals formed over several days of electrolysis. Crystalline mononuclear complexes prepared by this method were reported to be stable in air, enough to withstand several days of X-ray data collection. The oxidation state of the europium ion in the complexes and the stability in

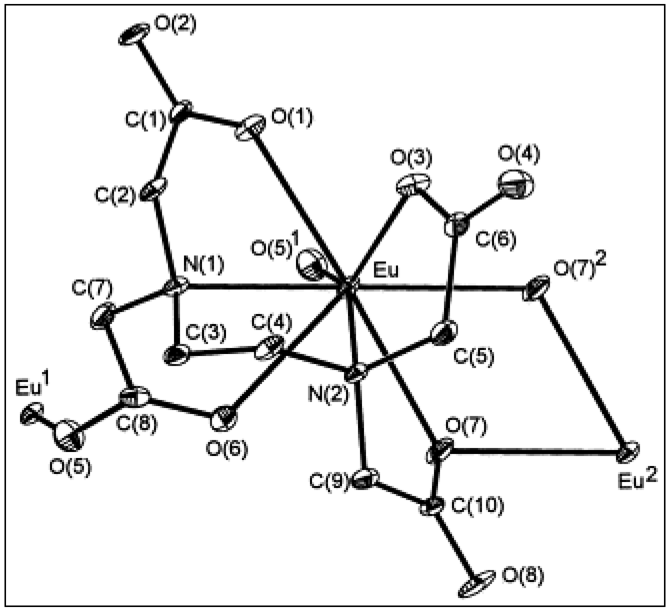

Figure 6.1: Coordination of europium and EDTA anion, together with atom numbering scheme.[82f]

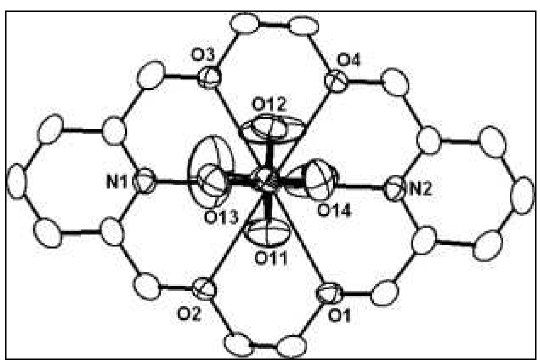

Figure 6.2: A view of bis(perchlorate)(bis-pyridino-18-crown)europium(II) with atom labeling. The Eu and Cl2 atoms are eclipsed by Cl1, and likewise O21 by O11, O23 by O24, and O24 by O23.[82h]

air was deduced by the reduction of iodine-starch paper and the lack of fluorescence characteristic of the Eu(II) ion. These papers discuss solid-state structure, with no solution chemistry reported.

Nonaqueous polynuclear divalent and mixed-valent europium complexes have been synthesized by dissolution of europium metal in alcohols.[52b] These complexes were isolated with alkoxides or phenoxides and quickly oxidize in air.[52b, c] Reactivity studies of these complexes have included ligand exchange reactions with other alkoxides or substituted phenols.[52b, c, 59d] Redox reactions of the mixed Eu(II)/Eu(III) alkoxide, $[Eu_4(OPr^i)_{10}(HOPr^i)_3]\cdot 2HOPr^i$ (Eu_4), and the Eu(III) alkoxide, $Eu_5O(OPr^i)_{13}$ (Eu_5), have shown that conversion from Eu_4 to Eu_5 is possible by oxidation of Eu_4 with oxygen gas, while reduction of Eu_5 with Eu metal does not yield the Eu_4 complex.[52c] This suggests that divalent polyeuropium complexes must be synthesized from lower-valent or divalent europium starting materials.

Divalent europium complexes are reactive species that are difficult to isolate. With a redox couple of -0.36 V, europium can be oxidized by dioxygen and must be handled under inert conditions. The photochemical oxidation of Eu(II) has also been demonstrated.[87, 95] Nonetheless, an interest within the Messerle group is the development of aqueous amino-acid-supported divalent polyeuropium chemistry. Herein is described (1) attempts to synthesize divalent polyeuropium complexes from lower-valent europium, and (2) attempts to chemically or electrochemically reduce trivalent polyeuropium(III) complexes.

Results and Discussion

Initial steps towards the isolation of divalent polyeuropium clusters began with approaches based on the reported europous isopropoxide.[52b, c] The synthesis of europous isopropoxide was straightforward, involving dissolution of europium metal in dried isopropanol and subsequent workup in tetrahydrofuran (THF). Reaction at elevated temperatures, higher than 45 ^{o}C, yields mixed-valent clusters. The isolated compound is described in the literature as $[Eu(O^{i}Pr)_2(THF)_x]_n$.[52b] Crystallographic data was not collected by the authors. Instead, they demonstrated that addition of phenols led to protonolysis of the alkoxides to yield new divalent polymeric phenoxide complexes. Discrete crystalline mixed-valent clusters were obtained by leaving the phenolate-substituted complex in the reaction mixture for months. It was our goal to substitute $O^{i}Pr$ ligands in $Eu(O^{i}Pr)_2$ with amino acids and isolate divalent, water-soluble clusters.

Reaction of $Eu(O^{i}Pr)_2$ with amino acids (proline, valine, glycine, or histidine) yielded noncrystalline material, similar to reactions of $Eu(O^{i}Pr)_2$ with alcohols and phenols reported in the literature. Amino acids are nearly insoluble in organic solvents and as such these reactions required long of reaction times. After several days of reaction the white amino acid would dissolve and the color of the solution would change from orange to yellow. However, crystalline product suitable for X-ray crystallography was not obtained. It is possible that, like the alkoxide and phenols, these complexes are oligomers, consistent with other reported lanthanide alkoxides.[52a] The light orange solid product obtained was insoluble in water and quickly turned white when exposed to oxygen. In attempts to obtain crystalline product and increase the solubility of the amino acids in organic solvents, Boc protected amino acids were used. Boc-proline was synthesized and found to be more soluble than L-proline in organic media such as THF. However, reaction with $[Eu(O^{i}Pr)_2(THF)_x]_n$ yielded solid product unsuitable for single-crystal X-ray characterization. The dry orange product was insoluble in H_2O and quickly turned white when exposed to oxygen. With these problems in mind the project shifted to more H_2O ‘friendly’ europous starting materials.

Europous carbonate was obtained by adaptation of literature methods.[96] $EuCO_3$ is an excellent source of aqueous europous ion, and the solid is stable in the divalent state in air for several months as the dry solid. Since most polylanthanide complexes reported in the literature are based on perchlorate as the supporting anion, initial attempts were performed by reacting $EuCO_3$ with perchloric acid. The resulting solutions were light yellow in color, indicative of aquated Eu(II). The solutions maintained the yellow color for extended periods of time (months) when kept under inert atmosphere. When exposed to oxygen, the solutions slowly lost color and clouded. Solutions of $Eu(ClO_4)_2$ and amino acid that were kept under inert atmosphere and concentrated to induce crystal growth usually formed insoluble white precipitate. The solid fluoresced in the visible when irradiated with long-wave UV light, and must be Eu(III) since Eu(II) does not fluoresce in the visible upon UV irradiation. The solid also yielded clear colorless solutions when dissolved in acid. Crystalline product was obtained on several occasions when L-proline and L-histidine were used. These crystals were determined to be the previously isolated and characterized trivalent molecules ($[Eu_4(\mu_3\text{-}OH)_4(pro)_6(OH)_2]^{6+}$ and $[Eu_{15}(\mu_5\text{-}X)(\mu_3\text{-}OH)_{20}(his^{+/-})_{10}(his^{-})_5(OH)_7]^{12+}$ (X = Cl, Br, $(I)_2$-OH)), based on single-crystal X-ray diffractometery. As stated earlier, perchlorate ion is an oxidizing agent and may not be a suitable anion for europous complexes, though $Eu(ClO_4)_2$ has been reported.[87a, 95]

Polynuclear lanthanide complexes without perchlorate anions have been reported. The iodide-supported complexes $[M_6(\mu_6\text{-}O)(\mu_3\text{-}OH)_8(OH_2)_{24}]I_8(H_2O)_8$ (M = Nd, Eu, Tb, and Dy) have been reported.[57, 97] This structure type does not have any organic supporting ligands. Perchlorate–free compounds with organic ligands have also been reported, such as $[Tb_2(DL\text{-}Cys)_4(OH_2)_8]Cl_2$, $[Eu_4(\mu_3\text{-}OH)_4(L\text{-}Asp)_2(L\text{-}HAsp)_3(OH_2)_7]Cl\cdot 11.5H_2O$, and $[Eu_8(HVal)_{16}(OH_2)_{32}]Cl_{24}\cdot 12.5H_2O$.[98] These compounds represent a small class of perchlorate-free polylanthanides. Adaptations of these syntheses were used in attempts to isolate perchlorate-free divalent polyeuropium complexes from $EuCO_3$. Reactions of $EuCO_3$ with HCl and amino acid (aspartic acid, glycine, proline, or histidine) under inert atmosphere produced light yellow solutions. Several of these reactions produced crystalline product that was later revealed to be previously characterized trivalent complex $[Eu_4(\mu_3\text{-}OH)_4(L\text{-}Asp)_2(L\text{-}HAsp)_3(OH_2)_7]^{+}$, by X-ray diffraction. Reactions of $EuCO_3$ with HI have not yet been performed. While

Eu(II) can be photooxidized, initial perchlorate-free attempts were carried out without any protection from light. It is possible that the reduced complexes photooxidized prior to crystallization, hence the isolation of trivalent products. Later reactions were performed with aluminum foil in order to prevent photooxidation. The solutions maintained a yellow color for extended periods of time (months). Several of these reaction mixtures, when concentrated via removal of solvent, produced insoluble white precipitate that fluoresced upon long-wave UV irradiation. Solutions that were not concentrated remained clear and maintained their yellow color but did not yield crystalline product. Furthermore the solutions did not fluoresce in the visible when irradiated with UV light. Yellow color and the lack of fluorescence supports the presence of Eu(II) and the lack of Eu(III) in these solutions. It is unclear at this time why crystalline Eu(II) product(s) could not be obtained.

Since direct synthesis of divalent polyeuropium complexes did not yield positive results, the research moved onto reduction of trivalent complexes. Initial attempts included the chemical reduction of trivalent $[Eu_4(\mu_3\text{-}OH)_4(pro)_6(OH)_2]^{6+}$, $[Eu_{14}(\mu_4\text{-}OH)_2(\mu_3\text{-}OH)_{16}(ser)_{20}(OH_2)_8]^{4+}$,[99] and $[Eu_{15}(\mu_5\text{-}X)(\mu_3\text{-}OH)_{20}(his^{+/-})_{10}(his^{-})_5(OH)_7]^{12+}$ (X = Cl, Br, $(I)_2$-OH, or OH). The chemical reduction was performed with a Jones reducing column as previously described in Chapter 5. An inherent problem occurs when employing a Jones reducer, as the chemical reduction of the analyte produces soluble Zn(II) which may hinder isolation of pure products. This is especially true if the ligands of the compound being reduced are labile as previously discussed. The change in the Lewis acidity of the europium ion may increase the lability of the ligands, allowing for exchange reactions and possible degradation of the compound of interest. White insoluble products that fluoresced with UV radiation were obtained in these experiments, suggesting Eu(III) and not Eu(II) was present. On several occasions, crystalline materials were obtained. However, the crystals fluoresced in the visible when irradiated with UV light and were determined to be unreduced starting material via single-crystal X-ray diffraction.

To bypass the possibility of by-products in solution after chemical reductions, electrochemical reductions were employed. Electrochemical techniques exist in the literature for the reduction of mononuclear chelated europium complexes. We adapted these procedures for synthesis of polynuclear complexes. Electrochemical data obtained for the polynuclear complexes discussed in this thesis demonstrated that these complexes are capable of multiple-one-electron reductions, although stability of the reduced products is questionable. The stability of these complexes after reduction is discussed at length in Chapter 5. In short, the reduction of Eu(III) to Eu(II) may change the Lewis acidity of the metal center enough to weaken the interaction with the Lewis base ligands, destabilizing the bonds and thus the complex.

Bulk electrolysis was performed on Eu_4 and Eu_{15}-his X clusters until the current reached an asymptote. The solutions turned yellow over the period of electrolysis. A steady potential was maintained during concentration of the solutions by inert gas flow. For Eu_{15}-his X, the solutions formed insoluble product prior to concentration. The Eu_4 complex maintained a clear solution until near dryness. Yellow crystals were collected from the latter and X-ray diffraction data obtained. The resulting crystals were trivalent polymeric $([(H_2O)_4Eu_2(\kappa^1\text{-pro})(\mu_2\text{-pro})_2](ClO_4)_{2.5})_n$ complex, Figure 6.1. This result has several interesting implications. Recrystallization of Eu_4 complexes in aqueous media has not yet been reported and would provide much more insight into these questions. However, it may be possible that the Eu_4 complex exists as the polymeric complex in solution or that upon reduction the Eu_4 complex unravels to form dinuclear polymeric units. Upon reduction, these polymeric units may form different oligomers. In either case, the polymeric complex is obtainable through direct synthesis of $Eu(ClO_4)_3$ with three equivalence of proline. In contrast, the Eu_4 complex is obtained through the synthesis of $Eu(ClO_4)_3$ with two equivalents of proline and the addition of base. With these two different reactions, one without base and one with base, two different products are obtained. This suggests that the Eu_4 complex, when reduced, undergoes a chemical process in which bonds are broken and reformed. With these results in mind, it is not hard to speculate that the reduction of Eu_{15}-his X would result in degradation and subsequent oligomerization to non-crystalline products.

Figure 6.3: Picture of actual H-cell employed for bulk electrolysis reactions. Two chambers are separated by a medium porosity fritted-glass. The chamber on the left has a Pt mesh CE submerged in a stock electrolyte solution. The chamber on the right has a pool of Hg as the WE with a Pt wire electrical contact (far right). The Hg pool is covered with a solution of analyte and a calomel RE is dipped into the analyte solution. A Teflon hose supplying inert gas was use to blanket the reaction in order to prevent oxidation by dioxygen and help concentrate the solution by evaporation of the solvent and to help alleviate some $O_{2(g)}$.

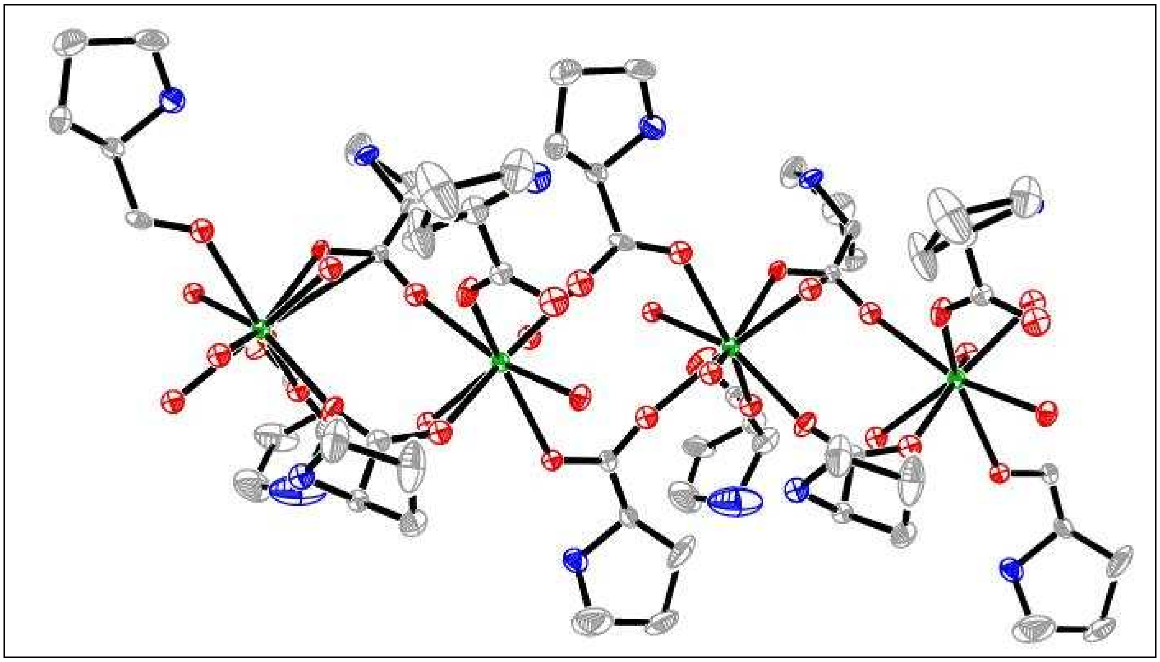

Figure 6.4: Depiction of polymeric trivalent $([(H_2O)_4Eu_2(\kappa^1\text{-pro})(\mu_2\text{-pro})_2](ClO_4)_{2.5})_n$. Color scheme: green, Eu(III); red, oxygen; gray, carbon; and blue, nitrogen.

Conclusions

Direct synthesis of divalent polyeuropium complexes has been unsuccessful to date. Literature methods provide routes towards mixed-valent complexes that are insoluble in water, and as such are unsuitable for application in MRI. Syntheses from $EuCO_3$ show the most promise because of the readily-accessible Eu(II) ion in aqueous solutions. However, standard methods for the formation of clusters have not succeeded. The target Eu_{15}-his X complexes in this research may be out of reach for divalent polyeuropium complexes because of the complex structure and Eu-ligand interactions. The structure is built upon ionic interactions, and the strength is dependent upon the Lewis acidity of the ions involved. Reduction of Eu(III) to Eu(II) may change the Lewis acidity of the Eu ion enough to weaken the ionic interactions with the oxygen ligands. If the interaction is weakened enough, the complex may degrade into smaller units or oligomerize. Studying the degradation of the large Eu_{15}-his X complexes would be very difficult because there may exist many different degradation pathways. Speculations on the degradation of Eu_{15}-his X were already discussed based on Eu_4. Studying smaller molecules such as Eu_2 or Eu_4 may provide insight into larger clusters.

Attempts towards divalent polyeuropium complexes may succeed with the syntheses of smaller more robust clusters such as the hexanuclear lanthanide clusters without perchlorate ion.[57, 97]

Reduction of trivalent polyeuropium complexes have produced mixed results. Chemical reduction with Zn amalgam contaminates solutions with soluble Zn(II) and have caused difficulties during crystallization. Electrochemical reductions have produced results that are not encouraging for the use of these complexes in biological systems. It seems that these complexes, when reduced, begin to degrade and rearrange to form new complexes. This is most likely because of the decrease in the Lewis acidity of the metal center.

Competitive oxidative processes have made the isolation of divalent complexes difficult under our conditions. If these competitive processes can be overcome, isolation of divalent polyeuropium complexes may be realized. Another challenge is overcoming the photooxidation of Eu(II).

Experimental

General Considerations:

Europium metal, stored in mineral oil, was obtained from Afla Aesar. The exterior surface was shaved off to reveal lustrous metal surface with a knife or wire cutters prior to use. Isopropanol was obtained from Fisher Chemical and distilled from Na (0.002 mole equivalent per mole of HO^iPr) prior to use. Zinc (20 mesh) was obtained from J.T. Baker Chemical and used as received. Tetrahydrofuran (THF, Aldrich) was dried over sodium. All other materials were used as received or dried by standard conditions prior to glove box use.

Electrochemical reductions were performed at 25+/-1 ^{o}C under $Ar_{(g)}$ atmosphere with a CH Instruments Model 700B Series Electrochemical Analyzer/Workstation. The vessel used was an H-shaped electrolyser with sintered glass diaphragm, a pool of mercury (Henry Schein Inc.) as the cathode with a platinum wire used for electrical contact, platinum wire (Alfa Aesar) anode, and saturated calomel reference electrode (Fisher, porous plug type). The reduction was conducted with the cathode potential set at -1.5 V.

All supporting electrolyte solutions were 100x the concentration of the analyte.

Synthesis of Europous Isopropoxide

$[Eu(O^{i}Pr)_2(THF)_n]_m$

$[Eu(O^{i}Pr)_2(THF)_n]_m$ was prepared based on an adaptation of the literature method.[52b] Eu metal was cut into small pieces (5 – 10 mm in diameter) and reacted with dry isopropanol at room temperature under $N_{2(g)}$ for six days, yielding an orange solution containing some insoluble material. Excess $HO^{i}Pr$ was removed *in vacuo* and the resulting paste dissolved in tetrahydrofuran (THF). The orange solution was filtered under inert conditions. The filtrate was dried *in vacuo* to a free-flowing orange powder that was stored in a dinitrogen glove box.

Attempted Synthesis of Polynuclear Europous Complex of L-Proline

In the glove box a Schlenk flask was charged with $[Eu(O^{i}Pr)_2(THF)_n]_m$ (0.64 g, ~ 2.0 mmol) and L-proline (0.23 g, 2.0 mmol). Anhydrous THF (10 mL) was added to the vessel to yield an orange solution with white solid at the bottom (presumed to be undissolved amino acid). The vessel was transferred to a Schlenk line and stirred under

$N_{2(g)}$ overnight at ambient temperature. Yellow/orange solid caked the walls of the reaction vessel. The solid was broken up by shaking the flask and the solution stirred for five days. It was later observed that the reaction mixtures received direct sunlight in the afternoon hours. Studies have shown that Eu(II) ion is susceptible to photochemical oxidation.[87, 95]

After five days, most of the solid had dissolved and the solution was filtered under inert conditions to yield clear orange solutions. The reaction vessel was placed into a freezer under positive $N_{2(g)}$ pressure in order to grow crystals. After a week, no crystalline product was obtained. Half of the solvent was removed i*n vacuo* and then the solutions returned to the freezer to grow crystals. No crystals were obtained. Yellow solid is obtained when the solution was brought to dryness. Dry yellow/orange solid was collected and stored in the glove box for future work.

A small amount of the yellow/orange solid was brought out of the glove box. When exposed to air, the yellow powder quickly turned white. The white solid was insoluble in water and very soluble in acids ($HClO_4$ and HCl).

Attempted Synthesis of Polynuclear Europous Complex of L-Glycine

In the glove box a Schlenk flask was charged with $[Eu(O^iPr)_2(THF)_n]_m$ (0.64 g, ~ 2.0 mmol) and L-glycine (0.15 g, 2.0 mmol). Anhydrous THF (10 mL) was added to the vessel to yield an orange solution with white solid at the bottom (presumed to be undissolved amino acid). The vessel was transferred to a Schlenk line and stirred under $N_{2(g)}$ overnight at ambient temperature. Red/orange solid caked the walls and bottom of the flask. The solid was broken up by shaking the flask and the solutions stirred for five days. It was later observed that the reaction mixtures received direct sunlight in the afternoon hours. Studies have shown that Eu(II) ion is susceptible to photochemical oxidation.[87, 95]

After five days, most of the solid had dissolved and the solution was filtered under inert conditions to yield clear orange solutions. The reaction vessel was placed into a freezer under positive $N_{2(g)}$ pressure in order to grow crystals. After a week, no crystalline product was obtained. Half of the solvent was removed i*n vacuo* and then the solution returned to the freezer to grow crystals. No crystals were obtained. Yellow solid is obtained when the solution was brought to dryness. Dry yellow/orange solid was collected and stored in the glove box for future work.

A small amount of the yellow/orange solid was brought out of the glove box. When exposed to air, the yellow powder quickly turned white. The white solid was insoluble in water and very soluble in acids ($HClO_4$ and HCl).

Attempted Synthesis of Polynuclear Europous Complex of L-Valine

In the glove box a Schlenk flask was charged with $[Eu(O^{i}Pr)_2(THF)_n]_m$ (0.64 g, ~ 2.0 mmol) and L-valine (0.234 g, 2.0 mmol). Anhydrous THF (10 mL) was added to the vessel to yield an orange solution with white solid at the bottom (presumed to be undissolved amino acid). The vessel was transferred to a Schlenk line and stirred under $N_{2(g)}$ overnight at ambient temperature. The solutions became darker orange and most of the valine appeared to dissolved. The solid was broken up by shaking the flask and the solutions stirred for five days. It was later observed that the reaction mixtures received direct sunlight in the afternoon hours. Studies have shown that Eu(II) ion is susceptible to photochemical oxidation.[87, 95]

After five days, most of the solid had dissolved and the solutions were filtered under inert conditions to yield clear orange solutions. The reaction vessel was pressurized with $N_{2(g)}$ and then placed into a freezer in order to grow crystals. After a week, no crystalline product was obtained. Half of the solvent was removed i*n vacuo* and then the solutions returned to the freezer to grow crystals. No crystals were obtained.

Yellow solid is obtained when the solution was brought to dryness. Dry yellow/orange solid was collected and stored in the glove box for future work.

A small amount of the yellow/orange solid was brought out of the glove box. When exposed to air, the yellow powder quickly turned white. The white solid was insoluble in water and are very soluble in acids ($HClO_4$ and HCl).

Synthesis of Boc-Proline[100]

Boc-Proline was synthesized in order to solubilize proline in organic solvents and aid in crystallization of europous complexes. To a solution of proline (2.878 g, 25 mmol) in a 1:1 mixture of THF/H_2O (150 mL), $NaHCO_3$ (6.3 g, 75 mmol) and di-*tert*-butyl dicarbonate (Boc anhydride, Boc_2O) (6.547 g, 30 mmol) were added consecutively at 0 ^oC. The solution was stirred for 30 min at 0 ^oC and then allowed to stir at ambient temperature overnight. The turbid solution was extracted with Et_2O (2x 100 mL) and the aqueous layer acidified to pH = 4 -5 with 30% (w/w) citric acid at 0 ^oC. This solution was then extracted with CH_2Cl_2 (3x 100 mL). The combined organic phases were dried with Na_2SO_4 and the solvent was removed using a rotovap. Dried white product, 3.9 g (18.139 mmol) with yield of 72.5% was obtained and used without further purification.

Attempted Synthesis of a Divalent Polynculear Europous Complex of Boc-Proline

A Schlenk flask was charged with $[Eu(O^iPr)_2(THF)_n]_m$ (0.64 g, ~ 2.0 mmol) and Boc-proline (0.4304 g, 2.0 mmol) and dissolved in 10 mL of anhydrous THF. The solution was stirred overnight and the orange color lightened over time. Most of the solids dissolved, and the solution was filtered under inert atmosphere to yield a clear orange solution. The reaction vessel were placed in a freezer under positive $N_{2(g)}$ pressure in order to grow crystals. After a week, no crystalline product was obtained. Half of the solvent was removed i*n vacuo* and then the solutions returned to the freezer to grow crystals. After a month, no crystals were obtained. Yellow/orange solid is obtained when the solution was brought to dryness. The solid was soluble in THF, CH_3CN, toluene, CH_2Cl_2, and Et_2O. The sample was dried and stored in the glove box.

Other Boc protected amino acids attempted include histidine and glycine. Boc-histidine was not soluble in THF. Boc-glycine gave similar results as Boc-proline.

All europous boc-amino acid samples were insoluble in H_2O and became white over time in air.

Preparation of Zinc Amalgam[96]

Amalgamated zinc was prepared by stirring 20-mesh zinc with $HgCl_2$ (10% w/w) dissolved in HCl (6.0 M). The mixture darkened and briefly became cloudy. With continued heating and stirring the solution cleared. The originally dull zinc metal became lustrous. The solution was decanted, washed several times with warm deionized H_2O, and allowed to dry under ambient conditions. The material was stored under a solution of HCl (0.1 M) until used in order to prevent clumping

Preparation of Europous Carbonate

Europous carbonate was prepared by literature methods.[96] Stock solutions of $EuCl_3$ (0.1 M) were prepared by digestion of Eu_2O_3 with HCl (12.1 M) and dilution with deionized H_2O. A Jones column containing 20-mesh amalgamated zinc in a column 6 inches tall and 2 cm in diameter was flushed out with 200 mL of 0.1 M HCl. Sufficient acid was left in the column just to cover the zinc. The outlet of the column was connected via a Claisen adapter with gas inlet and round bottom flask filled with concentrated H_2SO_4. The round bottom flask was purged with $N_{2(g)}$. A pressure-equalizing addition funnel charged with the $EuCl_3$ solution was attached to the top of the column. This solution was slowly passed through the column (~2.0 mL per minute). White feathery precipitate formed (α-$EuSO_4$) when the reduced solution reached the H_2SO_4. The α-product is light and feathery and the β-product is much denser. The precipitate becomes denser with stirring. Literature methods suggest heating the solution to obtain the β form of $EuSO_4$, however, sufficient heat is obtained through the interaction of H_2SO_4 and H_2O. The solid was filtered on a medium porosity glass fritted funnel and dried in air at 75 ^oC.

Dry β-$EuSO_4$ (5.0 g) was ground to a fine powder and then slowly added to a vigorously boiling, 300 mL solution that was normal with respect to sodium bicarbonate and 0.4 N in sodium hydroxide (12.6 g $NaHCO_3$ and 10.8 g NaOH). A violent reaction ensued and yellow powder formed. After the addition of β-$EuSO_4$, the solution was stirred and boiled for an additional 30 minutes. The $EuCO_3$ was then collected on a medium porosity glass fritted funnel and dried in air at 75 ^oC. Dry $EuCO_3$ can be stored at room temperature in air for several months without appreciable oxidation.

Attempted Synthesis of Divalent Polyeuropium Complexes from Europous Carbonate

In a typical reaction, an amino acid (2.0 mmol of proline, aspartic acid, or histidine; when histidine was the amino acid, 1 mmol of NaX, X = Cl, Br, or I was also added) and $EuCO_3$ (1.0 mmole, 0.211 g) were placed in a Schlenk flask with a magnetic stir bar and the vessel evacuated and backfilled with inert gas three times. The solids were covered with degassed deionized H_2O. Degassed HCl (1.0 M, 2.0 mL) or HI (1.0 M, 2.0 mL) was added via syringe. The yellow solid quickly dissolved with heating and stirring to produce a yellow solution with evolution of gas (presumed to be CO_2). Degassed NaOH (0.3 M) was added to the point of incipient precipitation. The solution was filtered under inert conditions via a double-ended inner standard tapered 19/22 fine porosity glass fritted funnel equipped with a Schlenk flask receiver. The resulting yellow solution was covered with aluminum foil and left to grow crystals. The yellow/white solid collected on the frit was kept for further analysis. This solid was insoluble in H_2O and effervesced when dissolved in acid.

The yellow solution were left to grow crystals and slowly lost color over time. When the solutions were concentrated, insoluble white solid formed. The white solid fluoresced in the visible (red/pink) when irradiated with long-wave UV light. No crystalline product was ever obtained.

Chemical Reduction of

$[Eu_4(\mu_3\text{-}OH)_4(pro)_6(OH)_2](ClO_4)_6$ with Zn(Hg)

$[Eu_4(\mu_3\text{-}OH)_4(pro)_6(OH)_2](ClO_4)_6$ (0.1 g) was dissolved in hot deionized H_2O (10.0 mL), degassed, and passed through a Jones column charged with Zn(Hg) (prepared as previously described). As the solution passed through the column a white precipitate formed. The rest of the dilute solution gave a light yellow tint after passing through the column. The solution was filtered or centrifuged under inert conditions in order to remove insoluble product. The solution was concentrated to 5.0 mL, covered with aluminum foil, and left to grow crystals. The yellow solution slowly lost all color and a white insoluble precipitate formed. The white solid fluoresced in the visible (red/pink) when irradiated with long-wave UV light.

Chemical Reduction of

$[Eu_{14}(\mu_4\text{-}OH)_2(\mu_3\text{-}OH)_{16}(ser)_{20}(OH_2)_8](ClO_4)_3(OH)$

with Zn(Hg)

This procedure followed the procedure for the chemical reduction of $[Eu_{14}(\mu_4\text{-}OH)_2(\mu_3\text{-}OH)_{16}(ser)_{20}(OH_2)_8](ClO_4)_3(OH)$ (Eu_{14}) with Zn(Hg). The solutions obtained after the reductions of Eu_{14} lost color over time and formed an insoluble white precipitate that fluoresced in the visible (red/pink) when irradiated with long-wave UV light.

Chemical Reduction of $[Eu_{15}(\mu_5\text{-}X)(\mu_3\text{-}OH)_{20}(his^{+/-})_{10}(his^{-})_5(OH)_7](ClO_4)_{12}$ (X = Cl, Br, $(I)_2$-OH, or OH) with Zn(Hg)

This procedure followed the procedure for the chemical reduction of Eu_4 with Zn(Hg). The solutions obtained after the reductions of Eu_{15}-his X (X = Cl, Br, $(I)_2$-OH, and OH) each lost color over time and formed insoluble white precipitates that fluoresced in the visible (red/pink) when irradiated with long-wave UV light.

Chemical Reduction of $EuCl_3$ with Zn(Hg) and Subsequent Reactions

In a typical reaction $EuCl_3$ (0.1 M, 1 mmol) was passed through a column charged with Zn(Hg) (as previously described) into a flask with a magnetic stir bar and an amino acid (2.0 mmol of proline, aspartic acid, or histidine; when histidine was the amino acid, 1.0 mmol of NaX, X = Cl, Br, or I was also added). The solution was stirred and heated. Degassed NaOH (0.3 M) was added via syringe until the point of incipient precipitation. The solution was filtered under inert conditions via a double ended male fine porosity glass fritted funnel equipped with a Schlenk flask receiver. The resulting yellow solution was covered with aluminum foil and allowed to grow crystals. The yellow/white solid collected on the frit was kept for further analysis. The yellow/white solid was insoluble in H_2O and dissolved in acid.

When the solution was concentrated, white insoluble precipitate was obtained and fluoresced in the visible (red/pink) when irradiated with long-wave UV light.

Electrochemical Reduction of Trivalent Polyeuropium Complexes

An H-shaped electrolyzer with sintered glass diaphragm, mercury pool cathode with a platinum wire used for electrical contact, platinum anode, and calomel reference electrode was used in these experiments. A solution of NaCl or KCl was used as the electrolyte. In a typical reduction, a Eu_n complex (n = 4 or 15) was dissolved in deionized H_2O and placed on top of the mercury pool. The solution was electrolyzed for several days and slowly gave a yellow color indicative of Eu(II) in solution. A stream of inert gas (Ar or N_2) was passed over the solution to aid in evaporation. Crystalline material or an insoluble precipitate was normally obtained after five or more days of electrolysis. Crystalline product from the electrolysis of Eu_4 did not fluoresce under long-wave UV radiation and were then characterized by single crystal X-ray diffraction. The product was determined to be polymeric $([(H_2O)_4Eu_2(\kappa^1\text{-pro})(\mu_2\text{-pro})_2](ClO_4)_{2.5})_n$ by X-ray diffraction. Crystalline product from the electrolysis of Eu_{15}-his X fluoresced in the visible when irradiated with long-wave UV light. X-ray crystallography was performed in order to assess the oxidation states of the multiple metal centers. The resulting compound was trivalent and matched the crystallographic data obtained from the recrystallized Eu_{15}-his X complexes.

X-Ray Diffractometry:

$([(H_2O)_4Eu_2(\kappa^1\text{-pro})(\mu_2\text{-pro})_2](ClO_4)_{2.5})_n$

A colorless needle with dimensions of 0.32 x 0.03 x 0.02 mm^3 was mounted via grease on the tip of a glass fiber (epoxied to a brass pin) and placed on the diffractometer with the long crystal dimension approximately parallel to the diffractometer phi axis. Data were collected on a Nonius KappaCCD diffractometer (Mo K_α radiation, graphite monochromator) at 220 K (cold N_2 gas stream) using standard CCD data collection techniques. Lorentz and polarization corrections were applied to the 6886 data. A correction for absorption using the multi-scan technique was applied (T_{max} = 0.9138, T_{min} = 0.3212). Equivalent data were averaged yielding 12622 unique data (R-int = 0.000, 10847 with $F > 4\sigma(F)$). Based on preliminary examination of the crystals, the space group P1 was assigned. The computer programs from the HKLint package were used for data reduction. Structure refinement was performed with the SHELXTL v6.1 software package.

The preliminary model of the structure was obtained using XS, a direct methods program. Least-squares refinement of the model vs. the data was performed with the XH program. Tables were made with the XCIF program. All non-hydrogen atoms were refined with anisotropic thermal parameters. All H atoms were included with the riding model using the XL program default values. Any restraints and constraints imposed on the data are described in the .cif files.

CHAPTER 7:
INNER LIGAND SUBSTITUTION CHEMISTRY OF HEXANCULEAR TANTALUM AND TUNGSTEN CHLORIDE CLUSTERS

Introduction

Transition metal clusters with π-donor ligands have been known and the subject of significant research interest for over 70 years. These clusters are of particular interest because of their potential use in photochemical energy storage,[101] as structural precursors to or analogues of the superconducting Chevrel phases,[102] as X-ray contrast agents in radiological imaging,[17b] as high-electron-density compounds in biomacromolecular crystallographic phase determination,[103] as chemical sensors,[104] and as catalysts.[105] The early transition metal halide clusters have been of most interest in research in the Messerle group. Clusters in Group 5 (Nb and Ta) typically consist of an octahedron of metal atoms with edge-bridging inner halides, $[M_6X_{12}Y_6]$ (Figure 7.1). Clusters in Group 6 (Mo and W) typically consist of an octahedron of metal atoms with face-bridging inner halides, $[M_6X_8Y_6]$ (Figure 7.2). In both cases, X represents an inner halide and Y represents ausser ligands, which are often halides.[106]

The ligand substitution chemistry of the ausser ligands is considerably more developed than the substitution chemistry of the inner ligands.[25, 79d] This is largely because of the robust nature of the M_6 core, which requires more forcing conditions in order to displace the inner ligands. Methods have been reported for ausser ligand substitutions with neutral ligands, including nitrogen donors,[107] oxygen donors,[107a, 107c, 108] phosphines,[107c, 109] and solvent molecules.[107c, 110] These substitutions are usually performed in refluxing solvents. Mixed halo clusters such as $(H_3O)_2[M_6Cl_8Y_6]$ (M = Mo, W; Y = F, Br, I) were prepared from the aqueous acids of HY and M_6Cl_{12}.[107a, 109a, 110b, 111] Weakly coordinated ligands such as triflate (trifluoromethanesulfonate),[112] tetrafluoroborate,[113] nitrate,[113c, 114] tosylate (*p*-toluenesulfonate),[112a] trifluoroacetate,[112a, 115] and perchlorate[110a] were prepared by heating the cluster in solvents in the presence of either the acid form or silver(I) salt of the anionic ligand.[110a]

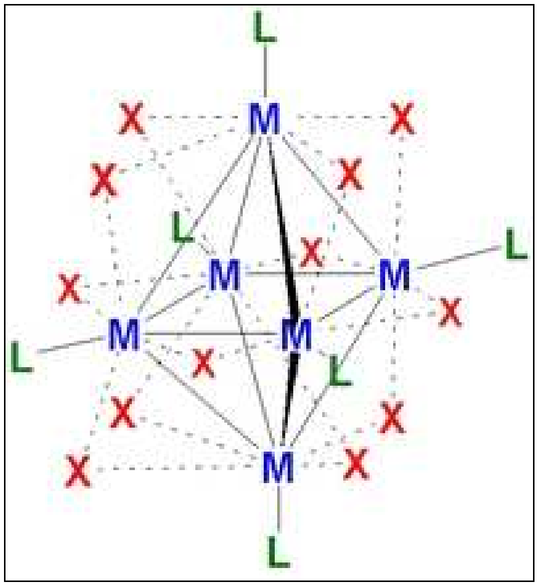

Figure 7.1: Depiction of the structure of discrete Group 5 (M= Nb and Ta) hexanuclear halide clusters, $M_6(\mu_2\text{-}X)_{12}Y_6$.

As implied earlier, inner ligands have lower lability than their ausser counterparts. Neither boiling *aqua regia* nor fuming sulfuric acid affects the octahedral core.[116] Basic solutions, however, disrupt the cubic array of inner ligands for face-bridged ligand clusters. The inner halide ligands of $[Mo_6Cl_8(OH)_6]^{2-}$ and $[Mo_6Br_8(OH)_6]^{2-}$ were partially displaced by hydroxide ions yielding $[Mo_6(X)_{8-z}(OH)_z(OH)_6]^{2-}$.[117] Full substitution of the inner chloride ligands of Mo_6Cl_{12} was affected by boiling solutions with sodium methoxide to dryness.[118] Heating the mixed halide cluster $Mo_6Cl_8Y_6$ (Y = Br, I) to 400 ^oC yielded mixed inner ligand species, $Mo_6(Cl)_{8-z}Y_z$ (ausser ligands omitted).[113d, e] Chalcogenides, on the other hand, have demonstrated facile face-bridged inner-ligand substitution reactions in hexarhenium cluster chemistry by the use of silylated reagents $(Me_3Si)_2E$ (E = O, S, Se, or Te).[119] These reactions replace inner halides with O, S, Se, or Te dianions.

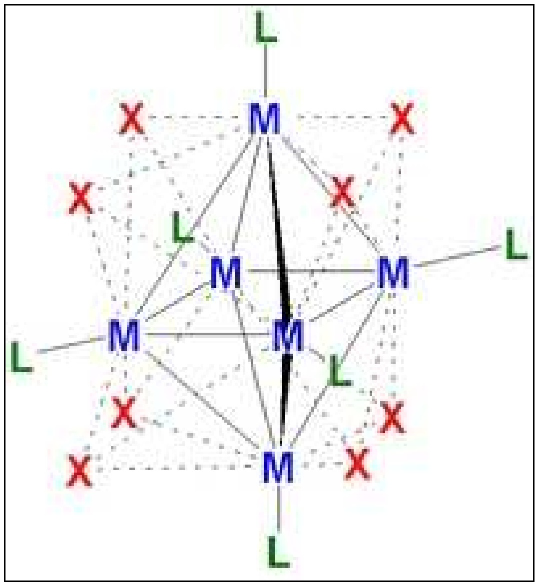

Figure 7.2: Depiction of the structure of discrete Group 6 (M = Mo and W) hexanuclear halide cluster, $M_6(\mu_3\text{-}X)_8Y_6$.

Direct solid-state synthesis has yielded mixed halide-oxide M_6 clusters.[120] Much of this work has been focused on the formation of two-dimensional materials. To date, phases have been identified as containing $[Nb_6OCl_{11}]^{1+}$, $[Nb_6O_nCl_{12-n}]^{(4-n)+}$ (n = 2 – 4), $[Ta_6O_3X_9]^{1+}$ (X = Cl, Br), $[Nb_6O_5Cl_7]^{1-}$ and $[Nb_6O_6Cl_6]^{1-}$ cluster cores. Most of these cluster-containing solid-state extended phases were prepared by solid-state stoichiometric reactions carried out at temperatures in excess of 700 ^{o}C. Similar chemistry for hexanuclear molybdenum and tungsten oxohalide clusters has thus far failed to emerge, with the exception of one report. Tungsten oxygen-halide clusters, with inner cores $[W_6O_6Cl_6]^{4+}$ and $[W_6O_7Cl_5]^{3+}$, have been prepared.[121] The synthesis of

$(Bu_4N)_2[\alpha\text{-}W_6O_6Cl_{12}]$ paralleled the method pioneered by the Messerle group to synthesize W_6Cl_{12}, as shown in Equation 7.1.[122] A $W_6O_6Cl_{10}$ parent phase was targeted by replacing WCl_6 with $WOCl_4$, Equation 7.2.[121] The discrete, zero-dimensional cluster $[W_6O_6Cl_{12}]^{2-}$ is excised from the solid-state reaction products by reaction with concentrated HCl.

$$6\ WCl_6 + 8\ Bi \rightarrow W_6Cl_{12} + 8\ BiCl_3 \tag{7.1}$$

$$18\ WOCl_4 + 14\ Bi \rightarrow 3\ W_6O_6Cl_{10} + 14\ BiCl_3 \tag{7.22}$$

The Messerle group's interest lie in the further investigation of hexanuclear early transition metal mixed oxohalide cluster chemistry. Herein are described attempts to further this chemistry by (1) solution-state reactions for inner-ligand substitutions, and (2) solid-state syntheses of hexanuclear mixed oxochloride clusters.

Results and Discussion

Solution-State Attempts Toward Inner-Ligand-Substitution of Hexanuclear Tantalum and Tungsten Chloride Clusters

Inner-ligand exchange chemistry of hexarhenium chalcogenides clusters is possible with silylated reagents, $(Me_3Si)_2E$, to replace inner chlorine anion ligands with oxygen, sulfur, selenium, or tellurium dianion ligands. The byproduct of these reactions is trimethylsilyl chloride, an easily removable, volatile compound. We postulated that analogous reactions of hexamethyldisiloxane (HMDS) with Ta_6 and W_6 complexes would afford inner-ligand substituted complexes, so the reactions of HMDS with fully-halide-substituted Ta_6 and W_6 complexes were examined at room temperature and at reflux in several solvents. However, none of these attempts afforded any observable signs that a reaction took place. The exchange of a single negatively-charged inner-chloride ligand with a double negatively-charged oxide ligand would have changed the overall charge of the molecule and most likely would have yielded a color change. Reaction progress was monitored by color change.

Further attempts were made using silver oxide (Ag_2O) as the oxygen transfer reagent via a metathesis reaction, in order to yield insoluble AgCl. These reactions were carried out much the same as those performed with HMDS. Ta_6 or W_6 was dissolved in various solvents and subsequently treated with Ag_2O. Ag_2O is a black/brown powder that is insoluble in organic solvents, so it was expected that reactions performed in organic solvents would proceed via heterogeneous reaction pathways. Ag_2O reactions with chloride ligands of Ta_6 or W_6 would yield a white insoluble powder, AgCl, in the case of a reaction. Several of these reactions gave white powder and observable color changes. Ta_6 complexes are forest-green when dissolved, while W_6 complexes are yellow in solution. The color changes observed were as follows: green Ta_6 would turn brown-red overnight or within several days in CH_3CN, CH_2Cl_2, and EtOH; yellow W_6 would turn golden yellow overnight or within several days in CH_3CN and THF. Crystallization yielded the known oxidized Ta_6 cluster, $(Bu_4N)_3[Ta_6Cl_{18}]$, and W_6 starting materials $[W_6(\mu_3\text{-}Cl)_8Cl_6]^{2-}$ (cations: H_3O^+ or NBu_4^+).

It was later thought that perhaps the ausser chlorides were interfering with the inner-ligand-exchange mechanism. With this is mind Ta_6 solvates ($[Ta_6(\mu_2\text{-}Cl)_{12}(EtOH)_6]Cl_2$ and $[Ta_6(\mu_2\text{-}Cl)_{12}(EtCN)_6]Cl_2$) were prepared and reacted with HMDS and Ag_2O in similar fashions as the halide Ta_6 and W_6 clusters. These Ta_6 reactants, while more soluble, yielded similar results as to those for the ausser chloride Ta_6 and W_6 clusters.

Solid-State Attempts Toward Hexatantalum Mixed Oxygen-Chlorine Clusters

Direct solid-state reactions were performed in attempts to produce hexatantalum mixed oxide-chloride clusters. Several literature reports describe the stoichiometry-controlled reactions of $NbCl_5$ with Nb_2O_5, Nb, and in some instances MCl (M = Na, K, Rb, Cs, or In) to produce hexaniobium mixed oxide-chloride clusters. These reactions are routinely performed at temperatures $\geq$ 700 ^oC. Very few literature reports discuss the synthesis of hexatantalum mixed oxide-chloride clusters. These reports generally react Ta_2O_5 with Ta, MCl, Ln_2O_3 (Ln = lanthanide), and in some cases $TaCl_5$. Again, these reactions are performed at temperatures $\geq$ 700 ^oC. It was unclear why the tantalum reactions were so few and far between when one would expect similar chemistry within the Group 5 transition metals.

The reactions studied in our research were performed in evacuated flame-sealed quartz ampules. Borosilicate ampules are only rated to withstand temperatures up to 500 ^oC. Explosions were the result for each reaction that was performed in quartz at or above 600 ^oC. It was later discovered that Ta metal and other tantalum chlorides react with SiO_2 at temperatures as low as 450 ^oC, and are reported to become severe at temperatures of 650 ^oC. It is quite possible that the reactions of Ta and $TaCl_5$ with the walls of the reaction vessel weaken the vessel, and as a result of increased internal pressure, the weakened walls rupture. It is unclear what type of vessels (volume, OD, and ID) were used to produce mixed oxide-halide clusters of tantalum in the literature reports. The reaction stoichiometry and starting material amounts are also not reported. In attempts to circumvent explosions, the reactions were performed with less starting material (under 0.5 g), however, these reactions again ended in ampule explosions. Reactions performed at 500 ^oC in quartz ampules also resulted in explosions. Reactions in borosilicate at 500 ^oC were also attempted but yielded infinite layered materials that did not consist of octahedral arrays of tantalum as confirmed by X-ray diffraction.

Solid-State Attempts Toward Hexatungsten Mixed Oxide-Chloride Clusters

Tungsten requires less forcing conditions to be reduced as compared to tantalum. Attempts to synthesize hexatungsten mixed oxide-chloride clusters were performed with stoichiometric control aimed towards specific products. Reactions were performed based on literature methods.[121] The reaction of $WOCl_4$ with WCl_6, Bi, and NaCl was performed at 350 ^oC in efforts to obtain $W_6(\mu_3\text{-O})_4(\mu_3\text{-Cl})_4$ and $Na_6[W_6(\mu_3\text{-O})_4(\mu_3\text{-Cl})_4Cl_6]$. Both stoichiometric reactions yielded the new α and β acid salts (Figure 7.3 and 7.4) of the previously reported $(Et_4N)_2[\alpha/\beta\text{-}W_6(\mu_2\text{-O})_6(\mu_2\text{-Cl})_6Cl_6]$. Solution workup of these reactions will be discussed later. The acid salt can be recrystallized from aqueous solution. The $(H_3O)_2[\alpha/\beta\text{-}W_6(\mu_2\text{-O})_6(\mu_2\text{-Cl})_6Cl_6]$ complexes are stable to H_2O and O_2 and are highly soluble in water. Indeed, the acid salt may be recrystallized after prolonged periods at room temperature in H_2O. However, after one month some insoluble yellow precipitate forms.

Figure 7.3 depicts the structure of the chloro acid $[\alpha\text{-}W_6(\mu_2\text{-O})_6(\mu_2\text{-Cl})_6Cl_6]^{2-}$ cluster, in which the edges of the W_6 octahedron are bridged by six oxo and six chloro ligands. The oxides are situated between two opposing triangular faces, resulting in a compression of the octahedron about a three-fold rotation axis. The chloro ligands are located on the two opposing triangular faces. Table 7.1 listed selected mean bond lengths for the D_{3d}-symmetry cluster. The bond lengths correlate well with the previously reported $(Et_4N)_2[\alpha/\beta\text{-}W_6(\mu_2\text{-O})_6(\mu_2\text{-Cl})_6Cl_6]$ clusters.[121] Oxo-bridged tungsten-tungsten bond distances are considerably shorter than those of chloro-bridged tungsten-tungsten bond distances. The shorter W-W bonds associated with oxo-bridged edges along the middle of the cluster result in an elongation of the octahedron along a 3-fold rotation axis. The oxo ligand positions can be considered a belt that squeezes and elongates the cluster.

The structure of the $[\beta\text{-}W_6(\mu_2\text{-O})_6(\mu_2\text{-Cl})_6Cl_6]^{2-}$ cluster (Figure 7.4) differs from that of the $[\alpha\text{-}W_6(\mu_2\text{-O})_6(\mu_2\text{-Cl})_6Cl_6]^{2-}$ cluster primarily in the arrangement of the core inner ligands. The oxo and chloro ligands switch positions, where the chloro ligands are now in the "belt" position. Since all of the oxygen ligands are on two faces of the octahedron, the distortion of the octahedron is considerably less.

Table 7.1: Selected mean bond lengths (Å) for $(H_3O)_2[\alpha\text{-}W_6(\mu_2\text{-}O)_6(\mu_2\text{-}Cl)_6Cl_6]$ and $(H_3O)_2[\beta\text{-}W_6(\mu_2\text{-}O)_6(\mu_2\text{-}Cl)_6Cl_6]$.

	$(H_3O)_2[\alpha\text{-}W_6(\mu_2\text{-}O)_6(\mu_2\text{-}Cl)_6Cl_6]$	$(H_3O)_2[\beta\text{-}W_6(\mu_2\text{-}O)_6(\mu_2\text{-}Cl)_6Cl_6]$
W-W (μ_2-Cl)	2.9075(7)	2.8854(6)
W-W (μ_2-O)	2.6966(6)	2.7091(6)
W-μ_2-Cl	2.454(3)	2.437(3)
W-μ_2-O	1.895(8)	1.923(9)
W-Cl	2.395(3)	2.4093)

Note: "W-W (μ_2-Cl)" denotes W-W bonds that are bridged by chloros and "W-W (μ_2-O)" denotes W-W bonds that are bridged by oxos.

Since the Bi reduction reactions starting with $WOCl_4$ or $WOCl_4$ and WCl_6 yielded the same complex reported in the literature,[121] reductions starting with higher oxides of tungsten were studied. Reactions were performed under similar conditions as described for $WOCl_4$ but with WO_2Cl_2 or WO_3. These reactions all ended with the same results as for $WOCl_4$, the $[\alpha/\beta\text{-}W_6(\mu_2\text{-}O)_6(\mu_2\text{-}Cl)_6Cl_6]^{2-}$ salts were obtained.

Assuming that $WOCl_4$, when reduced by Bi, will always yield $[\alpha/\beta\text{-}W_6(\mu_2\text{-}O)_6(\mu_2\text{-}Cl)_6Cl_6]^{2-}$, there are several possible explanations for its repeated isolation even when higher tungsten oxides and stoichiometries were used. WO_2Cl_2 may react with WCl_6 at low temperatures to exchange ligands and produce two equivalents of $WOCl_4$; also, WO_3 is know to react with WCl_6 to form $WOCl_4$ at 200 ^oC and WO_2Cl_2 at 350 ^oC.[123] These arguments strongly support the idea that $WOCl_4$ is present at some point during reaction and preferentially reacts with Bi to form $[\alpha/\beta\text{-}W_6(\mu_2\text{-}O)_6(\mu_2\text{-}Cl)_6Cl_6]^{2-}$ as a thermodynamic product.

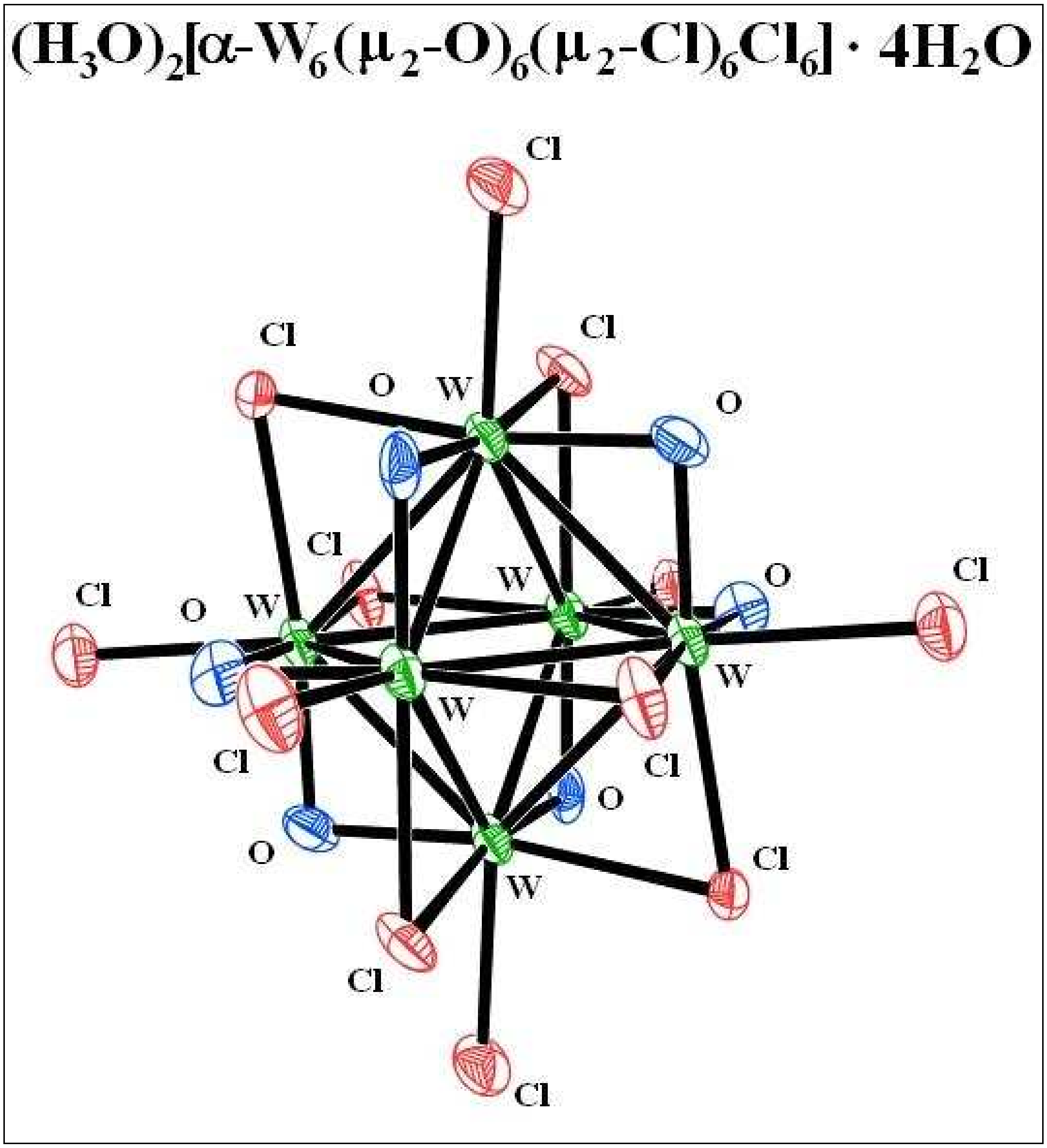

Figure 7.3: Solid-State molecular structure of $[\alpha\text{-}W_6(\mu_2\text{-}O)_6(\mu_2\text{-}Cl)_6Cl_6]^{2-}$, anion from $(H_3O)_2[\alpha\text{-}W_6(\mu_2\text{-}O)_6(\mu_2\text{-}Cl)_6Cl_6]$. Color scheme: green, tungsten; red, chlorine; blue, oxygen.

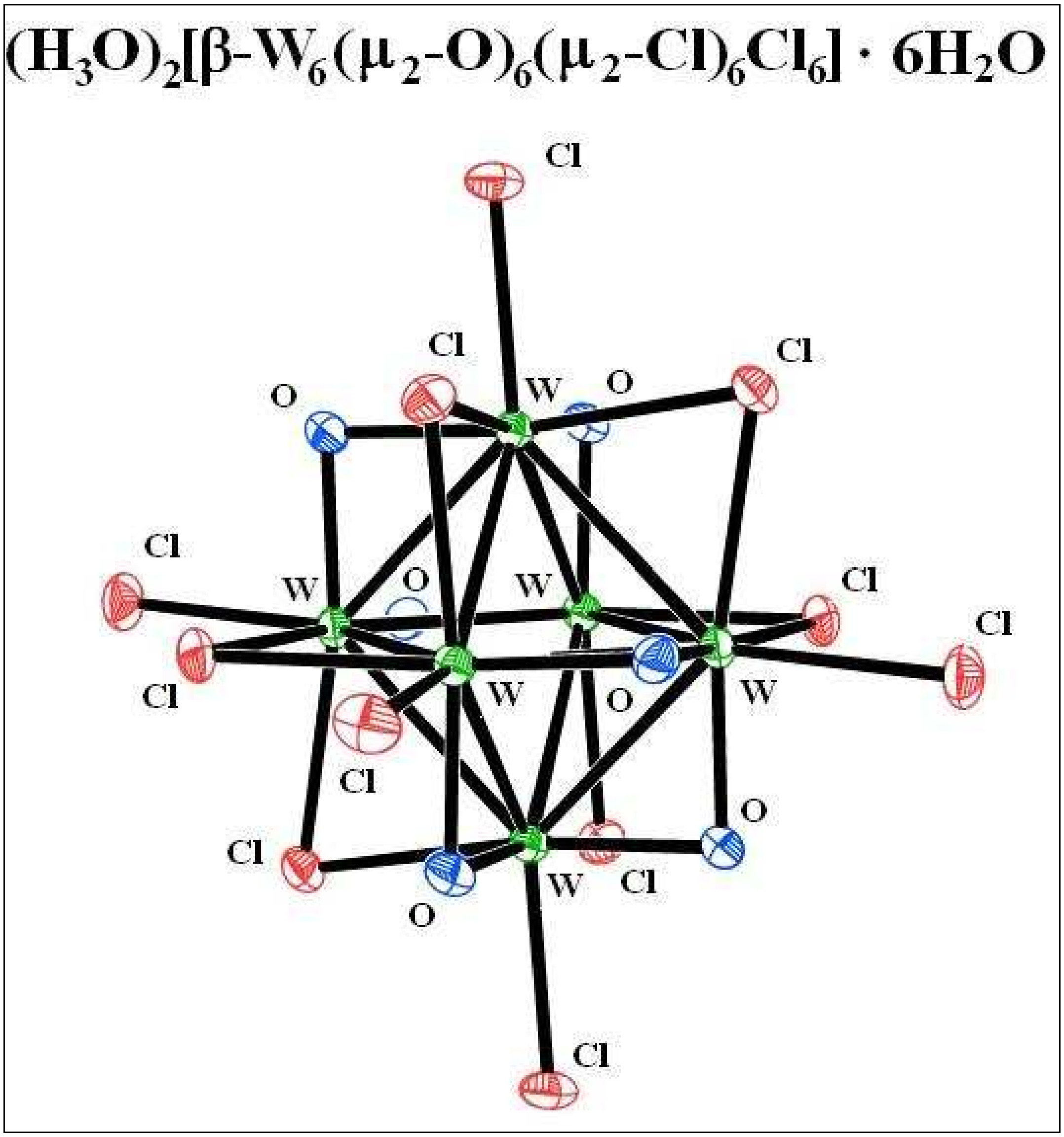

Figure 7.4: Solid-State molecular structure of $[\beta\text{-}W_6(\mu_2\text{-}O)_6(\mu_2\text{-}Cl)_6Cl_6]^{2-}$, anion from $(H_3O)_2[\beta\text{-}W_6(\mu_2\text{-}O)_6(\mu_2\text{-}Cl)_6Cl_6]$. Color scheme: green, tungsten; red, chlorine; blue, oxygen.

Hexanuclear tungsten clusters commonly possess face-bridged complexes. An interesting observation is that the average oxidation state of the tungstens in face-bridged clusters is +2, while the average oxidation state of the tungstens in $[\alpha/\beta\text{-}W_6(\mu_2\text{-}O)_6(\mu_2\text{-}Cl)_6Cl_6]^{2-}$ is +3.33. It may be possible that Bi is not an adequate reducing agent to reduce tungsten to the +2 oxidation state when oxides are present and thus adopt the face-bridged geometry. The oxidation state of the metal may play a large role in the geometry that is adopted by the complex. For example, niobium and tantalum halides tend to adopt structures with edge-bridged octahedral geometry in which 16 valence electrons participate in metal-metal bonding. In contrast, molybdenum and tungsten halides tend to exhibit structures with face-bridged octahedral geometry, where 24 valence electrons are involved in metal-metal bonding. Exceptions to these generalizations exist.[124] The $[\alpha/\beta\text{-}W_6(\mu_2\text{-}O)_6(\mu_2\text{-}Cl)_6Cl_6]^{2-}$ exhibits edge-bridged octahedral geometry, with a count of 14 tungsten-based valence electrons.

Solution Studies of $[\alpha/\beta\text{-}W_6(\mu_2\text{-}O)_6(\mu_2\text{-}Cl)_6Cl_6]^{2-}$

The repeated isolation of $[\alpha/\beta\text{-}W_6(\mu_2\text{-}O)_6(\mu_2\text{-}Cl)_6Cl_6]^{2-}$ led us to study these molecules in more detail. Each isomer (α-product or β-product) may be isolated separately based on workup conditions. The most common method employed in this research was workup with concentrated aqueous HCl. That is not to say that organic solvents do not allow for isolation of the α- or β-product; indeed, the α-product may be isolated from CH_3CN, and a mixture of the α- and β-products may be isolated from THF. If concentrated aqueous HCl solutions of the solid-state reaction material were heated, filtered, and then cooled to room temperature, $(H_3O)_2[W_6Cl_{14}]$ crystallized out of solution prior to isolation of the α- or β-product. After $(H_3O)_2[W_6Cl_{14}]$ was isolated and the filtrate allowed to slowly concentrate, α-product is obtained. The second crop was the β-product. The α-product can be preferentially isolated from the chloro acid and β-product by workup at room temperature with concentrated aqueous HCl solutions. The chloro acid and β-product are not soluble in room temperature aqueous HCl; these products can later be isolated by heating the undissolved reaction material from the α-product workup to boiling and subsequent cooling and concentration. It is also possible that applying heat to a solution of $[\alpha\text{-}W_6(\mu_2\text{-}O)_6(\mu_2\text{-}Cl)_6Cl_6]^{2-}$ may cause a structural rearrangement to β-form. This was not explored.

The majority of solution studies were performed on the α-product. The compound is very soluble and recrystallizable from H_2O. When the α-product is dissolved in H_2O and left for several weeks, yellow/tan precipitate forms and collects on the sides and bottom of the vial. Crystalline $(H_3O)_2[\alpha/\beta\text{-}W_6(\mu_2\text{-}O)_6(\mu_2\text{-}Cl)_6Cl_6]$ maintains crystallinity and its color when left in air for extended periods of time, suggesting stability towards dioxygen.

Conclusions

Inner-ligand-substitutions of hexanuclear tantalum and tungsten halides require more forcing reaction conditions than used in these experiments. Silylated chalcogenide reagents do not afford inner-chloro substitution in the hexanuclear tantalum and tungsten halide clusters under refluxing solvent conditions or with neat silylated reagent. Ag_2O only oxidized tantalum clusters and had no effect on tungsten clusters.

Solid-state reactions to prepare mixed oxo-chloro tantalum clusters have been reported, but the reaction vessels and conditions are not listed. Attempts reported here have all resulted in ampule explosions because of weakening of vessel walls from side reactions with starting materials. Thicker quartz vessels may be the key to alleviate this problem. However, thicker walled quartz has its own drawbacks, such as extremely high working temperatures of quartz (i.e. flame-sealing the quartz ampule is more difficult and requires extremely high temperatures).

Solid-state reactions that targeted mixed oxo-chloro tungsten clusters have yielded complexes previously reported in the literature. However, the acid salts discussed here are unreported, and solution chemistry has not been reported. The α- and β-complexes have greater H_2O and O_2 stability than $[W_6Cl_{14}]^{2-}$. The repeated isolation of the α/β clusters raises several questions: (1) does $WOCl_4$, when reacted with Bi, always form $[\alpha/\beta\text{-}W_6(\mu_2\text{-}O)_6(\mu_2\text{-}Cl)_6Cl_6]^{2-}$, even with stoichiometries aimed at different targets; (2) do WO_2Cl_2 and WO_3 undergo exchange reactions prior to any reduction by Bi; (3) can a stronger reducing agent, such as In or $Ga^+[GaCl_4]^-$, reduce the tungsten oxychlorides further than Bi and lead to face-bridged geometries?

Experimental

General Considerations:

Moisture-sensitive precursors and products were manipulated under inert atmosphere on a Schlenk line or in a glovebox under a N_2 atmosphere. Thermolyne Model 21100 single-zone (≤ 1200 °C), Marshall Model 1046 single-zone (≤ 2000 °C) tube furnaces controlled by Omega CN3251 Temperature/Process Controller equipped with positional thermocouples, or a Carbolite Type TZF (≤ 1200 °C) three-zone tube furnace controlled by a Eurotherm 2416 CG, 2416P8 programmer were used in solid-state synthesis. Most syntheses employed dual-chambered borosilicate glass ampules of 17 or 19 mm OD and 20-40 mL total chamber volume, with a 14/20 or 24/40 ground-glass joint at one end and constriction between the end reaction chamber and receiver chamber and between the receiver chamber and joint (Figure 7.5). Typically, double-chambered ampules were used for reactions with Bi. The second chamber allowed for the sublimation of $BiCl_3$ from the reaction product. Other syntheses employed a single-chamber borosilicate or quartz ampules of 17 or 19 mm OD and 10-20 mL total chamber value, with a 14/20 or 24/40 ground-glass joint at one end. Ampules were oven-dried at 135 °C overnight and then cooled under vacuum in the glovebox antechamber. Reactants were homogenized by mortar and pestle prior to ampule loading using a long-stem funnel in order to minimize contamination of interior surfaces other than the reaction chamber.

The ground-glass ends of the ampules were closed off with a gas inlet adapter and then removed from the glovebox. Ampules were evacuated using a Schlenk line and flame-sealed under dynamic vacuum. Double-chamber ampules were approximately 140-160 mm in length after flame sealing. Single-chamber ampules were approximately 30-50 mm in length after flame sealing.

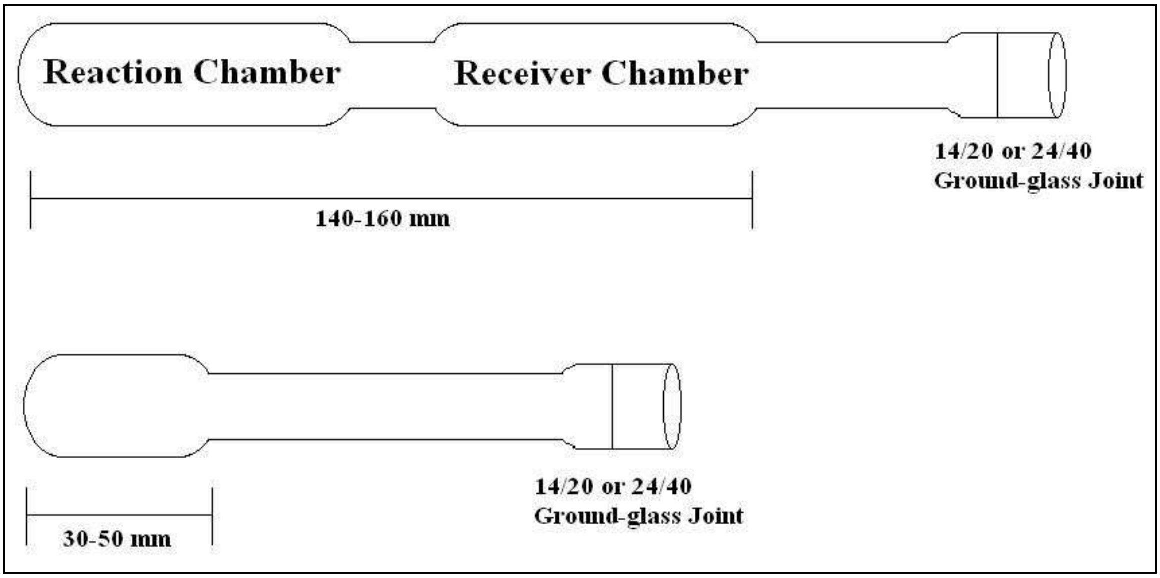

Figure 7.5: Depiction of the borosilicate/quartz ampules used in solid-state furnace reactions.

Tantalum powder (99.9 %, 325 mesh, Cerac), tantalum oxide (Ta_2O_5, Kawecki), tungsten hexachloride (WCl_6, 99.9 %, Strem), tungsten oxide (WO_3, Fluka or 20 micron, 99+ %, Aldrich) Bi (325 mesh, Cerac), indium powder (400 mesh, Ventron), gallium dichloride ($Ga^+[GaCl_4]^-$, Strem), hydrochloric acid (12.1 M, Fisher), tetrabutylammonium chloride (Aldrich), propionitrile (CH_3CH_2CN, Aldrich), hexamethyl-disiloxane (HMDS, d = 0.764 g/cm$_3$, 99.5 %, Aldrich), triethylsilane (99 %, Alrdich), silver oxide (Ag_2O, 99 %, Sigma Aldrich) sodium chloride (Fisher), and sodium hydroxide (Fisher) were used as received. Absolute ethanol (Decon Laboratories) was distilled from CaH_2 prior to use.

Tantalum pentachloride ($TaCl_5$, Cerac) was sublimed in double-chambered borosilicate glass ampules approximately 50 mm OD and 200-250 mL total chamber volume at 150 ^oC with one end of the ampule sticking out of the tube furnace. It is of importance to note that the $TaCl_5$ was contaminated with iron. Even after sublimation, the powder obtained is orange in color. The iron species was soluble in CH_2Cl_2 while the $TaCl_5$ was not. Washing with CH_2Cl_2 and subsequent washing with hexanes after sublimation yielded white free-flowing $TaCl_5$.

$[Ta_6(\mu_2\text{-}Cl)_{12}Cl_2(OH_2)_4]\cdot 4H_2O$ and $(Bu_4N)_4[Ta_6(\mu_2\text{-}Cl)_{12}Cl_6]$ were obtained from a published method.[125] $A_2[W_6(\mu_3\text{-}Cl)_8Cl_6]$ (A = H_3O^+ or Bu_4N^+)was obtained from a published method.[122]

Reactions using EtOH as a solvent were either performed using standard Schlenk line techniques or in an aqueous-glove box under $N_{2(g)}$ atmosphere.

Conversion of $[Ta_6(\mu_2\text{-}Cl)_{12}Cl_2(OH_2)_4]\cdot 4H_2O$ to $[Ta_6(\mu_2\text{-}Cl)_{12}(EtOH)_6]Cl_2$[126]

An-oven dried 250-mL Schlenk flask was charged with $[Ta_6(\mu_2\text{-}Cl)_{12}Cl_2(OH_2)_4]\cdot 4H_2O$ (Ta_6). Dry ethanol was added using standard Schlenk line techniques. The Ta_6 dissolved readily and was stirred for several days under inert atmosphere. The solvent was removed *in vacuo*. The resulting green solid was dissolved in dry ethanol and stirred overnight. The solvent was removed *in vacuo*; this procedure was repeated four times. After the last cycle, the dry product was stored in a glovebox prior to use.

Conversion of $[Ta_6(\mu_2\text{-}Cl)_{12}(EtOH)_6]Cl_2$ to $[Ta_6(\mu_2\text{-}Cl)_{12}(EtCN)_6]Cl_2$[127]

This procedure followed the procedure given for the conversion of $[Ta_6(\mu_2\text{-}Cl)_{12}Cl_2(OH_2)_4]\cdot 4H_2O$ to $[Ta_6(\mu_2\text{-}Cl)_{12}(EtOH)_6]Cl_2$. $[Ta_6(\mu_2\text{-}Cl)_{12}(EtOH)_6]Cl_2$ was dissolved in propionitrile. The solution was stirred for two hours, and solid began to form. The solution was then concentrated to approximately half volume by removal of solvent *in vacuo*. The solution slowly lost color to yield a light forest-green solid. The solvent was removed *in vacuo* and the solid stored in a glovebox.

Inner-Ligand-Substitution Reactions of $[Ta_6(\mu_2\text{-}Cl)_{12}Cl_2(OH_2)_4]\cdot 4H_2O$ with HMDS in a Variety of Solvents

$[Ta_6(\mu_2\text{-}Cl)_{12}Cl_2(OH_2)_4]\cdot 4H_2O$ (0.1 g, 3.7 x 10^{-2} mmol) was reacted with HMDS in 20 mL scintillation vials in the glove box in a variety of solvents (CH_3CN, CH_2Cl_2, THF, and EtOH). Varying amounts of HMDS (1, 2, 3, 5, or 10 equivalents of HMDS) were added to each reactant. Solutions of $[Ta_6(\mu_2\text{-}Cl)_{12}Cl_2(OH_2)_4]\cdot 4H_2O$ in the various solvents all gave dark forest-green colors. No observable reaction occurred when HMDS was introduced to the solution. Reaction progress was observed by color change. After 24 hrs the solutions were refluxed using standard Schlenk techniques. After reflux, no observable color change was noted for any of these reactions.

Inner-Ligand-Substitution Reactions of $[Ta_6(\mu_2\text{-}Cl)_{12}Cl_2(OH_2)_4]\cdot 4H_2O$ with Ag_2O in a Variety of Solvents

$[Ta_6(\mu_2\text{-}Cl)_{12}Cl_2(OH_2)_4]\cdot 4H_2O$ (0.1 g, 3.7 x 10^{-2} mmol) was reacted with Ag_2O in a 20 mL scintillation vial in the glove box with a variety of solvents (CH_3CN, CH_2Cl_2, THF, and EtOH). Ag_2O (1 or 2 equivalents) were added to each reaction. Solutions of $[Ta_6(\mu_2\text{-}Cl)_{12}Cl_2(OH_2)_4]\cdot 4H_2O$ in the various solvents all yielded dark forest-green colors. No observable reaction occurred when Ag_2O was introduced to the solution. Reaction progress was observed by color change. After 24 hrs the solutions were refluxed using standard Schlenk techniques. After reflux, no observable color change was noted for any of these reactions.

Inner-Ligand-Substitution Reactions of $(Bu_4N)_4[Ta_6(\mu_2\text{-}Cl)_{12}Cl_6]$ with HMDS in a Variety of Solvents

$(Bu_4N)_4[Ta_6(\mu_2\text{-}Cl)_{12}Cl_6]$ (0.1 g, 3.7 x 10^{-2} mmol) was reacted with HMDS in 20 mL scintillation vials in the glove box with a variety of solvents (CH_3CN, CH_2Cl_2, THF, and EtOH). Varying amounts of HMDS (1, 2, 3, 5, or 10 equivalents of HMDS) were added to each reaction. Solutions of $[Ta_6(\mu_2\text{-}Cl)_{12}Cl_2(OH_2)_4]\cdot 4H_2O$ in the various solvents all yielded dark forest-green colors. No observable reaction occurred when HMDS was introduced to the solution. Reaction progress was observed by color change. After 24 hrs the solutions were refluxed using standard Schlenk techniques. After reflux, no observable color change was noted for any of these reactions.

Inner-Ligand-Substitution Reactions of $(Bu_4N)_4[Ta_6(\mu_2\text{-}Cl)_{12}Cl_6]$ with Ag_2O in a Variety of Solvents

$(Bu_4N)_4[Ta_6(\mu_2\text{-}Cl)_{12}Cl_6]$ (0.1 g, 3.7 x 10^{-2} mmol) was reacted with Ag_2O in a 20 mL scintillation vial in the glove box with various solvents (CH_3CN, CH_2Cl_2, THF, and EtOH). Varying amounts of Ag_2O (1 or 2 equivalents) were added to each reaction. Solutions of $[Ta_6(\mu_2\text{-}Cl)_{12}Cl_2(OH_2)_4]\cdot 4H_2O$ in the various solvents all yielded dark forest-green colors. No observable reaction occurred when Ag_2O was added to the solution. Reaction progress was observed by color change. Reactions in CH_3CN and CH_2Cl_2 did change from green to brown-red and gave a white solid after 24 hrs. The white solid was presumed to be AgCl but was not characterized. Brown crystals were grown by layering with hexanes. The crystals were determined to be $(Bu_4N)_3[Ta_6(\mu_2\text{-}Cl)_{12}Cl_6]$ by X-ray diffractometery.

Inner-Ligand-Substitution Reactions of $[Ta_6(\mu_2\text{-}Cl)_{12}(EtOH)_6]Cl_2$ with HMDS in a Variety of Solvents

$[Ta_6(\mu_2\text{-}Cl)_{12}(EtOH)_6]Cl_2$ (0.1 g, 6.67 x 10^{-2} mmol) was reacted with HMDS in 20 mL scintillation vials in the glove box with various solvents (CH_3CN, CH_2Cl_2, THF, and EtOH). Varying amounts of HMDS (1, 2, 3, 5, or 10 equivalents of HMDS) were added to each reaction. Solutions of $[Ta_6(\mu_2\text{-}Cl)_{12}Cl_2(OH_2)_4]\cdot 4H_2O$ in the various solvents all yielded dark forest-green colors. No observable reaction occurred when HMDS was added to the solutions. Reaction progress was observed by color change. Reactions in CH_3CN would slowly lose color and while dark forest-green crystalline product grew on the sides and bottom of the reaction flask. Similar observations occur when the EtOH adduct was converted to the RCN adduct. The crystalline product was most likely $[Ta_6(\mu_2\text{-}Cl)_{12}(CH_3CN)_6]Cl_2$ based on crystal color and morphology. Other solvents did not give any visible indication of reaction. After 24 hrs the solutions were refluxed using standard Schlenk techniques. Under reflux, no observable color change was noted for any of these reactions.

Inner-Ligand-Substitution Reactions of $[Ta_6(\mu_2\text{-}Cl)_{12}(EtOH)_6]Cl_2$ with Ag_2O in a Variety of Solvents

$(Bu_4N)_4[Ta_6(\mu_2\text{-}Cl)_{12}Cl_6]$ (0.1 g, 3.7 x 10^{-2} mmol) was reacted with Ag_2O in a 20 mL scintillation vial in the glove box with various solvents (CH_3CN, CH_2Cl_2, THF, and EtOH). Varying amounts of Ag_2O (1 or 2 equivalents) was added to each reaction. Solutions of $[Ta_6(\mu_2\text{-}Cl)_{12}Cl_2(OH_2)_4]\cdot 4H_2O$ in the various solvents all yielded dark forest-green colors. No observable reaction occurred when Ag_2O was introduced to the solution. Reaction progress was observed by color change. Reactions in CH_3CN would slowly lose color, and crystalline product was obtained but not characterized. Similar observations occur when the EtOH adduct is converted to the RCN adduct. The crystalline product was most likely $[Ta_6(\mu_2\text{-}Cl)_{12}(CH_3CN)_6]Cl_2$ based on crystal color and morphology. All other solvents did not give any visible indication of reaction. After 24 hrs the solutions were refluxed using standard Schlenk techniques. Under reflux, no observable color change was noted for any of these reactions.

Inner-Ligand-Substitution Reactions of $[Ta_6(\mu_2\text{-}Cl)_{12}(EtCN)_6]Cl_2$ with HMDS in a Variety of Solvents

These reactions were performed as described above for the reaction of $[Ta_6(\mu_2\text{-}Cl)_{12}(EtOH)_6]Cl_2$ with HMDS. No observable reactions took place based on color.

Inner-Ligand-Substitution Reactions of $[Ta_6(\mu_2\text{-}Cl)_{12}(EtCN)_6]Cl_2$ with Ag_2O in a Variety of Solvents

These reactions were performed as described above for the reaction of $[Ta_6(\mu_2\text{-}Cl)_{12}(EtOH)_6]Cl_2$ with Ag_2O. No observable reactions took place based on color.

Solid-State Attempts to Prepare $A_x[Ta_6(\mu_2\text{-}Cl)_{12}(\mu_2\text{-}O)_2]$ (A = Cs, x = 0.938; or A = In, x = 0.634)

$TaCl_5$ (0.5 g, 1.393 mmol), Ta_2O_5 (0.1028 g, 0.2326 mmol), Ta (0.294 g, 1.6275 mmol), and In (0.0666 g, 0.580 mmol) or CsCl (0.0979 g, 0.580 mmol) were ground together and then placed in a quartz ampule. The ampule was flame-sealed under dynamic vacuum. The sealed ampule was placed in a tube furnace that was programmed to reach 750 ^oC over a two-hour period, after which the furnace was allowed to stabilize at 750 ^oC for 96 hours. After the allotted time, the furnace was allowed to slowly cool to room temperature over 96 hours. The reaction ampule was found to have exploded.

Attempts were performed at lower temperatures in quartz and in borosilicate ampules. The quartz ampule was heated to 600 ^{o}C over 15 hours, after which the temperature was held at 600 ^{o}C for 96 hours. After the allotted time, the furnace was allowed to slowly cool to room temperature over 36 hours. This ampule exploded. The borosilicate ampule was heated in a furnace programmed to reach 500 ^{o}C over 15 hours, after which the temperature was held at 500 ^{o}C for 24 hours. After the allotted time, the furnace was allowed to slowly cool to room temperature over 24 hours. This ampule was brought into the glovebox and worked up with various solvents.

Inside the glovebox, the solid-products were found to have some solubility in CH_3CN, CH_2Cl_2, and THF. The material was insoluble in diethyl ether, toluene, hexanes, and $ClCH_2CH_2Cl$. Separate extraction with CH_3CN, CH_2Cl_2, and THF was performed on the solid material. CH_3CN produced a brown yellow solution, CH_2Cl_2 produced a green solution with very fine white precipitate, and THF produced a tan solution. All solutions had black insoluble byproduct that was removed by filtration prior to attempts to grow crystals. The solutions that exhibited the brown color lost all color or become green over time, with the formation of brown precipitate. Layering the green solutions with hexanes produced crystalline material later determined to be $InCl_4[Ta_6Cl_{12}(CH_3CN)_6]$.

Solid-State Attempts to Prepare $In_6[Ta_6(\mu_2\text{-}Cl)_{10}(\mu_2\text{-}O)_2Cl_6]$

$TaCl_5$ (0.50 g, 1.393 mmol), Ta_2O_5 (0.077 g, 0.1741 mmol), Ta (0.1575 g, 0.871 mmol), and In (0.2999 g, 2.612 mmol) were ground together and then placed in a borosilicate ampule. The ampule was flame-sealed under dynamic vacuum. The ampule was heated in a furnace programmed to reach 500 ^{o}C over 15 hours, after which the temperature was held at 500 ^{o}C for 24 hours. The furnace was allowed to slowly cool to room temperature over 24 hours. The ampule’s walls were frosted, and a bluish black solid formed at the bottom. This ampule was brought into the glovebox and worked up with various solvents.

The material obtained from the solid-state reaction was insoluble in CH_3CN, THF, and CH_2Cl_2. No further characterization was performed.

Solid-State Attempts to Prepare

$Cs_6[Ta_6(\mu_2\text{-}Cl)_{10}(\mu_2\text{-}O)_2Cl_6]$

$TaCl_5$ (0.50 g, 1.393 mmol), Ta_2O_5 (0.123 g, 0.2786 mmol), Ta (0.403 g, 2.229 mmol), and CsCl (0.704 g, 4.179 mmol) were ground together and then placed in a borosilicate ampule. The ampule was flame-sealed under dynamic vacuum. The ampule was heated in a furnace programmed to reach 500 ^{o}C over 15 hours, after which the temperature was held at 500 ^{o}C for 24 hours. After the allotted time, the furnace was allowed to slowly cool to room temperature over 24 hours. A green-black crystalline solid was obtained from the solid-state reaction. Several crystals were isolated in the glovebox and single crystal X-ray diffraction was performed. The crystalline material was an extended structure with no Ta-Ta bonds. The rest of the material was worked up with several solvents. The material obtained from the solid-state reaction was insoluble in CH_3CN, THF, and CH_2Cl_2. No further characterization was performed.

Inner-Ligand-Substitution Reactions of

$(H_3O)_2[W_6(\mu_3\text{-}Cl)_8Cl_6]$ with HMDS in a Variety of

Solvents

$(H_3O)_2[W_6(\mu_3\text{-}Cl)_8Cl_6]$ (0.1 g, 6.11 x 10^{-2} mmol) was reacted with HMDS in 20 mL scintillation vials in the glove box with various solvents (CH_3CN, CH_2Cl_2, THF, and EtOH). Varying amounts of HMDS (1, 2, 3, 5, or 10 equivalents of HMDS) was added to each reaction. Solutions of $(H_3O)_2[W_6(\mu_3\text{-}Cl)_8Cl_6]$ in the various solvents all yieled a light yellow color ($(H_3O)_2[W_6(\mu_3\text{-}Cl)_8Cl_6]$ was only slightly soluble in CH_2Cl_2). No observable reaction occurred when HMDS was added to the solutions. Reaction progress was observed by color change. After 24 hrs, the solutions were refluxed using standard Schlenk techniques. Under reflux, no observable color change was noted for any of these reactions.

Inner-Ligand-Substitution Reactions of $(H_3O)_2[W_6(\mu_3\text{-}Cl)_8Cl_6]$ with Ag_2O in a Variety of Solvents

$(H_3O)_2[W_6(\mu_3\text{-}Cl)_8Cl_6]$ (0.1 g, 6.11 x 10^{-2} mmol) was reacted with Ag_2O in a 20 mL scintillation vial in the glove box with various solvents (CH_3CN, CH_2Cl_2, THF, and EtOH). Varying amounts of Ag_2O (1 or 2 equivalents) were added to each reaction. Solutions of $(H_3O)_2[W_6(\mu_3\text{-}Cl)_8Cl_6]$ in the various solvents all gave a light-yellow color ($(H_3O)_2[W_6(\mu_3\text{-}Cl)_8Cl_6]$ was only slightly soluble in CH_2Cl_2). No observable reaction occurred when Ag_2O was added to the solutions. Reaction progress was observed by color change. Reactions in CH_3CN and THF gave a golden-yellow color after 24 hrs. Crystals were obtained by vapor diffusion of Et_2O. Crystalline product was determined to be starting material by single-crystal X-ray diffractometry.

Crystalline starting material was also obtained when the reaction mixtures were refluxed.

Inner-Ligand-Substitution Reactions of $(Bu_4N)_2[W_6(\mu_3\text{-}Cl)_8Cl_6]$ with HMDS in a Variety of Solvents

$(Bu_4N)_2[W_6(\mu_3\text{-}Cl)_8Cl_6]$ (0.1 g, 4.79 x 10^{-2} mmol) was reacted with HMDS in 20 mL scintillation vials in the glove box with various solvents (CH_3CN, CH_2Cl_2, THF, and EtOH). Varying amounts of HMDS (1, 2, 3, 5, or 10 equivalents of HMDS) was added to each reaction. Solutions of $(Bu_4N)_2[W_6(\mu_3\text{-}Cl)_8Cl_6]$ in the various solvents all gave a light-yellow color ($(Bu_4N)_2[W_6(\mu_3\text{-}Cl)_8Cl_6]$ was only slightly soluble in CH_2Cl_2). No observable reaction occurred when HMDS was added to the solution. Reaction progress was observed by color change. After 24 hrs the solutions were refluxed using standard Schlenk techniques. After reflux, no observable color change was noted for any of these reactions.

Inner-Ligand-Substitution Reactions of $(Bu_4N)_2[W_6(\mu_3\text{-}Cl)_8Cl_6]$ with Ag_2O in a Variety of Solvents

$(Bu_4N)_2[W_6(\mu_3\text{-}Cl)_8Cl_6]$ (0.1 g, 4.79 x 10^{-2} mmol) was reacted with Ag_2O in a 20 mL scintillation vial in the glove box with various solvents (CH_3CN, CH_2Cl_2, THF, and EtOH). Varying amounts of Ag_2O (1 or 2 equivalents) was added to each reaction. Solutions of $(Bu_4N)_2[W_6(\mu_3\text{-}Cl)_8Cl_6]$ in the various solvents all obtained a light-yellow color ($(Bu_4N)_2[W_6(\mu_3\text{-}Cl)_8Cl_6]$ was only slightly soluble in CH_2Cl_2). No observable reaction occurred when Ag_2O was added to the solutions. Reaction progress was observed by color change. Reactions in CH_3CN and THF gave a golden-yellow color and after 24 hrs. Crystals were obtained by vapor diffusion of Et_2O. Crystalline product was determined to be starting material by single-crystal X-ray diffractometry.

Crystalline starting material was also obtained when the reaction mixtures were refluxed.

Solid-State Attempts to Prepare $[W_6(\mu_3\text{-}O)_4(\mu_3\text{-}Cl)_4]$ or $Bi_3[W_6(\mu_3\text{-}O)_4(\mu_3\text{-}Cl)_4Cl_6]$ via $WOCl_4$ Reduction

$WOCl_4$ (1.0 g, 2.9 mmol), WCl_6 (0.58 g, 1.5 mmol), and Bi powder (1.22 g, 5.85 mmol) were ground together and inserted into a double-chamber glass ampule via long-stem funnel. The ampule was closed off with a gas inlet adapter, brought out of the glovebox, and flame-sealed under dynamic vacuum. The vessel was placed in the center of a tube furnace. The furnace was programmed to heat to 350 ^{o}C over 4 hours, at which point the second chamber (receiver chamber) was removed from the furnace. The reaction chamber was allowed to heat at 350 ^{o}C for 24 hours and then allowed to slowly cool to room temperature. White crystalline material, presumably $BiCl_3$, sublimed into the receiving chamber. The ampule was brought into the glovebox to be opened and worked up.

The contents of the vessel were split into two equivalent portions. One was worked up in the glovebox while the other was worked up in concentrated HCl solution. Inside the glovebox, small portions were placed in small vials and mixed with CH_3CN, THF, or CH_2Cl_2 in attempts to determine solubility. Samples in CH_3CN and THF gave orange-red solutions with insoluble black material at the bottom, and samples in CH_2Cl_2 remained colorless with insoluble brown material at the bottom. The remainder of the original glovebox sample was divided into two portions and mixed with CH_3CN and with THF. These samples were shaken overnight to insure the dissolution of any soluble species. Clear red-orange solutions were obtained after filtering through Celite. No crystalline product was obtained.

Workup with concentrated HCl solution was performed in a hood. The majority of the solid dissolved in 12.1 M HCl (25 mL) to yield an amber solution. The solution was filtered through a medium porosity glass-fritted funnel to produce a clear amber solution. The solid obtained on the frit was grey-green. Cooling the sample in an ice bath did not induce crystallization, so the solution was heated to near boiling in order to concentrate the solution. The solution was left open to air for several days, and dark crystalline needles formed. The crystals were isolated, covered with mother liquor, and set aside for single crystal X-ray diffraction. The crystalline material was determined to be $(H_3O)_2[\alpha\text{-}W_6(\mu_2\text{-}O)_6(\mu_2\text{-}Cl)_6Cl_6]\cdot 4H_2O$ (0.267 g, 21.25 % yield based on $WOCl_4$). The rest of the sample was concentrated further by heating and accidently reduced to dryness. More concentrated HCl solution was added and the solution heated to dissolve the solid. The solution was filtered and allowed to cool to room temperature. Yellow needles formed when the solution cooled to room temperature; these were later determined to be $(H_3O)_2[W_6Cl_{14}]$ (0.105 g) by X-ray diffractometry. Further filtration provided a clear amber solutions that upon slow evaporation of solvent yielded $(H_3O)_2[\beta\text{-}W_6(\mu_2\text{-}O)_6(\mu_2\text{-}Cl)_6Cl_6]\cdot 6H_2O$ (0.113 g, 8.8 % yield based on $WOCl_4$) by X-ray diffractometry.

Recrystallization of $(H_3O)_2[\alpha\text{-}W_6(\mu_2\text{-}O)_6(\mu_2\text{-}Cl)_6Cl_6]$

$(H_3O)_2[\alpha\text{-}W_6(\mu_2\text{-}O)_6(\mu_2\text{-}Cl)_6Cl_6]\cdot 4H_2O$ (0.1 g, 5.765 x 10^{-2} mmol) was dissolved in a minimal amount of water and then allowed to slowly concentrate in a hood by evaporation in air. Crystalline product (0.0821 g, 82.1% yield) was obtained within one week and was determined to be $(H_3O)_2[\alpha\text{-}W_6(\mu_2\text{-}O)_6(\mu_2\text{-}Cl)_6Cl_6]\cdot XH_2O$.

X-Ray Diffractometry:

$(H_3O)_2[\alpha\text{-}W_6(\mu_2\text{-}O)_6(\mu_2\text{-}Cl)_6Cl_6]\cdot 4H_2O$

A dark red-orange needle with dimensions of 0.21 x 0.04 x 0.03 mm^3 from the solid-state reaction was mounted via grease on the tip of a glass fiber (epoxied to a brass pin) and placed on the diffractometer with the long crystal dimension approximately parallel to the diffractometer phi axis. Data were collected on a Nonius KappaCCD diffractometer (Mo K_α radiation, graphite monochromator) at 190 K (cold N_2 gas stream) using standard CCD data collection techniques. Lorentz and polarization corrections were applied to the 47572 data. A correction for absorption using the multi-scan technique was applied (T_{max} = 0.5174, T_{min} = 0.0761). Equivalent data were averaged yielding 3301 unique data (R-int = 0.0437, 2772 with $F > 4\sigma(F)$). Based on preliminary examination of the crystals, the space group P2(1)/n was assigned. The computer programs from the HKLint package were used for data reduction. Structure refinement was performed with the SHELXTL v6.1 software package.

The preliminary model of the structure was obtained using XS, a direct methods program. Least-squares refinement of the model vs. the data was performed with the XH program. Tables were made with the XCIF program. All non-hydrogen atoms were refined with anisotropic thermal parameters. All H atoms were included with the riding model using the XL program default values. Any restraints and constraints imposed on the data are described in the .cif files.

X-Ray Diffractometry:

$(H_3O)_2[\beta\text{-}W_6(\mu_2\text{-}O)_6(\mu_2\text{-}Cl)_6Cl_6]\cdot 6H_2O$

An orange blade with dimensions of 0.12 x 0.065 x 0.01 mm^3 from the second crop of the solid-state reaction was mounted via grease on the tip of a glass fiber (epoxied to a brass pin) and placed on the diffractometer with the long crystal dimension approximately parallel to the diffractometer phi axis. Data were collected on a Nonius KappaCCD diffractometer (Mo K_α radiation, graphite monochromator) at 190 K (cold N_2 gas stream) using standard CCD data collection techniques. Lorentz and polarization corrections were applied to the 3426 data. A correction for absorption using the multi-scan technique was applied (T_{max} =0.7887, T_{min} = 0.1539). Equivalent data were averaged yielding 3426 unique data (R-int = 0.0243, 3079 with $F > 4\sigma(F)$). Based on preliminary examination of the crystals, the space group P-1 was assigned. The computer programs from the HKLint package were used for data reduction. Structure refinement was performed with the SHELXTL v6.1 software package.

The preliminary model of the structure was obtained using XS, a direct methods program. Least-squares refinement of the model vs. the data was performed with the XH program. Tables were made with the XCIF program. All non-hydrogen atoms were refined with anisotropic thermal parameters. All H atoms were included with the riding model using the XL program default values. Any restraints and constraints imposed on the data are described in the .cif files.

X-Ray Diffractometry:

Recrystallized

$(H_3O)_2[\alpha\text{-}W_6(\mu_2\text{-}O)_6(\mu_2\text{-}Cl)_6Cl_6]\cdot 4H_2O$

A red orange plate with dimensions of 0.06 x 0.05 x 0.02 mm^3 was mounted via grease on the tip of a glass fiber (epoxied to a brass pin) and placed on the diffractometer with the long crystal dimension approximately parallel to the diffractometer phi axis. Data were collected on a Nonius KappaCCD diffractometer (Mo K_α radiation, graphite monochromator) at 190 K (cold N_2 gas stream) using standard CCD data collection techniques. Lorentz and polarization corrections were applied to the 3395 data. A correction for absorption using the multi-scan technique was applied (T_{max} = 0.7464, T_{min} = 0.4559). Equivalent data were averaged yielding 1391 unique data (R-int = 0.1262, 1047 with $F > 4\sigma(F)$). Based on preliminary examination of the crystals, the space group R-3 was assigned. The computer programs from the HKLint package were used for data reduction. Structure refinement was performed with the SHELXTL v6.1 software package.

The preliminary model of the structure was obtained using XS, a direct methods program. Least-squares refinement of the model vs. the data was performed with the XH program. Tables were made with the XCIF program. All non-hydrogen atoms were refined with anisotropic thermal parameters. All H atoms were included with the riding model using the XL program default values. Any restraints and constraints imposed on the data are described in the .cif files.

CHAPTER 8:
GENERAL SUMMARIES AND FUTURE WORK

High-nuclearity clusters have received considerable interest because of their intriguing variety of architectures and potential applications in magnetic materials, optical materials, catalysis, and biological and materials chemistry. The synthesis of high-nuclearity clusters is still a great challenge for chemists. The two types of clusters presented in this thesis include octahedral hexanuclear transition metal clusters and polynuclear lanthanide clusters. The latter have fewer well-characterized examples, and their syntheses are still characteristically viewed as self-assembly. However, common synthetic strategies have been developed for both classes of clusters.

Transition metal clusters are most commonly synthesized through stoichiometry-controlled solid-state syntheses. The resulting compounds are then isolated from side-products by various methods, such as solid-state crystallization or extraction of soluble products.

The tendency of lanthanide ions to form polynuclear aggregates in aqueous solutions is well known. However, the formation of insoluble aggregates can be avoided, and discrete polynuclear lanthanide clusters obtained by controlled hydrolysis of metal ions with the aid of supporting ligands. Hydrophilic groups such as oxo, hydroxo, and carboxylate bridge the metal ions to make up a cluster core, while hydrophobic groups take up the periphery, preventing cores from further aggregation. A wide variety of ligands have been used in this capacity, the more prominent being carboxylates, polyketonates, and alkoxides.

The solid-state structures of transition metal and polynuclear lanthanide clusters are better understood. Much of the work reported here involved attempts to understand the solution-state structure and chemistry of both types of clusters.

Part I: Polynuclear Lanthanide Complex Chemistry

General Conclusions

The synthesis of polynuclear lanthanide clusters was reported in Chapters 2 and 3. Chapter 2 focused on the synthesis and characterization of halide-templated L-histidine-supported pentadecanuclear lanthanide clusters (Ln_{15}-his X; Ln = Y, La, Nd, Eu, and Tb; X = Cl, Br, $(I)_2$-OH). In summary, Ln_{15}-his X was prepared by aqueous hydrolysis of $Ln(ClO_4)_3$ in the presence of L-histidine and NaX. All complexes were characterized by single-crystal X-ray diffraction. The core structure, $Ln_{15}(\mu_3\text{-}OH)_{20}$, remains relatively unchanged throughout the halide series. It was found that the central pentagonal cavity that is formed from the five vertex-sharing cubanes will expand slightly with increased halide size, but only to a small extent. The cavity does not expand in order to accommodate an iodide in the plane of the pentagon. Instead, a hydroxide localizes in the middle of the inner Ln_5 plane, and iodides sit above and below. Supporting L-histidine ligands were found to coordinate in three distinct coordination modes for Ln = Y, Eu, Gd, Tb. For complexes with large Ln(III) ions, such as Nd(III) or La(III), the L-histidine ligands adopted two new modes of coordination. The ability of separate clusters to link together into a one-dimensional extended structure was particularly noteworthy. Ln_{15}-his X complexes could be recrystallized from L-histidine buffered solutions (0.1 M, pH = 6.4).

The solution-state stability of these complexes was examined by NMR spectroscopy and ESI MS. Y(III) analogues were synthesized in order to characterize these complexes by ^{13}C and ^{89}Y NMR spectroscopy. ^{13}C NMR spectra were consistent with two unique histidine ligands in solution, one significantly further downfield than the other that matched the ^{13}C NMR spectrum of free L-histidine in aqueous solution. This suggests the possibility that some of the L-histidine ligands are labile. ^{89}Y NMR spectra of Y_{15}-his Cl exhibited two Y(III) resonances in solution with an integration of 1:2. The spectrum is consistent with the solid-state structure. The broadening of the downfield ^{89}Y signal, of relative ratio 2, was consistent with either ^{14}N quadrupolar coupling or a dynamic ^{89}Y environment (because of L-histidine lability). ESI mass spectra exhibited several envelopes with m/z values that were consistent with a fully-intact cluster core minus several anions and histidine ligands. NMR spectra and ESI-MS were consistent with solution-state stability of the Ln_{15}-his X complexes.

Chapter 3 discussed the first halide-free pentadecanuclear complex, Ln_{15}-his OH. It was previously thought that high-nuclearity lanthanide complexes were only obtainable by use of templating halides and that supporting ligands did not play a significant role other than to preclude extensive hydrolysis and aggregation. However, attempts to synthesize analogs of the Ln_{15}-his X (X = Cl, Br, $(I)_2$-OH) complexes with other amino acids (serine, glycine, valine, proline), in the presence of a halide were unsuccessful. The inability to obtain isostructural complexes with related amino acid ligands suggests that more than just anion-template effects influence the self-assembly of Ln(III) ions. The Ln_{15}-his OH complex demonstrates the need for a central negative charge density in order for these complexes to form. It was also shown that Ln_{15}-his OH complexes are capable of trapping halides. Recrystallization of Ln_{15}-his OH from L-histidine buffered solutions (0.1 M, pH = 6.0) in the presence of NaX yielded the corresponding Ln_{15}-his X.

Europium(III) analogues were synthesized for several reasons: (1) Eu(III) fluoresces in the visible, and this luminescence provides both qualitative and quantitative information, (2) Eu(III) has an accessible redox couple with Eu(II) that can be exploited to gain solution-state information, and (3) Eu(II)-based polynuclear clusters could provide excellent probes for redox-related physiological parameters. Chapter 4 discussed the fluorescence of Eu_{15}-his X complexes, Chapter 5 discussed the electrochemistry, and Chapter 6 explored the synthesis of divalent polyeuropium complexes.

Fluorescence profiles (excitation and emission) provided excellent qualitative information about Eu(III) complexes. The coordination environment for simple Eu(III) centers can be determined by emission splitting patterns. For complex molecules such as Eu_{15}-his X (X = Cl, Br, $(I)_2$-OH, OH), qualitative data is more readily observed. The emission profiles were consistent with coordinated inner-sphere ligands. In comparison with literature complexes, the Eu_{15}-his X fluorescence intensities suggest strong-field ligands, such as carboxylates, coordinated to the Eu(III) ions. Fluorescence data did not correspond to two unique Eu(III) centers in solution, as solid-state structural data suggests. This could be the result of very similar coordination environments for the Eu(III) centers, resulting in the two separate transitions overlapping, or major differences in solution structure.

Fluorescence lifetime measurements were obtained in order to ascertain the number of inner-sphere waters for Eu(III). Solution- and solid-state fluorescence lifetimes were measured for Eu_{15}-his X and perdeutero Eu_{15}-his X. The number of inner-sphere waters in the solution-state was determined to be between 22 and 24 per Eu_{15}-his X complex. This high number (20+ inner-sphere water molecules) was accounted for by the possible lability of the L-histidine ligands. The number of inner-sphere waters in the solid-state was also determined to be between 22 and 24. These values do not correlate with solid-state structure. It was concluded that the current equation used to determine the number of inner-sphere waters for mononuclear complexes requires alterations in order to provide an adequate estimation for the number of inner-sphere water molecules for polynuclear complexes. Similarities between the lifetimes of protio Eu_{15}-his X complexes dissolved in D_2O and solid perdeutero Eu_{15}-his X adducts suggested that the hydrogens of μ_3-OH ligands can exchange with bulk D_2O.

Chapter 5 examined the electrochemistry of polynuclear europium complexes. The redox potential of $Eu^{III}{}_{15}$-his X was determined to be irreversible. Data also suggests that these complexes were capable of multiple one-electron reduction steps. However, because the reduction potentials shift more negative as compared to aqueous Eu(III), these reduced complexes are not as electrochemically stable as their oxidized versions.

Cyclic voltammograms of Eu^{III}_{15}-his X complexes did not exhibit corresponding oxidative signals to reduction steps in DMSO. This could be the result of multiple consequences of reduction of the Eu^{III}_{15}-his X complexes. The most reasonable explanations include: (1) degradation of the complex, (2) rearrangement reactions, or (3) oxidation by other chemical species (e.g., perchlorate anion) in solution. Diffusion coefficients (D_o) were determined by CV and RDE measurements. Experimental D_o values were slower than theoretically-calculated values based on crystallographic radii. This suggests solute-solvent interaction. The diffusion coefficients are also much slower than that of $Eu(ClO_4)_3$ in DMSO, suggesting that the species observed in the Eu_{15}-his X studies is much larger than that of $Eu(ClO_4)_3$.

Chapter 6 explored the synthesis of divalent polyeuropium complexes by various methods: (1) direct synthesis of divalent polynuclear complexes from europium metal or divalent europium complexes, (2) chemical reduction of trivalent polyeuropium complexes with zinc amalgam, and (3) electrochemical reduction of trivalent polyeuropium complexes. Reaction of europous alkoxides with amino acids produced water-insoluble complexes.

Europous carbonate was examined as source of water-soluble Eu(II). Initial attempts started with the digestion of $EuCO_3$ in perchloric acid and subsequent hydrolysis in the presence of an amino acid. These attempts produced either insoluble precipitates or trivalent polyeuropium complexes. It is possible that perchlorate anions are not innocent, or that other oxidative processes were occurring. Suspecting perchlorate as the culprit, $EuCO_3$ was digested in aqueous HCl followed by hydrolysis in the presence of amino acids. These attempts did not produce isolable compounds.

Chemical reduction of trivalent polyeuropium complexes with zinc amalgam (Zn(Hg)) yielded trivalent starting materials. Reduction with Zn(Hg) has several draw-backs. The first is that these reactions are heterogenous and, as such, complete reduction may not be occurring. The second difficulty is that the reduction of Eu(III) by Zn(Hg) produces soluble Zn(II) in solution, and the chemistry of Zn(II) with the corresponding divalent polyeuropium complexes is unknown. Competitive chemical reactions occurring in solution may hinder crystallization of the desired complex.

Electrochemical reduction of trivalent europium complexes has been reported in the literature, and discussions with the pioneering author provided encouragement for the application of this method to polyeuropium complexes. Bulk electrolysis of trivalent polyeuropium compounds yielded either insoluble precipitates or polymeric crystalline product. The polymeric crystalline product obtained from the reduction of Eu_4-pro was determined to be trivalent. The polymeric compound is obtainable through stoichiometric reactions between Eu(III) and L-proline with no added base. However, Eu_4-pro is synthesized by base hydrolysis of Eu(III) in the presence of stoichiometric L-proline. With these two different reactions, one without base and one with base, two different products are obtained. This suggests that the Eu_4 complex, when reduced, undergoes a chemical process in which bonds are broken and reformed.

These experiments have demonstrated the difficulty of isolating divalent polyeuropium complexes. The difficulty may arise from oxidative processes, such as chemical oxidations and photooxidations.

Future Directions

In closing, the use of polygadolinium complexes with amino acid ligands as MRI contrast agents may be challenging because of the inherent toxicity of free Gd(III) ions that may be released from complexes with simple amino acid ligands. However, polynuclear lanthanide analogs may find other utility, as previously discussed. These complexes possess intriguing architectures and spectrochemical and electrochemical properties. This work has optimized reaction conditions for the isolation of discrete Ln_{15}-his X complexes, yielded the first halide-free pentadecanuclear lanthanide complex, and laid the foundation for spectrochemical analysis.

Future research directions could focus on:

(1) Ligand exchange reactions of Ln_{15}-his X with various amino acids or methylated histidine. Recrystallization of a structurally characterized complex in the presence of a different or labeled amino acid would be the simplest way to probe ligand-exchange reactions. Recrystallization of Ln_{15}-his X complexes from a ligand-buffered solution may yield isolable complexes with mixed ligand systems.

(2) Isolation of the first fluoride polynuclear lanthanide complex by means of trapping fluoride with Ln_{15}-his OH (LnF_3 compounds are insoluble and quickly precipitate out of solution when the free ions are present).

(3) Small molecule insertion reactions with Ln_{15}-his OH. Varying the size of the Ln(III) ion may provide interesting results in what type of small molecule may be inserted into the Ln_{15}-his cavity.

(4) Halide abstraction from Ln_{15}-his X (X = Cl, Br, $(I)_2$-OH) with silver salts ($AgClO_4$).

(5) Attempts to exchange the perchlorate anion of Ln_{15}-his X complexes with triflate, tosylate, nitrate, hexafluorophosphate, or tetrafluoroborate. Selecting a wide range of anions with various geometries may provide valuable information as to why initial attempts to synthesize polynuclear lanthanide triflates and tosylates have failed.

(6) Further understanding of the electrochemistry of Eu_{15}-his X. If these complexes have any possibility of being used in biomedical imaging, then their chemistry must be fully understood. Initial research should be performed in the modeling of the solution electrochemistry.

(7) Follow methods pioneered by Horrocks and co-workers to formulate an equation that is suitable for the determination of inner-sphere water molecules for polynuclear complexes.

(8) Exploring the fluorescence of polynuclear Tb(III) complexes in relation to the now established polynuclear Eu(III).

(9) Continued research in polynuclear Eu(II) chemistry, particularly in the synthesis of precursors from $EuCO_3$ with non-oxidizing acids such as triflic or para-toluenesulfonic acid, with weakly coordinated anions.

(10) Exploring the solution–state structure and "nearest neighbors" of the Ln(III) ions with X-ray absorption fine structure (XAFS).

(11) Determining the oxidation state of the metals and ligands with X-ray photoelectron spectroscopy (XPS) and electron paramagnetic resonance (EPR) spectroscopy.

Part II: Hexanuclear Tantalum and Tungsten Chemistry

General Conclusions

The primary goal of this research was to extend the chemistry of hexanuclear early transition metal mixed oxyhalide clusters. Chapter 7 was devoted to this chemistry. Initial attempts to produce mixed oxychloride clusters involved solution-state inner-ligand substitution reactions. These attempts followed literature precedent for reactions of silylated materials with hexarhenium chalcogenides, where inner chlorides were replaced by O^{2-}, S^{2-}, Se^{2-}, or Te^{2-}. Reaction of $[Ta_6(\mu_2\text{-Cl})_{12}Cl_2]^{4-}$, and various other adducts, or $[W_6(\mu_3\text{-Cl})_8Cl_6]^{2-}$ with hexamethyldisiloxane (HMDS) returned only starting materials. Reaction of $[Ta_6(\mu_2\text{-Cl})_{12}Cl_2]^{4-}$ with Ag_2O produced oxidized $[Ta_6(\mu_2\text{-Cl})_{12}Cl_2]^{3-}$. Reactions of $[W_6(\mu_3\text{-Cl})_8Cl_6]^{2-}$ with Ag_2O returned only starting material. Solution methods with these metathesis reagents did not seem to be a realistic approach to mixed oxychloride clusters.

Solid-state attempts to mixed oxychloride clusters of Ta and W gave differing results. Attempts to produce Ta clusters were unsuccessful because the temperatures required (>500 ^{o}C) for reaction also enabled undesirable side reactions to occur. The high temperatures required quartz ampoules and at these elevated temperatures, $TaCl_5$ reacts with SiO_2 to weaken the vessel and explode ampules.

Attempts towards mixed oxychloride clusters of tungsten via reduction of mixtures of WCl_6 and tungsten oxide or tungsten oxychlorides produced $[\alpha/\beta\text{-}W_6(\mu_2\text{-}O)_6(\mu_2\text{-}Cl)_6Cl_6]^{2-}$, a previously synthesized and structurally characterized core. We report our contribution to the chemistry of these compounds via the isolation of the acid salts $(H_3O)_2[\alpha/\beta\text{-}W_6(\mu_2\text{-}O)_6(\mu_2\text{-}Cl)_6Cl_6]$. The solution chemistry of these complexes was also explored. These chloroacids exhibit moderate H_2O and O_2 stability and may be recrystallized from H_2O. Inner-ligand substitution reactions of these complexes with HMDS and Ag_2O represent future directions.

Future Directions

Future research that could advance biomedical imaging goals are:

(1) Based on hexamolybdenum reports, explore the synthesis of hydroxide or alkoxide inner ligand substituted Ta_6 and W_6, followed by exchange of these new substituted clusters with stoichiometric halide or oxo ligand.

(2) Solid-state synthesis of mixed oxo-chloro tantalum clusters in thick-walled quartz ampoules.

(3) Solid-state synthesis of mixed oxygen-chlorine tungsten clusters with stronger reducing agents such as In or $Ga^+[GaCl_4]^-$, in efforts to force face-bridged geometry.

(4) Further solution-state inner-ligand substitution reactions of $[\alpha/\beta\text{-}W_6(\mu_2\text{-}O)_6(\mu_2\text{-}Cl)_6Cl_6]^{2-}$ and adducts thereof.

(5) Exploring the solution chemistry of $[\alpha/\beta\text{-}W_6(\mu_2\text{-}O)_6(\mu_2\text{-}Cl)_6Cl_6]^{2-}$ to determine if rearrangement reactions ($\alpha \rightarrow \beta$) occur at elevated temperatures.

(6) Perform solid-state reactions in attempts to isolate $[W_6(\mu_3\text{-}O)_4(\mu_3\text{-}Cl)_4]$ or $[W_6O_{10}Cl_2]$ from $WOCl_4$, WO_2Cl_2, or WO_3 with tungsten metal, in order to minimize possible side reactions with WCl_6.

APPENDIX A

CRYSTALLOGRAPHIC DATA FOR

$[Eu_{15}(\mu_5\text{-}Cl)(\mu_3\text{-}OH)_{20}(his^{+/-})_{10}(his^{-})_5(OH)_7](ClO_4)_{12}$

Identification code	mes82	
Empirical formula	C90 H120 Cl2 Eu15 N45 Na2 O75	
Formula weight	5428.59	
Temperature	190(2) K	
Wavelength	0.71073 Å	
Crystal system	Monoclinic	
Space group	$P2_1$	
Unit cell dimensions	a = 17.2041(18) Å	α= 90°.
	b = 31.384(4) Å	β= 92.185(5)°.
	c = 18.6881(19) Å	γ = 90°.
Volume	10083(2) $Å^3$	
Z	2	
Density (calculated)	1.788 Mg/m^3	
Absorption coefficient	4.701 mm^{-1}	
F(000)	5152	
Crystal size	0.36 x 0.26 x 0.18 mm^3	
Theta range for data collection	1.09 to 27.87°.	
Index ranges	-19<=h<=22, -39<=k<=41, -24<=l<=24	
Reflections collected	70673	
Independent reflections	44560 [R(int) = 0.0249]	
Completeness to theta = 27.87°	99.9 %	
Max. and min. transmission	0.4849 and 0.2824	
Refinement method	Full-matrix least-squares on F^2	
Data / restraints / parameters	44560 / 1 / 2392	
Goodness-of-fit on F^2	1.053	
Final R indices [I>2sigma(I)]	R1 = 0.0402, wR2 = 0.1141	
R indices (all data)	R1 = 0.0478, wR2 = 0.1301	
Absolute structure parameter	-0.013(9)	
Largest diff. peak and hole	2.993 and -1.927 e.$Å^{-3}$	

Atomic coordinates (x 10^4) and equivalent isotropic displacement parameters ($Å^2$x 10^3) for mes82. U(eq) is defined as one third of the trace of the orthogonalized U^{ij} tensor.

	x	y	z	U(eq)
Cl(2)	4290(1)	1584(1)	6936(1)	23(1)
Cl(3)	374(1)	2694(1)	8453(1)	29(1)
O(60)	4345(5)	2030(3)	7060(5)	37(2)
O(65)	247(5)	2336(3)	7977(6)	53(3)
Cl(4)	4742(2)	4459(1)	7937(2)	42(1)
Cl(10)	1539(2)	3351(1)	3681(2)	49(1)
O(85)	4915(7)	1435(4)	6561(6)	62(3)
O(50)	-326(5)	2864(4)	8706(7)	71(4)
O(37)	3586(6)	1483(4)	6555(6)	61(3)
O(97)	5545(7)	4403(4)	7787(7)	65(3)
O(80)	4547(7)	4894(4)	7898(7)	69(3)
O(71)	772(9)	3001(5)	8067(8)	87(4)
O(66)	4652(9)	4298(5)	8630(9)	91(4)
Cl(8)	1824(2)	-107(1)	10248(2)	48(1)
O(67)	2169(10)	-497(4)	9990(8)	86(4)
O(77)	726(9)	3465(5)	3582(11)	108(6)
O(94)	1888(9)	3381(5)	3019(9)	92(4)
O(95)	1616(9)	2916(6)	3921(10)	111(6)
O(59)	1892(9)	3629(6)	4162(9)	95(5)
Cl(12)	6421(1)	935(1)	6121(2)	36(1)
Cl(11)	-516(2)	512(1)	5212(2)	48(1)
O(103)	5759(5)	786(3)	5695(5)	49(2)
O(105)	6563(5)	1366(3)	6017(7)	60(3)
O(106)	4324(7)	1392(4)	7642(7)	67(3)
O(104)	6259(6)	886(5)	6866(6)	73(4)
O(101)	20(9)	364(5)	5796(9)	93(4)
O(91)	1548(15)	137(6)	9661(10)	148(10)
O(107)	7090(5)	696(4)	5914(9)	83(5)
O(109)	-362(8)	249(5)	4649(7)	90(5)
O(111)	884(9)	2597(5)	9033(8)	90(4)
O(110)	-1260(7)	432(5)	5423(8)	85(4)

O(108)	4328(8)	4230(5)	7452(8)	83(4)
O(115)	-409(12)	944(5)	5086(11)	122(7)
O(124)	1194(15)	-210(7)	10646(16)	189(14)
O(114)	2394(11)	87(9)	10717(18)	190(14)
Eu(1)	6772(1)	8087(1)	2306(1)	18(1)
Eu(2)	7972(1)	7604(1)	3873(1)	18(1)
Eu(6)	6210(1)	8212(1)	4334(1)	19(1)
Eu(15)	4998(1)	7932(1)	1182(1)	22(1)
Eu(4)	7962(1)	6292(1)	1357(1)	18(1)
Eu(9)	8244(1)	6623(1)	5195(1)	18(1)
Eu(5)	6821(1)	7284(1)	740(1)	18(1)
Eu(7)	7963(1)	8829(1)	3425(1)	22(1)
Eu(10)	10002(1)	5902(1)	2073(1)	21(1)
Eu(11)	8007(1)	5383(1)	2623(1)	22(1)
Eu(8)	9949(1)	7298(1)	4425(1)	21(1)
Eu(13)	6074(1)	6239(1)	160(1)	19(1)
Eu(12)	8109(1)	6601(1)	-551(1)	19(1)
Eu(3)	8706(1)	6507(1)	3272(1)	17(1)
Eu(14)	6871(1)	8437(1)	272(1)	23(1)
Cl(1A)	7658(1)	7148(1)	2305(1)	25(1)
O(1A)	7009(4)	7603(2)	4825(3)	25(1)
O(3A)	8169(4)	6044(2)	4244(3)	23(1)
O(2A)	5356(4)	8123(2)	2431(3)	26(2)
O(4A)	8954(4)	6252(3)	430(4)	29(2)
O(6A)	7437(4)	8763(2)	2153(4)	25(1)
O(5A)	5477(4)	6932(2)	433(4)	23(1)
O(9A)	8443(5)	6669(3)	-1842(4)	31(2)
N(11)	7221(4)	7093(2)	5617(4)	17(1)
O(14A)	7368(4)	7948(2)	1208(3)	21(1)
O(16A)	7432(4)	6091(2)	194(3)	22(1)
O(13A)	9087(4)	7231(2)	3416(3)	20(1)
O(15A)	6663(3)	6566(2)	1185(3)	19(1)
O(11A)	7771(4)	6855(2)	4015(3)	18(1)
O(10A)	8047(5)	5361(2)	3927(4)	30(2)
O(17A)	6040(4)	7512(2)	1678(3)	20(1)
O(18A)	7621(4)	8297(2)	4295(3)	23(1)

O(12A)	9080(4)	6489(2)	2022(3)	20(1)
O(20A)	6659(4)	7727(2)	3423(3)	20(1)
O(24A)	8012(5)	7336(3)	-988(4)	33(2)
O(21A)	8030(3)	8112(2)	2932(3)	19(1)
O(22A)	6215(4)	5525(3)	692(4)	29(2)
O(23A)	6247(4)	5874(2)	-935(4)	24(1)
O(19A)	6786(4)	6826(2)	-310(3)	22(1)
O(25A)	10884(4)	6825(3)	3881(4)	29(2)
O(29A)	8701(4)	7333(2)	4943(3)	21(1)
O(28A)	9249(4)	7971(2)	4141(4)	26(2)
O(26A)	8722(4)	5659(2)	1654(3)	21(1)
O(42A)	9329(3)	6612(2)	4418(3)	19(1)
O(27A)	10130(4)	6450(2)	3114(4)	24(1)
O(30A)	10443(5)	7009(3)	5507(4)	34(2)
O(31A)	9483(5)	6615(3)	5961(4)	34(2)
O(32A)	10011(4)	5877(3)	773(4)	35(2)
O(51A)	7428(4)	9246(2)	4353(4)	31(2)
O(53A)	7312(4)	6176(3)	-1390(4)	34(2)
O(55A)	4465(4)	7369(3)	406(4)	32(2)
O(58A)	5024(4)	8279(3)	3541(4)	32(2)
O(44A)	6043(4)	8430(2)	1304(3)	24(1)
O(52A)	7318(5)	9024(2)	1050(4)	32(2)
O(49A)	5004(5)	8606(3)	4847(5)	42(2)
O(56A)	9159(5)	8682(3)	4145(5)	37(2)
O(46A)	7403(4)	7723(2)	-175(3)	24(1)
N(10A)	5295(5)	7600(3)	4772(5)	29(2)
O(54A)	4433(5)	8360(3)	243(5)	45(2)
O(47A)	7723(3)	6129(2)	2606(3)	19(1)
O(48A)	5671(5)	8763(3)	-217(4)	34(2)
O(45A)	5952(4)	7836(2)	289(4)	24(1)
N(19A)	10252(6)	7942(3)	5241(5)	38(2)
O(62A)	6615(4)	8593(2)	3295(3)	22(1)
O(64A)	9136(4)	5796(2)	3036(3)	19(1)
O(63A)	8038(3)	6924(2)	629(3)	20(1)
O(41A)	9009(5)	4860(3)	2739(5)	38(2)
N(11A)	9563(6)	6849(3)	-619(5)	35(2)

N(16A)	6389(5)	8135(3)	5715(5)	29(2)
O(61A)	7147(4)	5642(2)	1533(4)	26(1)
N(14A)	8645(5)	5871(3)	5577(5)	29(2)
N(13A)	8885(5)	5931(3)	-875(4)	24(2)
O(38A)	6489(4)	8891(2)	4882(4)	29(2)
N(24A)	6943(7)	8308(3)	-1103(5)	39(2)
C(1A)	9629(6)	5871(4)	-479(5)	27(2)
N(1A)	6975(5)	6166(3)	5310(5)	32(2)
C(3A)	6942(6)	7447(3)	5434(5)	24(2)
C(2A)	7418(6)	9075(3)	1713(6)	26(2)
N(15A)	11160(5)	5823(3)	2995(5)	34(2)
N(28A)	5241(5)	5716(4)	-2912(6)	43(3)
C(44A)	3807(6)	6909(4)	2536(5)	27(2)
C(6A)	5970(6)	5082(4)	2458(6)	32(2)
C(4A)	4006(6)	6241(4)	613(6)	36(2)
N(12)	4968(5)	6475(3)	-702(5)	31(2)
C(8A)	10764(5)	6530(4)	3446(5)	27(2)
N(3A)	4087(5)	7494(3)	1948(5)	34(2)
N(2A)	4749(5)	6072(3)	732(5)	32(2)
N(6A)	10957(5)	6488(4)	1739(5)	39(2)
C(5A)	3684(5)	7605(4)	2556(6)	32(2)
O(89A)	10095(5)	5153(3)	2335(5)	42(2)
N(5A)	6580(6)	5278(4)	2855(5)	40(2)
C(7A)	8271(7)	5517(4)	5172(6)	31(2)
C(9A)	5274(7)	5176(4)	2748(8)	42(3)
C(20A)	6825(6)	5552(4)	-1957(5)	28(2)
C(10A)	11448(5)	6235(4)	3296(5)	26(2)
C(12A)	10230(6)	6610(4)	-697(5)	34(2)
C(11A)	11998(6)	6448(4)	2766(6)	33(2)
O(11B)	8833(6)	9492(4)	3856(7)	64(3)
C(14A)	10162(6)	6741(3)	5946(5)	27(2)
C(15A)	8160(6)	5647(3)	4376(5)	24(2)
N(27A)	11370(8)	7043(4)	1147(6)	56(3)
C(23A)	11621(6)	6643(4)	2093(5)	35(3)
C(21A)	5254(7)	7375(4)	5385(6)	33(2)
C(18A)	3772(6)	6501(4)	-17(7)	37(3)

C(16A)	11898(8)	6986(5)	1738(7)	47(3)
C(19A)	6788(6)	5902(4)	-1379(5)	26(2)
C(22A)	5683(6)	7489(4)	6076(6)	33(2)
C(27A)	6743(6)	4925(3)	1332(5)	26(2)
C(25A)	8747(7)	8403(4)	-537(6)	38(3)
N(7A)	8323(6)	8529(3)	38(5)	34(2)
N(17A)	4088(6)	8457(4)	1798(5)	37(2)
C(26A)	6697(6)	5394(3)	1165(5)	25(2)
C(24A)	6488(6)	7698(3)	5983(5)	29(2)
O(93A)	8123(8)	6668(5)	6517(5)	84(5)
C(28A)	4875(5)	8264(3)	2879(5)	23(2)
N(8A)	6251(6)	5225(3)	-1834(5)	36(2)
C(30A)	6678(6)	5753(4)	-2720(5)	33(2)
C(31A)	6852(6)	5726(4)	5320(5)	28(2)
C(32A)	7479(7)	5405(4)	5468(6)	36(2)
C(33A)	5918(6)	5966(4)	-2810(5)	32(2)
C(29A)	4809(5)	7046(4)	200(5)	25(2)
N(10)	7439(6)	9517(3)	2792(5)	36(2)
C(35A)	4069(5)	8392(4)	2584(5)	28(2)
C(38A)	10751(7)	6564(4)	6502(6)	37(3)
C(36A)	9523(6)	6011(4)	303(5)	27(2)
C(40A)	6078(8)	4795(4)	1816(7)	39(3)
N(12A)	7505(6)	4822(3)	1690(5)	34(2)
C(34A)	4158(6)	7065(4)	1956(7)	37(3)
C(37A)	10288(7)	6137(4)	-806(6)	39(3)
N(26A)	3979(8)	5860(5)	1588(7)	60(4)
N(25A)	5458(6)	5422(4)	3356(6)	46(3)
C(41A)	3546(9)	6116(5)	1134(8)	52(3)
C(39A)	6287(7)	6351(4)	5158(8)	44(3)
N(20A)	3518(6)	7229(4)	2935(7)	53(3)
N(23A)	10867(5)	7776(4)	3732(6)	37(2)
N(36A)	5727(6)	6037(4)	5084(7)	52(3)
C(45A)	9046(8)	9369(4)	2050(7)	48(3)
N(21A)	9031(6)	9040(4)	2544(6)	45(3)
C(47A)	7601(8)	8053(4)	-1314(5)	38(3)
N(29A)	5202(7)	9474(4)	4511(6)	52(3)

N(30A)	7502(6)	9877(3)	5276(6)	44(3)
C(48A)	6927(7)	9520(4)	5441(5)	33(2)
N(31A)	4473(6)	7074(4)	4588(6)	44(3)
N(50A)	11361(7)	7969(5)	2709(8)	56(3)
C(17A)	6952(6)	9191(3)	4837(5)	25(2)
C(49A)	6107(7)	9681(4)	5530(6)	37(3)
C(50A)	5664(9)	9779(5)	4849(7)	50(4)
C(52A)	4741(6)	7051(4)	5295(7)	37(3)
C(53A)	11088(7)	7650(6)	3067(8)	53(4)
C(51A)	4824(6)	7407(4)	4297(7)	36(3)
C(60A)	5649(7)	10126(4)	4416(6)	34(2)
N(33A)	5152(7)	10050(4)	3839(6)	49(3)
N(32A)	9578(6)	8530(4)	328(7)	47(3)
C(55A)	6246(7)	5492(5)	3390(7)	41(3)
C(59A)	9768(11)	9380(8)	1770(10)	79(6)
C(57A)	7543(8)	9513(3)	2016(6)	37(3)
C(56A)	4394(6)	6767(4)	-375(5)	28(2)
C(63A)	10420(11)	6552(11)	7246(8)	113(11)
C(58A)	9503(8)	8413(5)	-348(8)	52(3)
N(37A)	11507(7)	6788(5)	6478(6)	58(3)
C(46A)	6120(8)	5643(5)	5170(7)	47(3)
C(68A)	8853(7)	8608(4)	556(7)	40(3)
N(39A)	9418(8)	7175(5)	7376(8)	63(4)
N(40A)	10530(7)	7298(5)	-587(7)	58(3)
C(73A)	9739(7)	7261(5)	-538(8)	50(3)
C(75A)	9737(7)	4869(4)	2639(7)	40(3)
C(70A)	11048(6)	8190(4)	3801(9)	46(3)
C(76A)	10191(9)	4472(5)	2881(8)	54(4)
C(71A)	10200(10)	7073(6)	7409(8)	57(4)
C(74A)	10839(8)	6899(6)	-682(8)	59(5)
C(69A)	4712(8)	5847(5)	1324(7)	46(3)
C(72A)	10647(11)	7451(6)	7521(11)	73(5)
N(44A)	9752(10)	4198(4)	3323(7)	69(4)
C(86A)	9831(11)	4035(5)	1799(8)	58(4)
C(82A)	8349(9)	8309(5)	-1300(7)	47(3)
C(81A)	8363(9)	9687(5)	1847(9)	51(3)

N(45A)	10066(9)	7772(6)	7577(8)	72(4)
N(41A)	4960(9)	6405(4)	-2844(7)	61(3)
C(79A)	4670(8)	6012(6)	-2930(8)	53(4)
C(83A)	7692(6)	7667(3)	-783(5)	26(2)
C(78A)	3463(7)	8045(5)	2759(7)	46(3)
C(84A)	9310(12)	7568(7)	7515(10)	71(5)
C(80A)	9468(6)	8339(4)	4347(6)	30(2)
C(85A)	10484(10)	4228(5)	2219(8)	52(4)
C(90A)	5743(8)	6387(4)	-2761(8)	47(3)
C(89A)	10922(7)	8458(5)	4456(9)	53(4)
C(87A)	10173(7)	8356(4)	4866(8)	44(3)
C(88A)	10835(7)	6748(5)	1172(6)	42(3)
N(49A)	10190(8)	9061(6)	2113(9)	72(4)
O(10B)	11157(7)	5552(5)	1523(7)	86(5)
C(10B)	4860(10)	9658(5)	3900(8)	57(4)
C(10C)	9724(8)	8849(7)	2551(9)	65(5)
C(54A)	11377(8)	8305(8)	3138(14)	90(9)
C(10D)	8876(11)	3929(6)	1010(10)	65(5)
C(10E)	9521(9)	3636(6)	1913(8)	54(4)
N(52A)	8904(9)	3581(6)	1463(9)	78(5)
N(53A)	9405(15)	4201(7)	1232(11)	111(8)
N(54A)	6988(7)	9193(3)	-334(5)	38(2)
O(11C)	7621(13)	4632(6)	3164(9)	116(6)
C(61A)	5551(7)	9166(4)	-266(6)	35(2)
O(11D)	4933(6)	9331(3)	-384(6)	55(3)
C(13A)	6224(10)	9877(5)	-520(9)	57(4)
C(100)	6987(11)	10376(5)	277(10)	64(4)
C(13C)	6300(8)	9440(4)	-135(7)	43(3)
C(13D)	6930(13)	10135(5)	-323(12)	81(7)
N(56A)	7741(10)	10568(7)	333(12)	97(6)
C(101)	8119(18)	10425(9)	-230(20)	151(16)
Cl(1Q)	4579(2)	2531(1)	1766(2)	49(1)
O(12O)	4091(11)	2742(5)	2234(7)	102(6)
O(12P)	5152(9)	2342(6)	2168(8)	102(5)
O(12Q)	4006(14)	2183(7)	1680(20)	214(16)
O(12R)	4820(14)	2812(8)	1239(12)	152(9)

O(215)	7526(8)	4409(4)	7032(12)	114(7)
O(213)	7213(8)	7154(6)	7442(7)	90(4)
O(206)	7376(11)	10317(6)	7783(9)	110(6)
O(202)	2564(4)	5617(2)	6443(5)	39(2)
Cl(15)	2516(4)	5941(2)	7864(4)	108(2)
O(140)	4393(7)	10018(4)	463(5)	55(3)
O(142)	8954(8)	9387(4)	5405(7)	72(4)
O(138)	3621(8)	6957(6)	6671(8)	90(4)
O(144)	9029(13)	4572(7)	4449(12)	130(7)
Cl(55)	7369(3)	9889(2)	7458(3)	91(2)
O(309)	7876(9)	9926(9)	6839(10)	143(9)
O(310)	6551(8)	9789(6)	7259(9)	102(5)
O(146)	2449(19)	6126(11)	6982(19)	209(13)
O(401)	7004(5)	4118(3)	5637(6)	51(2)
N(57)	7450(20)	10157(13)	-700(20)	181(14)
O(250)	2738(19)	6235(11)	8464(18)	199(12)
O(300)	8696(17)	364(10)	3353(15)	172(10)
O(251)	3016(15)	5540(9)	7916(14)	152(8)
O(252)	1605(19)	5813(12)	7908(18)	198(12)
O(312)	4660(20)	8448(12)	6331(18)	207(13)
O(21O)	5646(9)	578(5)	1050(9)	97(5)
Cl(5E)	9190(3)	5399(2)	7381(2)	71(1)
O(30O)	8803(14)	5804(8)	7364(9)	160(11)
O(30P)	9760(16)	5371(9)	7939(15)	162(9)
O(40A)	9719(15)	5397(8)	6814(14)	150(8)
O(30T)	2461(10)	7142(6)	4394(10)	106(5)
O(30V)	488(13)	9537(8)	3975(12)	133(7)
O(30X)	3530(16)	8952(10)	9556(15)	170(10)
O(3ZZ)	2680(30)	6544(15)	5500(20)	261(18)
O(3ZY)	1828(16)	7800(9)	6178(15)	165(9)
O(31P)	3550(70)	7550(50)	6080(70)	860(110)
O(30Z)	1910(30)	8931(16)	6970(20)	269(19)
O(400)	7580(13)	9541(8)	7982(12)	134(7)
Cl(13)	1976(7)	8196(4)	592(6)	156(3)
O(403)	1480(20)	8520(12)	799(18)	205(13)
O(404)	1543(15)	7842(9)	210(14)	159(9)

O(405)	2137(10)	8080(6)	1315(9)	97(5)

APPENDIX B

CRYSTALLOGRAPHIC DATA FOR RECRYSTALLIZED $[Eu_{15}(\mu_5\text{-}Cl)(\mu_3\text{-}OH)_{20}(his^{+/-})_{10}(his^{-})_5(OH)_7](ClO_4)_{12}$

Identification code	mes1019	
Empirical formula	C60 H120 Cl5 Eu15 N45 O90	
Formula weight	5368.66	
Temperature	190(2) K	
Wavelength	0.71073 Å	
Crystal system	Orthorhombic	
Space group	$C222_1$	
Unit cell dimensions	a = 20.495(3) Å	α= 90°.
	b = 31.221(4) Å	β= 90°.
	c = 34.217(4) Å	γ = 90°.
Volume	21895(5) $Å^3$	
Z	4	
Density (calculated)	1.629 Mg/m^3	
Absorption coefficient	4.366 mm^{-1}	
F(000)	10180	
Crystal size	0.24 x 0.18 x 0.16 mm^3	
Theta range for data collection	2.61 to 25.36°.	
Index ranges	-24<=h<=24, -37<=k<=37, -41<=l<=39	
Reflections collected	64328	
Independent reflections	20049 [R(int) = 0.0461]	
Completeness to theta = 25.36°	99.8 %	
Max. and min. transmission	0.5418 and 0.4205	
Refinement method	Full-matrix least-squares on F^2	
Data / restraints / parameters	20049 / 0 / 762	
Goodness-of-fit on F^2	1.085	
Final R indices [I>2sigma(I)]	R1 = 0.0674, wR2 = 0.1793	
R indices (all data)	R1 = 0.0872, wR2 = 0.1962	
Absolute structure parameter	0.04(3)	
Largest diff. peak and hole	2.296 and -1.510 e.$Å^{-3}$	

Atomic coordinates (x 10^4) and equivalent isotropic displacement parameters ($Å^2$x 10^3) for mes1019. U(eq) is defined as one third of the trace of the orthogonalized U^{ij} tensor.

	x	y	z	U(eq)
Eu(1)	5031(1)	5000	10000	40(1)
Eu(2)	4407(1)	3885(1)	10127(1)	47(1)
Eu(3)	6102(1)	5897(1)	10388(1)	44(1)
Eu(4)	4613(1)	5639(1)	10928(1)	49(1)
Eu(5)	7278(1)	6759(1)	10156(1)	55(1)
Eu(6)	7882(1)	5556(1)	10245(1)	54(1)
Eu(7)	9155(1)	4665(1)	10496(1)	82(1)
Eu(8)	7460(1)	6130(1)	11155(1)	66(1)
Cl(9)	6579(2)	5000	10000	49(1)
O(50)	4370(5)	4588(3)	10512(3)	44(3)
O(5)	5420(4)	4288(3)	10154(3)	40(2)
O(3)	5472(5)	5280(3)	10587(3)	42(2)
O(6)	4259(4)	5492(3)	10274(3)	39(2)
O(51)	3943(6)	5005(4)	10981(4)	57(3)
O(4)	4984(5)	3823(3)	9515(3)	43(3)
O(2)	7014(5)	5595(3)	10727(4)	53(3)
O(201)	3570(6)	5965(4)	10930(4)	67(4)
O(7)	8008(5)	4814(3)	10379(4)	54(3)
O(1)	7061(4)	6009(3)	9983(4)	46(3)
O(54)	3793(7)	3203(4)	10222(7)	99(6)
N(10)	3314(7)	4107(4)	10445(5)	62(4)
O(53)	5102(6)	3239(4)	10183(5)	69(4)
O(52)	8301(6)	6666(4)	9764(4)	66(4)
O(200)	7588(9)	6860(6)	11288(5)	87(5)
O(60)	6414(7)	6223(5)	11504(4)	69(4)
N(3)	4955(9)	5278(7)	11556(6)	84(6)
O(56)	5734(6)	5908(4)	11101(4)	54(3)
O(58)	8266(6)	5570(5)	10933(4)	70(4)
N(1)	4523(10)	3752(4)	10862(6)	81(6)
C(4)	4161(10)	3873(7)	11187(6)	62(5)
O(9)	9025(6)	5367(4)	10205(4)	62(3)

O(202)	7550(9)	7223(5)	10726(6)	94(5)
O(57)	6085(5)	6580(3)	10035(4)	53(3)
C(1)	6443(11)	7212(7)	9291(8)	79(7)
C(2)	3386(9)	4358(6)	10804(6)	65(5)
N(2)	6989(10)	6951(6)	9445(6)	79(5)
O(300)	7877(8)	7439(4)	10005(7)	101(6)
O(8)	7962(6)	6275(4)	10533(4)	62(3)
C(3)	3514(9)	4070(6)	11164(6)	59(5)
O(61)	8493(6)	5968(4)	9741(5)	68(4)
N(5)	7534(17)	5629(11)	11657(9)	144(10)
N(6)	8731(11)	4247(7)	11078(8)	98(7)
C(61)	9231(19)	3521(12)	10880(11)	127(11)
N(11)	4658(10)	6245(6)	11432(6)	81(6)
C(5)	4495(15)	3784(10)	11501(8)	100(8)
N(4)	5025(14)	3589(9)	11404(8)	114(8)
C(7)	5063(16)	4888(11)	11582(9)	104(9)
C(6)	5076(14)	3565(9)	10994(8)	91(7)
N(7)	5354(15)	4762(10)	11922(8)	122(8)
C(8)	5228(16)	5444(11)	11907(9)	106(9)
N(13)	6439(8)	7374(6)	10179(7)	79(5)
C(10)	5500(17)	5134(11)	12094(9)	113(10)
C(9)	5234(14)	5940(10)	12000(8)	98(8)
C(12)	6003(12)	7492(8)	9532(7)	80(6)
C(14)	7263(11)	6777(7)	9167(6)	64(5)
N(8)	6965(11)	6855(8)	8837(10)	123(10)
C(15)	3930(9)	4670(6)	10770(5)	53(4)
O(10)	6713(6)	6458(3)	10714(4)	53(3)
N(9)	8606(11)	6235(8)	11385(7)	105(8)
C(17)	8461(19)	3702(12)	11462(11)	127(11)
O(203)	3443(8)	3751(7)	9669(5)	102(6)
N(14)	8141(15)	4107(10)	11591(8)	126(9)
C(20)	8810(20)	5602(15)	11819(12)	150(14)
C(19)	8124(13)	5420(9)	11871(8)	85(7)
C(13)	8810(16)	3783(10)	11162(9)	105(9)
C(21)	5656(8)	3148(5)	10063(5)	47(4)
C(13A)	6427(12)	7164(8)	8933(8)	75(6)

C(16)	8656(10)	6338(7)	9699(6)	61(5)
C(26)	7511(14)	7629(9)	11312(8)	91(7)
C(23)	5847(11)	6127(7)	11406(6)	69(5)
C(25)	7545(13)	7218(9)	11105(8)	89(7)
Cl(6)	5384(7)	2685(4)	8932(4)	159(4)
Cl(7)	5042(8)	8627(5)	9448(5)	182(5)
O(59)	9126(9)	5189(6)	11028(5)	90(5)
O(416)	5327(13)	3017(9)	9179(8)	144(8)
O(420)	4380(15)	8688(9)	9392(8)	154(9)
N(28)	2418(12)	6122(8)	11183(7)	104(7)
C(28)	2581(16)	6283(11)	10756(9)	108(9)
C(29)	3268(14)	6151(9)	10659(8)	88(7)
O(417)	5070(30)	2760(20)	8550(20)	320(30)
C(27)	5866(11)	7319(7)	9933(6)	68(5)
O(421)	5113(18)	8289(12)	9765(10)	194(13)
N(15)	9726(8)	3953(5)	10454(9)	114(10)
C(62)	8965(13)	5797(8)	11443(7)	83(7)
O(206)	10073(15)	4564(10)	11045(8)	163(10)
C(30)	5274(15)	6244(10)	11660(8)	98(8)
N(18)	7168(17)	5049(11)	12061(9)	142(10)
C(32)	9260(13)	3541(8)	10504(7)	83(6)
C(33)	7870(20)	5110(16)	12109(13)	158(15)
C(31)	8346(16)	4400(11)	11359(9)	104(8)
C(63)	8120(17)	7899(11)	11218(9)	111(9)
C(64)	8700(20)	7703(13)	11334(11)	128(12)
C(60)	8805(13)	5505(9)	11133(7)	87(7)
Cl(10)	4151(13)	2328(8)	10311(7)	300(11)
O(500)	1531(15)	1960(10)	1980(8)	157(10)
O(501)	5557(17)	4045(11)	2374(9)	182(12)
O(502)	6660(19)	4380(12)	2650(10)	198(13)
O(506)	7800(30)	1844(16)	7109(14)	270(20)
C(69)	2350(18)	6704(12)	10714(10)	115(10)
C(70)	2740(20)	6941(14)	10888(12)	140(13)
N(29)	9190(20)	7424(14)	11122(12)	175(14)
O(418)	6000(30)	2690(20)	8676(18)	320(30)
O(423)	5380(30)	9069(18)	9492(15)	290(20)

C(68)	9630(30)	7190(20)	11286(18)	200(20)
O(422)	5210(20)	8619(13)	9114(12)	210(14)
N(30)	9490(30)	7475(18)	11713(15)	216(19)
C(67)	8960(30)	7658(18)	11702(16)	172(18)
C(66)	7130(30)	5396(17)	11748(15)	171(17)
C(71)	3570(30)	7199(17)	11017(18)	174(18)
C(72)	2710(30)	7132(19)	11331(17)	200(20)
O(419)	5190(20)	2364(14)	9214(12)	219(15)
N(21)	3490(30)	7319(17)	11338(16)	213(19)
O(204)	10233(12)	4823(8)	10335(7)	125(7)
N(20)	3300(30)	7217(18)	10709(18)	240(20)
Cl(2A)	6549(2)	4400(2)	11089(2)	62(1)
O(40A)	6584(9)	4212(6)	11458(5)	90(5)
O(40B)	7060(11)	4242(7)	10837(6)	119(7)
O(40C)	6632(14)	4826(9)	11114(8)	153(9)
O(40D)	5930(20)	4340(13)	10919(11)	220(15)
Cl(5A)	6668(4)	8572(3)	10453(3)	113(2)
O(41A)	7164(14)	8276(9)	10275(8)	147(9)
O(41B)	6109(18)	8350(11)	10604(10)	186(12)
O(41C)	6590(20)	8899(14)	10193(12)	232(17)
O(41D)	7020(40)	8640(20)	10900(20)	400(40)
Cl(8A)	6862(5)	3980(4)	7160(3)	134(3)
O(42Z)	6680(16)	3704(11)	6842(9)	175(11)
O(43A)	6400(30)	4294(16)	7193(14)	260(20)
O(480)	7405(19)	4185(12)	7052(10)	198(13)
O(21)	7510(30)	6449(16)	11923(14)	270(20)
O(511)	5750(20)	3176(14)	2084(12)	233(18)
O(509)	9090(30)	1980(20)	2417(19)	350(30)
O(508)	8130(30)	3046(19)	7773(16)	300(30)
O(507)	5000	1190(30)	2500	280(30)
N(26)	7442(14)	7544(9)	11738(8)	116(8)
C(73)	10385(14)	5139(9)	9883(9)	93(8)
Cl(11)	2970(4)	5000	10000	72(2)
O(481)	7160(20)	3720(12)	7497(11)	260(14)

APPENDIX C

CRYSTALLOGRAPHIC DATA FOR

$[Eu_{15}(\mu_5\text{-}Br)(\mu_3\text{-}OH)_{20}(his^{+/-})_{10}(his^{-})_5(OH)_7](ClO_4)_{12}$

Identification code	mes923	
Empirical formula	C60 H120 Br Cl5 Eu15 N45 O80	
Formula weight	5288.57	
Temperature	150(2) K	
Wavelength	0.71073 Å	
Crystal system	Monoclinic	
Space group	$P2_1$	
Unit cell dimensions	a = 17.1771(18) Å	α= 90°.
	b = 31.430(4) Å	β= 91.823(5)°.
	c = 18.6633(19) Å	γ = 90°.
Volume	10071(2) $Å^3$	
Z	2	
Density (calculated)	1.744 Mg/m^3	
Absorption coefficient	4.938 mm^{-1}	
F(000)	5000	
Crystal size	0.36 x 0.32 x 0.16 mm^3	
Theta range for data collection	1.09 to 27.88°.	
Index ranges	-22<=h<=22, -41<=k<=41, -24<=l<=24	
Reflections collected	88998	
Independent reflections	47458 [R(int) = 0.0584]	
Completeness to theta = 27.88°	99.7 %	
Max. and min. transmission	0.5055 and 0.2694	
Refinement method	Full-matrix least-squares on F^2	
Data / restraints / parameters	47458 / 1 / 2437	
Goodness-of-fit on F^2	1.017	
Final R indices [I>2sigma(I)]	R1 = 0.0543, wR2 = 0.1377	
R indices (all data)	R1 = 0.0807, wR2 = 0.1584	
Absolute structure parameter	-0.021(11)	
Largest diff. peak and hole	2.483 and -1.301 e.$Å^{-3}$	

Atomic coordinates (x 10^4) and equivalent isotropic displacement parameters ($Å^2$x 10^3) for mes923.cif. U(eq) is defined as one third of the trace of the orthogonalized U^{ij} tensor.

	x	y	z	U(eq)
Cl(11)	2490(5)	3440(3)	2111(6)	125(3)
O(241)	3260(20)	3371(15)	1970(30)	330(40)
O(242)	2002(13)	3033(8)	2270(40)	400(50)
O(243)	2640(30)	3560(14)	3010(20)	390(40)
O(244)	2270(30)	3758(17)	1580(20)	280(30)
Eu(1)	2973(1)	105(1)	3885(1)	19(1)
Br(1A)	2650(1)	-351(1)	2309(1)	21(1)
Eu(5)	1764(1)	587(1)	2309(1)	20(1)
Eu(4)	1805(1)	-222(1)	733(1)	19(1)
Eu(15)	1207(1)	714(1)	4345(1)	21(1)
Eu(3)	2952(1)	-1219(1)	1358(1)	19(1)
Eu(7)	3238(1)	-877(1)	5208(1)	20(1)
Eu(8)	4995(1)	-1599(1)	2069(1)	23(1)
Eu(13)	-13(1)	430(1)	1190(1)	24(1)
Eu(14)	2964(1)	1328(1)	3422(1)	24(1)
Eu(9)	3008(1)	-2132(1)	2631(1)	23(1)
Eu(2)	3708(1)	-1002(1)	3284(1)	18(1)
Eu(11)	1062(1)	-1267(1)	161(1)	21(1)
Eu(6)	4952(1)	-207(1)	4431(1)	23(1)
Eu(10)	3105(1)	-908(1)	-554(1)	20(1)
Eu(12)	1862(1)	930(1)	265(1)	25(1)
O(10A)	343(5)	614(3)	2440(4)	24(2)
N(10A)	290(7)	119(4)	4781(6)	29(3)
C(10A)	974(9)	-2416(5)	2476(9)	35(3)
O(10B)	2013(5)	109(3)	4833(5)	26(2)
N(10B)	5963(7)	-1027(5)	1723(6)	40(3)
C(10B)	-134(7)	763(4)	2901(7)	21(3)
O(10C)	3171(6)	-1459(3)	4259(5)	25(2)
N(10C)	4020(8)	1533(5)	2545(7)	45(4)
C(10C)	5773(8)	-984(5)	3448(8)	29(3)
O(10D)	2389(6)	211(3)	-185(5)	26(2)

N(10D)	4542(7)	-664(4)	-625(6)	33(3)
C(10D)	6430(7)	-1271(5)	3264(7)	30(3)
O(10E)	449(5)	-566(3)	436(5)	26(2)
N(10E)	1570(8)	-2210(4)	2864(8)	40(3)
C(10E)	1847(8)	-1774(5)	5317(7)	29(3)
O(10F)	4080(5)	-1021(3)	2023(5)	21(2)
N(10F)	6155(7)	-1679(4)	2979(7)	29(3)
C(10F)	-210(7)	-458(4)	188(8)	25(3)
O(10G)	1657(5)	-944(3)	1181(4)	22(2)
N(10G)	1962(7)	-1326(4)	5321(7)	35(3)
C(10G)	3283(10)	-1979(4)	5198(8)	36(4)
O(10H)	2365(5)	443(3)	1204(4)	21(2)
N(10H)	-271(7)	-1426(4)	739(7)	36(3)
C(10H)	2471(9)	-2090(5)	5491(8)	33(3)
C(10I)	1745(8)	-2575(4)	1326(7)	27(3)
N(10I)	-928(9)	-9(4)	1951(8)	43(3)
O(10I)	3942(6)	-1257(3)	433(5)	29(2)
C(10J)	1074(9)	-2709(5)	1828(9)	39(4)
N(10J)	5869(7)	257(4)	3730(7)	34(3)
O(11A)	1618(5)	1093(3)	3301(5)	22(2)
C(11A)	275(9)	-2320(5)	2783(10)	42(4)
N(11A)	3301(9)	1031(4)	-2(8)	45(3)
O(11B)	3696(5)	-169(3)	4956(4)	20(2)
N(11B)	3635(7)	-1629(4)	5591(6)	30(3)
C(11B)	-1309(8)	106(6)	2566(8)	38(4)
O(11C)	3028(5)	618(3)	2935(4)	21(2)
C(11C)	-840(8)	-433(6)	1978(9)	39(4)
N(11C)	2493(8)	-2681(4)	1661(7)	38(3)
O(11D)	4089(5)	-274(3)	3422(5)	21(2)
C(11D)	2620(10)	544(5)	-1318(8)	35(3)
N(11D)	-919(8)	946(5)	1821(7)	40(3)
O(11E)	2451(6)	1262(3)	2155(5)	25(2)
N(11E)	1924(9)	786(4)	-1112(6)	38(3)
C(11E)	3707(10)	909(6)	-567(9)	42(4)
O(11F)	2204(5)	-404(3)	5630(5)	28(2)
N(11F)	3902(7)	-1567(4)	-888(6)	29(3)

C(11F)	4742(8)	-262(6)	-525(10)	47(5)
N(11G)	1386(7)	643(3)	5721(6)	27(2)
C(11G)	4635(8)	-1636(5)	-474(7)	33(3)
O(11G)	27(6)	785(3)	3556(5)	34(2)
C(11H)	1960(9)	-50(4)	5437(7)	27(3)
O(11H)	4163(6)	1172(3)	4122(6)	35(2)
N(11H)	-536(7)	-415(4)	4607(8)	39(3)
C(11I)	1476(9)	212(5)	5989(8)	34(3)
O(11I)	5887(5)	-677(3)	3894(5)	30(2)
C(11J)	677(8)	-12(5)	6099(8)	33(3)
N(11I)	-1186(8)	-598(5)	2558(7)	43(3)
O(12A)	1198(6)	-1980(3)	690(5)	32(2)
N(12A)	-29(6)	-1021(4)	-701(6)	26(2)
C(12A)	245(9)	-127(5)	5395(8)	34(3)
O(12B)	2994(6)	-177(3)	-1002(5)	31(2)
N(12B)	456(8)	-2062(5)	3361(7)	41(3)
C(12B)	-254(9)	-450(6)	5290(10)	43(4)
O(12C)	5024(6)	-1627(3)	777(5)	33(2)
C(12C)	-196(9)	-87(5)	4297(9)	35(3)
O(12D)	3461(6)	-839(3)	-1845(5)	28(2)
N(12C)	5529(9)	-216(6)	-622(10)	61(5)
C(12D)	-940(9)	882(5)	2612(8)	37(4)
O(12E)	2728(5)	-1388(3)	2617(5)	23(2)
C(12E)	-1559(9)	532(6)	2774(9)	42(4)
N(12D)	4556(9)	1014(5)	286(9)	52(4)
O(12F)	2774(5)	-641(3)	4030(4)	19(2)
N(12E)	6376(10)	-473(5)	1124(7)	57(4)
C(12F)	-614(8)	-738(4)	-367(8)	25(3)
O(12G)	1229(5)	-1627(3)	-944(5)	26(2)
C(12G)	-1259(9)	-1006(6)	-25(9)	40(4)
O(12H)	4245(5)	463(3)	4148(5)	27(2)
C(12H)	-992(9)	-1258(5)	607(9)	38(4)
O(12I)	4465(6)	-883(3)	5974(5)	34(2)
N(12F)	6373(10)	433(6)	2682(11)	62(5)
C(12I)	2432(8)	1564(4)	1716(7)	26(3)
O(12J)	5126(5)	-1056(3)	3112(5)	23(2)

N(12G)	2445(8)	2011(4)	2795(7)	37(3)
C(12J)	5231(9)	-900(6)	-705(8)	38(4)
O(13A)	1781(5)	-686(3)	-299(5)	21(2)
N(13A)	1208(8)	-2278(4)	-1832(7)	38(3)
C(13A)	6648(9)	-872(5)	2088(8)	36(3)
O(13B)	3721(5)	-1849(3)	1658(5)	22(2)
C(13B)	6915(12)	-519(7)	1733(10)	59(5)
N(13B)	235(9)	-1773(5)	-2924(9)	52(4)
O(13C)	2434(5)	-1409(3)	185(5)	22(2)
C(13C)	1805(8)	-1954(5)	-1967(8)	34(3)
N(13C)	-96(9)	-1085(5)	-2839(7)	47(4)
O(13D)	-10(6)	1099(3)	4866(6)	37(2)
C(13D)	6078(9)	138(7)	3092(10)	47(4)
N(13D)	730(9)	-1468(6)	5065(9)	55(4)
O(13E)	4323(5)	-886(3)	4430(4)	21(2)
C(13E)	1788(8)	-1599(5)	-1377(8)	31(3)
N(13E)	-1027(11)	-1642(5)	1577(8)	55(4)
O(13F)	1037(6)	922(3)	1305(5)	28(2)
C(13F)	916(9)	-1543(5)	-2823(8)	32(3)
N(13F)	2492(8)	2370(4)	5298(8)	45(3)
O(13G)	1015(5)	9(3)	1677(5)	24(2)
N(13G)	187(10)	1982(5)	4517(9)	56(4)
C(13G)	735(10)	-1120(5)	-2760(9)	42(4)
O(13H)	1654(5)	232(3)	3426(4)	19(2)
N(13H)	139(9)	2536(6)	3837(8)	52(4)
C(13H)	1676(7)	-2107(4)	1158(7)	25(3)
O(13I)	2617(5)	799(3)	4304(5)	25(2)
C(13I)	1239(9)	-2002(5)	3402(9)	38(4)
N(13I)	5164(11)	1558(9)	2084(12)	93(8)
O(13J)	4128(5)	-1718(3)	3033(4)	20(2)
C(13J)	2678(8)	156(4)	-779(8)	29(3)
N(13J)	4793(12)	-3284(5)	3344(11)	74(6)
O(14A)	2146(5)	-1866(3)	1524(5)	27(2)
N(14A)	2004(10)	1662(4)	-357(7)	46(4)
C(14A)	6997(8)	-1067(5)	2763(8)	35(3)
O(14B)	665(7)	1253(3)	-206(6)	37(2)

C(14B)	4469(8)	836(4)	4346(7)	27(3)
N(14B)	6478(10)	-683(7)	6490(10)	76(6)
O(14C)	-568(7)	859(4)	268(7)	51(3)
N(14C)	5276(9)	433(5)	5245(8)	44(3)
C(14C)	4534(9)	-1491(5)	289(8)	33(3)
O(14D)	2316(6)	-1338(3)	-1387(5)	35(2)
C(14D)	5287(9)	-1357(6)	-803(9)	41(4)
N(14D)	2055(12)	2878(6)	260(12)	81(6)
O(14E)	3046(6)	-2147(3)	3940(5)	33(2)
C(14E)	4486(12)	901(7)	-380(12)	57(5)
N(14E)	4542(15)	-3270(8)	1196(13)	99(8)
O(14F)	5430(6)	-483(3)	5516(5)	31(2)
C(14F)	3155(8)	-1858(4)	4380(7)	28(3)
N(14F)	3933(12)	-3895(11)	1462(13)	108(9)
O(14G)	2431(6)	1750(3)	4345(6)	32(2)
C(14G)	1287(10)	-1160(5)	5159(10)	45(4)
N(14G)	4373(14)	-277(9)	7395(15)	103(8)
O(14H)	1475(6)	1389(3)	4886(5)	29(2)
C(14H)	1111(11)	-1849(5)	5173(9)	45(4)
N(14H)	5043(14)	278(10)	7542(12)	100(8)
O(14I)	-546(6)	-136(3)	407(6)	35(2)
C(14I)	1661(9)	-1746(5)	-2731(7)	33(3)
N(14I)	3200(20)	2876(10)	-199(18)	147(14)
C(14J)	5165(10)	-739(5)	5947(9)	40(4)
O(15A)	2325(7)	1513(3)	1040(5)	37(2)
C(15A)	5759(10)	-920(5)	6534(8)	41(4)
O(15B)	3015(5)	-587(3)	612(5)	21(2)
C(15B)	1943(8)	1692(4)	4827(7)	24(3)
C(15C)	1914(9)	2015(6)	5442(9)	40(4)
O(15C)	4032(7)	-2647(3)	2705(6)	41(3)
C(15D)	1080(9)	2191(5)	5522(8)	38(4)
C(15E)	657(11)	2277(6)	4860(9)	46(4)
C(15F)	632(10)	2631(6)	4413(9)	43(4)
O(15D)	6181(15)	-1947(9)	1469(14)	141(10)
O(15E)	939(5)	335(3)	287(5)	24(2)
C(15G)	537(11)	1656(5)	-275(9)	43(4)

O(15F)	3833(8)	1986(4)	3815(9)	65(4)
C(15H)	-1483(12)	-1397(6)	1136(11)	54(5)
O(15G)	-73(8)	1838(4)	-352(8)	60(4)
C(15I)	-286(10)	-1662(5)	1331(9)	40(4)
O(15H)	5128(7)	-2346(4)	2311(8)	50(3)
C(15J)	-1481(9)	-284(6)	2947(9)	40(4)
O(16A)	2629(9)	-2866(5)	3178(8)	73(4)
C(16A)	3314(12)	791(5)	-1321(10)	49(5)
O(16B)	3085(10)	-855(6)	6534(6)	90(6)
C(16B)	3835(9)	1116(5)	549(9)	39(4)
C(16C)	4056(12)	1863(7)	2045(10)	55(5)
C(16D)	3372(11)	2164(5)	1804(13)	59(6)
C(16E)	4740(15)	1875(9)	1745(16)	87(8)
C(16F)	6041(9)	681(5)	3772(11)	45(4)
C(16G)	6362(12)	772(11)	3101(19)	109(14)
C(16H)	5168(12)	850(5)	4856(12)	56(6)
C(16I)	4785(10)	-2636(6)	2620(9)	42(4)
C(16J)	5240(11)	-3012(6)	2857(11)	56(5)
C(17A)	5525(12)	-3277(6)	2233(12)	54(5)
C(17B)	1294(14)	1934(6)	-151(11)	63(6)
C(17C)	1258(16)	2376(6)	-523(11)	65(6)
C(17D)	1972(16)	2630(6)	-320(13)	72(7)
C(17E)	5436(15)	-898(12)	7270(9)	104(11)
C(17F)	5225(17)	-409(9)	7389(12)	80(8)
C(17G)	5913(11)	943(7)	4439(12)	56(5)
C(17H)	5823(11)	-611(7)	-679(11)	59(6)
C(17I)	5862(11)	-765(6)	1138(9)	50(5)
C(17J)	4679(13)	1358(9)	2532(15)	81(8)
C(18A)	2559(11)	2007(5)	1989(10)	46(4)
C(18B)	-312(11)	-1481(8)	-2940(10)	60(6)
C(18C)	-162(15)	2151(7)	3896(12)	70(7)
C(18D)	2760(13)	3043(8)	289(15)	74(7)
C(18E)	4867(14)	-3450(6)	1758(13)	66(7)
C(18F)	4518(15)	-3825(9)	1940(13)	76(7)
C(18G)	3937(15)	-3538(9)	964(14)	81(8)
C(18H)	4280(20)	84(9)	7469(14)	102(12)

C(18I)	5650(20)	-25(10)	7500(20)	118(13)
C(18J)	2620(20)	2649(11)	-620(20)	118(13)
Cl(1A)	9295(2)	4087(1)	6925(2)	24(1)
O(20A)	9366(6)	4533(3)	7050(6)	32(2)
O(20B)	8595(7)	3975(4)	6548(8)	62(4)
O(21A)	9939(7)	3943(4)	6553(10)	74(5)
O(21B)	9286(11)	3885(4)	7608(7)	72(5)
Cl(2A)	5381(2)	5183(1)	8467(2)	30(1)
O(20E)	5246(7)	4823(4)	8014(8)	54(3)
O(20F)	4685(6)	5364(5)	8732(9)	72(5)
O(21E)	5907(13)	5103(6)	9006(8)	113(9)
O(23A)	5808(12)	5489(6)	8104(10)	107(7)
Cl(3A)	1428(2)	3441(1)	6107(2)	36(1)
O(20I)	766(6)	3291(4)	5708(7)	49(3)
O(20J)	1566(6)	3883(4)	5994(9)	58(4)
O(20K)	1259(8)	3390(6)	6858(8)	72(4)
O(22A)	2097(7)	3202(4)	5923(11)	81(6)
Cl(4A)	4491(2)	2996(2)	5212(2)	47(1)
O(21G)	4628(10)	2719(6)	4669(9)	83(5)
O(22C)	3732(8)	2931(5)	5401(10)	78(5)
O(23C)	4593(13)	3436(6)	5085(12)	115(7)
O(23D)	4974(12)	2854(7)	5790(12)	114(7)
Cl(5A)	3162(3)	7395(1)	9733(2)	42(1)
O(21I)	2837(10)	7010(5)	9998(8)	74(4)
O(23G)	3815(13)	7319(7)	9357(15)	136(10)
O(23H)	3425(13)	7644(6)	10302(9)	102(7)
O(23I)	2610(14)	7595(9)	9275(18)	177(15)
Cl(6A)	9740(3)	6958(1)	7940(2)	46(1)
O(21K)	10512(9)	6922(5)	7764(11)	82(5)
O(21L)	9567(9)	7392(4)	7901(8)	65(4)
O(22E)	9643(13)	6812(5)	8644(9)	97(6)
O(22F)	9315(9)	6742(6)	7418(10)	88(6)
Cl(7A)	399(3)	20(2)	8248(3)	54(1)
O(22I)	767(18)	275(7)	7776(10)	148(12)
O(23M)	95(16)	269(9)	8784(14)	152(11)
O(23N)	-211(11)	-173(9)	7861(10)	126(9)

O(24A)	858(15)	-269(9)	8492(14)	161(13)
Cl(8A)	3456(3)	851(1)	6325(2)	48(1)
O(20O)	4257(10)	957(6)	6403(12)	98(6)
O(20P)	3386(10)	407(6)	6116(12)	109(8)
O(22L)	3091(14)	883(7)	6972(9)	113(7)
O(22M)	3082(12)	1135(7)	5843(10)	111(8)
Cl(9A)	4208(4)	7880(2)	7367(3)	84(2)
O(22P)	3829(15)	8310(10)	7377(9)	159(13)
O(23S)	4623(16)	7876(9)	6817(10)	156(13)
O(23T)	4760(20)	7877(10)	7910(15)	195(17)
Cl(1C)	2389(3)	2396(2)	7444(3)	72(2)
O(21O)	2638(12)	2088(7)	7959(11)	112(7)
O(21P)	2867(9)	2402(7)	6845(9)	94(6)
O(21Q)	1586(9)	2274(6)	7223(9)	80(5)
O(22R)	2418(12)	2831(6)	7768(10)	94(6)
O(300)	2445(6)	3108(4)	3534(6)	42(3)
O(301)	9427(8)	2514(4)	445(8)	58(3)
O(302)	3954(8)	1881(5)	5415(8)	66(4)
O(303)	7976(9)	1590(5)	4365(9)	76(4)
O(305)	6910(10)	716(6)	604(10)	84(5)
O(306)	1396(10)	4449(6)	3271(10)	84(5)
O(307)	7775(11)	4657(7)	2543(11)	100(6)
O(308)	7476(14)	1940(8)	2894(13)	121(7)
O(309)	674(12)	3085(7)	1081(12)	106(6)
O(310)	7140(11)	579(6)	1312(11)	95(5)
O(311)	5508(13)	2032(7)	3928(12)	114(7)
O(312)	8894(13)	6577(8)	1880(13)	119(7)
O(313)	7423(14)	9650(8)	4397(14)	129(8)
O(314)	3951(13)	7055(7)	4482(12)	113(7)
O(315)	340(20)	6342(13)	3260(20)	213(15)
O(316)	1448(18)	6459(10)	478(17)	161(11)
O(317)	2469(17)	4425(10)	2187(17)	157(10)
O(318)	2390(20)	4142(13)	4430(20)	207(14)
O(319)	8490(30)	1627(15)	630(20)	245(18)

APPENDIX D

CRYSTALLOGRAPHIC DATA FOR

$[Eu_{15}(\mu_5\text{-}OH)(I)_2(\mu_3\text{-}OH)_{20}(his^{+/-})_{10}(his^-)_5(OH)_7](ClO_4)_{12}$

Identification code	mes85	
Empirical formula	C72 H72 Cl4 Eu12 I N8 O40	
Formula weight	3781.60	
Temperature	190(2) K	
Wavelength	0.71073 Å	
Crystal system	Monoclinic	
Space group	$P2_1$	
Unit cell dimensions	a = 17.1699(18) Å	α= 90°.
	b = 31.272(4) Å	β= 91.550(5)°.
	c = 18.6388(19) Å	γ = 90°.
Volume	10004.2(19) $Å^3$	
Z	4	
Density (calculated)	2.511 Mg/m^3	
Absorption coefficient	7.900 mm^{-1}	
F(000)	7028	
Crystal size	0.32 x 0.20 x 0.10 mm^3	
Theta range for data collection	2.93 to 27.84°.	
Index ranges	-22<=h<=22, -40<=k<=40, -24<=l<=24	
Reflections collected	90529	
Independent reflections	47012 [R(int) = 0.0286]	
Completeness to theta = 27.84°	99.7 %	
Max. and min. transmission	0.5055 and 0.1866	
Refinement method	Full-matrix least-squares on F^2	
Data / restraints / parameters	47012 / 1 / 2141	
Goodness-of-fit on F^2	1.095	
Final R indices [I>2sigma(I)]	R1 = 0.0455, wR2 = 0.1309	
R indices (all data)	R1 = 0.0520, wR2 = 0.1366	
Absolute structure parameter	0.013(8)	
Largest diff. peak and hole	2.196 and -2.348 e.$Å^{-3}$	

Atomic coordinates (x 10^4) and equivalent isotropic displacement parameters ($Å^2$x 10^3) for mes85. U(eq) is defined as one third of the trace of the orthogonalized U^{ij} tensor.

	x	y	z	U(eq)
Eu(1)	8232(1)	2947(1)	4276(1)	21(1)
Eu(11)	6793(1)	2278(1)	-218(1)	21(1)
Eu(2)	7058(1)	1937(1)	3627(1)	19(1)
Eu(13)	8811(1)	3884(1)	626(1)	22(1)
Eu(4)	7038(1)	3273(1)	1074(1)	20(1)
Eu(8)	5001(1)	1558(1)	2926(1)	22(1)
Eu(9)	7009(1)	1022(1)	2354(1)	23(1)
Eu(10)	5062(1)	2950(1)	559(1)	24(1)
Eu(12)	7038(1)	4499(1)	1556(1)	24(1)
Eu(5)	8268(1)	3774(1)	2667(1)	21(1)
Eu(3)	6301(1)	2150(1)	1699(1)	19(1)
Eu(6)	8952(1)	1897(1)	4805(1)	23(1)
Eu(14)	8133(1)	4103(1)	4709(1)	28(1)
Eu(7)	6909(1)	2260(1)	5536(1)	22(1)
Eu(15)	10031(1)	3609(1)	3783(1)	26(1)
I(1)	9089(1)	2323(1)	1983(1)	37(1)
I(2)	5665(1)	3282(1)	3341(1)	38(1)
Cl(3)	9475(4)	3176(3)	6620(4)	43(2)
Cl(2)	11405(2)	1639(1)	1113(2)	39(1)
Cl(7)	9671(3)	5110(1)	2936(2)	46(1)
Cl(5)	4532(2)	1165(1)	222(2)	44(1)
Cl(6)	6531(2)	3997(1)	-1333(2)	62(1)
Cl(4)	6805(2)	568(1)	5249(2)	57(1)
Cl(1)	3281(3)	3928(2)	4259(2)	67(1)
Cl(17)	2385(2)	563(2)	2459(3)	77(1)
O(51)	6561(5)	2346(2)	6821(4)	35(2)
O(40)	7806(4)	2759(2)	-654(4)	31(2)
O(5)	5943(3)	2151(2)	2953(3)	19(1)
O(39)	8014(4)	3263(2)	150(4)	27(1)
O(27)	5765(4)	3624(2)	846(4)	31(2)
O(17)	7651(4)	3590(2)	3755(3)	25(1)

O(38)	6958(5)	1009(2)	1038(4)	36(2)
O(31)	9662(4)	3795(2)	2541(4)	29(1)
O(18)	8954(4)	3184(2)	3295(3)	24(1)
O(33)	9539(3)	2587(2)	4529(4)	25(1)
O(20)	8961(4)	4110(2)	3667(4)	29(1)
O(37)	6845(4)	1693(2)	736(3)	23(1)
O(22)	6993(4)	2997(3)	5962(4)	36(2)
O(16)	8404(4)	4270(2)	1675(4)	23(1)
O(13)	7001(4)	3764(2)	2058(4)	26(1)
O(21)	7621(4)	3390(2)	5158(4)	28(1)
O(3)	8238(4)	2478(2)	5305(4)	27(1)
O(14)	8341(4)	3381(2)	1574(3)	23(1)
O(32)	9992(4)	3942(3)	1422(4)	34(2)
O(2)	8335(3)	2240(2)	3772(3)	21(1)
O(10)	5942(3)	2886(2)	1576(3)	22(1)
O(45)	5570(5)	2266(3)	-984(4)	42(2)
O(23)	6090(4)	1919(2)	4569(4)	29(1)
O(25)	4882(3)	2096(2)	1884(4)	26(1)
O(24)	5016(4)	1556(3)	4215(4)	33(2)
O(11)	6319(4)	2980(2)	34(4)	27(1)
O(9)	7265(3)	2518(2)	981(3)	20(1)
O(1)	7005(4)	2589(2)	4336(3)	23(1)
O(34)	10566(4)	3038(3)	4543(4)	38(2)
O(6)	7292(3)	1784(2)	2374(3)	20(1)
O(41)	7685(4)	1807(3)	6366(4)	37(2)
O(36)	8793(4)	1184(2)	4285(4)	32(2)
O(35)	7877(4)	1293(2)	3452(4)	25(1)
O(12)	5692(3)	2264(2)	564(3)	22(1)
O(29)	7559(4)	4427(2)	2831(4)	31(2)
O(4)	7589(4)	1753(2)	4787(3)	25(1)
O(26)	4133(4)	2468(2)	1095(4)	33(2)
O(42)	8778(4)	1538(2)	5907(4)	29(1)
O(47)	7582(5)	4926(3)	632(4)	39(2)
O(55)	6160(5)	5144(3)	1163(6)	56(2)
O(15)	7384(4)	3972(2)	685(3)	22(1)
O(7)	5870(3)	1438(2)	1961(3)	21(1)

O(28)	5839(5)	4329(2)	874(4)	39(2)
O(48)	8528(4)	4561(2)	98(4)	33(2)
O(44)	5980(4)	513(3)	2272(5)	37(2)
O(8)	6292(3)	1300(2)	3335(4)	25(1)
N(8)	4074(5)	2174(3)	3261(5)	33(2)
N(11)	4188(5)	3412(3)	1314(5)	34(2)
O(46)	4622(4)	2673(3)	-546(4)	39(2)
O(19)	9081(4)	3512(2)	4688(4)	25(1)
C(16)	3391(5)	2323(4)	2897(5)	30(2)
N(19)	10054(5)	2135(4)	5650(5)	42(2)
N(26)	8070(5)	1840(3)	-300(5)	35(2)
N(17)	10922(5)	3160(3)	2996(5)	36(2)
O(56)	9969(5)	4240(3)	45(6)	56(3)
N(5)	5452(5)	2510(3)	5595(5)	33(2)
N(4)	6126(5)	1596(3)	5870(4)	27(2)
N(28)	8616(6)	3805(3)	-745(4)	36(2)
N(22)	7483(6)	477(3)	3333(5)	38(2)
O(57)	10551(6)	4050(4)	4691(5)	63(3)
N(14)	5967(5)	4671(3)	2469(5)	38(2)
C(8)	5376(6)	1534(4)	5476(5)	29(2)
C(13)	4234(5)	2169(3)	1539(6)	29(2)
O(30)	7647(5)	4682(3)	3944(4)	41(2)
O(202)	11619(6)	2066(3)	919(7)	63(3)
C(31)	10132(5)	3929(3)	2051(6)	26(2)
O(200)	11193(6)	1654(4)	1850(6)	60(3)
N(1)	8055(6)	3977(3)	6079(5)	39(2)
O(43)	4904(4)	803(2)	2679(5)	38(2)
O(201)	10750(5)	1485(4)	668(6)	58(3)
O(203)	12061(5)	1372(3)	1017(8)	72(4)
N(10)	4729(5)	3605(3)	-224(6)	39(2)
C(34)	11332(5)	3267(4)	2398(6)	32(2)
C(51)	7582(6)	1062(4)	-509(6)	34(2)
N(25)	6411(6)	1522(3)	-614(5)	39(2)
N(29)	9695(6)	3275(3)	216(5)	35(2)
C(52)	8187(7)	1392(4)	-319(6)	39(3)
C(24)	3967(6)	3294(4)	1956(6)	38(2)

C(36)	10830(6)	2741(4)	2971(6)	37(2)
N(7)	3829(5)	1483(3)	2012(5)	35(2)
N(13)	7550(6)	5181(3)	2187(5)	39(2)
O(54)	6897(9)	2361(6)	-1539(9)	35(3)
O(54')	7087(9)	2176(6)	-1519(9)	35
O(49)	9323(5)	4425(3)	5206(5)	47(2)
C(14)	3546(5)	1886(3)	1720(5)	25(2)
C(50)	6774(6)	1184(3)	-197(5)	31(2)
N(18)	11207(5)	2573(4)	2405(5)	40(2)
C(62)	8221(7)	1216(4)	6933(6)	41(3)
C(45)	8939(7)	441(4)	3155(7)	45(3)
C(61)	8231(6)	1554(4)	6356(5)	31(2)
C(35)	11530(6)	2914(4)	2032(6)	37(2)
C(56)	8532(6)	3371(3)	-1008(5)	30(2)
C(44)	8262(7)	568(3)	3647(6)	36(2)
N(9)	3623(7)	2717(3)	3840(6)	49(3)
C(57)	9350(7)	3166(4)	-1085(6)	41(3)
C(17)	3102(7)	2655(4)	3271(7)	41(3)
C(63)	8361(7)	1421(4)	7688(6)	43(3)
C(55)	8078(5)	3112(3)	-456(5)	28(2)
O(53)	7455(8)	311(3)	1785(6)	73(3)
N(2)	6695(6)	4189(3)	4947(5)	38(2)
C(32)	10942(6)	4061(4)	2364(6)	32(2)
N(6)	4490(7)	2955(4)	5594(7)	57(3)
C(10)	4771(7)	2284(4)	5704(5)	37(2)
N(12)	3616(6)	3605(4)	2306(6)	51(3)
C(74)	4299(7)	2209(4)	-1507(6)	41(3)
C(12)	5234(7)	2904(4)	5540(8)	53(4)
C(54)	8750(7)	2014(4)	-152(7)	46(3)
C(22)	3966(6)	3852(4)	1244(8)	50(3)
C(37)	10203(5)	2709(3)	4756(5)	27(2)
C(73)	4887(6)	2398(4)	-953(6)	36(2)
C(6)	6177(6)	4245(4)	4403(7)	40(3)
N(31)	8840(7)	890(4)	6804(6)	53(3)
C(4)	6272(8)	4074(5)	5515(8)	54(4)
C(15)	3020(6)	2102(4)	2227(6)	35(2)

N(43)	8023(8)	4853(4)	5299(6)	53(3)
N(3)	5416(7)	4170(5)	4631(7)	59(3)
C(2)	7358(8)	3721(4)	6293(6)	45(3)
N(27)	9308(6)	1709(4)	-68(7)	54(3)
N(16)	10929(6)	4131(4)	3136(5)	41(2)
O(52)	3814(6)	1237(5)	3527(6)	79(4)
C(25)	7563(6)	4733(3)	3278(5)	29(2)
C(58)	9761(6)	3043(3)	-426(6)	33(2)
C(43)	8314(5)	1046(3)	3812(5)	26(2)
C(68)	4754(7)	139(4)	2144(7)	42(3)
C(40)	11017(7)	1899(4)	4359(8)	48(3)
N(34)	5282(10)	-150(4)	1664(8)	79(5)
C(23)	3612(6)	3952(4)	1897(9)	49(3)
C(28)	5905(8)	5024(4)	2927(7)	46(3)
C(79)	8091(6)	4861(3)	153(6)	29(2)
C(38)	10612(6)	2433(4)	5329(6)	35(2)
O(205)	4660(9)	900(6)	-375(7)	99(5)
C(5)	5486(8)	4062(5)	5355(8)	50(3)
C(11)	4144(7)	2556(5)	5737(7)	50(3)
O(204)	3715(7)	1102(5)	407(10)	112(6)
C(67)	5249(7)	526(4)	2371(6)	41(3)
C(19)	5529(6)	3995(3)	657(5)	27(2)
N(20)	10271(6)	1747(3)	4217(6)	40(2)
N(23)	8435(7)	973(4)	2092(8)	61(4)
C(21)	4077(6)	4119(4)	617(7)	40(3)
C(64)	9114(8)	1635(4)	7783(6)	42(3)
N(30)	10547(6)	2741(3)	360(7)	47(3)
C(18)	4182(7)	2413(4)	3808(6)	41(3)
C(20)	4802(7)	3995(4)	160(7)	43(3)
N(37)	3557(7)	2463(4)	-1465(7)	60(3)
C(33)	11570(6)	3715(4)	2185(7)	40(3)
C(53)	8975(7)	1324(5)	-177(8)	49(3)
C(60)	10197(7)	3068(4)	683(7)	42(3)
C(49)	6848(6)	1298(3)	600(6)	29(2)
C(3)	6639(8)	3967(4)	6260(7)	48(3)
C(65)	9805(8)	1413(5)	7893(9)	54(3)

C(46)	9054(6)	762(5)	2507(8)	49(3)
C(29)	5224(10)	5033(6)	3213(10)	67(4)
N(15)	4827(8)	4699(7)	2931(8)	88(6)
O(211)	2412(8)	1005(5)	2751(8)	95(5)
O(208)	2764(10)	4144(5)	4745(10)	110(5)
C(39)	11290(7)	2160(4)	4954(8)	50(3)
C(7)	5503(5)	1673(3)	4686(5)	27(2)
O(209)	2833(8)	3697(6)	3697(7)	92(4)
C(27)	6540(10)	5336(4)	3127(9)	62(4)
C(26)	7414(8)	5186(3)	2968(7)	45(3)
N(40)	7533(6)	5547(3)	-329(6)	41(2)
C(1)	7316(5)	3332(3)	5776(5)	26(2)
C(81)	8950(7)	5361(5)	-539(6)	45(3)
C(69)	4493(7)	-118(4)	2796(7)	45(3)
C(80)	8116(8)	5209(5)	-427(8)	53(4)
C(86)	8705(9)	5096(4)	5091(8)	55(3)
O(50)	10086(6)	4999(3)	5377(7)	65(3)
N(24)	9561(7)	1089(5)	1576(8)	66(4)
C(66)	10051(8)	2096(4)	7800(8)	48(3)
C(47)	9748(8)	831(5)	2189(9)	55(3)
C(87)	8757(12)	5529(5)	5457(12)	79(5)
C(9)	4725(7)	1796(5)	5804(7)	46(3)
C(85)	9398(9)	4824(4)	5248(7)	53(3)
N(32)	9250(15)	2055(9)	7827(14)	52(7)
N(32')	9275(15)	2023(9)	7566(16)	52
N(21)	11046(8)	1498(4)	3371(7)	60(3)
C(59)	10275(7)	2712(4)	-318(7)	44(3)
O(212)	6872(10)	4047(6)	-2007(7)	101(5)
O(214)	2913(10)	590(6)	1846(10)	114(6)
C(41)	11504(7)	1747(5)	3865(9)	57(4)
C(48)	8788(8)	1168(5)	1605(7)	52(3)
O(213)	6849(11)	4278(7)	-785(7)	117(6)
N(41)	9280(10)	5785(6)	640(8)	85(5)
C(83)	9927(14)	5177(7)	379(12)	99(8)
C(82)	9375(11)	5449(5)	133(8)	66(5)
O(230)	1602(7)	439(7)	2203(9)	110(6)

O(216)	2648(10)	247(6)	2965(10)	43(4)
C(42)	10303(9)	1507(5)	3613(8)	56(3)
C(30)	5287(8)	4482(6)	2474(8)	62(4)
O(218)	5724(8)	4109(5)	-1407(10)	104(5)
C(84)	9871(10)	5668(6)	1140(8)	67(4)
O(219)	6683(12)	3585(7)	-1129(12)	62(5)
O(221)	4692(11)	1582(5)	60(9)	109(6)
N(33)	10355(8)	1696(10)	7888(9)	121(9)
O(231)	3836(9)	4223(6)	3926(10)	108(5)
Cl(8)	7527(3)	6286(2)	1464(4)	104(2)
O(313)	2563(4)	5066(2)	2119(4)	32(2)
Cl(9)	6908(8)	-875(5)	1676(8)	208(5)
O(306)	7531(7)	6592(4)	2810(7)	76(3)
O(304)	6112(7)	5031(4)	-439(6)	67(3)
O(305)	2168(10)	2338(6)	-3074(10)	110(5)
O(302)	12449(9)	3161(5)	-68(8)	93(4)
O(303)	4526(8)	5207(5)	1138(8)	87(4)
O(300)	5987(9)	196(6)	475(9)	99(4)
O(309)	7813(9)	2811(6)	-2439(9)	102(5)
O(307)	10629(10)	5665(6)	4584(9)	103(5)
O(215)	6070(16)	1575(9)	7630(15)	171(9)
O(222)	7178(11)	175(7)	4989(10)	119(6)
O(308)	9345(13)	6268(8)	3897(12)	147(8)
O(311)	1457(13)	4703(8)	4427(13)	145(7)
O(312)	2969(13)	3381(8)	6265(13)	145(7)
O(301)	1120(20)	-271(14)	3100(20)	246(16)
O(224)	5055(9)	1019(6)	766(9)	102(5)
O(223)	3746(13)	3636(8)	4644(12)	140(7)
O(226)	6181(12)	504(7)	5717(11)	125(6)
N(42)	10203(12)	5327(7)	983(11)	98(5)
O(228)	6389(15)	789(9)	4598(14)	163(9)
O(225)	7437(16)	838(9)	5536(15)	174(9)
C(70)	5135(5)	-314(3)	3195(6)	48(3)
N(35)	5467(6)	-720(3)	3055(5)	70(4)
C(72)	6103(6)	-782(3)	3547(6)	63(4)
N(36)	6164(7)	-414(4)	3991(6)	97(5)

C(71)	5565(7)	-125(3)	3773(6)	74(5)
C(88)	8038(9)	5801(5)	5257(9)	84(5)
C(89)	7292(12)	5828(8)	5565(10)	147(12)
N(45)	6815(8)	6092(9)	5114(14)	206(16)
C(100)	7266(10)	6227(6)	4529(11)	113(8)
N(44)	8022(8)	6047(5)	4617(8)	92(5)
C(76)	4784(8)	2749(4)	-2390(10)	90(6)
C(77)	5593(7)	2837(5)	-2435(9)	82(5)
N(39)	5682(7)	3283(5)	-2544(11)	159(11)
C(78)	4928(9)	3471(4)	-2567(10)	79(5)
N(38)	4374(6)	3141(5)	-2472(9)	109(6)
O(238)	9554(10)	5548(6)	2910(10)	108(5)
O(237)	10517(10)	5078(6)	2758(10)	113(5)
O(235)	9680(11)	4955(7)	3631(11)	118(6)
O(232)	9530(7)	3130(4)	6531(8)	9(2)
O(236)	9563(6)	5085(4)	2694(5)	30(3)
C(75)	4588(17)	2170(10)	-2253(16)	114(8)
O(100)	7321(6)	2746(4)	2689(6)	59(2)
O(227)	7203(12)	5935(7)	1061(11)	130(6)
O(243)	6816(13)	-457(8)	2142(13)	145(7)
O(229)	7780(30)	6423(18)	510(30)	310(20)
O(244)	7306(17)	-1205(10)	2317(17)	191(11)
Cl(10)	5769(5)	1077(3)	-2351(5)	145(3)
O(245)	5000(20)	1230(13)	-1890(20)	246(14)

APPENDIX E

CRYSTALLOGRAPHIC DATA FOR

$[Nd_{15}(\mu_5\text{-}Cl)(\mu_3\text{-}OH)_{20}(his^{+/-})_{10}(his^{-})_5(OH)_8](ClO_4)_{12}$

Identification code	mes99	
Empirical formula	C90 H120 Cl6 N45 Nd15 O90	
Formula weight	5648.61	
Temperature	190(2) K	
Wavelength	0.71073 Å	
Crystal system	Orthorhombic	
Space group	$P2_12_12_1$	
Unit cell dimensions	a = 17.2891(18) Å	α= 90°.
	b = 28.868(3) Å	β= 90°.
	c = 40.359(5) Å	γ = 90°.
Volume	20143(4) $Å^3$	
Z	4	
Density (calculated)	1.863 Mg/m^3	
Absorption coefficient	3.961 mm^{-1}	
F(000)	10788	
Crystal size	0.26 x 0.26 x 0.25 mm^3	
Theta range for data collection	1.01 to 25.37°.	
Index ranges	-20<=h<=20, -34<=k<=34, -46<=l<=48	
Reflections collected	94682	
Independent reflections	34801 [R(int) = 0.0284]	
Completeness to theta = 25.37°	98.0 %	
Max. and min. transmission	0.4436 and 0.4257	
Refinement method	Full-matrix least-squares on F^2	
Data / restraints / parameters	34801 / 0 / 2008	
Goodness-of-fit on F^2	1.088	
Final R indices [I>2sigma(I)]	R1 = 0.0630, wR2 = 0.1762	
R indices (all data)	R1 = 0.0754, wR2 = 0.1960	
Absolute structure parameter	0.015(17)	
Extinction coefficient	0.00094(3)	
Largest diff. peak and hole	4.714 and -2.155 e.$Å^{-3}$	

Atomic coordinates (x 10^4) and equivalent isotropic displacement parameters ($Å^2$x 10^3) for mes99. U(eq) is defined as one third of the trace of the orthogonalized U^{ij} tensor.

	x	y	z	U(eq)
Cl(11)	4392(9)	5456(5)	1661(3)	164(5)
Nd(1)	3125(1)	5414(1)	9217(1)	29(1)
Nd(5)	1872(1)	5790(1)	8461(1)	28(1)
Nd(4)	1821(1)	4758(1)	7831(1)	31(1)
Nd(7)	3140(1)	6704(1)	8862(1)	31(1)
Nd(15)	1897(1)	5967(1)	7470(1)	32(1)
Nd(9)	5116(1)	5109(1)	9548(1)	35(1)
Nd(10)	3159(1)	2842(1)	8859(1)	39(1)
Nd(3)	3055(1)	3745(1)	8191(1)	33(1)
Nd(13)	3151(1)	3943(1)	7276(1)	36(1)
Nd(2)	3847(1)	4151(1)	9047(1)	32(1)
Nd(11)	5178(1)	3420(1)	8518(1)	36(1)
Nd(14)	-8(1)	5562(1)	8017(1)	38(1)
Nd(6)	1368(1)	6160(1)	9397(1)	33(1)
Nd(8)	3257(1)	4450(1)	9908(1)	36(1)
Nd(12)	1116(1)	3536(1)	7657(1)	41(1)
O(10A)	3087(7)	4392(3)	7788(2)	35(2)
O(2A)	3188(6)	5876(3)	8727(2)	33(2)
O(9A)	1729(6)	3991(3)	8110(3)	37(2)
O(10B)	2355(7)	3026(4)	8352(3)	43(3)
O(10C)	2150(6)	5503(4)	9694(2)	33(2)
O(1A)	1781(6)	5515(3)	9031(2)	35(2)
O(10D)	2371(7)	5136(4)	7311(2)	38(2)
O(10E)	4397(6)	5831(3)	9318(3)	37(2)
O(3A)	1762(6)	6441(3)	8853(2)	30(2)
O(10F)	5269(6)	4063(4)	8974(3)	37(2)
O(10G)	2398(7)	5064(4)	10147(3)	41(3)
O(7A)	930(7)	5344(4)	7577(3)	42(3)
O(5A)	2430(6)	5515(3)	7945(2)	33(2)
O(11A)	2914(7)	4655(4)	6949(3)	45(3)
O(8A)	1059(6)	5123(3)	8262(3)	34(2)

O(18A)	2851(6)	4609(4)	9350(3)	38(2)
O(10H)	2594(7)	6489(4)	8284(2)	39(2)
O(20A)	4455(6)	4356(4)	9602(2)	37(2)
O(20B)	759(6)	6376(4)	7242(3)	45(3)
O(14A)	4228(6)	4043(3)	8458(3)	33(2)
O(20C)	2444(8)	3518(4)	6862(3)	53(3)
O(17A)	4272(6)	4960(3)	9051(3)	32(2)
O(15A)	4281(6)	3340(4)	8993(3)	36(2)
O(11B)	5972(6)	4530(4)	9290(3)	46(3)
N(3A)	6172(8)	4081(5)	8352(4)	47(4)
O(6A)	1124(6)	6090(3)	7977(2)	30(2)
O(11C)	3074(9)	2986(4)	9459(3)	57(4)
O(11D)	1310(9)	2864(4)	8018(4)	59(3)
N(1A)	-814(9)	5189(6)	8500(5)	60(4)
O(19A)	3802(6)	5199(4)	9731(2)	37(2)
O(13A)	2869(6)	3676(3)	8792(3)	37(2)
O(20D)	2534(8)	7288(4)	9209(3)	53(3)
O(11E)	3261(6)	3740(4)	9540(2)	39(2)
O(11F)	5162(7)	3356(5)	7898(3)	49(3)
O(10I)	453(6)	5891(4)	8571(3)	35(2)
O(12A)	1822(6)	4165(4)	7390(3)	38(2)
O(20E)	-466(8)	6036(6)	7538(3)	66(4)
O(10J)	536(6)	4360(4)	7753(3)	40(3)
O(20F)	5321(7)	2606(4)	8655(3)	49(3)
O(10K)	186(7)	6180(5)	9066(3)	50(3)
N(2A)	-75(9)	3507(6)	8052(4)	52(4)
O(4A)	2784(6)	6231(3)	9347(3)	34(2)
O(11G)	2585(7)	6617(4)	7739(3)	46(3)
N(4A)	1983(8)	4016(5)	10039(4)	49(4)
O(11H)	4030(7)	3672(4)	7738(3)	46(3)
N(8A)	3309(9)	5989(5)	7210(4)	48(4)
O(11I)	4342(7)	6585(4)	9200(3)	50(3)
O(16A)	3910(6)	3099(3)	8372(3)	36(2)
N(6A)	6035(8)	5571(5)	9132(5)	54(4)
O(11J)	-482(6)	4834(4)	7787(3)	48(3)
O(20G)	5090(9)	5054(6)	10178(4)	71(4)

N(5A)	1680(10)	2731(6)	8999(4)	59(4)
N(7A)	4240(9)	6748(6)	8424(4)	49(4)
O(11K)	2521(6)	3420(4)	7667(3)	39(2)
O(20H)	1580(7)	6988(4)	9521(3)	51(3)
O(20I)	1282(8)	3310(6)	7075(4)	74(5)
Cl(9A)	-1534(6)	3193(3)	9400(2)	113(3)
C(10A)	6824(11)	4241(6)	8509(5)	51(4)
N(9A)	6536(8)	5731(7)	8650(4)	59(4)
C(10B)	5256(12)	1793(6)	8744(5)	53(5)
C(10C)	4909(11)	2267(6)	8739(4)	44(4)
C(10D)	15(9)	6095(5)	8784(4)	36(3)
C(10E)	3185(10)	3321(6)	9640(4)	43(4)
C(10F)	2662(9)	6757(5)	8040(4)	36(3)
C(10G)	6168(11)	6064(7)	9107(5)	54(5)
C(11A)	3587(12)	5820(6)	6903(5)	53(5)
C(10H)	4844(10)	6458(8)	8447(5)	58(5)
C(10I)	6091(13)	4299(7)	8058(5)	65(6)
C(10J)	6510(13)	6150(9)	8815(6)	71(7)
O(20J)	4222(9)	2272(5)	8819(4)	65(4)
O(21A)	4106(9)	4643(6)	10353(3)	68(4)
C(11B)	3096(15)	5626(7)	6635(5)	61(6)
O(12B)	131(8)	7034(4)	7151(4)	63(4)
N(10A)	2108(7)	6711(4)	7089(3)	32(3)
O(15B)	3979(8)	7445(4)	8977(4)	61(4)
O(15C)	359(9)	2802(5)	7494(4)	66(4)
O(19B)	2932(9)	2103(5)	9243(4)	72(4)
O(15D)	6460(9)	5065(6)	9829(4)	72(4)
C(11C)	1503(9)	7064(5)	7168(4)	35(3)
N(17A)	5392(10)	5926(5)	9821(3)	52(4)
N(12A)	1645(10)	6234(5)	10042(4)	54(4)
N(16A)	6293(9)	3389(5)	8950(4)	51(4)
N(19A)	1722(9)	5670(5)	6858(3)	45(3)
N(13A)	3617(11)	3645(5)	10166(4)	55(4)
C(11D)	729(10)	6822(5)	7177(4)	36(3)
N(11A)	740(10)	3916(8)	9986(6)	82(7)
O(15E)	171(9)	6558(6)	9684(4)	71(4)

N(20A)	4031(9)	3215(5)	7167(4)	56(4)
C(11E)	1497(9)	7489(5)	6925(5)	44(4)
C(11F)	1802(16)	3539(7)	10069(5)	66(6)
C(11G)	1097(13)	3445(9)	10062(6)	72(6)
C(11H)	1744(11)	5786(7)	10227(4)	48(4)
C(11I)	5287(11)	6344(6)	9597(5)	55(5)
N(18A)	2726(11)	7378(5)	8446(4)	56(4)
C(11J)	4652(9)	3436(5)	7687(4)	34(3)
O(15F)	-1543(10)	5479(7)	7866(6)	106(7)
N(31A)	2511(8)	7979(4)	7177(4)	41(3)
N(30A)	6610(8)	3053(5)	8217(4)	44(3)
N(25A)	-695(13)	3421(7)	8516(5)	80(6)
C(13A)	7206(11)	2776(6)	8330(4)	43(4)
C(12A)	2246(10)	7730(5)	6908(4)	37(4)
C(13B)	3177(10)	8166(6)	7082(4)	45(4)
C(12B)	-1216(12)	3640(6)	8300(5)	54(5)
N(22A)	-95(8)	3808(6)	7313(4)	52(4)
C(13C)	3896(9)	6120(7)	7382(5)	49(4)
N(29A)	6751(13)	4587(6)	8031(5)	73(5)
C(12C)	1844(13)	2751(6)	8225(5)	57(5)
C(12D)	-630(11)	4123(8)	7466(5)	57(5)
N(26A)	4567(10)	6036(6)	7206(5)	66(5)
C(12E)	-38(12)	3366(7)	8348(5)	60(6)
N(27A)	4526(9)	4290(6)	7197(5)	64(5)
C(13D)	7139(11)	4066(7)	8836(5)	55(5)
N(28A)	5390(13)	4859(7)	7250(7)	100(9)
N(23A)	-787(11)	6230(6)	8285(5)	71(6)
C(13E)	7155(12)	4550(7)	8308(5)	56(5)
C(13F)	5225(16)	4084(7)	7196(6)	71(7)
C(12F)	972(12)	5592(9)	10356(6)	67(6)
C(12G)	1288(12)	4230(7)	9984(5)	57(5)
C(13G)	5817(14)	4393(10)	7219(7)	85(8)
C(12H)	1997(16)	7296(7)	9436(5)	64(6)
N(24A)	472(10)	5564(7)	9690(8)	100(9)
N(21A)	2685(11)	2162(6)	8468(6)	70(5)
C(12I)	2317(10)	5341(7)	6746(4)	47(4)

C(12J)	1911(12)	2238(7)	8309(5)	58(5)
C(13H)	6044(10)	6414(7)	9384(6)	61(6)
C(14A)	3746(10)	7339(7)	8006(6)	62(6)
N(32A)	5317(11)	6507(8)	8163(5)	76(6)
C(14B)	2886(10)	7261(6)	8082(4)	40(4)
C(15A)	504(16)	5481(14)	10069(12)	140(20)
C(14C)	6579(10)	3859(6)	9076(4)	42(4)
C(15B)	3219(14)	3247(7)	10029(4)	58(5)
C(14D)	4294(11)	6999(7)	8135(5)	59(5)
C(15C)	2150(10)	5431(6)	10008(4)	41(4)
C(15D)	2383(17)	3155(8)	10154(6)	82(8)
C(15E)	-835(13)	3679(6)	8011(6)	65(6)
C(14E)	1988(17)	7724(8)	9647(8)	100(11)
N(33A)	551(12)	2873(8)	9220(6)	77(6)
C(15F)	-1189(10)	5382(8)	8768(5)	55(5)
C(14F)	1769(12)	3355(6)	6834(4)	48(4)
C(15G)	1313(14)	2951(8)	9224(6)	72(7)
C(15H)	-813(10)	6219(7)	8645(5)	50(4)
C(14G)	4362(12)	5849(7)	6914(7)	63(6)
C(14H)	5350(12)	3553(7)	7148(5)	56(5)
C(13I)	6259(11)	5387(7)	8855(5)	54(5)
C(14I)	2559(9)	5031(6)	7023(4)	39(4)
C(14J)	4965(13)	6843(9)	7963(6)	69(6)
C(13J)	4632(10)	6235(6)	9362(4)	42(4)
N(36A)	6362(13)	518(7)	9146(4)	63(5)
N(35A)	5171(13)	705(8)	8975(7)	95(8)
N(38A)	-1028(11)	4622(8)	8877(4)	70(5)
N(34A)	6061(9)	1833(6)	8605(4)	52(4)
C(15I)	5608(16)	1123(7)	9102(6)	76(7)
C(16A)	6328(14)	962(7)	9170(5)	60(5)
N(37A)	2800(16)	7989(9)	9607(6)	100(7)
C(16B)	-144(10)	4477(6)	7683(4)	45(4)
C(16C)	5660(20)	377(7)	9048(7)	99(11)
C(16D)	5887(9)	4177(6)	9122(4)	36(3)
C(16E)	4812(11)	3248(7)	7343(5)	53(5)
C(16F)	1244(17)	7982(10)	9662(7)	85(7)

C(16G)	-1173(12)	3848(7)	7694(7)	64(6)
C(17A)	-1408(11)	5900(11)	8767(6)	84(9)
C(15J)	5283(18)	1596(8)	9091(6)	80(8)
C(16H)	1083(15)	2454(8)	8825(7)	74(7)
O(32A)	-820(15)	3197(12)	9607(7)	149(11)
C(17B)	-704(12)	4729(7)	8574(6)	61(5)
C(16J)	443(14)	2525(15)	8995(7)	101(11)
C(17C)	-1356(14)	5045(12)	8983(7)	89(9)
O(32B)	-2330(30)	3137(17)	9623(12)	229(18)
C(17D)	4870(20)	4985(13)	10736(7)	128(16)
N(40A)	2075(15)	3404(10)	6232(5)	98(8)
N(41A)	4292(18)	4775(11)	10957(8)	117(9)
C(17E)	1502(17)	3182(11)	6495(6)	89(8)
C(17F)	1583(19)	2659(12)	6476(8)	100(9)
C(17G)	4705(14)	4908(9)	10408(6)	72(7)
N(42A)	-369(17)	5023(10)	9766(7)	105(8)
O(32C)	-1420(40)	3780(20)	9338(15)	320(30)
C(17H)	5630(30)	4845(15)	10821(10)	123(12)
C(18A)	1191(14)	2127(7)	8553(7)	75(7)
C(18B)	0(40)	5060(20)	10083(15)	180(20)
N(43A)	990(20)	8399(13)	8820(8)	119(9)
N(39A)	1400(30)	8678(17)	9297(11)	177(16)
C(18C)	890(30)	8071(16)	8990(11)	133(13)
C(18D)	1200(20)	8757(17)	8914(13)	145(16)
O(32D)	-1520(20)	3009(12)	9058(9)	165(12)
C(18E)	-20(20)	5349(13)	9564(9)	112(10)
C(18F)	4629(15)	4739(11)	7241(7)	89(8)
N(49A)	1549(13)	2105(8)	5631(5)	77(5)
N(44A)	5340(20)	4066(13)	10932(9)	142(12)
C(17I)	6370(30)	4270(20)	10482(14)	180(20)
C(17J)	600(30)	2389(15)	6043(11)	125(13)
C(18I)	2000(30)	2336(18)	5882(13)	157(17)
C(18J)	600(30)	2272(17)	5687(12)	152(16)
Cl(2A)	842(2)	4225(1)	9037(1)	42(1)
O(30A)	181(8)	4020(5)	9167(4)	72(5)
O(30B)	1527(8)	4043(7)	9188(5)	91(6)

O(30C)	814(9)	4710(5)	9086(8)	127(10)
O(30D)	875(12)	4138(10)	8710(5)	135(11)
Cl(3A)	4692(3)	5284(2)	8092(1)	44(1)
O(30Q)	5362(8)	5449(5)	7927(4)	63(4)
O(30R)	4484(11)	4841(6)	7963(6)	107(7)
O(30S)	4061(8)	5589(6)	8084(6)	99(7)
O(30T)	4863(14)	5234(8)	8411(6)	110(7)
Cl(1A)	2753(2)	4776(1)	8550(1)	38(1)
Cl(4A)	577(5)	7320(3)	8223(2)	99(2)
O(36A)	357(16)	7810(10)	8245(7)	131(8)
O(36B)	-128(18)	7143(10)	8071(7)	141(9)
Cl(6A)	8422(3)	1551(2)	8854(1)	49(1)
O(21L)	7667(10)	1648(6)	8695(4)	75(4)
O(21M)	8421(14)	1120(8)	9010(6)	113(7)
O(21N)	8996(11)	1558(8)	8603(4)	99(6)
O(31A)	8570(11)	1893(6)	9095(4)	83(5)
Cl(5A)	5402(5)	2936(3)	9775(2)	94(2)
O(37A)	6150(20)	2812(12)	9698(8)	164(11)
O(37B)	5143(19)	2798(11)	10096(8)	154(10)
O(37C)	5320(20)	3395(15)	9737(10)	208(16)
Cl(7A)	2356(4)	8641(2)	8072(2)	83(2)
O(34A)	1350(70)	8180(40)	7970(30)	550(70)
O(34B)	2830(20)	8549(13)	8314(9)	176(13)
Cl(8A)	8720(5)	8667(3)	9656(2)	102(2)
O(20Z)	8226(14)	8522(11)	9447(6)	153(12)
O(35A)	9518(14)	8522(14)	9632(8)	177(15)
O(35B)	8487(15)	8580(20)	9998(8)	360(40)
O(35C)	8690(30)	9149(15)	9653(11)	199(15)
Cl(1E)	8179(14)	6105(8)	9825(5)	229(8)
O(39A)	7530(20)	6238(12)	9962(8)	164(11)
Cl(1I)	6010(20)	7759(11)	8705(8)	312(14)
O(38A)	5070(70)	9020(40)	8950(30)	570(80)
O(38B)	5910(30)	8021(17)	8901(12)	214(17)
O(38C)	5600(30)	7526(17)	9087(12)	219(17)
C(200)	1170(30)	2495(16)	6136(11)	138(14)
O(23A)	3770(18)	3923(11)	6609(7)	149(10)

O(37D)	4990(30)	2655(15)	9550(11)	214(17)
O(34C)	2090(40)	8130(20)	7894(14)	270(20)
C(18H)	5840(20)	4366(14)	10739(10)	121(11)
O(39B)	8840(70)	5470(40)	9800(30)	580(60)
O(38D)	5030(50)	8160(30)	8780(20)	410(40)
C(16I)	1251(19)	8257(12)	9325(8)	95(8)
N(44B)	5990(20)	3699(13)	10564(9)	144(12)

APPENDIX F

CRYSTALLOGRAPHIC DATA FOR

$[Nd_{15}(\mu_5\text{-}Br)(\mu_3\text{-}OH)_{20}(his^{+/-})_{10}(his^{-})_5(OH)_8](ClO_4)_{12}$

Identification code	mes1024	
Empirical formula	C75 H120 Br Cl5 N45 Nd15 O90	
Formula weight	5512.92	
Temperature	150(2) K	
Wavelength	0.71073 Å	
Crystal system	Monoclinic	
Space group	$P2_1$	
Unit cell dimensions	a = 31.851(4) Å	α= 90°.
	b = 19.511(2) Å	β= 92.925(5)°.
	c = 33.390(4) Å	γ = 90°.
Volume	20723(4) $Å^3$	
Z	4	
Density (calculated)	1.767 Mg/m^3	
Absorption coefficient	4.027 mm^{-1}	
F(000)	10500	
Crystal size	0.19 x 0.19 x 0.09 mm^3	
Theta range for data collection	1.21 to 25.51°.	
Index ranges	-38<=h<=38, -23<=k<=23, -40<=l<=40	
Reflections collected	107484	
Independent reflections	69400 [R(int) = 0.0635]	
Completeness to theta = 25.51°	96.7 %	
Max. and min. transmission	0.7132 and 0.5073	
Refinement method	Full-matrix least-squares on F^2	
Data / restraints / parameters	69400 / 1 / 2371	
Goodness-of-fit on F^2	2.224	
Final R indices [I>2sigma(I)]	R1 = 0.1340, wR2 = 0.3353	
R indices (all data)	R1 = 0.1743, wR2 = 0.3576	
Absolute structure parameter	0.13(2)	
Largest diff. peak and hole	3.822 and -3.761 e.$Å^{-3}$	

Atomic coordinates (x 10^4) and equivalent isotropic displacement parameters ($Å^2$x 10^3) for mes1024. U(eq) is defined as one third of the trace of the orthogonalized U^{ij} tensor.

	x	y	z	U(eq)
Nd(1)	-2591(1)	6185(1)	5068(1)	29(1)
Nd(2)	-1597(1)	5177(1)	5558(1)	30(1)
Nd(4)	-1870(1)	3164(1)	5493(1)	26(1)
Nd(5)	-2965(1)	2973(1)	4955(1)	27(1)
Nd(7)	-2716(1)	1741(1)	5806(1)	27(1)
Nd(10)	-2024(1)	1615(1)	4802(1)	29(1)
Nd(11)	-1478(1)	6864(1)	4885(1)	33(1)
Nd(12)	-3233(1)	6340(1)	4021(1)	30(1)
Nd(15)	-3408(1)	4878(1)	4723(1)	30(1)
Nd(16)	-4195(1)	3511(1)	4965(1)	28(1)
Nd(17)	-3789(1)	6797(1)	5020(1)	39(1)
Nd(18)	-709(1)	3932(1)	5385(1)	33(1)
Nd(21)	-1896(1)	6894(1)	6006(1)	31(1)
Nd(22)	-1286(1)	3863(1)	6432(1)	33(1)
Nd(27)	-3560(1)	3309(1)	3970(1)	33(1)
Nd(3)	3098(1)	6975(1)	9545(1)	28(1)
Nd(6)	4273(1)	6196(1)	9596(1)	34(1)
Nd(8)	2224(1)	8403(1)	9249(1)	29(1)
Nd(9)	3003(1)	3239(1)	8970(1)	30(1)
Nd(13)	2068(1)	7150(1)	10096(1)	30(1)
Nd(14)	840(1)	6596(1)	10066(1)	33(1)
Nd(19)	1566(1)	6839(1)	11088(1)	36(1)
Nd(20)	3348(1)	4963(1)	9438(1)	29(1)
Nd(23)	2433(1)	3941(1)	9934(1)	35(1)
Nd(24)	1655(1)	5244(1)	10335(1)	38(1)
Nd(25)	3553(1)	3287(1)	10089(1)	35(1)
Nd(26)	3529(1)	6312(1)	8589(1)	32(1)
Nd(28)	1927(1)	3741(1)	10991(1)	40(1)
Nd(29)	3033(1)	8510(1)	10246(1)	32(1)
Nd(30)	1262(1)	3339(1)	9979(1)	51(1)
O(40)	-3462(7)	3847(12)	5185(6)	22(5)

O(41)	-3668(7)	2766(12)	4621(7)	25(5)
O(45)	-1869(7)	4238(12)	5926(7)	28(6)
O(201)	1379(6)	7342(12)	10411(6)	19(5)
O(204)	3062(8)	5901(14)	9071(7)	36(6)
O(300)	-2097(7)	405(15)	5092(8)	51(9)
O(44)	-2840(7)	5545(12)	4441(7)	26(5)
O(101)	-1414(7)	2440(12)	5079(7)	24(5)
O(203)	2378(8)	7135(14)	9400(8)	37(6)
O(400)	-2767(8)	746(14)	6345(8)	39(6)
O(205)	2895(7)	3046(14)	9703(7)	37(7)
O(202)	2283(8)	8450(14)	10014(7)	40(6)
O(100)	-2246(7)	2033(12)	6397(7)	30(6)
O(43)	-2629(8)	2998(15)	5647(8)	45(7)
O(301)	2892(7)	3340(13)	10510(7)	31(6)
O(200)	1550(6)	6297(11)	9903(6)	19(5)
O(42)	-3942(5)	4096(9)	4390(5)	7(4)
N(100)	-3203(9)	2190(15)	6362(8)	28(7)
Cl(1)	1815(3)	5613(5)	8814(3)	42(2)
Cl(2)	-1920(3)	4406(5)	4060(3)	41(2)
Cl(3)	3952(3)	8998(6)	8976(3)	46(3)
Cl(5)	3109(3)	9551(6)	3792(3)	43(3)
Cl(4)	-995(3)	1150(5)	6075(4)	48(3)
O(102)	-2540(7)	1683(13)	4178(7)	33(6)
N(101)	-1555(10)	2057(18)	4221(10)	43(9)
O(302)	3033(7)	7235(14)	8790(8)	40(7)
O(103)	-2590(8)	7580(14)	5992(8)	40(7)
Cl(6)	2393(3)	1247(5)	203(3)	48(3)
Cl(7)	3240(3)	5684(6)	945(3)	45(3)
O(105)	-737(8)	2792(12)	5058(8)	36(6)
O(305)	2094(7)	9385(12)	8708(7)	31(6)
O(108)	-1555(8)	7987(12)	5874(8)	35(6)
O(104)	-4032(9)	2444(13)	5441(9)	56(9)
O(107)	-3741(8)	4297(15)	3529(7)	37(7)
O(208)	1360(7)	4113(12)	10542(8)	30(6)
O(206)	3541(8)	6032(14)	9842(8)	42(7)
O(306)	3496(8)	5127(15)	8251(8)	47(7)

O(307)	3358(8)	2151(12)	9145(9)	45(8)
O(308)	2310(9)	2589(18)	9077(9)	64(10)
O(46)	-3043(7)	3925(12)	4423(6)	23(5)
O(207)	3800(7)	6909(12)	9208(7)	28(5)
O(247)	2596(8)	8460(14)	10849(8)	39(6)
O(106)	-2200(6)	6805(11)	4491(6)	18(5)
O(47)	-3097(6)	6857(11)	4690(6)	16(5)
O(304)	2468(7)	9647(15)	9261(8)	46(8)
Cl(8)	4912(4)	346(7)	6069(3)	58(3)
Cl(11)	3768(4)	5661(6)	5374(3)	52(3)
Cl(10)	5937(3)	5691(5)	9301(4)	49(3)
Cl(9)	2674(3)	3864(6)	5217(3)	47(3)
C(200)	4634(8)	6357(15)	8593(8)	10(6)
O(99)	-1933(8)	662(16)	4289(8)	50(8)
O(111)	-4305(8)	3053(14)	3811(8)	44(7)
N(200)	1642(7)	7998(14)	8692(8)	20(6)
C(100)	-4605(9)	3104(14)	3962(8)	9(6)
O(312)	3275(9)	9620(15)	3426(9)	46(7)
N(102)	-2960(13)	6090(30)	3327(10)	56(12)
O(114)	-1832(7)	2894(13)	6258(8)	35(7)
O(309)	-2161(11)	3866(15)	4190(9)	58(9)
N(104)	-1668(11)	7902(19)	4448(11)	53(10)
N(103)	-3869(11)	6177(16)	3527(9)	40(9)
O(310)	-2259(9)	4909(16)	3924(9)	54(8)
O(209)	3883(6)	5503(14)	9045(6)	28(6)
O(311)	3007(11)	6212(19)	785(11)	82(12)
O(49)	-2225(7)	5861(13)	5703(9)	39(7)
N(105)	-1399(10)	6570(20)	4113(11)	54(11)
C(101)	-1068(14)	2010(20)	4193(14)	53(12)
O(210)	3591(7)	3727(12)	9398(7)	26(6)
N(201)	3591(9)	3409(17)	8428(9)	37(8)
O(213)	4265(8)	3918(18)	10047(10)	59(9)
O(112)	-2517(11)	420(20)	5761(9)	75(12)
O(113)	-3352(7)	2332(14)	5469(7)	33(6)
O(110)	-3581(7)	7412(13)	3942(8)	35(6)
O(214)	4242(11)	6421(19)	8403(10)	71(10)

O(211)	1518(14)	5776(15)	11518(12)	89(13)
Cl(13)	4048(4)	2540(8)	7435(5)	76(4)
Cl(16)	1755(4)	2198(8)	7653(4)	67(3)
Cl(15)	1564(5)	9855(8)	1954(4)	81(4)
Cl(14)	4053(5)	7382(10)	7271(4)	91(5)
O(224)	2870(8)	2361(12)	8386(8)	36(7)
O(215)	3183(7)	4398(12)	10057(7)	29(6)
C(104)	-4861(10)	4974(17)	5078(10)	22(7)
O(116)	-1572(6)	5729(11)	6260(7)	24(5)
O(52)	-3341(8)	5831(11)	5227(9)	43(7)
O(119)	-4101(7)	4840(11)	5069(7)	31(6)
N(106)	-1919(8)	3907(18)	6882(10)	41(9)
O(220)	2689(7)	4227(12)	9285(9)	38(7)
O(118)	-3808(8)	7833(13)	4526(8)	36(6)
O(50)	-2077(6)	7109(10)	5289(6)	19(5)
O(221)	3718(8)	2283(11)	9696(8)	35(6)
O(223)	2954(8)	9696(13)	9902(8)	43(7)
O(216)	2957(7)	8217(12)	9519(6)	23(5)
O(115)	-2958(8)	6890(13)	5552(8)	42(7)
O(48)	-1146(6)	3233(10)	5801(6)	17(5)
O(225)	949(10)	7669(17)	9633(10)	64(9)
O(315)	3830(9)	8920(20)	8534(11)	77(11)
O(117)	-1282(13)	5105(18)	6698(12)	86(12)
O(316)	3947(11)	2383(16)	7053(8)	63(9)
O(51)	-2765(6)	1740(11)	5055(6)	19(5)
O(313)	-1699(9)	4252(13)	3721(8)	43(8)
O(222)	4279(7)	7333(13)	9929(7)	30(6)
O(218)	2048(8)	6227(12)	10638(7)	32(6)
C(103)	-4407(10)	5264(15)	5067(10)	22(8)
Cl(21)	261(7)	4821(13)	1100(6)	133(8)
Cl(20)	1327(5)	9482(7)	414(5)	93(5)
Cl(19)	4400(8)	7120(14)	2245(5)	157(12)
C(208)	507(13)	6980(20)	11018(13)	45(11)
O(123)	-4675(10)	3104(17)	4390(9)	64(9)
C(201)	3506(14)	3870(20)	8131(13)	51(11)
C(106)	-3658(12)	7140(20)	6129(12)	42(10)

O(124)	-513(10)	3552(17)	6571(10)	65(9)
C(105)	-3947(10)	6059(17)	5986(10)	23(8)
O(227)	596(10)	3210(19)	10002(10)	68(9)
O(317)	-1646(10)	4608(17)	4388(9)	58(8)
N(204)	2565(10)	3757(17)	8366(9)	39(8)
C(107)	-3496(10)	7929(17)	5373(9)	19(7)
O(228)	151(9)	7223(15)	9822(8)	49(7)
N(107)	-3825(9)	6657(16)	5823(9)	34(7)
O(226)	4677(9)	6412(15)	8960(8)	49(7)
O(229)	4054(7)	4938(13)	9814(7)	33(6)
O(122)	-4377(9)	7634(15)	5276(9)	50(8)
O(318)	3750(11)	2220(19)	7670(11)	76(10)
O(230)	830(9)	7129(14)	11148(8)	46(7)
C(154)	-931(7)	1619(13)	4830(7)	0(5)
Cl(25)	3908(8)	4487(13)	3497(8)	153(10)
O(127)	-1365(7)	7965(13)	5261(7)	32(6)
C(111)	-2053(11)	3400(20)	7110(11)	33(9)
O(321)	1783(19)	5050(30)	9040(18)	150(20)
O(53)	-1039(8)	4601(14)	5953(8)	39(7)
C(110)	-233(14)	3680(20)	6399(13)	50(11)
C(108)	-3856(10)	5439(18)	3345(10)	25(8)
O(324)	5779(12)	6410(20)	9327(12)	87(12)
O(319)	-740(30)	810(60)	5950(30)	210(50)
O(231)	2650(8)	8169(14)	8663(8)	42(7)
O(320)	-990(12)	1230(20)	6486(12)	83(11)
O(232)	2567(9)	2943(15)	11024(8)	46(7)
C(109)	-3597(9)	5530(16)	2953(9)	18(7)
O(233)	1401(10)	6980(17)	11823(9)	61(8)
C(112)	-3638(12)	2090(20)	6407(12)	37(9)
N(210)	3558(10)	7520(17)	8252(10)	38(8)
O(323)	2119(9)	826(15)	-90(8)	47(7)
O(235)	1740(7)	5015(12)	11107(7)	26(5)
O(54)	-2270(8)	2805(14)	4827(8)	43(7)
C(113)	-3036(13)	2620(20)	6661(13)	45(11)
O(134)	-2940(9)	2512(16)	4236(9)	52(8)
N(108)	-3820(10)	6124(17)	6363(10)	37(8)

O(128)	-4367(7)	5899(12)	5150(7)	26(5)
O(234)	1538(8)	2686(14)	11041(8)	42(7)
O(236)	3149(8)	9517(14)	10787(8)	38(6)
O(326)	2327(11)	4267(19)	5316(11)	73(10)
N(109)	-3353(14)	2870(20)	6897(13)	71(13)
O(55)	-1362(7)	6430(12)	5572(7)	26(5)
O(325)	253(16)	1520(30)	3230(16)	125(18)
O(322)	4275(14)	9400(20)	9053(13)	107(14)
N(112)	-3499(10)	2067(16)	3720(9)	36(8)
C(116)	-1912(11)	2455(19)	6460(11)	25(8)
N(208)	2906(10)	6422(18)	8033(10)	42(8)
O(335)	4912(14)	610(20)	6478(14)	102(14)
C(204)	2131(14)	4000(20)	8375(13)	48(11)
N(110)	-1242(11)	2631(18)	6769(11)	46(9)
O(336)	3566(11)	4961(19)	6642(11)	76(10)
N(111)	-3408(9)	956(16)	5726(9)	33(7)
O(237)	907(8)	5260(14)	10004(8)	42(7)
O(238)	3310(8)	4460(14)	8747(8)	44(7)
C(117)	-1680(12)	2400(20)	6876(12)	38(9)
C(206)	3119(11)	3872(19)	7852(10)	28(8)
C(205)	2690(12)	3990(20)	8013(12)	38(10)
O(333)	4314(13)	7030(20)	6994(13)	95(13)
C(119)	-3300(20)	8120(40)	5760(20)	110(20)
O(239)	1618(8)	7732(13)	9575(7)	35(6)
O(129)	-954(9)	5090(15)	5173(8)	49(7)
C(213)	1700(18)	7620(30)	8389(18)	81(16)
C(162)	-4195(10)	3745(18)	6019(10)	24(8)
C(301)	-4589(13)	4550(20)	6219(13)	44(11)
N(136)	-4315(10)	4109(17)	6327(10)	39(8)
C(161)	-4680(9)	4421(16)	5807(9)	15(7)
O(338)	-943(11)	1800(20)	5935(11)	75(10)
N(113)	-1219(13)	6810(20)	6531(12)	69(11)
N(213)	3055(11)	11018(18)	8203(10)	45(9)
N(214)	2543(10)	10973(16)	9136(9)	36(8)
C(219)	4110(7)	8527(13)	10195(7)	0(5)
N(215)	3372(9)	10020(16)	8101(9)	36(8)

C(216)	4119(11)	7814(19)	11165(11)	30(8)
C(120)	-2811(11)	5319(19)	2814(11)	30(8)
C(215)	746(11)	6390(20)	8989(11)	34(9)
N(114)	-2471(10)	5584(18)	2961(10)	44(9)
C(227)	2340(20)	6910(30)	7746(19)	99(18)
C(214)	2266(10)	9887(18)	8950(10)	25(8)
N(115)	-2484(12)	4340(20)	7135(12)	58(10)
C(223)	3029(13)	9910(20)	8251(12)	41(10)
C(221)	2341(19)	10740(30)	8395(18)	72(17)
N(209)	3875(17)	8890(30)	10121(16)	104(16)
N(212)	611(11)	6250(20)	9317(11)	53(10)
C(218)	4363(12)	8310(20)	10601(12)	44(10)
C(217)	4011(12)	8040(20)	10852(12)	39(10)
C(222)	2845(14)	10500(20)	8273(13)	50(11)
C(220)	2280(13)	10530(20)	8843(13)	48(11)
N(211)	3565(12)	8060(20)	10831(12)	62(11)
O(334)	1574(11)	5583(19)	8432(11)	73(10)
C(122)	-1426(11)	8214(19)	5595(11)	27(8)
O(339)	1554(16)	9990(30)	2402(16)	133(18)
C(123)	-2471(19)	3810(30)	7252(18)	80(17)
C(225)	2684(11)	6895(19)	7865(11)	31(8)
O(337)	4103(13)	5390(20)	5056(13)	95(13)
C(224)	3499(16)	10830(30)	8099(16)	68(14)
O(240)	1133(7)	6028(11)	10642(7)	24(5)
N(117)	-2450(9)	3724(16)	3155(9)	34(7)
N(218)	2767(11)	6454(19)	11896(10)	46(9)
N(223)	1040(9)	3938(16)	8631(9)	34(7)
C(234)	1173(13)	3330(20)	8544(12)	44(10)
N(120)	-4957(10)	2988(18)	3322(10)	42(8)
C(236)	1357(11)	2272(19)	8950(10)	28(8)
C(228)	2504(13)	6390(20)	11642(13)	46(11)
C(239)	5285(13)	6930(20)	8456(13)	51(11)
N(121)	-1519(9)	9365(16)	5949(9)	35(7)
N(227)	4958(15)	8210(30)	8587(15)	85(14)
C(125)	-2385(14)	3020(20)	3124(13)	49(11)
C(231)	2241(16)	8190(30)	11702(16)	71(15)

C(126)	-2788(13)	3900(20)	3402(13)	48(11)
N(224)	4928(19)	6200(30)	7875(18)	120(19)
N(226)	5213(13)	7960(20)	7970(12)	64(11)
O(241)	2257(8)	4569(14)	10568(8)	43(7)
C(235)	1226(12)	3030(20)	8891(12)	38(10)
C(241)	5054(16)	8700(30)	7948(16)	70(15)
N(221)	1122(9)	3495(16)	9167(9)	33(7)
C(230)	2374(14)	7400(20)	11734(13)	50(11)
C(240)	5138(15)	7720(30)	8393(15)	59(13)
O(242)	1972(6)	3255(11)	10338(6)	22(5)
O(328)	3693(19)	8040(30)	7030(18)	170(20)
N(119)	-139(11)	4941(19)	5328(10)	47(9)
C(232)	991(13)	3990(20)	9032(13)	48(11)
N(219)	4854(11)	5214(19)	9589(11)	51(9)
N(116)	-4859(10)	4310(17)	4815(10)	38(8)
C(124)	-2016(11)	7784(19)	4062(11)	33(9)
C(128)	-1346(11)	9095(18)	5582(10)	27(8)
N(217)	2213(13)	6910(20)	11579(13)	71(12)
C(238)	4989(15)	6490(30)	8407(15)	57(13)
C(237)	3170(9)	7864(16)	8201(9)	17(7)
N(220)	4554(11)	5910(19)	10373(11)	51(9)
O(131)	-4861(8)	2787(13)	5189(7)	35(6)
N(118)	-2960(11)	3330(19)	3456(10)	51(9)
C(127)	-5046(12)	2900(20)	3766(12)	38(9)
N(124)	-1384(11)	2595(19)	3670(11)	48(9)
N(123)	-2412(9)	-847(16)	5952(9)	33(7)
C(135)	-2672(11)	-506(19)	6186(11)	31(9)
N(303)	-1461(12)	100(20)	6890(12)	62(11)
N(304)	-1766(12)	-970(20)	6885(11)	57(10)
O(243)	1995(10)	3133(17)	9477(9)	60(9)
C(132)	-1116(13)	5990(20)	4033(12)	40(10)
C(245)	2079(11)	8430(20)	11305(11)	35(9)
O(132)	-813(9)	6186(16)	4876(9)	54(8)
N(228)	1477(15)	7250(30)	8248(14)	80(13)
O(244)	1244(8)	2299(14)	10488(8)	44(7)
C(136)	-3472(19)	7800(30)	5962(18)	76(17)

O(245)	3598(8)	7682(14)	9955(8)	42(7)
C(304)	-1410(13)	-590(20)	6908(13)	46(11)
N(229)	1983(11)	4182(19)	8035(11)	48(9)
O(329)	3792(12)	4620(20)	3906(12)	78(11)
C(244)	4016(11)	7717(18)	9999(10)	26(8)
C(131)	-3078(13)	1780(20)	3672(13)	46(10)
C(130)	-1712(13)	2440(20)	3944(13)	45(11)
C(133)	-1340(30)	6720(50)	3670(30)	150(30)
C(140)	-1231(12)	6340(20)	6779(11)	35(9)
C(139)	-1381(10)	5634(19)	6589(10)	23(8)
C(242)	299(11)	5618(19)	9275(11)	31(8)
O(130)	-3784(8)	5984(13)	4470(7)	35(6)
C(137)	-4003(19)	1520(30)	6150(18)	87(18)
N(222)	202(10)	7102(17)	11670(10)	39(8)
O(342)	3473(12)	5380(20)	664(12)	84(11)
C(247)	-116(12)	7910(20)	11111(12)	37(9)
N(129)	-5028(12)	1230(20)	3361(12)	61(11)
C(246)	116(13)	7100(20)	11179(13)	47(11)
O(343)	3465(9)	5786(16)	1292(9)	54(8)
C(142)	-2706(11)	2748(18)	3304(10)	26(8)
C(144)	-4971(12)	1640(20)	3739(12)	39(10)
O(246)	2845(9)	7354(15)	10202(8)	47(7)
O(142)	-3453(8)	5048(15)	3879(8)	45(7)
O(109)	-2602(7)	7110(12)	3942(7)	26(5)
O(340)	4073(12)	8350(20)	9170(12)	88(12)
C(141)	-3669(12)	4890(20)	3625(12)	37(9)
C(146)	-4752(14)	730(20)	3343(13)	48(11)
N(128)	-2230(15)	6440(30)	6621(14)	84(14)
O(344)	5680(13)	5270(20)	9042(12)	91(12)
O(56)	-1849(7)	5748(12)	4958(7)	28(6)
C(149)	509(15)	2980(30)	6458(15)	61(13)
C(150)	444(17)	2440(30)	6548(17)	72(15)
C(250)	155(11)	8520(20)	11285(11)	33(9)
C(263)	2344(12)	8160(20)	10953(11)	33(9)
O(146)	-1996(11)	7731(18)	6629(10)	70(10)
C(249)	1735(13)	2160(20)	9280(13)	50(11)

N(225)	3797(13)	3540(20)	10866(13)	70(12)
N(125)	-1268(15)	5910(20)	3613(14)	77(13)
O(346)	5143(11)	-330(20)	6071(11)	75(10)
N(131)	170(15)	3690(30)	6978(15)	87(14)
N(232)	1638(10)	8099(16)	11281(9)	37(8)
C(148)	240(16)	3620(30)	6579(15)	64(13)
C(152)	3770(19)	3510(30)	11533(19)	88(18)
O(148)	-974(11)	4023(18)	7206(10)	71(10)
N(133)	400(40)	1990(70)	7190(40)	280(60)
N(132)	131(12)	1900(20)	6349(11)	57(10)
C(252)	1306(17)	8020(30)	8613(15)	59(13)
N(130)	-1272(9)	1122(15)	4956(9)	32(7)
O(348)	3647(12)	9298(19)	9144(11)	76(10)
C(156)	-2103(15)	6220(30)	7009(14)	55(12)
C(158)	12(17)	1440(30)	6615(17)	72(15)
C(153)	-2858(16)	2000(30)	3353(16)	66(14)
C(254)	3965(13)	4170(20)	10933(12)	40(10)
C(155)	-691(12)	5570(20)	5017(12)	38(10)
C(253)	1600(30)	5220(50)	11420(30)	110(30)
O(349)	4314(17)	7680(30)	7600(16)	132(18)
C(255)	4326(11)	4410(20)	9893(11)	27(8)
O(149)	-746(12)	7410(20)	4729(12)	86(12)
Cl(30)	210(4)	1045(7)	3702(4)	67(4)
Cl(29)	3176(7)	2657(11)	2539(7)	129(8)
N(230)	1459(11)	1548(18)	11470(10)	46(9)
O(352)	-66(16)	1310(30)	3853(15)	118(15)
N(135)	-4629(13)	1330(20)	3861(13)	69(12)
C(159)	-3745(14)	2420(20)	6742(13)	50(11)
C(257)	1279(17)	1490(30)	11004(16)	71(15)
C(256)	1341(11)	2229(19)	10849(11)	30(9)
O(353)	3465(19)	3220(40)	2611(18)	150(20)
O(250)	468(10)	7109(17)	10626(10)	62(9)
O(354)	3070(30)	2490(60)	2080(30)	320(50)
C(160)	-2371(17)	6120(30)	7237(16)	73(15)
O(500)	-2777(8)	4905(14)	5221(8)	39(6)
C(262)	4943(11)	4900(20)	10274(11)	35(9)

N(234)	2890(20)	4460(40)	12010(20)	140(30)
C(265)	2772(14)	4050(20)	11661(14)	52(12)
C(275)	2740(20)	5730(40)	8130(20)	110(20)
O(59)	-2035(7)	1879(12)	5519(7)	27(5)
O(155)	-244(10)	3631(16)	5987(9)	58(8)
O(356)	2651(10)	3159(19)	5084(10)	69(9)
O(357)	1743(13)	6330(20)	8999(12)	91(12)
C(260)	2260(30)	4490(50)	7930(30)	140(30)
N(137)	-4430(11)	3956(19)	5720(11)	50(9)
O(358)	2066(16)	2420(30)	7332(15)	121(16)
C(163)	-2160(15)	4470(30)	6920(14)	54(12)
N(236)	2328(12)	4180(20)	11652(12)	58(11)
C(1=2)	4827(13)	4700(20)	9894(13)	44(11)
O(58)	-1485(8)	4071(13)	5189(7)	34(6)
O(359)	2875(13)	5120(20)	1081(12)	93(12)
O(403)	4177(9)	9043(16)	2782(9)	58(8)
O(402)	4812(9)	6547(15)	5137(8)	49(7)
N(139)	-3690(9)	8515(16)	3550(9)	34(7)
O(401)	2919(10)	2346(17)	7283(10)	62(9)
N(138)	-756(15)	4050(30)	3970(14)	84(14)
C(170)	-3783(11)	8560(20)	3923(11)	33(9)
C(172)	-2529(19)	-630(30)	6608(17)	77(16)
C(164)	-822(13)	3740(20)	4350(12)	43(10)
C(115)	-3788(7)	1579(13)	5749(7)	0(5)
C(166)	-490(20)	4570(40)	4090(20)	110(20)
N(134)	-548(11)	4260(19)	4615(11)	49(9)
C(167)	-821(16)	1740(30)	4484(15)	62(14)
C(169)	-3768(12)	7773(19)	4168(11)	32(9)
C(267)	382(15)	5570(30)	8814(15)	63(13)
C(174)	1860(30)	6300(50)	3440(30)	140(30)
C(269)	1145(11)	8565(18)	9293(10)	27(8)
O(364)	3870(20)	6970(40)	2260(20)	200(30)
C(268)	119(15)	8840(30)	11658(15)	60(13)
O(366)	3875(12)	6250(20)	5532(11)	81(11)
N(243)	3760(20)	4260(40)	11370(20)	160(30)
O(361)	3110(30)	9140(40)	3770(20)	200(30)

C(270)	2910(20)	7820(40)	7890(20)	110(20)
O(360)	4433(15)	340(30)	5958(14)	121(15)
C(271)	3414(15)	7620(20)	11172(14)	55(12)
N(240)	1502(11)	9155(19)	9410(11)	49(9)
O(365)	3801(13)	5190(20)	5689(13)	107(13)
N(242)	3362(12)	2200(20)	10526(12)	55(11)
N(241)	1486(10)	2181(17)	9658(10)	40(8)
O(369)	3942(13)	3350(20)	7370(12)	94(12)
N(301)	4916(17)	2870(30)	6764(16)	102(17)
C(178)	-3670(30)	6540(60)	6560(30)	160(40)
C(177)	-1780(20)	2670(40)	7200(20)	100(20)
O(368)	1720(20)	1610(40)	7550(20)	180(30)
C(302)	4752(16)	3410(30)	6691(15)	64(13)
C(274)	3431(13)	4560(20)	8392(13)	42(10)
N(238)	450(18)	9290(30)	11636(17)	103(17)
C(278)	2895(19)	7050(30)	11889(19)	89(18)
C(276)	2560(20)	4880(40)	12190(20)	120(30)
N(300)	4610(15)	2680(30)	6223(15)	83(15)
C(303)	4902(19)	2210(30)	6467(18)	89(18)
C(300)	4580(30)	3480(50)	6240(30)	150(30)
C(179)	-3760(13)	2180(20)	5538(12)	38(10)
C(176)	-2240(30)	-530(50)	6690(30)	140(30)
Cl(1B)	4627(3)	4143(6)	8672(4)	54(3)
O(31H)	4540(13)	3730(20)	8219(12)	94(13)
O(34F)	5016(18)	4190(30)	8719(16)	126(18)
Cl(12)	1022(4)	4448(7)	5722(4)	64(3)
O(404)	2869(9)	3068(16)	6609(9)	56(8)
O(405)	465(13)	6120(20)	7670(13)	99(13)
O(407)	3469(11)	858(19)	9057(11)	73(10)
O(406)	3478(11)	9164(18)	1629(10)	71(10)
C(180)	-5288(15)	2290(30)	3896(14)	59(13)
O(363)	3600(20)	7170(40)	7400(20)	200(30)
O(370)	560(40)	3780(70)	5390(40)	480(70)
O(367)	-190(20)	4350(40)	910(20)	200(30)
C(181)	3090(70)	10490(130)	3330(70)	260(140)
O(371)	1385(17)	4630(30)	5455(17)	138(19)

O(362)	1924(16)	2360(30)	7963(16)	124(16)
C(279)	4886(15)	8700(30)	8294(15)	54(12)
C(280)	2927(14)	7790(20)	8545(13)	46(11)
O(408)	999(9)	8148(15)	7281(8)	53(8)
O(409)	1280(11)	2600(20)	1999(11)	78(11)
O(410)	3971(12)	380(20)	2875(12)	89(12)
O(411)	1790(16)	9580(30)	7196(15)	129(17)
O(412)	4363(11)	2741(19)	2713(11)	76(10)
N(245)	2360(20)	6140(40)	7870(20)	150(20)
C(185)	-2666(16)	310(30)	6120(16)	68(14)
O(373)	4240(20)	6300(40)	1770(20)	220(30)
O(375)	3980(30)	5200(60)	3300(30)	300(50)
C(183)	-2850(30)	6530(50)	3410(30)	120(30)
C(184)	-1670(20)	7560(40)	3650(20)	110(20)
O(376)	1440(20)	9120(30)	1859(19)	160(20)
C(182)	-1900(20)	310(40)	6750(20)	120(30)
O(260)	664(10)	4268(17)	9849(9)	60(9)
O(372)	296(17)	4570(30)	1534(17)	134(19)
O(374)	1470(20)	9760(30)	815(19)	180(20)
O(251)	2128(11)	7607(18)	10801(10)	66(9)
O(413)	252(11)	4781(19)	2678(11)	77(10)
O(414)	3720(12)	5400(20)	7447(11)	82(11)
C(284)	1698(17)	4490(30)	12065(17)	76(16)
N(265)	1361(14)	4020(20)	11481(13)	69(13)
C(282)	1117(16)	7660(30)	8425(16)	64(14)
C(186)	-3168(18)	5590(30)	3031(17)	82(16)
O(263)	1666(10)	4322(17)	9848(10)	58(9)
O(377)	2907(15)	2670(30)	2892(15)	110(15)
O(379)	2657(13)	820(20)	362(12)	93(12)
O(378)	2653(15)	9950(30)	3789(15)	123(16)
C(187)	-2927(13)	7470(20)	5787(13)	45(11)
C(283)	1310(20)	4520(30)	11698(19)	88(18)
O(355)	2980(20)	4440(40)	4858(19)	190(20)
N(266)	3685(17)	7460(30)	11340(16)	97(16)

APPENDIX G

CRYSTALLOGRAPHIC DATA FOR

$[Tb_{15}(\mu_5\text{-}Cl)(\mu_3\text{-}OH)_{20}(his^{+/-})_{10}(his^{-})_5(OH)_7](ClO_4)_{12}$

Identification code	mes98	
Empirical formula	C90 H120 Cl6 N45 O90 Tb15	
Formula weight	5868.81	
Temperature	190(2) K	
Wavelength	0.71073 Å	
Crystal system	Monoclinic	
Space group	C2	
Unit cell dimensions	a = 30.908(4) Å	α= 90°.
	b = 20.174(3) Å	β= 93.220(5)°.
	c = 32.213(4) Å	γ = 90°.
Volume	20054(5) $Å^3$	
Z	4	
Density (calculated)	1.944 Mg/m^3	
Absorption coefficient	5.385 mm^{-1}	
F(000)	11088	
Crystal size	0.13 x 0.12 x 0.03 mm^3	
Theta range for data collection	2.92 to 25.33°.	
Index ranges	-28<=h<=37, -24<=k<=24, -38<=l<=38	
Reflections collected	38553	
Independent reflections	27514 [R(int) = 0.1448]	
Completeness to theta = 25.33°	89.4 %	
Max. and min. transmission	0.8551 and 0.5301	
Refinement method	Full-matrix least-squares on F^2	
Data / restraints / parameters	27514 / 1 / 144	
Goodness-of-fit on F^2	3.374	
Final R indices [I>2sigma(I)]	R1 = 0.3345, wR2 = 0.6524	
R indices (all data)	R1 = 0.4408, wR2 = 0.6773	
Absolute structure parameter	0.34(14)	
Largest diff. peak and hole	33.034 and -4.836 e.$Å^{-3}$	

Atomic coordinates (x 10^4) and equivalent isotropic displacement parameters ($Å^2$x 10^3) for mes98. U(eq) is defined as one third of the trace of the orthogonalized U^{ij} tensor.

	x	y	z	U(eq)
Tb(2)	4116(1)	4482(2)	5411(1)	21(1)
Tb(3)	4455(2)	6265(2)	5258(2)	45(2)
Tb(4)	3887(2)	2789(3)	4891(2)	58(2)
Tb(5)	4435(2)	2995(3)	5999(2)	60(2)
Tb(7)	3260(2)	5667(2)	5175(2)	56(2)
Tb(8)	5374(2)	7517(3)	5519(2)	89(2)
Tb(9)	3954(2)	5870(3)	6217(2)	57(2)
Tb(10)	0	4033(19)	0	540(20)
Tb(11)	-903(2)	5239(4)	373(2)	103(2)
Cl(10)	5671(8)	5003(13)	6166(8)	60(7)
Cl(11)	5000	1290(20)	5000	74(12)
O(30)	4604(17)	2740(30)	4505(16)	43(16)
O(2)	3811(17)	3410(30)	5569(15)	28(15)
O(81)	3640(20)	1560(30)	5230(20)	60(19)
N(1)	3630(30)	3080(40)	4070(30)	90(30)
O(31)	4990(30)	2400(40)	6000(20)	100(30)
O(80)	4006(16)	1820(30)	5905(16)	28(14)
O(23)	3219(14)	3460(20)	4854(13)	13(12)
O(25)	3302(14)	6740(20)	4740(13)	14(12)
N(2)	7070(30)	5120(40)	5730(20)	60(20)
O(104)	2704(19)	5960(30)	5728(18)	55(18)
O(105)	3120(20)	5940(40)	6350(20)	80(20)
C(2)	6600(30)	5480(50)	5870(30)	50(30)
N(3)	3980(20)	7210(30)	3790(20)	40(20)
C(1)	3900(30)	1520(40)	5580(30)	40(30)
O(5)	4658(13)	7346(19)	5143(12)	0(10)
O(22)	4116(13)	6724(19)	4753(12)	0(10)
O(21)	4844(13)	6946(19)	5810(12)	0(10)

APPENDIX H

CRYSTALLOGRAPHIC DATA FOR

$[Tb_{15}(\mu_5\text{-}Br)(\mu_3\text{-}OH)_{20}(his^{+/-})_{10}(his^{-})_5(OH)_7](ClO_4)_{12}$

Identification code	mes1027	
Empirical formula	C60 H120 Br Cl5 N45 O90 Tb15	
Formula weight	5552.97	
Temperature	190(2) K	
Wavelength	0.71073 Å	
Crystal system	Triclinic	
Space group	P1	
Unit cell dimensions	a = 17.3380(18) Å	α= 66.436(5)°.
	b = 18.4078(19) Å	β= 78.976(5)°.
	c = 18.5112(19) Å	γ = 88.649(5)°.
Volume	5306.2(9) $Å^3$	
Z	1	
Density (calculated)	1.738 Mg/m^3	
Absorption coefficient	5.257 mm^{-1}	
F(000)	2610	
Crystal size	0.19 x 0.15 x 0.12 mm^3	
Theta range for data collection	3.47 to 25.34°.	
Index ranges	-20<=h<=20, -22<=k<=21, -22<=l<=22	
Reflections collected	28166	
Independent reflections	28166 [R(int) = 0.0000]	
Completeness to theta = 25.34°	94.6 %	
Max. and min. transmission	0.5831 and 0.4349	
Refinement method	Full-matrix least-squares on F^2	
Data / restraints / parameters	28166 / 3 / 940	
Goodness-of-fit on F^2	1.247	
Final R indices [I>2sigma(I)]	R1 = 0.1345, wR2 = 0.3323	
R indices (all data)	R1 = 0.2243, wR2 = 0.3866	
Absolute structure parameter	0.23(4)	
Largest diff. peak and hole	4.075 and -2.232 e.$Å^{-3}$	

Atomic coordinates (x 10^4) and equivalent isotropic displacement parameters ($Å^2$x 10^3) for mes1027. U(eq) is defined as one third of the trace of the orthogonalized U^{ij} tensor.

	x	y	z	U(eq)
Tb(1)	9249(2)	-7227(1)	10624(1)	55(1)
O(1)	8705(14)	-8518(14)	10993(14)	24(6)
Tb(2)	10075(2)	-5201(1)	10275(2)	55(1)
O(2)	8274(14)	-8376(15)	9602(15)	28(6)
Tb(3)	8465(2)	-7076(2)	8792(1)	56(1)
O(3)	9279(19)	-4110(20)	9520(20)	61(9)
Tb(4)	8811(2)	-4919(2)	7284(2)	60(1)
O(4)	9734(15)	-2726(16)	6899(16)	36(7)
Tb(5)	9030(2)	-6718(2)	12388(1)	58(1)
O(5)	8897(16)	-3605(16)	6358(16)	37(7)
Tb(6)	9795(2)	-3752(2)	8206(2)	60(1)
O(6)	9813(17)	-7426(19)	11704(18)	51(8)
Tb(7)	9455(2)	-8937(2)	10050(2)	61(1)
O(7)	9319(16)	-6196(16)	7530(16)	37(7)
Tb(8)	9648(2)	-3165(2)	10049(2)	61(1)
O(8)	8946(15)	-6093(16)	10985(16)	35(6)
Tb(9)	11121(2)	-6908(2)	11283(2)	61(1)
O(9)	10290(20)	-6020(20)	11600(20)	71(10)
Tb(10)	8935(2)	-6720(2)	6655(2)	65(1)
O(10)	8540(20)	-4090(20)	7960(20)	63(9)
Tb(11)	7367(2)	-8360(2)	10752(2)	65(1)
O(11)	8083(14)	-7133(15)	10131(15)	29(6)
Tb(12)	11596(2)	-3528(2)	8822(2)	65(1)
O(12)	8260(20)	-5580(30)	6590(30)	89(12)
Tb(13)	6988(2)	-5974(2)	7492(2)	63(1)
O(13)	10716(18)	-4580(20)	8900(20)	58(9)
Cl(3)	10493(6)	-1148(6)	6981(6)	31(2)
Tb(14)	8323(2)	-2806(2)	7072(2)	81(1)
O(14)	9535(15)	-7488(16)	9426(16)	36(7)
Tb(15)	10258(2)	-3312(2)	5924(2)	79(1)
O(15)	7801(19)	-5860(20)	8300(20)	57(8)

Br(16)	9285(3)	-5640(3)	9041(3)	59(1)
O(16)	10071(15)	-4324(16)	7270(16)	36(6)
O(17)	10413(17)	-6469(18)	10255(17)	45(7)
O(18)	7860(16)	-7015(17)	7748(17)	44(7)
O(19)	10695(19)	-4030(20)	10100(20)	61(9)
O(20)	10350(30)	-2870(30)	8730(30)	91(13)
C(161)	13090(30)	-6430(30)	10100(30)	63(14)
C(163)	13540(40)	-6430(40)	9530(40)	90(20)
C(162)	13230(40)	-5930(40)	10620(40)	90(20)
O(100)	6997(19)	-7476(19)	9420(19)	54(8)
O(101)	8220(20)	-7490(20)	11900(20)	65(10)
N(101)	7570(20)	-6540(20)	12730(20)	45(9)
O(102)	10260(20)	-8240(20)	10660(20)	65(10)
N(103)	12710(30)	-3790(30)	7940(40)	92(16)
O(104)	11150(20)	-8225(19)	11331(19)	63(10)
N(105)	12450(20)	-6900(30)	10350(30)	62(11)
O(105)	9450(20)	-8960(20)	8720(20)	65(10)
O(106)	8910(20)	-2270(20)	9150(20)	77(11)
O(107)	6210(20)	-7080(20)	8570(20)	70(10)
O(108)	8960(20)	-5350(20)	12380(20)	78(11)
O(109)	9370(20)	-4570(20)	11120(20)	76(11)
O(110)	9740(20)	-5580(20)	5560(20)	72(10)
O(111)	11488(19)	-5475(19)	10308(19)	50(8)
C(111)	13030(30)	-3550(40)	7200(40)	80(20)
O(112)	11250(40)	-3430(40)	7510(40)	150(20)
N(112)	10080(30)	-3390(30)	4640(30)	80(14)
C(112)	13520(30)	-4020(40)	7000(40)	72(16)
N(113)	8760(20)	-8180(30)	6880(30)	60(11)
O(113)	8790(20)	-2790(30)	8270(20)	82(12)
C(113)	6950(30)	-6990(30)	13040(30)	56(13)
O(114)	9770(20)	-4670(20)	6100(20)	64(9)
C(114)	6280(30)	-6610(30)	12950(30)	58(13)
O(115)	7274(19)	-8460(20)	12110(20)	63(9)
N(115)	12090(20)	-6210(30)	11640(20)	59(11)
O(116)	9129(19)	-7750(20)	8000(20)	55(8)
N(116)	10040(20)	-9690(30)	11180(30)	60(11)

C(117)	7890(50)	-10250(50)	11300(50)	90(20)
O(117)	7200(30)	-3180(30)	6680(30)	101(14)
O(118)	12360(20)	-4450(30)	9760(20)	73(10)
C(119)	8510(70)	-1840(80)	8120(80)	160(50)
C(120)	7420(30)	-5850(30)	12420(30)	52(12)
N(121)	8320(30)	-8040(30)	13400(30)	93(16)
N(123)	9760(20)	-3390(30)	11470(30)	64(12)
C(123)	9270(30)	-3980(30)	12030(30)	48(12)
C(124)	9270(30)	-4720(40)	11830(40)	67(15)
N(124)	12140(20)	-2270(30)	7550(30)	60(11)
C(126)	11450(30)	-9650(30)	10720(30)	69(15)
C(128)	9270(30)	-8690(30)	7360(30)	59(13)
C(129)	9860(30)	-4950(30)	5530(30)	45(11)
C(130)	6880(30)	-7970(30)	13530(30)	51(12)
O(130)	11380(30)	-2720(30)	6150(30)	103(14)
C(131)	11520(30)	-2320(30)	9780(30)	57(13)
N(131)	6450(20)	-4930(30)	6360(30)	65(11)
N(132)	6250(30)	-8870(40)	10270(40)	100(17)
C(133)	8360(30)	-3770(40)	12300(40)	79(17)
N(133)	6450(30)	-5850(30)	12590(30)	79(14)
C(134)	7690(30)	-8280(30)	13230(30)	61(13)
C(135)	7760(30)	-8010(30)	12320(30)	54(13)
C(136)	7130(30)	-6810(30)	6220(30)	39(10)
N(136)	5860(40)	-5380(40)	8010(40)	120(20)
C(137)	11990(20)	-1910(30)	10140(20)	37(10)
C(164)	11930(40)	-990(40)	9830(40)	81(18)
N(138)	12890(30)	-2050(40)	9890(30)	98(17)
N(139)	13400(30)	-4740(40)	7650(40)	100(17)
C(139)	13090(40)	-2650(40)	6740(40)	85(18)
C(141)	10220(40)	-4220(40)	4720(40)	90(20)
C(142)	7720(30)	-11100(30)	12010(30)	58(13)
N(143)	6930(20)	-11170(30)	12580(30)	67(12)
C(143)	6860(40)	-7180(50)	5810(40)	100(20)
N(144)	8460(30)	-1500(30)	7150(30)	89(15)
C(144)	12200(30)	-2240(30)	6790(30)	68(15)
C(150)	12920(40)	-4650(40)	8280(40)	80(17)

C(153)	6430(30)	-7610(30)	9150(30)	46(11)
C(154)	5930(40)	-8290(40)	9650(40)	92(19)
C(156)	8210(30)	-1550(40)	8010(30)	59(14)
C(157)	7440(30)	-1590(30)	8340(30)	51(12)
C(158)	9360(30)	-8380(30)	8090(30)	59(13)
C(159)	11160(30)	-4440(40)	4440(40)	77(16)
C(160)	5260(40)	-8050(40)	10250(40)	84(18)
O(202)	11040(20)	-7600(20)	12670(20)	80(11)
O(255)	6730(20)	-6670(20)	6680(20)	78(11)
O(256)	8440(30)	-10080(30)	10900(30)	105(15)
O(257)	7490(20)	-9780(30)	11470(30)	85(12)
O(258)	7760(30)	-6890(30)	6150(30)	96(13)
O(260)	8780(20)	-6620(30)	13710(20)	83(11)
O(261)	9440(30)	-1850(30)	10140(30)	99(14)
O(262)	9250(20)	-6760(20)	5310(20)	73(10)
O(263)	11970(20)	-2710(20)	9420(20)	67(10)
O(303)	10780(20)	-2420(20)	9970(20)	66(9)
Cl(1)	7121(8)	-5136(8)	10076(8)	60(3)
Cl(2)	11448(8)	-6161(9)	8019(8)	65(4)
Cl(4)	11261(13)	5410(13)	1904(13)	107(6)
Cl(6)	4429(10)	4259(12)	-3506(14)	105(6)
Cl(9)	8119(14)	796(14)	5618(14)	115(6)
O(300)	6396(19)	-5030(30)	10350(20)	79(12)
O(304)	10970(40)	-6170(40)	7580(40)	140(20)
O(302)	8040(40)	350(50)	6680(50)	180(30)
O(305)	11630(20)	5680(30)	1970(20)	77(11)
O(306)	14348(18)	7920(19)	-1870(19)	54(8)
O(311)	11150(30)	-6760(30)	8790(30)	92(13)
Cl(11)	530(19)	7990(20)	2290(20)	184(12)
O(313)	12210(30)	-6320(30)	7710(30)	110(15)
O(309)	160(30)	8270(30)	1460(30)	123(17)
O(281)	7610(40)	-4590(40)	9920(40)	140(20)
N(150)	13190(30)	-7090(30)	9450(30)	79(14)
C(167)	12650(40)	-5620(50)	10950(50)	100(20)
O(310)	8630(40)	330(40)	5220(40)	150(20)
Cl(8)	9113(8)	-9422(6)	12810(6)	32(3)

Cl(10)	8113(6)	-3871(6)	4914(6)	39(2)
C(172)	11540(30)	-2830(40)	6830(40)	66(14)
N(114)	8241(19)	-3330(30)	10810(30)	101(18)
C(121)	7580(30)	-3210(30)	10440(20)	100(20)
N(142)	6891(19)	-3480(30)	11060(30)	95(16)
C(152)	7130(30)	-3750(30)	11810(20)	100(20)
C(168)	7970(30)	-3660(30)	11660(30)	100(20)
N(111)	11440(20)	-4040(20)	5600(30)	90(15)
C(155)	12000(20)	-4230(30)	6110(20)	82(18)
N(149)	12480(20)	-4800(30)	5950(30)	91(15)
C(166)	12220(30)	-4970(30)	5340(30)	180(50)
C(170)	11570(30)	-4490(30)	5130(30)	76(16)
N(100)	10899(17)	-8910(20)	9500(20)	66(12)
C(145)	11180(20)	-8540(30)	8660(20)	100(20)
N(109)	12010(20)	-8440(30)	8520(20)	110(19)
C(101)	12247(17)	-8750(30)	9270(30)	85(18)
C(140)	11560(20)	-9040(30)	9883(18)	89(19)
Cl(5)	7208(9)	-8989(9)	8408(9)	76(4)
O(220)	8690(30)	1000(30)	5410(30)	112(16)
O(286)	8810(50)	-5390(60)	10500(60)	220(40)
O(119)	7380(30)	-4410(30)	7070(30)	115(16)
C(192)	10790(30)	-8550(30)	11080(30)	61(14)
C(188)	6940(50)	-4120(50)	6860(50)	110(20)
C(189)	6290(30)	-4180(30)	6530(30)	66(15)
C(171)	5540(30)	-4250(40)	7060(40)	75(16)
O(270)	9820(20)	-10200(20)	9890(20)	75(11)
O(289)	7110(30)	-5380(30)	9510(30)	119(16)
N(171)	5800(40)	-7270(40)	6230(40)	120(20)
C(146)	10130(30)	-8700(30)	6950(30)	67(15)
N(176)	5260(30)	-4990(30)	9050(30)	87(15)
C(197)	5470(40)	-4620(40)	7770(40)	79(17)
C(127)	10640(40)	-9370(40)	11260(40)	90(20)
C(198)	5160(40)	-4490(40)	8450(40)	81(17)
O(254)	8520(40)	-1950(40)	6010(40)	150(20)
N(102)	6180(20)	-7710(20)	10960(20)	66(12)
C(151)	6150(20)	-7210(30)	11390(30)	76(16)

N(175)	5440(30)	-6820(30)	11340(30)	150(30)
C(191)	5020(20)	-7070(30)	10880(40)	130(30)
C(190)	5480(30)	-7620(30)	10650(30)	100(20)
N(141)	10300(20)	-7170(30)	6420(30)	140(30)
C(148)	10940(30)	-6590(20)	6120(30)	73(16)
N(181)	11640(20)	-7000(30)	6270(30)	130(20)
C(169)	11430(30)	-7830(30)	6650(40)	130(30)
C(147)	10600(30)	-7930(20)	6750(30)	89(19)
O(265)	9980(20)	-7420(30)	13290(20)	83(12)
C(202)	12440(40)	-7270(40)	9830(40)	82(17)
N(135)	7140(20)	-2650(20)	8000(20)	88(15)
C(175)	6570(20)	-3310(20)	8380(30)	66(15)
N(180)	6100(20)	-3230(20)	9060(20)	150(30)
C(174)	6380(20)	-2530(30)	9100(20)	68(15)
C(173)	7020(20)	-2170(20)	8450(30)	85(18)
C(176)	6570(30)	-6080(20)	4630(30)	130(30)
N(178)	7040(20)	-5400(30)	4510(30)	120(20)
C(199)	6610(30)	-4720(20)	4190(30)	110(20)
N(179)	5880(20)	-4970(20)	4100(30)	96(17)
C(200)	5860(20)	-5810(20)	4370(30)	69(15)
C(125)	12050(50)	-5020(50)	10060(50)	110(20)
C(207)	9020(30)	-1850(30)	5230(30)	54(13)
O(293)	7610(40)	-5620(50)	10900(40)	170(30)
O(290)	4480(50)	4630(50)	-4310(60)	190(30)
C(203)	5790(50)	-5650(60)	8740(60)	140(30)
O(230)	9340(40)	-2220(40)	5250(40)	150(20)
O(283)	9466(15)	-9341(12)	12790(12)	6(5)
C(208)	6850(40)	-7020(40)	5000(40)	89(19)
C(193)	7150(30)	-11510(30)	11030(30)	110(20)
N(200)	7190(20)	-11000(30)	10210(30)	106(18)
C(177)	6410(30)	-10990(30)	10060(20)	85(18)
N(170)	5910(20)	-11490(30)	10780(30)	140(20)
C(194)	6360(30)	-11810(30)	11380(20)	110(30)
C(205)	7700(50)	-11520(50)	11350(50)	110(20)
C(213)	11280(50)	-7210(60)	14340(50)	130(30)
N(210)	11460(40)	-8700(40)	13870(40)	114(19)

C(211)	10640(40)	-8360(40)	14180(40)	90(19)
C(212)	10460(70)	-7650(80)	14560(80)	180(40)
C(210)	10640(40)	-7680(40)	13340(40)	82(18)
C(204)	12020(40)	-500(40)	8930(20)	170(40)
C(209)	12750(30)	-110(40)	8450(40)	120(20)
N(208)	12720(30)	90(30)	7640(30)	120(20)
C(206)	11960(30)	-170(40)	7610(30)	110(20)
N(199)	11530(30)	-530(40)	8410(40)	160(30)
C(215)	7630(30)	-6030(20)	7380(20)	26(9)
C(217)	7280(40)	-990(40)	4960(50)	100(20)
N(212)	6830(60)	-1650(70)	5540(70)	210(40)
C(218)	7730(50)	-940(50)	5390(50)	100(30)
N(211)	9240(60)	-600(70)	3350(70)	220(40)
C(214)	8500(50)	-1260(60)	4560(60)	130(30)
C(216)	7650(90)	-1200(90)	4370(90)	250(60)

APPENDIX I

CRYSTALLOGRAPHIC DATA FOR

$[La_{15}(\mu_5\text{-}Br)(\mu_3\text{-}OH)_{20}(his^{+/-})_{10}(his^{-})_5(OH)_{11}](ClO_4)_{12}$

Identification code	mes1050	
Empirical formula	C60 H120 Br Cl15 La15 N45 O90	
Formula weight	5607.32	
Temperature	220(2) K	
Wavelength	0.71073 Å	
Crystal system	Orthorhombic	
Space group	$P2_12_12_1$	
Unit cell dimensions	a = 17.5356(19) Å	α= 90°.
	b = 29.203(3) Å	β= 90°.
	c = 40.376(5) Å	γ = 90°.
Volume	20676(4) $Å^3$	
Z	4	
Density (calculated)	1.801 Mg/m^3	
Absorption coefficient	3.497 mm^{-1}	
F(000)	10640	
Crystal size	0.30 x 0.07 x 0.07 mm^3	
Theta range for data collection	1.01 to 25.38°.	
Index ranges	-19<=h<=20, -32<=k<=34, -47<=l<=48	
Reflections collected	76896	
Independent reflections	31448 [R(int) = 0.1020]	
Completeness to theta = 25.38°	89.4 %	
Max. and min. transmission	0.7919 and 0.4202	
Refinement method	Full-matrix least-squares on F^2	
Data / restraints / parameters	31448 / 0 / 1204	
Goodness-of-fit on F^2	1.027	
Final R indices [I>2sigma(I)]	R1 = 0.1319, wR2 = 0.3281	
R indices (all data)	R1 = 0.2359, wR2 = 0.4005	
Absolute structure parameter	0.16(5)	
Largest diff. peak and hole	2.527 and -2.407 e.$Å^{-3}$	

Atomic coordinates (x 10^4) and equivalent isotropic displacement parameters ($Å^2$x 10^3) for mes1050. U(eq) is defined as one third of the trace of the orthogonalized U^{ij} tensor.

	x	y	z	U(eq)
La(1)	8216(2)	10299(1)	2802(1)	55(1)
Br(1)	7286(3)	10279(2)	3554(1)	62(1)
O(1)	8968(12)	9904(7)	3228(7)	44(6)
N(1)	3780(20)	10927(12)	3353(8)	61(9)
C(1)	3190(30)	10776(17)	3522(11)	74(13)
La(2)	6914(2)	9620(1)	4238(1)	57(1)
N(2)	6640(19)	9078(11)	2194(7)	52(9)
O(2)	9091(15)	9694(9)	2543(9)	73(9)
C(2)	8230(20)	11760(13)	1768(9)	43(9)
La(3)	8175(2)	9243(1)	3450(1)	54(1)
O(3)	8897(12)	8941(10)	2942(6)	51(7)
N(3)	10130(20)	11535(13)	3059(9)	69(10)
C(3)	3890(30)	8988(18)	4071(13)	75(15)
La(4)	6181(2)	10909(1)	4070(1)	64(1)
C(4)	3620(40)	8940(20)	3758(15)	100(18)
O(4)	5820(20)	11027(9)	3466(7)	81(11)
La(5)	6884(2)	8314(1)	3862(1)	58(1)
O(5)	8303(16)	9518(8)	4038(5)	49(7)
C(105)	6950(40)	11780(20)	5030(15)	103(19)
C(102)	4240(30)	10640(20)	2245(13)	88(16)
La(6)	6978(2)	11328(1)	3184(1)	62(1)
O(6)	6859(13)	9163(8)	3714(6)	51(7)
C(6)	8260(20)	12358(14)	3230(9)	49(10)
C(101)	5420(30)	10330(20)	2206(13)	89(16)
La(7)	8107(2)	9069(1)	2438(1)	58(1)
O(7)	8264(13)	8583(7)	3837(6)	42(6)
N(7)	4560(30)	9058(18)	4806(12)	109(16)
La(8)	6876(2)	12234(1)	3875(1)	69(1)
O(8)	5757(16)	10074(8)	4059(7)	56(7)
C(8)	7350(20)	8319(12)	3007(10)	36(8)
N(8)	3990(40)	9550(20)	4158(15)	140(20)

La(9)	6875(2)	11133(1)	2233(1)	65(1)
O(9)	7184(15)	11407(8)	3810(6)	50(7)
La(10)	10069(2)	9460(1)	2978(1)	63(1)
O(10)	6119(15)	11984(8)	3379(6)	44(6)
N(10)	5840(30)	8252(16)	3399(11)	92(13)
La(11)	8682(2)	8848(1)	4403(1)	63(1)
O(11)	5584(14)	10693(10)	4612(7)	62(8)
N(11)	3660(20)	11629(14)	3958(10)	79(11)
N(5)	6550(30)	11449(18)	5247(12)	108(16)
La(12)	4888(2)	9930(1)	4566(1)	67(1)
O(12)	6935(15)	10687(8)	2767(6)	52(7)
C(12)	6270(30)	7680(15)	3002(10)	61(12)
N(12)	10660(30)	11647(16)	3533(11)	94(13)
La(13)	6766(2)	10591(1)	4967(1)	77(1)
O(13)	8220(18)	10899(8)	2355(7)	61(8)
C(13)	6100(30)	8963(17)	2423(12)	77(14)
N(13)	8430(30)	12359(16)	3983(11)	89(13)
La(14)	8926(2)	11547(1)	2639(1)	67(1)
O(14)	7608(17)	9502(8)	2906(8)	64(8)
C(14)	6350(30)	9296(15)	1903(10)	58(11)
La(15)	4837(2)	11655(1)	3522(1)	67(1)
O(15)	8307(16)	11052(9)	3088(6)	58(7)
C(15)	6740(30)	9459(18)	1612(12)	87(15)
C(107)	9920(40)	9710(20)	4526(16)	110(20)
C(16)	10900(30)	11369(15)	3022(11)	60(12)
N(16)	7304(19)	7645(11)	3408(8)	49(8)
O(16)	6253(16)	9864(9)	4775(6)	59(8)
C(108)	9560(30)	9627(19)	5021(12)	74(14)
O(17)	7298(19)	8810(10)	4364(6)	68(9)
C(17)	11140(30)	11389(19)	3341(13)	85(16)
N(102)	10450(30)	10000(15)	4784(10)	87(13)
N(18)	3510(30)	12019(16)	3228(11)	92(14)
C(18)	8990(40)	12640(20)	3873(16)	103(19)
O(19)	5740(20)	11727(12)	4017(8)	86(10)
O(21)	7396(17)	8507(8)	3284(7)	58(8)
O(22)	5620(20)	9196(12)	4331(8)	82(10)

C(22)	9230(50)	9470(30)	5353(19)	150(30)
O(23)	4716(17)	11006(10)	3980(7)	60(8)
C(23)	10070(30)	8913(17)	3793(13)	74(14)
N(23)	10200(20)	11299(13)	2300(9)	69(10)
O(24)	6028(14)	11435(9)	2721(8)	71(9)
C(24)	3330(30)	11886(16)	2899(10)	65(12)
N(15)	9610(20)	9431(13)	4730(9)	67(10)
O(25)	7891(15)	9508(9)	4717(6)	51(7)
C(25)	2940(20)	12305(14)	3354(9)	53(11)
O(26)	9544(18)	10679(10)	2738(7)	65(8)
C(26)	2440(40)	12270(20)	3111(15)	100(20)
O(27)	7728(17)	12044(11)	3363(11)	99(14)
C(27)	3760(30)	9630(20)	3828(14)	91(16)
C(28)	5300(40)	8510(20)	3461(16)	105(19)
O(29)	3999(18)	10552(11)	4322(7)	71(9)
N(29)	2590(30)	12008(15)	2822(10)	83(12)
C(29)	3420(30)	11225(18)	4095(12)	79(15)
C(100)	2870(30)	11005(17)	3834(12)	76(14)
O(30)	4844(19)	11716(9)	2897(7)	70(9)
N(30)	8430(30)	8784(17)	5070(11)	102(14)
O(31)	7129(17)	10387(10)	1898(7)	68(8)
C(31)	10680(30)	10953(17)	2474(11)	69(13)
N(31)	10910(30)	9792(16)	3510(11)	94(14)
N(32)	11070(20)	10356(14)	3844(9)	75(11)
C(32)	11160(40)	11230(20)	2705(16)	110(20)
O(33)	6780(20)	11319(11)	4568(7)	80(10)
C(33)	10750(30)	10297(17)	3561(11)	70(13)
N(33)	7920(20)	8316(13)	2037(9)	71(10)
O(34)	7645(18)	9944(12)	5153(7)	74(9)
O(35)	9874(18)	8879(13)	4065(8)	84(10)
C(35)	11210(30)	9662(16)	3772(11)	63(12)
O(36)	9650(20)	9142(12)	3563(8)	88(11)
C(36)	11480(40)	9150(20)	3787(15)	110(20)
O(37)	5635(17)	8473(10)	4187(7)	63(8)
O(38)	10480(20)	10225(13)	2764(8)	90(11)
O(39)	8650(20)	12247(13)	3012(9)	100(11)

C(40)	8460(20)	7975(14)	2137(9)	52(11)
C(111)	6920(30)	11720(20)	4673(12)	81(14)
O(41)	7663(15)	9892(9)	2272(6)	53(7)
C(41)	5740(30)	8048(18)	3098(13)	80(15)
O(42)	7386(16)	8397(9)	2735(7)	57(7)
O(20)	7519(19)	11634(12)	2652(8)	80(10)
C(104)	4800(40)	10990(20)	2208(14)	101(18)
N(104)	8200(30)	9378(15)	1805(10)	93(13)
N(128)	9540(40)	12150(20)	4213(14)	129(19)
N(100)	5500(20)	10752(15)	2184(10)	79(12)
N(103)	10850(30)	8732(16)	3282(11)	90(13)
O(50)	7620(20)	11610(11)	1838(8)	82(10)
O(51)	9234(18)	8643(10)	2193(7)	71(8)
C(106)	8350(40)	9270(20)	5240(14)	101(19)
O(52)	10464(15)	8879(10)	2539(8)	68(9)
O(18)	7189(17)	10413(10)	4369(7)	66(8)
O(53)	8790(40)	11794(12)	2017(8)	150(20)
O(54)	7520(20)	7706(13)	4238(9)	92(11)
O(114)	5560(30)	10486(17)	5394(11)	134(16)
C(110)	10840(30)	8769(19)	3585(14)	90(16)
O(58)	4650(20)	12481(12)	3686(12)	112(16)
O(81)	11580(19)	9514(12)	2831(12)	116(16)
O(82)	3470(20)	9926(17)	4820(10)	118(15)
O(84)	9870(20)	8458(13)	4625(13)	132(18)
O(86)	6050(20)	7562(10)	3953(9)	87(11)
O(87)	9750(20)	12246(13)	2500(10)	109(14)
Cl(1)	813(7)	5810(4)	989(3)	71(3)
Cl(2)	5350(7)	9766(4)	3096(4)	68(3)
Cl(3)	641(7)	2805(5)	1803(4)	88(4)
O(200)	4730(20)	9602(11)	2945(10)	96(12)
O(203)	200(30)	5990(15)	883(10)	115(14)
O(201)	5330(40)	9759(18)	3408(13)	160(20)
Cl(7)	9457(12)	390(6)	1719(5)	127(6)
O(206)	1450(20)	6029(18)	863(13)	170(20)
N(107)	8080(20)	11698(14)	1223(9)	76(11)
C(114)	9070(70)	11670(40)	5010(30)	190(40)

N(106)	9200(30)	11170(20)	4937(13)	117(17)
O(100)	8474(19)	8040(11)	4540(7)	77(9)
C(112)	7850(40)	11890(20)	5127(17)	120(20)
C(118)	2940(30)	10452(19)	3321(13)	86(16)
N(110)	3530(30)	9365(17)	3639(11)	95(14)
C(119)	5140(30)	8258(19)	2915(12)	81(15)
N(105)	7400(30)	12942(16)	3489(11)	91(13)
C(115)	8690(40)	10860(20)	4947(15)	104(19)
O(207)	850(30)	5826(15)	1330(11)	115(13)
C(117)	8940(50)	12360(30)	1420(20)	150(30)
Cl(5)	2321(11)	1414(7)	1950(6)	141(7)
Cl(8)	8230(20)	3860(14)	233(12)	330(30)
O(204)	5560(30)	10192(17)	2991(11)	125(15)
C(124)	5400(30)	8808(17)	4366(11)	63(12)
C(123)	5390(30)	11666(15)	2682(10)	55(11)
O(205)	5970(50)	9610(30)	3046(19)	230(30)
C(127)	4980(40)	12840(20)	3766(13)	89(16)
N(111)	5980(30)	11866(15)	2115(10)	88(13)
C(120)	7460(30)	10035(16)	1987(11)	61(12)
C(125)	4050(30)	10863(19)	4132(13)	80(15)
C(126)	9990(30)	11650(20)	3349(13)	89(16)
C(122)	5210(40)	11810(20)	2329(14)	97(17)
N(112)	3940(30)	13241(17)	3613(11)	103(15)
Cl(9)	8680(20)	1344(12)	298(8)	220(13)
N(130)	321(19)	7929(11)	-210(7)	47(8)
O(221)	2870(30)	1620(20)	1705(13)	160(20)
C(11)	7200(30)	7754(18)	3110(13)	80(15)
O(222)	8650(120)	1480(70)	740(50)	590(130)
C(131)	9870(50)	9900(30)	5100(20)	150(30)
C(133)	5660(40)	9240(20)	1862(17)	120(20)
C(132)	8110(40)	12830(19)	3314(13)	90(16)
N(113)	5520(40)	9110(20)	2241(15)	140(20)
C(130)	7600(50)	9840(30)	1690(20)	150(30)
N(101)	4510(30)	10190(20)	2243(13)	121(18)
O(220)	1880(50)	1820(30)	2143(18)	230(30)
O(226)	1100(50)	5380(30)	870(20)	250(40)

O(108)	9730(20)	7972(13)	2092(9)	90(11)
C(39)	9280(30)	8152(17)	2141(11)	64(13)
C(160)	4630(40)	8640(20)	4543(15)	110(20)
C(187)	230(60)	7950(30)	120(20)	170(30)
C(162)	7940(30)	9553(17)	5008(12)	71(13)
C(161)	4350(110)	9040(70)	3960(50)	340(100)
C(180)	1180(90)	7670(50)	-430(30)	240(60)
O(55)	4880(30)	10076(16)	5205(11)	131(15)
C(165)	10240(30)	10646(18)	2666(12)	78(14)
O(110)	7230(30)	10624(16)	5607(11)	126(15)
C(166)	9610(40)	12530(30)	3993(18)	120(20)
C(164)	8610(50)	11880(30)	1417(17)	130(20)
N(109)	5010(60)	8600(30)	3180(20)	220(40)
Cl(11)	8440(20)	6921(13)	585(9)	239(14)
O(113)	7130(30)	13006(15)	4262(10)	115(14)
N(108)	3330(30)	10460(20)	3057(14)	125(18)
C(34)	11450(40)	9940(20)	3960(15)	98(18)
Cl(4)	3726(14)	7777(8)	2232(5)	141(7)
Cl(6)	8070(16)	8479(8)	1149(6)	148(9)
C(140)	8520(20)	7530(14)	1882(10)	54(11)
O(230)	8498(15)	8495(7)	1156(5)	26(5)
C(167)	4780(50)	13410(30)	4161(19)	130(30)
C(163)	4840(60)	13270(30)	3840(20)	160(30)
O(229)	3282(16)	7738(8)	2345(6)	39(6)
N(6)	8160(30)	11052(15)	5040(9)	81(11)
N(131)	640(90)	8070(60)	-260(40)	190(80)
O(227)	8300(40)	6930(20)	957(16)	200(20)
O(228)	8280(70)	6140(40)	650(30)	360(50)
O(99)	7060(20)	12019(14)	4485(10)	105(12)
C(168)	8860(40)	12910(20)	3550(15)	107(19)
C(183)	8880(40)	6770(20)	4332(15)	92(17)
C(182)	8710(40)	6960(20)	4594(15)	104(19)
N(129)	7200(30)	7022(19)	4612(13)	112(17)
C(172)	4520(50)	13940(30)	4050(20)	140(30)
N(120)	3930(30)	14174(19)	4198(12)	101(15)
C(185)	9190(80)	6890(50)	3730(30)	230(50)

N(124)	9190(70)	6920(40)	4030(30)	270(50)
C(181)	7960(60)	7270(30)	4680(20)	160(30)
N(125)	8800(50)	6520(30)	3850(20)	190(30)
C(184)	8670(50)	6370(30)	4250(20)	140(30)
C(103)	4490(50)	11470(30)	2140(20)	150(30)
O(118)	6350(30)	11119(17)	1599(11)	134(16)
C(171)	8400(40)	11490(20)	5043(16)	110(20)
O(231)	7730(60)	3900(40)	80(30)	270(40)
N(123)	4380(60)	14850(30)	3980(20)	220(40)
C(176)	4910(50)	14380(30)	3965(18)	130(20)
C(178)	3730(50)	14540(30)	4110(20)	150(30)
C(175)	3920(30)	10747(17)	3059(11)	67(13)
O(131)	5750(30)	12821(17)	3871(12)	139(16)
C(188)	1080(60)	8700(30)	320(20)	200(30)
C(179)	7980(30)	7640(20)	4463(14)	91(16)
C(20)	8840(50)	12120(20)	4236(17)	120(20)
C(186)	1190(60)	8250(30)	130(20)	190(30)

APPENDIX J

CRYSTALLOGRAPHIC DATA FOR

$[Eu_{15}(\mu_5\text{-}OH)(\mu_3\text{-}OH)_{20}(his^{+/-})_{10}(his^{-})_5(OH)_7](ClO_4)_{12}$

Identification code	mes914	
Empirical formula	C90 H120 Cl5 Eu15 N45 O90	
Formula weight	5728.96	
Temperature	190(2) K	
Wavelength	0.71073 Å	
Crystal system	Monoclinic	
Space group	$P2_1$	
Unit cell dimensions	a = 17.2255(18) Å	α= 90°.
	b = 31.567(4) Å	β= 89.816(5)°.
	c = 18.6710(19) Å	γ = 90°.
Volume	10152(2) $Å^3$	
Z	2	
Density (calculated)	1.874 Mg/m^3	
Absorption coefficient	4.714 mm^{-1}	
F(000)	5450	
Crystal size	0.27 x 0.11 x 0.11 mm^3	
Theta range for data collection	1.09 to 27.92°.	
Index ranges	-22<=h<=22, -41<=k<=41, -24<=l<=24	
Reflections collected	84005	
Independent reflections	47244 [R(int) = 0.0345]	
Completeness to theta = 27.92°	99.0 %	
Max. and min. transmission	0.6251 and 0.3626	
Refinement method	Full-matrix least-squares on F^2	
Data / restraints / parameters	47244 / 1 / 2110	
Goodness-of-fit on F^2	1.181	
Final R indices [I>2sigma(I)]	R1 = 0.0568, wR2 = 0.1425	
R indices (all data)	R1 = 0.0702, wR2 = 0.1646	
Absolute structure parameter	0.005(15)	
Extinction coefficient	0.00259(6)	
Largest diff. peak and hole	4.074 and -2.185 e.$Å^{-3}$	

Atomic coordinates (x 10^4) and equivalent isotropic displacement parameters ($Å^2$x 10^3) for mes914. U(eq) is defined as one third of the trace of the orthogonalized U^{ij} tensor.

	x	y	z	U(eq)
Eu(1)	1930(1)	-333(1)	4215(1)	32(1)
O(1)	1188(7)	-582(4)	3236(6)	32(2)
N(1)	3471(11)	-1544(5)	4986(9)	46(4)
Cl(1)	796(2)	279(2)	1897(2)	41(1)
Eu(2)	1855(1)	-1179(1)	2659(1)	26(1)
O(2)	2478(8)	-984(3)	3753(5)	31(2)
N(2)	4691(12)	-1556(8)	4726(12)	64(5)
Eu(3)	3062(1)	-698(1)	1069(1)	25(1)
N(3)	2084(13)	-1354(5)	6051(9)	55(5)
O(3)	1169(6)	-1497(4)	3655(6)	31(2)
Cl(3)	410(3)	7462(2)	2935(3)	56(1)
Eu(4)	3837(1)	430(1)	1679(1)	26(1)
N(4)	4138(9)	-2070(5)	2518(9)	45(4)
Cl(4)	4728(3)	9288(2)	3470(2)	42(1)
O(4)	1062(8)	-885(4)	4635(6)	37(3)
Eu(5)	3087(1)	653(1)	3605(1)	27(1)
O(5)	3106(7)	-1170(3)	2072(6)	30(2)
Cl(5)	2450(4)	6303(2)	1464(4)	63(2)
N(5)	5277(13)	-2043(11)	2991(14)	81(7)
Eu(6)	3214(1)	360(1)	5530(1)	30(1)
O(6)	2672(6)	-1385(3)	674(5)	24(2)
Cl(6)	6743(3)	7009(2)	4801(3)	51(1)
Eu(7)	5133(1)	1031(1)	2911(1)	29(1)
N(7)	5934(10)	-849(5)	1315(9)	39(3)
O(7)	1772(6)	-786(3)	1556(6)	29(2)
Cl(7)	6477(3)	3562(2)	1319(3)	56(1)
Eu(8)	5028(1)	-384(1)	578(1)	28(1)
N(8)	6528(9)	-1036(6)	2288(11)	56(5)
O(8)	1706(6)	-1675(3)	1680(6)	29(2)
Cl(8)	2397(6)	6634(3)	4933(6)	99(3)
Eu(9)	3043(1)	-1911(1)	1574(1)	28(1)

O(9)	4126(6)	-317(3)	1596(5)	23(2)
N(9)	5358(9)	-1033(5)	-159(9)	39(3)
Eu(10)	1985(1)	-1476(1)	4704(1)	35(1)
N(10)	6106(10)	468(6)	3256(8)	45(4)
O(10)	4426(6)	303(4)	546(6)	28(2)
Cl(10)	5569(3)	1417(2)	202(3)	56(1)
Eu(11)	1180(1)	708(1)	4743(1)	29(1)
O(11)	3760(6)	-420(3)	49(5)	24(2)
N(11)	6593(11)	-84(6)	3874(10)	52(4)
Cl(11)	7506(6)	7479(3)	2037(9)	133(5)
Eu(12)	3122(1)	1545(1)	2310(1)	29(1)
O(12)	2869(6)	45(3)	978(5)	24(2)
N(12)	6276(9)	1089(5)	2011(7)	35(3)
C(12)	6520(14)	-1377(9)	1913(17)	67(7)
Cl(12)	176(10)	3068(5)	1873(9)	149(5)
Eu(13)	3309(1)	281(1)	-230(1)	27(1)
O(13)	4197(7)	434(3)	2948(6)	31(2)
C(13)	6206(13)	-718(7)	1935(11)	49(5)
Eu(14)	1280(1)	-1300(1)	616(1)	27(1)
Cl(14)	8666(3)	925(2)	994(4)	55(1)
O(14)	2845(6)	779(3)	2341(5)	22(2)
Eu(15)	123(1)	-1000(1)	3750(1)	35(1)
O(15)	3856(6)	1272(4)	3295(6)	28(2)
N(15)	4027(8)	1020(5)	5862(7)	34(3)
O(16)	2561(6)	840(4)	4750(6)	27(2)
N(16)	-791(9)	-578(6)	2980(9)	42(4)
Cl(16)	7095(11)	-1581(6)	4042(10)	161(6)
O(17)	1793(7)	371(3)	3715(5)	28(2)
N(17)	-1131(11)	-13(6)	2353(9)	47(4)
Cl(18)	7761(5)	1943(3)	2344(5)	86(2)
O(18)	1893(7)	123(3)	5242(6)	29(2)
N(18)	-759(10)	-1544(6)	3149(10)	50(4)
O(19)	4255(7)	1129(4)	1912(6)	29(2)
N(19)	370(8)	-701(5)	131(9)	38(3)
Cl(19)	9502(5)	4424(2)	3340(4)	68(2)
O(20)	3160(7)	23(3)	4320(7)	36(3)

N(20)	-455(11)	-189(6)	271(10)	55(5)
O(21)	475(7)	-1193(4)	2497(6)	38(3)
N(21)	1444(8)	-1227(5)	-751(8)	37(3)
O(22)	113(7)	-1360(4)	1391(6)	33(2)
N(22)	2048(9)	712(5)	-332(9)	42(3)
O(23)	2070(6)	-687(3)	146(6)	29(2)
N(23)	797(11)	825(8)	-119(12)	61(5)
O(24)	2304(7)	-203(4)	-675(7)	38(3)
N(24)	1672(10)	1553(6)	2011(9)	47(4)
O(25)	3262(7)	864(4)	712(6)	30(2)
O(26)	3157(9)	1544(4)	985(7)	44(3)
N(26)	567(11)	1388(11)	1552(12)	86(10)
O(27)	2271(7)	1275(3)	3379(6)	30(2)
O(28)	1303(8)	1396(5)	4145(8)	50(4)
O(29)	572(7)	13(4)	4471(7)	37(3)
O(30)	-393(8)	-445(5)	4511(7)	46(3)
N(30)	851(16)	552(9)	7685(16)	83(7)
O(31)	2502(8)	-2067(4)	3956(7)	40(3)
O(32)	2563(7)	-1830(4)	2841(6)	36(3)
N(32)	540(11)	-3195(7)	621(10)	55(5)
O(33)	4239(7)	-1750(4)	903(8)	38(3)
N(33)	6435(11)	50(7)	-1556(11)	62(5)
O(34)	4300(6)	-1049(4)	874(7)	34(2)
O(35)	5961(8)	86(4)	1111(7)	41(3)
O(36)	5238(7)	459(4)	1885(6)	33(2)
O(37)	5138(7)	1043(5)	4217(6)	38(3)
O(38)	4078(6)	685(4)	4553(6)	36(3)
O(39)	3158(9)	-373(4)	5942(7)	50(3)
O(40)	2533(8)	-768(4)	5129(6)	39(3)
N(40)	-161(9)	885(5)	4190(11)	48(4)
N(50)	2632(11)	2099(5)	3271(10)	46(4)
N(51)	1189(12)	1701(7)	6707(11)	62(5)
N(53)	2477(11)	-2991(5)	-252(10)	47(4)
N(54)	-213(18)	-2697(10)	1157(17)	96(8)
N(56)	2494(11)	-2575(5)	2240(8)	43(4)
N(61)	-246(16)	920(19)	8000(20)	140(20)

O(100)	1328(8)	1065(4)	5821(7)	41(3)
C(100)	343(10)	-486(5)	-486(9)	35(4)
O(101)	4129(7)	2073(4)	2262(8)	41(3)
N(101)	4220(10)	931(5)	-2452(8)	42(4)
C(101)	4637(10)	933(5)	4695(9)	35(3)
C(102)	2808(10)	-705(6)	5754(9)	35(4)
N(102)	4610(10)	1527(6)	-1999(11)	53(4)
O(103)	2441(7)	-2351(4)	657(7)	37(3)
O(104)	1524(7)	-1973(4)	74(7)	40(3)
C(104)	4746(10)	1065(7)	5461(9)	42(4)
O(105)	2449(8)	832(4)	6324(7)	38(3)
N(105)	129(11)	452(5)	5609(9)	49(4)
C(105)	5409(13)	856(8)	5788(10)	50(5)
C(106)	5144(14)	143(6)	-992(11)	52(6)
O(106)	5428(9)	-121(4)	-534(9)	51(4)
C(107)	5758(9)	341(5)	-1485(9)	33(3)
C(108)	5858(9)	393(5)	1545(8)	29(3)
C(109)	6560(9)	690(5)	1716(10)	33(3)
C(110)	7100(10)	479(8)	2195(11)	49(5)
C(111)	5408(16)	475(8)	-2235(11)	57(6)
C(112)	4969(10)	890(6)	-2191(11)	41(4)
C(113)	5182(14)	1258(8)	-1875(13)	55(6)
O(114)	-322(11)	-1475(7)	4609(10)	70(5)
C(115)	2024(10)	-533(5)	-489(8)	30(3)
C(116)	1570(12)	-797(5)	-1038(11)	42(4)
C(118)	4823(12)	-1860(9)	2541(15)	59(6)
C(119)	-5(10)	-1347(5)	2044(8)	28(3)
C(120)	4547(10)	-1396(5)	690(9)	33(3)
C(121)	3896(13)	-1431(7)	5557(13)	51(5)
C(122)	6023(13)	231(7)	3842(11)	48(5)
C(123)	7073(14)	-34(7)	3283(11)	54(6)
C(124)	1061(13)	1792(9)	2447(19)	75(9)
C(125)	1198(13)	2102(7)	3012(14)	55(5)
C(127)	-177(12)	-161(6)	-387(12)	46(4)
C(128)	4671(15)	-1435(7)	5390(13)	59(6)
C(129)	412(14)	1689(11)	2070(15)	71(8)

O(131)	3516(9)	263(4)	6825(7)	45(3)
C(133)	-420(11)	168(8)	5308(15)	65(8)
C(134)	2734(14)	-1075(7)	6282(10)	50(5)
O(135)	3893(8)	-2570(5)	1197(9)	54(4)
C(136)	3968(13)	-1635(7)	4489(12)	50(5)
O(139)	1997(13)	-2186(5)	5252(10)	71(5)
O(140)	3019(9)	339(6)	-1532(7)	58(4)
C(140)	3455(15)	-1329(9)	6325(14)	62(6)
N(100)	3699(10)	1017(5)	-615(7)	41(3)
C(141)	1813(9)	1532(6)	3712(8)	34(4)
O(142)	4480(8)	257(5)	-1005(7)	43(3)
C(142)	-844(10)	-1482(6)	2308(10)	40(4)
C(143)	-219(14)	1115(8)	3562(13)	57(5)
O(143)	6307(11)	1401(7)	3502(9)	69(5)
O(144)	5256(8)	1773(4)	2599(8)	45(3)
C(144)	4148(14)	-2407(7)	3002(12)	52(5)
O(145)	33(9)	-1666(4)	71(8)	47(3)
C(145)	-1212(9)	-702(7)	2329(12)	44(4)
C(146)	-707(14)	-155(6)	2968(12)	51(5)
O(147)	2643(10)	2271(6)	1751(10)	64(4)
C(147)	-1418(12)	-329(8)	1985(12)	54(5)
C(148)	760(10)	-589(6)	-1123(10)	40(4)
C(150)	1360(12)	538(7)	-161(12)	49(5)
C(151)	4873(13)	2065(8)	2383(12)	51(5)
C(152)	5254(10)	-1436(5)	212(10)	35(3)
C(154)	-1424(12)	-1156(9)	2165(11)	54(5)
C(157)	1866(11)	1998(6)	3539(12)	46(5)
C(158)	6770(10)	297(6)	2888(11)	41(4)
C(159)	1973(8)	-2308(5)	157(11)	37(4)
C(160)	1889(10)	-2636(5)	-421(8)	33(3)
C(161)	1076(12)	-2785(7)	-503(9)	45(5)
C(163)	-903(9)	695(7)	4361(13)	48(5)
C(164)	5306(14)	2445(9)	2109(16)	67(8)
N(409)	-938(11)	1093(6)	3335(10)	52(4)
C(166)	626(11)	-2851(7)	209(11)	45(4)
C(167)	166(12)	-2547(6)	515(12)	46(5)

C(168)	1876(12)	1075(5)	6281(10)	40(4)
C(169)	-69(10)	-96(6)	4701(9)	36(4)
C(170)	1720(14)	1196(6)	7628(9)	45(5)
C(171)	984(11)	985(8)	7761(9)	46(4)
C(172)	286(12)	1201(8)	7944(14)	56(6)
C(174)	1813(12)	1407(6)	6882(8)	39(4)
C(175)	-15(14)	502(8)	7807(11)	52(5)
C(176)	5752(19)	2651(10)	2739(16)	79(9)
C(177)	5999(10)	-1528(6)	683(13)	48(5)
C(178)	6138(10)	-1266(6)	1283(12)	44(4)
C(179)	3352(10)	1358(7)	-211(11)	43(4)
C(180)	2536(12)	1461(6)	-542(12)	48(5)
O(180)	760(9)	-1677(6)	5266(9)	58(4)
C(181)	1928(12)	1131(6)	-340(9)	43(4)
C(182)	1163(12)	1203(9)	-247(13)	59(6)
C(183)	74(14)	-3090(6)	1179(11)	48(5)
C(185)	-1142(11)	466(9)	4914(14)	62(6)
C(186)	3556(15)	-2706(7)	3180(13)	56(6)
C(187)	2666(14)	-2582(6)	3013(11)	48(5)
C(188)	3224(9)	1247(5)	546(9)	34(4)
C(190)	4810(20)	-2431(14)	3430(30)	140(20)
C(191)	71(18)	-1603(9)	5172(16)	69(7)
C(192)	-490(20)	-1720(11)	5821(19)	79(8)
C(193)	-146(10)	-526(7)	584(11)	43(4)
C(195)	1373(15)	1289(12)	1563(17)	83(10)
C(196)	4070(13)	1300(9)	-2360(10)	53(6)
O(200)	1585(10)	307(10)	1798(12)	103(10)
C(200)	-1378(17)	833(9)	3771(16)	69(7)
O(201)	570(10)	497(5)	2550(10)	61(4)
C(201)	2549(9)	-2129(5)	3287(9)	29(3)
O(202)	634(9)	-172(4)	1965(9)	52(4)
O(203)	365(12)	433(6)	1371(12)	75(5)
O(204)	8870(11)	934(7)	1741(11)	76(5)
O(205)	8022(8)	1179(6)	830(17)	114(11)
O(213)	9296(8)	1081(7)	606(12)	80(6)
O(215)	703(18)	7678(10)	2422(16)	116(9)

O(219)	1967(18)	6133(10)	879(15)	109(8)
O(222)	8444(13)	516(7)	885(16)	103(8)
O(226)	2935(14)	5975(10)	1730(20)	127(11)
O(230)	1937(19)	6438(10)	2069(17)	118(9)
O(232)	2826(18)	6664(10)	1227(17)	115(9)
O(234)	6431(16)	6785(9)	5345(16)	101(7)
O(236)	5154(19)	1536(10)	681(17)	117(9)
O(237)	6357(12)	1415(9)	406(10)	88(7)
O(239)	5442(18)	993(8)	38(14)	116(11)
O(240)	7210(20)	1954(11)	1686(19)	129(10)
O(241)	5449(13)	1698(6)	-370(10)	74(5)
O(243)	7260(20)	7635(13)	1420(20)	142(12)
O(245)	5709(12)	3435(9)	1423(13)	98(8)
O(246)	6889(16)	3586(8)	1943(14)	98(7)
O(247)	2770(40)	40(30)	-580(40)	250(30)
O(248)	6970(30)	3256(14)	970(20)	165(14)
O(250)	-363(14)	7479(8)	2841(14)	91(7)
O(251)	5340(14)	9014(8)	3566(13)	97(8)
O(252)	4054(19)	9163(11)	3181(18)	118(9)
O(253)	4954(12)	9609(7)	2992(11)	73(5)
O(254)	4340(30)	9382(12)	4101(12)	200(20)
O(255)	7022(15)	7410(6)	5007(16)	103(8)
O(257)	9790(20)	4266(14)	4020(20)	155(13)
O(258)	525(18)	7619(10)	3640(17)	114(9)
O(259)	8980(30)	4241(15)	2710(20)	163(14)
O(260)	7302(17)	-1178(10)	3662(16)	111(8)
O(268)	3290(30)	6552(16)	4760(30)	187(17)
O(269)	700(20)	7087(11)	2896(18)	124(9)
O(271)	9044(15)	4451(8)	3174(13)	85(6)
O(272)	9980(20)	4678(11)	3044(18)	127(10)
O(275)	150(40)	3550(20)	1430(40)	240(30)
O(400)	2817(16)	-158(9)	2718(15)	104(7)
O(402)	7750(40)	8940(20)	10(30)	220(30)
O(405)	2338(18)	5218(10)	587(17)	121(9)
O(406)	680(40)	6750(20)	2830(40)	380(30)
O(407)	8760(40)	1850(20)	2290(40)	230(30)

C(132)	5315(13)	349(7)	5744(12)	51(5)
N(6)	4638(10)	112(5)	5639(9)	44(4)
C(410)	4837(15)	-277(8)	5655(14)	58(5)
N(70)	5593(16)	-324(9)	5728(15)	81(7)
N(67)	5730(50)	2410(30)	1600(40)	220(30)
N(62)	4980(30)	2599(15)	3820(20)	131(13)
C(202)	5050(20)	2874(13)	3230(20)	94(10)
N(63)	3850(30)	3048(18)	3630(30)	159(17)
C(203)	4620(30)	3143(18)	3070(30)	124(15)
O(411)	8400(40)	7800(20)	1970(40)	260(30)
O(413)	540(30)	6406(19)	3750(30)	190(20)
C(411)	5870(20)	69(11)	5793(19)	82(8)
O(221)	5850(40)	7120(20)	4420(30)	230(20)
O(412)	7720(30)	1449(16)	2500(30)	194(16)
O(220)	7150(60)	2100(30)	2550(50)	380(50)
O(229)	5600(70)	-1780(40)	4890(70)	620(70)
O(228)	6740(40)	-1860(30)	3190(40)	300(30)
O(227)	7940(40)	-1930(20)	4220(30)	250(20)
C(300)	-480(40)	-2210(20)	5880(40)	190(20)
O(360)	6620(20)	4038(12)	1080(20)	136(11)
N(200)	-1150(40)	-1490(20)	5920(40)	250(30)

APPENDIX K

CRYSTALLOGRAPHIC DATA FOR

$[Tb_{15}(\mu_5\text{-}OH)(\mu_3\text{-}OH)_{20}(his^{+/-})_{10}(his^{-})_5(OH)_7](ClO_4)_{12}$

Identification code	mes1023	
Empirical formula	C75 H120 Cl5 N45 O90 Tb15	
Formula weight	5653.21	
Temperature	150(2) K	
Wavelength	0.71073 Å	
Crystal system	Monoclinic	
Space group	$P2_1$	
Unit cell dimensions	a = 18.5329(19) Å	α= 90°.
	b = 31.022(4) Å	β= 106.282(5)°.
	c = 18.6075(19) Å	γ = 90°.
Volume	10269(2) $Å^3$	
Z	2	
Density (calculated)	1.828 Mg/m^3	
Absorption coefficient	5.242 mm^{-1}	
F(000)	5330	
Crystal size	0.28 x 0.12 x 0.11 mm^3	
Theta range for data collection	1.14 to 25.40°.	
Index ranges	-22<=h<=18, -37<=k<=37, -22<=l<=22	
Reflections collected	53183	
Independent reflections	36087 [R(int) = 0.0622]	
Completeness to theta = 25.40°	99.3 %	
Max. and min. transmission	0.5963 and 0.3215	
Refinement method	Full-matrix least-squares on F^2	
Data / restraints / parameters	36087 / 1 / 1343	
Goodness-of-fit on F^2	1.032	
Final R indices [I>2sigma(I)]	R1 = 0.1053, wR2 = 0.2679	
R indices (all data)	R1 = 0.1849, wR2 = 0.3383	
Absolute structure parameter	0.05(3)	
Largest diff. peak and hole	3.287 and -2.684 e.$Å^{-3}$	

Atomic coordinates (x 10^4) and equivalent isotropic displacement parameters ($Å^2$x 10^3) for mes1023. U(eq) is defined as one third of the trace of the orthogonalized U^{ij} tensor.

	x	y	z	U(eq)
Cl(5)	6081(6)	6426(4)	4465(5)	80(3)
Cl(6)	7527(10)	9437(7)	3355(10)	144(6)
O(404)	5700(20)	6470(12)	3690(20)	116(11)
O(405)	6380(30)	6808(16)	4730(30)	148(15)
O(406)	6630(20)	6115(14)	4656(19)	118(12)
Tb(1)	3353(1)	578(1)	3069(1)	48(1)
Tb(2)	1653(1)	596(1)	3774(1)	53(1)
Tb(3)	5394(1)	758(1)	3379(1)	54(1)
Tb(4)	4044(1)	919(1)	1385(1)	52(1)
Tb(5)	-359(1)	849(1)	3365(1)	64(1)
Tb(6)	1084(1)	1782(1)	3931(1)	56(1)
Tb(7)	3902(1)	1689(1)	2810(1)	57(1)
Tb(8)	370(1)	2753(1)	2848(1)	62(1)
Tb(9)	2522(1)	2479(1)	3311(1)	59(1)
Tb(10)	3188(1)	2740(1)	1717(1)	68(1)
Tb(11)	3016(1)	-283(1)	4468(1)	71(1)
Tb(12)	4670(1)	2710(1)	3687(1)	68(1)
Tb(13)	1902(1)	-235(1)	2351(1)	56(1)
Tb(14)	955(1)	1043(1)	5380(1)	81(1)
Tb(15)	1871(1)	2865(1)	4857(1)	82(1)
O(10A)	4515(11)	259(7)	3860(12)	50(5)
O(10B)	463(11)	327(7)	2904(13)	53(6)
O(10C)	-87(12)	2024(7)	3083(12)	52(5)
O(10D)	3424(14)	233(7)	934(14)	62(6)
O(21A)	2792(11)	2118(6)	2317(14)	54(6)
O(11A)	4359(11)	-308(7)	4490(12)	54(6)
O(10E)	2034(11)	2836(8)	2118(15)	69(7)
N(10A)	-338(16)	2444(9)	1553(16)	59(7)
O(22A)	3245(10)	1091(7)	2124(10)	44(5)
O(10F)	-980(11)	1539(9)	2885(12)	62(7)
O(10G)	2805(14)	150(7)	1824(12)	55(6)

O(20A)	5029(12)	492(9)	1219(14)	68(7)
O(10H)	5998(11)	1443(7)	3814(13)	59(6)
O(10I)	5078(13)	1942(7)	3636(13)	58(6)
O(10J)	575(14)	-275(8)	2264(14)	69(7)
O(11B)	3715(12)	2334(7)	845(14)	63(6)
C(10A)	-1098(19)	2219(13)	1350(20)	63(10)
N(10B)	5933(18)	668(11)	4782(19)	73(9)
O(23A)	2987(12)	465(8)	4176(15)	65(6)
N(10C)	1223(18)	-71(10)	1028(18)	70(8)
O(24A)	1825(11)	-149(7)	3602(13)	56(6)
O(25A)	3077(10)	-199(8)	3202(13)	56(6)
C(10B)	3910(20)	1934(12)	840(20)	63(9)
O(20B)	1851(13)	-951(8)	2746(17)	74(8)
N(10E)	3074(18)	1050(12)	162(15)	72(9)
O(28A)	4328(11)	478(6)	2497(11)	46(5)
O(26A)	1311(11)	2168(7)	2866(13)	56(6)
O(20C)	-90(15)	655(15)	5572(14)	125(16)
O(27A)	1781(11)	1171(8)	4658(12)	55(6)
N(10F)	5400(20)	2496(12)	4960(20)	85(10)
O(11C)	908(11)	3110(8)	1945(14)	62(6)
O(22B)	6779(12)	725(10)	3622(19)	92(9)
N(10G)	5774(17)	-33(9)	3588(18)	65(8)
O(11D)	4178(16)	3141(10)	4510(20)	109(12)
N(11A)	6006(15)	2611(11)	3637(19)	72(9)
O(36A)	3430(14)	2933(7)	2975(19)	85(9)
O(31A)	664(12)	548(9)	4313(14)	67(7)
O(11E)	2122(13)	218(11)	4991(13)	82(9)
N(10H)	2059(19)	2602(11)	576(19)	79(9)
O(34A)	4848(12)	1273(7)	2428(13)	59(6)
O(33A)	161(12)	1362(9)	4313(12)	67(7)
N(10I)	1990(30)	1230(15)	6510(30)	109(13)
O(20D)	4091(14)	3243(9)	1650(20)	94(10)
O(32A)	825(11)	1173(8)	3171(13)	61(6)
C(10D)	3000(30)	1431(15)	-350(30)	87(13)
O(29A)	4331(12)	1111(8)	3623(16)	72(7)
O(20E)	5879(13)	513(12)	2318(15)	87(9)

O(30A)	2252(14)	2165(9)	4393(13)	73(7)
O(35A)	4227(11)	2373(7)	2480(11)	50(5)
O(11F)	3743(11)	1702(8)	1357(14)	62(6)
N(11B)	-952(19)	2668(11)	2900(20)	84(11)
C(11B)	6710(30)	2184(15)	4840(30)	86(13)
O(11G)	2004(11)	506(7)	2649(14)	58(6)
N(11C)	2536(14)	3454(11)	1460(20)	79(10)
O(20F)	4983(15)	3257(12)	2819(19)	102(10)
O(20G)	930(20)	3388(12)	4860(20)	120(11)
C(10H)	6070(20)	283(14)	5250(30)	79(12)
C(11D)	6370(19)	2156(12)	3960(20)	66(10)
C(10I)	6100(20)	-152(13)	4980(20)	76(11)
N(11D)	3740(20)	-56(14)	5750(20)	113(16)
C(10J)	1380(30)	2794(18)	250(30)	104(18)
O(11H)	3055(14)	2893(8)	4431(17)	79(8)
O(37A)	765(13)	2508(7)	4144(14)	65(6)
N(134)	-370(20)	3400(13)	2030(20)	95(11)
N(11E)	4682(17)	1376(12)	627(18)	77(10)
O(11I)	1390(20)	2487(14)	5735(17)	107(12)
N(12A)	3110(30)	1256(17)	7260(30)	134(17)
N(10J)	2547(18)	-658(12)	1590(20)	102(14)
C(11F)	2080(30)	1582(15)	7020(30)	89(13)
C(11G)	2360(30)	1450(15)	-790(30)	94(14)
C(11H)	2500(30)	1030(20)	6640(30)	105(16)
N(12C)	2570(20)	3598(12)	5020(20)	92(11)
C(12A)	-1190(20)	2046(13)	688(19)	70(11)
C(12B)	-1131(19)	-80(18)	1830(30)	130(30)
C(13A)	2730(20)	-448(14)	1000(20)	78(11)
O(12A)	1572(18)	423(15)	5875(15)	124(14)
C(13B)	2979(19)	35(11)	1320(20)	53(8)
C(13C)	940(30)	2539(15)	-270(30)	81(12)
C(12D)	-1630(20)	2248(14)	1830(30)	90(14)
N(12E)	-530(20)	2159(12)	500(20)	84(10)
O(20H)	2472(19)	-1014(11)	3906(19)	108(10)
N(12D)	-936(19)	728(13)	1910(20)	97(12)
O(12B)	1289(16)	1824(11)	5315(13)	82(9)

C(12F)	4720(20)	-100(12)	4250(20)	59(9)
C(12H)	4370(30)	206(18)	5900(30)	105(16)
N(12F)	-755(16)	68(11)	3220(20)	84(11)
C(12I)	3440(30)	-74(17)	6490(30)	101(15)
O(20I)	-820(20)	672(13)	4510(20)	127(13)
C(12J)	1400(30)	3301(19)	520(30)	117(17)
O(39A)	1643(14)	2999(9)	3513(15)	75(7)
N(12G)	4450(30)	346(19)	6550(30)	138(18)
O(40A)	3741(12)	2158(7)	3788(17)	76(8)
O(21B)	170(17)	3415(9)	3500(17)	90(9)
C(13E)	4290(19)	1789(13)	360(20)	71(11)
C(13F)	2880(30)	-322(18)	6600(30)	103(15)
Cl(1)	1087(4)	1369(3)	1185(5)	58(2)
O(40F)	644(15)	1413(11)	491(16)	98(10)
O(40G)	1400(20)	1789(9)	1502(16)	118(13)
O(40H)	1740(20)	1074(12)	1340(20)	115(11)
Cl(8)	5345(8)	4221(4)	7777(8)	98(4)
Cl(9)	3910(10)	7269(5)	8242(10)	122(5)
Cl(4)	7594(11)	9132(7)	6829(12)	161(7)
C(100)	-1340(20)	2248(14)	2680(30)	80(13)
C(102)	1200(20)	2126(18)	5680(20)	71(11)
O(300)	-1760(20)	836(12)	3060(20)	109(10)
C(115)	5770(20)	1814(11)	3790(20)	58(8)
C(109)	3690(30)	1654(16)	-400(30)	92(13)
C(106)	-790(20)	1919(12)	2800(20)	60(9)
C(120)	6170(30)	79(16)	1440(30)	97(14)
C(104)	203(17)	-49(10)	2563(18)	46(7)
C(108)	1770(20)	3436(14)	1330(20)	81(12)
C(116)	-70(20)	2406(9)	1068(19)	61(11)
C(113)	2040(30)	-386(15)	5860(30)	88(13)
C(119)	5690(20)	403(12)	1700(20)	66(10)
N(101)	370(20)	1598(13)	6120(20)	92(11)
C(105)	-581(19)	-173(11)	2660(30)	80(13)
C(111)	740(20)	1960(13)	6280(20)	78(11)
C(103)	2110(20)	-386(13)	260(20)	76(11)
C(107)	1520(20)	3101(14)	1850(30)	79(12)

C(114)	5530(30)	-253(15)	4190(30)	88(12)
C(118)	5270(30)	3578(16)	1820(30)	99(14)
C(117)	4790(30)	3346(15)	2190(30)	89(13)
N(102)	2160(30)	-564(16)	5300(30)	122(15)
O(100)	2990(50)	1370(30)	3580(40)	260(30)
C(124)	6970(20)	390(20)	1440(30)	104(17)
N(110)	4890(20)	3665(13)	1030(20)	100(12)
N(121)	5670(20)	-38(13)	450(20)	99(12)
N(122)	1940(20)	1114(14)	-520(20)	99(12)
O(401)	580(40)	1230(20)	1550(30)	190(20)
C(126)	2370(30)	867(19)	-30(40)	130(20)
C(123)	3560(30)	3171(14)	4620(30)	82(12)
N(123)	1230(30)	2099(17)	-250(30)	130(16)
O(400)	3700(30)	-881(16)	5170(30)	151(15)
C(101)	2720(30)	1648(17)	7470(30)	105(15)
O(411)	5670(30)	6348(15)	4920(30)	145(15)
O(410)	4270(50)	6890(30)	8090(50)	280(30)
O(301)	5440(30)	3371(15)	4260(30)	149(15)
O(413)	5740(30)	4372(16)	7350(30)	157(17)
C(130)	5460(30)	4080(20)	2220(30)	121(18)
O(414)	4830(20)	3999(14)	7210(20)	135(13)
O(416)	3290(40)	7350(20)	7640(40)	230(30)
O(415)	5070(30)	4460(20)	8330(30)	200(20)
C(133)	6230(30)	2131(18)	5930(30)	107(16)
C(134)	6110(20)	2295(14)	5220(20)	80(12)
N(132)	5530(30)	2264(19)	6100(30)	146(18)
C(135)	2030(20)	2249(14)	310(30)	82(12)
O(417)	650(20)	9315(14)	3890(20)	129(13)
C(112)	1890(30)	146(15)	5550(30)	85(12)
O(421)	7590(30)	3359(16)	3730(30)	150(16)
O(422)	7230(30)	3337(18)	4300(30)	180(20)
O(111)	-170(20)	4079(13)	3540(20)	120(11)
C(141)	910(30)	183(14)	-200(30)	81(12)
N(137)	430(20)	315(12)	150(20)	93(11)
C(142)	610(20)	169(11)	870(20)	60(9)
C(136)	0(40)	3770(20)	2540(40)	160(30)

C(138)	4020(30)	195(18)	6800(30)	106(16)
C(140)	1420(30)	-130(18)	420(30)	107(16)
C(139)	5080(40)	2490(20)	5490(40)	124(19)
C(137)	-60(30)	3755(17)	3200(30)	93(14)
Cl(7)	8891(14)	2371(8)	4849(13)	165(8)
N(142)	-1070(20)	871(14)	840(20)	97(11)
O(420)	5850(40)	3980(20)	8530(40)	220(30)
C(145)	-1200(30)	499(16)	860(30)	89(13)
C(127)	-1160(30)	360(20)	1510(30)	110(17)
C(143)	1410(40)	1820(20)	7090(40)	130(20)
O(423)	7590(150)	2740(100)	4800(150)	800(200)
O(424)	9080(50)	2860(30)	5010(50)	300(40)
O(425)	500(40)	9730(30)	5060(40)	240(30)
C(148)	-260(30)	4180(19)	1270(30)	116(17)
C(132)	3360(30)	3566(16)	5160(30)	97(14)
C(147)	-360(30)	4193(17)	1990(30)	99(14)
C(152)	3070(30)	2461(17)	6320(30)	97(14)
C(146)	-1000(30)	1050(20)	1520(30)	109(17)
N(147)	3060(30)	2794(16)	6020(30)	113(13)
C(150)	3700(40)	3050(20)	6180(40)	130(20)
O(428)	4500(50)	7720(30)	8510(50)	280(40)
Cl(11)	1437(17)	8149(10)	638(17)	219(11)
N(48)	3830(30)	2592(15)	6850(30)	121(15)
O(444)	1630(70)	7410(40)	940(70)	390(60)
N(81)	190(30)	4240(16)	260(30)	125(16)
C(201)	1800(40)	5530(30)	4480(40)	150(20)
N(80)	480(40)	4490(20)	1070(40)	180(20)
C(202)	1970(50)	5760(30)	4310(50)	150(30)
N(200)	2020(50)	6040(30)	3660(50)	250(40)
C(204)	1760(40)	6400(20)	4450(40)	140(20)
C(203)	1820(30)	6490(20)	3290(40)	123(18)
C(153)	1050(60)	4610(40)	430(60)	250(50)
C(151)	-1550(170)	4520(120)	-380(170)	1000(200)
N(201)	1730(40)	6740(30)	3870(50)	210(30)
N(11)	6170(20)	802(13)	5950(20)	89(10)
N(40)	7010(50)	1210(30)	1300(50)	240(40)

N(39)	6960(30)	809(19)	330(30)	147(19)
C(125)	6930(40)	690(20)	1050(40)	114(18)
C(128)	6840(40)	1330(20)	620(40)	130(20)
C(20)	5980(30)	961(17)	5240(30)	102(15)
O(427)	3410(70)	7190(50)	8980(80)	460(70)
C(21)	6140(30)	440(20)	5900(30)	112(16)
Cl(10)	7489(15)	7861(10)	1595(14)	197(10)
Cl(12)	270(30)	9160(20)	4490(30)	410(30)
C(154)	3850(40)	3460(30)	5940(40)	150(30)
O(445)	7460(40)	7460(30)	1490(40)	270(40)
O(447)	-620(120)	8710(70)	4390(120)	770(140)
O(446)	8340(40)	7890(20)	1970(40)	260(30)

APPENDIX L

CRYSTALLOGRAPHIC DATA FOR

$[Eu_{15}(\mu_5\text{-}Cl)(\mu_3\text{-}OH)_{20}(his^{+/-})_{10}(his^{-})_5(OH)_7](ClO_4)_{12}$

FROM

$[Eu_{15}(\mu_5\text{-}OH)(\mu_3\text{-}OH)_{20}(his^{+/-})_{10}(his^{-})_5(OH)_7](ClO_4)_{12}$

RECRYSTALLIZED FROM L-HISTIDINE BUFFER

SOLUTION WITH NaCl

Identification code	mes1020a	
Empirical formula	C60 H120 Cl5 Eu15 N45 O90	
Formula weight	5368.66	
Temperature	293(2) K	
Wavelength	0.71073 Å	
Crystal system	Orthorhombic	
Space group	$C222_1$	
Unit cell dimensions	a = 20.466(4) Å	α= 90°.
	b = 31.161(6) Å	β= 90°.
	c = 34.175(7) Å	γ = 90°.
Volume	21795(8) $Å^3$	
Z	4	
Density (calculated)	1.636 Mg/m^3	
Absorption coefficient	4.386 mm^{-1}	
F(000)	10180	
Crystal size	? x ? x ? mm^3	
Theta range for data collection	1.19 to 25.35°.	
Index ranges	-24<=h<=21, -37<=k<=37, -40<=l<=41	
Reflections collected	46863	
Independent reflections	19911 [R(int) = 0.0441]	
Completeness to theta = 25.35°	99.8 %	
Refinement method	Full-matrix least-squares on F^2	
Data / restraints / parameters	19911 / 0 / 440	
Goodness-of-fit on F^2	2.082	
Final R indices [I>2sigma(I)]	R1 = 0.1544, wR2 = 0.4484	
R indices (all data)	R1 = 0.1704, wR2 = 0.4578	
Absolute structure parameter	0.28(6)	
Largest diff. peak and hole	2.353 and -7.248 e.$Å^{-3}$	

Atomic coordinates (x 10^4) and equivalent isotropic displacement parameters ($Å^2$x 10^3) for mes1020a. U(eq) is defined as one third of the trace of the orthogonalized U^{ij} tensor.

	x	y	z	U(eq)
Eu(1)	33(1)	0	5000	42(1)
Cl(1)	1592(5)	0	5000	56(3)
Eu(2)	-588(1)	1118(1)	4874(1)	52(1)
Eu(3)	1108(1)	-895(1)	4609(1)	48(1)
Eu(4)	-388(1)	-640(1)	4068(1)	55(1)
Eu(5)	2288(1)	-1762(1)	4834(1)	61(1)
Eu(6)	2891(1)	-557(1)	4756(1)	62(1)
Eu(7)	4167(1)	337(1)	4505(1)	99(1)
Eu(8)	2467(1)	-1124(1)	3839(1)	74(1)
C(119)	-270(30)	-970(20)	2986(17)	99(16)
O(50)	2074(10)	-1018(6)	5035(5)	39(4)
O(51)	2060(9)	-586(7)	4287(7)	47(5)
O(52)	471(11)	-291(7)	4413(6)	46(5)
O(53)	2980(13)	200(9)	4577(7)	59(6)
O(54)	428(13)	694(8)	4846(7)	58(6)
O(55)	-30(13)	1203(8)	5469(7)	56(5)
O(56)	-767(9)	-487(5)	4725(7)	47(6)
O(57)	1736(11)	-1453(6)	4293(8)	52(6)
N(59)	-1634(15)	905(9)	4550(7)	51(6)
N(62)	2850(50)	-510(30)	3280(30)	170(30)
N(64)	-335(18)	-1230(12)	3580(9)	64(8)
C(120)	2580(40)	-2650(30)	3660(20)	110(20)
O(100)	3287(12)	-535(9)	4035(11)	78(9)
O(101)	1451(13)	-1165(12)	3458(8)	73(8)
O(102)	747(11)	-918(8)	3914(6)	54(6)
O(103)	-586(13)	424(7)	4456(12)	89(12)
O(104)	-1024(15)	11(10)	4015(11)	90(11)
O(106)	1124(12)	-1601(8)	4948(6)	51(5)
O(107)	119(12)	1758(8)	4812(6)	52(5)
O(108)	3300(20)	-1616(9)	5234(14)	135(19)
O(109)	2500(20)	-1874(16)	3738(12)	107(12)

O(110)	2620(20)	-2241(13)	4285(14)	112(14)
O(111)	-1430(20)	-905(13)	4117(10)	84(9)
C(111)	-1470(20)	947(13)	3862(11)	60(9)
O(112)	-1740(30)	1270(20)	5333(16)	135(18)
O(113)	5210(20)	188(14)	4684(11)	99(10)
C(113)	-1610(20)	625(15)	4165(12)	70(10)
C(114)	-1070(20)	340(20)	4219(10)	100(20)
C(115)	2330(30)	-2520(40)	4030(30)	220(70)
C(117)	-1760(14)	-1288(15)	4257(15)	81(16)
O(400)	-1400(20)	1807(8)	4786(16)	120(16)
O(410)	2877(11)	-2451(10)	5003(17)	123(18)
Cl(2)	8447(5)	611(3)	1079(3)	68(2)
Cl(5)	8143(13)	-1051(9)	2867(7)	142(7)
Cl(3)	4608(15)	2624(9)	1084(8)	153(8)
O(203)	8450(20)	-1352(15)	3093(12)	106(12)
O(204)	7590(60)	-740(40)	2940(30)	250(50)
O(200)	4960(30)	2954(19)	1521(16)	133(16)
O(201)	4860(20)	2904(15)	689(12)	108(12)
Cl(6)	3412(16)	1343(10)	352(8)	167(9)
O(205)	8540(30)	860(19)	1397(15)	135(16)
O(300)	2760(30)	1620(20)	243(16)	137(17)
O(301)	3830(40)	1770(20)	680(20)	170(20)
O(302)	3010(30)	1130(17)	803(14)	120(14)
O(206)	8630(30)	170(20)	1114(17)	150(19)
O(207)	7880(20)	782(15)	824(12)	105(11)
Cl(7)	7018(6)	5000	0	87(5)
C(126)	4110(40)	1420(30)	4070(20)	120(20)
C(123)	3640(100)	-640(60)	3050(50)	240(80)
C(125)	300(30)	-1373(16)	3354(13)	78(11)
N(53)	-486(15)	1241(10)	4141(6)	64(8)
C(108)	111(16)	1434(15)	4022(11)	130(20)
N(63)	135(18)	1426(16)	3607(11)	160(30)
C(110)	-450(20)	1229(14)	3469(6)	91(14)
C(107)	-830(13)	1115(11)	3799(7)	58(8)
N(68)	2440(20)	-2623(12)	3310(10)	70(9)
N(51)	-90(20)	-318(10)	3427(10)	91(12)

C(100)	-26(18)	135(9)	3412(8)	73(10)
N(55)	354(18)	240(10)	3078(9)	93(12)
C(101)	530(20)	-148(13)	2886(10)	95(15)
C(118)	250(30)	-493(9)	3102(14)	2000(1300)
C(127)	4220(20)	1498(13)	4372(11)	58(8)
Cl(8)	4970(30)	-1466(17)	580(14)	257(19)
O(305)	5290(30)	-2124(17)	454(14)	117(14)
O(307)	4760(50)	-1340(30)	1150(30)	210(40)
O(306)	5610(40)	-1220(30)	720(20)	180(30)
O(304)	4570(20)	-1044(16)	273(13)	114(13)
C(130)	1050(30)	-2554(18)	5491(15)	84(13)
N(60)	2026(19)	-1986(13)	5559(8)	90(12)
C(109)	2210(20)	-1689(12)	5855(10)	91(13)
N(61)	1870(20)	-1798(13)	6202(8)	170(30)
C(122)	1470(16)	-2161(11)	6121(9)	53(8)
C(129)	1570(20)	-2278(12)	5724(9)	180(40)
N(50)	3780(30)	785(18)	3900(16)	170(30)
C(121)	3340(30)	653(17)	3599(18)	110(20)
N(65)	3160(30)	1020(20)	3384(16)	250(60)
C(133)	3470(30)	1383(16)	3552(18)	130(20)
C(128)	3860(30)	1237(18)	3871(16)	110(20)
O(310)	3640(30)	-1230(20)	3655(16)	147(17)

APPENDIX M

CRYSTALLOGRAPHIC DATA FOR

$[Eu_{15}(\mu_5\text{-}Br)(\mu_3\text{-}OH)_{20}(his^{+/-})_{10}(his^{-})_5(OH)_7](ClO_4)_{12}$

FROM

$[Eu_{15}(\mu_5\text{-}OH)(\mu_3\text{-}OH)_{20}(his^{+/-})_{10}(his^{-})_5(OH)_7](ClO_4)_{12}$

RECRYSTALLIZED FROM L-HISTIDINE BUFFER

SOLUTION WITH NaBr

Identification code	mes1113	
Empirical formula	C60 H120 Br Cl5 Eu15 N45 O90	
Formula weight	5448.57	
Temperature	150(2) K	
Wavelength	0.71073 Å	
Crystal system	Monoclinic	
Space group	$P2_1$	
Unit cell dimensions	a = 17.1935(18) Å	α= 90°.
	b = 31.402(4) Å	β= 91.598(5)°.
	c = 18.6504(19) Å	γ = 90°.
Volume	10066(2) $Å^3$	
Z	2	
Density (calculated)	1.798 Mg/m^3	
Absorption coefficient	4.947 mm^{-1}	
F(000)	5160	
Crystal size	0.22 x 0.14 x 0.12 mm^3	
Theta range for data collection	1.09 to 27.84°.	
Index ranges	-22<=h<=22, -41<=k<=41, -24<=l<=24	
Reflections collected	79668	
Independent reflections	46113 [R(int) = 0.0342]	
Completeness to theta = 27.84°	98.5 %	
Max. and min. transmission	0.5882 and 0.4091	
Refinement method	Full-matrix least-squares on F^2	
Data / restraints / parameters	46113 / 1 / 1145	
Goodness-of-fit on F^2	1.392	
Final R indices [I>2sigma(I)]	R1 = 0.0597, wR2 = 0.1695	
R indices (all data)	R1 = 0.0743, wR2 = 0.1892	
Absolute structure parameter	0.028(12)	
Largest diff. peak and hole	5.304 and -2.238 e.$Å^{-3}$	

Atomic coordinates (x 10^4) and equivalent isotropic displacement parameters ($Å^2$x 10^3) for mes1113. U(eq) is defined as one third of the trace of the orthogonalized U^{ij} tensor.

	x	y	z	U(eq)
Eu(1)	-2037(1)	-5530(1)	-1106(1)	20(1)
Eu(2)	-3237(1)	-5045(1)	-2684(1)	21(1)
Eu(3)	-3198(1)	-5854(1)	-4262(1)	19(1)
Eu(4)	-5011(1)	-5195(1)	-3803(1)	25(1)
Eu(5)	-1784(1)	-6512(1)	216(1)	21(1)
Eu(6)	-3946(1)	-6898(1)	-4831(1)	21(1)
Eu(7)	-3803(1)	-4914(1)	-642(1)	22(1)
Eu(8)	-2059(1)	-6853(1)	-3635(1)	19(1)
Eu(9)	-2006(1)	-7770(1)	-2364(1)	24(1)
Eu(10)	-19(1)	-7231(1)	-2932(1)	24(1)
Eu(11)	-2037(1)	-4308(1)	-1573(1)	26(1)
Eu(12)	-1307(1)	-6638(1)	-1709(1)	19(1)
Eu(13)	-1897(1)	-6544(1)	-5552(1)	21(1)
Eu(14)	-58(1)	-5843(1)	-562(1)	25(1)
Eu(15)	-3125(1)	-4702(1)	-4731(1)	27(1)
Br(1)	-2356(1)	-5987(1)	-2684(1)	24(1)
Cl(1)	-4312(2)	-6543(1)	-1913(2)	24(1)
Cl(9)	-6452(2)	-7184(1)	-1093(2)	37(1)
Cl(3)	-1543(3)	-4792(2)	1334(2)	52(1)
Cl(4)	-1850(3)	-8241(1)	-5267(2)	44(1)
Cl(5)	486(3)	-7642(2)	-226(2)	48(1)
Cl(6)	-4730(3)	-3675(1)	-2945(3)	53(1)
Cl(7)	-4567(4)	-5617(2)	-6721(3)	65(1)
O(101)	-3013(5)	-5533(3)	-141(5)	22(2)
O(1)	-2644(5)	-5186(3)	-3795(5)	21(2)
O(5)	-3355(5)	-6567(3)	-3803(5)	22(2)
O(105)	-749(6)	-5166(3)	-859(5)	30(2)
O(9)	-942(5)	-6648(3)	-2972(5)	22(2)
O(100)	-4663(6)	-5007(3)	-2540(5)	26(2)
O(102)	-2801(6)	-6031(3)	651(5)	27(2)
O(13)	-908(5)	-5915(3)	-1574(5)	20(2)

O(104)	-3828(6)	-7606(3)	-4299(5)	27(2)
O(103)	-554(6)	-6519(4)	994(6)	36(2)
O(107)	-1837(5)	-7093(3)	-742(5)	22(2)
O(130)	-1552(6)	-6471(3)	-6835(5)	30(2)
O(122)	-2589(5)	-5422(3)	-5176(5)	21(2)
O(108)	-1945(6)	-7781(3)	-1049(5)	31(2)
O(2)	-3974(5)	-5617(3)	-3312(5)	20(2)
N(101)	-470(9)	-6305(5)	-5623(8)	41(3)
O(15)	-687(5)	-6527(3)	-568(4)	20(2)
O(14)	-1333(5)	-5802(3)	-36(5)	23(2)
O(124)	-1046(6)	-6896(3)	-4570(5)	32(2)
O(113)	-3766(6)	-7262(3)	-5923(5)	26(2)
O(120)	-2534(6)	-4376(3)	-2847(5)	28(2)
O(18)	-1982(5)	-5028(3)	-2063(5)	24(2)
O(6)	-3223(5)	-6313(3)	-5313(5)	20(2)
O(117)	-2561(6)	-3879(3)	-644(6)	32(2)
O(7)	-2584(5)	-7045(3)	-4813(5)	24(2)
O(127)	858(6)	-6322(3)	-1121(6)	33(2)
O(20)	-3374(6)	-4530(3)	-1693(5)	26(2)
O(106)	-4991(6)	-4851(3)	-1442(6)	33(2)
O(126)	123(6)	-6692(3)	-1891(5)	27(2)
O(125)	4(6)	-7272(3)	-4224(6)	34(2)
O(110)	-4553(6)	-6201(3)	-4549(5)	28(2)
O(128)	-5017(7)	-4522(4)	-88(6)	42(3)
O(123)	-1989(6)	-5812(4)	-5984(6)	35(2)
O(17)	-3352(6)	-5396(3)	-1563(5)	25(2)
O(11)	-878(5)	-7357(3)	-1965(5)	22(2)
O(114)	-2696(7)	-6975(4)	-6394(6)	41(3)
O(111)	-5551(6)	-5761(3)	-4588(5)	32(2)
O(19)	-2374(6)	-4830(3)	-687(5)	26(2)
O(119)	-818(7)	-4446(4)	-862(6)	43(3)
O(10)	-2288(5)	-7021(3)	-2374(5)	23(2)
O(109)	-2869(6)	-7495(3)	-3462(5)	25(2)
O(3)	-3953(6)	-4700(3)	-3678(5)	31(2)
N(104)	-4760(7)	-5520(4)	-195(7)	31(3)
O(116)	-3526(6)	-4230(3)	-109(5)	31(2)

N(102)	987(8)	-6660(5)	-3289(8)	40(3)
O(115)	-4307(6)	-4377(3)	-5224(5)	32(2)
O(112)	-947(7)	-8276(4)	-2279(6)	38(2)
O(121)	-2643(6)	-4115(3)	-3948(6)	34(2)
O(118)	417(7)	-6127(4)	505(6)	41(3)
Cl(2)	-381(2)	-5450(1)	-3460(2)	33(1)
O(300)	-4368(6)	-6094(3)	-2041(5)	29(2)
O(305)	-256(8)	-5820(4)	-3005(7)	51(3)
O(8)	-1973(5)	-6220(3)	-4365(5)	24(2)
O(301)	-4914(8)	-6691(5)	-1491(8)	55(3)
O(16)	-2245(5)	-6274(3)	-957(5)	22(2)
O(310)	-5776(7)	-7335(4)	-692(7)	44(3)
O(4)	-4053(6)	-5295(3)	-4705(5)	30(2)
O(129)	-5542(8)	-4752(4)	-4714(7)	47(3)
C(102)	-4043(9)	-8033(5)	-2533(8)	34(3)
C(106)	-6023(9)	-6899(5)	-4380(8)	31(3)
O(302)	-3594(7)	-6644(4)	-1554(7)	45(3)
N(103)	-3608(8)	-4982(4)	732(7)	34(3)
O(303)	-4337(9)	-6740(5)	-2614(8)	57(3)
N(105)	-3062(8)	-6966(4)	319(7)	35(3)
N(106)	-3448(8)	-7850(4)	-2126(7)	38(3)
N(107)	-5270(8)	-7068(4)	-4243(7)	35(3)
C(103)	-4744(10)	-7947(6)	-2213(9)	39(4)
O(12)	-1295(6)	-7486(3)	-3330(5)	25(2)
N(111)	857(8)	-5382(5)	-1268(8)	39(3)
N(109)	-5915(8)	-5627(4)	-3049(7)	35(3)
C(104)	-3970(9)	-8343(5)	-3145(8)	34(3)
C(100)	-5128(8)	-4863(4)	-2093(7)	24(3)
O(304)	327(10)	-5275(6)	-3731(9)	70(4)
N(108)	-5037(8)	-6652(4)	-5698(7)	32(3)
N(113)	-938(11)	-4090(6)	-2444(9)	55(4)
N(110)	-3093(8)	-4847(4)	-6112(7)	38(3)
O(311)	-6601(8)	-6745(4)	-957(7)	52(3)
O(135)	-1140(10)	-3646(5)	-1176(9)	69(4)
C(105)	-3292(8)	-8214(4)	-3666(7)	26(3)
C(101)	-3181(9)	-7405(5)	339(8)	35(3)

Cl(10)	-7393(3)	-8230(2)	-2441(3)	66(1)
Cl(11)	-9202(5)	-2760(3)	-2356(4)	93(2)
N(124)	-3790(8)	-7922(4)	-6834(7)	36(3)
C(129)	-3202(9)	-7587(5)	-6949(8)	31(3)
C(123)	1887(11)	-6156(6)	-3296(10)	47(4)
C(130)	-3369(9)	-7383(5)	-7723(8)	31(3)
N(120)	1384(10)	-6118(5)	-3935(9)	51(4)
C(119)	-375(9)	-7280(5)	-5495(8)	34(3)
C(113)	-1745(9)	-7615(5)	191(8)	31(3)
C(110)	-4327(9)	-5635(5)	1099(8)	32(3)
N(119)	1135(8)	-7316(4)	-2024(7)	36(3)
C(122)	1621(9)	-6499(5)	-2931(8)	36(3)
N(122)	1344(10)	-5163(6)	-2258(9)	56(4)
N(118)	-1121(7)	-7212(4)	-5871(6)	26(2)
O(314)	-2145(10)	-8622(6)	-5026(9)	75(5)
C(131)	-4105(11)	-7166(6)	-7825(10)	43(4)
C(118)	-6310(9)	-5521(5)	-2399(8)	35(3)
C(107)	-3334(8)	-7750(4)	-3820(7)	24(3)
C(128)	-3228(9)	-7253(5)	-6377(8)	30(3)
N(116)	-1402(7)	-7262(4)	608(6)	29(3)
C(121)	729(10)	-6629(5)	-1566(9)	38(3)
N(117)	-4573(9)	-7707(5)	-1625(8)	41(3)
C(125)	1034(10)	-5493(6)	-1913(9)	41(4)
O(315)	-5514(11)	-3715(6)	-2781(9)	76(5)
C(108)	-3067(9)	-5683(5)	470(8)	31(3)
C(109)	-3518(9)	-5428(5)	1008(8)	30(3)
C(114)	-2564(9)	-7728(5)	491(8)	35(3)
C(127)	-2378(10)	-5101(5)	-6315(9)	37(3)
N(115)	-5567(9)	-6055(5)	-360(9)	49(4)
O(136)	117(8)	-7985(4)	-2716(7)	49(3)
C(112)	-5247(10)	-6078(5)	371(9)	39(4)
N(114)	-5906(8)	-4677(4)	-3163(7)	36(3)
N(121)	226(9)	-5199(5)	250(8)	46(3)
C(111)	-4782(10)	-5758(5)	417(9)	38(4)
C(120)	1419(9)	-6913(5)	-1719(8)	34(3)
N(123)	-1668(9)	-4601(5)	-5008(8)	46(4)

C(126)	-1252(10)	-4728(6)	-5582(9)	41(4)
C(124)	-546(9)	-4796(5)	-648(8)	30(3)
O(134)	-2382(10)	-8509(5)	-1836(9)	70(4)
O(312)	345(10)	-7945(5)	343(9)	67(4)
O(313)	1253(11)	-7683(6)	-437(10)	77(5)
Cl(8)	-2524(7)	-2522(3)	-1442(9)	161(5)
N(129)	-6164(8)	-6228(5)	-2437(8)	40(3)
N(126)	542(10)	-5840(6)	-5602(9)	57(4)
N(112)	-2547(9)	-3620(5)	-2186(8)	40(3)
C(140)	716(10)	-6570(6)	1518(9)	40(4)
C(143)	-3956(12)	-7471(7)	188(11)	51(5)
C(144)	-3790(10)	-7629(5)	-1619(9)	36(3)
C(146)	-5610(8)	-6363(4)	-5363(7)	26(3)
C(133)	-2560(9)	-4064(5)	-3296(8)	33(3)
O(317)	-4520(10)	-3236(6)	-2899(9)	73(4)
C(139)	114(11)	-6389(6)	957(10)	44(4)
O(138)	-1891(13)	-6460(7)	1538(11)	94(6)
C(147)	-6250(11)	-6630(6)	-5002(10)	47(4)
C(137)	239(10)	-6554(5)	-5712(9)	38(3)
C(134)	2001(10)	-6699(6)	-2234(9)	40(4)
N(127)	-2520(8)	-8327(4)	-3339(7)	36(3)
C(149)	-5843(9)	-6064(5)	-3004(8)	35(3)
C(142)	-3739(11)	-6794(6)	158(9)	43(4)
O(316)	-6260(8)	-7236(5)	-1840(8)	58(3)
O(318)	-6575(11)	-8355(6)	-2212(10)	78(5)
N(128)	-4311(10)	-7082(5)	69(9)	50(4)
C(148)	-5928(10)	-4727(5)	-2375(9)	36(3)
C(136)	272(10)	-6993(6)	-5818(9)	41(4)
N(141)	-2978(8)	-3969(4)	-5357(8)	39(3)
C(141)	-5191(10)	-5699(5)	-658(9)	38(3)
C(145)	-5202(8)	-6081(4)	-4780(7)	24(3)
C(150)	-6480(10)	-5897(5)	-2038(9)	39(4)
C(132)	-1164(11)	-4534(6)	-4459(10)	45(4)
N(125)	-390(10)	-4616(6)	-4712(9)	56(4)
C(135)	-2285(9)	-5483(5)	-5765(8)	29(3)
C(138)	-271(12)	-5885(7)	-5576(11)	52(4)

Cl(12)	-2423(10)	-2167(4)	-2955(9)	202(7)
O(137)	-5047(9)	-3789(5)	-5376(8)	57(3)
N(144)	-6037(9)	-7271(5)	-3380(8)	47(4)
N(139)	-2497(9)	-3251(5)	306(8)	47(4)
N(142)	-4775(9)	-7417(5)	-7899(8)	43(3)
N(143)	-5095(11)	-6726(6)	-7847(10)	61(4)
N(140)	-4841(12)	-3612(6)	-444(10)	65(5)
C(161)	-3075(10)	-3597(5)	440(9)	37(3)
C(171)	-5294(10)	-7289(5)	-3649(9)	38(4)
C(163)	-3911(10)	-3438(5)	543(9)	37(3)
C(165)	-4423(10)	-3964(5)	-5283(9)	38(4)
O(306)	-896(11)	-5536(6)	-4047(10)	82(5)
C(170)	-1855(8)	-7502(4)	-614(7)	25(3)
C(160)	-3056(10)	-3938(5)	-156(9)	35(3)
O(322)	-7869(11)	-8247(6)	-1849(10)	81(5)
C(159)	-472(8)	-7143(4)	-4701(7)	25(3)
C(157)	-1623(11)	-4824(6)	-6319(10)	46(4)
C(164)	-4350(12)	-3328(6)	-144(11)	50(4)
C(166)	-3673(12)	-3699(7)	-5172(11)	51(4)
C(151)	180(12)	-4786(6)	-128(11)	50(4)
O(320)	-7357(11)	-7810(6)	-2792(10)	81(5)
O(319)	-7125(9)	-7421(5)	-892(9)	67(4)
C(153)	989(13)	-4936(7)	-1228(11)	56(5)
O(324)	-754(12)	-4702(7)	1506(11)	91(6)
C(167)	-3747(12)	-3271(7)	-5515(11)	51(4)
C(154)	-874(11)	-3784(6)	-2983(10)	46(4)
C(156)	-1637(12)	-3461(6)	-3139(11)	51(4)
C(152)	889(13)	-4662(7)	-582(11)	56(5)
C(168)	-4274(11)	-6755(6)	-7731(10)	49(4)
C(155)	-261(16)	-3770(9)	-3269(14)	74(7)
O(323)	-4730(12)	-3814(7)	-3672(11)	86(5)
C(173)	-6516(12)	-7029(7)	-3862(11)	51(4)
C(169)	-6541(10)	-5100(5)	-2174(9)	38(4)
O(321)	-7611(14)	-8591(7)	-2968(12)	101(6)
C(158)	-527(12)	-4729(7)	-5421(11)	53(5)
N(146)	-3016(17)	-2763(10)	-4717(15)	103(8)

N(149)	-187(12)	-8885(7)	-1662(11)	70(5)
N(152)	-4852(10)	-3093(6)	-1183(9)	55(4)
C(186)	261(13)	-8634(7)	-2093(12)	58(5)
C(188)	-111(13)	-9082(7)	-3201(12)	56(5)
C(185)	-216(11)	-8270(6)	-2358(10)	45(4)
C(187)	514(13)	-8902(7)	-2781(11)	55(5)
C(180)	-2226(15)	-2553(8)	-4647(13)	67(6)
O(326)	-30(13)	-7790(8)	-806(12)	102(6)
N(145)	212(15)	-4078(8)	-2912(14)	90(7)
N(148)	1464(15)	-6369(8)	1461(13)	85(6)
C(181)	812(13)	-6270(7)	-5696(12)	57(5)
C(182)	870(12)	-6406(7)	-3889(11)	53(5)
N(150)	-419(17)	-9430(9)	-3080(15)	102(8)
C(178)	-3008(13)	-2994(7)	-5320(12)	56(5)
C(176)	-2410(11)	-3621(6)	-2955(10)	43(4)
N(147)	-1835(17)	-2715(10)	-5234(16)	107(8)
O(307)	-750(11)	-5114(6)	-3056(10)	81(5)
O(330)	-1939(13)	-4741(7)	1988(11)	96(6)
C(191)	-4325(12)	-3009(7)	-599(11)	52(5)
O(329)	-1605(13)	-5191(7)	1131(12)	100(6)
C(174)	1308(16)	-4810(9)	-1840(14)	74(7)
C(183)	380(20)	-6551(11)	2308(17)	95(9)
O(325)	-4314(13)	-3915(8)	-2535(12)	102(6)
O(328)	-1960(14)	-4497(8)	840(13)	107(7)
O(331)	-5190(16)	-5763(9)	-7169(14)	124(8)
C(192)	-5379(13)	-7096(7)	-7923(12)	59(5)
O(332)	-4180(15)	-5376(8)	-7224(13)	113(7)
C(175)	-265(16)	-4252(9)	-2376(14)	74(7)
O(327)	318(13)	-7237(7)	-63(12)	101(6)
C(189)	-413(16)	-8913(9)	-3885(14)	75(7)
C(190)	-5139(15)	-3448(8)	-1068(13)	67(6)
C(184)	170(20)	-6092(12)	2370(20)	111(11)
N(151)	-1014(18)	-9164(10)	-4019(16)	109(9)
C(179)	-2310(20)	-2973(11)	-5597(18)	95(9)
N(155)	-660(14)	-5916(8)	2399(13)	84(6)
C(195)	-1087(15)	-9506(8)	-3555(13)	67(6)

C(193)	657(19)	-5669(11)	2524(17)	94(9)
C(194)	-800(30)	-5538(16)	2420(20)	137(14)
N(154)	17(19)	-5334(10)	2545(17)	115(9)
O(150)	1110(20)	-7582(12)	-3640(19)	169(12)

APPENDIX N

CRYSTALLOGRAPHIC DATA FOR

$[Eu_{15}(\mu_5\text{-}OH)(I)_2(\mu_3\text{-}OH)_{20}(his^{+/-})_{10}(his^{-})_5(OH)_7](ClO_4)_{10}$

FROM

$[Eu_{15}(\mu_5\text{-}OH)(\mu_3\text{-}OH)_{20}(his^{+/-})_{10}(his^{-})_5(OH)_7](ClO_4)_{12}$

RECRYSTALLIZED FROM L-HISTIDINE BUFFER SOLUTION WITH NaI

Identification code	mes1051	
Empirical formula	C60 H120 Cl7 Eu15 I2 N45 O90	
Formula weight	5693.36	
Temperature	220(2) K	
Wavelength	0.71073 Å	
Crystal system	Monoclinic	
Space group	$P2_1$	
Unit cell dimensions	a = 17.2128(18) Å	α= 90°.
	b = 31.428(4) Å	β= 91.410(5)°.
	c = 18.6837(19) Å	γ = 90°.
Volume	10104(2) $Å^3$	
Z	2	
Density (calculated)	1.871 Mg/m^3	
Absorption coefficient	5.063 mm^{-1}	
F(000)	5370	
Crystal size	0.34 x 0.18 x 0.16 mm^3	
Theta range for data collection	1.09 to 27.85°.	
Index ranges	-22<=h<=22, -41<=k<=41, -24<=l<=24	
Reflections collected	81541	
Independent reflections	46273 [R(int) = 0.0218]	
Completeness to theta = 27.85°	99.3 %	
Max. and min. transmission	0.4980 and 0.2779	
Refinement method	Full-matrix least-squares on F^2	
Data / restraints / parameters	46273 / 1 / 2102	
Goodness-of-fit on F^2	1.206	
Final R indices [I>2sigma(I)]	R1 = 0.0436, wR2 = 0.1325	
R indices (all data)	R1 = 0.0493, wR2 = 0.1439	
Absolute structure parameter	0.021(9)	
Largest diff. peak and hole	2.732 and -2.525 e.$Å^{-3}$	

Atomic coordinates (x 10^4) and equivalent isotropic displacement parameters ($Å^2$x 10^3) for mes1051. U(eq) is defined as one third of the trace of the orthogonalized U^{ij} tensor.

	x	y	z	U(eq)
Eu(1)	-2034(1)	-9224(1)	-1076(1)	20(1)
Eu(14)	-1796(1)	-10212(1)	220(1)	21(1)
Eu(3)	-3242(1)	-9559(1)	-4270(1)	21(1)
Eu(4)	-2058(1)	-10562(1)	-3616(1)	19(1)
Eu(6)	-3797(1)	-8610(1)	-624(1)	23(1)
Eu(13)	5(1)	-10928(1)	-2924(1)	24(1)
Eu(7)	-2033(1)	-8003(1)	-1576(1)	24(1)
Eu(10)	-3951(1)	-10609(1)	-4784(1)	23(1)
Eu(12)	-1990(1)	-11478(1)	-2343(1)	22(1)
Eu(2)	-3271(1)	-8729(1)	-2669(1)	21(1)
Eu(8)	-5040(1)	-8898(1)	-3772(1)	26(1)
Eu(15)	-58(1)	-9543(1)	-556(1)	25(1)
Eu(5)	-1296(1)	-10346(1)	-1694(1)	19(1)
Eu(11)	-1916(1)	-10243(1)	-5529(1)	22(1)
Eu(9)	-3146(1)	-8410(1)	-4720(1)	27(1)
I(16)	-674(1)	-9216(1)	-3355(1)	40(1)
I(17)	-4081(1)	-10177(1)	-1969(1)	39(1)
O(39)	-2996(4)	-9224(2)	-143(4)	28(1)
O(40)	-2801(5)	-9728(2)	666(4)	32(2)
O(21)	-772(4)	-8870(2)	-855(4)	31(2)
O(6)	-3974(4)	-8405(2)	-3667(4)	31(2)
O(16)	-872(4)	-11056(2)	-1951(3)	20(1)
O(9)	-2008(4)	-9915(2)	-4335(3)	23(1)
O(13)	-944(3)	-10340(2)	-2954(3)	19(1)
O(1)	-1997(4)	-8746(2)	-2068(3)	24(1)
O(38)	-1950(5)	-11480(2)	-1030(4)	34(2)
O(7)	-2653(4)	-8918(2)	-3748(3)	25(1)
O(17)	-941(4)	-9608(2)	-1587(4)	23(1)
O(27)	-1085(4)	-10585(2)	-4561(3)	26(1)
O(31)	-4679(4)	-8707(2)	-2533(4)	31(2)
O(37)	-1832(4)	-10800(2)	-722(3)	24(1)

O(10)	-3241(4)	-10026(2)	-5293(4)	27(1)
O(25)	-2641(4)	-9123(2)	-5166(4)	29(1)
O(5)	-3958(4)	-9322(2)	-3277(4)	24(1)
O(36)	-3791(4)	-11318(3)	-4260(4)	34(2)
O(23)	-2556(5)	-8077(2)	-2847(4)	30(2)
O(33)	-4522(4)	-9913(2)	-4508(4)	31(2)
O(28)	-11(4)	-10929(3)	-4230(4)	39(2)
O(35)	-2869(4)	-11213(2)	-3428(4)	27(1)
O(26)	-2029(5)	-9513(3)	-5982(4)	36(2)
O(18)	-2256(3)	-9975(2)	-984(3)	21(1)
O(2)	-3392(4)	-8234(2)	-1685(3)	22(1)
O(11)	-3346(3)	-10268(2)	-3753(3)	21(1)
O(30)	864(4)	-10026(2)	-1101(4)	35(2)
O(29)	116(4)	-10400(2)	-1873(4)	28(1)
O(14)	-2283(3)	-10715(2)	-2350(3)	20(1)
O(34)	-5556(4)	-9475(3)	-4525(5)	38(2)
O(22)	-818(5)	-8168(2)	-906(5)	38(2)
O(3)	-3332(4)	-9122(2)	-1574(4)	24(1)
C(100)	-5135(5)	-8571(3)	-2054(6)	28(2)
Cl(1)	-6397(2)	-851(1)	-1070(2)	40(1)
Cl(2)	-5444(2)	-4349(1)	-3382(2)	49(1)
Cl(3)	-4664(5)	-7385(2)	-2957(4)	58(2)
Cl(4)	-9522(2)	-1351(1)	-219(2)	48(1)
Cl(5)	-8181(2)	-6919(1)	-4748(2)	50(1)
O(106)	-1581(5)	-10155(2)	-6822(4)	38(2)
O(108)	-600(5)	-10223(3)	999(4)	43(2)
O(102)	-3773(4)	-10969(2)	-5895(4)	32(2)
O(100)	-2697(5)	-10696(3)	-6370(4)	43(2)
N(107)	-5053(5)	-10374(3)	-5624(5)	36(2)
O(12)	-2588(4)	-10746(2)	-4771(3)	24(1)
N(13)	1152(5)	-11012(3)	-2002(5)	35(2)
O(24)	-2630(5)	-7837(3)	-3958(4)	39(2)
O(109)	-4953(5)	-8235(4)	-44(7)	62(3)
O(107)	-939(4)	-11976(2)	-2252(5)	38(2)
O(32)	-4986(4)	-8561(3)	-1414(4)	35(2)
O(20)	-691(3)	-10225(2)	-550(3)	22(1)

O(4)	-2377(4)	-8523(2)	-695(4)	27(1)
N(2)	804(6)	-9081(3)	-1340(6)	39(2)
O(111)	-1149(5)	-7353(3)	-1167(5)	49(2)
C(28)	1629(5)	-10179(4)	-2902(5)	33(2)
O(15)	-1279(3)	-11185(2)	-3330(4)	25(1)
C(101)	-3224(6)	-10949(3)	-6351(5)	31(2)
N(5)	-955(6)	-7839(3)	-2508(6)	42(2)
N(10)	-1100(5)	-10899(3)	-5869(5)	32(2)
O(105)	-5551(6)	-8449(4)	-4690(6)	63(3)
O(103)	-2599(5)	-7571(3)	-657(4)	37(2)
N(108)	-4685(6)	-9220(3)	-199(5)	37(2)
N(14)	920(5)	-10315(3)	-3243(5)	36(2)
O(19)	-1322(4)	-9510(2)	-35(3)	25(1)
N(11)	-471(6)	-9981(3)	-5563(6)	43(2)
N(111)	-2479(5)	-12020(3)	-3311(5)	33(2)
C(10)	-927(8)	-7496(4)	-2968(6)	44(3)
N(110)	-1415(5)	-10963(3)	610(5)	34(2)
C(7)	-2554(6)	-7777(3)	-3280(5)	29(2)
O(8)	-4099(4)	-8998(2)	-4678(4)	27(1)
N(109)	-3066(5)	-10645(3)	309(5)	35(2)
O(200)	-7053(5)	-1114(4)	-948(8)	70(4)
C(26)	1446(5)	-10612(4)	-1710(5)	30(2)
O(110)	-2390(7)	-12201(3)	-1789(6)	61(3)
O(201)	-6617(7)	-435(3)	-879(7)	67(3)
O(104)	-3505(5)	-7939(2)	-97(5)	39(2)
Cl(6)	-7371(2)	-1903(1)	-2414(2)	59(1)
Cl(7)	-8481(3)	-3509(2)	-1347(2)	67(1)
N(105)	-6201(6)	-9937(3)	-2394(6)	41(2)
C(25)	760(5)	-10320(3)	-1537(5)	27(2)
O(112)	346(5)	-9808(3)	569(5)	43(2)
C(122)	-3230(8)	-11288(4)	-6924(6)	42(3)
N(106)	-3599(6)	-8682(3)	751(5)	38(2)
C(119)	-6322(5)	-9233(4)	-2363(6)	34(2)
O(113)	-4338(5)	-8073(3)	-5197(5)	44(2)
C(121)	-3074(5)	-9378(3)	475(5)	22(2)
N(112)	-3846(7)	-11618(4)	-6790(7)	53(3)

O(114)	126(4)	-11686(3)	-2684(6)	47(2)
N(8)	-1710(6)	-8337(3)	-4982(6)	40(2)
C(30)	1920(8)	-9843(4)	-3255(8)	46(3)
N(104)	-5915(6)	-9337(3)	-2980(6)	40(2)
C(113)	-3205(8)	-11091(4)	332(6)	40(3)
C(112)	-2595(8)	-11419(4)	489(7)	43(3)
N(103)	-3412(7)	-11525(4)	-2078(7)	53(3)
O(115)	-2045(7)	-10251(5)	1542(5)	75(4)
C(123)	-3349(7)	-11089(5)	-7660(6)	45(3)
C(117)	-4045(8)	-11738(4)	-2484(7)	42(3)
N(4)	-2538(6)	-7327(3)	-2230(5)	38(2)
C(111)	-1774(8)	-11315(3)	202(5)	36(2)
C(4)	1005(6)	-8643(5)	-1271(9)	56(4)
C(120)	-5825(7)	-9764(4)	-2964(7)	37(2)
N(7)	-3099(6)	-8550(3)	-6102(6)	40(2)
N(15)	1421(7)	-9784(4)	-3857(7)	54(3)
C(114)	-3968(8)	-11163(4)	208(7)	48(3)
C(20)	-358(6)	-10946(4)	-5473(5)	35(2)
O(202)	-6184(8)	-865(5)	-1783(7)	78(3)
C(22)	189(7)	-10215(5)	-5694(6)	43(3)
C(116)	-3252(7)	-11925(3)	-3643(6)	35(2)
O(203)	-5750(6)	-1021(4)	-671(6)	63(3)
C(118)	-3903(8)	-12066(4)	-3123(8)	49(3)
C(110)	-1855(6)	-11190(3)	-593(5)	29(2)
C(5)	1002(8)	-9203(4)	-1968(7)	47(3)
C(115)	-3303(5)	-11454(3)	-3775(6)	27(2)
N(1)	272(6)	-8882(3)	207(6)	42(2)
C(16)	-1315(8)	-8457(4)	-5595(8)	50(3)
C(131)	-6025(6)	-10602(4)	-4333(6)	40(2)
C(135)	-4319(8)	-9315(5)	1104(7)	47(3)
C(134)	-3524(7)	-9113(3)	1015(5)	32(2)
N(117)	-4318(7)	-10774(4)	93(7)	50(3)
C(128)	666(7)	-10278(4)	1522(6)	43(3)
C(27)	1984(7)	-10380(4)	-2234(6)	41(3)
N(12)	466(8)	-9521(4)	-5594(7)	58(3)
C(130)	-5618(6)	-10084(4)	-5285(6)	34(2)

C(132)	-6507(7)	-9592(5)	-2018(7)	45(3)
N(3)	1345(7)	-8890(4)	-2347(6)	51(3)
N(113)	-4547(7)	-11392(4)	-1561(7)	55(3)
C(133)	-5941(6)	-8432(4)	-2345(7)	37(2)
C(125)	-192(7)	-11960(3)	-2360(6)	35(2)
N(131)	-3017(6)	-7678(4)	-5326(6)	44(2)
N(9)	-437(7)	-8337(4)	-4733(7)	56(3)
C(1)	-532(6)	-8506(3)	-672(6)	30(2)
N(114)	-5270(6)	-10763(4)	-4188(6)	44(2)
N(115)	-5936(6)	-8373(4)	-3136(6)	44(2)
C(136)	-4725(7)	-9435(4)	454(7)	41(3)
O(213)	-9646(8)	-1635(4)	351(7)	75(3)
C(23)	-293(9)	-9583(5)	-5478(10)	64(4)
O(210)	-7861(10)	-7313(4)	-5003(10)	99(5)
O(211)	-7434(7)	-1490(4)	-2749(7)	70(3)
N(116)	-5531(7)	-9750(4)	-351(7)	53(3)
C(18)	-552(8)	-8435(6)	-5431(11)	68(5)
C(138)	-3760(6)	-10473(4)	147(8)	45(3)
C(127)	101(8)	-10089(4)	971(6)	39(3)
C(126)	294(8)	-12321(5)	-2133(8)	49(3)
C(137)	-5263(8)	-9771(4)	350(9)	54(3)
O(122)	1192(6)	-11213(5)	-3537(6)	76(4)
C(129)	-4717(8)	-11655(5)	-2172(9)	56(4)
C(9)	-1564(11)	-7185(4)	-3166(7)	63(5)
O(212)	-7856(7)	-1888(5)	-1791(7)	80(4)
N(127)	-2527(6)	-6940(4)	305(6)	48(2)
C(141)	-3950(7)	-7141(5)	536(8)	49(3)
N(126)	-6012(8)	-11027(4)	-3344(8)	60(3)
C(139)	-3074(6)	-7629(3)	-177(6)	33(2)
C(15)	-1720(9)	-8553(5)	-6317(7)	55(4)
C(142)	-4111(9)	-10883(5)	-7765(7)	52(3)
C(3)	900(7)	-8394(4)	-647(8)	43(3)
C(6)	1392(7)	-8546(5)	-1958(11)	62(4)
C(19)	-477(5)	-10808(3)	-4701(5)	28(2)
C(148)	579(8)	-12585(4)	-2733(10)	57(4)
C(144)	-5207(6)	-9797(3)	-4740(6)	32(2)

O(217)	-7642(9)	-2232(6)	-2926(7)	99(5)
C(140)	-3115(8)	-7280(4)	411(7)	49(3)
C(8)	-2414(9)	-7329(3)	-2995(6)	43(3)
C(21)	283(7)	-10684(5)	-5797(7)	46(3)
O(215)	-8749(7)	-1404(6)	-410(9)	100(5)
C(13)	-2367(6)	-9182(4)	-5787(6)	32(2)
C(2)	173(8)	-8479(4)	-204(8)	48(3)
C(147)	-6543(6)	-8788(4)	-2174(6)	39(2)
O(216)	-9942(12)	-1494(6)	-835(8)	116(7)
C(143)	-4798(8)	-11110(5)	-7853(9)	57(4)
C(14)	-2460(8)	-8804(4)	-6320(6)	41(3)
C(145)	-6281(7)	-10335(4)	-4933(8)	47(3)
C(146)	-6474(8)	-10760(5)	-3792(10)	62(4)
C(29)	837(7)	-10072(5)	-3805(7)	48(3)
N(125)	-4288(12)	-10425(7)	-7712(11)	100(6)
O(140)	-5039(7)	-7504(3)	-5392(7)	64(3)
C(158)	-3668(12)	-7413(4)	-5129(7)	64(5)
N(157)	-1027(11)	-12851(6)	-4007(10)	88(5)
C(151)	-5175(6)	-9422(4)	-668(7)	39(3)
C(149)	-4363(10)	-7053(5)	-142(8)	57(4)
C(159)	-3693(10)	-6966(4)	-5469(10)	60(4)
C(164)	-398(12)	-12616(6)	-3778(12)	79(6)
N(130)	-4836(10)	-6823(6)	-1169(10)	81(4)
C(17)	-1177(8)	-8273(4)	-4484(8)	49(3)
C(157)	-4428(9)	-7680(4)	-5252(8)	49(3)
N(129)	-4924(11)	-7334(7)	-348(11)	92(5)
N(6)	208(10)	-7861(6)	-2950(10)	82(4)
N(124)	-202(12)	-12596(7)	-1628(11)	99(5)
C(152)	-3747(8)	-11327(5)	-1568(7)	48(3)
O(218)	-6578(7)	-2013(7)	-2213(9)	107(6)
C(12)	-197(10)	-7505(7)	-3264(10)	77(5)
O(219)	-9689(11)	-923(5)	-74(12)	126(7)
C(154)	-67(11)	-12756(5)	-3213(12)	82(6)
C(24)	826(8)	-9898(7)	-5706(9)	75(5)
C(153)	-5069(10)	-10429(5)	-7827(8)	56(3)
C(155)	-5233(13)	-7192(6)	-972(13)	97(8)

C(150)	-5279(10)	-11008(5)	-3571(8)	58(3)
Cl(8)	-8288(3)	-8563(2)	-4285(2)	81(1)
Cl(9)	-2495(3)	-6216(2)	-1517(4)	88(2)
N(148)	-2939(9)	-6451(5)	-4661(9)	73(4)
O(236)	-7758(11)	-8359(6)	-4741(9)	106(6)
N(151)	1409(8)	-10050(5)	1506(8)	66(3)
O(238)	-5535(9)	-7422(5)	-2877(12)	118(7)
C(163)	-121(10)	-10822(9)	2181(9)	81(7)
N(149)	-1781(15)	-6464(9)	-5046(14)	122(8)
O(240)	-4545(13)	-6934(5)	-2959(9)	111(6)
O(237)	-8843(10)	-8274(8)	-4014(13)	143(9)
O(222)	-9285(10)	-3371(7)	-1431(12)	120(6)
C(160)	-3042(14)	-6702(5)	-5249(9)	76(5)
O(234)	-8062(12)	-3485(7)	-1942(8)	122(7)
C(161)	-2251(13)	-6268(8)	-4564(13)	97(7)
O(239)	-4550(12)	-7429(7)	-2753(13)	95(9)
O(220)	-8774(18)	-6975(8)	-4232(16)	231(18)
O(221)	-8079(14)	-3178(8)	-809(13)	140(7)
C(162)	404(11)	-10347(11)	2242(8)	114(11)
O(235)	-7879(12)	-8758(8)	-3668(10)	128(7)
N(156)	-427(13)	-13160(8)	-3006(12)	104(6)
C(11)	-301(9)	-8042(6)	-2521(8)	58(4)
N(150)	-5367(12)	-10784(7)	-7881(12)	100(6)
O(241)	-1940(30)	-6512(7)	-1219(15)	270(20)
O(223)	-8282(18)	-3890(9)	-1085(13)	194(12)
C(168)	-1046(10)	-13201(8)	-3526(10)	79(6)
Cl(11)	-7592(4)	-7421(2)	-2213(6)	128(3)
Cl(10)	-2695(8)	-5210(4)	-3226(7)	209(7)
O(400)	-2315(7)	-9754(5)	-2683(7)	75(3)
C(165)	-4343(8)	-6736(5)	-656(8)	51(3)
O(227)	-4752(16)	-7532(6)	-3707(11)	144(9)
O(225)	-7579(12)	-6706(8)	-4310(20)	236(19)
O(224)	-8441(15)	-6678(5)	-5301(8)	134(8)
C(166)	-2331(15)	-6667(10)	-5507(19)	132(11)
O(232)	-4734(15)	-4481(11)	-2810(20)	218(16)
O(226)	-8820(20)	-8823(15)	-4590(20)	220(17)

O(231)	-2494(13)	-4929(13)	-2691(12)	198(16)
O(242)	-5860(50)	-4072(14)	-2792(18)	430(50)
O(228)	-6100(50)	-7570(40)	-4460(50)	700(60)
O(233)	-5860(50)	-3830(30)	-2760(40)	390(40)
O(230)	-3070(110)	-3740(80)	-5210(100)	700(200)
O(229)	-2200(30)	-5901(9)	-3005(19)	310(30)
O(250)	-3380(40)	-6210(30)	-1610(40)	470(40)
O(251)	-2390(30)	-5810(17)	-600(20)	270(20)
O(252)	-6770(20)	-7281(12)	-2373(19)	212(14)
O(301)	8901(7)	2547(4)	418(7)	71(3)
N(160)	-886(10)	-10860(6)	2432(9)	79(4)
O(303)	5642(9)	8139(6)	4635(9)	97(4)
O(304)	3111(11)	1306(6)	-40(10)	110(5)
O(305)	7149(10)	306(6)	2432(10)	104(5)
O(306)	9512(10)	7704(6)	1138(9)	103(5)
O(308)	1931(11)	1686(7)	1679(11)	118(6)
O(309)	2570(13)	666(7)	80(12)	134(7)
O(310)	6477(12)	7206(7)	4413(11)	124(6)
O(311)	9192(16)	553(9)	2560(14)	160(9)
C(167)	94(13)	-11229(7)	1961(12)	83(5)
N(161)	-559(13)	-11489(7)	2076(12)	98(6)
C(169)	-904(15)	-11363(8)	2384(13)	72(6)

APPENDIX O

CRYSTALLOGRAPHIC DATA FOR

$([(H_2O)_4Eu_2(\kappa^1\text{-pro})(\mu_2\text{-pro})_2](ClO_4)_{2.5})_n$

Identification code	mes104	
Empirical formula	C20 H20 Cl2 Eu2 N8 O20	
Formula weight	1067.26	
Temperature	190(2) K	
Wavelength	0.71073 Å	
Crystal system	Triclinic	
Space group	P1	
Unit cell dimensions	a = 9.8865(11) Å	α= 109.680(5)°.
	b = 13.0234(14) Å	β= 110.403(5)°.
	c = 13.5691(15) Å	γ = 100.847(5)°.
Volume	1446.5(3) $Å^3$	
Z	2	
Density (calculated)	2.450 Mg/m^3	
Absorption coefficient	4.591 mm^{-1}	
F(000)	1032	
Crystal size	0.32 x 0.03 x 0.02 mm^3	
Theta range for data collection	2.22 to 27.88°.	
Index ranges	-13<=h<=12, -17<=k<=17, -17<=l<=17	
Reflections collected	12622	
Independent reflections	12622 [R(int) = 0.0000]	
Completeness to theta = 27.88°	99.8 %	
Max. and min. transmission	0.9138 and 0.3212	
Refinement method	Full-matrix least-squares on F^2	
Data / restraints / parameters	12622 / 3 / 656	
Goodness-of-fit on F^2	1.010	
Final R indices [I>2sigma(I)]	R1 = 0.0476, wR2 = 0.1283	
R indices (all data)	R1 = 0.0619, wR2 = 0.1414	
Absolute structure parameter	0.000(12)	
Largest diff. peak and hole	1.577 and -1.251 e.$Å^{-3}$	

Atomic coordinates (x 10^4) and equivalent isotropic displacement parameters ($Å^2$x 10^3) for mes104. U(eq) is defined as one third of the trace of the orthogonalized U^{ij} tensor.

	x	y	z	U(eq)
Eu(1)	14117(1)	8017(1)	6364(1)	15(1)
Eu(2)	9249(1)	8473(1)	6337(1)	15(1)
Cl(4)	3486(4)	2720(3)	9524(3)	35(1)
Cl(1)	5325(3)	4174(2)	-3200(2)	27(1)
Cl(2)	3066(3)	6561(2)	1695(2)	29(1)
O(1)	14425(8)	6397(6)	5082(7)	22(2)
O(2)	15782(8)	7217(6)	7532(6)	18(2)
O(9)	8751(8)	7797(7)	7690(7)	25(2)
O(15)	9041(7)	10158(6)	7696(6)	17(2)
O(3)	14607(8)	8701(6)	4972(6)	20(2)
O(4)	11788(8)	7095(6)	4475(6)	20(2)
O(16)	11629(8)	9496(6)	8160(6)	22(2)
O(17)	7556(8)	9219(7)	5146(7)	23(2)
O(5)	14303(8)	8918(7)	8336(7)	23(2)
O(18)	9078(8)	7452(7)	4335(6)	24(2)
O(102)	16611(8)	9328(6)	7271(6)	21(2)
O(19)	6853(8)	7039(7)	5336(7)	29(2)
O(20)	10889(8)	9837(6)	6110(6)	23(2)
O(7)	12481(7)	6446(6)	6417(6)	20(1)
O(8)	13050(8)	9449(6)	6382(6)	23(2)
O(21)	10678(7)	7229(6)	6382(6)	21(2)
C(3)	12874(12)	11100(9)	5996(9)	17(2)
C(1)	12218(12)	10030(9)	6184(9)	20(2)
C(2)	11244(10)	6451(8)	6466(8)	13(2)
C(4)	10382(11)	5494(8)	6622(10)	18(2)
O(100)	2706(11)	1962(9)	9848(9)	48(2)
O(101)	5319(12)	3664(10)	-2409(10)	59(3)
N(3)	6418(12)	5840(9)	1278(10)	33(2)
O(22)	7129(8)	7744(6)	3139(6)	32(2)
N(1)	13631(9)	10757(7)	5234(7)	23(2)
O(105)	3782(8)	6635(6)	924(7)	36(2)

O(103)	4795(8)	3231(6)	-4356(7)	40(2)
O(104)	1498(9)	5900(8)	991(8)	50(2)
N(2)	10924(9)	4496(6)	6358(7)	23(2)
C(9)	8008(12)	6290(10)	2268(9)	29(2)
C(8)	8059(10)	7235(8)	3335(8)	19(2)
Cl(5)	7217(3)	1937(2)	5119(3)	35(1)
Cl(7)	856(3)	9519(2)	832(2)	34(1)
O(106)	6835(9)	4933(8)	-2814(10)	53(3)
O(109)	8235(9)	1314(8)	4904(10)	59(3)
O(108)	7115(11)	1995(11)	6170(10)	69(3)
O(112)	3246(10)	7719(8)	2452(8)	48(2)
O(111)	3813(12)	6008(9)	2354(9)	62(3)
O(107)	4294(9)	4816(7)	-3262(9)	50(2)
C(10)	11680(11)	11496(8)	5325(9)	27(2)
O(110)	5724(10)	1340(8)	4183(8)	54(2)
Cl(6)	23(4)	3678(3)	2999(3)	38(1)
C(20)	7866(11)	10126(8)	7896(9)	13(2)
C(15)	15628(12)	6252(8)	5027(9)	18(2)
N(4)	14001(9)	4151(7)	3914(8)	32(2)
N(5)	9590(9)	11940(7)	9699(7)	28(2)
O(116)	814(9)	8451(7)	0(7)	43(2)
C(17)	13736(15)	3286(11)	2778(11)	41(3)
C(25)	8037(18)	13068(12)	9465(15)	53(4)
C(24)	9590(20)	13078(14)	9610(20)	76(6)
O(117)	17(11)	9257(9)	1449(8)	60(3)
C(23)	7970(9)	11107(8)	8966(8)	23(2)
C(16)	15627(10)	5017(8)	4484(8)	22(2)
C(26)	6969(15)	11769(12)	8558(12)	49(3)
C(18)	15375(16)	3432(12)	2821(12)	44(3)
C(27)	10693(13)	5877(9)	7904(10)	36(2)
C(19)	16166(12)	4726(9)	3543(10)	32(2)
O(113)	778(17)	3547(13)	4010(10)	109(6)
O(114)	-444(19)	2677(10)	1997(11)	117(6)
O(115)	-1210(20)	3944(17)	3020(30)	211(14)
O(23)	15213(9)	7937(6)	9339(6)	37(2)
C(33)	14642(11)	8677(8)	9214(8)	27(2)

C(34)	14414(12)	9446(10)	10230(9)	33(2)
C(28)	6546(13)	5953(12)	242(9)	44(3)
C(32)	11323(14)	4170(11)	7326(12)	43(3)
C(29)	11076(13)	10615(13)	4054(11)	50(3)
C(30)	12405(13)	10222(13)	3989(10)	48(3)
C(31)	10555(15)	4775(11)	8071(11)	46(3)
O(118)	2435(9)	10194(7)	1636(7)	45(2)
C(21)	9088(12)	6828(15)	1833(10)	57(4)
O(121)	7796(9)	3081(7)	5233(9)	45(2)
O(119)	192(14)	10100(9)	203(9)	71(3)
O(120)	5132(13)	3194(15)	10239(15)	112(6)
O(122)	1060(10)	4633(8)	3003(9)	47(2)
C(22)	8255(16)	6304(17)	573(13)	76(5)
C(37)	14606(11)	8980(8)	11100(8)	24(2)
C(36)	16267(17)	9532(12)	11990(11)	61(4)
N(6)	15690(20)	10658(12)	10899(13)	93(5)
C(35)	16967(17)	10541(14)	11709(15)	67(5)
O(127)	3760(40)	1930(17)	8607(18)	360(30)
O(128)	3020(30)	3655(18)	9650(30)	251(18)

APPENDIX P

CRYSTALLOGRAPHIC DATA FOR

$(H_3O)_2[\alpha\text{-}W_6(\mu_2\text{-}O)_6(\mu_2\text{-}Cl)_6Cl_6]\cdot 4H_2O$

Identification code	mes1114	
Empirical formula	C H2 Cl6 O6 W6	
Formula weight	1425.83	
Temperature	190(2) K	
Wavelength	0.71073 Å	
Crystal system	Monoclinic	
Space group	$P2_1/n$	
Unit cell dimensions	a = 8.3379(9) Å	α= 90°.
	b = 11.9803(13) Å	β= 90.588(5)°.
	c = 13.9222(15) Å	γ = 90°.
Volume	1390.6(3) $Å^3$	
Z	2	
Density (calculated)	3.405 Mg/m^3	
Absorption coefficient	25.295 mm^{-1}	
F(000)	1204	
Crystal size	0.21 x 0.04 x 0.03 mm^3	
Theta range for data collection	2.24 to 27.92°.	
Index ranges	-10<=h<=10, -15<=k<=15, -18<=l<=18	
Reflections collected	11708	
Independent reflections	3301 [R(int) = 0.0437]	
Completeness to theta = 27.92°	99.2 %	
Max. and min. transmission	0.5174 and 0.0761	
Refinement method	Full-matrix least-squares on F^2	
Data / restraints / parameters	3301 / 0 / 145	
Goodness-of-fit on F^2	1.293	
Final R indices [I>2sigma(I)]	R1 = 0.0501, wR2 = 0.1598	
R indices (all data)	R1 = 0.0596, wR2 = 0.1665	
Largest diff. peak and hole	4.453 and -4.439 e.$Å^{-3}$	

Atomic coordinates (x 10^4) and equivalent isotropic displacement parameters ($Å^2$x 10^3) for mes1114. U(eq) is defined as one third of the trace of the orthogonalized U^{ij} tensor.

	x	y	z	U(eq)
W(1)	1261(1)	1403(1)	-4(1)	18(1)
W(2)	1247(1)	-697(1)	-1047(1)	19(1)
W(3)	1297(1)	-694(1)	1043(1)	19(1)
Cl(4)	2631(4)	3162(2)	-9(2)	27(1)
Cl(3)	2633(4)	-1612(3)	-2328(2)	38(1)
Cl(2)	2729(4)	-1604(3)	2329(2)	36(1)
O(1)	-51(10)	2033(6)	-1006(6)	23(2)
O(2)	-17(10)	2032(7)	996(6)	26(2)
O(3)	-12(10)	-5(6)	-2031(6)	27(2)
Cl(5)	3190(4)	810(2)	-1206(2)	23(1)
Cl(6)	3253(4)	817(2)	1193(2)	27(1)
Cl(7)	3250(4)	-1577(2)	-2(2)	27(1)
O(10)	983(13)	930(9)	6045(8)	42(2)
O(11)	1079(15)	951(11)	3943(8)	51(3)
O(12)	842(17)	5785(10)	1400(14)	82(5)
O(13)	773(16)	5728(10)	8779(18)	108(8)

APPENDIX Q

CRYSTALLOGRAPHIC DATA FOR

$(H_3O)_2[\beta\text{-}W_6(\mu_2\text{-}O)_6(\mu_2\text{-}Cl)_6Cl_6]\cdot 6H_2O$

Identification code	mes1046	
Empirical formula	C2 H6 Cl10 N Na2 O4 W6	
Formula weight	1611.66	
Temperature	190(2) K	
Wavelength	0.71073 Å	
Crystal system	Triclinic	
Space group	P-1	
Unit cell dimensions	a = 8.7223(10) Å	α= 102.464(5)°.
	b = 8.9895(10) Å	β= 102.253(5)°.
	c = 10.4878(11) Å	γ = 109.907(5)°.
Volume	717.49(14) $Å^3$	
Z	1	
Density (calculated)	3.730 Mg/m^3	
Absorption coefficient	24.919 mm^{-1}	
F(000)	693	
Crystal size	0.12 x 0.07 x 0.01 mm^3	
Theta range for data collection	2.09 to 27.99°.	
Index ranges	-11<=h<=11, -11<=k<=11, -13<=l<=13	
Reflections collected	6225	
Independent reflections	3426 [R(int) = 0.0243]	
Completeness to theta = 27.99°	98.9 %	
Max. and min. transmission	0.7887 and 0.1539	
Refinement method	Full-matrix least-squares on F^2	
Data / restraints / parameters	3426 / 0 / 146	
Goodness-of-fit on F^2	1.252	
Final R indices [I>2sigma(I)]	R1 = 0.0526, wR2 = 0.1256	
R indices (all data)	R1 = 0.0671, wR2 = 0.1704	
Extinction coefficient	0.0098(7)	
Largest diff. peak and hole	8.514 and -7.536 e.$Å^{-3}$	

Atomic coordinates (x 10^4) and equivalent isotropic displacement parameters ($Å^2$x 10^3) for mes1046. U(eq) is defined as one third of the trace of the orthogonalized U^{ij} tensor.

	x	y	z	U(eq)
W(1)	16840(1)	15973(1)	14210(1)	16(1)
W(2)	13401(1)	15079(1)	13398(1)	16(1)
W(4)	15340(1)	17194(1)	16179(1)	16(1)
Cl(1)	19221(4)	16120(4)	16017(3)	22(1)
Cl(2)	17660(4)	18884(3)	15481(3)	22(1)
Cl(4)	11592(4)	15179(4)	11343(3)	26(1)
Cl(3)	13427(4)	17763(3)	14486(3)	22(1)
Cl(5)	15697(4)	19775(4)	17734(4)	28(1)
Cl(6)	18921(4)	16975(4)	13091(3)	28(1)
O(1)	15239(12)	16161(11)	12745(9)	21(2)
O(2)	12958(11)	12854(11)	12328(9)	20(2)
O(3)	16568(12)	13802(11)	13208(9)	22(2)
O(10)	12382(13)	17382(13)	18976(11)	36(2)
O(11)	14598(14)	22723(13)	19550(12)	41(2)
O(13)	11971(16)	20143(14)	18692(12)	47(3)
O(12)	-164(14)	11290(14)	9304(12)	46(3)

APPENDIX R

CRYSTALLOGRAPHIC DATA FOR

RECRYSTALLIZED

$(H_3O)_2[\alpha\text{-}W_6(\mu_2\text{-}O)_6(\mu_2\text{-}Cl)_6Cl_6]\cdot 4H_2O$

Identification code	mes116	
Empirical formula	C2 H4 Cl10 O6 W6	
Formula weight	1581.65	
Temperature	190(2) K	
Wavelength	0.71073 Å	
Crystal system	Hexagonal	
Space group	R-3	
Unit cell dimensions	a = 9.1077(16) Å	α= 90°.
	b = 9.1077(16) Å	β= 90°.
	c = 48.023(7) Å	γ = 120°.
Volume	3449.8(10) $Å^3$	
Z	3	
Density (calculated)	2.284 Mg/m^3	
Absorption coefficient	15.531 mm^{-1}	
F(000)	2034	
Crystal size	0.06 x 0.05 x 0.02 mm^3	
Theta range for data collection	1.27 to 25.38°.	
Index ranges	-10<=h<=10, -10<=k<=10, -56<=l<=56	
Reflections collected	4970	
Independent reflections	1391 [R(int) = 0.1262]	
Completeness to theta = 25.38°	98.8 %	
Max. and min. transmission	0.7464 and 0.4559	
Refinement method	Full-matrix least-squares on F^2	
Data / restraints / parameters	1391 / 0 / 67	
Goodness-of-fit on F^2	3.322	
Final R indices [I>2sigma(I)]	R1 = 0.2217, wR2 = 0.5017	
R indices (all data)	R1 = 0.2542, wR2 = 0.5098	
Largest diff. peak and hole	17.155 and -8.135 e.$Å^{-3}$	

Atomic coordinates (x 10^4) and equivalent isotropic displacement parameters ($Å^2$x 10^3) for mes116. U(eq) is defined as one third of the trace of the orthogonalized U^{ij} tensor.

	x	y	z	U(eq)
W(1)	1670(5)	6965(5)	1447(1)	23(1)
W(2)	-8315(4)	1969(5)	218(1)	22(1)
Cl(3)	1150(20)	4870(30)	1098(5)	23(6)
Cl(4)	-7770(30)	360(30)	559(6)	30(7)
Cl(1)	-320(30)	7430(30)	1198(7)	40(7)
Cl(5)	-6290(30)	4490(40)	464(7)	42(7)
O(2)	-8430(50)	4580(60)	-223(11)	0(10)
O(10)	-310(60)	7890(60)	1442(11)	0(10)
O(1)	-180(80)	5140(90)	1638(14)	28(16)

REFERENCES

1. Roberts, T. P. L., *Basic Principles In Magnetic Resonance Imaging of the Body*. Third ed.; Lippincott-Raven Press: New York, 1997.

2. Wolbarst, A. B., *Physics of Radiology*. Medical Physics Publishing: Madison, 1993.

3. Alliance, M. I. a. T. Medical Imaging Primer. http://www.medicalimaging.org/medical-imaging-primer/ (accessed March).

4. (a) Roobottom, C. A.; Mitchell, G.; Morgan-Hughes, G., Radiation-reduction strategies in cardiac computed tomographic angiography. *Clinical Radiology* **2010,** *65* (11), 859-867; (b) De Santis, M.; Cesari, E.; Nobili, E.; Straface, G.; Cavaliere, A. F.; Caruso, A., Radiation effects on development. *Birth Defects Research Part C: Embryo Today: Reviews* **2007,** *81* (3), 177-182.

5. Galanti, L. X-ray Photography as Art: Hidden Faces of The Inner Space. http://www.cultcase.com/2008/05/x-ray-photography-as-art-hidden-faces.html (accessed March).

6. Oldendorf, W., *Basics of Magnetic Resonance Imaging*. Martinus Nijoff Publishing: Boston, 1988.

7. Krause, W.; Schneider, P., Chemistry of X-Ray Contrast Agents. In *Contrast Agents II*, Krause, W., Ed. Springer Berlin / Heidelberg: 2002; Vol. 222, pp 107-150.

8. Sprawls, P. Physical Principles of Medical Imaging Online, Resources for Learning and Teaching. http://www.sprawls.org/resources/.

9. Skucas, J., *Radiographic Contrast AGents*. 2nd ed.; Aspen Publishers: Rockville, Madison, 1989.

10. Busch, U., Progress in Radiology in1896. *The Newsletter of the Radiology History and Heritage Charitable Trus* 1999, pp 1-24.

11. Alsalam, H. Right Sided Aortic Arch. http://radiopaedia.org/cases/right-sided-aortic-arch (accessed March).

12. Davidson, J. K. Oxford Companion to the Body: X-rays. http://www.answers.com/topic/x-ray (accessed March).

13. Chellquist, E. W., S. Strasters, J. Wolfe, H. Stroflor, H., The effect of glucose and coppe on teh stability of diatrizoic acid. *PDA J ournal of Pharmaceutical Science and Technology* **1999,** *5* (53), 247-251.

14. Priebe, H.; Aukrust, A.; Bjørsvik, H. R.; Tønseth, C. P.; Wiggen, U. N., Stability of the X-ray contrast agent iodixanol=3,3′,5,5′-tetrakis(2,3-dihydroxypropylcarbamoyl)-2,2′,4,4′,6,6′-hexaiodo-N,N′-(2-hydroxypropane-1,3-diyl)-diacetanilide towards acid, base, oxygen, heat and light. *Journal of Clinical Pharmacy and Therapeutics* **1999,** *24* (3), 227-235.

15. Jacobsen, P. B., Larsen, A., Konarboland, R., Skotland, T., Biotransformation of nonionic X-ray contrast agents in vivo and in vitro. *Drug Metabolism and Disposition* **1999,** *27* (10), 1205-1213.

16. (a) Helaine, A. MRI Contrast Problems. http://www.ehow.com/about_5474651_mri-contrast-problems.html (accessed March); (b) Committee, A., ACR Committee on Drugs and Contrast Media. In *ACR Manual on Contrast Media*, 2010; pp 1-81; (c) Brasch, R., Contrast media toxicity in children. *Pediatric Radiology* **2008,** *38* (0), 281-284.

17. (a) Messerle, L.; Nolting, D.; Bolinger, L.; Stolpen, A. H.; Mullan, B. F.; Swenson, D.; Madsen, M., Transition Metal Cluster and Polygadolinium Compounds as a New Paradigm For High Attenuation and/or Relaxivity in Contrast Media Design: Crashing The Molecular r1 = 100 Barrier. *Academic radiology* **2005,** *12* (5), S46-S47; (b) Brian F. Mullan, M. T. M., Louis Messerle, Vladimir Kolesnickenko, Jason Kruger, X-ray Attenuation Coefficients of High-Atomic-Number, Hexanuclear Transition Metal Cluster Compounds: A New Paradigm for Radiographic Contrast Agents. *Academic radiology* **2000,** *7* (4), 254-259; (c) Yu, S.-B.; Watson, A. D., Metal-Based X-ray Contrast Media. *Chemical Reviews* **1999,** *99* (9), 2353-2378.

18. (a) Merbach, A. E., *The Chemistry of Contrast Agents in Medicical Magnetic Resonance Imaging*. John Wiley and Sons, LTD: Chichester, 2001; (b) Hornak, J. P. The Basics of MRI. http://www.cis.rit.edu/htbooks/mri/index.html.

19. Gould, T. A., How MRI Works. **2011**.

20. Caravan, P.; Ellison, J. J.; McMurry, T. J.; Lauffer, R. B., Gadolinium(III) Chelates as MRI Contrast Agents: Structure, Dynamics, and Applications. *Chemical Reviews* **1999,** *99* (9), 2293-2352.

21. Tóth, É.; Helm, L.; Merbach, A., Relaxivity of MRI Contrast Agents. In *Contrast Agents I*, Krause, W., Ed. Springer Berlin / Heidelberg: 2002; Vol. 221, pp 61-101.

22. Hohenschuh, E. W., A.D., *Contrast Media: Theory and Mechanisms of Contrast-Enhancing Agents. In Magnetic Resonance Imaging of the Body*. Third ed.; Lippin-Raven Press: New York, 1997.

23. Bea, The commercial chemist. In *MRI contrast agent approved*, July 31, 2008 ed.; RSC: 2008.

24. Moore, E. C. a. E. Metals in Medicine. http://prospect.rsc.org/metalsandlife/index.html (accessed March).

25. Propkop, M., CT and MR to Assess the Response of Liver Tumors to Hepatic Perfusion. *Recent Results in Cancer Research* **1998,** *147*, 136-154.

26. Lauffer, R. B., Paramagnetic metal complexes as water proton relaxation agents for NMR imaging: theory and design. *Chemical Reviews* **1987,** *87* (5), 901-927.

27. Aime, S.; Fasano, M.; Terreno, E., Lanthanide(III) chelates for NMR biomedical applications. *Chemical Society Reviews* **1998,** *27* (1), 19-29.

28. Aime, S.; Botta, M.; Fasano, M.; Paoletti, S.; Terreno, E., Relaxometric Determination of the Exchange Rate of the Coordinated Water Protons in a Neutral GdIII Chelate. *Chemistry – A European Journal* **1997,** *3* (9), 1499-1504.

29. Lauffer, R. B., Magnetic Resonance Contrast Media: Principles and Progress. *Magnetic Resonance Quarterly* **1990,** *2* (6), 65-84.

30. (a) Desreux, J. F.; Merciny, E.; Loncin, M. F., Nuclear magnetic resonance and potentiometric studies of the protonation scheme of two tetraaza tetraacetic macrocycles. *Inorganic Chemistry* **1981,** *20* (4), 987-991; (b) Desreux, J. F., Nuclear magnetic resonance spectroscopy of lanthanide complexes with a tetraacetic tetraaza macrocycle. Unusual conformation properties. *Inorganic Chemistry* **1980,** *19* (5), 1319-1324.

31. Lauffer, R. B.; Brady, T. J., Preparation and water relaxation properties of proteins labeled with paramagnetic metal chelates. *Magnetic Resonance Imaging* **1985,** *3* (1), 11-16.

32. (a) Abe, A. S. H. H. M., Synthesis and applications of magnetic nanoparticles for biorecognition and point of car medical diagnostics. *Nanotechnology* **2010,** *21* (44), 442001/1-442001/22; (b) Khemtong, C.; Kessinger, C. W.; Gao, J., Polymeric nanomedicine for cancer MR imaging and drug delivery. *Chemical Communications* **2009,** (24), 3497-3510.

33. Della Rocca, J.; Lin, W., Nanoscale Metal–Organic Frameworks: Magnetic Resonance Imaging Contrast Agents and Beyond. *European Journal of Inorganic Chemistry* **2010,** *2010* (24), 3725-3734.

34. Krause, W., *Magnetic Resonance Imaging*. Springer: Germany, 2002; Vol. 221.

35. Broome, D. R.; Girguis, M. S.; Baron, P. W.; Cottrell, A. C.; Kjellin, I.; Kirk, G. A., Gadodiamide-Associated Nephrogenic Systemic Fibrosis: Why Radiologists Should Be Concerned. *Am. J. Roentgenol.* **2007,** *188* (2), 586-592.

36. (a) Gibson, S. E., Farver, C.F., Prayson, R.A., Multiorgan involvement in nephrogenic fibrosing dermopathy: an autopsy case and review of the literature. *Archives of Pathology and Laboratory Medicine* **2006,** *130* (2), 209-212; (b) Daram, S. R., Cortese, C.M., Bastani, B., Nephrogenic fibrosing dermopathy/nehprogenic systemic fibrosis: report of a new case with literature review. *American Journal of Kidney Diseases* **2005,** *46* (4), 754-759.

37. (a) Giester, G.; Unfried, P.; ák, Z., Syntheses and crystal structures of some new rare earth basic nitrates II: $[Ln_6O(OH)_8(H_2O)_{12}(NO_3)_6](NO_3)_2{\cdot}xH_2O$, Ln=Sm, Dy, Er; x(Sm)=6, x(Dy)=5, x(Er)=4. *Journal of Alloys and Compounds* **1997,** *257* (1-2), 175-181; (b) Zák, Z.; Unfried, P.; Giester, G., The structures of some rare earth basic nitrates $[Ln_6(\mu_6\text{-}O)(\mu_3\text{-}OH)_8(H_2O)_{12}(NO_3)_6](NO_3)_2 \cdot xH_2O$, Ln = Y, Gd, Yb, x(Y, Yb) = 4; x(Gd) = 5. A novel rare earth metal cluster of the M_6X_8 type with interstitial O atom. *Journal of Alloys and Compounds* **1994,** *205* (1-2), 235-242.

38. Lam, A. W.-H.; Wong, W.-T.; Wen, G.; Zhang, X.-X.; Gao, S., Synthesis, crystal structure and magnetic properties of μ_4-oxo-centered tetranuclear lanthanide clusters. *New Journal of Chemistry* **2001,** *25* (4), 531-533.

39. Wang, R.; Carducci, M. D.; Zheng, Z., Direct Hydrolytic Route to Molecular Oxo−Hydroxo Lanthanide Clusters. *Inorganic Chemistry* **2000,** *39* (9), 1836-1837.

40. Xiao-Ming, C.; Yu-Luan, W.; Ye-Xiang, T.; Ziming, S.; Hendrickson, D. N., Tetra(μ_3-hydroxo)hexa(μ_2-carboxylato-O,O')-bridged tetranuclear terbium(III) cubane complex. *Polyhedron* **1997,** *16* (24), 4265-4272.

41. Zhang, D.-S.; Ma, B.-Q.; Jin, T.-Z.; Gao, S.; Yan, C.-H.; Mak, T. C. W., Oxo-centered regular octahedral lanthanide clusters. *New Journal of Chemistry* **2000,** *24* (2), 61-62.

42. Zheng, X.-J.; Jin, L.-P.; Gao, S., Synthesis and Characterization of Two Novel Lanthanide Coordination Polymers with an Open Framework Based on an Unprecedented $[Ln_7(\mu_3\text{-}OH)_8]^{13+}$ Cluster. *Inorganic Chemistry* **2004,** *43* (5), 1600-1602.

43. Wang, R.; Selby, H. D.; Liu, H.; Carducci, M. D.; Jin, T.; Zheng, Z.; Anthis, J. W.; Staples, R. J., Halide-Templated Assembly of Polynuclear Lanthanide-Hydroxo Complexes†. *Inorganic Chemistry* **2002,** *41* (2), 278-286.

44. Wang, R.; Zheng, Z.; Jin, T.; Staples, R. J., Coordination Chemistry of Lanthanides at "High" pH: Synthesis and Structure of the Pentadecanuclear Complex of Europium(III) with Tyrosine. *Angewandte Chemie International Edition* **1999,** *38* (12), 1813-1815.

45. (a) Zheng, Z., Ligand-controlled self-assembly of polynuclear lanthanide-oxo/hydroxo complexes: from synthetic serendipity to rational supramolecular design. *Chemical Communications* **2001,** (24), 2521-2529; (b) Wang, R.; Liu, H.; Carducci, M. D.; Jin, T.; Zheng, C.; Zheng, Z., Lanthanide Coordination with α-Amino Acids under Near Physiological pH Conditions: Polymetallic Complexes Containing the Cubane-Like $[Ln_4(\mu_3\text{-}OH)_4]^{8+}$ Cluster Core. *Inorganic Chemistry* **2001,** *40* (12), 2743-2750.

46. (a) Choppin, J.-C. G. B. a. G. R., *Lanthanide Probes in Life, Chemical and Earth Sciences Theory and Practice*. Elsevier Sceince Publishing Company Inc.: New York, 1989; (b) Cotton, S., *Lanthanide and Actinide Chemistry*. John Wiley and Sons, Ltd: Chichester, 2005.

47. (a) Gatteschi, D.; Caneschi, A.; Sessoli, R.; Cornia, A., Magnetism of large iron-oxo clusters. *Chemical Society Reviews* **1996,** *25* (2), 101-109; (b) Decurtins, S.; Gross, M.; Schmalle, H. W.; Ferlay, S., Molecular Chromium(III)−Lanthanide(III) Compounds (Ln = La, Ce, Pr, Nd) with a Polymeric, Ladder-Type Architecture: A Structural and Magnetic Study. *Inorganic Chemistry* **1998,** *37* (10), 2443-2449; (c) Peng, J.-B.; Ren, Y.-P.; Kong, X.-J.; Long, L.-S.; Huang, R.-B.; Zheng, L.-S., A series of di-, tri- and tetranuclear lanthanide clusters with slow magnetic relaxation for Dy2 and Dy4. *CrystEngComm* **2011,** *13* (6), 2084-2090.

48. (a) Major, J. L.; Meade, T. J., Bioresponsive, Cell-Penetrating, and Multimeric MR Contrast Agents. *Accounts of Chemical Research* **2009,** *42* (7), 893-903; (b) Aime, S.; Castelli, D. D.; Crich, S. G.; Gianolio, E.; Terreno, E., Pushing the Sensitivity Envelope of Lanthanide-Based Magnetic Resonance Imaging (MRI) Contrast Agents for Molecular Imaging Applications. *Accounts of Chemical Research* **2009,** *42* (7), 822-831.

49. Schuetz, S. A.; Day, V. W.; Clark, J. L.; Belot, J. A., Direct synthesis of a tetranuclear erbium(III) hydroxo cluster bearing a saturated Schiff base. *Inorganic Chemistry Communications* **2002,** *5* (9), 706-710.

50. (a) Squire, R. C.; Aubin, S. M. J.; Folting, K.; Streib, W. E.; Christou, G.; Hendrickson, D. N., Octadecanuclearity in Manganese Carboxylate Chemistry: Preparation and Properties of $K_4[Mn_{18}O_{16}(O_2CPh)_{22}(phth)_2(H_2O)_4]\cdot 10MeCN$. *Inorganic Chemistry* **1995,** *34* (26), 6463-6471; (b) Watton, S. P.; Fuhrmann, P.; Pence, L. E.; Lippard, S. J.; Caneschi, A.; Cornia, A.; Abbati, G. L., A Cyclic Octadecairon(III) Complex, the Molecular 18-Wheeler. *Angewandte Chemie International Edition in English* **1997,** *36* (24), 2774-2776.

51. Tasiopoulos, A. J.; O'Brien, T. A.; Abboud, K. A.; Christou, G., Mixed Transition-Metal—Lanthanide Complexes at Higher Oxidation States: Heteronuclear CeIV–MnIV Clusters. *Angewandte Chemie International Edition* **2004,** *43* (3), 345-349.

52. (a) Helgesson, G.; Jagner, S.; Poncelet, O.; Hubert-Pfalzgraf, L. G., Synthesis and molecular structure of $Nd_5(\mu_5\text{-}O)(\mu_3\text{-}OR)_2(\mu_2\text{-}OR)_6(OR)_5(ROH)_2$ (R = Pri). The first example of a trigonal bipyramidal metal oxoalkoxide. *Polyhedron* **1991,** *10* (13), 1559-1564; (b) Evans, W. J.; Greci, M. A.; Ziller, J. W., Reactivity of "$Eu(O^iPr)_2$" with Phenols:□ Formation of Linear Eu_3, Square Pyramidal Eu_5, Cubic Eu_8, and Capped Cubic Eu_9 Polymetallic Europium Complexes. *Inorganic Chemistry* **2000,** *39* (15), 3213-3220; (c) Westin, G.; Moustiakimov, M.; Kritikos, M., Synthesis, Characterization, and Properties of Three Europium 2-Propoxides:□ $[Eu_4(OPr^i)_{10}(HOPr^i)_3]$*2HOPri, $Eu_5O(OPr^i)_{13}$, and $EuAl_3(OPr^i)_{12}$. *Inorganic Chemistry* **2002,** *41* (12), 3249-3258.

53. Caneschi, A.; Cornia, A.; Lippard, S. J., A Cyclic Hexairon(III) Complex with an Octahedrally Coordinated Sodium Ion at the Center, an Example of the [12]Metallacrown-6 Structure Type. *Angewandte Chemie International Edition in English* **1995,** *34* (4), 467-469.

54. Abbati, G. L.; Cornia, A.; Fabretti, A. C.; Caneschi, A.; Gatteschi, D., A Ferromagnetic Ring of Six Manganese(III) Ions with a S = 12 Ground State. *Inorganic Chemistry* **1998,** *37* (7), 1430-1431.

55. Zucchi, C.; Shchegolikhina, O. I.; Borsari, M.; Cornia, A.; Gavioli, G.; Fabretti, A. C.; Rentschler, E.; Gatteschi, D.; Ugo, R.; Psaro, R.; Pozdniakova, Y. A.; Lindeman, S. V.; Zhdanov, A. A.; Pályi, G., Cyclooligosiloxanolate cluster complexes of transition metals and lanthanides. *Journal of Molecular Catalysis A: Chemical* **1996,** *107* (1-3), 313-321.

56. Liu, J.; Meyers, E. A.; Shore, S. G., An Unusual Cyanide Bridging Lanthanide−Transition Metal Complex that Contains the One-Dimensional Cationic Array $\{[(DMF)_{16}Yb_6(\mu_6\text{-}O)(\mu_3\text{-}OH)_8(\mu\text{-}NC)Pd(\mu\text{-}CN)(CN)_2]^{6+}\}\infty$. *Inorganic Chemistry* **1998,** *37* (21), 5410-5411.

57. Mudring, A.-V.; Babai, A., $[Nd_6(\mu_6\text{-}O)(\mu_3\text{-}OH)_8(H_2O)_{24}]I_8(H_2O)_{12}$ - the First Basic Rare Earth Iodide with an Oxygen-centred M6X8-Cluster Core. *Zeitschrift für anorganische und allgemeine Chemie* **2005,** *631* (2-3), 261-263.

58. Kong, X.-J.; Wu, Y.; Long, L.-S.; Zheng, L.-S.; Zheng, Z., A Chiral 60-Metal Sodalite Cage Featuring 24 Vertex-Sharing $[Er_4(\mu_3\text{-}OH)_4]$ Cubanes. *Journal of the American Chemical Society* **2009,** *131* (20), 6918-6919.

59. (a) Anwander, R., "Self-Assembly" in Organolanthanide Chemistry: Formation of Rings and Clusters. *Angewandte Chemie International Edition* **1998,** *37* (5), 599-602; (b) Kretschmer, W. P.; Teuben, J. H.; Troyanov, S. I., Novel, Highly Symmetrical Halogen-Centered Polynuclear Lanthanide Complexes: $[Cp_6Yb_6Cl_{13}]^-$ and $[Cp_{12}Sm_{12}Cl_{24}]$. *Angewandte Chemie International Edition* **1998,** *37* (1-2), 88-90; (c) Watson, P. L.; Tulip, T. H.; Williams, I., Defluorination of perfluoroolefins by divalent lanthanoid reagents: activating carbon-fluorine bonds. *Organometallics* **1990,** *9* (7), 1999-2009; (d) Evans, W. J.; Sollberger, M. S., Synthetic and structural studies on the formation of a tetradecametallic yttrium oxide alkoxide chloride complex: an example of how molecular yttrium oxygen frameworks form extended arrays. *Inorganic Chemistry* **1988,** *27* (24), 4417-4423; (e) Andersen, R. A.; Templeton, D. H.; Zalkin, A., Synthesis and crystal structure of a neodymium isopropoxide chloride, $Nd_6[OCH(CH_3)_2]_{17}Cl$. *Inorganic Chemistry* **1978,** *17* (7), 1962-1965; (f) Xiong, R.-G.; Zuo, J.-L.; Yu, Z.; You, X.-Z.; Chen, W., $Eu_5(\mu_4\text{-}OH)(\mu_3\text{-}OH)_4(\mu\text{-}DBM)_4(DBM)_6$ (DBM=dibenzoylmethide): a novel Eu_5 square-pyramid polynuclear complex with a rare μ_4-OH bridging mode. *Inorganic Chemistry Communications* **1999,** *2* (10), 490-494; (g) Pernin, C. G.; Ibers, J. A., Octanuclear Rare-Earth Clusters. *Journal of Cluster Science* **1999,** *10* (1), 71-90.

60. Deschamps, P.; Kulkarni, P. P.; Gautam-Basak, M.; Sarkar, B., The saga of copper(II)-l-histidine. *Coordination Chemistry Reviews* **2005,** *249* (9-10), 895-909.

61. Hill, R. W., The specific heats of Tb_2O_3 and Tb_4O_7 between 0.5 and 22 K. *Journal of Physics C: Solid State Physics* **1986,** *19*, 673-682.

62. McCaldin, D. J., The Chemistry of Ninhydrin. *Chemical Reviews* **1960,** *60* (1), 39-51.

63. (a) Ma, B.-Q.; Zhang, D.-S.; Gao, S.; Jin, T.-Z.; Yan, C.-H., The formation of Gd_4O_4 cubane cluster controlled by L-valine. *New Journal of Chemistry* **2000,** *24* (5), 251-252; (b) Ma, B.-Q.; Zhang, D.-S.; Gao, S.; Jin, T.-Z.; Yan, C.-H.; Xu, G.-X., From Cubane to Supercubane: The Design, Synthesis, and Structure of a Three-Dimensional Open Framework Based on a Ln_4O_4 Cluster. *Angewandte Chemie International Edition* **2000,** *39* (20), 3644-3646.

64. Wang, R.; Song, D.; Wang, S., Toward Constructing Nanoscale Hydroxo-lanthanide Clusters: Syntheses and Characterizations of Novel Tetradecanuclear Hydroxo-lanthanide Clsuters. *Chemical Communications* **2002,** *4*, 368-369.

65. (a) Kong, X.-J.; Long, L.-S.; Zheng, Z.; Huang, R.-B.; Zheng, L.-S., Keeping the Ball Rolling: Fullerene-Like Molecular Clusters. *Accounts of Chemical Research* **2010,** *43* (2), 201-209; (b) Kong, X.-J.; Ren, Y.-P.; Chen, W.-X.; Long, L.-S.; zheng, Z.; Huang, R.-B.; zheng, L.-S., A Four-Shell, Nesting Doll-Like 3d-4f Cluster Containing 108 Metal Ions. *Angewandte Chemie International Edition in English* **2008,** *47* (13), 2398-2401.

66. (a) Brennan, J. G.; Sella, A., Scandium, Yttrium and the Lanthanides. In *Organometallic Chemistry*, The Royal Society of Chemistry: 2010; Vol. 36, pp 121-147; (b) Norton, K.; Banerjee, S.; Heubner, L.; Das, S.; Emge, T. J.; Brennan, J. G., Lanthanide Oxochlcogenido Clusters. *Dalton Transactions* **2010,** *39*; (c) Banerjee, S.; Huebner, L.; Romanelli, M. D.; Kumar, G. A.; Riman, R. E.; Emge, T. J.; Brennan, J. G., Oxoselenido Clusters of the Lanthanides: Rational Introduction of Oxo Ligands and Near-IR Emission from Nd(III). *Journal of the American Chemical Society* **2005,** *127*.

67. Horrocks, W. D.; Sudnick, D. R., Lanthanide ion luminescence probes of the structure of biological macromolecules. *Accounts of Chemical Research* **1981,** *14* (12), 384-392.

68. (a) Sommerville, L. E.; Resnick, R. M.; Thomas, D. D.; Nelsestuen, G. L., Terbium probe of calcium-binding sites on the prothrombin-membrane complex. *Journal of Biological Chemistry* **1986,** *261* (14), 6222-6229; (b) Richardson, F. S., Terbium(III) and europium(III) ions as luminescent probes and stains for biomolecular systems. *Chemical Reviews* **1982,** *82* (5), 541-552.

69. Tanguay, J. F.; Suib, S. L., Luminescence as a Probe of Rare Earth Ions in Zeolites. *Catalysis Reviews: Science and Engineering* **1987,** *29* (1), 1 - 40.

70. Albin, M.; Farber, G. K.; Horrocks, W. D., Europium(III) luminescence excitation spectroscopy. A species-specific method for the quantitation of lanthanide ion binding to chelating agents. Complexes of (1,2-ethanediyldioxy)diacetate. *Inorganic Chemistry* **1984,** *23* (12), 1648-1651.

71. (a) McNemar, C. W.; Horrocks, W. D., The determination of the $Mg^{2+}\cdot$ATP dissociation constant by competition with Eu^{3+} ion using laser-induced Eu^{3+} ion luminescence spectroscopy. *Analytical Biochemistry* **1990,** *184* (1), 35-38; (b) Ling Wu, S.; DeW. Horrocks, W., Direct determination of stability constants of lanthanide ion chelates by laser-excited europium(III) luminescence spectroscopy: application to cyclic and acyclic aminocarboxylate complexes. *Journal of the Chemical Society, Dalton Transactions* **1997,** (9), 1497-1502.

72. Ozaki; Arisaka; Kimura; Francis; Yoshida, Empirical method for prediction of the coordination environment of Eu(III) by time-resolved laser-induced fluorescence spectroscopy. *Analytical and Bioanalytical Chemistry* **2002,** *374* (6), 1101-1104.

73. (a) Frey, S. T.; Horrocks, W. D., On correlating the frequency of the $^7F_0 \longrightarrow {}^5D_0$ transition in Eu^{3+} complexes with the sum of `nephelauxetic parameters' for all of the coordinating atoms. *Inorganica Chimica Acta* **1995,** *229* (1-2), 383-390; (b) Albin, M.; Horrocks, W. D., Europium(III) luminescence excitation spectroscopy. Quantitive correlation between the total charge on the ligands and the $^7F_0 \longrightarrow {}^5D_0$ transition frequency in europium(III) complexes. *Inorganic Chemistry* **1985,** *24* (6), 895-900.

74. (a) Haas, Y.; Stein, G., Pathways of radiative and radiationless transitions in europium(III) solutions. The role of high energy vibrations. *The Journal of Physical Chemistry* **1971,** *75* (24), 3677-3681; (b) Haas, Y.; Stein, G., Pathways of radiative and radiationless transitions in europium(III) solutions. Role of solvents and anions. *The Journal of Physical Chemistry* **1971,** *75* (24), 3668-3677; (c) Heller, A., Formation of Hot OH Bonds in the Radiationless Relaxations of Excited Rare Earth Ions in Aqueous Solutions. *Journal of the American Chemical Society* **1966,** *88* (9), 2058-2059.

75. (a) Stein, G.; Wurzberg, E., Energy gap law in the solvent isotope effect on radiationless transitions of rare earth ions. *The Journal of Chemical Physics* **1975,** *62* (1), 208-213; (b) Kropp, J. L.; Windsor, M. W., Luminescence and Energy Transfer in Solutions of Rare-Earth Complexes. I. Enhancement of Fluorescence by Deuterium Substitution. *The Journal of Chemical Physics* **1965,** *42* (5), 1599-1608.

76. Supkowski, R. M.; Horrocks, W. D., On the determination of the number of water molecules, q, coordinated to europium(III) ions in solution from luminescence decay lifetimes. *Inorganica Chimica Acta* **2002,** *340*, 44-48.

77. Durham, D. A.; Frost, G. H.; Hart, F. A., Lanthanide complexes-VIII tris(2,2'6',2''-terpyridine)lanthanide(III)perchlorates: Fluorescence and structure. *Journal of Inorganic and Nuclear Chemistry* **1969,** *31* (3), 833-838.

78. (a) Allen J. Bard, L. R. F., *Electrochemical Methods Fundamentals and Applications* Second Addition ed.; John Wiley and Sons, INC: New York, 2001; (b) Tóth, É.; Burai, L.; Merbach, A. E., Similarities and differences between the isoelectronic GdIII and EuII complexes with regard to MRI contrast agent applications. *Coordination Chemistry Reviews* **2001,** *216-217*, 363-382; (c) Botta, M.; Ravera, M.; Barge, A.; Bottaro, M.; Osella, D., Relationship between ligand structure and electrochemical and relaxometric properties of acyclic poly(aminocarboxylate) complexes of Eu(ii). *Dalton Transactions* **2003,** (8), 1628-1633.

79. (a) Sadakane, M.; Steckhan, E., Electrochemical Properties of Polyoxometalates as Electrocatalysts. *Chemical Reviews* **1998,** *98* (1), 219-238; (b) Boujtita, M.; Boixel, J.; Blart, E.; Mayer, C. R.; Odobel, F., Redox properties of hybrid Dawson type polyoxometalates disubstituted with organo-silyl or organo-phosphoryl moieties. *Polyhedron* **2008,** *27* (2), 688-692; (c) Shriver, N. P. a. D. F., The Octahedral M_6Y_6 and M_6Y_{12} Clusters of Group 4 and 5 Transition Metals. In *Advances in Inorganic Chemistry*, Academic Press: New York, 1999; Vol. 46; (d) Long, E. J. W. a. J. R., Atomlike Building Units of Adjustable Character: Solid-State and Solution Routes to Manipulating Hexanuclear Transition Metal Chalcohalide Clusters. In *Progress in Inorganic Chemistry*, Karlin, K. D., Ed. John Wiley and Sons, Inc.: New York, 2005; Vol. 54.

80. Morsomme, P.; Slayman, C. W.; Goffeau, A., Mutagenic study of the structure, function and biogenesis of the yeast plasma membrane H+-ATPase. *Biochimica et Biophysica Acta (BBA) - Reviews on Biomembranes* **2000,** *1469* (3), 133-157.

81. (a) Espenson, J. H.; McCarley, R. E., Oxidation of Tantalum Cluster Ions1. *Journal of the American Chemical Society* **1966,** *88* (5), 1063-1064; (b) Espenson, J. H., Kinetic study of the two-stage oxidation of the tantalum halide cluster ion $(Ta_6Br_{12})^{2+}$ by vanadium(V). *Inorganic Chemistry* **1968,** *7* (4), 631-635; (c) Espenson, J. H.; Boone, D. J., Kinetics and mechanism of oxidation of the tantalum halide cluster ion $(Ta_6Cl_{12})^{2+}$ by cobalt(III) complexes and by miscellaneous oxidizing agents. *Inorganic Chemistry* **1968,** *7* (4), 636-640; (d) Eisenbraun, R.; Schäfer, H., Drei Wege zur Oxydation von $[Ta_6Cl_{12}]^{2+}$ ($[Ta_6Br_{12}]^{2+}$ und $[Nb_6Cl_{12}]^{2+}$). *Zeitschrift für anorganische und allgemeine Chemie* **1985,** *530* (11), 222-226; (e) Hussey, C. L.; Quigley, R.; Seddon, K. R., Electrochemical and Spectroscopic Characterization of $\{Ta_6Cl_{12}\}^{2+}$ Chloride Clusters in Acetonitrile and in The Aluminum Chloride-1-Methyl-3-ethylimidazolium Chloride Molten Salt. *Inorganic Chemistry* **1995,** *34* (1), 370-377; (f) Penicaud, A.; Batail, P.; Coulon, C.; Canadell, E.; Perrin, C., Novel redox properties of the paramagnetic hexanuclear niobium cluster halide $Nb_6Cl_{18}^{3-}$ and the preparation, structures, and conducting and magnetic properties of its one-dimensional mixed-valence tetramethyltetra(selena and thia)fulvalenium salts: $[TMTSF and TMTTF]_5[Nb_6Cl_{18}](CH_2Cl_2)_{0.5}$. *Chemistry of Materials* **1990,** *2* (2), 123-132.

82. (a) Seibig, S.; Tóth, É.; Merbach, A. E., Unexpected Differences in the Dynamics and in the Nuclear and Electronic Relaxation Properties of the Isoelectronic $[Eu^{II}(DTPA)(H_2O)]^{3-}$ and $[Gd^{III}(DTPA)(H_2O)]^{2-}$ Complexes (DTPA = Diethylenetriamine Pentaacetate)1. *Journal of the American Chemical Society* **2000,** *122* (24), 5822-5830; (b) Nagaishi, R.; Arisaka, M.; Kimura, T.; Kitatsuji, Y., Spectroscopic and electrochemical properties of europium(III) ion in hydrophobic ionic liquids under controlled condition of water content. *Journal of Alloys and Compounds* **2007,** *431* (1-2), 221-225; (c) Starynowicz, P., Structure and spectroscopy of diaqua(μ_3-acetato)(acetato-O)(acetic acid-O)europium(II), $[Eu(OAc)_2(AcOH)(H_2O)_2]$. *Polyhedron* **1995,** *14* (23-24), 3573-3577; (d) Starynowicz, P., Crystal structure of triaquadihydrogen triaquatris(oxydiacetato)dieuropate(II). *Journal of Alloys and Compounds* **1995,** *224* (2), 217-219; (e) Starynowicz, P., Crystal structure of triaqua(oxydiacetato-O,O',O")europium(II) hydrate. *Journal of Alloys and Compounds* **1995,** *225* (1-2), 406-408; (f) Starynowicz, P., Synthesis and structure of trisodium (ethylenediaminetetraacetato)europate(II) chloride heptahydrate. *Journal of Alloys and Compounds* **1998,** *269* (1-2), 67-70; (g) Starynowicz, P., Synthesis and crystal structure of europium(II) diacetate hemihydrate, $Eu(CH_3COO)_2 \cdot 0.5H_2O$. *Journal of Alloys and Compounds* **1998,** *268* (1-2), 47-49; (h) Starynowicz, P., Europium(II) complexes with unsubstituted crown ethers. *Polyhedron* **2003,** *22* (2), 337-345.

83. Kissinger, P. T.; Heineman, W. R., Cyclic voltammetry. *Journal of Chemical Education* **1983,** *60* (9), 702-null.

84. (a) Jiang, J.; Higashiyama, N.; Machida, K.-i.; Adachi, G.-y., The luminescent properties of divalent europium complexes of crown ethers and cryptands. *Coordination Chemistry Reviews* **1998,** *170* (1), 1-29; (b) Yee, E. L.; Gansow, O. A.; Weaver, M. J., Electrochemical studies of europium and ytterbium cryptate formation in aqueous solution. Effects of varying the metal oxidation state upon cryptate thermodynamics and kinetics. *Journal of the American Chemical Society* **1980,** *102* (7), 2278-2285.

85. Bicknell, R. T. M.; Davies, D. B.; Lawrence, K. G., Density, refractive index, viscosity and ^{1}H nuclear magnetic resonance measurements of dimethyl sulphoxide at 2 ^{o}C intervals in the range 20-60 ^{o}C. Structural implications. *Journal of the Chemical Society, Faraday Transactions 1: Physical Chemistry in Condensed Phases* **1982,** *78* (5), 1595-1601.

86. (a) Urbansky, E., Perchlorate as an environmental contaminant. *Environmental Science and Pollution Research* **2002,** *9* (3), 187-192; (b) Bond, A. M., Novel Aspects of Electrochemical Oxidation of Inorganic Nompounds in Non-Coordinating Media. *Pure and Applied Chemistry* **1990,** *62* (2), 1043-1046.

87. (a) Davis, D. D.; Stevenson, K. L.; King, G. K., Photolysis of europium(II) perchlorate in aqueous acidic solution. *Inorganic Chemistry* **1977,** *16* (3), 670-673; (b) Douglas, D. L.; Yost, D. M., Photo-Chemical Reduction of Water by Europium (II) Ion, and the Magnetic Susceptibilities of Europium (II) and (III) Ions. *The Journal of Chemical Physics* **1949,** *17* (12), 1345-1346.

88. Peter Dawson, D. O. C., Ronald G. Grainger, *Textbook of Contrast Media*. Isis Medical Media Ltd.: Oxford, 1999.

89. Aime, S.; Botta, M.; Gianolio, E.; Terreno, E., A p(O2)-Responsive MRI Contrast Agent Based on the Redox Switch of Manganese(II□/□III)□–□Porphyrin Complexes. *Angewandte Chemie International Edition* **2000,** *39* (4), 747-750.

90. Caravan, P.; Tóth, É.; Rockenbauer, A.; Merbach, A. E., Nuclear and Electronic Relaxation of $Eu^{2+(aq)}$: An Extremely Labile Aqua Ion1. *Journal of the American Chemical Society* **1999,** *121* (44), 10403-10409.

91. (a) Meyer, G., Superbulky Ligands and Trapped Electrons: New Perspectives in Divalent Lanthanide Chemistry. *Angewandte Chemie International Edition* **2008,** *47* (27), 4962-4964; (b) Girard, P.; Namy, J. L.; Kagan, H. B., Divalent lanthanide derivatives in organic synthesis. 1. Mild preparation of samarium iodide and ytterbium iodide and their use as reducing or coupling agents. *Journal of the American Chemical Society* **1980,** *102* (8), 2693-2698.

92. (a) Greedan, J. E.; McCarthy, G. J.; Sipe, C., Complex oxides containing divalent europium. II. Europium metal metal' oxide ($Eu(M,M')O_3$) phases. *Inorganic Chemistry* **1975,** *14* (4), 775-779; (b) Greedan, J. E.; Johnston, R. G.; McCarthy, G. J., Magnetic properties of the divalent europium scheelites europium molybdate and europium tungstate and the mixed-valence phases Eu_xMoO_4 and Eu_xWO_4. *Inorganic Chemistry* **1976,** *15* (5), 1238-1240; (c) Machida, K.; Hata, H.; Okuno, K.; Adachi, G.; Shiokawa, J., Synthesis and characterization of divalent-europium (Eu^{2+}) compounds, EuB_4O_7, EuB_2O_4 and $Eu_2B_2O_5$. *Journal of Inorganic and Nuclear Chemistry* **1979,** *41* (10), 1425-1430.

93. Mitzi, D. B.; Liang, K., Preparation and Properties of $(C_4H_9NH_3)_2EuI_4$: A Luminescent Organic−Inorganic Perovskite with a Divalent Rare-Earth Metal Halide Framework. *Chemistry of Materials* **1997,** *9* (12), 2990-2995.

94. Burai, L.; Tóth, É.; Seibig, S.; Scopelliti, R.; Merbach, A. E., Solution and Solid-State Characterization of EuII Chelates: A Possible Route Towards Redox Responsive MRI Contrast Agents. *Chemistry – A European Journal* **2000,** *6* (20), 3761-3770.

95. Adin, A.; Sykes, A. G., The kinetics of the oxidation of europium(II) with vanadium(III) and chromium(III) in aqueous perchloric acid solutions. *Journal of the Chemical Society A: Inorganic, Physical, Theoretical* **1966**, 1230-1236.

96. Cooley, R. A.; Yost, D. M.; Stone, H. W., *Europium(II) Salts*. John Wiley & Sons, Inc.: 2007; p 69-73.

97. Mudring, A.-V.; Timofte, T.; Babai, A., Cluster-Type Basic Lanthanide Iodides $[M_6(\mu_6\text{-}O)(\mu_3\text{-}OH)_8(H_2O)_{24}]I_8(H_2O)_8$ (M = Nd, Eu, Tb, Dy)†. *Inorganic Chemistry* **2006,** *45* (13), 5162-5166.

98. Zhang, H.-y.; Yu, H.-j.; Xu, H.-x.; Ren, J.-s.; Qu, X.-g., Structural diversity of lanthanide-amino acid complexes under near physiological pH conditions and their recognition of single-stranded DNA. *Polyhedron* **2007,** *26* (18), 5250-5256.

99. Nolting, D. D. Polynuclear Lanthanide and Yttrium Complex and Tungsten Bromide CLuster Chemistries Relevant to Diagnostic Imaging and Protien Crystallographic Phasing. The University of Iowa, Iowa City, 2005.

100. Deepak M. Shendage, R. F., and Günter Haufe, Highly Efficient Stereoconservative Amidation and Deamidation of α-Amino Acids. *Organic Letters* **2004,** *6* (21), 3675-3678.

101. Maverick, A. W.; Gray, H. B., Luminescence and redox photochemistry of the molybdenum(II) cluster $Mo_6Cl_{14}^{2}$. *Journal of the American Chemical Society* **1981,** *103* (5), 1298-1300.

102. Zhang, X.; McCarley, R. E., High-Yield Synthesis of the W_6S_8 Cluster Unit as the Pyridine Complex $(W_6S_8)(py)_6$ and Attempts To Prepare Tungsten Analogs of the Chevrel Phases. *Inorganic Chemistry* **1995,** *34* (10), 2678-2683.

103. Hay, D. N. T. M., L., Low-Temperature, High Yield Synthesis, and Convient Isolation of the High-Electron-Density Cluster Compound $Ta_6Br_{14}8H_2O$ for Use in Biomacromloecular Crystallographic Phase Determination. *Journal of Structural Biology* **2002,** *139* (3), 147-151.

104. Gray, T. G.; Rudzinski, C. M.; Meyer, E. E.; Holm, R. H.; Nocera, D. G., Spectroscopic and Photophysical Properties of Hexanuclear Rhenium(III) Chalcogenide Clusters. *Journal of the American Chemical Society* **2003,** *125* (16), 4755-4770.

105. (a) Gray, H. B.; Maverick, A. W., Solar Chemistry of Metal Complexes. *Science* **1981,** *214* (4526), 1201-1205; (b) Simon, A., Cluster valenzelektronenarmer Metalle – Strukturen, Bindung, Eigenschaften. *Angewandte Chemie* **1988,** *100* (1), 163-188; (c) Golden, J. H.; Deng, H.; DiSalvoa, F. J.; Fréchet, J. M. J.; Thompson, P. M., Monodisperse Metal Clusters 10 Angstroms in Diameter in a Polymeric Host: The "Monomer as Solvent' Approach. *Science* **1995,** *268* (5216), 1463-1466.

106. Wikipedia Octahedral cluster. http://en.wikipedia.org/wiki/Octahedral_cluster (accessed March).

107. (a) Hogue, R. D.; McCarley, R. E., Chemistry of polynuclear metal halides. V. Reactions and characterization of compounds containing tungsten halide cluster species. *Inorganic Chemistry* **1970,** *9* (6), 1354-1360; (b) Sheldon, J. C., 208. Chloromolybdenum(II) compounds. *Journal of the Chemical Society (Resumed)* **1960**, 1007-1014; (c) Fergusson, J. E.; Robinson, B. H.; Wilkins, C. J., Complex formation by molybdenum(II) chloride. *Journal of the Chemical Society A: Inorganic, Physical, Theoretical* **1967**, 486-490; (d) Carmichael, W. M.; Edwards, D. A., Complexes of octa-$[\mu]_3$-chlorohexamolybdenum(II) chloride with nitrogen donors. *Journal of Inorganic and Nuclear Chemistry* **1967,** *29* (6), 1535-1538.

108. Field, R. A.; Kepert, D. L.; Taylor, D., Metal atom clusters III. The acceptor properties and bonding of $(Mo_6Cl_8)^{4+}$ and $(Nb_6Cl_{12})^{2+}$ clusters. *Inorganica Chimica Acta* **1970,** *4*, 113-117.

109. (a) Hamer, A. D.; Smith, T. J.; Walton, R. A., Complex halides of the transition metals. XXI. Evidence for the existence of tertiary phosphine derivatives of the new octachlorohexamolybdate(2+) cluster cation. *Inorganic Chemistry* **1976,** *15* (5), 1014-1017; (b) Saito, T.; Nishida, M.; Yamagata, T.; Yamagata, Y.; Yamaguchi, Y., Synthesis of hexanuclear molybdenum cluster alkyl complexes coordinated with trialkylphosphines: crystal structures of trans-$[(Mo_6Cl_8)Cl_4\{P(n\text{-}C_4H_9)_3\}_2]$ and all-trans-$[(Mo_6Cl_8)Cl_2(C_2H_5)_2\{P(n\text{-}C_4H_9)_3\}_2]$ $2C_6H_5CH_3$. *Inorganic Chemistry* **1986,** *25* (8), 1111-1117.

110. (a) Cotton, F. A.; Curtis, N. F., Some New Derivatives of the Octa-μ_3-chlorohexamolybdate(II),$[Mo_6Cl_8]_4^+$, Ion. *Inorganic Chemistry* **1965,** *4* (2), 241-244; (b) Schäfer, H.; Plautz, H.; Abel, H.-J.; Lademann, D., Einige Reaktionen mit $[Mo_6Cl_8]Cl_4$. *Zeitschrift für anorganische und allgemeine Chemie* **1985,** *526* (7), 168-176.

111. Preetz, W.; Braack, P.; Harder, K.; Peters, G., 15N- und 19F-NMR-spektroskopischer Nachweis und Xa-Austauschreaktionen der Clusteranionen [(Mo6Cl□i8)(15NCS)□an X□a6−n]2−, Xa = F, Cl, Br, I; n = 1–6. *Zeitschrift für anorganische und allgemeine Chemie* **1992,** *612* (6), 7-13.

112. (a) Johnston, D. H.; Gaswick, D. C.; Lonergan, M. C.; Stern, C. L.; Shriver, D. F., Preparation of bis(tetrabutylammonium) octa(μ_3-chloro)hexakis(trifluoromethanesulfonato)-octahedro-hexamolybdate(2-), $(Bu_4N)_2[Mo_6Cl^{i8}(CF_3SO_3)^{a6}]$: a versatile starting material for substituted molybdenum(II) clusters containing the $[Mo_6Cl^{i8}]^{4+}$ core. *Inorganic Chemistry* **1992,** *31* (10), 1869-1873; (b) Johnston, D. H.; Stern, C. L.; Shriver, D. F., Synthesis of 12-metal clusters based on the $([Mo_6Cl_8]^{4+})$ core. X-ray structure of $(PPN)_2[Mo_6Cl^{i8}\{(\mu\text{-NC})Mn(CO)_2Cp\}^{a6}]$. *Inorganic Chemistry* **1993,** *32* (23), 5170-5175.

113. (a) Harder, K.; Peters, G.; Preetz, W., 19F-NMR-spektroskopischer Nachweis und Xa-Austauschreaktionen der Clusteranionen [(Mo6Cl□8i)F□naX□6-na]2−, Xa = Cl, Br, I; n = 1 – 6. *Zeitschrift für anorganische und allgemeine Chemie* **1991,** *598* (1), 139-149; (b) Preetz, W.; Harder, K.; von Schnering, H. G.; Kliche, G.; Peters, K., Synthesis, structure and properties of the cluster anions $[(Mo_6Cl_8^{i})X_6^{a}]^{2-}$ with Xa[triple bond; length as m-dash]F, Cl, Br, I. *Journal of Alloys and Compounds* **1992,** *183*, 413-429; (c) Preetz, W.; Bublitz, D.; Von Schnering, H. G.; Saßmannshausen, J., Darstellung, Kristallstruktur und spektroskopische Eigenschaften der Clusteranionen [(Mo6Br□8i)X□6a]2− mit Xa = F, Cl, Br, I. *Zeitschrift für anorganische und allgemeine Chemie* **1994,** *620* (2), 234-246; (d) Brückner, P.; Peters, G.; Preetz, W., 19F-NMR-spektroskopischer Nachweis und Berechnung der statistischen Bildung der gemischten Clusteranionen [(Mo6Br□niCl□8−ni)F□6a]2−, n = 0 – 8. *Zeitschrift für anorganische und allgemeine Chemie* **1993,** *619* (3), 551-558; (e) Brückner, P.; Peters, G.; Preetz, W., 19F-NMR-spektroskopischer Nachweis und statistische Untersuchung zur Bildung der gemischten Clusteranionen [(Mo6I□niCl□8−ni)F□6a]2−, n = 0–7, und Darstellung von (TBA)2[(Mo6I□8i)F□6a]. *Zeitschrift für anorganische und allgemeine Chemie* **1993,** *619* (11), 1920-1926.

114. (a) Bublitz, D.; Preetz, W.; Simsek, M. K., Darstellung, Kristallstrukturen und spektroskopische Eigenschaften der Clusteranionen [(Mo6X□8i)(N3)□6a]2−; Xi = Cl, Br. *Zeitschrift für anorganische und allgemeine Chemie* **1997,** *623* (1-6), 1-7; (b) Simsek, M. K.; Preetz, W., Darstellung, Kristallstrukturen, Schwingungsspektren und Normalkoordinatenanalyse von (TBA)2[(Mo6X□8i)Y□6a]; Xi = Cl, Br; Ya = NCO, NCSe. *Zeitschrift für anorganische und allgemeine Chemie* **1997,** *623* (1-6), 515-523.

115. Harder, K.; Preetz, W., Darstellung und spektroskopische Charakterisierung des Clusteranions $[(Mo_6Cl_8^{i})(CF_3COO)_6^{a}]^{2-}$. *Zeitschrift für anorganische und allgemeine Chemie* **1992,** *612* (6), 97-100.

116. Sheldon, J. C., Polynuclear Complexes of Molybdenum(II). *Nature* **1959,** *184* (4694), 1210-1213.

117. (a) Sheldon, J. C., 252. Sterically hindered SN2 hydroxide attack of the bromomolybdenum (II) group. *Journal of the Chemical Society (Resumed)* **1964**, 1287-1291; (b) Sheldon, J. C., 791. SN2 hydroxide attack on the chloromolybdate(II) group. *Journal of the Chemical Society (Resumed)* **1963**, 4183-4186.

118. (a) Nannelli, P.; Block, B. P., Molybdenum(II) cluster compounds involving alkoxy groups. *Inorganic Chemistry* **1968,** *7* (11), 2423-2426; (b) Chisholm, M. H.; Heppert, J. A.; Huffman, J. C., Octahedral Mo_6 clusters supported by methoxide ligands. *Polyhedron* **1984,** *3* (4), 475-478.

119. (a) Gabriel, J.-C. P.; Boubekeur, K.; Uriel, S.; Batail, P., Chemistry of Hexanuclear Rhenium Chalcohalide Clusters. *Chemical Reviews* **2001,** *101* (7), 2037-2066; (b) Yaghi, O. M.; Scott, M. J.; Holm, R. H., Rhenium-selenium-chlorine solid phases: cluster excision and core substitution reactions of molecular species. *Inorganic Chemistry* **1992,** *31* (23), 4778-4784; (c) Uriel, S.; Boubekeur, K.; Batail, P.; Orduna, J.; Canadell, E., Solution Chemistry of Chalcohalide Hexanuclear Rhenium Cluster Monoanions: Substitution Reactions and Structural and LSIMS Characterization of the Heterosubstituted Cluster Dianions, $(n\text{-}Bu_4N)_2[Re_6Q_5ECl_8]$ (Q = S, E = O, S, Se; Q = Se, E = S, Se, Te). *Inorganic Chemistry* **1995,** *34* (21), 5307-5313.

120. (a) Cordier, S.; Perrin, C.; Sergent, M., A new series of oxyhalides based on $(Nb_6Cl_{11}^iO^i)Cl_6$a units with oxygen in statistical occupancy: $M_2renb_6Cl_{17}O$. The crystal structure of $Cs_2LuNb_6Cl_{17}O$. *Materials Research Bulletin* **1996,** *31* (6), 683-690; (b) Cordier, S.; Perrin, C.; Sergent, M., New series of niobium oxychlorides, $M_2RENb_6Cl_{15}O_3$ (M = monovalent cation, RE = rare earth) and $M_2UNb_6Cl_{15}O_3$. The crystal structure of $Cs_2UNb_6Cl_{15}O_3$. *Materials Research Bulletin* **1997,** *32* (1), 25-33; (c) Cordier, S.; Perrin, C.; Sergent, M., An Original Series in the Tantalum Cluster Oxohalide Chemistry with Isolated $(Ta_6Br_{15}O_3)^{5-}$ Units: Crystal Structure of $Cs_2LaTa_6Br_{15}O_3$. *Journal of Solid State Chemistry* **1995,** *120* (1), 43-48; (d) Perrin, C.; Cordier, S.; Ihmaine, S.; Sergent, M., Recent investigations on the $(Me_6L_{18})_n$ unit based halides and oxyhalides (Me = Nb, Ta and L = Cl, Br, O) with rare earths as countercations: Electronic and steric effects. *Journal of Alloys and Compounds* **1995,** *229* (1), 123-133; (e) Anokhina, E. V.; Day, C. S.; Lachgar, A., A New Quasi-One-Dimensional Niobium Oxychloride Cluster Compound $Cs_2Ti_4Nb_6Cl_{18}O_6$: Structural Effects of Ligand Combination. *Inorganic Chemistry* **2001,** *40* (20), 5072-5076; (f) Anokhina, E. V.; Day, C. S.; Meyer, H.-J.; Ströbele, M.; Kauzlarich, S. M.; Kim, H.; Whangbo, M.-H.; Lachgar, A., Preparation, structure, and properties of a series of anisotropic oxychloride cluster compounds $A_xNb_6Cl_{12}O_2$ (A=K, Rb, Cs, or In). *Journal of Alloys and Compounds* **2002,** *338* (1-2), 218-228; (g) Gulo, F.; Perrin, C., The crystal structure of CsNbClO, a novel niobium cluster oxychloride with interconnected NbClO units. *Journal of Materials Chemistry* **2000,** *10* (7), 1721-1724.

121. Crawford, N. R. M.; Long, J. R., Edge-Bridged Octahedral Tungsten−Oxygen−Chlorine Clusters: Synthesis and Characterization of Two D_{3d}-Symmetric $[W_6O_6Cl_{12}]^{2-}$ Isomers and $[W_6O_7Cl_{11}]^{3-}$. *Inorganic Chemistry* **2001,** *40* (14), 3456-3462.

122. Kolesnichenko, V.; Messerle, L., Facile Reduction of Tungsten Halides with Nonconventional, Mild Reductants. 2. Four Convenient, High-Yield Solid-State Syntheses of the Hexatungsten Dodecachloride Cluster W_6Cl_{12} and Cluster Acid $(H_3O)_2[W_6(\mu_3\text{-}Cl)_8Cl_6](OH_2)_x$, Including New Cation-Assisted Ternary Routes. *Inorganic Chemistry* **1998,** *37* (15), 3660-3663.

123. Tillack, J., *Inorganic Syntheses*. McGraw-Hill, Inc.: 1973; Vol. XIV.

124. (a) Imoto, H.; Simon, A., Structural study of the spin-crossover transition in the cluster compounds niobium iodide (Nb_6I_{11}) and hydrogen niobium iodide (HNb_6I_{11}). *Inorganic Chemistry* **1982,** *21* (1), 308-319; (b) Zheng, Y.-Q.; Jonas, E.; Nuss, J.; Schnering, H. G. v., The DMSO Solvated octahedro-[W6Cl□i12]Cl□6a Cluster Molecule. *Zeitschrift für anorganische und allgemeine Chemie* **1998,** *624* (9), 1400-1404; (c) Siepmann, R.; v. Schnering, H. G.; Schäfer, H., Tungsten Trichloride [W_6Cl_{12}]Cl_6. *Angewandte Chemie International Edition in English* **1967,** *6* (7), 637-637.

125. Hay, D. N. T.; Swenson, D. C.; Messerle, L., Gallium and Gallium Dichloride, New Solid-State Reductants in Preparative Transition Metal Chemistry. New, Lower Temperature Syntheses and Convenient Isolation of Hexatantalum Tetradecachloride Octahydrate, $Ta_6(\mu\text{-}Cl)_{12}Cl_2(OH_2)4.4H_2O$, and Synthesis and Solid-State Structure of a Tetraalkylammonium Derivative, $[N(CH_2Ph)Bu_3]_4[Ta_6(\mu\text{-}Cl)_{12}Cl_6]$, of the Reduced $[Ta_6(\mu\text{-}Cl)_{12}]^{2+}$ Cluster Core1. *Inorganic Chemistry* **2002,** *41* (18), 4700-4707.

126. Kashta, A.; Brniceaic, N.; McCarley, R. E., Reactions of niobium and tantalum clusters with aliphatic alcohols. Synthesis and properties of $[M_6X_{12}(ROH)_6]X_2$, M = Nb or Ta, X = Cl or Br, R = Me, Et, i-Pr or i-Bu. *Polyhedron* **1991,** *10* (17), 2031-2036.

127. Planinić, P.; Rastija, V.; Širac, S.; Vojnović, M.; Frkanec, L.; Brničević, N.; McCarley, R. E., Nitrile Cluster Compounds $[(M_6X_{12})X_2(RCN)_4]$ (M=Nb, Ta; X=Cl, Br; R=Et, -Pr, -Bu). *Journal of Cluster Science* **2002,** *13* (2), 215-222.